

# Birla Central Library

PILANI (Rajasthan)

Class No. 541 3452  
Book No. K 957 A V 3  
Accession No. 42262

Acc. No . . . . .

## ISSUE LABEL

Not later than the latest date stamped below.

--	--	--





ADVANCES IN COLLOID SCIENCE  
VOLUME III

# Advances in COLLOID SCIENCE

Inaugurated by the late ELMER O. KRAEMER

VOLUME I: Edited by E. O. Kraemer, F. E. Bartell,  
and S. S. Kistler. "Out of print."

VOLUME II: *Scientific Progress in the Field of Rubber  
and Synthetic Elastomers.* Edited by H.  
Mark and G. S. Whitby.

VOLUME III: Edited by H. Mark and L. J. W. Verwey.

# Advances in Colloid Science'

VOLUME III

Edited by

H. MARK

*Polymer Research Institute  
Polytechnic Institute of Brooklyn  
Brooklyn, New York*

E. J. W. VERWEY

*N. V. Philips' Gloeilampenfabrieken  
Eindhoven, Holland*



INTERSCIENCE PUBLISHERS, INC., NEW YORK  
INTERSCIENCE PUBLISHERS LTD., LONDON

Copyright, 1950, by  
INTERSCIENCE PUBLISHERS, INC.

*All Rights Reserved*

This book or any part thereof must not be reproduced in any form without permission of the publisher in writing. This applies specifically to photostat and microfilm reproductions.

INTERSCIENCE PUBLISHERS, INC.  
215 Fourth Avenue, New York 3, N. Y.

*For Great Britain and Northern Ireland*  
INTERSCIENCE PUBLISHERS LTD.  
2a Southampton Row, London W. C. 1

Printed in the United States of America  
by Mack Printing Co., Easton, Pa.

## PREFACE

The second volume of *Advances in Colloid Science*, which appeared in 1946, was devoted to a field of special and actual interest at that time—the analysis and characterization of the rubbery state. It appeared to the editors that the third volume should cover a series of topics, and should attempt to give an approximate cross section through those branches of colloid science that have grown rapidly or shown unexpected developments during the last few years. Three articles, “Electrokinetic Research at the University of Ghent,” by A. J. Rutgers and M. de Smet, “Ion-Exchange Resins,” by H. P. Gregor, and “Ultrasonics and Sonic Phenomena in Colloid and High Polymer Research,” by H. S. Sack, had originally been scheduled for Volume III but shortage of time and space made necessary postponing these to Volume IV. The editors are eager to express their sincerest thanks to the individual authors and to the publishers, whose continued efforts made it possible to bring out Volume III at this time.

March, 1950

H. MARK  
E. J. W. VERWEY

### CONTRIBUTORS TO VOLUME III

A. E. ALEXANDER, *The New South Wales University of Technology,  
Sydney, N. S. W., Australia*

STRATHMORE R. B. COOKE, *School of Mines and Metallurgy, University  
of Minnesota, Minneapolis, Minnesota*

J. H. DE BOER, *Laboratorium voor Chemische Technologie der Technische  
Hoogeschool, Delft, Netherlands*

J. H. DILLON, *The Textile Foundation and Textile Research Institute,  
Princeton, New Jersey*

E. A. HAUSER, *Department of Chemical Engineering, Massachusetts  
Institute of Technology, Cambridge, and Worcester Polytechnic Institute,  
Worcester, Massachusetts*

PER-OLOF KINELL, *Institute of Physical Chemistry, University of Upp-  
sala, Sweden*

D. S. LE BEAU, *Midwest Rubber Reclaiming Company, East St. Louis,  
Illinois*

J. TH. G. OVERBEEK, *Van't Hoff-Laboratorium der Rijksuniversiteit,  
Utrecht, Netherlands*

BENGT G. RÅNBY, *Institute of Physical Chemistry, University of  
Uppsala, Sweden*

## CONTENTS

	PAGE
<b>Preface .....</b>	<b>v</b>
<b>Atomic Forces and Adsorption. By J. H. DE BOER, Delft, Netherlands.....</b>	<b>1</b>
I. Combination of Attraction and Repulsion Forces.....	2
1. Various Forces and Summation of Their Effects.....	2
2. Structure of the Surface.....	4
3. Repulsion Forces.....	6
4. Distance between Adsorbed Molecule and Surface.....	7
II. Interaction between a Surface and Adsorbed Ions or Radicals.....	8
1. Coulomb Interaction between Surface of an Ionic Compound and an Adsorbed Ion.....	8
2. Interaction between an Ion and a Metal Surface.....	11
3. Polarization of a Dielectric Surface by an Adsorbed Ion.....	13
4. Atoms and Free Radicals on Surfaces.....	17
III. Van der Waals' Forces between a Surface and a Visiting Molecule.....	20
1. Physical Adsorption.....	20
2. Nature of Nonpolar van der Waals' Forces.....	21
3. Adsorption of Atoms by Nonpolar van der Waals' Forces.....	24
4. Some Results of Additive Character of Nonpolar van der Waals' Forces.....	27
5. Adsorption on Metal Surfaces by van der Waals' Forces.....	29
6. Polar van der Waals' Forces.....	32
7. Polar van der Waals' Forces. Electrostatic Polarization of an Ad- sorbed Molecule.....	36
IV. Collaboration between Various Forces.....	38
1. Various Attraction Forces Collaborating in Adsorption of a Single Atom or Molecule.....	38
A. Nonpolar van der Waals' Forces and Electrostatic Polariza- tion.....	39
B. Molecule with a Nonperipheral Dipole on an Ionic Surface...	40
C. Molecule with a Peripheral Dipole on an Ionic Surface.....	41
D. Dipole Molecule on a Metallic Surface.....	41
E. Ion on an Ionic Surface.....	42
F. Ion on a Metallic Surface.....	44
G. Covalent Bonds and Nonpolar van der Waals' Forces.....	45
2. Various Forms of van der Waals' Interaction at Different Spots of the Surface.....	46
3. Mutual van der Waals' Forces between Adsorbed Molecules. Re- orientation.....	49



4. Additional Forces Emanating from Chemisorbed Molecules.....	52
5. Ions Next to Ions on Ionic Surfaces.....	54
6. Multimolecular Adsorption.....	55
7. Significance of Entropy Changes.....	56
V. Reactions with or on Surfaces.....	58
1. Changes in Adsorbing Surface. Swelling.....	58
2. Changes in Adsorbed Molecule. "Activated" Adsorption.....	60
3. Reactions on Surfaces.....	63
References.....	63
 <b>Surface Chemistry and Colloids. By A. E. ALEXANDER, <i>Cambridge, England</i></b>	67
I. Introduction.....	67
II. Principal Experimental Techniques.....	68
III. Applications of Surface Chemistry to Problems in Colloidal Systems....	70
1. Proteins.....	71
Molecular Weights from Monolayer Measurements.....	71
Protein Monolayers at Air-Water and Oil-Water Interfaces....	73
Adsorbed Films of Proteins.....	75
Hydrogen Bonding in Proteins and Protein Monolayers.....	76
2. Polymers.....	78
3. Foams and Emulsions.....	80
Kinetics of Adsorption at Air-Water and Oil-Water Interfaces	80
Desorption from Interfaces.....	82
Structure of the Stabilizing Film in Foams and Emulsions....	83
Reactions in Emulsion Systems.....	89
4. Pastes.....	89
5. Biological Problems.....	91
Biological Activity of Homologous Series.....	91
Mechanism of Fat Absorption.....	91
Anthelmintic Activity of Hexylresorcinol in the Presence of	
Soaps.....	92
Bactericidal Activity of Soap-Phenol Mixtures.....	94
References.....	95
 <b>Quantitative Interpretation of the Electrophoretic Velocity of Colloids. By J. TH.</b>	
<b>G. OVERBEEK, <i>Utrecht, Netherlands</i></b> .....	97
I. Introduction.....	97
II. Classical Concepts of Electrophoretic Velocity.....	99
1. Equation of Helmholtz-Smoluchowski.....	99
2. Hückel Equation.....	103
3. Henry Solution of the Contradiction between Smoluchowski and	
Hückel Theories.....	104
4. Influence of Conductivity of Particles.....	107
5. Electrophoresis of Liquid Droplets.....	108
III. Influence of Deformation of Double Layer upon Electrophoresis.....	109
1. Relaxation Effect.....	109

2. Influence of Surface Conductance. ....	117
3. Summary of Conditions in Which Zeta Potential Can Be Evaluated from Electrophoresis. ....	118
4. Experimental Work. ....	119
IV. Electrophoretic Velocity and Charge of Particles. ....	120
1. Charge and Potential. ....	120
2. Spherical Particles. ....	122
3. Nonspherical Particles. ....	127
4. Applications. ....	128
5. Comparison of Electrophoretic Charge with Charge Determined by Other Means. ....	130
6. General Conclusions. ....	133
References. ....	134
 <b>Lyogels.</b> By E. A. HAUSER, <i>Cambridge, Massachusetts</i> , and D. S. LE BEAU, <i>East St. Louis, Illinois</i> . ....	137
1. Introduction. ....	137
II. Older Theories of Lyogel Structure. ....	139
III. Modern Theories of Lyogel Structure. ....	139
IV. Special Types of Lyogels. ....	143
1. Thixotropy. ....	144
2. Rheopexy. ....	145
3. Dilatancy. ....	146
V. Elasticity of Lyogels. ....	147
1. X-Ray Diffraction. ....	148
2. Electron Microscopy. ....	150
3. Ultramicroscopy with Incident Light. ....	150
VI. Summary. ....	158
References. ....	159
 <b>Ultracentrifugal Sedimentation of Polymolecular Substances.</b> By PER-OLOF KINELL and BENGT G. RÅNBY, <i>Uppsala, Sweden</i> . ....	161
I. Introduction. ....	161
II. Ultracentrifugal Method. ....	163
III. Sedimentation Properties of Threadlike Molecules. ....	166
1. Threadlike Molecules in Solution. ....	166
2. Change of Shape in a Centrifugal Field. ....	168
3. Influence of Branching on Sedimentation Velocity. ....	170
4. Interaction between Molecules. Solvation. ....	172
5. Influence of Shielding Ratio. ....	176
6. Sedimentation as a Rate Process. ....	177
7. Concentration Dependence. ....	177
8. Effects of Polymolecularity. ....	181
IV. Information on Polymolecularity from Sedimentation Measurements. ....	183
1. Average Sedimentation Constants. ....	184
2. $dB/dx$ Method According to Gralén. ....	185

3. Frequency Functions from Sedimentation Diagrams.....	188
4. Use of Parameter Functions.....	192
V. Polymolecularity Measurements and Fractionation.....	194
1. Cellulose Nitrate.....	198
Selectivity of Fractionation.....	198
Properties of Cellulose Nitrate Molecules.....	202
Frequency Functions.....	204
2. Polymeric Methyl Methacrylate.....	208
3. Polystyrene.....	212
VI. General Conclusions.....	215
References.....	215

## **Fatigue Phenomena in High Polymers.** By J. H. DILLON, *Princeton, N. J.*.... 219

I. Definitions of Fatigue.....	220
II. Classification of High Polymers.....	221
III. Basic Phenomena Occurring with Fatigue.....	222
1. Molecular Flow and Secondary Bond Slippage.....	222
2. Physical Rupture of Molecular Chains.....	223
3. Orientation.....	223
4. Crystallization.....	225
5. Second-Order Transition.....	226
6. Chemical Scission and Cross Linking.....	226
IV. Generalized Fatigue Tests.....	227
1. Class A Fatigue.....	229
2. Class B Fatigue.....	229
3. Class C Fatigue.....	229
4. Class D Fatigue.....	229
5. Class E Fatigue.....	232
6. Class F Fatigue.....	232
V. Fatigue of Rubbers.....	233
1. General Characteristics.....	233
2. Fatigue Tests with Hysteretic Temperature Rise.....	233
3. Hysteresis.....	237
4. Stress-Strain Characteristics.....	243
5. Dynamic Fatigue Experiments.....	246
6. Qualitative Theory of the Effect of Strain Magnitudes and Limits upon Dynamic Fatigue Life.....	254
7. Fatigue of Rubbers as Related to Weathering.....	263
8. Fatigue Effects as Influenced by Oxidation.....	265
9. Static Fatigue at Intermediate and Low Temperatures.....	270
VI. Fatigue of Fibers.....	272
1. General Characteristics.....	272
2. Resilience.....	273
3. Stress-Strain and Primary Creep Characteristics.....	275
4. Static Fatigue-Rupture, Long-Term Creep, and Relaxation.....	282
5. Dynamic Fatigue.....	286

VII. Fatigue of Plastics.....	306
1. General Characteristics.....	306
2. Stress-Strain, Creep, and Hysteresis.....	307
3. Static and Dynamic Fatigue to Rupture.....	309
VIII. Summary.....	315
References.....	316
<b>Flotation.</b> By STRATHMORE R. B. COOKE, <i>Minneapolis, Minnesota</i> .....	321
I. Introduction.....	321
II. Colloid Production in Grinding.....	323
III. Flotation Reagents.....	324
1. Frothers.....	325
Two-Phase Systems.....	325
Structure of Frothers.....	328
Three-Phase Systems.....	330
Aeration.....	331
Frothers in Practice.....	334
2. Collectors.....	336
Mechanism of Collection.....	338
Orientation of the Collector Coating on the Mineral.....	346
Effect of Slimes on Collection.....	347
Flocculation and Collection.....	353
Classification of Flotation Collectors.....	354
3. Activators.....	357
4. Depressants.....	368
References.....	372
<b>Subject Index</b> .....	375



# ATOMIC FORCES AND ADSORPTION

J. H. DE BOER

*University of Delft, Netherlands*

---

I. Combination of Attraction and Repulsion Forces.....	2
1. Various Forces and Summation of Their Effects.....	2
2. Structure of the Surface.....	4
3. Repulsion Forces.....	6
4. Distance between Adsorbed Molecule and Surface.....	7
II. Interaction between a Surface and Adsorbed Ions or Radicals.....	8
1. Coulomb Interaction between Surface of an Ionic Compound and an Adsorbed Ion.....	8
2. Interaction between an Ion and a Metal Surface.....	11
3. Polarization of a Dielectric Surface by an Adsorbed Ion.....	13
4. Atoms and Free Radicals on Surfaces.....	17
III. Van der Waals' Forces between a Surface and a Visiting Molecule.....	20
1. Physical Adsorption.....	20
2. Nature of Nonpolar van der Waals' Forces.....	21
3. Adsorption of Atoms by Nonpolar van der Waals' Forces.....	24
4. Some Results of Additive Character of Nonpolar van der Waals' Forces.....	27
5. Adsorption on Metal Surfaces by van der Waals' Forces.....	29
6. Polar van der Waals' Forces.....	32
7. Polar van der Waals' Forces. Electrostatic Polarization of an Ad- sorbed Molecule.....	36
IV. Collaboration between Various Forces.....	38
1. Various Attraction Forces Collaborating in Adsorption of a Single Atom or Molecule.....	38
A. Nonpolar van der Waals' Forces and Electrostatic Polariza- tion.....	39
B. Molecule with a Nonperipheral Dipole on an Ionic Surface.....	40
C. Molecule with a Peripheral Dipole on an Ionic Surface.....	41
D. Dipole Molecule on a Metallic Surface.....	41
E. Ion on an Ionic Surface.....	42
F. Ion on a Metallic Surface.....	44
G. Covalent Bonds and Nonpolar van der Waals' Forces.....	45
2. Various Forms of van der Waals' Interaction at Different Spots of the Surface.....	46
3. Mutual van der Waals' Forces between Adsorbed Molecules. Re- orientation.....	49

IV. Collaboration between Various Forces, <i>contd.</i>	
4. Additional Forces Emanating from Chemisorbed Molecules.....	52
5. Ions Next to Ions on Ionic Surfaces.....	54
6. Multimolecular Adsorption.....	55
7. Significance of Entropy Changes.....	56
V. Reactions with or on Surfaces.....	58
1. Changes in Adsorbing Surface. Swelling.....	58
2. Changes in Adsorbed Molecule. "Activated" Adsorption.....	60
3. Reactions on Surfaces.....	63
References.....	63

---

## I. Combination of Attraction and Repulsion Forces

### 1. Various Forces and Summation of Their Effects

One of the first statements that has to be made before discussing atomic forces and adsorption is that there are no special adsorption forces. The various forces that hold a visiting molecule for a shorter or longer time at a surface are exactly the same as those that form molecules from atoms, crystals from molecules, and, *e.g.*, rocks from crystals. They are of the same nature as the forces that cause the cohesion in solids and liquids, or which are responsible for the deviation of the behavior of real gases from the laws of ideal gases. All the various molecular or atomic forces known to us from the study of physical or chemical phenomena may give rise to adsorption when the mutual arrangement of the participating molecules leads to it. When two atoms attract each other and one of them happens to be a constituent atom of a surface and the other is part of a free gaseous or dissolved molecule, the result of their interaction will be that they are bound together for a shorter or longer time; hence the molecule is adsorbed at the surface. The other, neighboring, constituent atoms of the surface may, however, exert a dominant influence on the magnitude of the force of attraction. They may greatly increase this force or they may seriously decrease its magnitude. The resulting "adsorption force" may, therefore, be far higher or far lower than the force that would have been experienced if the attracting atom had been on its own. It is just the result of this adding together of the contributions of all the constituent atoms which makes worth while devoting a special study to the attraction of atoms by surfaces—and therefore to the subject of atomic forces and adsorption.

Though all molecular and atomic forces ultimately find their root in the mutual behavior of the constituent parts of the atoms, *viz.*, the nuclei and the electrons and though, theoretically, they all may be derived from the

fundamental wave equations describing the atoms, it is here, as in other branches of physics and chemistry, still convenient to treat the various forms of mutual interaction of atoms as different forces, acting independently. Such a procedure, which deliberately ignores the theoretical knowledge that all forces are already included in the wave function describing the mutual behavior of the atoms, is only permitted because of the good empirical results obtained with it. Hence we will in the following sections treat such forces as the exchange forces leading to covalent bonds, the Coulomb forces between ions or dipoles, the electrostatic polarization of atoms or molecules by ions, the nonpolar van der Waals' (dispersion) forces, the repulsion forces due to interpenetration of electronic clouds together with the Pauli principle, as different, independently acting forces. In nearly all cases, two or more of these forces act simultaneously; summation of the contributions to the adsorption energy over all participant atoms, however, has to be done for each of these forces separately.

Assuming a known regular pattern for the constituent atoms of the surface and assuming known values for their mutual distances and for the distance of the adsorbed atom from the surface, such summations of all individual contributions can, in many cases, be evaluated with any desired degree of accuracy. This, however, does not mean that we will in practice be able to evaluate the adsorption energy with the same degree of accuracy. On the contrary, we will be only too glad if in many cases the right order of magnitude results from our calculations. Three main reasons for this are:

- (a) We have little knowledge of the real structure of the surface.
- (b) We know little about the magnitude of the repulsion forces, which check the attraction forces at short distances.
- (c) We know little about the real distance of the adsorbed atom from the surface.

Despite these three setbacks, with which we will deal separately, we will see that present knowledge enables us to understand the nature of adsorption forces and the magnitude of adsorption energies. These adsorption energies vary widely, from a few hundred calories per mole, which enables a molecule to stay just long enough at a surface to exchange thermal energy with it, up to, in some cases, a few hundred kilocalories per mole. We will, in the following sections, deal only with surfaces of solids and examine the mutual interaction of such surfaces and adsorbed molecules. Adsorption phenomena at liquid-air or liquid-liquid interfaces are, therefore, excluded, as well as problems arising from a competition between adsorption forces and solvation forces as they occur in adsorption from solutions.



## 2. *Structure of the Surface*

In most calculations of adsorption energies the surface of a crystalline adsorbent is idealized as a smooth two-dimensional network of atoms or ions with exactly the same mutual distances as are found inside the crystal. It is also generally assumed that the distances between the atoms or ions of this outer plane and those of the second plane just underneath are the same as those inside the crystal. The surface atoms or ions, however, are not symmetrically surrounded by others as are the atoms or ions inside the crystal. Compared with the distances prevailing in the crystal, those at the surface may be expected to deviate.

Dealing with a crystal like that of sodium chloride, various authors contend that the distance of the ions of the outer layer to those of the second layer is smaller than the normal distance in the crystal, and the ions in the outer layer also tend to have a smaller mutual distance. For the older literature we refer to some compilations (1,100); quite recently Verwey (115), in reconsidering the problem of the free surface of alkali halide crystals, came to the conclusion that the negative surface ions are generally displaced outwardly, over a very short distance, while the positive surface ions are displaced toward the inside of the lattice. For NaCl Verwey found that the sodium ions of the surface are not placed at the normal distance, 2.81 Å. above the chloride ions of the second layer underneath them, but that this distance is 0.15 Å. shorter; the chloride ions of the outer layer, however, are, according to his calculations, 0.05 Å. further away from the sodium ions underneath them. The electric double layer, which results from the fact that the negative ions form a plane 0.20 Å. higher than the sodium ions, is nearly compensated by the effect of the dipoles set up in the negative ions. The result that the negative ions form the outside layer of the surface is in accordance with experimental results obtained with the adsorption of iodine and phenols on salt layers (6d).

Specular reflection experiments with beams of hydrogen or helium (67) show that cleavage surfaces of LiF or NaCl are very smooth surfaces, the inequalities only being of the order of  $10^{-8}$  cm. (as caused by the temperature movement). Diffraction spectra obtained with such material waves may give us the experimental proof that the mutual distance of two fluorine ions *in* the outer layer of LiF is exactly the same as in the crystal. The angles of diffraction, which are measured experimentally, are just slightly smaller than those calculated theoretically from the wave length and the ionic distances. This means that either the actual effective wave length is just slightly smaller than the theoretical one or that the ionic distance in

the outer surface layer of ions is just slightly greater than the distance inside the crystal. The latter would be highly improbable; if anything, just the reverse might have been expected. The effective wave length, however, will be slightly smaller, because there will be a slight increase in velocity when the atom approaches the surface, due to the attraction exercised on it by the ions of the crystal. From a careful experiment by Estermann, Frisch, and Stern (65) the wavelength corresponding to the helium beam may be calculated to  $0.599 \times 10^{-8}$  cm. The beam was homogenized and had a velocity of 1635 m./sec., from which the wave length can be calculated to be  $0.610 \times 10^{-8}$  cm. In order to account for the somewhat lower experimental figure of  $0.599 \times 10^{-8}$  cm., one has to assume that the velocity of the helium atoms increases from 1635 m./sec. to 1665 m./sec., when they approach the surface, hence an increase of kinetic energy of about 45 cal./mole, which is of the right order of magnitude for the adsorption energy in this case.

We may, therefore, conclude that the distances *in* the outer layer are unaltered but that the distances of the ions of the outer layer to those of the second layer have undergone material alterations.

Similarly we may expect the atoms of the outer layer of a metal surface to be somewhat closer to the second layer than corresponding to the distances in the metal lattice. The same is true for the edge atoms of the two-dimensional layers, which constitute the lattice of graphite. In very small graphite particles, where a great proportion of the atoms are really outside edge atoms, this smaller distance is even noticeable (11).

In all these cases the above-mentioned deviations occur at smooth surfaces. The majority of experimental figures for heats of adsorption, however, are not obtained with smooth surfaces. Technical adsorbents certainly have anything but smooth surfaces. We will learn (Sect. III.4) that for many cases of adsorption a rough surface is not only desirable in order to get a high adsorption capacity, but that a roughness is often essential to get adsorption at all. The occurrence of badly developed surfaces with many corners, ribs, edges, cavities, and lattice disturbances is sometimes of major importance. Very often adsorption occurs between two surfaces which are only a very small distance apart, and in many cases the adsorbed molecules have to widen this distance, thus creating the surface at which they will be adsorbed. This phenomenon is closely related to the well-known swelling phenomena.

We will, despite all this, very often consider the adsorption at a smooth idealized surface, because this is the only way in which we can hope to learn something about the nature of the forces that cause the adsorption.

### 3. Repulsion Forces

Whatever the detailed nature of attraction forces between atoms or molecules may be, when they approach each other, repulsion forces will check the attraction forces, and at a certain distance (equilibrium distance), these forces will balance each other. The repulsion forces arise from the interpenetration of the electronic clouds of the atoms and they may be expected to be the stronger and also to increase the more with decreasing distance of the atoms, the more electrons there are in the outer shells of the atoms. It must theoretically be expected that these repulsion forces increase exponentially with decreasing distance. Born and Mayer (45) suggested the following simple expression for the contribution to the potential energy, due to the repulsion forces:

$$E_{rep} = + be^{-r/\rho} \quad (1)$$

where  $b$  and  $\rho$  are constants and  $r$  is the distance between the atoms (the above expression is given a positive sign, because it gives an increase of the energy content of the system; the contributions to the potential energy given by attraction forces will, therefore, be provided by negative signs).

Expression (1) gives good results in calculations of lattice energies of the ionic lattices of the alkali halides and the oxides of the alkaline earths (42,92), but it fails completely when the formation of alkali halide molecules and their condensation to alkali halide crystals is considered. In this case the older empirical expression:

$$E_{rep} = + \frac{b}{r^n} \quad (2)$$

where  $b$  and  $n$  are constants gives excellent quantitative results (117). As the character of the phenomenon of the adsorption on surfaces is something in between the formation of molecules and the condensation of molecules to crystals, we feel inclined to use expression (2) rather than (1). In the case of the alkali halides the value of  $n$  is 12 throughout the whole series (117). When molecules attract each other by van der Waals' forces, the checking repulsion forces show a strong increase with decreasing distances, hence demand a high figure for  $n$ , ranging from 9 for hydrogen and helium with only few electrons in the outer shell, to over 20 for oxygen and nitrogen, and 100 for carbon dioxide (107,120).

In many cases the adsorption energy may be given by the expression:

$$E = - \frac{a}{r^p} + \frac{b}{r^n} \quad (3)$$

where  $p$  and  $a$  are constants of the attraction forces, which we will discuss later.  $b$  may be eliminated from this expression by the condition for the equilibrium:

$$\left(\frac{dE}{dr}\right)_{r=r_m} = \frac{pa}{r_m^{p+1}} - \frac{nb}{r_m^{n+1}} = 0$$

hence:

$$\frac{b}{r_m^n} = \frac{pa}{nr_m^p}$$

The energy content,  $E_m$ , at the equilibrium distance,  $r_m$ , therefore, is:

$$E_m = -\frac{a}{r_m^p} \left(1 - \frac{p}{n}\right) \quad (4)$$

The influence of the repulsion forces on the adsorption energy is greater the smaller the value of  $n$ . In case  $p$  is 3 (a value that we will often meet), and  $n$  is 12, the repulsion forces cause a correction of 25% of the adsorption energy. When two molecules attract each other by van der Waals' forces,  $p = 6$  and the correction would be 50% if  $n$  were 12.

Several authors either neglect the influence of the repulsion forces or take account of them by just subtracting a fixed percentage, as 40%, from the adsorption energy, as calculated with the attraction forces only (48a). The magnitude of the contribution arising from the repulsion forces gives an additional degree of uncertainty to many numerical figures of calculated adsorption energies.

We will see in Section III.2 that, when adsorption is caused by van der Waals' forces only, the contribution of the repulsion forces is nearly completely counterbalanced by the contribution of correction terms of the attraction forces. There is some justification in such a case to use a simple equation and to omit the contribution of the repulsion forces (10,69).

#### 4. Distance between Adsorbed Molecule and Surface

The equilibrium distance,  $r_m$ , is closely related to the repulsion forces. Calculations of lattice energies of ionic crystals and of sublimation energies of solidified gases can successfully be made in good accordance with experimentally known figures, because the distance of the ions or molecules in the crystals is known from other sources. Unfortunately in the case of adsorption phenomena, the distance between adsorbed molecule and surface is not known experimentally. Very often this distance,  $r_m$ , is assumed to be the sum of the "radii" of the adsorbed atom and a surface atom, these radii being derived from experimentally known figures for distances of the

same atoms in other combinations. The distance of an argon atom, adsorbed at a metallic surface, is assumed to be the sum of the radius of argon (as derived from the closest distance between two argon atoms in an argon crystal), and the radius of an atom of the metal, derived similarly from the metal crystal. It will be clear that such a figure will only give a rough approximation. As the adsorption energy is inversely proportional to a high power (at least 3) of the distance, a small uncertainty in the distance (of approximately 5%) gives a far greater uncertainty (at least 15%) in the calculated value of the adsorption energy. In most cases the uncertainty in the values for the distance, which we use, is far greater.

We will encounter still another difficulty when discussing the adsorption on metallic surfaces. A metallic surface is very often considered as a surface of an ideally conducting body or rather a body of ideal polarizability. The difficulty in doing this, is to assess from which distance the region of ideal polarizability starts. It is not clear, when we speak of the distance of an adsorbed atom from a metal surface, whether we have to take the distance between the center of the atom and the outer periphery of the atoms of the metal surface, or whether we must assume the metallic properties to start not at the outer surface but at a plane through the centers of the surface atoms of the metal. The first assumption may lead to only half the figure for the "distance" than the second assumption would give. Consequently the calculated values for the adsorption energies may differ up to a few hundred per cent, depending on the choice of the "distance" in this case. This difficulty is discussed further in Sections II.2, III.6, and IV.1.F.

## **II. Interaction between a Surface and Adsorbed Ions or Radicals**

In this section various forces between adsorbed ions or radicals and the adsorbing surface will be discussed. The adsorbed particles under discussion, therefore, have a surplus electron (negative ion), or they have lost their valency electron (positive ion), or they have an unpaired electron available which may combine with another unpaired electron of a surface atom. Forces between a surface and neutral saturated molecules will be discussed in Section III.

### ***1. Coulomb Interaction between Surface of an Ionic Compound and an Adsorbed Ion***

The distance between the two ions in isolated molecules of alkali halides, in the gas phase (91), is shorter than the distances of the ions in the

corresponding crystals of these salts. The ratio is 0.88 for all alkali halides that crystallize in the rock salt type (117). If we idealize the surface of a cubic face of an alkali halide crystal as a two-dimensional network of ions, without the deviations that we discussed in Section I.2, and we assume a negative ion adsorbed just on top of one of the positive ions of the surface, we will easily see that the attraction of this negative adsorbed ion by the surface is far weaker than it would be if the positive ion with which it has direct contact would have been on its own. If we denote the shortest interionic distance in the crystal as  $r_c$ , we see that the attraction of the adsorbed ion by the nearest positive ion at a distance  $r$  is opposed by a repulsion of 4 negative surface ions, at a distance  $\sqrt{r^2 + r_c^2}$ . The next nearest 4 positive surface ions at a distance  $\sqrt{r^2 + 2r_c^2}$  exert an attraction and so do the following 4 positive surface ions at a distance  $\sqrt{r^2 + 4r_c^2}$ . Next follow, however, 8 negative surface ions at a distance  $\sqrt{r^2 + 5r_c^2}$ , which repel the negative adsorbed ion, etc. In addition to these actions of all the ions of the surface layer, there are the actions of the ions of the second layer. The nearest of these, at a distance  $(r + r_c)$  repels the negative adsorbed ion, then follow 4 attracting positive ions at a distance  $\sqrt{(r + r_c)^2 + r_c^2}$ , etc. The result is that the adsorbed negative ion takes an equilibrium position, which is further away from its nearest positive partner than if the partner had not been part of a surface. A calculation, which we will not give here, or a simple consideration of the equilibrium, shows that in the case in which the adsorbed negative ion is the same as the negative ion partner of the crystal, for example, chloride ion on a sodium chloride surface, the distance is not  $0.88 r_c$ , as in the case of the molecule, but just equal to  $r_c$ , itself. The result is also that the "adsorption" energy is far smaller than the energy of combination of the two ions to form a molecule. If we take NaCl as an example, the adsorption energy contribution arising from these coulomb attractions and repulsions is  $0.54 \times 10^{-12}$  erg, whereas the combination energy in a NaCl molecule is  $9.2 \times 10^{-12}$  erg, nearly 17 times as much. There are, of course, other forces that have a great influence on the adsorption energy, working as well (see especially Sect. IV.1.E) but it is a striking result that the electrostatic field emanating from a cubic face of the surface of an alkali halide crystal is so small.

Hückel (71) introduced an equation for this field, derived from original calculations by Madelung. We will use this equation in the form:

$$F = \frac{8\pi\epsilon}{r_c^2} \cdot \exp\left(-\pi\sqrt{2}\frac{r}{r_c}\right) \quad (5)$$

where  $r_c$  and  $r$  have the same significance as above and  $\epsilon$  is the charge of an

electron (univalent ion). Putting the equilibrium distance of the adsorbed ion, as indicated above, equal to  $r_e$ , we get for the energy contribution of these coulomb forces:

$$E_c = \int_0^{r_e} \epsilon F dr = - \frac{\epsilon^2}{r_e} \left( \frac{8}{\sqrt{2}} \exp(-\pi\sqrt{2}) \right)$$

$$F_c = -0.0662 \frac{\epsilon^2}{r_e} \quad (6)$$

As, according to equation (5), the force shows a strong dependence on the distance, we see that the collaboration of all the ions of the surface results in a very short range force; at a distance  $r = 2r_e$  the force is negligibly small.

When an ion approaches the surface, following a line perpendicular to the surface and ending in a surface ion of the same charge as its own, it will be repelled, the force being equal in magnitude to the one given by equation (5) but of opposite sign. On lines, perpendicular to the surface and ending either just between a positive and a negative surface ion or just in the center of a square of 4 surface ions, 2 of which are positively and 2 negatively charged, no electrostatic force will be exercised. At the short distances that the electrostatic surface forces work, therefore, they cause a periodical inhomogeneous field. The movement of a single adsorbed ion over the surface may be hampered by these variations (see also Sects. IV.1. E and IV.5).

The small value for the adsorption energy as given by equation (6) holds only for positions in the middle of a cubic face of a crystal of the NaCl type. A similar position at an edge of the crystal results in a stronger bond, the electrostatic part being:

$$E_{C(edge)} = -0.0903 \frac{\epsilon^2}{r_e} \quad (7)$$

Still stronger are the electrostatic forces at the corners of the crystals, the contribution to the energy being:

$$E_{C(cor)} = -0.2470 \frac{\epsilon^2}{r_e} \quad (8)$$

When the process of growing of a crystal suddenly stops, the last ionic layer of a cubic face will not be a complete one. Several rows of ions may have been laid on in the process of forming this last ionic layer and adjacent to that part an uncompleted row may be present. The next open position

—the position of an ion on top of a crystal, adjacent to a part of a new ionic layer already formed and as a continuation of a row that was in progress of forming—is one in which an ion will be bound very firmly. The energy, due to the electrostatic contributions at such a place is:

$$E_{C(end)} = -0.8737 \frac{e^2}{r_c} \quad (9)$$

The importance of such positions, which we will call “end” positions, has often been stressed in the literature (1, 6b, 48b, 106). For the purpose of our considerations it will therefore be sufficient to mention that such positions, one of which at least will always occur on every freshly formed crystal face, are extremely “active spots” for adsorption by electrostatic forces.

Other crystallographic faces, which do not generally occur in well-developed crystals, may exercise stronger forces than the normal faces. The adsorption energy of an ion of the same kind as one of the constituents of the crystal at a rhombic dodecahedron face of an alkali halide is:

$$E_{C(rh)} = -0.2082 \frac{e^2}{r_c} \quad (10)$$

The electrostatic forces will be extremely strong at all places where the normal periodicity of constituent ions of the crystal is interrupted. Crystal or lattice disturbances, occurring at the surface will, therefore, also be “active spots” for adsorption by electrostatic forces.

Although the above-mentioned figures are derived for crystals of the rock salt type, it may generally be stated that “active spots” for electrostatic adsorption will be given by: (1) remnants of other crystallographic faces, (2) edges and especially corners of the crystals, (3) “end positions,” and (4) lattice disturbances at the surface. All four species, mentioned in order of increasing importance, are, in particular, present in quickly made finely powdered preparations in fresh condition. They all tend to disappear or to decrease in number with time, especially at higher temperatures or in the presence of a solvent. “Healing,” sintering, and recrystallization tend to decrease the number and the “activity” of such “active spots.”

## 2. *Interaction between an Ion and a Metal Surface*

An electric charge polarizes a metal in such a way that the action may be described as if an electric charge of opposite sign were formed (electric image) at a distance below the surface equal to the distance between the actual inducing charge and the metal surface. The attraction experienced



by an inducing charge at distance  $r$  from the metal surface may, therefore, be described as the attraction between this charge and its image at distance  $2r$ . Hence, when an ion of charge  $\epsilon$  is adsorbed on a metal surface, the force due to this induction effect is given by:

$$F_i = \frac{\epsilon^2}{(2r)^2} \quad (11)$$

and the contribution to the adsorption energy is:

$$E_i = \int_{\infty}^{r_0} \frac{\epsilon^2}{4r^2} dr = - \frac{\epsilon^2}{4r_0} \quad (12)$$

where subscript  $i$  represents "image," and  $r_0$  is the equilibrium distance between the ion and the metal surface.

This energy, it may be noticed at once, is greater than the energy contributions due to the mutual coulomb attraction of an ion and the surface of an ionic crystal. If  $r_0$  has the same value as  $r_e$ , equation (12) gives a figure of the same order of magnitude as equations (8) and (10), representing "active spots" of an ionic surface. The difference becomes even greater when we make the right choice of  $r_0$ . In the case of the adsorption of ions just on top of surface ions of ionic surfaces, the distance  $r_e$  is composed of the sum of the radii of the surface ion and the adsorbed ion. In the case of the adsorption of an ion on a metal surface the van der Waals' forces direct the ion to a position above the center of an elementary cell of the surface, where it touches 3 or 4 atoms.  $r_0$ , the distance between the adsorbed ion and the plane through the centers of the surface atoms of the metal, therefore, is substantially smaller than the sum of the radii of a surface atom and the adsorbed ion (see also Sect. IV.1.F).

Active places, as previously mentioned, have no or far less influence in the case of adsorption on metal surfaces. Other crystallographic faces give, according to the image force conception, exactly the same adsorption energy. Edges and corners of crystals tend to give even smaller energy contributions and are, therefore, certainly not active spots in this case (in case the metallic crystal forms part of a charged electrode or is electrically charged in another way, ions of opposite charge will be preferentially attracted by any sharp edge or point, because the charge density will be greater there). The "end positions" (Sect. II.1) will also here lead to a somewhat increased value for the adsorption energy, the effect will, however, be less important than with ionic crystals. Lattice disturbances, which may give very active spots in the case of ionic crystals, are also of

less importance here. They may, depending on their nature, lead to either a somewhat higher or a somewhat lower adsorption energy.

The conception of an image force leads to some correction of equation (11) when the dimensions of the metal particles that serve as adsorbent are of the same order of magnitude as the distance between the adsorbed ion and the surface. An electric charge  $\epsilon$  at distance  $r$  from a conductive sphere with radius  $R$  polarizes the sphere in such a way that the image charge will be at a distance:

$$r' = \frac{Rr}{R + r}$$

behind the surface, while the charge of the image is:

$$\epsilon' = \frac{\epsilon R}{R + r}$$

Denoting:

$$\frac{R}{R + r} = \rho$$

we get for the image force in this case:

$$F_i = \frac{\epsilon\epsilon'}{(r + r')^2} = \frac{\epsilon^2\rho}{r^2(1 + \rho)^2} \quad (13)$$

The correction  $\rho/(1 + \rho)^2$  does not lead to serious deviations of the adsorption energy. As the correction factor increases with increasing values of  $r$  the effect is to decrease the force especially at greater distances. If an ion were adsorbed on a metallic particle of spherical form and a radius of 10 Å. only, and the distance of the ion to the particle were 2.8 Å., the adsorption energy would be 26 kcal./mole, instead of 29.5 kcal./mole in case of a plane metallic surface.

### ***3. Polarization of a Dielectric Surface by an Adsorbed Ion***

The adsorption of ions on metallic surfaces has been treated as the problem of the polarization of an ideally polarizable structure by the ion. We must expect a similar phenomenon to happen when the adsorbent has a more restricted polarizability, in other words, when an ion is adsorbed on the surface of a dielectric. In the latter case the shifting of the electrons due to the polarization, however, is restricted to the atoms of the dielectric or to a group of atoms to which they belong. An ion of charge  $\epsilon$

at a distance  $r$  from an atom with a polarizability  $\alpha$  induces a dipole in the atom, the dipole moment being:

$$\mu_{\alpha} = \frac{\alpha \epsilon}{r^2} \quad (14)$$

Taking into account the energy needed to separate the charges in forming this dipole and the energy gained by the mutual attraction of the ion and the dipole, the total decrease of the energy content of the system, hence the binding energy of the ion and the atom due to this electrostatic polarization is:

$$E_{\epsilon, \alpha} = - \frac{\alpha \epsilon^2}{2 r^4} \quad (15)$$

If a sodium ion were adsorbed by the surface of an aromatic organic compound, say a synthetic resin of the phenol-formaldehyde type, and we take  $r_0 = 2.8 \text{ \AA.}$  and  $\alpha = 1.45 \times 10^{-24}$  for the mean polarizability (10) of one of the attraction centers of the adsorbent (C, CH, CH<sub>2</sub>, or OH groups), equation (15) gives a contribution of 3.9 kcal./mole toward the adsorption energy by the polarization of the nearest center of attraction only. The other atoms or groups (attraction centers), however, will also be polarized. All the induced dipoles will tend to be directed toward the polarizing ion, but they influence each other, repelling each other when they are nearly parallel or attracting each other when they are more or less in alignment. It would be a rather complicated task to calculate by a direct summation the adsorption energy due to the setting up of this swarm of dipoles and to the mutual repulsions and attractions. The dielectric constant  $K$  and especially the expression for the total molar polarization of a dielectric by an electric charge, however, may be used instead. Consequently the adsorption energy contribution due to this electrostatic induction of a dielectric by an adsorbed ion may be written as:

$$E_{\epsilon, \alpha} = - \frac{\epsilon^2}{4 r_0} \frac{K - 1}{K + 2} \quad (16)$$

If the polarizability of the dielectric is only due to electronic shifts and not to displacement of ions or dipoles so that:

$$K = n^2$$

where  $n$  is the index of refraction, we may write:

$$E_{\epsilon, \alpha} = - \frac{\epsilon^2}{4 r_0} \frac{n^2 - 1}{n^2 + 2} \quad (17)$$

Because of the relation between the mean polarizability  $\bar{\alpha}$  and refraction:

$$\bar{\alpha} = \frac{3}{4\pi N_s} \frac{n^2 - 1}{n^2 + 2} \quad (18)$$

we may also use the expression:

$$E_{e, \alpha} = - \frac{\pi N_s \bar{\alpha} \epsilon^2}{3r_0} \quad (19)$$

where  $N_s$  is the number of atoms (or centers of refraction or polarization) per cubic centimeter.

Following up the above-mentioned example of a sodium ion on the surface of a phenol-formaldehyde condensation product, we may apply equation (17). With  $r_0 = 2.8 \text{ \AA.}$  and  $n = 1.65$ , the value for  $E_{e, \alpha}$  is calculated to be 10.7 kcal./mole.

The polarization of the adsorbent by an adsorbed ion will take place with any adsorbent, hence also when an ion is adsorbed on ionic surfaces. When a sodium ion is adsorbed on top of a chloride ion of a cubic face of sodium chloride, the polarization of this chloride ion and the mutual attraction of its dipole and the inducing adsorbed ion contribute  $0.57 \times 10^{-12}$  erg toward the adsorption energy, as calculated with equation (15), and if  $\alpha = 3.05 \times 10^{-24}$ , the polarizability of the chloride ion. Application of equation (17) and with  $n = 1.5442$  leads to  $0.65 \times 10^{-12}$  erg. Thus we see that in this case the major part of the energy contribution is given by the polarization of the nearest ion. (When a chloride ion is adsorbed on top of a sodium ion it is the polarization of the 4 nearest chloride ions of the surface that gives the main contribution.) We see further that this energy contribution is of the same order of magnitude as that which results from the direct Coulomb attraction of the ion, since equation (6) of Section II.1 gives  $0.54 \times 10^{-12}$  erg. The figure may even be expected to be higher, because of the possibility of polarization by shifting of ions; the dielectric constant of NaCl,  $K = 5.62$ , is higher than  $n^2$ . Equation (16) gives  $1.24 \times 10^{-12}$  erg. Adsorption of an ion on one of the surface ions counteracts, however, the existing polarization of the ions of the surface (referred to in Sect. I.2). According to Verwey's (115) calculations a peripheral chloride ion of the surface of NaCl has a dipole, with a moment of  $0.9 \times 10^{-18}$  e.s.u., the positive pole of which points outward. By adsorption of a sodium ion on top of such a chloride ion a dipole of opposite direction is induced with a moment of  $1.87 \times 10^{-18}$  e.s.u. Moreover it may be expected that the action of the adsorbed ion will also cause a change in the distances of the surface ions with respect to the rest of the crystal. It may, never-

theless, be expected that the contribution of this induction effect will lead to a figure somewhat higher than  $1 \times 10^{-12}$  erg, or somewhere in the neighborhood of 15 kcal./mole.

With respect to the "active spots," which we encountered in Section II.1, it may be said that: (1) on remnants of other crystallographic faces this contribution will virtually be the same; (2) on edges or corners of the crystals it will be somewhat less; (3) it will be negligibly small or zero on the active spots caused by end positions; and (4) it may, in some cases, even be higher on active spots caused by lattice disturbances.

In the case of "end positions" the polarization caused by the newly added "adsorbed" ion is counterbalanced by the existing polarization due to the last ion of the row to which the "adsorbed" ion is added. It may be stated in general that when an ion is adsorbed next to another (adsorbed) ion of opposite sign, the effects of polarization by both ions compensate each other nearly completely.

For lattice disturbances the arrangement of surface ions may well be so that a far greater contribution results from ionic shifts. "Active spots" of this kind may be expected to play an important role in some catalytic processes, especially when electrostatic action is involved.

In all cases where  $K > n^2$ , equation (16) must be used instead of equations (17) or (19). For alkali halides the dielectric constant for static fields  $K$  is about 5, whereas  $n^2$  is about 2 to 2.5. The oxides of the alkaline earths have a value for  $K$  of about 10 ( $n^2$  is about 3), the same is the case for silver halides. Thallium halides have a value for  $K$  of about 30 and some oxides, titanium oxide, for instance, have very high values for  $K$ .  $\text{TiO}_2$  in the form

TABLE I

Energy Contributions by Various Forces to an Ion at a Distance of 2.81 Å.

Surface	Ergs/ion $\times 10^{12}$	Kcal./mole
NaCl, smooth cubic face		
Coulomb force.....	0.54	7.8
Induction of adsorbent.....	$\sim 1.0$	$\sim 15$
NaCl, cubic face, "end position" (coulomb).....	7.15	103
Metal surface (induction).....	2.04	29.5
Dielectric surface		
$n = 1.5$ (induction).....	0.60	8.6
$K = 10$ (induction).....	1.53	22
$K = 110$ (induction).....	1.98	28.5

of rutile has a value of  $K = 114$  ( $n^2 = 7.35$ ). In cases like this the adsorption energy due to this induction effect is practically the same as for metal surfaces. A similar phenomenon occurs when an ionic group, attached to a hydrophobic residue, which prevents the ion from dissolving, is adsorbed on the surface of water. The full static polarizability of water comes into play and the orientation of the water dipoles (which cause the dielectric constant to be as high as 80), giving rise to surface hydration, cause a high adsorption energy.

#### *4. Atoms and Free Radicals on Surfaces*

Graphite consists of parallel layers of carbon atoms. The layers are only one atom thick. There are no covalent or ionic bonds between these layers; they are held together by van der Waals' forces. The atoms *in* the layers are arranged in a regular hexagonal pattern, each carbon atom is directly bound to three others. This leaves each carbon atom with a "free" valency electron. As in metals these "free" valency electrons do not belong to specific atoms in particular, they are not localized, but they are mobile over the whole layer and are responsible for the metallic character of graphite layers.

According to another way of describing these bonds, graphite is a resonance hybrid of several canonical structures in each of which two bonds of each hexagon are double bonds, while the others are single. Each bond in graphite may accordingly be described as  $1/3$ rd double bond and  $2/3$ rd single bond; the interatomic distance of  $1.42 \text{ \AA}$ . is in accordance with this picture (97).

When an atom or a radical comes into contact with the surface of graphite the same may happen as when such an atom or radical is "added" to an organic molecule having a double bond. One of the double bonds of the surface "opens," a normal covalent link is formed between one of the surface carbon atoms and the adsorbed atom or radical (chemisorption). If the atom is monovalent only one of the "free" valency electrons of the surface is used, hence one atom of hydrogen or a halogen may be adsorbed per surface carbon atom by this mechanism or one oxygen atom per two surface carbon atoms. We will see later (Sect. V.1) that in extreme cases such atoms penetrate in between the graphite layers, thus swelling the graphite and forming stoichiometric compounds as extreme saturation cases of this adsorption phenomenon.

The carbon atoms of the edges and corners of the hexagon layers in the graphite crystals—the carbon atoms of the hexagonal prism faces—are bound not to 3 other atoms, but only to 2 (11). Accordingly, there are

more "free" valencies available at the corners and one oxygen atom may be bound to one such carbon atom.

A similar phenomenon occurs at the surface of metal. There is at least one "free" valency electron (conduction electron) available per metal atom, and in many metals there are more. In describing the process of forming a bond with atoms that come into contact with a metal surface, we may either approach the picture from the ionic end or we may describe it again as the formation of covalent bonds. In the first case we consider the metal as a structure that can give off electrons provided a certain amount of energy is supplied (work function, comparable with ionization potential in the case of single metal atoms (6a)), or which has an electron affinity numerically equal to the value of the work function (6a,39). In the second case it may be more convenient to start from the picture that the metallic bond (in the metal) itself is closely related to a covalent bond, the number of covalent bonds which are possible resonating among the available interatomic positions (96). This number of covalent bonds per atom is equal to the number of "free" electrons in the other picture and is *less* than the number of available positions about an atom. The bond order is therefore *less than one* and, consequently, the interatomic distance in the metals is greater than the distance which two of the metal atoms would observe if they were bound together as a pair by a single covalent bond. Pauling (96) calculates that, while in cesium metal the radius of an atom is 2.67 Å., the radius of a cesium atom, shown in a single covalent bond, would be 2.35 Å.

The first, ionic, picture is the best approach for the adsorption of alkali metal atoms on metal surfaces (39). The alkali atom gives its valency electron to the metal, which acts as the electronegative partner of the bond, the metal playing the role of, for instance, a halogen atom. The alkali metal ion is attracted by its image (Sect. II.2) and also by van der Waals' forces. The resulting adsorption of positive ions sets up an electric double layer on the surface, the positive part of which points outward.

The adsorption of an oxygen atom may better be described by picturing the bond as a covalent one. It may be assumed that the surface metal atom with which the oxygen is in direct contact combines 2 electrons with 2 electrons of the oxygen atom to form 2 shared pairs (116). The binding of an electron is shown by the increase of the secondary electron emission (16,47), while conductivity measurements (34) and measurements of contact resistances (112,118) show that conduction electrons have been occupied by this bond. Although covalent, the bond still has a dominant polar character. The surface metal atoms and the adsorbed oxygen

atoms, or in other words, the molecules of the surface oxide, form an electric double layer, the negative end of which points outward; dipole moments per surface oxide molecule of the order of magnitude of  $10^{-18}$  e.s.u. may occur (46,116).

We cannot calculate theoretically the adsorption energy in cases like this, nor do we know the distance between the adsorbed atom and its direct neighbor. It is clear from experimental figures that the adsorption energy will be high in most cases. For an oxygen atom on a tungsten surface 162 kcal./mole may be calculated for the first atoms on the most active places (80), for further atoms the value may be somewhat smaller (74), and as an average, 128 kcal./mole may be calculated (7a, 102). The distances are mostly assumed to be the same as in similar covalent bonds in molecules or crystals where the bond length is known. It may be remarked that, as in the comparison between ionic and covalent bonds, the bond length for the same energy of combination is far shorter in the case of the covalent bonds.

Not only oxygen atoms may be adsorbed by covalent bonds. Other "electronegative" atoms, like the halogens, sulfur, or nitrogen, may also enter into similar bonds with surface atoms of metals, thus forming surface compounds. The bond of nitrogen atoms to surface atoms of tungsten for example, is stronger than the above-mentioned bond of oxygen atoms (63).

Attention may be drawn to the special case of hydrogen. Atomic hydrogen is very well adsorbed on the surfaces of many metals by covalent bonds. In some cases the surface hydride forms a double layer with the negative side pointing outward (alkali and alkaline earth metals, zirconium, titanium, tungsten), in other cases the hydrogen is the electropositive partner (platinum, nickel, iron) (7a).

In many cases these atoms, under suitable conditions, do not restrict themselves to the surface of the metals, but may dissolve homogeneously in the lattice of the metal, like oxygen in silver or zirconium (28,30), hydrogen in nickel, platinum, or iron (29), and nitrogen in iron or zirconium (see also Sect. V.2).

A molecule, like CO, which has electrons available for forming covalent bonds, shows a great tendency for chemisorption. The chemisorption of CO on the surface of cobalt and the formation of chemisorbed carbon atoms from it is one of the principal steps in the well-known Fischer-Tropsch synthesis of hydrocarbons (59).

When a  $\text{CH}_3$  radical, formed by thermal decomposition of an organo-metallic compound, strikes a metallic surface, the radical may also share its free valency electron with one of the metallic electrons and be adsorbed by a covalent bond. The adsorption of organic radicals on metal surfaces is



mostly a result of a reaction of an organic molecule with the metal surface. Ethylenic linkage may be adsorbed by one covalent link (*e.g.*, one of the carbon atoms with one nickel atom of a nickel surface), or by two (both carbon atoms with two adjacent nickel atoms). We will consider some of these reactions in Section. V.2.

It may be assumed that metal atoms of edges or corners of the crystals or of superficial lattice disturbances, which have far less direct neighbors than normal surface atoms, enter more easily into a covalent bond with an adsorbed atom than normal surface atoms do. "Active places" in this kind of adsorption will be formed by protruding points of the surface, when the atoms have as few direct neighbors as possible.

Similar considerations lead to the view that adsorption by forming covalent bonds may also be expected at surfaces of many semiconductors. Graphite (55) as well as thin metallic layers (of a few atoms thick (33)), which are semiconductors, show this adsorption very pronouncedly. Semiconductors of the oxide or halide type (7c,43), which crystallize in ionic lattices but which contain ions still having free valencies, may serve as adsorbents of the type discussed in this subsection. As these free valency electrons form the conduction electrons of the semiconductor, a picture as shown in this subsection, may be used to describe the adsorption of atoms or radicals from the ionic bond end or from the covalent bond end.

### III. Van der Waals' Forces between a Surface and a Visiting Molecule

#### 1. *Physical Adsorption*

Apart from the more "chemical" adsorption forces dealt with in Section II and which are of a specific nature, there are always forces of a more general character operating in any adsorption phenomenon. Any atom or molecule is attracted by any other atom or molecule by van der Waals' forces. Hence any atom or molecule is attracted by any surface by means of these forces. While adsorption caused by ionic action or by formation of covalent bonds is often referred to as *chemisorption*, the van der Waals' forces, when operating alone, produce what is commonly called *physical adsorption* or *van der Waals' adsorption*. In general the energy liberated by physical adsorption is much smaller than that connected with chemisorption. There are, however, exceptions to this general rule and a distinction between the two types of adsorption would be better based upon another criterion.

Like Margenau (89) in an excellent survey, we will adhere to the defini-

tion that van der Waals' forces are those forces which give rise to the constant  $a$  in van der Waals' equation. This includes forces between molecules possessing dipoles or quadrupoles (Keesom's alignment effect (77)), attraction forces caused by the polarization of molecules by static dipole or quadrupole fields of other molecules (Debye's induction effect (60)) as well as the nonpolar van der Waals' forces, also referred to as dispersion forces, since London (85) discovered the close connection between their nature and the cause of optical dispersion. It is also logical that the forces between an ionic or, more general, a polar surface and dipole molecules and the electrostatic induction of atoms and molecules by polar surfaces are included in the definition of van der Waals' adsorption forces. Doing this we follow closely Brunauer's (48) concept of physical adsorption. We therefore include all cases in which neutral atoms or molecules—they may be spherically symmetrical or they may be polar—interact with surfaces without sharing of electrons taking place, thus preserving the individuality of the adsorbed neutral atoms or molecules.

The nature of van der Waals' forces does not, of course, exclude them from causing intra- or intermolecular bonds in cases that may be considered to belong to the field of chemistry. There are some molecules in which the atoms are held together by van der Waals' forces. In many complex molecules, water, ammonia, or organic molecules are bound by van der Waals' forces (dipole, induction as well as dispersion). Van der Waals' forces cause hydration or more generally solvation; they are responsible for the cohesion of the molecules in, *e.g.*, the crystals of practically all organic compounds and they are, in conjunction with ionic or covalent bonds, a determining factor for the crystal structure of many inorganic or organic salts or for the spatial arrangement of organic molecules. Due to their general character they embrace an enormous field of binding phenomena where physics and chemistry not only meet, but are indistinguishable.

## ***2. Nature of Nonpolar van der Waals' Forces***

In the following three subsections we will consider the interaction of adsorbed molecules and surfaces by the nonpolar van der Waals' forces. These forces are always present in any combination of molecule and surface and they always lead to attraction. They result from the polarization of each one of the participating molecules of any pair by the continuously changing field, arising from the electronic movements in the other partner. From a more general equation, London (85) has derived the following ap-

proximation formula for the mutual energy of interaction of a pair of atoms:

$$E_W = -\frac{3}{2r^6} \cdot \alpha_1 \alpha_2 \frac{h\nu_1 \nu_2}{\nu_1 + \nu_2} \quad (20)$$

where  $\alpha_1$  and  $\alpha_2$  are the polarizabilities,  $h$  is Planck's constant, and  $\nu_1$  and  $\nu_2$  characteristic frequencies from the optical dispersion curve of the atoms, hence  $h\nu_1$  and  $h\nu_2$  are characteristic energies in the dispersion equation. If the two atoms are identical, equation (20) turns into:

$$E_W = -\frac{3}{4r^6} \alpha_0^2 h\nu_0 \quad (21)$$

where  $\alpha_0$  is the polarizability and  $h\nu_0$  the characteristic energy of the atom.

Equations (20) and (21) are only approximation equations in the derivation of which it has been assumed that the dispersion equation of the atom may be described by one term, with one characteristic frequency only:

$$\frac{n_\nu^2 - 1}{n_\nu^2 + 2} \frac{V}{N} = \frac{4\pi}{3} \alpha = \frac{\epsilon^2}{3\pi m} \frac{f_0}{\nu_0^2 - \nu^2} \quad (22)$$

where  $n_\nu$  is the index of refraction for the frequency  $\nu$ ,  $V$  is the molecular volume,  $N$  the number of Avogadro,  $\epsilon$  and  $m$  the charge and the mass, respectively, of an electron, and  $f_0$  a constant, measuring the strength of the light absorption.

Other simplifications used in the derivation of equations (20) and (21) are the conception of spherical symmetry with respect to the polarizability and the assumption that only the attraction forces between the continuously changing inducing dipoles in each of the atoms and the continuously changing induced dipoles in the other partner contribute toward the interaction energy and that poles of higher order than dipoles may be neglected.

In many cases energies  $h\nu_1$  and  $h\nu_2$  are nearly equal to the ionization energies, and, if the dispersion data are not known, the ionization energies  $I_1$  and  $I_2$  may be taken instead:

$$E_W = -\frac{3}{2r^6} \alpha_1 \alpha_2 \frac{I_1 I_2}{I_1 + I_2} \quad (23)$$

Slater and Kirkwood (103) derived another equation for the van der Waals' interaction energy:

$$E_W = -\frac{3}{4\pi r^6} \cdot \frac{\epsilon h}{m^{1/2}} \cdot \frac{\alpha_1 \alpha_2}{(\alpha_1/n_1)^{1/2} + (\alpha_2/n_2)^{1/2}} \quad (24)$$

where  $n_1$  and  $n_2$  are the numbers of electrons in the outer shells of the atoms and all other symbols have the same significance as before. For equal atoms, we find:

$$E_W = - \frac{3}{8\pi r^6} \cdot \frac{\epsilon h}{m^{1/2}} \cdot \alpha_0^{3/2} n_0^{1/2} \quad (25)$$

We can see the connection between equations (25) and (21) when we derive the static polarizability  $\alpha_0$  from equation (22) by having  $\nu = 0$ :

$$\frac{4\pi}{3} \alpha_0 = \frac{\epsilon^2}{3\pi m} \cdot \frac{f_0}{\nu_0^2} \quad (26)$$

hence:

$$\nu_0 = \frac{\epsilon}{2\pi m^{1/2}} \cdot \left( \frac{f_0}{\alpha_0} \right)^{1/2} \quad (27)$$

Substituting this expression for  $\nu_0$  in equation (21) gives us:

$$E_W = - \frac{3}{8\pi r^6} \cdot \frac{\epsilon h}{m^{1/2}} \cdot \alpha_0^{3/2} f_0^{1/2} \quad (28)$$

Equation (28) is identical with equation (25) but for the substitution of  $f_0$  for  $n_0$ . As  $f_0$  is always smaller than  $n_0$  the formula of Slater-Kirkwood gives somewhat higher figures than that of London (89).

Very often, however, both equations may be used with advantage to get an impression of the order of magnitude of the van der Waals' forces.

Sometimes an equation is used in which the atomic diamagnetic susceptibility,  $\chi$  is introduced instead of  $n$  or  $\nu$ :

$$E_W = - \frac{6mc^2}{r^6} \frac{\alpha_1 \alpha_2}{(\alpha_1/\chi_1) + (\alpha_2/\chi_2)} \quad (29)$$

The results obtained with this equation, however, are not very good. The mechanism of the interaction of the electrons with a magnetic field is too different from the mechanism to which the dispersion forces owe their existence (89), and we will not make use of this approximation.

As can be seen from the above-mentioned equations, the main contribution to the van der Waals' interaction energy between two atoms is given by an expression of the form:

$$E_W = - \frac{C}{r^6} \quad (30)$$

where  $C$  is a constant depending on the properties of the atoms. Apart from this term, which arises from the interaction of continuously changing

inducing dipoles and induced dipoles, there are terms inversely proportional to higher powers of distance  $r$ , which arise from the interaction of continuously changing quadrupoles with dipoles and quadrupoles with quadrupoles:

$$E_w = -\frac{C}{r^6} - \frac{D}{r^8} - \frac{E}{r^{10}} \quad (31)$$

The contribution of the second term in this equation may amount to 15% to 30% of the first term. In some cases, however, as with atomic hydrogen or with the alkali metals, it is far higher (89) and its contribution may be even more important than that of the first term. In most normal cases, however, the effect of these additional terms is largely counterbalanced by the repulsion term (Sect. I.3), with the result that in many practical calculations sufficiently good numerical results are obtained by using the so-called "dipole-dipole" term only and evaluating the constant  $C$  by the approximation equations of either London or Slater and Kirkwood (10,69).

### 3. Adsorption of Atoms by Nonpolar van der Waals' Forces

The nonpolar van der Waals' forces (dispersion forces) are additive, so that when an atom is adsorbed at a surface by these forces the energy of adsorption may be evaluated by calculating the mutual interaction energies of the adsorbed atom with all the individual atoms of the adsorbent and to add these contributions together. Instead of carrying out such elaborate calculations, Polanyi and London (99) replaced this summation by an integration:

$$E_w = \int \int \int -\frac{C}{r^6} N_s dv = -\frac{N_s \pi C}{6} \frac{1}{r_0^3} \quad (32)$$

where  $N_s$  is the number of atoms of the adsorbent per cubic centimeter and  $r_0$  is the shortest distance of the adsorbed atom to the surface. Instead of being inversely proportional to the sixth power of the distance, we get here the third power and in addition the number  $N_s$  (compare Sect. II.3, Eq. 19). If we choose as an imaginary adsorbent a closely packed cubic lattice (face-centered) of atoms, such that there are  $10^{23}$  per cubic centimeter,  $N_s = 0.1 \times 10^{24}$ . The shortest distance between such atoms would be 2.42 Å., and we represent the surface atoms by spheres of a radius  $r_s = 1.21$  Å. We will now imagine an atom of helium ( $r_{\text{He}} = 1.47$  Å.), argon ( $r_{\text{A}} = 1.8$  Å.), and xenon ( $r_{\text{Xe}} = 2.1$  Å.), respectively, to be adsorbed on the surface of this lattice. We will use equation (23) for the

evaluation of  $C$  of equation (32) and we assume the following data for the atoms of the adsorbent:  $\alpha_2 = 1 \times 10^{-24}$  cm.<sup>3</sup>,  $I_2 = 10$  electron volts (230 kcal./mole). In Table II we give the interaction energy of the 3 rare gas atoms with 1 atom of the adsorbent (Eq. 23) and the interaction energy with the surface, according to equation (32). In order to evaluate the distance  $r_0$  we must bear in mind that the rare gas atom can approach to 4 surface atoms to a distance,  $r_m$ , equal to the sum of the radii of the surface atom and of itself;  $r_0$  is the shortest distance of the adsorbed atom to the plane through the centers of the surface atoms.

TABLE II

Atom	$\alpha \times 10^{24}$ cm. <sup>3</sup>	$I_1$ , kcal./mole	$r_m \times 10^8$ cm.	$C/r_m^6$ kcal./mole.	$r_0 \times 10^8$ cm.	$N_s \pi C/6r_0^3$ kcal./mole	$E_{ads}$ , kcal./mole
He.....	0.2	563	2.68	0.13	2.1	0.27 <sup>b</sup>	0.7
A.....	1.68	361	3.01	0.49	2.4 <sup>b</sup>	1.25	3.1 <sup>b</sup>
Xe.....	4.17	178	3.31	0.61	2.8 <sup>b</sup>	1.77	4.6

According to London (86) the integration of equation (32) is allowed only if  $r_0 \gg 1/(N_s)^{1/3}$ . This is certainly not the case with He (see Table II), and for the other rare gas atoms the integration also gives too small results. A better method to follow, therefore, is to evaluate the interaction energies of the adsorbed atom with all the individual atoms of the adsorbent within a certain distance  $r_D$ , to add all these contributions, and then to add the contributions of the rest of the atoms of the adsorbent beyond the chosen distance by integrating (10,18). Using this method, the values indicated in the last column of Table II under  $E_{ads}$  are obtained; they are about 2.5 times the values calculated with equation (32). This is a general result and the procedure, given above, should always be followed. Another conclusion which may be drawn from these calculations, also a general one, is that the ratio of the adsorption energy  $E_{ads}$ , and the interaction energy with one atom of the adsorbent,  $C/r_m^6$ , is greater for greater atoms. The bigger the atom the more it benefits from the additive character of the nonpolar van der Waals' forces.

Since the adsorbent in our example is only a hypothetical one, the actual numerical values in Table II are not important. Even if, however, this adsorbent did represent a real case, the calculated values would probably be too high. The figures for  $r_m$  which we used are obtained as the sum of the "radius" of the rare gas atom, derived from the equation of state of this gas and the "radius" of an atom of the adsorbent. This latter value was taken to be identical to the radius of the atoms of the adsorbent

as operating *in* the lattice. The atoms in most adsorbents are bound together by covalent or ionic forces and their mutual distances will be appreciably smaller than the distances observed when van der Waals' forces are operating. The figures for  $r_m$  will, therefore, certainly be higher, and therefore the adsorption energy will be lower. It is only in case of an adsorbent like graphite where the two-dimensional hexagon layers are also mutually bound by van der Waals' forces only that such a procedure may be followed.

Let us, therefore, consider the adsorption of an argon atom on a smooth surface of graphite. The strongest van der Waals' adsorption forces will be exercised by the basal face of graphite and not by the hexagonal prism faces. The two-dimensional layers of hexagons in graphite are about 3.6 Å. apart and we may, tentatively, take a value of 1.8 Å. for the operating "radius" of a carbon atom in van der Waals' interactions. The actual value will be rather higher than lower. If we again take also 1.8 Å. for the "radius" of an argon atom (from the equations of state, as we did in Table II), the distance of an adsorbed argon atom to the *six* nearest carbon atoms of the basal plane of graphite will be 3.6 Å. The distance to the next six is 4.37 Å., etc. Summations over the 24 nearest carbon atoms and integration over the rest and using the following numerical data:

$$\begin{aligned}\alpha_C &= 1 \times 10^{-24} \text{ cm.}^3 & \alpha_A &= 1.68 \times 10^{-24} \text{ cm.}^3 \\ I_C &= 258 \text{ kcal./mole} & I_A &= 361 \text{ kcal./mole} \\ N_A &= 1.13 \times 10^{23}\end{aligned}$$

leads to an adsorption energy of 1.9 kcal./mole. The best experimental value for argon on a smooth surface of graphite is 2.2 kcal./mole (4). Direct integration, using equation (32) with  $r_0 = 3.31$  Å. would have resulted in 0.62 kcal./mole, a far too low value. The numerical result of such calculations depends, of course, very much on the choice of the constants. If the polarizability of a carbon atom were  $1.4 \times 10^{-24}$  cm.<sup>3</sup> (about the highest value we can assume it to be), we would get the same numerical result again by increasing  $r_m$  from 3.6 Å. to 3.8 Å. The only conclusion we are allowed to draw is that the order of magnitude of adsorption energies is well explained by van der Waals' forces.

If we had followed the same procedure for helium, we would have obtained considerably too high a value. With helium we may not assume that the effect of the second and third term of equation (31) will be nearly compensated by the effect of the repulsion term. Helium has only two electrons and therefore a low value for  $n$  in equation (2) (see Sect. I.2). The effect of the repulsion force on the adsorption energy of helium is very

dominant and overcompensates by far the effects of the second and third term of equation (31), which make only a very small contribution here. As a result the adsorbability of helium is very low, even at low temperatures.

It may be expected that the influence of the repulsion term will also be high in the case of atomic hydrogen. On the other hand the polarizability of atomic hydrogen ( $\alpha_A = 0.664 \times 10^{-24}$ ) (69) is 3.5 times that of helium, while the effective radius (about 0.8 Å.) is far smaller. The influence of the higher terms of the van der Waals' forces (Eq. 31) is, moreover, extremely strong in this case, their contribution may exceed that of the dipole-dipole term by some hundred per cent (89). Consequently the adsorbability of atomic hydrogen by van der Waals' forces is very high (35,73,78).

The atoms of the alkali metals have also a high polarizability, as compared with their "radius," hence, a high adsorbability (25,36), which is again enhanced by the influence of the higher terms of the van der Waals' interaction. In Table III values for the polarizability and the radius of some atoms are given for comparison, as well as the ratios between  $\alpha$  and the third power of the radius.

TABLE III

Value	Atom					
	H	He	A	Xe	K	Cs
$\alpha \times 10^{24} \text{ cm.}^3 \dots$	0.664	0.20	1.68	4.17	46	61
$r \times 10^8 \text{ cm.} \dots \sim$	0.8	1.47	1.8	2.1	2.35	2.67
$\alpha/r^3 \dots \dots \dots$	1.3	0.06	0.29	0.45	3.5	3.2

#### 4. Some Results of Additive Character of Nonpolar van der Waals' Forces

When a molecule, consisting of two or more atoms, is adsorbed, the adsorption energy will be higher the more direct contacts there are between the atoms of the adsorbent and the atoms of the adsorbed molecule. It is a consequence of the additivity of the van der Waals' forces that all polyatomic molecules tend to lie flat on the surface of the adsorbent. This is despite the fact that the anisotropy of the polarizability would tend to place them with the axis of greatest polarizability, which in the majority of the cases means the long axis of the molecules, perpendicular to the surface. The effect of the additivity outweighs largely the effect of the anisotropy (10,31).

As a consequence, rod-shaped molecules, which are adsorbed by van



der Waals' forces, often show a higher index of refraction in a direction parallel to the surface (birefringence) (93) or a preferential light absorption for light vibrating parallel to the surface (dichroism) (21,93).

Organic molecules with double bonds or, still better, with conjugated double bonds show an increased power to be adsorbed. This higher adsorbability is to be ascribed not so much to the higher polarizability of these bonds, but to the flat configurations resulting from them, thus enabling the molecules to approach the surface closely and in a more favorable position than saturated molecules can. It is for similar reasons that aromatic molecules have a higher degree of adsorbability. Due to their flat configuration all their atoms may come into direct contact with the surface.

The better an adsorbed molecule can be "fitted" into the pattern of the surface atoms of the adsorbent, the better it will be adsorbed. The increased attraction may result in a shorter distance to the surface for the same reason that the distance between hydrocarbon chains in paraffin crystals decreases with increasing length of the chains (114).

The surface of an adsorbent is often not smooth but shows a roughness of molecular or higher dimensions. There will be many places on such a surface where an adsorbed molecule can get into direct contact with more atoms of the adsorbent than would be possible if the surface were an ideal smooth face. Crevices, cavities, capillaries, the inside of cracks, etc., are "active places" for adsorption by nonpolar van der Waals' forces (18). The first molecules to be adsorbed on the surface of an adsorbent will, therefore, often show a higher adsorption energy. The usual trend of adsorption energies of various gases on powders with increasing amount of adsorptive reveals this phenomenon.

The differential heat of adsorption for the first molecules of argon on graphite is 3.9 kcal./mole; with increasing amount of adsorption this value falls to 2.2 kcal./mole, which may be considered to be the heat of adsorption on a flat graphite surface (4). For nitrogen the corresponding figures are 4.4 and 2.3 kcal./mole., for hydrogen 1.8 and 0.9 kcal./mole.

Many figures for adsorption energies on technical adsorbents can only be explained by assuming that adsorption has taken place in such "active places" where the adsorbed molecule is surrounded by a maximum amount of atoms of the adsorbent (18). The same properties assist effectively in promoting swelling phenomena as we will see in Section V.1.

In many cases van der Waals' forces between like molecules are responsible for the heat of sublimation of solids or the heat of evaporation of liquids. Comparison of equations (20) and (21) shows that the mutual forces between like molecules of a very small polarizability will be smaller

than the adsorption forces between such molecules and the atoms of an average adsorbent. We saw in Section III. 3 that the adsorption energy of helium on any adsorbent is very small. Stout and Giauque (105) estimated the heat of adsorption of helium on nickel sulfate as 0.14 kcal./mole. The heat of evaporation of the liquid is still far lower, namely, 0.02 kcal./mole. A similar ratio holds for molecular hydrogen (48e). On the other hand when the polarizability of a molecule is very high we may expect the heat of evaporation or of sublimation to be higher than the heat of adsorption on an average adsorbent. Thus, for iodine, the heat of sublimation is 15.5 kcal./mole; the differential heat of adsorption of iodine on  $\text{BaCl}_2$  when 57% of the surface is covered is 11.8 kcal./mole (9,14). For many gases, such as nitrogen and carbon monoxide, and for many organic vapors, the heat of adsorption on adsorbents such as charcoal and silica gel is roughly twice the heat of liquefaction.

### 5. Adsorption on Metal Surfaces by van der Waals' Forces

In a first attempt to understand the nature of the adsorption on metal surfaces by van der Waals' forces, Lennard-Jones (82) used an "image-force" picture, similar to the one we used in describing the adsorption of ions on metal surfaces (Sect. II.2, Eq. 11). The continuously changing dipoles in the adsorbed atom, originating from the movements of the electrons with respect to the nucleus, induce similar continuously changing "image" dipoles. The mutual attraction of inducing and induced dipoles leads to the following expression for the interaction energy:

$$E_w = - \frac{\epsilon^2 \bar{r}^2}{12r_0^3} \quad (33)$$

where  $\bar{r}^2$  is the mean square displacement of all electrons in the atom, hence  $\epsilon^2 \bar{r}^2$  the mean square dipole moment, and  $r_0$  the distance of the atom from the metal surface.

Equation (33) leads to numerical figures, which are far too high. Bardeen (3), by introducing various corrections, mainly due to the interaction of the electrons in the metal, derives the expression:

$$E_w = - \frac{\epsilon^2 \bar{r}^2}{12r_0^3} \cdot \frac{C\epsilon^2/2r_s\hbar\nu_0}{1 + (C\epsilon^2/2r_s\hbar\nu_0)} \quad (34)$$

where  $C$  is a numerical constant approximately equal to 2.5,  $r_s$  is the radius of a sphere in the metal containing one conduction electron, and  $\hbar\nu_0$  is the characteristic energy of the adsorbed atom or molecule as in equations

(20) and (21). Equation (34) gives very often numerical values that are only one-half to one-third of those obtained by equation (33).

In order to evaluate adsorption energies by his equation, Lennard-Jones (82) used the diamagnetic susceptibility and obtained the expression:

$$E_w = - \frac{mc^2\chi}{2r_0^3} \quad (35)$$

where  $m$  is the mass of an electron,  $c$  the velocity of light, and  $\chi$  the atomic diamagnetic susceptibility. It was mentioned in Section III.2 (Eq. 29) that figures obtained from diamagnetic susceptibility are far too high.

As pointed out by Margenau and Pollard (90), there is a far more serious objection to the use of the "image" picture in this case. Such a picture may describe the polarization of the metal when we are dealing with static or slowly alternating fields. The inducing fields of the continuously changing instantaneous dipoles in a nonpolar molecule, however, change so rapidly that the conduction electrons in the metal are incapable of following their movements. With respect to van der Waals' forces a metal behaves as a dielectric body rather than as an ideally polarizable structure.

Margenau and Pollard (90) consider the interaction energies between the adsorbed atom (molecule) and elementary portions of the metal, which are small with respect to the wave length of radiation corresponding to the main resonance frequencies of the atom, but large enough to possess the bulk properties of the metal. The total interaction energy, which is then obtained by summing over all the elementary portions consists of two portions:

$$E_w = E_1 + E_2 \quad (36)$$

$E_1$  results from the polarization of the metal by the continuously changing dipoles in the adsorbed atom. They derive the expression:

$$E_1 = - \frac{\epsilon^2 h}{2\pi m} \alpha_m(\nu_0) \frac{f_0}{\nu_0} \frac{1}{8r_0^3} \quad (37)$$

where  $\alpha_m(\nu_0)$  is the polarizability of the metal for the frequency  $\nu_0$  and  $f_0$  and  $\nu_0$  are properties of the adsorbed atom, which have the same meaning as in equation (22). If for  $\alpha_m(\nu_0)$  the *static* polarizability of the metal is taken, equation (37) leads to equation (33). To see this we may express  $(f_0/\nu_0)$  in terms of the average dipole moment:

$$\frac{\epsilon^2 h f_0}{2\pi m \nu_0} = \frac{4\pi}{3} \epsilon^2 r^2 \quad (38)$$

Substituting this in equation (37).

$$E_1 = - \frac{\pi \epsilon^2 \bar{r}^2}{6 r_0^3} \alpha_m (\nu_0) \quad (39)$$

and introducing the *static* polarizability:

$$\alpha_m(\nu_0) = \frac{1}{2\pi}$$

gives equation (33).

The polarizability  $\alpha_m(\nu_0)$  for high values of  $\nu_0$  as they are operating in van der Waals' forces has, however, a quite different value. If we take for  $\nu_0$  the resonance frequencies of the adsorbed atoms (molecules)—values in general far greater than the frequencies of the absorption bands of the metals—it is found that the polarizability of the metal is even negative and may be written:

$$\alpha_m(\nu_0) = \frac{-n_0 \epsilon^2}{4\pi^2 m \nu_0^2} \quad (40)$$

where  $n_0$  is the number of conduction electrons per cubic centimeter.

According to equation (26) we may write for  $f_0$ :

$$f_0 = \frac{4\pi^2 \alpha_0 \nu_0^2 m}{\epsilon^2} \quad (41)$$

where  $\alpha_0$  is the polarizability of the adsorbed atom. Substituting (40) and (41) into (37) gives:

$$E_1 = + \frac{\epsilon^2 h n_0 \alpha_0}{2\pi m \nu_0} \cdot \frac{1}{8 r_0^3} \quad (42)$$

The contribution  $E_2$  of equation (36) results from the polarization of the adsorbed atom by the electronic movements in the metal. Margenau and Pollard derive the following expression:

$$E_2 = - \frac{C \epsilon^2 \alpha_0}{2 r_e} \cdot \frac{1}{8 r_0^3} \quad (43)$$

where  $\alpha_0$  is the (static) polarizability of the adsorbed atom and  $C$  and  $r_e$  have the same meaning as in Bardeen's equation (34).

Adding the expressions of equations (42) and (43) we obtain for the total energy of interaction:

$$E_w = - \frac{\epsilon^2 \alpha_0}{16 r_0^3} \left( \frac{C}{r_e} - \frac{h n_0}{\pi m \nu_0} \right) \quad (44)$$

There are very few experimental data available of adsorption energies of gases, adsorbed on metals by van der Waals' forces only. The heat of

adsorption of hydrogen on nickel at low temperatures (20°K.) is 1200 cal./mole in the initial stages of adsorption, which value decreases to 400 cal./mole (66). Taking this latter value as the heat of adsorption of H<sub>2</sub> on a flat surface of nickel and using the following data:

$$\text{H}_2: \alpha_0 = 0.775 \times 10^{-24}$$

$$\nu_0 = 3.95 \times 10^{13}$$

$$\text{Ni}: r_e = 1.1 \text{ \AA. (2 electrons per Ni atom)}$$

$$n_0 = 18 \times 10^{22}$$

and further:

$$C = 2.5$$

$$h = 6.62 \times 10^{-27}$$

$$m = 9.11 \times 10^{-28}$$

we may calculate which value would have to be given to  $r_0$  in equation (44) in order to obtain this figure. The result of such a calculation is  $r_0 = 3.56 \text{ \AA.}$ , a very reasonable value indeed for the distance of H<sub>2</sub> from the Ni surface in van der Waals' adsorption.

We will give some other examples of the use of equation (44) in Section IV.1.

### 6. Polar van der Waals' Forces

When a molecule has a permanent dipole, we may expect it to be attracted by the electrostatic field of the surface of ionic dielectrics. Such fields, however, when emanating from smooth surfaces, are not very strong (Sect. II.1). A significantly high contribution to the adsorption energy is only experienced, therefore, when a dipole of sufficiently high dipole moment is situated at such a place in the polar molecule that it can approach to within a short distance of the surface. Water, ammonia, organic hydroxy-compounds, amines, and acids have dipoles that are near the periphery of the molecules. Such peripheral dipoles may well be oriented and bound by ionic surfaces (18), or by surfaces having similar dipoles of their own (carbohydrates, proteins).

Surfaces of inorganic salts and oxides have a great tendency to adsorb water molecules tenaciously (27); they also adsorb remarkably well organic alcohols and phenols. As the ionic arrangement of most of these surfaces is such that their negative ions form the outer layer (Sect. I.2), and as the positive end of the peripheral dipoles under consideration (the H atom of the OH and NH dipoles) is very close to the periphery of the molecule, such dipoles will take up an oriented position (18) perpendicular to the surface and with the H atom in direct contact with one of the negative surface ions, which may be a halide ion or an oxide ion.

The polar sites of carbohydrate or protein surfaces have either their negative part pointing outward (the oxygen of CO groups or oxygen bridges) and peripheral dipole molecules may be adsorbed in a similar way as in the case of the inorganic surfaces described above, or they show peripheral dipoles themselves (OH groups, NH groups) with their positive end close at the surface, thus attracting easily dipole molecules as water and ammonia (24). In the latter case the oxygen of an adsorbed water molecule comes into direct contact with the hydrogen atom of a surface dipole.

The type of binding described here is often called "hydrogen-bonding" (119). It is the same type of linkage that plays a dominant role in the formation of many association complexes or complex inorganic or organic molecules, and in the mutual bonding of water molecules in liquid water and ice. For the purpose of this article, however, there is no reason to consider this example of polar van der Waals' forces as a special type of linkage, though it is only in the case of the peripheral OH, NH, and similar dipoles that the effect of this force is strong enough to dominate the orientation of the adsorbed molecule.

When the electrostatic field of the surface is denoted by  $F$  and the polar molecule has a dipole moment,  $\mu$ , the adsorption energy contribution caused by the orientation and binding of the dipole is given by:

$$E_{\mu} = -F\mu \quad (45)$$

The electrostatic field over a surface ion of the cubic face of a crystal of the sodium chloride type is given by equation (5) in Section II.1. Let us take an OH dipole as an example and let us assume it to be oriented and bound by a chloride ion of the surface of a NaCl crystal. The radius of the OH group may be taken as 1.4 Å., the distance between the O and the H in this dipole group may be 1.0 Å. As the radius of the chloride ion is 1.8 Å., the positive end of the dipole is 2.2 Å. and the negative end 3.2 Å. apart from the center of the chloride ion. The distance between the chloride ion and the center of the dipole is, therefore, 2.7 Å. The strength of the electrostatic field of the surface at this distance is, according to equation (5)  $0.215 \times 10^6$  e.s.u. As the dipole moment may be taken as  $1.7 \times 10^{-18}$  e.s.u. (1.7 debyes), the value of  $E_{\mu}$  according to equation (45) will be  $0.366 \times 10^{-12}$  erg/mole or 5.25 kcal./mole.

We may ask whether at such short distances the dipole conception still gives the right answer. If, instead with a dipole moment,  $\mu$ , we calculate the energy with charges  $\epsilon'$ , which are a distance  $l$  apart, so that  $\epsilon'l = \mu$ , we may use the following expression:

$$E_{e'l} = - \int_{r_0+(l/2)}^{r_0-(l/2)} \frac{F_\mu}{l} dr \quad (46)$$

where  $r_0$  is the distance between the center of the dipole and the center of the nearest surface ion and  $l$  is the dipole length. With, as above,  $r_0 = 2.7 \text{ \AA.}$  and  $l = 1.0 \text{ \AA.}$ , we obtain the value  $E_{e'l} = 5.8 \text{ kcal./mole}$ , nearly 10% greater than the calculated value for  $E_\mu$ .

The order of magnitude of this adsorption energy is quite appreciable if we compare it with the energy with which an ion is bound by the same surface and at approximately the same distance (see Sect. II.1 and II.3). Active places of the surface, as discussed in Section II.1, have also the effect to increase the energy of combination with a peripheral dipole, the relative influence of the effect is, however, far smaller. The strength of the bond with a peripheral dipole, oriented perpendicular to the surface is, apart from being dependent on the magnitude of the field, also dependent on the gradient of the field. The most ideal "active place" would be a single ion, not counteracted by other ions of opposite charge. An *ion* at a distance of  $2.8 \text{ \AA.}$  from such an idealized "active place" would show an energy of combination of  $118 \text{ kcal./mole}$  as against  $7.8 \text{ kcal./mole}$  by the electrostatic forces of a smooth surface, hence a ratio of 15:1. The energy of combination between a *dipole* with a dipole moment  $1.7 \times 10^{-18} \text{ e.s.u.}$  and such an "active place" at a distance  $2.7 \text{ \AA.}$  would be  $16.6 \text{ kcal./mole}$  as against  $5.8 \text{ kcal./mole}$  as shown by the smooth surface, hence a ratio of less than 3:1. For actually occurring active places of the character of the "end positions" as described in Section II.1, the ratios would be 13:1 in case of an ion and 2.5:1 in case of an oriented peripheral dipole. The influence of active places is, therefore, less dominant with peripheral dipoles.

Polar molecules that have dipoles of a nonperipheral character, such as organic ketones (the CO group), organic halides, ethers, and nitro compounds, will also be attracted by the electrostatic field of ionic surfaces. In all those cases, however, the dominant contribution to the adsorption energy will be given by the nonpolar van der Waals' forces and, in general, no orientation will take place as a result of dipole action, the molecules lying as flat as possible on the surface.

The same holds for molecules which (like  $\text{CO}_2$ ) have no resultant dipole when viewed from a great distance, but which possess partial dipole moments, compensating each other entirely in the molecule. In adsorption phenomena the partial dipole moments are far more important than the resultant dipole.  $\text{CO}_2$  must also be assumed to take up a flat position when adsorbed on ionic surfaces. Nevertheless the dipole may contribute

to the total adsorption energy. Lenel (81) calculates a contribution of 2.7 kcal./mole from this source in the adsorption of  $\text{CO}_2$  on KCl (total heat of adsorption 6.35 kcal./mole) (see also Sect. IV.1).

When a polar molecule is adsorbed on the surface of a metal, we may assume that, as in the case of adsorption of ions (Sect. II.2), the attraction may be described by the image picture. It is interesting to note that, at the time that Keesom tried to explain van der Waals' forces as an interaction of dipoles (77), Lorenz and Landé (87), followed by Magnus (88) were the first to explore the nature of adsorption forces by picturing it as the mutual attraction of a dipole molecule and its image. The energy of interaction may be given by the expression:

$$E_\mu = -\frac{\mu^2}{16r_0^3} (1 + \cos^2 \beta) \quad (47)$$

where  $\mu$  is the dipole moment,  $r_0$  the distance to the metal surface, and  $\beta$  the angle between the direction of the dipole and the normal to the surface. The energy is a maximum when  $\beta = 0$ , hence the dipole is oriented perpendicularly to the surface. Even in this position, however, the energy of interaction is negligibly small. If one tries to explain adsorption by this effect only, one can only attain the right order of magnitude of adsorption energies by using improbably low values for the distance  $r_0$  (of the order of 1 Å.). Let us take as an example again the dipole of an organic alcohol OH group or of water, with  $\mu = 1.7$  debyes and assume  $r_0$  to be again 2.7 Å. We may take  $\beta = 0^\circ$ , hence:

$$E_\mu = -\frac{2\mu^2}{16r_0^3} \quad (48)$$

which amounts to 0.26<sup>5</sup> kcal./mole. Even if the distance  $r_0$  were appreciably smaller than in the case of adsorption of an OH dipole on a chloride ion of an NaCl surface and were as low as 1.5 Å., the energy would only amount to 1.55 kcal./mole.

At small distances like this the calculations should be made with charges  $\epsilon'$  separated by the length of the dipole  $l$  rather than with the dipole moment  $\mu$ . Instead of equation (48) we should use:

$$F_{\epsilon'l} = -\frac{(\epsilon'l)^2}{8r_0^3 - 2r_0l^2} \quad (49)$$

where  $r_0$  is the distance of the center of the dipole from the metal surface.

With  $r_0 = 1.5$  Å. (the lowest possible figure),  $l = 1.0$  Å., and  $\epsilon'l = \mu = 1.7$  debyes, we obtain 1.73 kcal./mole, still a relatively low figure.

While, therefore, an ion is much more strongly bound by a metallic



surface (Sect. II.1) than by the electrostatic action of the surface of an ionic crystal (Sect. II.1), it is just the reverse in the case of a polar molecule.

Polar molecules, adsorbed in such a position that the dipoles are parallel to the surface, get even less contribution from the dipole-induction force. In this case  $\beta = 90^\circ$  and the energy contribution is only:

$$E_\mu = -\mu^2/16r_0^3 \quad (50)$$

An organic molecule with a CO group, like the aliphatic ketones, lying flat on a metal surface would, according to equation (50), receive a contribution of only 0.15<sup>5</sup> kcal./mole to its adsorption energy from the mutual attraction of the CO dipole and its image, if  $\mu = 2.7$  debyes and  $r_0 = 3.5$  Å.

It will be clear from the above discussion that the polarization of a *dielectric* adsorbent by an adsorbed polar molecule, may, in general, be neglected. The energy contributions in such cases would always be smaller than in the adsorption by metals (see Sect. II.2 and II.3).

### 7. Polar van der Waals' Forces. Electrostatic Polarization of an Adsorbed Molecule

On various occasions we have discussed the polarization of the adsorbent by an adsorbed ion or polar molecule (Sects. II.2, II.3, and III.6). In this subsection we will deal with the polarization of an adsorbed molecule by the electrostatic field of the surface of an adsorbent. When the electrostatic field at the distance  $r_0$  is  $F$  (Eq. 5) and the polarizability of the adsorbed molecule is  $\alpha$ , the energy of combination due to this effect is:

$$E_\alpha = -F^2\alpha/2 \quad (51)$$

Usually the contribution by this electrostatic polarization is small. Let us consider the adsorption of an argon atom on top of a potassium ion of the cubic face of KCl. The distance  $r_0$  of the center of the argon atom to the center of the potassium ion is roughly the same as the distance between a potassium ion and its nearest chloride ion in the crystal:  $r_c = 3.14$  Å. The electrostatic field at this distance above the surface, calculated by equation (5) is  $0.145 \times 10^6$  e.s.u.

Taking  $\alpha = 1.68 \times 10^{-24}$  cm.<sup>3</sup> for the polarizability of the argon atom, equation (51) gives us 0.25<sup>5</sup> kcal./mole. Lenel (81) pointed out that the electrostatic field of the surface of the ionic lattice is too unhomogeneous to treat the argon atom as a whole with one mean value for the polarizability. In that part of the electronic cloud of the argon atom bordering the potassium ion, the field is nearly ten times that in the center of the argon

atom (Eq. 5). Lenel divided the argon atom in volume elements  $dv$ , calculated the electron density  $\rho$  in these volume elements, and assessed the potential due to the electric field for each of them separately. In case of an infinite number of volume elements, the expression takes the following form, derived by Teller (48d):

$$E_{\alpha} = - \int \frac{(P - P_0)^2 \rho}{I} dv \quad (52)$$

where  $P_0$  is the potential at the center of the argon atom,  $P$  is the potential in the volume element  $dv$ , and  $I$  the characteristic energy for the argon atom, for which as in equation (23) the ionization energy may be taken. Instead of 0.25<sup>5</sup> kcal./mole as given by equation (51), Lenel's method gives about 0.45 kcal./mole for an argon atom on top of a potassium ion.

Equation (51) when applied to an argon atom adsorbed just over the center of a square of 4 surface ions (2 positive and 2 negative) would give no contribution of this polarization effect, because the electric field in the center of the adsorbed atom is zero in this position. Lenel's method, however, gives a contribution of 0.37 kcal./mole for an argon atom adsorbed at such a spot, because the electric field is certainly not zero in those parts of the argon atom that touch the surface ions.

The energy contribution by the electrostatic polarization of the adsorbed molecule or atom is far more important on "active spots" of the kind discussed in Section II.1. An atom with a polarizability  $\alpha = 1 \times 10^{-24}$  cm.<sup>3</sup>, when placed on top of an ion of the cubic face of NaCl at a distance 2.8 Å., will, according to equation (51) show an amount of 0.23<sup>5</sup> kcal./mole toward its adsorption energy, as caused by this polarization. When bound at an active spot of the "end-position" character, the energy contribution will, however, be about 2.7 kcal./mole. The ratio between these two values is 11.5:1, nearly the same ratio as in the case of adsorption of ions and far greater than in case of dipoles (see Sect. III.6). While on smooth and flat surfaces the effect of the nonpolar van der Waals' forces (Sects. III.2-4) is always far more important than the effect of the electrostatic polarization (or influence effect), on active places of ionic surfaces, especially on projecting corners, edges, or points of the surface, on points of lattice disturbances with strong electrostatic fields, and on active places of the character of "end positions," the order may be reversed and the main contribution to the adsorption energy may be given by the electrostatic polarization (18). In such cases the physical properties of the adsorbed atoms or molecules may be drastically changed as we will see in Section IV.2.

In Section IV.1 we will discuss an example of electrostatic polarization of an adsorbed ion ( $\text{Cs}^+$ ) by its image. Jaquet (72) introduced a similar effect in discussing the adsorption of dipole molecules at metal surfaces. The adsorption energy in his calculations is enlarged by one-third of its value by this polarization. The total amount, however, is too small to account for the experimental values of adsorption energies and Jaquet's successful attempt to calculate dipole moments from adsorption energies is only explainable by the improbably low values of the distance  $r_0$ , which are used.

In Section IV.4 we will encounter cases in which an adsorbed ion serves as an "active spot" for electrostatic polarization, enforcing an induced dipole moment on another adsorbed atom or molecule.

#### IV. Collaboration between Various Forces

After having discussed in Sections II and III the forces leading to chemisorption and to physical adsorption, we will in the present section deal with the collaboration of these various forces in adsorption phenomena. The first subsection will be concerned with cases where various attraction forces collaborate in the adsorption of a single atom or molecule, while in Section IV.2 examples will be given in which the adsorbing forces working at different spots of the surface differ, changing the character of the adsorption when the adsorption proceeds. In subsequent subsections problems resulting from the mutual interaction of forces emanating from the adsorbed molecules themselves will be discussed.

##### *1. Various Attraction Forces Collaborating in Adsorption of a Single Atom or Molecule*

Any adsorption phenomenon is a result of the cooperation of at least one of the attraction forces discussed in the previous sections, and the repulsion forces mentioned in Section I.3. Of the various attraction forces the nonpolar van der Waals' forces (Sects. III.2-4) are always present and one or more of the other attraction forces may collaborate with them. The nonpolar van der Waals' forces dominate in many cases and the choice of the precise spot on the surface where the atom or molecule will be adsorbed is often governed by them. They tend to direct an adsorbed atom or molecule to such a place and also tend to orient it in such a position that a maximum number of neighboring atoms of surface and adsorbate is achieved. On a smooth surface they promote, therefore, the adsorption above the center of an elementary cell of the surface instead of on top of just a single surface atom.

It was shown in Sections III.4 and 5 that the magnitude of the adsorption energy of neutral nonpolar molecules on nonpolar surfaces could very well be explained by the nonpolar van der Waals' forces. In the following examples we will discuss some cases of adsorption in which either the molecule, or the surface, or both, have a polar character. Examples *A*, *B*, *C*, and *D* deal with the collaboration of nonpolar van der Waals' forces with various forms of polar van der Waals' forces. In examples *E*, *F*, and *G*, forces which lead to chemisorption cooperate with van der Waals' forces.

#### *A. Nonpolar van der Waals' Forces and Electrostatic Polarization*

When an argon atom is adsorbed on a smooth surface of a cubic face of potassium chloride, it has, theoretically, the choice between 4 different sites: on top of a potassium ion, on top of a chloride ion, above the mid-point of a lattice edge, or above the center of a lattice cell. The electrostatic polarization forces (Sect. III.7) would promote the first two positions, the nonpolar van der Waals' forces favor the latter one. Lennard-Jones and Dent (84) have already pointed out that at equilibrium distance the electrostatic field of the surface is only a fraction of the nonpolar van der Waals' field, amounting to 10% at a maximum in the most favorable position for electrostatic polarization. The nonpolar van der Waals' forces dominate and the equilibrium position of the adsorbed atom is above the center of a lattice cell. Lenel (81) calculated the contribution of the electrostatic polarization in this position by his method, mentioned in Section III.7 and found 0.37 kcal./mole while the contribution of the nonpolar van der Waals' forces in the same position amounted to 1.50 kcal./mole. The total amount, 1.87 kcal./mole, is well in accordance with the experimental figure of 2.08 kcal./mole, as found by Lenel, or 2.10 kcal./mole as determined by Orr (94). Similar calculations were made by Orr (95), using equation (51) for the electrostatic polarization and making use of the diamagnetic susceptibility (Eq. 29) for the van der Waals' forces. This latter method tends to give too high results, which are more than offset, however, by introducing the repulsion forces in the form of equation (1), as Orr does. As a result his calculated figures are on the low side, 1.593 kcal./mole for argon above the center of a lattice cell. The contribution of the electrostatic polarization, even in the most favorable positions amounted only to 4% of the contribution by the nonpolar van der Waals' forces. It is remarkable that, even on a surface as that of the cubic face of CsI, assuming cesium ions in the outer layer, the contribution by the electrostatic

polarization comes not higher than 22% of the contribution by the nonpolar van der Waals' forces as calculated by Orr's method (95) or 46% as calculated by Lenel (81). Lenel obtained the following figures:

Contribution by nonpolar van der Waals' forces.....	2.40 kcal./mole
Contribution by electrostatic polarization.....	1.10 kcal./mole
<i>Total</i> .....	<i>3.50 kcal./mole</i>

The experimental figure is 3.56 kcal./mole.

Similar considerations hold for the adsorption of other nonpolar atoms or molecules on smooth surfaces of ionic crystals. It is only in case of surfaces with protruding active spots (see Sect. III.7) that the electrostatic polarization may dominate over the nonpolar van der Waals' forces (18) (see also Sect. IV.2).

### *B. Molecule with a Nonperipheral Dipole on an Ionic Surface*

The dipole moment of carbon dioxide is zero because the partial dipoles in the molecule compensate each other entirely. Such a molecule, however, must be considered as a polar molecule in adsorption phenomena where polarity in molecular distances plays an important role. Lenel (81) has calculated the adsorption energy of CO<sub>2</sub> on potassium chloride. The contributions of the nonpolar van der Waals' forces (2.90 kcal./mole) and of the electrostatic polarization (0.74 kcal./mole) give only 3.64 kcal./mole, while the experimental figure is 6.35 kcal./mole. The difference, 2.7 kcal./mole, may be ascribed to the effect of the two oppositely directed partial dipoles or, in other words, to the quadrupole of the molecule. Lenel used this figure to calculate the various contributions to the adsorption energy of CO<sub>2</sub> on potassium iodide with the following results:

Nonpolar van der Waals' forces.....	3.30 kcal./mole
Electrostatic polarization.....	1.14 kcal./mole
Dipole forces.....	3.25 kcal./mole
<i>Total</i> .....	<i>7.69 kcal./mole</i>

The experimental figure for the adsorption energy of CO<sub>2</sub> on KI- is 7.45 kcal./mole.

A similar situation may be found with many other inorganic or organic molecules, independent of whether they have a permanent dipole moment or not. It is the partial dipoles which matter in adsorption phenomena. In all these cases we may assume the position on the surface to be governed mainly by the nonpolar van der Waals' forces, forcing the molecules in a flat position on the surface. The exact location on the surface may be modified by the polar forces.

### C. Molecule with a Peripheral Dipole on an Ionic Surface

When a molecule such as phenol is adsorbed on an ionic surface, it may be expected that the benzene ring lies flat on the surface, while the adjoining dipole containing hydroxyl group is pointed toward one of the negatively charged surface ions in such a way that its positive end (the H atom) is in direct contact with this negative surface ion.

Some years ago an analysis of the various contributions to the adsorption energy was given (18). When corrections are made in accordance with present knowledge, we obtain the following figures for the adsorption of a phenol molecule on a cubic face of NaCl with the OH dipole perpendicular to the surface and on top of a chloride ion.

Nonpolar van der Waals' forces of $C_6H_5$ group.....	3.4	kcal./mole
Dipole forces of OH group.....	5.3	kcal./mole
Nonpolar van der Waals' forces of OH group.....	0.60 <sup>b</sup>	kcal./mole
Electrostatic polarization of OH group.....	0.06 <sup>b</sup>	kcal./mole
<i>Total</i> .....	9.3 <sup>b</sup>	kcal./mole

For the calculation of the contribution of the  $C_6H_5$  group an average distance of 3.2 Å. has been assumed. The dipole contribution has been calculated with equation (46) using the following numerical figures:  $\mu = 1.56$  debyes,  $r_0 = 2.7$  Å.,  $l = 1.0$  Å.

The main contribution is given by the dipole force. A similar behavior may be expected in all cases of adsorption of organic molecules with peripheral dipoles (alcohols, acids, and amines) on ionic surfaces and especially for the adsorption of water or ammonia on these surfaces (27).

### D. Dipole Molecule on a Metallic Surface

Let us assume an  $NH_3$  molecule to be adsorbed on a copper surface. The experimental value for the adsorption energy is stated to be 9.2 kcal./mole for the first molecules, which value decreases to 6.6 kcal./mole in later stages of the adsorption (61). We may assume that the latter figure represents the adsorption energy on a flat part of the copper surface; the real adsorption energy for a single molecule will then be *lower* than 6.6 kcal./mole (see Sect. IV.3.)

The dipole of ammonia is composed of charge distributions connected with the nitrogen in the center of the molecule and the hydrogen atoms, which form a pyramid with the nitrogen on top. The N—H distance is about 1.05 Å.; the height of the pyramid is about 0.3 Å. Copper crystallizes in a face-centered lattice; the parameter of the elementary cell is 3.60 Å.; the shortest distance between two copper atoms is 2.55 Å. If a  $NH_3$  molecule is adsorbed on a cubic face over the mid-point of a lattice

edge, it is situated over the center of a square of 4 copper atoms (the edge of this square being 2.55 Å.). Assuming 1.7 Å. for the radius of  $\text{NH}_3$  and 1.27<sup>5</sup> Å. for the radius of a copper atom, the vertical distance of the center of  $\text{NH}_3$  to the plane through the centers of the surface atoms of the copper surface is 2.37 Å.

We may calculate the contribution of the nonpolar van der Waals' forces to the adsorption energy with equation (44), using the following numerical data:

$$\begin{aligned}\text{NH}_3: \alpha_0 &= 2.26 \times 10^{-24} \\ \nu_0 &= 2.7 \times 10^{15} \text{ (calculated from } h\nu_0 = 257 \text{ kcal./mole)} \\ \text{Cu: } r_e &= 1.41 \times 10^{-8} \text{ (one electron per atom)} \\ n_0 &= 8.55 \times 10^{23}\end{aligned}$$

and the usual figures for  $C$ ,  $h$ , and  $m$ . With  $r_0 = 2.37$  Å., we obtain for this contribution 3.55 kcal./mole.

The contribution arising from the dipole attraction may be calculated with the aid of equation (49), using the following numerical data:  $\epsilon' l = \mu = 1.46$  debyes,  $l = 0.6$  Å., and  $r_0 = 2.07$  Å. ( $2.37$  Å.  $-\frac{1}{2}l$ ).

Equation (49) gives 0.45 kcal./mole. Hence we obtain for the total adsorption energy a figure of  $3.55 + 0.45 = 4.0$  kcal./mole, a figure appreciably lower than the above-mentioned 6.6 kcal./mole (see also Sect. IV.3).

It may be noted that the dipole contribution only amounts to 11% of the total adsorption energy. Quite in accordance with the results of Section III.6, this contribution is small even in an extremely favorable case like this example.

### E. Ion on an Ionic Surface

When an ion is adsorbed on top of one of the constituent ions of an ionic surface, there will be a collaboration of various attraction forces, *viz.*, the Coulomb attraction of the ion by the electrostatic field of the surface, the induction of the adsorbent by the ion, the electrostatic polarization of the ion by the field of the surface, and the van der Waals' forces.

If we take as an example a chloride ion adsorbed on top of a sodium ion of a smooth idealized cubic face of NaCl at a distance 2.81 Å., we obtain the following figures:

Coulomb force (Eq. 6 in Sect. II.1).....	7.8 kcal./mole
Induction of the adsorbent (Eq. 16 in Sect. II.3).....	17.9 kcal./mole
Electrostatic polarization of ion (Eq. 51).....	0.7 kcal./mole
Nonpolar van der Waals' forces (Sect. III.3).....	2.1 <sup>6</sup> kcal./mole
<b>Total (approximately).....</b>	<b>28.5<sup>5</sup> kcal./mole</b>

In this case, however, the contribution of the repulsion forces (Sect. I.3.) may not be neglected. This contribution amounts to about 3.08 kcal./mole, hence the total adsorption energy is calculated to be about 25.5 kcal./mole.

If the chloride ion were not adsorbed on top of a sodium ion, but over the center of an elementary cell of the surface, the electrostatic field would be zero (neglecting the influence of the unhomogeneity as introduced by Lenel) (see Sect. III.7), hence the only contributions would be:

Induction of the adsorbent.....	16.8 kcal./mole
Nonpolar van der Waals' forces.....	9.4 kcal./mole
<i>Total</i> .....	<i>26.2 kcal./mole</i>

The effect of the induction of the adsorbent, when applying equation (16) is less in this case, because the vertical distance,  $r_0$ , between a chloride ion in such a position and the plane through the centers of the surface ions of the idealized surface is governed by the chloride ions only and is therefore greater than when the chloride ion is adsorbed on top of a sodium ion. Instead of  $r_0 = 2.81 \text{ \AA}$ ., we had to take  $r_0 = 3.03 \text{ \AA}$ .

The adsorption energy of a chloride ion in a position on top of a sodium ion is therefore of the same order of magnitude as in a position over the center of an elementary cell.

If we calculate similarly the adsorption energy of a sodium ion on top of a chloride ion of the surface, we obtain:

Coulomb forces (Eq. 5).....	7.8 kcal./mole
Induction of adsorbent (Eq. 16 with $r_0 = 2.81 \text{ \AA}$ ).....	17.9 kcal./mole
Electrostatic polarization of ion (Eq. 51).....	0.04 <sup>5</sup> kcal./mole
Nonpolar van der Waals' forces.....	0.43 kcal./mole
<i>Total</i> .....	<i>26.17<sup>5</sup> kcal./mole</i>
Less contribution of repulsion forces (approximately).....	3.08 kcal./mole
<i>Total (approximately)</i> .....	<i>23.1 kcal./mole</i>

For a sodium ion over the center of a lattice cell:

Induction of adsorbent (Eq. 16, with $r_0 = 1.99 \text{ \AA}$ ).....	25.2 kcal./mole
Nonpolar van der Waals' forces.....	0.86 kcal./mole
<i>Total</i> .....	<i>26.0 kcal./mole</i>

Again the adsorption energy in a position on top of an ion of opposite charge or over the middle of an elementary cell is of the same order of magnitude.

The above result is caused by a compensation of various effects and it is doubtful whether the calculations are exact enough to generalize the result, which would mean that a migration of an adsorbed ion over the sur-



face would demand only a relatively small activation energy. The application of equation (16) may lead to erroneous results in view of the real structure of the surface (see Sect. II.3) and it is just this equation that is responsible for the similarity of the adsorption energies calculated above.

In Section IV.5 we will see that the adsorption of a sodium ion next to a singly adsorbed chloride ion or of a chloride ion next to a single adsorbed sodium ion, hence the adsorption of an ion pair results in a far less dominant influence of the polarization of the dielectric adsorbent.

### *F. Ion on a Metallic Surface*

The adsorption energy of a single cesium ion on a tungsten surface is known to be 54.5 kcal./mole (39,40,110). The total adsorption energy results from the collaboration of the induction of the metal by the ion (image force), the nonpolar van der Waals' forces, the electrostatic polarization of the ion by its own electric image, the induction of the metal by the induced dipole in the ion, and the repulsion force.

The first two effects are given by equations (12) and (44), respectively, the third by an equation similar to equation (15) with  $(2r)^4$  instead of  $r^4$  and an extra factor, 2, in the denominator, because the polarization arises from an image charge. The fourth effect is given by equation (48) and the repulsion contribution by equation (2). The constant  $b$  of equation (2) may be eliminated in the way indicated in the derivation of equation (4) from equation (3). Hence the complete equation for the adsorption energy in our case reads:

$$E = -\frac{n-1}{n} \frac{\epsilon^2}{4r_0} - \frac{n-3}{n} \frac{\epsilon^2 \alpha_0}{16r_0^3} \left( \frac{C}{r_e} - \frac{h n_0}{\pi m \nu_0} \right) - \frac{n-4}{n} \frac{\alpha_0 \epsilon^2}{64r_0^4} - \frac{n-7}{n} \frac{\alpha_0^2 \epsilon^2}{128r_0^7}$$

With  $E = 54.5$  kcal./mole  $= 3.78 \times 10^{-12}$  erg/ion,  $n = 12$ ,  $\alpha_0 = 2.46 \times 10^{-24}$ ,  $r_e = 1.55 \times 10^{-8}$  cm. (1 electron per tungsten atom),  $n_0 = 6.4 \times 10^{22}$ ,  $\nu_0 = 5.63 \times 10^{15}$  (from  $h\nu_0 = 540$  kcal./mole, the ionization energy of a cesium ion),  $C = 2.5$ , and giving  $h$  and  $m$  their normal values, we can calculate  $r_0$ . We find  $r_0 = 1.74$  Å. If this value of  $r_0$  is taken to be the vertical distance of the cesium ion to the plane through the centers of the tungsten atoms of the surface and if we consider the surface to consist of dodecahedral faces, and the cesium ion to be adsorbed above a triangle of tungsten atoms with edges of 2.72 Å., 2.72 Å., and 3.15 Å., the closest distance of the adsorbed cesium ion to its 3 direct tungsten neighbors is 2.42 Å.,

which is a reasonable value for the sum of the radii of a tungsten atom and a cesium ion in this sort of bond.

It is interesting to see to what extent the various forces contribute to the adsorption energy. The following data may be given:

Image force (induction of metal by ion).....	47.5 kcal./mole
Nonpolar van der Waals' forces.....	13.3 kcal./mole
Induction of ion by its own image.....	1.4 kcal./mole
Induction of metal by the induced dipole in ion.....	0.3 kcal./mole
<i>Total</i> .....	62.5 kcal./mole
Less contribution by repulsion forces.....	8.0 kcal./mole
<i>Total</i> .....	54.5 kcal./mole

As in Section IV.1.E, the induction of the adsorbent by the adsorbed ion is the most important contribution.

The value  $r_0 = 1.74 \text{ \AA}$ . fits also very well the experimentally found dipole moment  $\mu = 6.8 \times 10^{-18} \text{ e.s.u.}$  (40). This dipole is set up by the adsorbed cesium ion and its image and it lowers the work function of the tungsten metal. The active dipole moment effective in reducing the work function is given by the product of the charge of the ion and its distance from the metal surface, diminished by the dipole moment induced in the cesium ion by its image charge (40):

$$\mu_{eff} = e r_0 - (\alpha_0 e / 4 r_0^2)$$

with  $r_0 = 1.74 \text{ \AA}$ . and  $\alpha = 2.46 \times 10^{-24}$ , we find  $\mu_{eff} = 7.37 \times 10^{-18} \text{ e.s.u.}$ , which is in good accordance with the above-mentioned experimental value. If for  $r_0$  a value  $1.65 \text{ \AA}$ . were taken, the accordance would be better. This value happens to be the radius of the cesium ion in cesium halides and if this figure were taken it might mean that we had to assume the "metal surface" to start with its full polarizability (conductivity) at the outer periphery of its surface atoms. This might represent the right picture in a case where by the adsorption of a positive ion the conduction electrons are, on an average, more forced to the outside of the metal (39, 40). On the other hand the radius of a cesium ion in a bond like the one under consideration where it is not surrounded by other ions might well be smaller than  $1.65 \text{ \AA}$ . and be about 0.83 this value (117):  $1.37 \text{ \AA}$ .

### *G. Covalent Bonds and Nonpolar van der Waals' Forces*

A free methyl radical has a flat structure (98). If it were adsorbed by van der Waals' forces only, it would take up a flat position on the surface and its distance to a metal surface, *e.g.*, a nickel surface, would probably be about  $3 \text{ \AA}$ . or more. When the carbon atom of this free radical enters into a

covalent bond with one of the nickel atoms of the surface, the distance of this nickel atom to the carbon atom will be diminished to about 1.82 Å. (113). At the same time, because the fourth valency of the carbon atom is then saturated, the plane triangular arrangement of the free radical will be altered into the regular tetrahedral arrangement. The hydrogen atoms will, therefore, assume a vertical distance of 2.46 Å. above the plane through the centers of the nickel atoms of the surface. A hydrogen atom of the chemisorbed methyl group cannot, therefore, come nearer to a free nickel atom of the surface than 2.92 Å. This distance is far greater than the equilibrium distance, which the nonpolar van der Waals' forces would establish, when working alone, hence there will be a relatively small van der Waals' action between the 3 hydrogen atoms of the methyl group and the surface.

If, however, we consider a radical  $CR_1R_2R_3$  and  $R_1$ ,  $R_2$ , and  $R_3$  are groups that are bound with a carbon atom to the central carbon atom, the situation is far more favorable. Assuming again the distance between the central carbon atom and nickel atom to which it is bound by a covalent bond to be 1.82 Å. and assuming the normal tetrahedron angle of  $109^\circ 28'$  and a C—C distance of 1.54 Å., the vertical distance from the surface of a carbon atom next to the one involved in the chemisorption is 2.72 Å. Such a carbon atom may take up a position in which it is 3.0 Å. apart from the nickel atom to which the radical is bound as well as from its nearest neighbor. It, therefore, may take up an excellent position for attraction by non-polar van der Waals' forces. The further parts of the groups  $R_1$ ,  $R_2$ , and  $R_3$  will try to take up positions as flat as possible with respect to the surface.

## ***2. Various Forms of van der Waals' Interaction at Different Spots of the Surface***

There is an antagonistic character between "active spots" promoting nonpolar van der Waals' adsorption (Sect. III.4) and those promoting adsorption by electrostatic polarization (Sect. III.7). The latter consist, for example, of protruding parts of an ionic surface, where strong ionic fields are operating while the former are found in cracks, crevices, and other recessed parts of the surface where a maximum number of direct neighbors can be found. Interesting examples of both kinds of van der Waals' adsorption can be found on surfaces of inorganic salts obtained by sublimation in a high vacuum (6d,8) and may be described in the following lines as they give a clear experimental evidence of the simultaneous exist-

ence of different sorts of adsorption forces on the same surface. When a salt like  $\text{CaF}_2$  is sublimed in a high vacuum on a glass wall, it forms an optically clear film, which consists of very thin lamellae, which are on the average only a few molecules thick (23,35,62). Such salt layers are very suitable for studying light absorption spectra of adsorbed molecules. When iodine is adsorbed at such low pressures that only a few isolated molecules are adsorbed on the surface (less than 0.5% of the maximum amount that can be adsorbed at higher pressures), these iodine molecules are colorless to the eye. Their absorption spectrum is completely shifted to the ultraviolet, a strong light absorption being exhibited with two maxima at 343 and 284  $m\mu$  (17). This absorption spectrum resembles that of an iodine molecule, bound to an iodide ion in the tri iodide ion or bound to a bromide ion in the  $(\text{BrI}_2)^-$  ion and is to be ascribed to iodine molecules adsorbed by electrostatic polarization on active spots with strong ionic fields of fluoride ions. The light absorption constant per molecule per square centimeter is very high ( $> 1000 \times 10^{-18}$ ).

At higher iodine pressures nonpolar van der Waals' adsorption makes itself manifest. The light absorption of molecules adsorbed at these higher pressures is far lower (about  $10 \times 10^{-18}$ ) and less far shifted to the ultraviolet. This nonpolar van der Waals' adsorption starts on active spots of other character (see above) and spreads with increasing iodine pressure over the whole surface until it is covered with a unimolecular layer of adsorbed iodine molecules. The light absorption spectra are simultaneously shifted toward longer wave length as may be illustrated (58) by the position of the first maximum at various degrees of covering of the surface with adsorbed iodine.

0.5– 9%, first maximum at 363  $m\mu$

9–16%, first maximum at 374  $m\mu$

16–26%, first maximum at 395  $m\mu$

The color of the adsorbed molecules is now visible to the eye, the layers turn brown, and the absorption spectrum is approaching more and more that of solid iodine as the adsorption increases.

Adsorbed bromine behaves in an analogous manner. Here, again, the first molecules, adsorbed at very low pressures, are bound by electrostatic polarization and show a very pronounced absorption spectrum (56) with maxima at 267 and 252  $m\mu$ . At higher pressures adsorption by nonpolar van der Waals' forces sets in on different parts of the surface.

The nonpolar van der Waals' forces between the ions of these surfaces and the iodine molecules are weaker than the mutual forces between iodine

molecules in solid iodine. The heat of adsorption even on these highly porous surfaces, where the iodine molecules can get direct contact with many surface ions, is lower than the heat of sublimation of solid iodine (9, 14) (see also Sect. III.4). Other inorganic compounds, which, on sublimation, do not give lamellar, porous structures but which form compact layers, do not possess crevices or recessed parts that can act as "active" spots for nonpolar van der Waals' adsorption. Layers of  $\text{SiO}_2$ ,  $\text{Al}_2\text{O}_3$ ,  $\text{AgCl}$ , etc., formed by sublimation in a high vacuum, when exposed to iodine vapor, do not give the visible nonpolar van der Waals' adsorption. They have, however, still active spots for electrostatic polarization and consequently adsorb a few isolated molecules of iodine, showing the characteristic, very strong, light absorption analogous to the light absorption of the first molecules of iodine on layers of  $\text{CaF}_2$ ,  $\text{BaF}_2$ , etc. (20). The position of the two maxima is given for a few examples.

<u>Adsorbed on</u>	<u><math>m\mu</math></u>
$\text{CaF}_2$ .....	343 and 284
$\text{SrF}_2$ .....	349 and 283
$\text{BaF}_2$ .....	352 and 285
$\text{SiO}_2$ .....	355 and 290

A similar behavior is shown when cesium is adsorbed instead of iodine. In equilibrium with extremely low pressures of cesium vapor only a few isolated cesium atoms are adsorbed by electrostatic polarization on salt layers, such as  $\text{CaF}_2$ . Their light-absorption spectrum shows maxima in the ultraviolet region between 200 and 300  $m\mu$  (22). Although they do not show a visible color, they nevertheless absorb some visible light, for their presence is responsible for a photoelectric activity of these layers (36, 37). The photoelectric emission increases linearly with the amount of cesium atoms adsorbed in this manner; the photoelectric threshold is at about 700  $m\mu$ , as compared with the ionization threshold of 318.4  $m\mu$  for a cesium atom in cesium vapor. When by increasing the vapor pressure the adsorption of cesium on the salt layer increases, nonpolar van der Waals' adsorption sets in. The absorption spectrum of these new cesium atoms is completely different; their main light absorption is in the visible region, the color of the layers turns blue, the adsorbed layer shows electric conductivity, and the photoelectric activity decreases (36,37). At higher cesium pressures the adsorbed cesium layer is 3 atoms thick on the average (62) and shows the light absorption of thin metallic layers of cesium.

Nonporous, compact, layers of  $\text{SiO}_2$ ,  $\text{Al}_2\text{O}_3$ , etc., again show only the adsorption of isolated cesium atoms by electrostatic polarization. The same substances, in powder form, however, give nonpolar van der Waals'

adsorption as well, and show a deep blue color when cesium is adsorbed (20).

The striking difference in behavior between salts forming layers with a porous lamellar structure and those forming layers with a compact structure, both by sublimation in a high vacuum, is probably connected with the structure of the molecules of these substances in the gaseous state. When these molecules consist of ions, a porous structure consisting of lamellae is obtained; when the molecules consist of atoms bound by covalent forces, a compact layer is formed (13).

The greatly decreased ionization energy of cesium atoms adsorbed on isolated active spots of a cesium oxide surface by electrostatic polarization is the cause of the high photoelectric emission of modern photoelectric emission cathodes (6e,38). Similarly, the reduced ionization energy of barium atoms adsorbed on isolated active spots of barium oxide surfaces is responsible for the electron emission of "thermionic" cathodes (6f).

### ***3. Mutual van der Waals' Forces between Adsorbed Molecules. Reorientation***

Up till now we have considered mainly the adsorption of single molecules not influenced by forces emanating from other adsorbed molecules. Two molecules, however, adsorbed on the same surface, will attract each other with van der Waals' forces. The contribution of these mutual attraction forces between adsorbed molecules may in some cases lead to an important increase in the total adsorption energy.

As already mentioned in Section III.4, the differential heat of adsorption of many gases on porous adsorbents has a general tendency to *decrease* with increasing amount of adsorbed molecules. This is caused by the simple fact that the first molecules are adsorbed at active places, where the adsorption energy is greater, while molecules added at later stages find less active places. This trend, however, is counteracted by the mutual van der Waals' forces between the adsorbed molecules. Consequently there is often a minimum in the differential heat of adsorption as a function of the amount of molecules adsorbed. Thus the first molecules of  $N_2$  on charcoal show a differential heat of adsorption of 8.35 kcal./mole, this figure decreases to 4.1 kcal./mole when more  $N_2$  is adsorbed, and increases again to 4.8 kcal./mole on further adsorption (111). Similarly, the first molecules of  $NH_3$  on charcoal show a differential heat of adsorption of 11.27 kcal./mole, the figure passes through a minimum of 7.83 kcal./mole and then increases to 8.71 kcal./mole when more  $NH_3$  is adsorbed (111).

As mentioned in Section III.4, the differential heat of adsorption of iodine on  $\text{BaCl}_2$  is 11.8 kcal./mole when the surface is covered to the extent of 57%. The heat of adsorption increases to 13.7 kcal./mole when 74% of the surface is covered (9,14).

As a result of both effects *all* experimental figures for the differential heat of adsorption will be higher than the figure that would correspond to the adsorption of one single molecule on a smooth surface of the adsorbent. The experimental figure of 6.6 kcal./mole for  $\text{NH}_3$  on copper, which we mentioned in Section IV.1.D. must, therefore, also be considered as the sum of the heat of adsorption of  $\text{NH}_3$  on a smooth copper surface and the energy resulting from mutual interaction with other  $\text{NH}_3$  molecules, and it is not surprising that our calculated figure is lower (4.0 kcal./mole). The nonpolar van der Waals' interaction energy of two  $\text{NH}_3$  molecules at a mutual distance of 3.6 Å. (as prescribed by the Cu lattice, see Sect. IV.1.D) is, according to equation (21), 0.455 kcal./mole. If we assume that on the average every  $\text{NH}_3$  molecule at that stage of the adsorption has two such neighbors, we obtain an increase of the adsorption energy of 0.91 kcal./mole. When two molecules of  $\text{NH}_3$  are adsorbed next to each other on the surface, we may expect a reorientation of their dipoles. Instead of being oriented toward the metal surface, two molecules will tend to place their dipoles in alignment. When this happens, the interaction energy caused by the mutual attraction of their dipoles would be  $2\mu^2/r^3$ . With  $\mu = 1.46$  debyes and  $r = 3.6$  Å., this is 1.32 kcal./mole. The interaction energy would be  $\mu^2/r^3 = 0.66$  kcal./mole if the dipoles are antiparallel.

Let us assume that the dipole of one of the two neighbors mentioned above is in alignment, and the dipole of the other antiparallel to the dipole of an average  $\text{NH}_3$  molecule. The energy of adsorption would then be increased by 1.98 kcal./mole by this effect. However, since through this reorientation the dipoles are not directed to the metal surface, but only parallel to it, the dipole contribution of 0.45 kcal./mole, mentioned in Section IV.1.D, must be halved. Hence, instead of 4 kcal./mole, we obtain:

$$3.55 + 0.22^5 + 0.91 + 1.98 = 6.67 \text{ kcal./mole}$$

which is a figure very close to the experimental one.

When the pressure of the gas, which is in equilibrium with the adsorbed layer, increases and approaches the saturation pressure at the temperature of the experiment, the properties of the adsorbed layer will approach those of the solid or the liquid of the gas that is adsorbed. As we saw in Section IV.2, the optical properties of iodine or cesium adsorbed on salt layers indeed approach those of solid iodine or solid cesium. Very often, however,

we must expect that the influence of the lattice of the adsorbent is still dominant for the mutual distances of the adsorbed molecules, as we assumed in the above-mentioned example of  $\text{NH}_3$  on copper. Consequently the properties of the adsorbed layer when reaching saturation will approach the properties of the solid or the liquid of the same substance, without, however, becoming exactly equal to them. There is *no* continuity between the adsorbed layer and the condensed one in such a case. Very often the liquid of the same substance does *not* wet the adsorbed layer. When cesium or iodine crystallizes, distinct crystals are found either on top of or next to the adsorbed layer, without there being a continuous transition from the one into the other phase. Water very often does *not* wet a surface, although this has already bound a great number of water molecules in the adsorbed state (2,52).

In the above-mentioned example of the adsorption of  $\text{NH}_3$  on copper, we assumed that a reorientation of the dipole molecules might take place, decreasing the energy content of the system. A reorientation of dipole molecules also takes place in the adsorption of molecules of fatty acids on metals (104) or on ionic surfaces. When a single fatty acid molecule is adsorbed, the dipole will be oriented toward the surface and the hydrocarbon chain will assume a position as flat as possible on the surface, like the phenol molecules in Section IV.1.C. When more molecules are adsorbed a reorientation will take place in such a way that the dipoles are still directly bound and oriented toward the surface, but that the hydrocarbon chains are desorbed orienting each other to parallel chains, pointing away from the surface. Such an orientation is similar to the mutual arrangement of these molecules in their crystals. The same molecules show an analogous behavior when adsorbed on a water surface. The total energy content of the system decreases considerably by this reorientation, because of the contribution of the mutual van der Waals' attraction forces of the hydrocarbon chains and by the fact that more dipoles can come into direct contact with the surface. It is true that the parallel orientation of the dipoles leads to a repulsion; this, however, is considerably overcompensated by the other contributions.

*o*-Nitrophenol molecules, adsorbed on a  $\text{CaF}_2$  surface show a similar behavior (27). *p*-Nitrophenol molecules remain adsorbed in a flat position (27), even when the adsorbed layer gets completely filled up. It could be shown by the study of the light-absorption spectra that the first molecules have their dipoles oriented toward the fluoride ions of the surface. On top of the first layer a second layer of *p*-nitrophenol molecules is adsorbed, purely bound by nonpolar van der Waals' forces. When adsorbed on  $\text{CaF}_2$



(19), the light-absorption maximum of the molecules of the first layer is  $370\text{ m}\mu$ , that of the second layer of  $316\text{ m}\mu$ ; when adsorbed on  $\text{BaF}_2$  (57), the absorption maximum of the molecules of the first layer is at  $413\text{ m}\mu$  and that of the molecules of the second layer varies between  $355$  and  $320\text{ m}\mu$ .

#### *4. Additional Forces Emanating from Chemisorbed Molecules*

A cesium ion adsorbed on a metal surface forms together with its image an electric dipole (see Sect. IV.1.F). By the presence of such dipoles, with their positive end pointing outward, the work function of the metal is lowered (5,79); hence it requires less energy to remove an electron from the metal. We come back to this phenomenon in Section V.2.

Because the double layer, formed by the adsorption of ions, consists of discrete ions and their images, there is already an electric field manifesting itself a very short distance above the metal surface, which field attracts other positive ions. Thus by the presence of a certain number of adsorbed positive ions, the adsorption energy of other ions is *raised* (6c,39,41). The adsorption energy of a  $\text{Cs}^+$  ion on a tungsten surface is  $54.5\text{ kcal./mole}$  (Sect. IV. 1.F). When 10% of the available places have been covered with cesium ions, the adsorption energy is raised to  $67.2\text{ kcal./mole}$ .

In Section V.2 we will see that cesium atoms, when coming into contact with a metal surface like that of tungsten, ionize, and are adsorbed as ions. After about 13.5% of the available adsorption places have been covered, the work function of the tungsten metal is lowered to such an extent that the ionization of a new cesium atom and the adsorption of the formed ion would lower the energy content of the system less than the straightforward adsorption as an atom (6c,39,41). The cesium atoms are then adsorbed next to the adsorbed ions. They are bound by van der Waals' forces emanating from the metal and from the neighboring cesium ion while, moreover, the cesium ion and its image polarize the cesium atom. As a consequence of this latter electrostatic polarization the adsorbed atoms acquire an induced dipole moment, which assists the dipoles resulting from the ions and their images in further lowering the work function of the metal. Four atoms can be adsorbed on the average around every cesium ion, which brings the degree of covering to about 67%, which is the degree of covering where the work function gets its minimum value (109).

The description of these phenomena as if discrete atoms are adsorbed next to discrete ions, is of course a very rough one. A better description would perhaps be that after about 13.5% of the available adsorption places

have been covered by ions and no more electrons will be taken up by the metal, any further arriving cesium atom will settle next to one of the adsorbed ions and share its electron with it, so that one might speak of an adsorbed  $\text{Cs}_2^+$  ion. The more cesium atoms added, the more dominating will be the atomic character.

On further adsorption more cesium atoms are placed in between those already present and they are bound by nonpolar van der Waals' forces emanating from these other atoms and from the metal surface. The electric double layer, consisting of ions and their images and polarized atoms, results in a polarization of these newly adsorbed atoms in such a way that their dipoles are oriented with their negative end pointing outward (41), thus increasing the work function.

Similar phenomena are observed with other metals as adsorbents (molybdenum, tantalum, silver, etc.) and with the alkali atoms, alkaline earth atoms, or thorium atoms as adsorbates.

In all these cases adsorbed ions form "active places" next to which atoms can be adsorbed by van der Waals' forces (nonpolar and electrostatic polarization). We saw in Section II.4 that oxygen atoms adsorbed by chemisorption form dipoles with the metal atoms to which they are bound. Such oxygen atoms and the electric fields they cause may similarly act as "active places" for further adsorption. When oxygen molecules are adsorbed next to or on top of the chemisorbed oxygen atoms, these oxygen molecules will also be polarized, thus increasing the strength of the double layer (negative end pointing outward). Oxygen molecules adsorbed on tungsten next to or on top of chemisorbed oxygen atoms are responsible for one-third of the potential drop in the double layer (63).

Active places of this kind may also adsorb other atoms or molecules. Cesium ions or ions of other alkali or alkaline earth metals are far stronger adsorbed next to oxygen atoms, which are chemisorbed on a metal surface, than they are on a clean metal surface. Alkali atoms are strongly adsorbed on metal surfaces when chemisorbed hydrogen is present, which has formed a surface hydride with the metal atoms underneath. Water molecules, which are not very strongly bound by metal surfaces in general, are very well adsorbed when hydrogen is present in and on the metal forming a double layer with the positive end pointing outward. The water dipoles become oriented in the same way, assisting the photoelectric emission of those surfaces. All these composite adsorption phenomena have up till now been investigated mainly because of their importance for electron emission phenomena (6).

### 5. Ions Next to Ions on Ionic Surfaces

It was shown in Sections II.3 and IV.1.E that the induction of the adsorbent by the adsorbed ion gives the most important part of the adsorption energy. When an ion of opposite sign is adsorbed next to it, however, this polarization is nearly completely neutralized.

The adsorption energy of a *pair* of ions is about the same, when the constituent ions are adsorbed just over ions of opposite sign or when they are situated over the centers of elementary cells of the surface. For a pair of a  $\text{Na}^+$  and a  $\text{Cl}^-$  ion on a  $\text{NaCl}$  surface, this energy amounts to about 15 kcal./mole. (The energy of the mutual attraction between the  $\text{Na}^+$  and the  $\text{Cl}^-$  ion, about 110 kcal./mole, is not included in this figure.)

While it may be rather difficult for a single ion to migrate over the surface (Sect. IV.1.E), a pair of ions is in a far better position to move. As a result of such migrations the pair of ions may reach the edge of the crystal or the corner of the crystal face on which it is adsorbed. The adsorption energy is far greater at such a point. Actually it is only one of the two ions of the pair in the corner position; the other ion has a position on the edge of the crystal. For a pair of  $\text{Na}^+$  and  $\text{Cl}^-$  ions on a cubic face of  $\text{NaCl}$ , the adsorption energies may be calculated as:

$\text{Na}^+$ in corner, $\text{Cl}^-$ next to it.....	35.5 kcal./mole
$\text{Cl}^-$ in corner, $\text{Na}^+$ next to it.....	35.3 kcal./mole

If we consider a cubic face of  $\text{NaCl}$  with linear dimensions of  $n$  ionic distances, then there are  $n^2$  ions in that face. It will be easily seen that there are then  $6n^2$  possible positions for a pair of ions to be adsorbed somewhere on that face. There are, however, only 4 corner positions. The ratio of the probabilities to find an ion pair (after migration) at a corner position or somewhere on the face itself is proportional to the ratio of the possible positions multiplied by an  $e$  power of the difference of the adsorption energies over  $RT$ :

$$\frac{P_{cor}}{P_{mid}} = \sim \frac{4}{6n^2} \cdot \exp \left( \frac{E_{cor} - E_{mid}}{RT} \right)$$

With  $E_{cor} = 34.4$  kcal./mole,  $E_{mid} = 15$  kcal./mole, and  $T = 290^\circ\text{K.}$ , we get:

$$\frac{P_{cor}}{P_{mid}} = \frac{2 \times 10^{16}}{3n^2}$$

The influence of the difference in adsorption energy would be balanced by the geometrical factor with  $n = 2.6 \times 10^7$ , hence a linear dimension of

about  $\frac{3}{4}$  cm. Even for crystals of macroscopic dimensions, therefore, the probability of finding a pair of ions at a corner position is greater than finding it somewhere on the cubic face.

### 6. Multimolecular Adsorption

Due to the forces emanating from adsorbed molecules, other molecules may be adsorbed, not only next to them but also on top of them. In such cases the adsorption is not restricted to a unimolecular film but several layers may be adsorbed on top of each other. In Sections 2, 3, and 4 above we encountered a few examples of multimolecular adsorption (cesium, nitrophenol, and oxygen).

The adsorption isotherms, in cases of multimolecular adsorption, have very often a sigmoid shape. When the amount of adsorbed material is plotted as a function of the relative pressure (*i.e.*, the actual pressure of the gas divided by the saturation pressure of the gas at the temperature of the experiment), the curve first rises rather steeply, then slows, passes through an inflection point, and starts to rise steeply again when the relative pressure approaches unity. This sigmoid shape is the basis of the well-known method for the determination of the size of surface areas given by Brunauer, Emmett, and Teller (48c,49,64), based on multimolecular adsorption of nitrogen or another inert gas at low temperatures.

A sigmoid shape of adsorption isotherm is, conversely, often taken as a proof for multimolecular adsorption. Such a conclusion, however, is not valid (12). A sigmoid shape may be expected in many cases—as where the heat of adsorption falls at first with increasing amount of adsorbed material and then passes through a minimum in order to rise again when more molecules are adsorbed. As we saw in Section 3 above this often happens when adsorption first takes place on spots active for nonpolar van der Waals' forces, then on less active spots, etc., while simultaneously the adsorption energy increases again by the mutual nonpolar van der Waals' forces between the adsorbed molecules.

De Boer and Zwikker (44) derived an equation for a sigmoid form of adsorption isotherm, assuming multimolecular adsorption caused by electrostatic polarization. Since then, however, it has been realized that electrostatic polarization forces are not nearly strong enough to account for multimolecular adsorption (49) (see also Sect. III.7). It has also been shown experimentally that the adsorption of iodine on  $\text{CaF}_2$  and similar salts, though showing an adsorption isotherm of a sigmoid type, fitting in with the above-mentioned theory, leads to unimolecular layers only (9,27,35).

Adsorption in multimolecular layers, however, may well be promoted

when small molecules with a large permanent dipole (water and ammonia) are adsorbed on ionic surfaces or on polar sites of other adsorbents. The mutual dipole forces between molecules of successive layers will assist materially in increasing the heat of adsorption, while simultaneously in the case of water molecules the entropy may be greater than in the liquid state. Multimolecular adsorption may well be favored under such circumstances. We may, in this connection, mention the adsorption of water on the surfaces of gel-forming substances, such as silica gel, or on carbohydrate and protein surfaces (24). The adsorption isotherm has a pronounced sigmoid character in these cases (76).

However, as already mentioned, such a shape may also be experienced in cases where no multimolecular adsorption does occur. Recently Cassie (52) has shown that on the assumption that molecules are first bound on isolated sites (far apart), and that further molecules are adsorbed next to these to form clusters of molecules, all far apart from each other, the same equation for the adsorption isotherm may be derived as was obtained by Brunauer, Emmett, and Teller for multimolecular adsorption. Cassie applied this isotherm successfully to the binding of water by keratin. There is no multimolecular adsorption in the sense of continuous layers of adsorbed molecules on top of each other in such a case.

### *7. Significance of Entropy Changes*

In all cases in which adsorption takes place from the gaseous state (the subject of this article), the adsorption process is accompanied by a decrease in entropy, since in a gas the molecules always have more freedom of movement than in the adsorbed state. As the free energy of the system always decreases when adsorption takes place, it is obvious that *all* these adsorption phenomena are exothermic in character.

We saw in Section III.4 that the heat of adsorption may in some cases be lower than the heat of condensation (to the liquid or to the solid). Adsorption nevertheless takes place in such cases in equilibrium with pressures lower than the saturation pressure, because the decrease of entropy in case of adsorption is far less than the decrease of entropy when condensation to the solid or liquid phase takes place. The molecules have, in general, more freedom of movement in the adsorbed state than in the solid or sometimes even than in the liquid state, hence the entropy is higher in the adsorbed state. We may especially expect this to happen, when the molecules are bound to the surface by nonpolar van der Waals' forces, which do not differ much from spot to spot. The molecules may then migrate over the surface—provided the temperature is high enough to overcome

the small differences of binding energy at various spots of the surface—thus giving the molecules freedom of movement in two directions.

When water molecules are adsorbed on a nonpolar substance, like charcoal, the heat of adsorption is given by nonpolar van der Waals' forces only; the dipoles have practically no effect (Sects. III.6 and IV.1.D). When water molecules condense to liquid water or to ice, the contribution of the mutual attraction by the dipoles is a very large one. Consequently the heat of adsorption is smaller than the heat of condensation (54). Water molecules, adsorbed on a charcoal surface, however, have a great freedom of movement and behave as a two-dimensional gas. The entropy is so much greater than in the liquid or solid state that adsorption takes place in equilibrium with unsaturated water pressures, despite the lower heat of adsorption. The shape of the adsorption isotherm is convex toward the pressure axis, in complete agreement with the shape that may be expected from statistical considerations (51).

Another example where the heat of condensation (to the solid) is greater than the heat of adsorption (Sects. III.4 and IV.3), is the adsorption of iodine on  $\text{BaCl}_2$ . When 57% of the adsorption has taken place, the heat of adsorption is 11.8 kcal./mole, and the relation between the equilibrium pressure  $p_{0.57}$  and the absolute temperature  $T$  is given by the equation of the adsorption isostere (9):

$$\log p_{0.57} = - \frac{11,800}{4.57T} + 7.7$$

The relation between the saturation pressure  $p_s$  and the absolute temperature is given by:

$$\log p_s = - \frac{15,500}{4.57T} + 10.9$$

The heat of sublimation is 15.5 kcal./mole.

Subtracting both equations gives us:

$$\log \frac{p_{0.57}}{p_s} = \frac{3700}{4.57T} - 3.2$$

Since  $\log p_{0.57}/p_s$  must be negative, the temperature must be higher than 253°K. (−20°C.) to enable this adsorption to take place.

Similarly when 74% of the adsorption places have been filled, the adsorption isostere is given by (9):

$$\log p_{0.74} = - \frac{13,700}{T} + 9.35$$

hence:

$$\log \frac{p_{0.74}}{p_s} = \frac{1800}{4.57T} - 1.5^5$$

and  $T$  must again be higher than  $253^\circ\text{K}$ .

## V. Reactions with or on Surfaces

### 1. Changes in Adsorbing Surface. Swelling

We saw in Section II.4 that the hexagon layers of graphite are held together by nonpolar van der Waals' forces only. Therefore, it does not involve much work to separate these layers or to increase their mutual distance. Some atoms or molecules may be adsorbed by such hexagon layers of graphite so strongly that the energy content of the system and the free energy are decreased if these atoms or molecules push the layers apart and are bound in between them. In doing so the mutual distance of the layers will be increased materially and the graphite is swollen. The additive character of the nonpolar van der Waals' forces favors such a swelling phenomenon, because the strongly bound atoms or molecules can gather a maximum amount of direct neighbors by working their way in between the layers and pushing them apart.

Adsorption phenomena of this kind are far slower than the normal, practical instantaneous adsorption on free surfaces. It takes a certain amount of energy to push the layers apart, to create the new surface. The phenomenon will, therefore, be associated with a certain amount of activation energy, which has to be overcome before the full advantage may be experienced from the increased adsorption energy. The reaction will be slower, the higher the activation energy; increase in temperature will increase the rate of this adsorption, hence the rate of swelling.

When this interlamellar adsorption takes place in the small graphitic grains of active charcoal or similar adsorbents with a layer lattice structure, it manifests itself as an increased adsorption with a slow rate, while often hysteresis phenomena may be expected, because when desorption takes place, the broken up structure need not return to its original state. When this swelling takes place in a well-formed graphite lattice, it may lead to stoichiometric compositions, because the lamellae are exactly one atom of carbon thick and the adsorbate may find definite places in between the carbon atoms of the hexagons of two successive layers. Thus "alloys," such as  $\text{C}_{16}\text{K}$  or  $\text{C}_8\text{K}$ , or even a compound as  $\text{CF}$ , may be formed. The fluorine atoms are bound by chemisorption forces in this latter case (see Sect. V. 2).

Similar reactions may be found with other adsorbents. Layers of in-

organic salts, obtained by sublimation in a high vacuum have a lamellar structure (Sect. IV.2). When such layers are heated at temperatures between  $150^{\circ}$  and  $350^{\circ}\text{C.}$ , a decrease in the surface takes place due to sintering (23). The salt films remain completely optically clear by this sintering process. The lamellae merely become more or less firmly attached to each other by mutual van der Waals' forces. The size of the lamellae is unchanged after the sintering; ionic forces have not played a role in the phenomenon; they are *not* grown together to form one crystal lattice. A growing together to an enlarged or to a new crystal lattice (pure recrystallization), takes place at higher temperatures and is favored by the presence of water vapor. The sintering, however, means merely a decrease in free accessible surface due to mutual van der Waals' interaction of the lamellae. For each salt, sintering takes place to a certain degree for each temperature, which may be estimated by the study of the adsorption of molecules, adsorbed by relatively weak forces such as iodine and atomic hydrogen (35). Molecules or atoms that are strongly adsorbed, however, are able to overcome these forces again and thus abrogate the effect of the sintering. A lamellar  $\text{CaF}_2$  film whose surface has been sintered down nearly completely by heating at  $350^{\circ}\text{C.}$  so that practically no adsorption of iodine can be measured is fully restored to its original free surface by the adsorption of cesium (62). The cesium atoms work their way between the lamellae and push them apart again thus swelling the sintered film. When after this swelling the cesium is removed at a low temperature the open lamellar structure stays open and iodine is adsorbed to the same amount as it was before the sintering had taken place.

Other inorganic salts (*e.g.*, the alkali halides) sinter more easily than  $\text{CaF}_2$ , but the sintered surfaces are also reopened more easily by adsorbed molecules. In the case of sodium bromide, adsorbed iodine molecules are capable of swelling the sintered structure and, following this, of recrystallizing it completely (6d).

The swelling of gelatin with water shows some striking similarities to the above-described phenomena. It is possible, by means of a heat treatment, to increase the mutual bonds between the micelles and to reduce the capacity of the gelatin to swell in water accordingly (24).

Fibrous systems such as cellulose materials, wool, and nylon often consist of parallel chains, which may be considered to be partly in a crystalline state, partly in an amorphous one. The cohesive forces between the chains are stronger in the crystalline parts; hence when swelling takes place it is far easier to push the chains apart in the amorphous parts. Swelling, therefore, takes place preferentially in the amorphous parts.



When discussing the swelling of graphite, we mentioned the formation of stoichiometric compounds. Swelling phenomena provide us with examples of cases in which the border lines between adsorption and absorption, or between absorption and dissolution have been crossed. The binding of water by gelatin or wool may be better described as an absorption phenomenon (52); the swelling of rubber in organic media may be described as a dissolution process (68).

## **2. Changes in Adsorbed Molecule. "Activated" Adsorption**

Chemisorption is sometimes identified with the so-called phenomenon of "activated adsorption." When brought into contact with a metallic surface at not too low temperatures, an oxygen molecule reacts with the surface and splits into atoms that are adsorbed by chemisorption as described in Section II.4. Energy must be supplied to overcome the bond between the oxygen atoms in the molecule and to enable them to combine separately with the surface atoms of the metal. Just as in Section V.1, therefore, this adsorption phenomenon will be of a relatively slow rate (more slow the higher the activation energy). Taylor (108) pointed out that the rate of chemisorption increases exponentially with the temperature. Because of the activation energy involved in this type of adsorption, he introduced the name "activated adsorption." The amount of activation energy is far lower than the bond energy of the atoms in the molecule, because the whole process takes place in close proximity to the surface and occurs under the influence of the atoms of the metallic surface (or surface of a dielectric) (83).

In many cases the activation energy is so low that the chemisorption reaction takes place at quite low temperatures. In other cases it may amount to several kilocalories per mole. Oxygen molecules are adsorbed by nonpolar van der Waals' forces only when brought into contact with a charcoal surface at temperatures lower than  $-80^{\circ}\text{C}$ . Studies of the ortho-para hydrogen conversion or measurements of magnetic susceptibilities have revealed that above this temperature a very slow reaction sets in leading to the chemisorption of oxygen atoms. The activation energy in this case is about 5 kcal./mole (75). When oxygen is adsorbed on very thin molybdenum layers at very low temperatures only oxygen molecules will be adsorbed by nonpolar van der Waals' forces. At higher temperatures, however, chemisorption takes place and covalent bonds are established between molybdenum and oxygen atoms, thus occupying conduction electrons of the metal and consequently decreasing the conductivity of the very thin film (34). Measurements of contact resistances lead to similar

conclusions (112,118). On the other hand when oxygen molecules come into contact with metallic cesium, chemisorption takes place readily at  $-180^{\circ}\text{C}$ . as shown by the photoelectric properties of the metal (7b). When nitrogen molecules enter into a reaction with an iron surface, the reaction leads to the chemisorption of nitrogen atoms on iron, the activation energy in this case is as high as 15 kcal./mole (50).

At higher temperatures many of these gases dissolve in the metal in the atomic state. The activation energy for this dissolution process (or for diffusion through the metal lattice) is higher than for the activated adsorption. In many cases the interatomic distances in the metal lattices are increased by the formation of such a solution, the metal is swollen. The dissolved atoms may in some cases be moved through the lattice under the influence of an electric field, thus hydrogen atoms move in platinum toward the negative pole (53), oxygen atoms in zirconium are drawn toward the positive pole (30).

For graphite as adsorbent or absorbent, the gases, split up in the atomic state, may arrange themselves between the layers, where they are bound by covalent bonds to the carbon atoms. In such cases this activated adsorption leads also to swelling. When fluorine is adsorbed (absorbed), the ultimate product is the solid  $\text{CF}$ . All conduction electrons of the graphite are then used for covalent bonds and the conductivity of graphite has disappeared.

It is not only with diatomic molecules like  $\text{O}_2$ ,  $\text{N}_2$ , or  $\text{H}_2$  that activated adsorption may be found; more complicated molecules may also show a similar behavior.  $\text{NH}_3$  molecules may be split into an  $\text{NH}_2$  radical and a hydrogen atom, both of which will be chemisorbed. The same may happen when  $\text{CH}_4$  comes into contact with a metallic surface at a sufficiently high temperature; a chemisorbed  $\text{CH}_3$  radical and a chemisorbed hydrogen atom result from this reaction. A reaction of this type proceeds relatively easily when a  $\text{CH}_2$  group is situated in between two double  $\text{C}=\text{C}$  bonds, as in linoleic acid (32). This specific adsorption gives the explanation for the so-called "selective hydrogenation," in which molecules of this kind are hydrogenated (70).

When molecules with a double  $\text{C}=\text{C}$  bond are adsorbed by chemisorption by some metals ( $\text{Ni}$ ,  $\text{Pt}$ ,  $\text{Pd}$ , etc.), the double bond may go, and both  $\text{C}$  atoms enter into a covalent bond with the metal atoms. Such a "double" chemisorption is possible only when the interatomic distance of the surface atoms of the metal falls within certain limits. Twigg and Rideal (113) calculated that the most ideal distance would be  $2.73 \text{ \AA}$ . With this distance chemisorption would be possible without distortion of the tetrahedral

angles of the valences. This distance must be considered as a *lower* limit for, by turning one of the valencies around the C—C axis (single bond after chemisorption) with preservation of the tetrahedron angle, greater distances might be covered. Platinum and palladium have interatomic distances of exactly this value. In the case of nickel and cobalt the normal distances are just somewhat smaller (*ca.* 2.5 Å.). It has been suggested that active nickel catalysts are activated by oxygen atoms in the crystal lattice, which have increased the interatomic distance (113).

In chemisorption phenomena ionization of an atom may be the major factor. When an alkali metal atom comes into contact with a metallic surface, the alkali atom ionizes to a positive alkali ion and is bound by the mirror image force (Sect. II.4) while the electron is taken up by the metal. The metal surface plays in this chemisorption phenomenon a similar role as a halogen atom does when it forms a salt molecule with an alkali metal atom (39). The condition for such a chemisorption by ionization to occur is that the sum of the electron affinity of the metal (the reverse of the energy for electron emission) and the adsorption energy of the positive ion is greater than the sum of the ionization energy of the atom and the adsorption energy of the atom. Na, Ba, Th, etc. are adsorbed in such a manner. By their adsorption an electric double layer is set up which alters the values that make up the above-mentioned conditions. The work function of the metal decreases; hence the electron affinity of the metal decreases and the adsorption energy of the positive ion increases. As a result of these changes a point will be reached where the inequality mentioned above no longer holds. From such a point, which for cesium on tungsten occurs when about 13.5% of the adsorption places have been covered (40), atoms will be adsorbed next to the ions (Sect. IV.4).

Adsorbed molecules may sometimes enter into chemical reactions with the constituents of the surface. Alizarin, quinizarin, and similar highly colored molecules are strongly adsorbed on the surfaces of inorganic salts. Their OH dipoles are oriented and strongly bound by negative ions of the salt surfaces. At higher temperatures a chemical reaction sets in, hydrogen halide molecules evaporate, and the resulting alizarin ions are strongly bound by ionic forces in the place of the escaped halide ions (15). These reactions are restricted to the surface only and are accompanied by characteristic color changes. Before the reaction the color of the physically adsorbed alizarin molecule on the surfaces of  $\text{CaF}_2$ ,  $\text{SrF}_2$ , and  $\text{BaF}_2$  is yellow. After the reaction the colors of the chemisorbed alizarin ions are:

On  $\text{CaF}_2$ , red, light absorption maximum at 482  $\mu$

On  $\text{SrF}_2$ , red-violet, light absorption maximum at 495  $\mu$

On  $\text{BaF}_2$ , blue-violet, light absorption maximum at 520  $\mu$

Reactions of this kind may be used to estimate the size of a surface. In the reaction with  $\text{BaCl}_2$ , two molecules of  $\text{HCl}$  escape for every alizarin molecule that enters into the reaction. By estimating either the  $\text{HCl}$  or the alizarin, the surface of the  $\text{BaCl}_2$  may be found (9).

Water molecules, strongly adsorbed by their dipoles on a  $\text{CaF}_2$  surface, give a similar reaction. At higher temperatures  $\text{HF}$  molecules evaporate and the fluoride ions of the surface are replaced by hydroxyl ions. At a still higher temperature this surface hydroxide is converted into a surface oxide (27).

These reactions have a certain analogy to ion exchange reactions between surfaces and solutions of electrolytes, the discussion of which falls, however, beyond the scope of this article.

### 3. Reactions on Surfaces

Atoms or molecules, when adsorbed on surfaces, are sometimes far more reactive than when in the solid or liquid state or even in the gaseous state. This is due partly to the fact that they are more readily accessible for other molecules and partly also to the fact that the surface may facilitate the reaction by taking up the heat of the reaction. On the other hand the molecules or atoms are also often in a state more prone to reaction. The ionization energy of atoms, *e.g.*, alkali metal atoms, may be decreased considerably, as is known from electron emission phenomena (6). Solid cesium does not react with hydrogen (apart from the surface); in the adsorbed state cesium reacts spontaneously and vigorously with hydrogen (26).

Reactions between adsorbed atoms or molecules, or between adsorbed molecules and gaseous molecules, or molecules in the liquid state are the subjects of all reactions of heterogeneous catalysis. The discussion of catalytic reactions on surfaces does not fall in the scope of this article. It may only be remarked here that in many cases one of the partners seems to be bound by chemisorption and the other by van der Waals' adsorption forces (101).

### References

1. van Arkel, A. E., and de Boer, J. H., *La Valence et l'Electrostatique*. Librairie Alcan, Paris, 1936, Chapter XI.
2. Bangham, D. H., and Razouk, R. I., *Trans. Faraday Soc.*, **33**, 1463 (1937).
3. Bardeen, J., *Phys. Rev.*, **58**, 727 (1940).
4. Barrer, R. M., *Proc. Roy. Soc. London*, **A161**, 476 (1937).
5. Becker, J. A., *Trans. Faraday Soc.*, **28**, 148 (1932).
6. de Boer, J. H., *Electron Emission and Adsorption Phenomena*. Cambridge Univ.

- Press, London, 1935. (a) *Loc. cit.*, Chapter I. (b) *Loc. cit.*, Chapter II. (c) *Loc. cit.*, Chapter III. (d) *Loc. cit.*, Chapter VIII. (e) *Loc. cit.*, Chapter IX. (f) *Loc. cit.*, Chapter XIV.
- 7(a). de Boer, J. H., *Elektronenemission und Adsorptionserscheinungen*. Barth, Leipzig, 1937, Chapter VI (b) *Loc. cit.*, Chapter IX. (c) *Loc. cit.*, Chapter XII.
  8. de Boer, J. H., *Proc. Roy. Acad. Sci. Amsterdam*, **31**, 906 (1928); *Z. physik. Chem.*, **B13**, 134 (1931); **B14**, 149 (1931); **B15**, 300 (1932); **B17**, 161 (1932); **B20**, 11 (1933).
  9. de Boer, J. H., *Z. physik. Chem.*, **B15**, 300 (1932).
  10. de Boer, J. H., *Trans. Faraday Soc.*, **32**, 10 (1936).
  11. de Boer, J. H., *Rev. trav. chim.*, **59**, 826 (1940).
  12. de Boer, J. H., *ibid.*, **65**, 576 (1946).
  13. de Boer, J. H., *Proc. Roy. Acad. Sci. Amsterdam*, **39**, 1103 (1946).
  14. de Boer, J. H., and Broos, J., *Z. physik. Chem.*, **B14**, 457 (1931).
  15. de Boer, J. H., and Broos, J., *ibid.*, **B15**, 281 (1932).
  16. de Boer, J. H., and Bruining, H., *Physica*, **6**, 941 (1939).
  17. de Boer, J. H., and Custers, J. F. H., *Z. physik. Chem.*, **B21**, 208 (1933).
  18. de Boer, J. H., and Custers, J. F. H., *ibid.*, **B25**, 225 (1934).
  19. de Boer, J. H., and Custers, J. F. H., *ibid.*, **B25**, 238 (1934).
  20. de Boer, J. H., and Custers, J. F. H., *Physica*, **4**, 1017 (1937).
  21. de Boer, J. H., and Custers, J. F. H., in J. H. de Boer, *Z. Elektrochem.*, **1938**, 494.
  22. de Boer, J. H., Custers, J. F. H., and Dippel, C. J., *Physica*, **1**, 935 (1934).
  23. de Boer, J. H., and Dippel, C. J., *Z. physik. Chem.*, **B21**, 198 (1933).
  24. de Boer, J. H., and Dippel, C. J., *Rec. trav. chim.*, **52**, 214 (1933).
  25. de Boer, J. H., and Dippel, C. J., *Z. physik. Chem.*, **B21**, 278 (1933).
  26. de Boer, J. H., and Dippel, C. J., *Naturwissenschaften*, **21**, 204 (1933).
  27. de Boer, J. H., and Dippel, C. J., *Z. physik. Chem.*, **B25**, 399 (1934).
  28. de Boer, J. H., and Fast, J. D., *Rec. trav. chim.*, **55**, 459 (1936).
  29. de Boer, J. H., and Fast, J. D., *ibid.*, **58**, 984 (1939).
  30. de Boer, J. H., and Fast, J. D., *ibid.*, **59**, 161 (1940).
  31. de Boer, J. H., and Heller, G., *Physica*, **4**, 1045 (1937).
  32. de Boer, J. H., Houtman, J. P. W., and Waterman, H. J., *Proc. Roy. Acad. Sci. Amsterdam*, **50**, 1181 (1947).
  33. de Boer, J. H., and Kraak, H. H., *Rec. trav. chim.*, **55**, 941 (1936).
  34. de Boer, J. H., and Kraak, H. H., *ibid.*, **56**, 1103 (1937).
  35. de Boer, J. H., and Lehr, J. J., *Z. physik. Chem.*, **B22**, 423 (1933); **B24**, 98 (1934).
  36. de Boer, J. H., and Teves, M. C., *Z. Physik*, **65**, 489 (1930).
  37. de Boer, J. H., and Teves, M. C., *ibid.*, **73**, 192 (1931); **74**, 624 (1932).
  38. de Boer, J. H., and Teves, M. C., *ibid.*, **83**, 521 (1933).
  39. de Boer, J. H., and Veenemans, C. F., *Physica*, **1**, 753 (1934).
  40. de Boer, J. H., and Veenemans, C. F., *ibid.*, **1**, 953, 960 (1934).
  41. de Boer, J. H., and Veenemans, C. F., *ibid.*, **2**, 521, 529, 915 (1935).
  42. de Boer, J. H., and Verwey, E. J. W., *Rec. trav. chim.*, **55**, 443 (1936).
  43. de Boer, J. H., and Verwey, E. J. W., *Proc. Phys. Soc.*, **49**, Extra Part, 59 (1937).
  44. de Boer, J. H., and Zwikker, C., *Z. physik. Chem.*, **B3**, 407 (1929).
  45. Born, M., and Mayer, J. E., *Z. Physik*, **75**, 1 (1932).
  46. Bosworth, R. C. L., in D. D. Eley and E. K. Rideal, *Proc. Roy. Soc. London*, **A178**, 429 (1941).

47. Bruining, H., and de Boer, J. H., *Physica*, **4**, 473 (1937); Bruining, H., *ibid.*, **8**, 1161 (1941).
48. Brunauer, S., *The Adsorption of Gases and Vapors*, Oxford Univ. Press, London, 1943. (a) *Loc. cit.*, Chapter IV. (b) *Loc. cit.*, Chapter X. (c) *Loc. cit.*, p. 140. (d) *Loc. cit.*, p. 208. (e) *Loc. cit.*, pp. 231-235.
49. Brunauer, S., Emmett, P. H., and Teller, E., *J. Am. Chem. Soc.*, **60**, 309 (1938); Brunauer, S., Deming, L. S., Deming, W. E., and Teller, E., *ibid.*, **62**, 1723 (1940).
50. Brunauer, S., and Emmett, P. H., *ibid.*, **62**, 1732 (1940).
51. Cassie, A. B. D., *Trans. Faraday Soc.*, **41**, 450 (1945).
52. Cassie, A. B. D., *ibid.*, **43**, 615 (1947).
53. Coehn, A., *Z. Elektrochem.*, **35**, 676 (1929). Coehn, A., and Specht, W., *Z. Physik*, **62**, 1 (1930). Coehn, A., and Jürgens, H., *ibid.*, **71**, 179 (1931).
54. Coolidge, A. S., *J. Am. Chem. Soc.*, **49**, 703 (1927).
55. Coulson, C. A., *Nature*, **159**, 265 (1947).
56. Custers, J. F. H., and de Boer, J. H., *Physica*, **1**, 265 (1934).
57. Custers, J. F. H., and de Boer, J. H., *ibid.*, **3**, 407 (1936).
58. Custers, J. F. H., and de Boer, J. H., *ibid.*, **3**, 1021 (1936).
59. Craxford, S. R., *Trans. Faraday Soc.*, **42**, 576, 580 (1946).
60. Debye, P., *Physik. Z.*, **21**, 178 (1920).
61. Dew, W. A., and Taylor, H. S., *J. Chem. Phys.*, **31**, 277 (1927).
62. Dippel, C. J., and de Boer, J. H., *Rec. trav. chim.*, **57**, 277, 1087 (1938).
63. Eley, D. D., and Rideal, E. K., *Proc. Roy. Soc. London*, **A178**, 429 (1941).
64. Emmett, P. H., in E. O. Kraemer, ed., *Advances in Colloid Science*. Vol. I, Interscience, New York, 1942, p. 7.
65. Estermann, J., Frisch, R., and Stern, O., *Z. Physik*, **73**, 348 (1931).
66. Eucken, A., and Hunsmann, W., *Z. physik. Chem.*, **B44**, 163 (1939).
67. Fraser, R. G. J., *Molecular Rays*. Cambridge Univ. Press, London, 1931.
68. Gee, G., *Trans. Faraday Soc.*, **38**, 276 (1942).
69. Hellmann, H., *Einführung in die Quantenchemie*. Deuticke, Leipzig-Vienna, 1937, Chapter V.
70. Hilditch, T. P., *Nature*, **157**, 586 (1946).
71. Hückel, E., *Adsorption und Kapillarkondensation*. Akad. Verlagsgesellschaft Leipzig, 1928, p. 126.
72. Jaquet, E., *Fortschr. Chem., Physik u. physik. Chem.*, **B18**, (1925).
73. Johnson, M. C., *Proc. Roy. Soc. London*, **A123**, 603 (1929).
74. Johnson, M. C., and Vick, F. A., *ibid.*, **A157**, 308 (1935).
75. Juza, R., and Langbein, R., *Z. Elektrochem.*, **45**, 689 (1939).
76. Katz, J. R., *Proc. Roy. Acad. Sci. Amsterdam*, **15**, 449 (1912).
77. Keesom, W. H., *Physik. Z.*, **22**, 129 (1921).
78. Langmuir, I., *J. Am. Chem. Soc.*, **34**, 1310 (1912); **38**, 2270 (1916).
79. Langmuir, I., and Kingdon, K. H., *Proc. Roy. Soc. London*, **A107**, 61 (1925).
80. Langmuir, I., and Villars, D. S., *J. Am. Chem. Soc.*, **53**, 486 (1931).
81. Lenel, F. V., *Z. physik. Chem.*, **B23**, 379 (1933).
82. Lennard-Jones, J. E., *Trans. Faraday Soc.*, **28**, 333 (1932).
83. Lennard-Jones, J. E., *ibid.*, **28**, 341 (1932).
84. Lennard-Jones, J. E., and Dent, B. M., *ibid.*, **24**, 92 (1928).
85. London, F., *Z. Physik*, **63**, 245 (1930).

86. London, F., *Z. physik. Chem.*, **B11**, 246 (1931).
87. Lorenz, R., and Landé, A., *Z. anorg. allgem. Chem.*, **125**, 47 (1922).
88. Magnus, A., *Z. physik. Chem.*, **142**, 401 (1922).
89. Margenau, H., *Rev. Modern Physics*, **11**, 1 (1939).
90. Margenau, H., and Pollard, W. G., *Phys. Rev.*, **60**, 128 (1941).
91. Maxwell, L. R., Hendricks, S. B., and Mosley, V. M., *ibid.*, **52**, 968 (1937).
92. Mayer, J. E., and Maltbie, M., *Z. Physik*, **75**, 748 (1932).
93. Morton, T. H., *J. Soc. Dyers Colourists*, **62**, 272 (1946).
94. Orr, W. J. C., *Proc. Roy. Soc. London*, **A173**, 349 (1939).
95. Orr, W. J. C., *Trans. Faraday Soc.*, **35**, 1247 (1939).
96. Pauling, L., *Phys. Rev.*, **54**, 899 (1938); *J. Am. Chem. Soc.*, **69**, 542 (1947).
97. Pauling, L., Brockway, L. O., and Beach, J. Y., *J. Am. Chem. Soc.*, **57**, 2705 (1935); Pauling, L., and Brockway, L. O., *ibid.*, **59**, 1223 (1937).
98. Penney, W. G., *Trans. Faraday Soc.*, **31**, 734 (1935).
99. Polanyi, M., and London, F., *Naturwissenschaften*, **18**, 1099 (1930).
100. Rideal, E. K., *An Introduction to Surface Chemistry*. Cambridge Univ. Press, London, 1930, Chapter V.
101. Rideal, E. K., *Proc. Cambridge Phil. Soc.*, **35**, 130 (1938); *Nature*, **161**, 461 (1948).
102. Roberts, J. K., *Proc. Roy. Soc. London*, **A152**, 452 (1935); *Trans. Faraday Soc.*, **35**, 941 (1939).
103. Slater, J. C., and Kirkwood, J. G., *Phys. Rev.*, **37**, 682 (1931).
104. Smith, H. A., and Fuzek, J. F., *J. Am. Chem. Soc.*, **68**, 229 (1946).
105. Stout, J. W., and Giauque, W. F., *ibid.*, **60**, 393 (1938).
106. Stranski, I. N., *Z. physik. Chem.*, **136**, 259 (1928); *Z. Elektrochem.*, **36**, 25 (1930).
107. Stuart, H. A., *Molekülstruktur*. Springer, Berlin, 1934, Chapter II.
108. Taylor, H. S., *J. Am. Chem. Soc.*, **53**, 578 (1931).
109. Taylor, J. B., and Langmuir, I., *Phys. Rev.*, **44**, 423 (1933).
110. Taylor, J. B., and Langmuir, I., *ibid.*, **44**, 433 (1933). See also J. H. de Boer and C. F. Veenemans, ref. (40).
111. Titoff, A., *Z. physik. Chem.*, **74**, 641 (1910). See also Hückel, E., *Adsorption und Kapillarkondensation*, Akad. Verlagsgesellschaft, Leipzig, 1928, pp. 22-35.
112. Twigg, G. H., *Trans. Faraday Soc.*, **42**, 657 (1946).
113. Twigg, G. H., and Rideal, E. K., *ibid.*, **36**, 533 (1940).
114. Vand, V., and de Boer, J. H., *Proc. Roy. Acad. Sci. Amsterdam*, **50**, 991 (1947).
115. Verwey, E. J. W., *Rev. trav. chim.*, **65**, 521 (1946).
116. Verwey, E. J. W., and de Boer, J. H., *ibid.*, **55**, 675 (1936).
117. Verwey, E. J. W., and de Boer, J. H., *ibid.*, **59**, 633 (1940).
118. Went, J. J., *Physica*, **8**, 233 (1941).
119. Wheland, G. W., *The Theory of Resonance*. Wiley, New York, 1945.
120. Wohl, K., *Z. physik. Chem.*, **B14**, 36 (1931); *B (Bodenstein-Festband)*, 807 (1931).

# SURFACE CHEMISTRY AND COLLOIDS

A. E. ALEXANDER

*The University, Cambridge, England*

---

I. Introduction.....	67
II. Principal Experimental Techniques.....	68
III. Applications of Surface Chemistry to Problems in Colloidal Systems.....	70
1. Proteins.....	71
Molecular Weights from Monolayer Measurements.....	71
Protein Monolayers at Air-Water and Oil-Water Inter- faces.....	73
Adsorbed Films of Proteins.....	75
Hydrogen Bonding in Proteins and Protein Monolayers.....	76
2. Polymers.....	78
3. Foams and Emulsions.....	80
Kinetics of Adsorption at Air-Water and Oil-Water In- terfaces.....	80
Desorption from Interfaces.....	82
Structure of the Stabilizing Film in Foams and Emulsions.....	83
Reactions in Emulsion Systems.....	89
4. Pastes.....	89
5. Biological Problems.....	91
Biological Activity of Homologous Series.....	91
Mechanism of Fat Absorption.....	91
Anthelmintic Activity of Hexylresorcinol in the Presence of Soaps.....	92
Bactericidal Activity of Soap-Phenol Mixtures.....	94
References.....	95

---

## I. Introduction

Surface chemistry, or surface physical chemistry as it might more appropriately be termed, is concerned with the study of interfaces and interfacial phenomena, generally with interfaces of macroscopic area. Although the importance of the interface in colloidal systems had long been recognized, as for example by Graham, nevertheless "surface chemistry" as now understood is a comparatively new field; its basis being laid only some



three decades ago by the work of Hardy, Langmuir, Harkins, and others. Its subsequent development was both rapid and considerable, and an extensive literature now appertains to it. A great deal of this accumulated data upon interfaces is naturally very valuable in attempts to analyze the behavior of macroscopic colloidal systems, although remarkably few investigations can be said to have been specifically directed toward this end. The present article attempts to survey and to summarize certain aspects of the study of the air-water, oil-water, and solid-liquid interfaces, these interfaces being of particular relevance in such typical colloidal systems as foams, emulsions, proteins, suspensions, pastes, as well as bacteria and other biological systems.

For an adequate appreciation of the experimental findings some outline of the principal techniques, particularly those of more recent development, is essential. This is given in Section II, which may be omitted by those already moderately conversant with the practical aspects.

## II. Principal Experimental Techniques

The study of insoluble monolayers at an air-water interface undoubtedly forms the basis of much of our present knowledge of surface phenomena. The film-forming substance is usually spread from petroleum ether or benzene solution, using a micrometer syringe to measure the volume and hence the number of molecules placed on the surface.

The earliest, and still the principal, measured quantity of the monolayer is the lowering of surface tension, often termed the "surface pressure" or "force,"  $\Pi$ , where  $\Pi = \gamma(\text{water}) - \gamma(\text{film})$ , which is determined as a function of the molecular area,  $A$ . ( $A$  is usually expressed in square angstroms per molecule or as square meters per milligram.) The  $\Pi$   $A$  curve is usually built up point by point, although for certain purposes, particularly for examining phase changes and stability ranges in condensed monolayers, automatic recording is preferable. (Apparatus for automatic recording have been described by Dervichian (25), Stenhagen *et al.* (15), and Alexander (10).) The increasing interest in insoluble monolayers has led to the development of numerous pressure-measuring devices to replace the commonly employed torsion balance (see, for example, Puddington (45) and Stenhagen (55).) A simple apparatus recently devised by the author makes accurate determination of  $\Pi$  *versus*  $A$  curves readily accessible. In this method the pressure due to the monolayer displaces the float to a small extent ( $> 1$  mm.), and this movement is then amplified optically by means of a long optical path (about 2 m.). The principle readily lends itself to auto-

matic recording and in addition can be utilized for measuring surface or interfacial tension by means of the maximum pull on a ring or frame (9).

The "surface potential,"  $\Delta V$ , where  $\Delta V = V(\text{water}) - V(\text{film})$ , and the mechanical properties (viscosity, and in some condensed films, the elasticity), both measured as a function of  $A$ , are also of great importance. The former is the change in the air-water phase boundary potential produced by spreading the monolayer, and its chief importance arises from the fact that for a given molecular surface density,  $n$  ( $n = 1/A$ ),  $\Delta V$  is characteristically determined by the nature and orientation of the polar groups in the molecule. The principle of vectorial summation can be applied to the constituent linkages in a complex molecule, often with informative results concerning structure, orientation, and disposition of the polar groups.

The "surface viscosity,"  $\eta_s$ , where  $\eta_s = \eta(\text{film}) - \eta(\text{water})$ , is usually determined by one of two methods depending upon the nature of the film. With films of low viscosity, as encountered in the gaseous and expanded states ( $A > ca. 30$  sq. angstroms for simple paraffin-chain derivatives), the rate of flow through a narrow slit or canal is measured, whence  $\eta_s$  follows from the two-dimensional analog of Poiseuille's equation. For condensed films, where the viscosity may rise to quite high values, the damping of a suitable oscillating system, such as a disc or vane attached to a vertical torsion wire, is employed. The same apparatus can also be utilized to measure the shear rigidity modulus for those films exhibiting elasticity, such as proteins, polymers, and many substances when in the condensed state.

In the case of condensed monolayers only, it is usually possible to transfer them, by a simple dipping process, to a metal, glass, or other solid surface. By continued repetition, layers many molecules thick, termed "multilayers" or "built-up films," have been obtained. These multilayers have found a number of applications, particularly where very thin layers of accurately known thickness are required, as in the study of boundary lubrication, as absorbing screens in radioactive work, and for measuring the thickness of thin films such as red-cell "ghosts." In addition they are of interest owing to their high degree of orientation, which can be turned to good account as a means of inducing crystallization in intractable long-chain compounds and polymers.

The study of the air-water interface is clearly very pertinent to foams and similarly the oil-water interface is directly related to emulsion and biological systems. Despite its great intrinsic interest it is only comparatively recently that insoluble monolayers have been quantitatively studied at oil-water interfaces and the relevant data are therefore rather meager. The technique found most suitable employs the ring method to follow the

changes in interfacial tension (and hence  $\Pi$ ), the film-forming material, in a suitable solvent, being spread at the interface from the usual micrometer syringe. In contrast to the ordinary film balance method the area per molecule is decreased by injecting further amounts of spreading solution. Accurate  $\Pi$  versus  $A$  curves for a number of phospholipides such as lecithin, lysolecithin, and cephalin, and for some synthetic soaps, proteins, and polymers, are on record, and in addition some preliminary results of "interfacial potentials" ( $\Delta V$ ) and interfacial viscosities and rigidities.

Recent interest in *adsorbed* films at mobile interfaces has been largely concerned with the kinetics of adsorption and desorption. The standard techniques for boundary tension, such as capillary rise, pendant drop, hanging plate, and ring method, usually suffice for following slow changes; for rapid adsorptions the oscillating jet technique, recently developed and extended to oil-water interfaces by Addison (2), and a method utilizing surface potentials (3,4) appear to be the most suitable.

The solid-liquid interface is much less amenable to quantitative study than either the air-water or oil-water, for in addition to the formidable difficulties involved in preparing and maintaining clean surfaces there is also the problem of determining the true surface area. In the latter connection mention may be made of a simple method recently developed for fine powders, which utilizes long-chain polar compounds (*e.g.*,  $C_{16}H_{33}OH$ ) as adsorbates (35). The long-chain compound is dissolved in an organic solvent such as benzene and its concentration before and after adding the powder determined by spreading an aliquot as a monolayer on a film balance. The adsorption isotherm and the saturation uptake, giving the specific surface, are then deduced in the usual way, assuming a value of 20 square angstroms per long-chain molecule at the saturation limit. Equilibrium appears to be rapidly attained and the method seems a convenient one for speed and accuracy (see also (28,52)). For further discussion of the experimental techniques, see (1,7,8,49), where detailed references will also be found.

### III. Applications of Surface Chemistry to Problems in Colloidal Systems

As previously indicated the questions that will now be considered are certain aspects of such typical colloidal systems as proteins, polymers, foams, emulsions, pastes, and bacteria. Where, as in some cases, the literature is rather extensive, only a few key references or summarizing articles will be given.

### 1. *Proteins*

In addition to their obvious biological importance, proteins have marked stabilizing powers for foams and emulsions (see section on Foams and Emulsions below).

Although frequently very soluble in water (being typical hydrophilic colloids) many proteins can nevertheless be spread quantitatively as homogeneous monolayers at both air-water and oil-water interfaces. The best spreading medium so far devised appears to be 60% propyl (or isopropyl) alcohol with 0.5 *M* sodium acetate (54), for not only does this appear not to denature many proteins but it has the additional advantage of dissolving many lipides, so that mixed lipid-protein monolayers can be prepared. By use of this spreading medium many of the complications previously associated with protein monolayers are overcome; for example, the degree of spreading obtained no longer depends upon the time factor, pH, or salt concentration.

Protein monolayers have received a good deal of attention in the past, in the hopes of throwing some light upon the structure of the native protein molecule as well as upon the formation and structure of protein membranes.

#### *Molecular Weights from Monolayer Measurements*

Before considering the above points, however, some reference may be made to an interesting suggested use of protein monolayers—namely, for molecular weight determination. This involves measuring the  $\Pi$  *versus*  $A$  curve in the gaseous state, that is at very low film pressures ( $< 1$  dyne/cm.), and extrapolating to zero pressure where it is assumed that the ideal gas equation:

$$\Pi A = nRT$$

is applicable. As would be imagined the technique is not simple owing to the minute pressures involved and consequent troubles due to contamination.

Guastalla (30), who first developed this method, uses various modifications of the film balance principle, and extrapolates  $C/\Pi$  against  $C$  to zero  $C$ , where  $C$  is the surface concentration of protein in milligrams per square meter. Bull (17), using a Wilhelmy plate method over the range 0.1 to 1.0 dyne per centimeter, plots  $\Pi A$  against  $\Pi$  and extrapolates to zero  $\Pi$ . From the extrapolated value of  $\Pi A$ , molecular weights are then calculated from the relation:

$$\Pi A = nRT = (W/M)RT$$

where  $R$  is the gas constant ( $8.3 \times 10^7$  ergs/degree/mole),  $n$  the number of moles,  $A$  the area of the film in square centimeters,  $W$  the weight of the film in grams, and  $M$  the molecular weight.

The data of Table I summarize the results so far obtained by this technique.

TABLE I  
Molecular Weight of Proteins in Monolayers

Protein	Substrate	Molecular Weight	Ref. No.
Egg albumin.....	0.01 <i>N</i> HCl	40,000	(30)
Egg albumin.....	35% (NH <sub>4</sub> ) <sub>2</sub> SO <sub>4</sub>	44,000	(19)
Gliadin.....	0.01 <i>N</i> HCl	27,000	(30)
Hemoglobin.....	0.01 <i>N</i> HCl	12,000	(30)
$\beta$ -Lactoglobulin.....	20% (NH <sub>4</sub> ) <sub>2</sub> SO <sub>4</sub>	17,100	(17)
$\beta$ -Lactoglobulin.....	20% (NH <sub>4</sub> ) <sub>2</sub> SO <sub>4</sub> + 2.5 $\times 10^{-4}$ <i>M</i> CuSO <sub>4</sub>	34,300	(17)
Zein.....	20% (NH <sub>4</sub> ) <sub>2</sub> SO <sub>4</sub>	20,100	(19)

It will be observed that in some cases (*e.g.*, egg albumin), the film molecular weight agrees closely with the accepted value for this protein in solution (as obtained by osmotic pressure and ultracentrifuge for example), whereas in others it suggests that spreading the protein molecule has brought about splitting into a number of fragments (*e.g.*, 5 or 6 in the case of hemoglobin). (The behavior of hemoglobin at the air-water interface is to be contrasted with that at an oil-water interface, as discussed below.)

In addition to the experimental difficulties already mentioned there are also problems connected with the equation of state that is assumed, and with the extrapolation procedure. Un-ionized substances will presumably obey the equation of state:

$$\Pi(A - A_0) = xRT$$

and in some systems such as simple linear polymers  $x$  may reasonably be assumed to be unity, but with ionized substances such as proteins, and with polymers containing long side chains, this may be far from the truth. If, however, these points can be cleared up the method will undoubtedly be of considerable value for substances that can be spread as homogeneous monolayers, owing to the comparative simplicity of the apparatus and the speed of measurement.

*Protein Monolayers at Air-Water and Oil-Water Interfaces*

Considering now protein monolayers at an air-water interface under more usual film pressures (about 1–30 dynes/cm.), it is rather striking how proteins differing widely in molecular size and composition nevertheless give remarkably similar  $\Pi$  versus  $A$  curves. Other notable features are the ready formation of elastic gel films and the ease of compression to areas which appear much too small for a close-packed monolayer. (The monolayers are often reversible down to approximately 10 square angstroms per

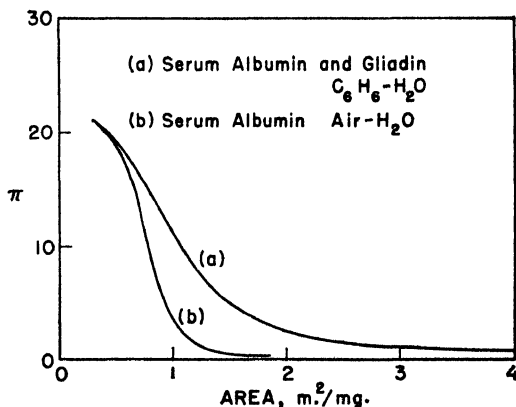


Fig. 1.  $\Pi$  vs.  $A$  curves for serum albumin and gliadin at benzene-water interface, and for serum albumin at air-water interface ( $\Pi$  in dynes/cm.) (12a). Aqueous substrate pH 7.4 (universal buffer) + 0.1  $M$  NaCl.

amino acid residue, as compared with a calculated minimum area of approximately 30 square angstroms.) A typical  $\Pi$  versus  $A$  curve is shown in Figure 1, the pressure rising rapidly at an area of about 1  $\text{m}^2/\text{mg}.$  where the molecules are believed to come into contact, and the previously liquid film "gelling" at somewhat smaller areas. If compressed to high pressures the monolayer collapses to a visible thread, which shows no tendency to re-expand when the pressure is removed. Despite their similarities in  $\Pi$  versus  $A$  curves, different proteins are, however, often clearly differentiated by their mechanical properties (viscosity and elasticity), and by the hysteresis phenomena which these films invariably manifest.

The spreading of a protein at an air-water interface appears to be accompanied by the complete loss of solubility and in general of enzymic and specific immunological reactions, indicating very radical and irrevers-

ible changes in structure. (The change is therefore frequently referred to as "surface denaturation.") In the case of solubility some workers have reported some reversal at high pressures, but this appears to be due to some unspread material and is not observed when spreading is known to be complete.

A number of studies of purified crystalline enzymes have been reported. For example, Langmuir and Schaefer spread urease and pepsin as monolayers, deposited these on metal plates, and then tested for enzymic activity. In their first experiments some activity was observed, but this was later (36) traced to some unspread protein incorporated in the monolayer. Where other enzymes have been deposited after spreading, as with catalase (32,36) and saccharase (53), varying degrees of loss of activity have been reported, but since in these cases the film thicknesses are all very much greater than the value of approximately 10 angstroms expected for a fully spread monolayer, it seems that the proteins were only partially spread. Further work with greater precautions to ensure complete spreading seems very desirable.

The effect of spreading an antigen or an antibody at the air-water interface upon the specific immunological reaction has also been examined in a few cases and with very similar conclusions. Thus Danielli, Danielli, and Marrack (23) were unable to detect any sign of reaction (using surface pressures and surface potentials for this purpose) in the two systems studied, namely, with horse-serum globulin as monolayer and rabbit antiserum in the subsolution, and with pneumococcus (type II) antibody as monolayer and specific polysaccharide in the subsolution (see also 48).

Despite the great interest that protein monolayers have evoked in the past, early speculations concerning their molecular structure were not very conclusive. The chief reasons were undoubtedly the lack of knowledge of how the linear polypeptide chains would behave at interfaces, and of the bonding between the principal polar groups present, particularly between  $\text{>C=O}$  and  $\text{H-N<}$  in the main chain, and those such as  $\text{—COO}^-$  and  $\text{NH}_3^+$ — in the side chains. Recently some information on both these questions has become available, from the study of synthetic linear polymers on the one hand (see section on Polymers) and from monolayers of long-chain amides, ureas, etc. on the other (see below).

The very radical changes referred to above, and termed "surface denaturation," are believed to arise from the polypeptide chains, originally coiled or folded up as they must be in the native corpuscular proteins, being unrolled and reoriented under the action of the surface forces. This

leads to the hydrophobic side chains (*e.g.*,  $-\text{CH}_2\text{C}_6\text{H}_5$ ,  $-\text{CH}_3$ , etc.) and the hydrophilic ones (*e.g.*,  $-\text{CH}_2\text{COOH}$ ,  $-\text{C}_6\text{H}_5\text{OH}$ ) being respectively oriented away from and toward the aqueous phase. At areas below the cohering point the evidence from long-chain amides, etc. suggests that the polypeptide chains are largely associated through the keto-imido groups by intermolecular hydrogen bonding.

Artificial lipide-protein films, although not so far extensively studied, are of considerable interest. One of gliadin and cholesterol is rather striking in that the gel film formed at low pressures liquefies sharply at pressures above approximately 20 dynes/cm., the process being reversible (51). The interaction between ionized soaps and proteins, which has been much studied recently in the bulk phase, can also be detected in monolayers. Bull (18), for example, has presented evidence of complex formation between sodium dodecyl sulfate and proteins such as  $\beta$ -lactoglobulin spread on 35%  $(\text{NH}_4)_2\text{SO}_4$  solution (see also (19,40).)

In comparison with air-water monolayers, little has been done upon protein monolayers at oil-water interfaces. As Figure 1 clearly shows, the films are much more expanded at low pressures, due to the oil molecules effectively eliminating the van der Waals attractive forces between the non-polar side chains. At high film pressures the two *II versus A* curves come into coincidence, showing that the oil phase is ultimately squeezed out entirely from the interface, a point of importance in connection with the structure of emulsion systems. (For further accounts see (19,40).)

### *Adsorbed Films of Proteins*

Soluble proteins appear to adsorb spontaneously at most interfaces, and it is by virtue of this adsorption that they can act as stabilizers for foams and emulsions, an aspect considered in more detail in Section 3 below. Their adsorption upon solid surfaces has been examined in a number of instances by using techniques developed in the study of multilayers. Thus a multilayer of barium stearate "conditioned" by thorium or aluminum salts (which presumably coats the outer surface with a thin layer of the hydrous oxide), dipped successively into solutions of diphtheria toxin and antitoxin, deposits alternate layers. Very similar observations have been made with other antigen-antibody pairs. For example, conditioned metal slides will adsorb antibodies against types I, II, or III pneumococci, giving an increment in thickness of about 50 angstroms, and then after treatment with homologous pneumococci polysaccharide will again adsorb a similar thickness of antibody (44). (An increment of 50 angstroms shows



that the antibody molecule can have undergone little unrolling during adsorption, for a fully spread protein monolayer would give, at most, a value of 10–15 angstroms.)

With the system catalase–anticatalase, the compound formed by alternate deposition shows only slightly lower activity than adsorbed catalase alone, and is about one-fifth to one-tenth less active than catalase in solution. The thickness of the first layer of catalase deposited was found to be approximately 53 angstroms, for the following anticatalase layer about 56 angstroms, indicating adsorption in the globular form in both cases (see also (19,40,48)).

### *Hydrogen Bonding in Proteins and Protein Monolayers*

The extent to which the protein molecule is stabilized by association between its polar groups, in particular by hydrogen bonding between the keto-imido groups, leading to  $\diagup\text{C}=\text{O}\cdots\text{H}-\text{N}\diagdown$ , has been the subject of much discussion. It has also been suggested that this linkage is of great importance in protein monolayers. Simple organic molecules containing the  $-\text{CONH}-$  group (e.g., amides and ureas) are well known to be associated in organic solvents, but in the presence of an aqueous environment, itself capable of forming hydrogen bonds with both  $\diagup\text{C}=\text{O}$  and  $\diagup\text{N}-\text{H}$  groups, as with the proteins in solution, determination of the extent of association by standard physical methods, such as distribution and infrared spectroscopy, is extremely difficult. Surface chemical techniques are, however, particularly suited to such problems, and in this case a comparison can be made between insoluble monolayers of long paraffin-chain acetamides, amides, ureas, etc., and closely similar compounds where intermolecular hydrogen bonding is impossible, such as the long-chain esters and ketones.

If we confine our attention to the acetamides  $\text{RNHCOCH}_3$ , the acetates  $\text{ROCOCH}_3$ , and the methyl ketones  $\text{RCH}_2\text{COCH}_3$ , which differ only in that the  $-\text{NH}-$  group in the first molecule has been replaced by  $-\text{O}-$  and  $-\text{CH}_2-$ , respectively, some very striking differences are observed, particularly in the condensed films (6). Acetates and methyl ketones show marked similarities: in the condensed state they both give fluid films showing little or no hysteresis and no evidence of any head-group reorientation. On the other hand, condensed monolayers of the long-chain acetamides exist in two forms, of which one, the high-area form, resembles closely in all respects the acetates and methyl ketones (see Fig. 2, configuration II). The

other, the low-area form, is an extremely rigid solid film of quite remarkable stability and showing considerable hysteresis, and the surface potential indicates that the head-group has been reoriented as shown in Figure 2, con-

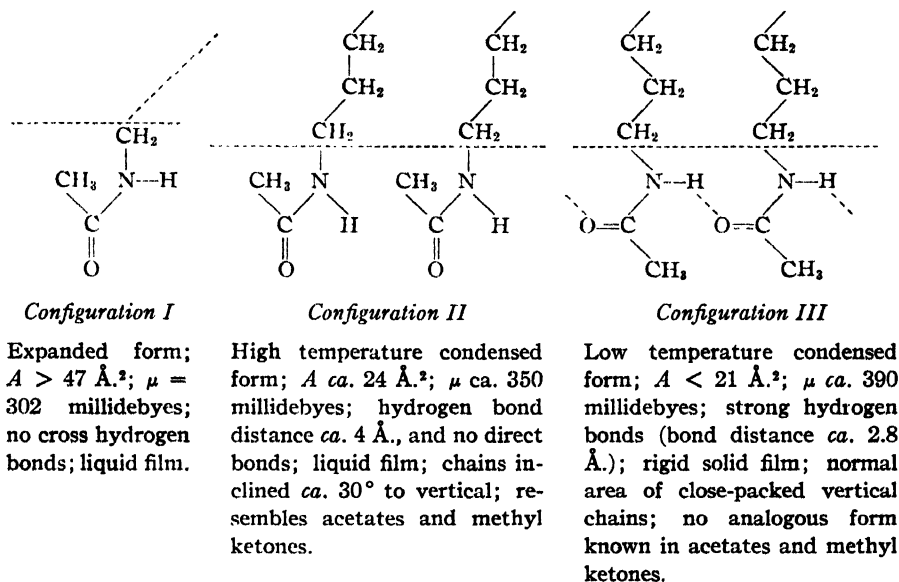


Fig. 2. Configurations of acetamide monolayers in the expanded state and in the two condensed forms (6). (The water surface is to be taken as parallel to the horizontal dotted line.)

figuration III. This latter configuration, which does not exist in the acetates and methyl ketones, appears to be possible because it is stabilized by intermolecular hydrogen bonding, the N to O distance between the  $\text{>CO}$  and  $\text{>NH}$  groups being about  $2.8$  angstroms, close to the x-ray value for related compounds in the crystal. Very similar conclusions have been reached with monolayers of other compounds, such as the long-chain ureas, amides, and acetanilides. The influence of the pH upon the strength of the hydrogen bonding has been demonstrated and that of other reagents such as urea is being examined.

The long-chain  $\alpha$ -amino acids are also of interest since they are believed to exist in the zwitterionic form e.g.,  $\text{C}_{16}\text{H}_{33}\text{CH}(\text{NH}_3^+)(\text{COO}^-)$ , and are

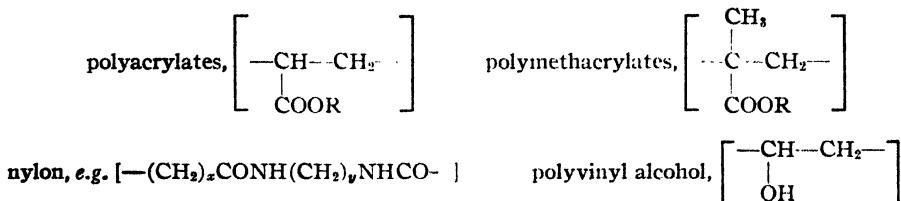
thus useful for assessing the strength of the "salt linkages" in proteins. They also form unusual monolayers, resembling the acetamides in their marked hysteresis, but being distinctive in forming elastic "gel" films at comparatively large areas, even up to approximately 35 square angstroms. The gelation power disappears if the  $\text{—NH}_2$  group is replaced by  $\text{—Br}$ , as in the  $\alpha$ -bromo acids.

Intermolecular hydrogen bonding between  $\text{>C=O}$  and  $\text{H—N<}$  groups in condensed monolayers, despite the competitive action of the water molecules, thus appears to be established, and it is certainly one factor giving rise to hysteresis in protein monolayers. It also seems reasonable to conclude that such a bonding between polar groups of different molecules will be of considerable value for stabilizing the native protein molecule.

## 2. Polymers

As previously mentioned the study of monolayers of synthetic linear polymers has helped to clarify the structure of protein monolayers. This work is also interesting in its relation to the structure of polymers and to their behavior in bulk.

A recent publication (21) deals with a number of linear polymers of known and varied structures, such as:



Here the formula given inside the square bracket denotes the repeating unit of the polymer and R a side chain—methyl, ethyl, etc.

In contrast with the behavior at extremely low pressures, the molecular weight (or chain length) of the polymer has little influence upon the monolayer behavior over the usual range of film pressures (*i.e.*  $> ca. 1$  dyne/cm.). Variation in the side-chain grouping (R), however, brings about considerable changes. Some typical  $\Pi$  *versus*  $A$  curves, shown in Figures 3a and b, are clearly not dissimilar to those given by the proteins (*e.g.*, Fig. 1), which they further resemble in giving gel films, in their marked hysteresis, and in the small areas (often  $< 10$  square angstroms per residue), to which they can be reversibly compressed. Since any marked association between the polar groups in ester films is improbable it follows that one factor in-

volved in the hysteresis phenomena of protein monolayers arises from the presence of the long polypeptide chains on the surface. The very low areas observed in the high pressure region of polymer films arise from the expulsion of segments of the long chains, leading to the formation of a thickened layer or overfilm. Although proteins in general possess more hydrophilic groups than these ester polymers, nevertheless a similar behavior can be inferred for protein monolayers, rather than a looping of the chains beneath the surface as previously held by some workers.

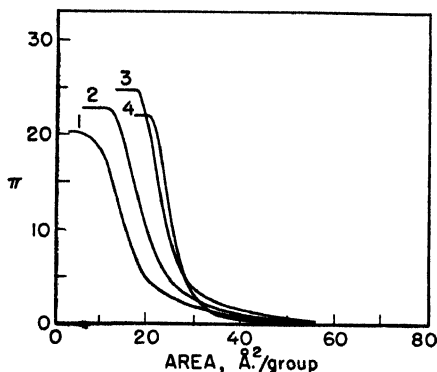


Fig. 3a.  $\Pi$  vs.  $A$  curves for polyacrylates ( $\Pi$  in dynes/cm.) (21): (1) polymethyl acrylate; (2) polyethyl acrylate; (3) polyisopropyl acrylate; (4) poly-*n*-butyl acrylate.

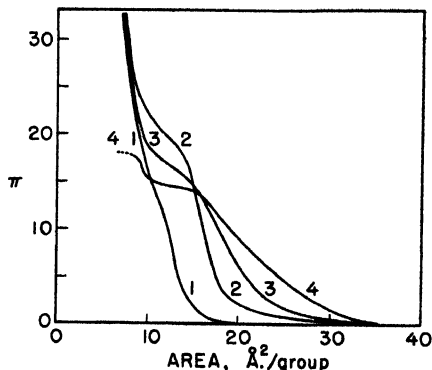


Fig. 3b.  $\Pi$  vs.  $A$  curves for polymethacrylates (21): (1) polymethyl methacrylate; (2) polyethyl methacrylate; (3) poly-*n*-propyl methacrylate; (4) poly-*n*-butyl methacrylate.\*

An alteration in the side chain ( $R$ ) is reflected not only in the  $\Pi$  versus  $A$  curves, as Figures 3a and b show, but also in the viscosity and elasticity of the monolayer. The latter changes often, although not invariably, run parallel to changes in the bulk properties of the polymer. Thus, increasing the length of the side chain (*e.g.*, from methyl to propyl) causes a rise in the gelation pressure, whereas very long or ring side chains (*e.g.*, octadecyl and cyclohexyl) have the converse effect: in the solid the first change renders the plastic softer and more rubberlike (internal plasticization) and the second more rigid, owing to the increased cohesive forces. Similarly the differences in bulk properties between the acrylate and methacrylate series show up clearly, the latter forming much more coherent monolayers in line with their greater bulk rigidity.

\* All readings taken slowly to avoid hysteresis.

One interesting use of the multilayer technique has come in connection with polymers. With the so-called "amorphous" polymers (*e.g.*, the acrylates), thin films obtained by the usual methods such as evaporation from solution give, when examined by electron diffraction, very broad diffuse rings indicating a truly amorphous molecular arrangement. On the other hand, films formed by deposition from monolayers exhibit much sharpened diffraction rings, showing that they possess a much higher degree of order (20).

### 3. Foams and Emulsions

These two types of colloidal systems, despite their importance and long-known existence, are still by no means thoroughly understood. The principal problems arising are as follows: (1) the adsorption of the stabilizing agent during the dispersion process, (2) the structure of the adsorbed stabilizing film and its importance in relation to the gross stability of the system, and (3) the desorption of stabilizing agent as the colloidal particles recombine. As might be anticipated the information arising from surface chemistry is of particularly direct application to the problems arising in these systems.

#### *Kinetics of Adsorption at Air-Water and Oil-Water Interfaces*

The question of *rate* of adsorption of capillary-active substances, which can readily be followed by measuring the boundary tension as a function of time, has been examined in some detail at the air-water interface. Comparison of the observed rate with that calculated either from the approximate or the more recently developed accurate theory (59) of diffusion shows considerable discrepancies (see also (47).) In the case of soaps and dyes, for example, provided the concentration is too low for micelles to be present, the time required for equilibration may be hours or days instead of the calculated fractions of a second, the ratio of calculated to observed rate often being  $10^6$  or more.

Most of the systems used in the early studies of this "surface aging" phenomenon, as it has been termed, were aqueous solutions of ionized substances such as natural and synthetic soaps, and dyes, and the hindrance to diffusion was generally ascribed to an electrostatic potential barrier at the surface, due to the adsorbed organic ions (26). On this theory the rate of adsorption would be reduced by the factor  $e^{Q\psi/kT}$ , where  $Q$  is the charge on the organic ion and  $\psi$  the electrostatic potential barrier (34). That an electrostatic barrier does exist in the case of soap monolayers is shown by

the hydrolysis of long-chain esters with strong sodium hydroxide (11), where the reaction goes as shown in Figure 4. The velocity constant falls progressively as reaction proceeds, at 50% reaction being about one-quarter of the initial rate, and at 100% reaction about one-tenth (an extrapolated value) (see also (24).)

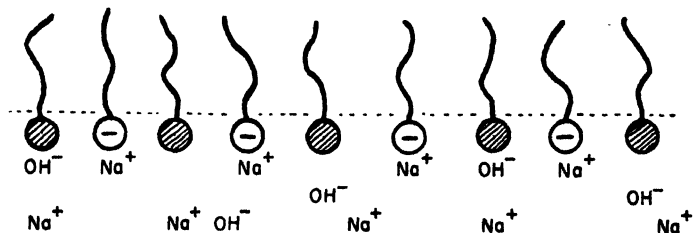


Fig. 4. Structure of a monolayer of long-chain ester after 50% hydrolysis with  $N$  NaOH. The soap ions in the film give rise to an electrostatic potential barrier for the diffusing  $\text{OH}^-$  ions.

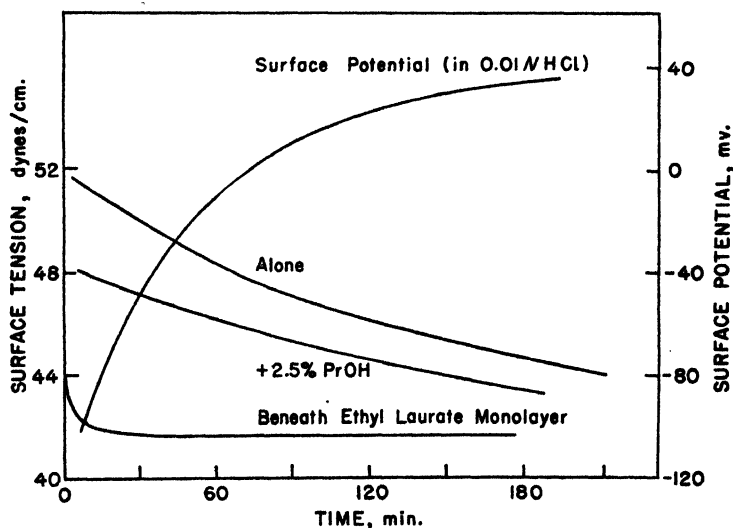


Fig. 5. Adsorption of hydrocinnamic acid (4 g./liter in 0.01  $N$  HCl) at the air-water interface (4).

The above results show that the electrostatic energy barrier is of insufficient magnitude to explain the whole discrepancy in adsorption rates, and the fact that the anomalies are by no means restricted to ionized compounds confirms that this type of barrier is certainly not the major factor

involved. Figure 5 shows the adsorption of hydrocinnamic acid ( $\text{C}_6\text{H}_5\text{-CH}_2\text{CH}_2\text{COOH}$ ) at pH 2 where the carboxyl group would be completely un-ionized. Both with ionized and un-ionized compounds the attainment of equilibrium is accelerated by other surface-active substances, whether freely soluble or as insoluble monolayers (see Fig. 5). Although in this case the additives by themselves are much less surface active than the hydrocinnamic acid, they nevertheless reduce the aging time enormously.

From such experiments as the above it would appear that the main factor in these slow adsorptions arises from a potential barrier of a different type: the steric hindrance that the hydrocarbon part of the molecule encounters when it endeavors to penetrate a comparatively close-packed monolayer (4). For the system shown in Figure 5 the area per molecule at 47 dynes/cm. is about 36 square angstroms, compared with approximately 25 square angstroms for close packing. This suggestion is further supported by the fact that the anomaly increases with chain length in homologous series, and is particularly pronounced in branched-chain compounds.

Anomalously slow adsorption of long-chain polar compounds may also occur from an oil phase to an aqueous interface, the ratio of calculated to observed rates being about  $10^8$  for 1% palmitic acid in hexane (58). In such systems the polar compound is usually aggregated in the oil phase (e.g., as dimers in the case of the fatty acids), whereas the entity present in the interface will certainly be the monomeric form. Adsorption of the aggregated units as such would probably occur at a negligible rate, since the long chains would effectively prevent the polar groups from coming into contact with the aqueous phase. The monomer would not suffer from this disadvantage, but on the other hand its concentration in nonpolar solvents is extremely low. The slow rate of adsorption may thus arise indirectly from the aggregation phenomenon, an explanation supported by the diminished anomaly in more polar solvents such as nitrobenzene where the association is reduced (12). In addition to this factor, it seems likely that in the higher concentrations, where the lowerings of interfacial tension are considerable, the same steric factor advanced above for aqueous systems would also be of importance.

### *Desorption from Interfaces*

Compared with the amount of work done upon adsorption, the question of the rates of desorption from interfaces has received little attention, particularly at the oil-water interface. The data available do, however, show that desorption may be an equally hindered process, even with not

particularly complex molecules such as hydrocinnamic acid. In some cases the process is so slow that if a film adsorbed at an air-water interface is compressed (as may be done very conveniently with a surface trough), the adsorbate actually separates out on the surface as a crystalline or liquid aggregate (5).

It is undoubtedly because of hindered desorption that many substances of quite detectable solubility can be studied as monolayers (*e.g.*, lauric acid at an air-water interface, and sodium cetyl sulfate at an oil-water interface). In addition this factor may be of considerable importance in delaying the breaking of foams and emulsions, since many common types of stabilizers would be expected to show the phenomenon to an extreme degree.

Some preliminary kinetics of desorption, using substances such as lauric acid spread as monolayers on a film balance, show that at constant pressure a unimolecular law is obeyed, as would be expected under these conditions (31).

### *Structure of the Stabilizing Film in Foams and Emulsions*

Let us now consider the final problem mentioned above—the information provided by surface studies upon the structure of the stabilizing film and its relation to the over-all stability. One particularly important question is the thickness of the stabilizing film, whether monomolecular or multimolecular.

In the case of water-soluble compounds (*e.g.*, soaps and detergents, lower fatty acids or alcohols) the amount of adsorption, if the adsorbed film is monomolecular, can readily be calculated assuming an equation of state deduced from the study of the homologous longer chain compounds, which form insoluble monolayers. For example, a reasonable equation of state for un-ionized compounds at an air-water interface would be:

$$\Pi(A - A_0) = xkT$$

and for an ionized soap at an oil-water interface:

$$\Pi(A - A_0) = C$$

where the symbols have the same significance as in earlier equations.  $A_0$ ,  $x$ , and  $C$  are known (or deduced) from experiments on insoluble monolayers, so that  $A$ , and hence the adsorption, can be determined as a function of  $\Pi$ , and therefore at any particular surface tension. Values of the adsorption have thus been worked out for the two compounds, hydrocinnamic acid



and lauryl sulfonic acid, under the conditions where their experimental adsorptions have been accurately determined by the microtome and other methods (38,39). The data given in Table II show that the observed and calculated adsorptions are in good agreement.

TABLE II

Solute	Adsorption, g./cm. <sup>2</sup>	
	Calculated	Observed
Hydrocinnamic acid.....	$8.3 \times 10^{-8}$	$7.7 \times 10^{-8}$
Lauryl sulfonic acid.....	$14.4 \times 10^{-8}$	$13.0-14.2 \times 10^{-8}$

The above results, typical of a number of systems, lead us to the conclusion that in foams, and by analogy also in emulsions of the oil-in-water type, stabilized by water-soluble soaps, the interfacial stabilizing film is no more than monomolecular in thickness. It also follows that this monolayer is in a highly compressed gaseous (and hence fluid) state, with a molecular area of about 30 square angstroms for straight paraffin-chain derivatives. The study of insoluble monolayers at oil-water interfaces shows that with stable oil-water emulsions (*i.e.* in systems in which the interfacial tension has been considerably reduced), the oil phase will be effectively displaced from the interface by the adsorbed monolayer of stabilizer. This can clearly be seen with the protein monolayer of Figure 1.

It would be anticipated from surface chemistry that stabilization in foams and emulsions would result, in addition to the question of rates of adsorption and desorption discussed above, from two principal factors: the reduction in surface energy of the system brought about by adsorption; and the mechanical properties (viscosity and elasticity) of the stabilizing film. On the whole these anticipations appear to be borne out in practice, although the experimental data are extremely scanty. Pankhurst (41), for example, has compared the foaming power and foam stability of a number of synthetic soaps with their lowerings of surface tension, and it is clear from his results that the surface tension factor is not the only one operative. Data on interfacial viscosity are very scanty, although the increasing foam stability with increasing chain length in an homologous series may well arise from this factor. Certain mixtures greatly increase foam stability, for example, lauryl alcohol with sodium laurate at pH 10 (37), due undoubtedly to "surface complex" formation as discussed in more detail below.

In the case of synthetic soaps, branched-chain compounds are fre-

quently much more efficacious emulsifiers than the straight-chain homologs, the interfacial tension sometimes being reduced to values as low as 0.1 dyne/cm. as compared with 3-5 dynes for the straight-chain compounds. Hartley (33) has suggested that the difference arises from the greater difficulty that the branched-chain compounds have in forming the micelle, since micelle formation sets a very effective limit to surface activity. This difference in packing between straight- and branched-chain compounds is also shown in studies of insoluble monolayers (56).

The close connection between the lowering of interfacial tension and emulsion stability is shown particularly well by systems stabilized by "interfacial complexes" formed between a water-soluble soap and organic compounds containing  $\text{—OH}$  or  $\text{—NH}_2$  groups (*e.g.*, cholesterol, cetyl alcohol, and long-chain amines), dissolved in the oil phase (50). These "complexes" were discovered when studying the effect of injecting a water-soluble soap, such as sodium cetyl sulfate, beneath various types of insoluble monolayers (51). With monolayers of long-chain alcohols or cholesterol, the soap penetrates very rapidly, as shown by the lowering of surface tension if the monolayer is held at constant area (as in Fig. 6), or by the increase in area if held at constant pressure. If, however, the  $\text{—OH}$  group is esterified, as in cholesterol acetate, or if the straight chain in cetyl alcohol is replaced by a kinked chain as in oleyl alcohol, then the penetration is enormously reduced (see Fig. 6), and with it the emulsifying power (see Fig. 7 and (50)). The stabilizing action thus seems to arise from a type of hydrogen bonding, requiring first, the presence of a dative hydrogen as in  $\text{—OH}$  or  $\text{—NH}_2$ , and, second, that this dative hydrogen can be brought sufficiently close to the organic ion, which is clearly much less easy if either long chain is kinked, as in the *cis*-unsaturated compounds (see Fig. 7).

With the heavy-metal or oil-soluble soaps (*e. g.*, magnesium oleate and zinc stearate), which form excellent stabilizers for the water-in-oil type of emulsion, the question of the nature of the stabilizing film can also be inferred from surface studies. Measurements of the equilibrium spreading pressures between monolayer and solid phase for these systems have recently been carried out by spreading fatty acids upon substrates containing the heavy-metal cation at suitable pH (3). The values so obtained, which are clearly the maximum surface pressures at equilibrium, were invariably quite small ( $>$  a few dynes per centimeter), and thus of a different order of magnitude from the water-soluble soaps. This shows quite definitely that stabilization by an adsorbed monolayer is quite out of the question in these systems (42). The spontaneous formation at an oil-water interface of visible rigid films or "skins" of the soap, formed when the aqueous phase

contains heavy-metal cations and the oil phase some fatty acid, indicates that stabilization in these water-in-oil emulsions stabilized by heavy-metal

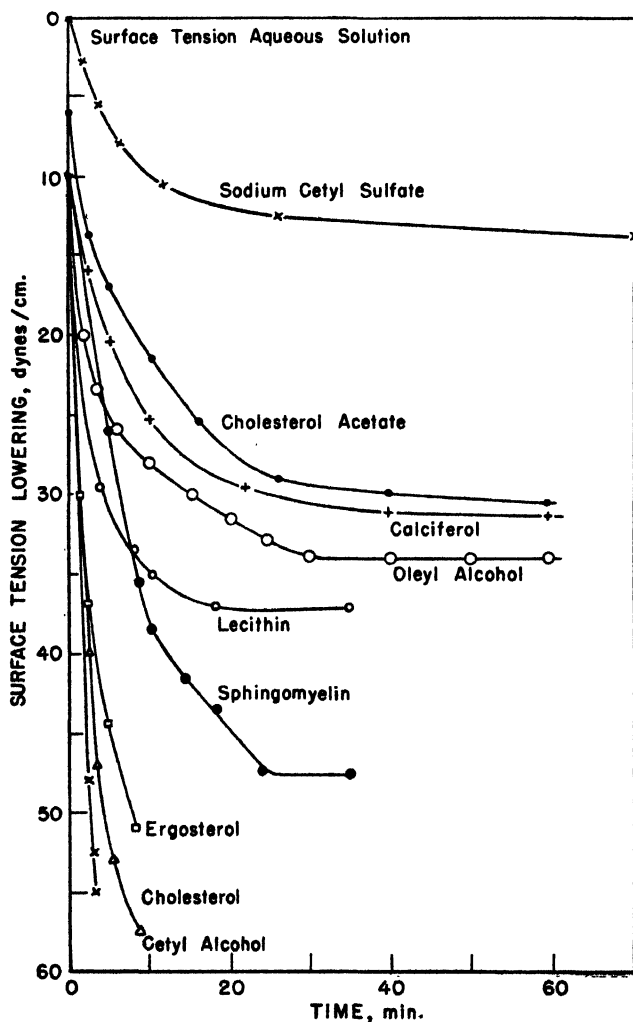


Fig. 6. Penetration of sodium cetyl sulfate ( $3.3 \times 10^{-4}\%$ ) into various monolayers at pH 7.2 and 10 dynes/cm. surface pressure (51).

soaps is due to a three-dimensional rather than a monolayer at the interface. The systems are thus analogous to emulsions stabilized by solid powders in

general. The above conclusion accords with that reached by Pink (43) from the study of benzene solutions of the pure heavy-metal soaps. He found that for such soaps to be efficient emulsifiers (water-in-oil), it was es-

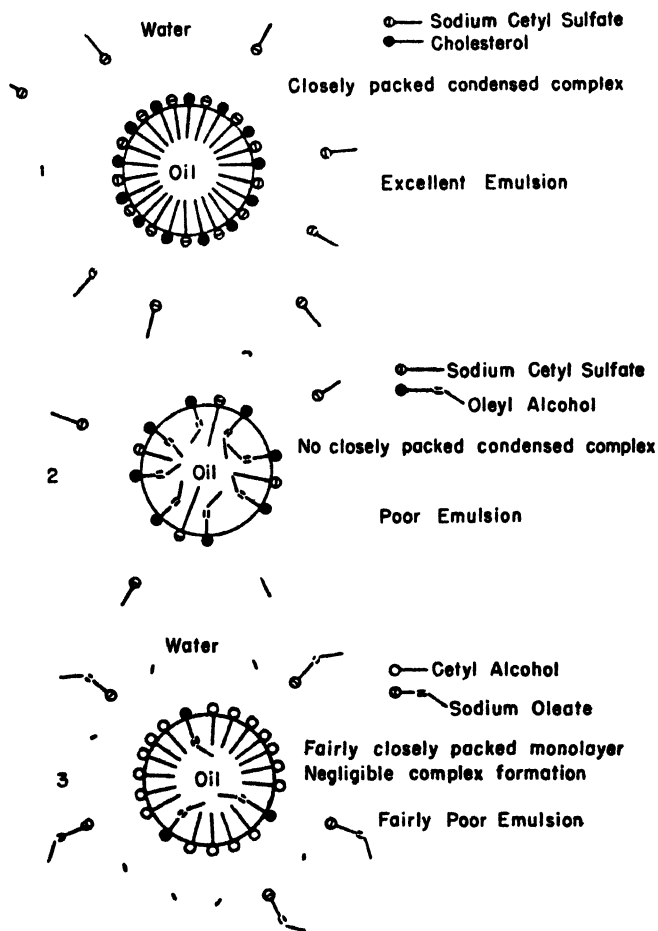


Fig. 7. Diagrammatic picture illustrating how the introduction of kinked chains into one constituent of the emulsifying complex reduces the interfacial packing and the emulsion stability (50).

sential for them to be precipitated at the interface, in the form of hydrated soap, by the action of the water.

Proteins, although frequently extremely soluble in water, are well known for their ability to impart great stability to both foams and emul-

sions (oil-in-water type), as in meringue and milk for example. This power is undoubtedly linked to the fact that a protein solution in contact with an air-water or an oil-water interface readily gives rise to a tough visible "skin" or membrane, a phenomenon first investigated by Ascherson over a century ago, and still very imperfectly understood. In the case of an air-water interface, this adsorption and "surface denaturation" continue until all the protein present has been removed as a coagulum practically devoid of surface activity. This phenomenon also forms the basis of the method for removing proteins from solution by bubbling air through, and also for the inversion of cream to butter by surface denaturing the protein in solution and in the stabilizing films.

Surface denaturation of proteins also occurs at oil-water interfaces, but the rate, and apparently also the extent, of the changes diminish with decreasing interfacial tension (22). Thus oils such as medicinal paraffin or benzene (interfacial tensions against water about 55 and 35 dynes/cm., respectively), show more marked effects than ones such as oleic acid or oleyl alcohol (interfacial tension about 7 dynes/cm.). Closely related is the adsorption of proteins upon charged emulsions stabilized by detergents, which appears to be reversible. It has been shown (27) that, if hemoglobin is desorbed (by changing the pH from below to above the isoelectric point and thus reversing its charge) from the surface of a fine negatively charged emulsion stabilized by sodium cetyl sulfate, the molecular weight is unaffected but the frictional ratio (from ultracentrifugal behavior) has increased from 1.16 to 1.33, indicating some, but by no means complete, unfolding of the molecule (see also (40)).

Some mention of the behavior and structure of protein monolayers at air-water and oil-water interfaces has been given earlier. Comparison of these *monolayers* with the films adsorbed (*i.e.*, formed spontaneously) from protein solutions suggests very strongly that proteins stabilize foams and emulsions by the formation of polymolecular films or "skins" rather than by a monolayer, these "skins" conferring mechanical protection owing to their elastic nature and high viscosity.

The occurrence of elasticity (a property characteristic of solid bodies) in adsorbed films is important in relation to the question of thermodynamic stability of foams and emulsions. *Monolayers* only exhibit elasticity when in the condensed state, and from the study of equilibrium spreading pressures of crystals it would appear that all *condensed* monolayers are *potentially* unstable with respect to their bulk phase. (In monolayer studies the rate of change-over is often too slow to cause any trouble.) Accordingly, if an *adsorbed* film exhibits elasticity (as with protein or saponin (60) solutions,

and with heavy-metal soaps formed by metathesis at an interface, as described above), it would seem probable that its structure is poly- rather than monomolecular, and that the system is not in thermodynamic equilibrium. (The inapplicability of thermodynamics to such systems as saponin solutions explains certain discrepancies observed in the experimental testing of the Gibbs adsorption isotherm.)

Mention may be made here of Hardy's technique for studying foam stability by measuring the lifetime of an air bubble liberated beneath an adsorbed or insoluble monolayer. By using insoluble monolayers the effect of such variables as molecular density, viscosity, and elasticity of the monolayer can be accurately examined without being complicated by adsorption and desorption processes. With simple paraffin-chain compounds appreciable stabilization is only obtained with coherent monolayers (in the expanded or condensed states), and the bubble stability decreases in the highly condensed state where such monolayers become unstable (57).

#### *Reactions in Emulsion Systems*

To conclude this section, one further use of surface techniques may be briefly mentioned—namely, for studying reactions in certain heterogeneous systems. For example, the alkaline hydrolysis of fats and long-chain esters shows very complicated kinetics, the reaction often appearing to be autocatalytic in nature, due to the emulsifying action of the soap formed tending to increase the total area of reacting interface. By spreading the ester as a monolayer upon an aqueous substrate containing sodium hydroxide, the velocity constant can be measured without this complication, and its dependence upon the molecular density and orientation of the monolayer, sodium hydroxide concentration, etc., readily found (8,46).

#### *4. Pastes*

With pastes, concentrated dispersions of finely divided solids in a liquid continuum, two properties of particular interest are the flow behavior and the sedimentation volume. It has long been known that small amounts of surface-active substances may modify these properties in a very striking manner. For example, the addition of a fatty acid or an aluminum soap to dispersions of polar solids (*e.g.*,  $\text{SiO}_2$ ,  $\text{TiO}_2$  and inorganic pigments) in oils increases the fluidity and decreases the sedimentation volume (*i.e.*, decreases the "oil absorption" as it is termed in paint technology). Water-soluble soaps act similarly with many aqueous dispersions such as clays and colloidal graphite.

The resistance to flow in these systems, with their high concentrations of disperse phase, arises chiefly from contact between the solid particles, and hence would be expected to depend a great deal upon the forces between them. Some recent work (35) has shed a good deal of light upon the influence of surface-active substances upon paste flow. Using finely powdered ionic crystals such as  $\text{NaNO}_3$  as adsorbents, and long-chain polar compounds in benzene or organic solution as adsorbates, the adsorption was measured by the film balance technique as described earlier. Some

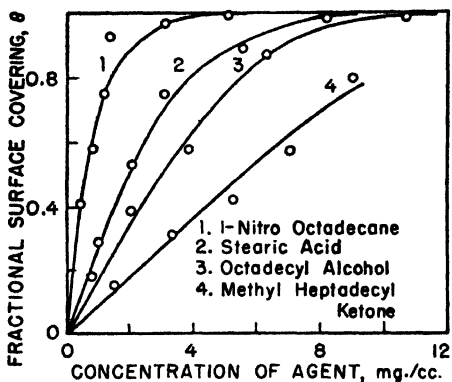


Fig. 8. Adsorption isotherms of various long-chain compounds upon sodium nitrate (35a).

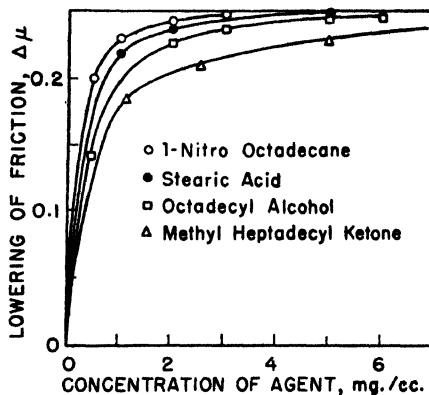


Fig. 9. Lowering of friction between  $\text{NaNO}_3$  crystals produced by various long-chain compounds (35a).

typical isotherms, reproduced in Figure 8, show that the adsorption decreases in the following order:  $-\text{NO}_2 > -\text{COOH} > -\text{OH} > >\text{C}=\text{O}$ . Parallel measurements of the coefficient of friction between large crystals showed that the friction was lowered in the same order (see Fig. 9). With increasing adsorption the ease of flow increases and the sedimentation volume decreases. Adsorption in these systems takes place with the polar groups of the adsorbate molecules oriented toward the polar surfaces of the crystal, and with the hydrocarbon chains extending into the organic liquid. This outer surface of hydrocarbon reduces the interaction between the polar faces of the crystal and leads to the observed changes in macroscopic properties (see also (16)). The initial amounts of adsorption are seen to exert a proportionately greater influence upon the friction, a not unexpected behavior in view of the long-chain structure of the adsorbates.

### 5. *Biological Problems*

It has often been stated that a thorough understanding of surface phenomena is absolutely vital in the detailed analysis of almost all biological phenomena. So far, however, the number of biological systems that have proved amenable to this approach is not considerable, although some advances can be recorded. Only a few of the more clear-cut examples can be discussed here.

#### *Biological Activity of Homologous Series*

One of the oldest, and still a very important contribution, was in connection with the activity of homologous series of paraffin-chain derivatives. As Traube first pointed out the narcotic activity of different alcohols varied with their power of lowering the surface tension of water, *i.e.*, with their adsorption at an air-water interface. A similar parallelism between biological and surface activity has been noted in other systems, such as the germicidal activity of phenyl alkyl acids, and of substituted resorcinols. Such results were interpreted on the reasonable theory that the biological response was determined by the amount of adsorption at the biological-aqueous interface, which was reasonably assumed to parallel that at the air-water interface. With the development of more detailed knowledge of surface behavior, it is now known that adsorption is a much more specific phenomenon, depending not only upon the chain length of the "drug," but also upon the chemical and physical nature of the adsorbing surface. Also the biological response will only run parallel to the adsorption if the slowest step involved is the diffusion from the adsorbing surface. Many of the apparent anomalies to Traube's generalization can be explained on this more detailed analysis.

#### *Mechanism of Fat Absorption*

It has been shown by Frazer and co-workers that, when a liquid fat is ingested, it emulsifies spontaneously in the intestine, and is subsequently absorbed through the intestinal wall. For spontaneous emulsification to occur it is essential that the interfacial tension of the system be extremely low, less than about 1 dyne/cm. An examination (29) of the substances present in that part of the intestine where emulsification occurs has shown that only one combination (bile salt (taurocholate)-monoglyceride-fatty acid) was capable of producing the requisite low interfacial tension over the required pH range of 6.0 to 8.5 (see Table III). This combination is seen



to be very analogous to those showing "complex" formation discussed earlier.

TABLE III  
Comparative Study of Possible Intestinal Emulsifying Systems

Emulsifying systems	pH					
	6.0	6.5	7.0	7.5	8.0	8.5
1. Bile salts.....	—	—	—	—	+ <sup>a</sup>	+ <sup>a</sup>
2. Oleic acid (soap).....	—	—	—	+ <sup>b</sup>	++	+++
3. Monostearate.....	—	—	—	—	+	+
4. Cholesterol.....	—	—	—	—	—	—
5. Bile salt-oleic acid.....	—	—	—	+	++	+++
6. Oleic acid-monostearate.....	—	—	+	++	++	+++
7. Soap-cholesterol.....	—	—	—	+	++	+++
8. Bile salts-monostearate..	—	—	—	—	++ <sup>a</sup>	++ <sup>a</sup>
9. Bile salts-cholesterol....	—	—	—	—	+ <sup>a</sup>	+ <sup>a</sup>
10. Cholesterol - monostearate.....	—	—	+	+	+	+
11. Oleic acid-bile salts-monostearate.....	+++	+++	+++	+++	+++	+++
12. Bile salt-oleic acid-cholesterol.....	—	—	—	+	++	+++
13. Oleic acid-cholesterol-monoglyceride.....	—	—	+	++	++	+++

— No emulsification.  
 + Emulsification on agitation: particles average more than 2  $\mu$ .  
 ++ Some spontaneous emulsification: particles on agitation exceed an average of 1  $\mu$ .  
 +++ Spontaneous emulsification: dispersion of particles less than 0.5  $\mu$  average.

<sup>a</sup> Effect probably due to soap impurities.

<sup>b</sup> Effect obtained with excess oleic acid.

### *Anthelmintic Activity of Hexylresorcinol in the Presence of Soaps*

Hexylresorcinol is a well-known and widely used drug for *Ascaris* and other intestinal worms. A systematic *in vitro* examination of the effect of normal intestinal constituents showed that if bile salts were present the rate of entry of hexylresorcinol was reduced, the inhibition becoming complete at approximately 1% in the case of sodium cholate.

Other soaps, such as sodium oleate and cetyl trimethyl ammonium bromide (C.T.A.B.), resembled the bile salt in producing complete inhibition above a certain concentration, but differed in giving a marked *acceleration* at low concentrations (14). The rate curve thus passes through a maximum as can clearly be seen in Figure 10. The surface activities of

the various mixtures, against medicinal paraffin, also plotted in Figure 10, showed that the maximum rate of hexylresorcinol penetration occurs just at the point where soap micelles start to form in the bulk of the solution.

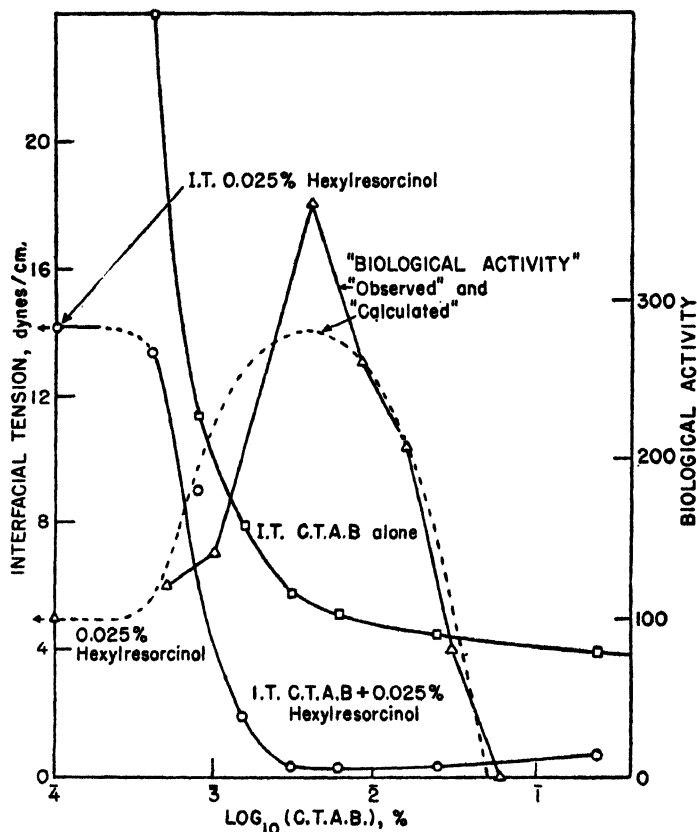


Fig. 10. Cetyl trimethyl ammonium bromide (C.T.A.B.)-0.025% hexylresorcinol mixtures in 0.9% NaCl (14). Interfacial tension against paraffin and biological activity measured by the penetration of hexylresorcinol as percentage of control (0.025% hexylresorcinol alone).

(The onset of micelle formation is shown by the sudden flattening of the interfacial tension curve.) The fall-off in the rate beyond this point arises from the soap micelles competing with the biological surface for the fixed amount of drug. The adsorption of hexylresorcinol into the soap micelles, and hence the "cut-off" soap concentration, can actually be calculated from surface chemical considerations, and the latter is in good agreement with the experimental value (see Fig. 10).

The activation of drug penetration produced by low soap concentrations is linked up with the increased surface activity of the mixture (another example of "interfacial complex" formation, in this case between the hexylresorcinol molecule and the soap ion). This increased surface activity leads to the surface of the worm being opened up or modified in some way, thus facilitating the entry of the phenol.

### *Bactericidal Activity of Soap-Phenol Mixtures*

The idea of improving the disinfectant action of phenols by utilizing the detergent power of soap is a very old one, but when various workers

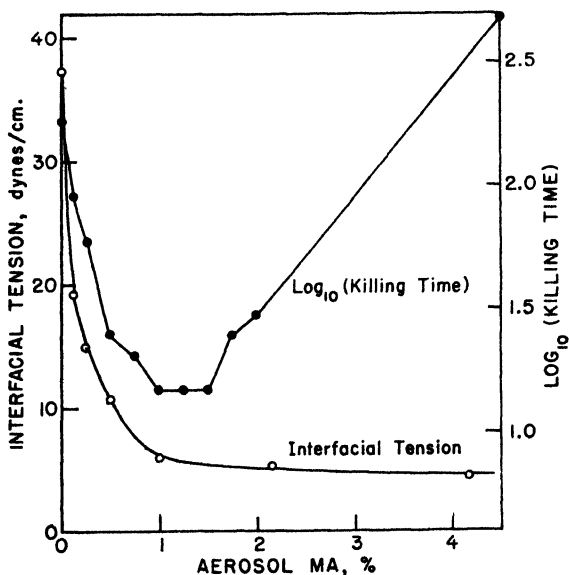


Fig. 11. Bactericidal and interfacial activities of Aerosol MA-0.5% phenol mixtures (13).

tested it quantitatively, very varied and conflicting results were obtained, some reporting an increase, others an equally definite decrease. The above work upon the anthelmintic activity of hexylresorcinol in the presence of soaps led to the bactericidal question being reinvestigated (13). Using mixtures of 0.5% phenol with Aerosol MA (dihexyl sodium sulfosuccinate) and *Escherichia coli* as test organism, the bactericidal activity was measured by both Rideal-Walker tests and by rates of killing. Figure 11 shows a typical result for the time for complete kill (Rideal-Walker test), and the

interfacial tension against medicinal paraffin, both plotted as a function of soap concentration. The maximum biological activity at the point where micelles start to form is again apparent and a precisely similar theory to that advanced in the case of *Ascaris* appears to hold in this system also. Thus the conflicting results obtained by the earlier workers are seen to depend upon their arbitrarily chosen soap concentration, whether this happened to be below or much above the micelle point.

### References

1. Adam, N. K., *The Physics and Chemistry of Surfaces*. 3rd ed., Oxford Univ. Press, London, 1941.
2. Addison, C. C., *Phil. Mag.*, **36**, 73 (1945) (gives references to earlier work).
3. Alexander, A. E., *unpublished work*.
4. Alexander, A. E., *Trans. Faraday Soc.*, **37**, 15 (1941).
5. Alexander, A. E., *ibid.*, **38**, 54 (1942).
6. Alexander, A. E., *Proc. Roy. Soc. London*, **A179**, 470 (1942).
7. Alexander, A. E., *Repts. Progress Phys.*, **9**, 158 (1943).
8. Alexander, A. E., *Ann. Repts. Chem. Soc. London*, **41**, 5 (1944).
9. Alexander, A. E., *Nature*, **159**, 304 (1947).
10. Alexander, A. E., *Faraday Discussion on "Surface Chemistry."* Bordeaux, 1947. Butterworth, London; Interscience, New York, 1949.
11. Alexander, A. E., and Rideal, E. K., *Proc. Roy. Soc. London*, **A163**, 70 (1937).
12. Alexander, A. E., and Rideal, E. K., *Nature*, **155**, 18 (1944).
- 12a. Alexander, A. E., and Teorell, T., *Trans. Faraday Soc.*, **35**, 734 (1939).
13. Alexander, A. E., and Tomlinson, A. J. H., *Faraday Discussion on "Surface Chemistry."* Bordeaux, 1947. Butterworth, London; Interscience, New York, 1949.
14. Alexander, A. E., and Trim, A. R., *Proc. Roy. Soc. London*, **B133**, 220 (1946).
15. Andersson, K., Stållberg-Stenhagen, S., and Stenhagen, E., in A. Tiselius and K. O. Pedersen eds., *Svedberg, 1884-1944*. Almqvist & Wiksells, Uppsala, 1944.
16. Bigelow, W. C., Pickett, D. L., and Zisman, W. A., *J. Colloid Sci.*, **1**, 513 (1946).
17. Bull, H. B., *J. Am. Chem. Soc.*, **68**, 745 (1946).
18. Bull, H. B., *ibid.*, **68**, 747 (1946).
19. Bull, H. B., *Advances in Protein Chemistry*. Vol. III, Academic Press, New York, 1947, p. 95.
20. Coumoulos, G. D., *Proc. Roy. Soc. London*, **A182**, 166 (1943).
21. Crisp, D. J., *J. Colloid Sci.*, **1**, 49, 161 (1946).
22. Danielli, J. F., *Cold Spring Harbor Symposia Quant. Biol.*, **6**, 190 (1938).
23. Danielli, J. F., Danielli, M., and Marrack, J. R., *Brit. J. Exptl. Path.*, **19**, 393 (1938).
24. Davies, J. T., *Faraday Discussion on "Surface Chemistry."* Bordeaux, 1947.
25. Dervichian, D. G., *Thesis*, Paris, 1936.
26. Doss, K. S. G., *Kolloid-Z.*, **86**, 205 (1939) (and earlier papers).
27. Elkes, J. J., Frazer, A. C., Schulman, J. H., and Stewart, H. C., *Proc. Roy. Soc. London*, **A184**, 102 (1945).
28. Ewing, W. W., *J. Am. Chem. Soc.*, **61**, 1317 (1939).
29. Frazer, A. C., Schulman, J. H., and Stewart, H. C., *J. Physiol. London*, **103**, 306 (1944).

30. Guastalla, J., *Compt. rend.*, **208**, 1078 (1939).
31. Guastalla, J., and Mibashan, L., *Faraday Discussion on "Surface Chemistry."* Bordeaux, 1947. Butterworth, London; Interscience, New York, 1949.
32. Harkins, W. D., Fourt, L., and Fourt, P. C., *J. Biol. Chem.*, **132**, 111 (1940).
33. Hartley, G. S., *Trans. Faraday Soc.*, **37**, 130 (1941).
34. Hartley, G. S., and Roe, J. W., *ibid.*, **36**, 101 (1940).
35. Hutchinson, E., *ibid.*, **43**, 435, 439, 443 (1947). See also Verwey, E. J. W., and de Boer, J. H., *Rec. trav. chim.*, **57**, 383 (1938).
- 35a. Hutchinson, E., *Doctoral Dissertation*, Cambridge, 1945.
36. Langmuir, I., and Schaefer, V. J., *Chem. Revs.*, **24**, 181 (1939).
37. Miles, G. D., and Ross, J., *J. Phys. Chem.*, **48**, 280 (1944).
38. McBain, J. W., Ford, T. F., and Mills, G. F., *J. Am. Chem. Soc.*, **62**, 1319 (1940).
39. McBain, J. W., and Wood, L. A., *Proc. Roy. Soc. London*, **A174**, 286 (1940).
40. Neurath, H., and Bull, H. B., *Chem. Revs.*, **23**, 391 (1938).
41. Pankhurst, K. G. A., *Trans. Faraday Soc.*, **37**, 496 (1941).
42. Pink, R. C., *J. Chem. Soc.*, 1939, 619.
43. Pink, R. C., *Trans. Faraday Soc.*, **37**, 180 (1941).
44. Porter, E. F., and Pappenheimer, A. M., *J. Exptl. Med.*, **69**, 755 (1939).
45. Puddington, I. E., *J. Colloid Sci.*, **1**, 505 (1946).
46. Rideal, E. K., *J. Chem. Soc.*, 1945, 423.
47. Ross, S., *J. Am. Chem. Soc.*, **67**, 990 (1945).
48. Rothen, A., *Advances in Protein Chemistry*. Vol. III, Academic Press, New York, 1947, p. 123.
49. Schulman, J. H., *Ann. Repts. Chem. Soc.*, **36**, 94 (1939).
50. Schulman, J. H., and Cockbain, E. G., *Trans. Faraday Soc.*, **36**, 651 (1940).
51. Schulman, J. H., and Rideal, E. K., *Proc. Roy. Soc. London*, **B122**, 29 (1937).
52. Smith, H. A., and Fuzek, J. F., *J. Am. Chem. Soc.*, **68**, 229 (1946).
53. Sobotka, H., and Bloch, E., *J. Phys. Chem.*, **45**, 9 (1941).
54. Stållberg, S., and Teorell, T., *Trans. Faraday Soc.*, **35**, 1413 (1939).
55. Stållberg-Stenhagen, S., and Stenhagen, E., *Nature*, **159**, 814 (1947).
56. Stenhagen, E., *Trans. Faraday Soc.*, **36**, 597 (1940).
57. Trapeznikov, A. A., *Acta Physicochim. U. R. S. S.*, **13**, 265 (1940).
58. Ward, A. F. H., and Tordai, L., *Nature*, **154**, 146 (1944).
59. Ward, A. F. H., and Tordai, L., *J. Chem. Phys.*, **14**, 453 (1946).
60. Van Wazer, J. R., *J. Colloid Sci.*, **2**, 223 (1947).

# QUANTITATIVE INTERPRETATION OF THE ELECTROPHORETIC VELOCITY OF COLLOIDS

J. TH. G. OVERBEEK

*Van't Hoff-Laboratorium der Rijksuniversiteit, Utrecht, Netherlands*

---

I. Introduction.....	97
II. Classical Concepts of Electrophoretic Velocity.....	99
1. Equation of Helmholtz-Smoluchowski.....	99
2. Hückel Equation.....	103
3. Henry Solution of the Contradiction between Smoluchowski and Hückel Theories.....	104
4. Influence of Conductivity of Particles.....	107
5. Electrophoresis of Liquid Droplets.....	108
III. Influence of Deformation of Double Layer upon Electrophoresis.....	109
1. Relaxation Effect.....	109
2. Influence of Surface Conductance.....	117
3. Summary of Conditions in Which Zeta Potential Can Be Evaluated from Electrophoresis.....	118
4. Experimental Work.....	119
IV. Electrophoretic Velocity and Charge of Particles.....	120
1. Charge and Potential.....	120
2. Spherical Particles.....	122
3. Nonspherical Particles.....	127
4. Applications.....	128
5. Comparison of Electrophoretic Charge with Charge Determined by Other Means.....	130
6. General Conclusions.....	133
References .....	134

---

## I. Introduction

When an electric field is applied to a colloidal solution, in many cases, the colloidal particles are observed to migrate to one of the electrodes. This phenomenon, described in 1861 by Quincke (56), is termed cataphoresis or, better and more generally, electrophoresis.

In the development of colloid science, electrophoretic experiments have played a very great part indeed. There probably is not a single other

method of investigation that has been so widely applied in pure as well as in applied research of colloids. This may be explained by the fact that a number of techniques for the determination of the electrophoretic mobility are available, which ask only for a comparatively simple experimental setup. Another factor in favor of electrophoresis certainly has been the attractive and simple interpretation of Helmholtz (33) and Smoluchowski (61,62), permitting calculation of the *zeta potential* from the electrophoretic mobility.

The classical investigations of Hardy (32), Powis (55), and Burton (15) introduced the concept that the stability of hydrophobic colloids is closely related to the zeta potential as calculated from electrophoresis. A specified minimal zeta potential (the *critical potential*) was found to be necessary to keep the hydrophobic suspension stable. This concept has been very widely used, and, although in more recent concepts of the stability of colloids (71,73,74) the zeta potential has a less predominant position, electrophoresis still remains an important source of information about hydrophobic colloids.

With hydrophilic colloids the relation between stability and electrophoresis is much less prominent because many hydrophilic colloids may remain in colloidal solution even when their electrophoretic mobility is reduced to zero. Nevertheless, in this domain also electrophoresis retains its significance for the determination of the isoelectric point and of the charge of the particles outside the isoelectric point. In mixtures of hydrophilic colloids, again, stability is related to electrophoresis. Complex coacervation—that is, a phase separation in which a mixture of hydrophilic colloids is precipitated in the form of a very concentrated liquid—occurs only if the two colloids are oppositely charged and if the charge of each is sufficiently high (14). This charge can be, and is actually in most cases, evaluated from electrophoresis.

Although the usual methods of determining electrophoretic mobility of hydrophobic colloids are not directly applicable to hydrophilic systems, because the scattering of light by the latter is much slighter than that of hydrophobic colloids, the technique of measuring electrophoresis of hydrophilic colloids adsorbed on small inert particles as coal, quartz, oil droplets, etc. (2) is widely applicable and easy to manage.

Moreover, the method of Tiselius (65,66), which uses the difference in optical density between a colloidal solution and its dialyzate, and thereby adapts the moving boundary technique to hydrophilic colloids, enjoys a continually increasing interest especially in the field of proteins. It has been very frequently used for the determination of purity of protein prepa-

rations, and for the quantitative analysis and separation of protein mixtures. In the application of this method, however, the interpretation of the electrophoretic mobility in terms of the charge or potential of the particles has somewhat fallen into the background. Not so much because the evaluation of the electrophoretic mobility would be difficult in this method (it may be so in dilute solutions), but perhaps because in many applications of the Tiselius technique (quantitative separations, proof of purity), the relation between electrophoretic mobility and charge of the particles is inessential.

In every textbook on colloid science and in many books on general physical chemistry, electrophoresis is treated. Moreover, two excellent monographs of Abramson on the subject exist. The first of these (1), however, dates back to 1934; the second (4), published in 1942, deals especially with proteins.

In the following pages we shall direct our attention particularly to the quantitative interpretation of the electrophoretic mobility. Such a survey seems not to be wholly superfluous as, even in recent times, there exist many controversial opinions on the subject and, although by far not all the problems presented here have been completely solved, the situation seems to be cleared sufficiently to justify a review of this type.

## II. Classical Concepts of Electrophoretic Velocity

In 1879 Helmholtz (33) presented a theory of electrokinetic phenomena, one of which is electrophoresis, and made clear that the electrophoretic velocity is proportional to the zeta potential and not, as one might imagine upon first thought, to the charge of the colloidal particle.

### 1. Equation of Helmholtz-Smoluchowski

The derivation of Helmholtz has been improved and extended by Smoluchowski without, however, essentially altering the final result. Smoluchowski's analysis was in the first instance directed upon electro-osmosis and he derived his electrophoresis equation by simply remarking that electrophoresis is the reverse phenomenon from electro-osmosis, so that, for the relative motion of liquid and solid the same equation applies to both phenomena. As we are concerned here especially with electrophoresis, we will give Smoluchowski's derivation in an abridged form and in direct application to electrophoresis.

In a solution of electrolyte, a suspended particle assumes as a rule a certain charge, a compensating charge of the opposite sign and equal magnitude staying in the solution in the neighborhood of the charged particle.



The extension of this compensating charge in the solution is of the same order as the thickness,  $1/\kappa$ , of the Debye-Hückel ionic atmosphere:

$$\frac{1}{\kappa} = \left( \frac{\epsilon k T}{4\pi e^2 \sum n_i z_i^2} \right)^{1/2} \quad (1)$$

in which  $\epsilon$  is the dielectric constant,  $e$  the elementary charge,  $z_i$  the valency,  $n_i$  the number of ions of species  $i$  per cubic centimeter,  $k$  Boltzmann's constant, and  $T$  the absolute temperature.

By application of Poisson's equation:

$$\Delta\psi = -4\pi\rho/\epsilon \quad (2)$$

in which  $\Delta$  is the operator of Laplace,  $\psi$  the potential, and  $\rho$  the charge density in the double layer and Boltzmann's theorem, the distribution of charge and potential around the particle, can be derived, but since in Smoluchowski's derivation, an explicit expression for the distribution of charge is superfluous, we will postpone this point until Section 3.

With Smoluchowski we assumed a rigid particle of *arbitrary form* embedded in a solution. The surface of the particle has a potential  $\zeta$  with respect to the liquid far from the particle. If one wishes to assume that a layer of liquid adheres so firmly to the particle that it cannot be set into motion either by an applied electric field, or by a motion of the liquid, this layer shall be considered as forming part of the particle, the potential  $\zeta$  being found now at the boundary of the fixed and the free liquid.

The existence of such a fixed layer of liquid was postulated by Smoluchowski (61) in order to explain the difference between the total potential in the double layer ( $\epsilon$ -potential) obeying the equation of Nernst, and the  $\zeta$  potential. The difference between these two potentials is located in the adhering liquid layer and perhaps in the solid phase too.

Lamb (41), contrary to Helmholtz and Smoluchowski, assumed the possibility of a slip between solid and liquid in the electrokinetic movements. The experimental arguments for such a slip are, however, far from convincing and, as far as our knowledge of the boundary phenomena goes at present, slip does not seem to occur.

Bikerman (7) recently discussed the theory of the adhering liquid layer and tried to explain the difference between  $\epsilon$  and  $\zeta$  potentials by the surface roughness of solids. A layer of liquid, without being in the true sense fixed to the solid, would be kept from moving with the bulk of the liquid by the protruding parts of the surface. It should be kept in mind, however, that in Smoluchowski's analysis the form of the particles is immaterial. Roughness of the surface could only influence the electrokinetic phenomena if the roughness is on a scale smaller than the thickness of the double layer, thereby invalidating Smoluchowski's next assumption on the dimensions of the particle.

The *dimensions* of the particle are so large that the radius of curvature at any point of the surface is large compared to the extension of the double layer.

The particle is considered to be *nonconducting*, whereas the *electric conductance* of the liquid, its *dielectric constant*, and *viscosity* are assumed to have the same value in the double layer as in the bulk of the liquid.

All three assumptions are debatable. The electric conductance in the surface layer may be higher than the bulk conductance (see Sect. III.2).

The viscosity might well be influenced by the presence of the solid surface. This effect, however, is at least formally accounted for by the assumption of the adhering water layer (in which the viscosity would be infinitely high).

The dielectric constant in the double layer might be changed by a loss of mobility of the liquid molecules adsorbed to the surface and by a change in composition of the liquid near the surface. As long as there is no direct experimental evidence of this change in dielectric constant, which there is not at present, it seems not useful to introduce a change in dielectric constant as an extra complication in the theory.

The *electric field* applied to produce electrophoresis may be distorted by the presence of the particle but is otherwise additively superimposed upon the field of the double layer.

As the radius of curvature of the particle surface is large, the potential gradient of the double layer is to a good approximation perpendicular to the surface. The applied electric field has only a component parallel to the surface, because the particle is nonconducting. If we call this field strength  $\mathbf{E}$ , it is easy to demonstrate that just outside the double layer the velocity of the liquid with respect to the particle is directed along  $\mathbf{E}$  (parallel to the surface) and has the value:

$$\mathbf{v} = - \frac{\epsilon \zeta}{4\pi\eta} \mathbf{E} \quad (3)$$

where  $\eta$  is the viscosity of the liquid.

The derivation of equation (3) can be given along the following lines. The charge density,  $\rho$ , in the double layer is given by Poisson's equation (2), which may be written:

$$\rho = - \frac{e}{4\pi} \frac{d^2\psi}{dn^2}$$

in which  $n$  is the outward normal on the surface. A volume element of the liquid is subjected to two equal forces of opposite directions, one due to the applied electric field working on the charge in the double layer, the other due to viscous friction.

As in the neighborhood of the surface, the motion of the liquid is parallel to the surface, the force exerted by viscous friction on a thin layer of liquid,  $dn$ , is equal to the difference in the forces transmitted on both sides of the thin layer, that is equal to:

$$\left( \eta \frac{d\mathbf{v}}{dn} \right)_{n=n} - \left( \eta \frac{d\mathbf{v}}{dn} \right)_{n=n+dn} = -\eta \frac{d^2\mathbf{v}}{dn^2} dn$$

The force exerted by the external field on the net charge present in this layer is given by  $\rho \mathbf{E} dn$ . Equalizing the two forces we get the equation:

$$\rho \mathbf{E} = -\frac{\epsilon}{4\pi} \frac{d^2\psi}{dn^2} \mathbf{E} = -\eta \frac{d^2\mathbf{v}}{dn^2}$$

Integrating once we find:

$$\frac{\epsilon}{4\pi} \frac{d\psi}{dn} \mathbf{E} = \eta \frac{d\mathbf{v}}{dn} + c_1$$

$c_1 = 0$  because for  $n \rightarrow \infty$ ,  $(d\psi/dn) = (d\mathbf{v}/dn) = 0$ .

The second integration gives:

$$\frac{\epsilon}{4\pi} (\psi_\infty - \psi) \mathbf{E} = \eta (\mathbf{v}_\infty - \mathbf{v}_0)$$

With  $\psi_\infty = 0$  and  $\mathbf{v}_0 = 0$ , this is equivalent to equation (3).

Under the influence of the applied electric field, the particle moves with a certain constant speed,  $u$ , in the direction of the field. With respect to a system of coordinates fixed to the particle, the liquid at a great distance from the particle moves with velocity  $-u$ . In the immediate neighborhood of the particle, the velocity of the liquid is given by equation (3), and in intermediate regions the velocity has to satisfy the condition of incompressibility, *viz.*:

$$\text{div } \mathbf{v} = 0 \quad (4)$$

The solution of equation (4) and therewith the value of  $u$  is easily found by remarking that the applied electric field obeys an equation analogous to equation (4):

$$\text{div } \mathbf{E} = 0 \quad (5)$$

and that the boundary conditions at the surface of the particle for  $\mathbf{v}$  and  $\mathbf{E}$  are proportional to each other according to equation (3). Consequently the velocity of the liquid is everywhere parallel and proportional to the electric field  $\mathbf{E}$  and especially at a large distance from the particle:

$$v = -\frac{\epsilon\zeta}{4\pi\eta} E$$

where  $E$  is the value of the applied field at some point far from the particle. Returning to a resting system of coordinates, the electrophoretic velocity  $u$  of the particle with respect to this system is given by:

$$u = \frac{\epsilon\zeta}{4\pi\eta} E \quad (6)$$

completely independent of the form and dimensions of the particle, if large enough.

With regard to the uncertainty in the value of  $\epsilon$  (see above), there have been proposals by Bull and Gortner (12) and Guggenheim (31), among others, to characterize the electrokinetic phenomena by the product of  $\epsilon$  and  $\zeta$ —being the electric moment of the double layer. Guggenheim even made a formal proposal to introduce the quantity  $\epsilon\zeta/12\pi$  and to call the unit of this quantity the *Helmholtz*. Although these proposals have a certain advantage in that they allow the double layer to be characterized unhampered by uncertainties in the dielectric constant, it should not be forgotten that we turn to electrokinetic experiments for information on the potential or the charge of the surface. To that end we must make some assumption (more or less well founded) on the value of  $\epsilon$  in the double layer.

## 2. Hückel Equation

In Smoluchowski's theory, the motion of the particle is governed by three different types of forces, although they have not been explicitly introduced into the calculation. The equation:

$$\frac{\epsilon}{4\pi} \cdot \frac{d\psi}{dn} \mathbf{E} = \eta \frac{d\mathbf{v}}{dn}$$

occurring in the derivation of Smoluchowski's equation, when applied to  $n = 0$ , is equivalent to:

$$-\sigma \mathbf{E} = \eta \left( \frac{d\mathbf{v}}{dn} \right)_{n=0}$$

in which  $\sigma$  is the charge density on the surface. This means that the electrical force on the surface charge is just counterbalanced by a viscous friction. This viscous friction can be regarded as consisting of two components.

(1) The viscous friction that would also be present if the liquid surrounding the particle would contain no charges.

(2) The force that would be exerted on the particle by that component of the motion of the liquid which is caused exclusively by the action of the applied field on the charges in the liquid part of the double layer. This force is called the "electrophoretic retardation." It is always retarding because the charge in the liquid is the opposite of that on the particle. These same forces are treated in the theory of conductance of strong electrolytes (20,50); Debye and Hückel (21) also applied to colloidal particles the method of calculation used in the theory of strong electrolytes. They confirmed Smoluchowski's equation (6) except for the factor  $1/4\pi$ , which should only have this value for a cylindrical particle migrating with its axis parallel to the field, whereas for other forms the factor should have another value. For a spherical particle Hückel (36) derived a factor  $1/6\pi$ .

Since Debye and Hückel stated that they used the same assumptions

of Smoluchowski, but did not show where the analysis of the latter was in error, there was a contradiction (remaining unsolved for several years) until Henry (34), in a renewed analysis of the whole problem, reconciled the two contradictory points of view.

### ***3. Henry Solution of the Contradiction between Smoluchowski and Hückel Theories***

The difference between the concepts of Smoluchowski and Debye and Hückel is to be found in the geometry of the applied electric field. Whereas Smoluchowski considers the particle as an insulator and takes the deformation of the applied field by the particle explicitly into account, Debye and Hückel simply assume that the value and the direction of the electric field have the same value throughout the whole system. The conception of Debye and Hückel is quite justified in the case of electrolytic solutions, because there the extension of the double layer is so much larger than the dimensions of the ions that the deformation of the field, which is only felt in the immediate neighborhood of the ions, is practically without influence upon the electrophoretic retardation.

In colloidal systems, however, which of the two concepts must be applied depends wholly upon the ratio of the extension of the double layer and the dimensions of the particles. If the particle is relatively large, the deformation of the lines of force has to be taken into account, which results in a smaller value of the electrophoretic retarding force. Hence Smoluchowski's value for the electrophoresis is larger than Hückel's.

Henry (34) worked out an electrophoresis equation for any ratio between the thickness of the double layer and the dimensions of the particle.

It is impossible to solve this problem with the same generality used by Smoluchowski; it is necessary to restrict the analysis to certain specified forms of the particle. Henry's calculations are restricted to spherical particles and cylinders with their axis parallel to, or perpendicular to, the direction of the applied field.

For the motion of the liquid Henry uses the same assumption as Smoluchowski and Debye and Hückel, *viz.*, the equations of Navier and Stokes, with a constant viscosity, incompressibility of the liquid, and a relative velocity zero at the spherical (or cylindrical) surface, where the potential of the double layer has the value  $\zeta$ . Henry, too, assumes that the outwardly applied field, although deformed by the presence of the particle, and the field of the double layer are simply additive.

Without any further approximation he thus derives the following

equation (7) for the electrophoretic mobility of a spherical isolating particle of radius  $a$ .

$$u = \frac{\epsilon E}{4\pi\eta} \left[ \zeta + 5a^5 \int_{\infty}^a \frac{\psi}{r^6} dr - 2a^3 \int_{\infty}^a \frac{\psi}{r^4} dr \right] \quad (7)$$

In order to work out the integrals in expression (7) it is necessary to introduce explicitly the dependence of potential  $\psi$  on distance  $r$ , measured from the center of the sphere. So apart from Poisson's equation (2), which has been used in the derivation of (7), it is necessary to introduce Boltzmann's theorem to establish a relation between the charge density,  $\rho$ , and the potential,  $\psi$ :

$$\rho = n_+ z_+ e \exp(-z_+ e\psi/kT) - n_- z_- e \exp(+z_- e\psi/kT) \quad (8)$$

where  $n_+$  and  $n_-$  are the concentrations,  $z_+$  and  $z_-$  the valencies of the positive and negative ions present in the solution. It is well known that an explicit solution of the combination of equations (2) and (8) can be found only when the exponents in (8) are so low that the exponentials may be developed and only the first term of the development is used, leading to:

$$\rho = - \frac{e^2}{kT} (n_+ z_+^2 + n_- z_-^2) \psi \quad (9)$$

When this approximation is used:

$$\psi(r) = \zeta a \frac{e^{\kappa(a-r)}}{r} \quad (10)$$

Inserting equation (10) into (7), relation (11) is found for the velocity of a spherical isolating particle:

$$u = \frac{\epsilon \zeta E}{6\pi\eta} \left[ 1 + \frac{\kappa^2 a^2}{6} - \frac{5\kappa^3 a^3}{48} - \frac{\kappa^4 a^4}{96} + \frac{\kappa^5 a^5}{96} - \left( \frac{\kappa^4 a^4}{8} - \frac{\kappa^5 a^5}{96} \right) e^{\kappa a} \int_{\infty}^{\kappa a} \frac{e^{-t}}{t} dt \right] \quad (11)$$

in which  $\kappa a$  gives the ratio between the extension of the double layer ( $(1/\kappa)$ , see Eq. 1) and the radius of the sphere,  $a$ .

In Figure 1 the equation of Henry is represented graphically. It will be clear that the deformation of the applied field is strongly dependent upon the electric conductance of the particle. Henry showed that this deformation and its influence upon the electrophoretic velocity is determined by the ratio  $\mu$  of the electrical conductivities of the particle and the surrounding liquid. His results for three typical cases,  $\mu = 0$ ,  $\mu = 1$ , and  $\mu = \infty$ , are given in Figure 1.

For cylindrical particles with their axis parallel to the field, the electrophoretic velocity is given by Smoluchowski's equation (proportionality factor  $1/4\pi$ ), independent of the thickness of the double layer or the conductivity of the particles.

For cylinders placed transverse to the field, Henry has given an electrophoresis equation analogous to equation (7), but he has only worked out

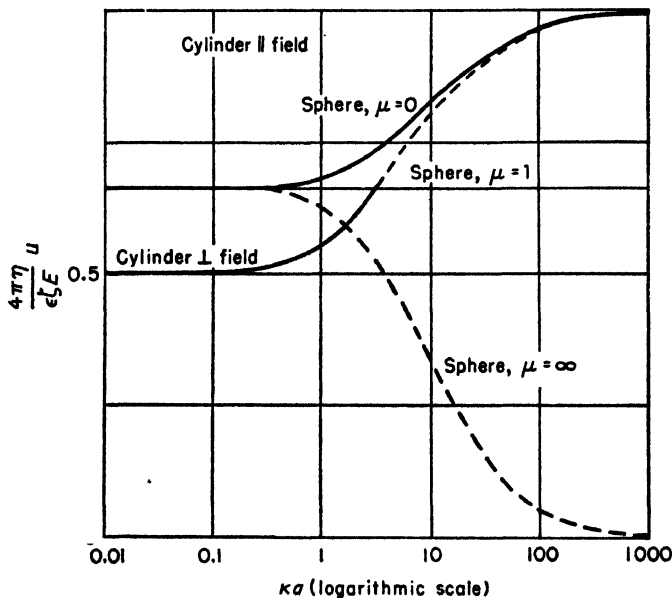


Fig. 1. Factor of proportionality between electrophoretic velocity  $u$  and zeta potential according to the theory of Henry (34).

the solution for the extreme cases that  $\kappa b = 0$  or  $\kappa b = \infty$  ( $b$  is the radius of the cylinder), finding for insulating particles a proportionality factor  $1/8\pi$  when the double layer is very extended and  $1/4\pi$  for a very thin double layer. When the cylinder is conducting the electrophoretic velocity in the case of a very thin double layer is zero, just as in the case of a conducting sphere.

Gorin (26) extended Henry's calculations on cylinders and determined the proportionality factor for intermediate values of  $\kappa b$ . His results are reproduced in Table I and Figure 1.

In applications to cylindrical particles, cylinders oriented randomly are often involved. Gorin (4, p. 127) determined an average mobility factor for random orientation by applying the relation:

$$\frac{3}{u_{\text{random}}} = \frac{2}{u_{\perp}} + \frac{1}{u_{\parallel}} \quad (12)$$

The reasons given for averaging the reciprocal values of the mobility rather than the mobility itself are not very convincing. Gorin defends this procedure by mentioning that, in the averaging, stress should be placed upon the distortion of the external field rather than on the mobility.

TABLE I

Electrophoretic Mobility of Infinitely Long Cylindrical Particles (26)

$\kappa b$	$(4\pi\eta/e\xi E)u$	
	Cylinder $\perp$ to field	Cylinder in random orientation
0	0.50	0.60
0.4	0.518	0.616
1.0	0.544	0.639
1.4	0.582	0.676
2.0	0.615	0.705
2.4	0.631	0.719
3.0	0.656	0.741
$\infty$	1	1

For particle forms other than cylinders, spheres, and flat plates no calculations have been made. Neither does there exist a theory of the electrophoresis of a randomly kinked long-chain molecule—of which colloids like gum arabic, pectic acid, and polyacrylic acid are interesting examples.

#### 4. Influence of Conductivity of Particles

In experiments on the electrophoretic displacement of a cylindrical silver wire in a solution of silver nitrate where polarization had been carefully excluded, Henry (34) could confirm the fact predicted by the theory that the electrophoretic velocity is zero for conducting cylinders, which are large in comparison to the thickness of the double layer.

It remains questionable, however, whether for true colloidal suspensions the case  $\mu = \infty$  is ever realized even for metallic particles, because the passing of an electric current through the particles necessarily entails a polarization of the surface, which may easily be large enough to stop completely any further current through the particle. Consequently the particle behaves as an insulator and the electrophoretic velocity should be calculated putting  $\mu = 0$ .

Mercury droplets, which certainly are large compared to the extensions



of the double layer, nevertheless show a normal electrophoretic mobility (13), which proves, as has already been remarked by Verwey (69), that they behave as insulators.

### 5. *Electrophoresis of Liquid Droplets*

Up to this point the considerations have been restricted to rigid particles. If this condition is dropped and one turns to the electrophoresis of the droplets of an emulsion, the state of the theory is rather disappointing. The friction experienced by a liquid droplet is certainly less than that of a

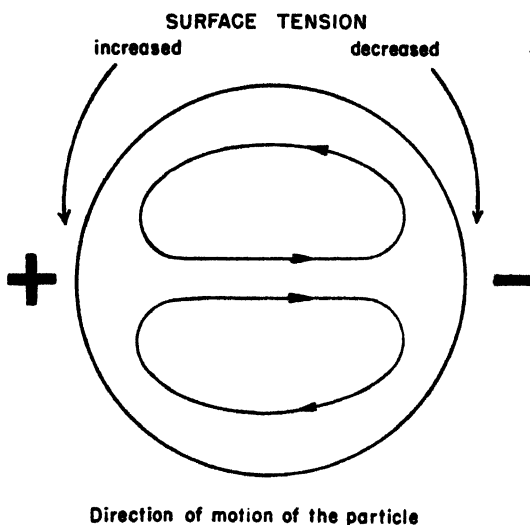


Fig. 2. Schematic representation of the motions in a drop of mercury placed in an electric field (23).

solid sphere of the same dimensions, because the drop of liquid can more or less adapt itself to the movements of the surrounding medium (10,60). On the other hand, the double layer at the interface of two liquids extends in both phases (70,72), and the part of it present in the droplet would be expected to play an active role in electrophoresis, giving rise to a circulating motion in the drop. The case has not, however, been analyzed theoretically.

A recent investigation of Frumkin (23) on the electrophoresis of mercury drops should be mentioned here too. Frumkin shows that in this case the mercury droplet is completely polarized by the applied field, so

that actually it behaves like an insulator. The polarization, however, alters the surface tension on the poles of the particle thereby generating motions of the mercury along the interface. If the mercury is positively charged (as is normally the case), the surface at the pole facing the positive electrode is negatively polarized, whereby its surface tension increases, whereas at the other pole it decreases. The motion of mercury generated by this difference in surface tension is schematically represented in Figure 2. It can be seen that this motion would support the motion of the particle to the negative electrode thus enhancing the electrophoretic velocity.

Frumkin has shown by experiments and theoretically that, especially when the surrounding medium is very viscous, the electrophoretic velocity may be increased enormously above the value calculated from Smoluchowski's equation by a factor of the order of  $10^4$  or  $10^5$ , so that in this special case the velocity is practically given by the simple equation of Stokes, where  $Q$  is the charge of the drop:

$$u = QE/6\pi\eta a$$

### III. Influence of Deformation of Double Layer upon Electrophoresis

#### 1. Relaxation Effect

In the considerations of the two foregoing sections, an essential supposition was that the electric field due to the double layer and the externally applied field may be simply superimposed on each other. This is certainly not exactly the case, as the particle and the outer part of the double layer, having opposite signs of charge, move in opposite directions, by which means the original symmetry of the double layer is disturbed. By electric conduction and diffusion, the double layer tends to restore its symmetry but this restoration takes a certain time, the *time of relaxation*, and the outer part of the double layer lags somewhat behind the particle. This gives rise to an additional electric field, which is directed oppositely to the applied field, and retards the electrophoretic motion.

In the conductance of strong electrolytes, the influence of this *relaxation effect* is of the same order of magnitude as the retardation caused by the motion of the ions of the atmosphere, *electrophoretic retardation* (20,50). Hence, in order to arrive at a complete description of electrophoresis, it seems necessary to include this relaxation effect.

Several investigators have approached this problem. The first was Paine (54), who applied the equation of Debye and Hückel directly to colloidal particles. However, as in the theory of electrolytic conductance

no account is taken of the deformation of the applied field (see above), this theory is valid only for small values of  $\kappa a$  ( $\kappa a < 1/10$ ). It can be seen from Figure 3 that the field of interest of colloid science, *viz.*, particles of dimensions between  $10 \text{ \AA.}$  and  $1 \mu$  and values of  $\kappa$  between  $10^5$  and  $10^{7.5}$  (concentrations of electrolyte in water from  $10^{-5}$  to  $1 N$ ) only coincides for a very small area with the region in which  $\kappa a < 1/10$ .

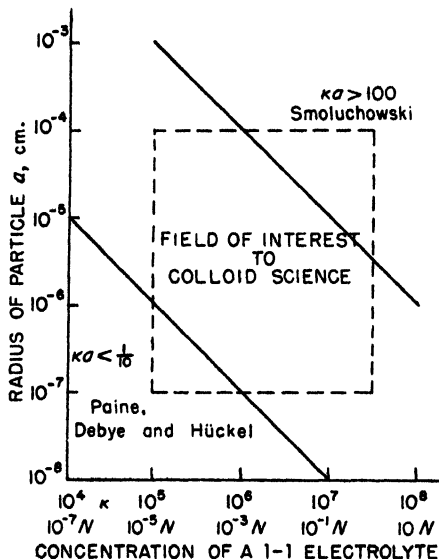


Fig. 3. Field of interest to colloid science compared to fields in which  $\kappa a$  is larger than 100 or is smaller than 0.1 (51, 53, 54).

On the other hand, it is possible to show that for large values of  $\kappa a$  ( $\kappa a > 100$ ), where  $a$  is one of the main dimensions of a particle of arbitrary form, the correction due to the relaxation effect is less than a few per cent. (In this region Henry's correction, too, is of the order of 3% or less.)

We repeat here the proof of this theorem given by Overbeek (51) in an abridged and somewhat simplified form.

The relaxation effect can be described as an extra field  $F$  (opposing the applied field  $E$ ), which is generated by the transport of charge along the particle. This transport of charge is effected by the applied field and by the electrophoretic motion itself, and it is counteracted by diffusion and conduction. When the double layer is thin, diffusion plays only a secondary role, so that in the stationary state of electrophoresis the conduction should just balance the two first-named effects.

The primary transport of charge by the applied field is proportional to the circum-

ference of the particle, the field strength  $E$ , and the charge density of the surface, which itself is proportional to  $\kappa\zeta$ . Consequently this transport can be expressed as a current  $i_I$ .

$$i_I \sim E\zeta\kappa a$$

The transport of charge by the electrophoresis itself is likewise proportional to the circumference of the particle, the charge density of the surface, and the velocity  $u$  of the particle, which itself is proportional to  $E$ . Therefore the second current is:

$$i_{II} \sim E\zeta\kappa a$$

The conduction current balancing these two currents  $i_I$  and  $i_{II}$  is not restricted to the surface of the particle but passes in the surrounding medium through a cross section of the order of  $a^2$  and is proportional to:

$$i_{III} \sim Fna^2$$

where  $n$  is the number of ions per cubic centimeter. As  $\kappa^2 \sim n$ :

$$i_{III} \sim F\kappa^2 a^2$$

Consequently, by putting  $i_{III} = i_I + i_{II}$  we find:

$$F\kappa^2 a^2 \sim E\zeta\kappa a$$

or:

$$F/E \sim \zeta/\kappa a$$

To take the relaxation effect into account, we must replace  $E$  in the equation of Smoluchowski by  $E - F$  and we find:

$$u = \frac{\epsilon\zeta}{4\pi\eta} (E - F) = \frac{\epsilon\zeta E}{4\pi\eta} \left\{ 1 - \frac{\text{const. } \zeta}{\kappa a} \right\} \quad (13)$$

which immediately shows that the correction for relaxation goes to zero when  $\kappa a$  becomes large enough. By a somewhat more accurate reasoning than the one given above, it is possible to obtain an idea about the magnitude of the constant in equation (13), which is of the order of  $e/kT$ . This means that the correction amounts to about 1% when  $\kappa a = 100$  and  $\zeta = 25$  mv.

The fact that for relatively large particles Smoluchowski's (or Henry's) equation retains its validity, even if account is taken of the relaxation correction, explains a very interesting series of observations summarized by Abramson (1). It was observed that the electrophoretic mobility of *microscopic* particles of widely divergent shapes and dimensions is exactly the same when the surface of the particles may be considered to be identical. In many cases the identity of the surfaces has been attained by covering the particles, which may have very different chemical properties (oil, graphite, iron oxide, quartz, asbestos, etc.) by a layer of protein. In the circumstances of these experiments, the thickness of the double layer (which varied between  $\sim 0.1 \mu$  (distilled water) and  $0.001 \mu$  (solutions)

was always small compared to the dimensions of the particles (which varied between 0.5 and several hundred microns). So it is in complete accord with the theoretical developments given above that all show the same electrophoretic mobility, which, incidentally, is the same as the electro-osmotic mobility. This, however, does not imply that the relaxation effect may also be neglected for smaller particles. It can be seen in Figure 3 that there still exists a large region of interest to colloid science (between  $\kappa a = 1/10$  and  $\kappa a = 100$ ) in which the influence of the relaxation effect may be expected to be more important.

In the existing literature there are relatively few papers on the relaxation effect of colloids. Only three deal with the case of large  $\kappa a$ . Of these, Mooney (48) and Bikerman (8,9) come to equations analogous to our equation (13), Mooney, however, without stating clearly how his equation has been derived and Bikerman only for a very special case, *viz.*, a long, but not infinitely long, cylinder parallel to the field. The third author, Hermans (35) treats the case of a spherical particle and arrives at a much larger relaxation effect than that given by equation (13). It seems that his derivations contain an omission, namely, the relative influence of the relaxation effect and the electrophoretic retardations, which makes his results of too large an order of magnitude (see also (52)). The work of Paine (54) for the case of very small values of  $\kappa a$  has already been mentioned.

Komagata (39) calculated the influence of the relaxation effect including any values of  $\kappa a$ . Although his basic work is sound, the calculations contain several mistakes, which make his results valueless.

Overbeek (52,53) has given a derivation of the relaxation effect for spherical particles valid for arbitrary values of  $\kappa a$ . Very recently Booth (11) in a short communication announced independent work on the same subject, which, in the main lines, seems to confirm Overbeek's analysis. As details of Booth's work are not yet available, a short description of Overbeek's method of approach and the most important of his results are given.

The calculations of electrophoretic mobility (including relaxation) for intermediate values of  $\kappa a$ , although in principle not more difficult than for the extreme cases of small or large  $\kappa a$ , are in practice very laborious and time consuming. This is, among other things, due to the fact that for intermediate and large values of  $\kappa a$  we may no longer consider the effects of relaxation and electrophoretic retardation separately, as we do for electrolytes (small  $\kappa a$ ). For larger values of  $\kappa a$ , it is essential to include in the calculations the mutual influence of the two effects. Moreover, it can be inferred from the considerations on the relaxation effect for very small and

very large  $\kappa a$  that the correction for the relaxation effect will be proportional to the square, and possibly higher powers, of the zeta potential. This implies that also in the distribution of the potential around the particle higher powers of zeta must be included.

In Overbeek's calculations the particle is assumed to be a rigid sphere with a surface potential  $\zeta$  and a charge  $ne$  spread out uniformly over the surface. (Booth used a more general assumption about the charge of the surface.) The particle is embedded in a solution of a  $(z_+ - z_-)$  valent electrolyte. It is surrounded by a diffuse double layer of the Gouy-Chapman type (18,29), which, however, is deformed by the electrophoresis.

The motion of the ions is governed by displacement in the electric field, by diffusion in concentration gradients, and by being dragged along by the movements of the liquid. During electrophoresis a stationary state is attained in which, relative to the moving particle, the concentration of each sort of ion remains constant. The particle is considered to acquire a constant velocity  $u$  in the direction of the applied field.

The equations for the stationary state are:

$$\begin{aligned} \operatorname{div} \left[ -\frac{n_+ z_+ e}{\rho_+} \operatorname{grad} \psi - \frac{kT}{\rho_+} \operatorname{grad} n_+ + n_+ \mathbf{v} \right] &= 0 \\ \operatorname{div} \left[ +\frac{n_- z_- e}{\rho_-} \operatorname{grad} \psi - \frac{kT}{\rho_-} \operatorname{grad} n_- + n_- \mathbf{v} \right] &= 0 \end{aligned} \quad (14)$$

where  $n_+$  and  $n_-$  represent the number of ions per cubic centimeter,  $\rho_+$  and  $\rho_-$  their friction constants, and  $\psi$  the electric potential due to the combined effects of double layer, applied field, and deformation by the relaxation effect.

By assuming a uniform motion for the central particle, its Brownian movement is neglected. This analysis is thus more in accord with the original Debye and Hückel theory (20) of conductance of strong electrolytes than with the later improved analysis of Onsager (50). In solutions of a single electrolyte, the correction of Onsager is essential because in the original version of the theory, which leaves the Brownian movement of the central ion out of account, the relaxation forces on the positive and negative ions are different, whereas, of course, the equality of action and reaction requires that the two forces are of equal magnitude. In a colloidal solution, however, the particles with their double layers are always embedded in a solution of electrolyte and, except in the cases of very concentrated and highly dialyzed sols, the total charge on the colloidal particles is only a very small fraction of the total charge of all the ions present in the solution.

Consequently the colloidal solution can be compared to a solution of electrolyte to which a small proportion of a second electrolyte has been added. Bennewitz, Wagner, and K  chler (6) have given an evaluation of the relaxation effects for such a mixture taking

Brownian motion into account. From their analysis one finds, neglecting the Brownian motion of the ion present in small quantity, an increase of the relaxation correction with a factor of the order:

$$1 + \rho_1/\rho_2$$

in which  $\rho_1$  and  $\rho_2$  are the frictional constants of the ions present in large and small quantity, respectively. As the diameter of a colloidal particle is at least 10 times and often 100 or more times as large as that of an ion, neglecting the Brownian motion in the case of colloids is completely justified.

The relations between charge density and potential in equation (14) are again given by Poisson's equation (2). Since the particle is considered to be an insulator, no discharge of either type of ions occurs at the surface of the particles. (For a consideration of a conducting particle see (52).)

The above considerations define the electric field and the ionic concentrations in the double layer, except for the value of the motion of liquid,  $\mathbf{v}$ , in equation (14). The motion of the liquid can be completely described by the fundamental hydrodynamic equations:

$$\begin{aligned} \operatorname{div} \mathbf{v} &= 0 \\ \eta \operatorname{rot} \operatorname{rot} \mathbf{v} + \operatorname{grad} p + \rho \operatorname{grad} \psi &= 0 \end{aligned} \quad (15)$$

By a method of successive approximations it is possible to solve equations (14) and (15) and the resulting equation for the electrophoretic mobility is, including all terms up to  $\zeta^3$ .

$$\begin{aligned} u = \frac{\epsilon \zeta E}{6\pi\eta} & \left[ f_1(\kappa a) - (z_- - z_+) \frac{e\zeta}{kT} f_2(\kappa a) + (z_+ - z_-) \left( \frac{e\zeta}{kT} \right)^2 g_1(\kappa a) - \right. \\ & (z_+^2 - z_+ z_- + z_-^2) \left( \frac{e\zeta}{kT} \right)^2 g_2(\kappa a) + (z_- - z_+)^2 \left( \frac{e\zeta}{kT} \right)^2 g_3(\kappa a) - \\ & \left. \frac{z_+ \rho_+ + z_- \rho_-}{(z_+ + z_-)e} \cdot \frac{\epsilon kT}{6\pi\eta e} \cdot \left( \frac{e\zeta}{kT} \right)^2 f_4(\kappa a) \right] \quad (16) \end{aligned}$$

The functions  $f(\kappa a)$  and  $g(\kappa a)$  except  $g_3(\kappa a)$  have been calculated. For symmetrical electrolytes the electrophoretic equation can be simplified to:

$$u = \frac{\epsilon \zeta E}{6\pi\eta} \left[ f_1(\kappa a) - z^2 \left( \frac{e\zeta}{kT} \right)^2 f_3(\kappa a) - \frac{\rho_+ + \rho_-}{2e} \frac{\epsilon kT}{6\pi\eta e} \left( \frac{e\zeta}{kT} \right)^2 f_4(\kappa a) \right] \quad (17)$$

and for unsymmetrical electrolytes, neglecting all contributions proportional to  $\zeta^3$  except the last term, which is preponderant even over the  $\zeta^2$  terms for small values of  $\kappa a$ :

$$u = \frac{e\xi E}{6\pi\eta} \left[ f_1(\kappa a) - (z_- - z_+) \frac{e\xi}{kT} f_2(\kappa a) - \frac{z_+ \rho_+ + z_- \rho_-}{(z_+ + z_-)e} \frac{\epsilon kT}{6\pi\eta e} \left( \frac{e\xi}{kT} \right)^2 f_4(\kappa a) \right] \quad (18)$$

Figure 4 and Table II show the values of the functions  $f(\kappa a)$ .  $f_1(\kappa a)$  has not been included in Figure 4 because it is identical with Henry's function  $f(\kappa a, \mu = 0)$ , which can be read from Figure 1. The broken line in Figure 4 shows the values of  $f_2$  and  $f_4$  as they follow from Debye and Hückel's theory of the conductivity of strong electrolytes.

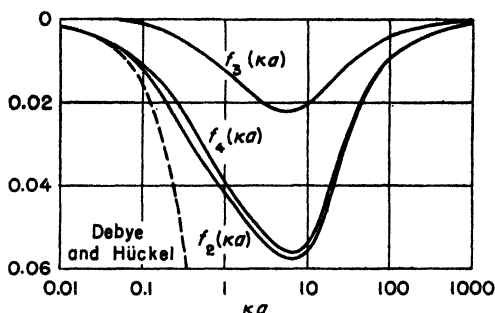


Fig. 4. Values of the functions  $f(\kappa a)$  for use in the electrophoresis equations (17) and (18).

TABLE II  
Values of Correction Terms in Equations (17) and (18)

$\kappa a$	$f_1(\kappa a)$	$f_2(\kappa a)$	$f_3(\kappa a)$	$f_4(\kappa a)$
0.01	1.000006	0.0006	0.00009	0.0006
0.1	1.000545	0.0125	0.00090	0.0107
0.3	1.00398	0.0279	0.0044	0.0218
1	1.0267	0.0411	0.0116	0.0387
3	1.1009	0.053	0.020	0.051 <sub>6</sub>
5	1.160	0.057	0.022	0.054 <sub>6</sub>
10	1.239	0.05 <sub>6</sub>	0.021	0.05 <sub>6</sub>
20	1.34	0.04	0.014 <sub>6</sub>	0.04
50	1.424	0.0188	0.00796	0.0177
100	1.458	0.0102	0.00444	0.00992
1000	1.495	0.0011	0.0005	0.0011

To illustrate the total influence of the correction of Henry and the relaxation effect on the electrophoretic velocity, Figures 5 and 6 are given. Both have been drawn for an equivalent conductance of the positive and negative ions equal to  $70 \Omega^{-1} \text{ cm.}^2$  per gram equivalent (this value is not



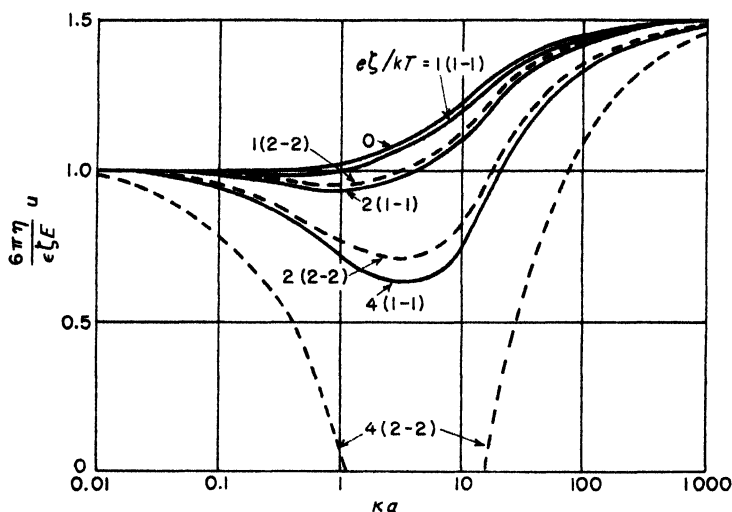


Fig. 5. Electrophoretic mobility in symmetrical electrolytes (Eq. 17). Values of  $e\zeta/kT$  are 1, 2, and 4 or  $\zeta$  about 25, 50, and 100 mv., respectively. The line marked 0 forms the limit for very small values of the zeta potential. Full lines for monovalent and broken lines for bivalent electrolytes.

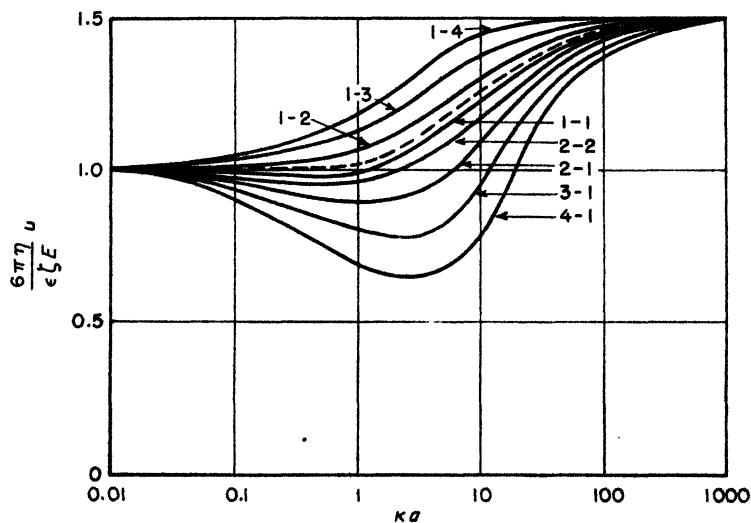


Fig. 6. Electrophoretic mobility in unsymmetrical electrolytes (Eq. 18). For all the curves  $e\zeta/kT$  values equal 2 or  $\zeta$  about 50 mv.

very critical), and a temperature of 25°C. Figure 5 represents equation (17) for symmetrical electrolytes; Figure 6 gives equation (18) for unsymmetrical electrolytes. In Figure 5,  $e\zeta/kT$  varies from very small values ( $e\zeta/kT \rightarrow 0$ ) to 4, which means that the zeta potential varies from 0 to about 100 mv. For the higher values of  $\zeta$  it would have been necessary to include more terms of the series; they should be seen only as a rough illustration of the trend of the electrophoretic velocity. In Figure 6,  $\zeta$  is fixed at 50 mv. ( $e\zeta/kT = 2$ ) but the type of electrolyte has been varied.

It is conspicuous that the correction for relaxation is largest for intermediate values of  $\kappa a$ , which are of the order of 5–10. Since the corrections are proportional to the second and higher powers of  $\zeta$ , they tend to reach zero for small values of  $\zeta$ . With increasing potentials and increasing valency of the ions, the corrections increase rapidly. But for monovalent electrolyte and zeta potentials smaller than 25 mv. the relaxation effect is small for any  $\kappa a$  and the corrections to Henry's equation never exceed 3%.

This small value of the relaxation effect justifies many an application of Henry's equation to proteins, for which the electrophoretic mobility often remains smaller than  $1 \mu \text{ cm. v.}^{-1} \text{ sec.}^{-1}$ , which is equivalent to a zeta potential smaller than 20 mv. at 25°C., or 35 mv. when the electrophoresis has been carried out at 0°.

Figure 6 shows the remarkable fact that, with unsymmetrical electrolytes, the relaxation effect may be accelerating instead of retarding if it is the ion bearing the same charge as the particle that is polyvalent.

## 2. Influence of Surface Conductance

It is to be expected that the double layer is a source of surface conductance and we should investigate in what respects surface conductance influences the electrophoretic mobility.

In 1903 Smoluchowski (62) pointed out that the net charge of the double layer results in a specific surface conductivity equal to (for small values of  $\zeta$ ):

$$\frac{1}{\eta d} \left( \frac{e\zeta}{4\pi} \right)^2$$

in which  $d$  is the thickness of the double layer. Moreover, the concentrations of ions in the double layer are different from those in the bulk of the liquid, and as the changes in concentrations for positive and negative ions are different, a second contribution to the surface conductance results. Both these effects are incorporated in the theory of relaxation and, therefore, no extra corrections are needed.

In several experiments, especially on glass-water interfaces (see Table III), however, surface conductivities have been measured which far exceed the values to be expected from the simple theory of the diffuse double layer. Just as, according to Henry's calculations, the mobility is decreased by a certain conductivity of the particle as a whole, an excessively large surface conductance would have the same effect, lowering the mobility of a spherical particle with a factor (11):

$$1 + \lambda_s/\lambda a$$

in which  $\lambda_s$  is the specific surface conductance and  $\lambda$  the bulk conductance of the liquid. However, as long as there are such wide divergencies in the experimental values as shown in Table III, any further discussion of this effect seems to be premature.

TABLE III

Specific Surface Conductivities (in  $10^{-9} \Omega^{-1}$ ) of Glass in Contact with Solutions of 0.0005 *N* Electrolytes

Reported by	KCl	KNO <sub>3</sub>	HCl	HNO <sub>3</sub>
McBain (45-47).....	95	—	—	—
White (68,75,76).....	2.2-4.3	—	—	—
Fricke (22).....	1	—	—	—
Rutgers (57,59).....	95	—	225	—
Wijga (77).....	—	8	—	50

Recently Booth (11a) and Henry (34a) independently discussed the influence of surface conductance on electrophoresis. They concluded that, especially with small particles, the electrophoretic velocity could be very much lower than that given by equation (6).

### ***3. Summary of Conditions in Which Zeta Potential Can Be Evaluated from Electrophoresis***

The practical consequence of the theoretical developments in this section is that in certain well-defined cases  $\zeta$  can be confidently evaluated from the electrophoretic mobility. They are:

(1) For any value of  $\kappa a$  if the  $\zeta$  potential is smaller than 25 mv. and the particle is spherical or nearly so. Application of Henry's equations is essential; the correction for relaxation can be calculated by the above theory or may be neglected if an inaccuracy of a few per cent is not essential.

(2) For large values of  $\kappa a$  and any value of  $\zeta$  irrespective of the form of the particle, by application of Smoluchowski's equation.

In both cases the particle should be an insulator or at least behave as such. There should be no excessive surface conductance. In analogy to the results obtained for spherical particles, it seems safe to assume that also for other forms of the particles (especially for cylinders for which the calculations of Henry and Gorin are available) the relaxation effect remains small in the two conditions mentioned above. In all other cases the quantitative evaluation of zeta potentials from electrophoresis has the element of great uncertainty.

#### 4. *Experimental Work*

Experiments allowing a quantitative test of the theory are unfortunately very scarce. Even the simple equations of Smoluchowski and Henry have never been really tested, and even a convincing test of the theory of the relaxation effect does not exist.

One of the reasons is that it is very difficult to determine zeta potential in an independent way. De Bruyn (19) has indicated an interesting method of determining the zeta potential by potentiometry which, as far as order of magnitude is concerned, confirms the values by electrokinetic methods. But a closer comparison of the two principles is still lacking.

Other electrokinetic phenomena, especially electro-osmosis and streaming potential, may be used to determine  $\zeta$ , but then the identity of the surfaces in the two types of experiments is hard, if not impossible, to insure.

The most satisfying results are obtained by a comparison of electro-osmosis and electrophoresis of relatively large particles covered with a layer of protein to insure identity of the surfaces. These experiments give ample confirmation of the reliability of the factor of proportionality in Smoluchowski's equation, that is, for the identity of the electro-osmotic and electrophoretic velocity for large  $\kappa a$  (4). In many of the experiments of this type the electrophoretic velocity was rather low ( $< 1 \mu\text{cm. v.}^{-1} \text{sec.}^{-1}$ ), so that the relaxation effect would be expected to be small anyway.

Mooney (48) did some experiments on the electrophoresis of oil drops of different diameter in which a lowering of the electrophoretic velocity with decreasing radius of the particles was established. Qualitatively this is in accord with equations (13) and (16). Quantitatively the effects of Mooney seem to be larger than the theoretical predictions. His experiments, however, are not so exact that they form a serious test of the theory. Moreover, the fact that they have been performed with emulsions may have caused complications (see Sect. II.5.)

For very small particles of  $\text{CuO}$ ,  $\text{Fe}_2\text{O}_3$ , and  $\text{As}_2\text{S}_3$  sols at very low elec-

trolyte concentrations ( $\kappa a < 1/10$ ), Paine found a linear dependence of the mobility from  $\kappa$ , which is in accord with the applicability of the theory of Debye and Hückel if the charge of the particles is assumed to be constant. The slope of the  $u$  versus  $\kappa$  line determines the value of the radius of the particles, which seemed to be of the right order of magnitude, but has not been determined independently.

In view, however, of the arguments given in the beginning of the next section (see also (73)), it is rather doubtful whether in this case the charge is really independent of  $\kappa$ , so that the arguments of Paine cannot be considered to be decisive.

Other experimental data will be treated at the end of Section IV.

Finally it may be mentioned that the maxima often found in electrophoretic mobility as a function of the concentration of the electrolyte may perhaps be explained as an increase of the relaxation effect on the low-concentration side of the maximum and a real decrease of  $\zeta$  at the other side. The fact that those maxima are usually found in colloids with relatively large particles, where the "pure sols" may have a value of  $\kappa a$  of the order of 1–10, corroborates this explanation. In principle the same explanation has already been given by Bikerman (8,9).

## IV. Electrophoretic Velocity and Charge of Particles

### 1. Charge and Potential

In the foregoing sections attention has been concentrated on the evaluation of the zeta potential. The charge of the particles necessary to generate this potential has been treated as a magnitude of only secondary importance. This point of view seems entirely justified in the case of hydrophobic suspensions, emulsions and the like because, in all probability, their surface potential is much more characteristic than the surface charge. Indeed, if the particle is considered to be in thermodynamic equilibrium with the surrounding liquid, its potential is completely determined by the distribution of certain ions, which are present in both phases (38,43). Consider, as an example, a particle of a silver halide in contact with its saturated solution, which may contain an excess of the silver or halide ions and, in addition, any amount of other electrolytes. Then for equilibrium the chemical potential  $\mu_{Ag^+}$  of the silver ions must have the same value in both phases. In the solid phase the chemical potential depends only upon the characteristic structure of the solid and upon its potential:

$$\mu_I = \mu_I^0 + e\psi_I$$

where the index I designates the silver halide phase. In the solution

$\mu_{II}$  depends on the potential of the liquid and moreover on the ionic activity:

$$\mu_{II} = \mu_{II}^0 + e\psi_{II} + kT \ln a_{Ag}$$

In equilibrium,  $\mu_I = \mu_{II}$ , or

$$e(\psi_I - \psi_{II}) = \mu_{II}^0 - \mu_I^0 + kT \ln a_{Ag} \quad (19)$$

which means, that if the activity of the silver ions in the solution (the potential-determining ions) is given (43), the potential difference between the two phases is fixed, whereas the charge density on the surface may still vary widely dependent on the thickness of the double layer.

On the other hand the situation changes completely if, instead of considering particles of hydrophobic sols, we turn our attention to the electrophoresis of large molecules like proteins. Here the whole concept of zeta potential loses much of its attraction, and, on the contrary, the charge of the molecule seems a more fundamental characteristic.

In regard to the electrophoresis of proteins the foregoing sections do not lose their interest. In fact, in this case there is an additional problem. If the zeta potential has been evaluated from electrophoretic data, it must be converted into a value for the charge of the particles. And apart from other complications still to be mentioned, evaluating the charge of the particles is essentially more difficult than evaluating the zeta potential. In the case of the zeta potential, the value of the radius of the particles enters into the calculations (see Figs. 1, 4, 5, and 6) as a correction factor, which only changes logarithmically with the dimensions of the particles. For a given zeta potential, however, the particle charge is proportional to the radius (small  $\kappa a$ ) or the surface (large  $\kappa a$ ) of the particle. Consequently the charge is very sensitive to the right choice of the radius and it is by no means easy to determine this radius or an equivalent radius, if the particle is known to be nonspherical.

A second difficulty in interpreting electrophoresis in terms of charge is based upon the fact that in principle an electrokinetic experiment is only informative on the charge of the particles within the surface of shear. This charge, however, is not necessarily identical with the total charge of the particle, just as in general the zeta potential is not always identical with the total potential drop between the particle and the bulk of the liquid. Part of the counterions may be present within the surface of shear, thereby reducing the electrophoretic charge below the charge as determined analytically for example, by titration. This effect may be expected to be especially large in high concentrations of electrolyte, where the double layer is very much compressed. In very dilute solutions, on the

contrary, the double layer is so extended that only a negligible part of its charge is present near the surface of the particles and thus might be included within the surface of shear.

## 2. Spherical Particles

If, for a moment, we leave the above-mentioned difficulties, it is possible to formulate a relation between charge and zeta potential, or between charge and electrophoretic mobility.

For a spherical particle of radius  $a$ , the charge  $Q$  can be simply expressed by noting that it is equal to the opposite of the total charge of the diffuse double layer:

$$\begin{aligned} Q &= - \int_a^\infty \rho \cdot 4\pi r^2 dr = \int_a^\infty \frac{\epsilon}{4\pi} \cdot \frac{1}{r^2} \frac{d}{dr} \left( r^2 \frac{d\psi}{dr} \right) \cdot 4\pi r^2 dr \\ &= - \epsilon a^2 \left( \frac{d\psi}{dr} \right)_{r=a} \end{aligned} \quad (20)$$

Applying the approximative equation of Debye and Hückel for the potential in the double layer:

$$\psi = \zeta \cdot a \cdot e^{\kappa(a-r)} / r \quad (21)$$

which is allowed when the zeta potential is small,  $d\psi/dr$  in equation (20) may be transformed into:

$$\left( \frac{d\psi}{dr} \right)_{r=a} = - \frac{\zeta}{a} (1 + \kappa a) \quad (22)$$

leading for the charge to:

$$Q = \epsilon \zeta a (1 + \kappa a) \quad (23)$$

For large particles the charge density,  $\sigma$ , may be important:

$$\sigma = \frac{\epsilon \zeta}{4\pi a} (1 + \kappa a) \quad (24)$$

which for very large values of  $a$  transforms to the equation for the charge density of flat surfaces:

$$\sigma = \frac{\epsilon \zeta \kappa}{4\pi} \quad (25)$$

Two important corrections to equation (23) have to be considered. The first one concerns the case in which  $\zeta$  is not small, so that the approximation of Debye and Hückel:

$$\Delta\psi = \kappa^2\psi$$

must be replaced by the complete equation:

$$\Delta\psi = \kappa^2 \frac{kT}{e(z_+ + z_-)} (e^{z_- e\psi/kT} - e^{-z_+ e\psi/kT}) \quad (26)$$

Unfortunately equation (26) cannot be integrated for a case of spherical symmetry. Müller (49) has given numerical integrations for a number of values of  $\kappa a$  and  $\zeta$  from which the relation between charge and potential can be derived. Gronwall, LaMer, and Sandved (30) and LaMer, Gronwall, and Greiff (42) have solved equation (26) in a series of ascending powers of the charge of the central particle. Numerical values of the coefficients of the first to fifth (symmetric electrolytes) or third (unsymmetric electrolytes) power of the charge are available from their work.

Gorin (24) also applied the work of Gronwall, LaMer, and Sandved to find the correction for larger  $\zeta$  potentials but his equation in the original paper as well as in the book by Abramson, Gorin, and Moyer (4), is inconsistent, as it contains a sum of two quantities of which one has a zero dimension and the other the dimension of velocity.

In Table IV some values of the quantity  $f$  are given, this being the quotient of the charge calculated according to Müller's or LaMer's method (which lead to practically identical results) to the charge calculated in accordance with the approximate equation (23).

In Müller's terminology factor  $f$  is given by:

$$f = \frac{\varphi'(y)}{\varphi(y)} \cdot \frac{y}{1 + \frac{1}{y} \left( \frac{\sum c_i z_i^2}{\sum c_i} \right)^{1/2}}$$

Gronwall, LaMer, and Sandved give the following relation between the  $\zeta$  potential and charge  $Q$ :

$$\zeta = \sum_{m=1}^{\infty} \left( \frac{Q}{ea} \right)^m \left( -\frac{e}{kT} \right)^{m-1} \cdot \psi_m(\kappa a) \quad (27)$$

in which:

$$\begin{aligned} \psi_1(x) &= \frac{1}{1+x} \\ \psi_2(x) &= \frac{c_+ z_+^3 - c_- z_-^3}{c_+ z_+^2 - c_- z_-^2} X_2(x) \\ \psi_3(x) &= \left( \frac{c_+ z_+^3 - c_- z_-^3}{c_+ z_+^2 + c_- z_-^2} \right)^2 X_3^*(x) + \frac{c_+ z_+^4 + c_- z_-^4}{c_+ z_+^2 + c_- z_-^2} X_3(x) \\ \psi_3(x) &= z^4 X_3(x), \text{ for symmetrical electrolytes only.} \end{aligned}$$



The functions  $X(x)$  are available in tabular form (30,42). Correction factor  $f$  now becomes:

$$f = Q(\text{Eq. 27})/Q(\text{Eq. 23})$$

Unfortunately the calculations of Müller and Gronwall *et al.* extend only to relatively small values of  $\kappa a$ . For very large values of  $\kappa a$  the relation between charge and potential can be approximated by the unidimensional case of equation (26), which can be solved exactly, leading to equation (28) for charge density  $\sigma$ , and equation (29) for  $f$ .

$$\sigma = \frac{\epsilon \kappa}{4\pi} \frac{kT}{e} (2)^{1/2} \left( \frac{\exp(z_- e\zeta/kT) - 1}{z_- (z_+ + z_-)} + \frac{\exp(-z_+ e\zeta/kT) - 1}{z_+ (z_+ + z_-)} \right)^{1/2} \quad (28)$$

$$f = \frac{kT}{e\zeta} (2)^{1/2} \left( \frac{\exp(z_- e\zeta/kT) - 1}{z_- (z_+ + z_-)} + \frac{\exp(-z_+ e\zeta/kT) - 1}{z_+ (z_+ + z_-)} \right)^{1/2} \quad (29)$$

It is seen in Table IV that the corrections increase with increasing  $\kappa a$ , increasing zeta potential, and increasing valency of the counterions. For  $e\zeta/kT < 1$ , that is, for zeta potentials smaller than 25 mv., and for monovalent electrolytes, the corrections remain under 5%.

TABLE IV

$f = Q_{\text{exact}}/Q_{\text{approx}}$  for Different Values of  $\kappa a$  and  $\zeta$   
For a Sphere with Radius  $a$  Å., the Charge  $Q_{\text{exact}}$  is Equal to  
 $0.1395 a(1 + \kappa a) (e\zeta/kT)f$  at 25°C.

$\kappa a$ values	$e\zeta/kT$			
	0	1	2	3
1-1 electrolyte				
$\kappa a = 0$	1	1	1	1
0.3	1	1.004	1.019	1.048
0.6	1	1.010	1.041	1.107
1.0	1	1.015	1.063	1.14
2.0	1	1.023	1.13	*
3.0	1	1.029	1.17 <sup>b</sup>	*
$\infty$	1	1.042	1.17 <sub>4</sub>	1.42
2-1 electrolyte				
$\kappa a = 0$	1	1	1	1
0.2	1	1.022	1.064	1.146
0.4	1	1.05	1.19	1.7
0.7	1	1.09	1.4	*
1.0	1	1.12	*	*
$\infty$	1	1.30 <sub>7</sub>	2.079	3.88

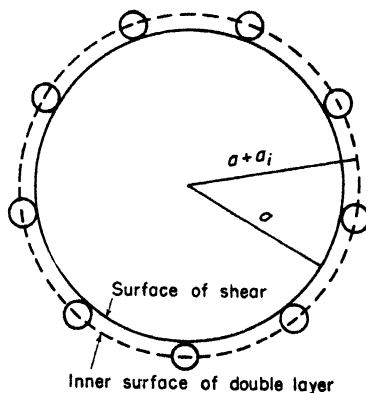
\* No data available.

One might doubt whether it is consistent to use these data for the charge at high potentials when the zeta potential is calculated from an

electrophoresis equation like Henry's or Overbeek's, which are only valid for low potentials. The answer is that Henry's equation is not very sensitive to the exact course of the potential curve. Higher potentials act as if the double layer were more compressed, as if  $\kappa a$  were somewhat larger. In the equations of Overbeek, more terms of the development of equation (26) have been included in the correction terms so that Table IV may indeed be directly combined with the zeta potential as calculated from electrophoresis.

Another correction of equation (23) of a somewhat more speculative character has been given by Gorin (25). In all developments given up to this point, the electrolytic ions have been considered to be point charges,

Fig. 7. Spherical particle with counterions showing the difference between surface of shear and limiting surface of the charge of the double layer.



which can approach the surface of the particles to infinitesimally small distances. In 1923 Stern (64), in his theory of the electrocapillary curve, indicated how a correction for the finite dimensions of the ions could be applied. In the same paper he took account of a specific adsorption potential for the ions of the double layer and of the fact that for the ions, which are very near to the surface, the dielectric constant is much lower than that in the bulk of the solution. Gorin applied a similar idea to the interpretation of electrophoresis, using, however, a much simpler theory than that of Stern, in which he took account only of the finite dimensions of the ions, leaving aside the other corrections introduced by Stern.

In Figure 7 a spherical particle has been sketched, surrounded by a number of counterions at the distance of closest approach. The ions of the diffuse part of the double layer have not been indicated in the figure. The surface of shear is formed by a sphere of radius  $a$  (to be determined, for example, from diffusion experiments). The charge of the double layer is

located between the radii  $(a + a_i)$  and  $\infty$ ; the shell between  $a$  and  $(a + a_i)$  is free of charge.

With this picture the relation between charge and potential is easily found and turns out to be:

$$Q = \epsilon \zeta a \left[ \frac{1 + \kappa(a + a_i)}{1 + \kappa a_i} \right] \quad (30)$$

in which  $Q$  is the total charge enclosed within the surface of shear and  $\zeta$  the potential at that surface.

Compared with equation (23), this new equation gives a correction factor in the charge equal to:

$$f = \frac{1 + \kappa(a + a_i)}{(1 + \kappa a)(1 + \kappa a_i)} \quad (31)$$

Assuming for  $a_i$  a value of 2.5 Å. and for  $a$ , alternatively, 25 Å. (for example, a protein molecule with a molecular weight of the order of 40,000) and  $\infty$  (flat surface), the correction factor has been tabulated for different values of the ionic strength in Table V. The influence of the finite dimensions of the ions is seen to result always in a decrease of the charge (the more pronounced, the higher the ionic concentrations). In contrast to the correction mentioned in Table IV the influence of the ionic dimensions is independent of the zeta potential and should be taken into account even for very weakly charged particles.

TABLE V

Correction Factors ( $f = Q_{\text{exact}}/Q_{\text{approx}}$ ) for an Ionic Radius of 2.5 Å.

$\omega = \frac{1}{2} \sum c_i z_i^2$	$\kappa a_i$	$f$ for $a = 25 \text{ Å.}$	$f$ for $a = \infty$
0.00001	0.00259	0.99994	0.9974
0.0001	0.00819	0.9994	0.992
0.001	0.0259	0.995	0.975
0.005	0.0579	0.980	0.945
0.01	0.0819	0.966	0.924
0.02	0.1159	0.944	0.896
0.05	0.1831	0.899	0.846
0.1	0.2592	0.851	0.794
0.2	0.3662	0.789	0.732

Combination of equation (30) or (31) with an electrophoretic equation like Henry's, which has been derived without taking account of the dimensions of the ions, is nevertheless allowed because closer inspection shows that by Gorin's correction not only has the value of  $\zeta$  for a given

charge been increased by a factor  $1/f$ , but the potential at any point of the double layer has been increased in the same proportion (provided that  $\kappa a_1 \ll 1$ ).

A difficulty in the application of equation (30) is the choice of radius  $a_i$ . There is no accord in the literature on the values of radii of hydrated ions (which should be used here), and even if the particle as a whole is spherical its surface will certainly contain local hills and valleys of atomic dimensions, and by going into the valleys the counterions can approach the average surface of shear at a shorter distance than would follow from their radii.

So probably the best thing to do at the moment is to consider the ionic radii  $a_i$  as an additional parameter whose value must be determined by experiments and cannot be predicted without a far greater knowledge than we now have on the constitution and interaction of surfaces of particles in electrophoresis.

### 3. *Nonspherical Particles*

In practice it will seldom occur, except in the case of emulsions, that the particles are exactly spherical. Unfortunately there are no theoretical investigations on the electrophoresis of ellipsoids of a moderate ratio (say 1:2 or 1:3) of the long and short axis. The only nonspherical forms on which data are available are a flat surface and infinitely long cylinders, as has been mentioned in Section III. The best way of handling nonspherical particles now is to assume that electrophoresis may be represented as that of cylinders of finite length, neglecting the end effects. The degree of validity of this approximation, however, is difficult to estimate.

The additional problem of evaluating the charge of the cylinder when the zeta potential is known has been solved by Gorin (27). Applying the approximation of Debye and Hückel, the charge  $Q$  of a cylinder of length  $l$  and radius  $a$  is given by:

$$Q = e\zeta \left( \frac{1}{2}l + a \right) \kappa a \frac{K_1(\kappa a)}{K_0(\kappa a)} \quad (32)$$

in which  $K_0$  and  $K_1$  are Bessel functions for which tables are available.

For very large particles, the situation is more favorable. The zeta potential can be found, as treated in Section III from Smoluchowski's equation (6), and the charge density on the surface by application of the equation for flat surfaces (Eqs. 25 and 28). These equations may be useful in the interpretation of the electrophoresis of microscopic particles, which may or may not be covered with a layer of proteins.

For particles that are very small compared to the extension of the double layer again the problem is simpler. Irrespective of the form of the particles, the symmetry of the double layer is practically spherical and all our developments for spherical particles may be applied. The equivalent radius of the particle necessary to estimate the charge according to equation (23) may be taken from diffusion data. Unfortunately, measurements on small particles in dilute solutions where the charge of the particles is known from another, independent, method are very rare. The moving boundary technique of Burton, as modified and ameliorated by Tiselius, and which is especially adapted to small particles like protein molecules, is unsuitable for measurements in systems containing little or no electrolyte. The microscope method, on the other hand, which is easiest to handle in solutions of low conductivity, is restricted by the demand of visibility in the microscope or ultramicroscope to comparatively large particle dimensions. It would certainly be of interest to investigate protein systems, nearly free of electrolyte by the Hittorf method of determining electrophoretic mobility.

#### *4. Applications*

The application of the relation between charge and zeta potential to "inert" surfaces by Abramson and Müller (3) is very well known. They find that for these surfaces (oil, graphite,  $\text{SiO}_2$ , etc.) the charge as a function of the electrolyte concentration can be represented by a curve resembling very much an adsorption isotherm. Although the accuracy of the  $\zeta$  values at the lower concentrations may be open to doubt (8,9), the fact that the charge of the surface increases with increasing concentration of electrolyte has been established by independent means. De Bruyn (19) and Kruyt and Klompé (40) found, by analytical determinations, that the addition of any electrolyte produced an increase of the charge of silver iodide. This fact, however, should not be interpreted as a specific adsorption of one of the added ions. As soon as ionic equilibria between the liquid and the material of the suspended particles are possible, the potential difference between surface and liquid is fixed (see Sect. III). The zeta potential will be a more or less accurate image of this potential difference, and the increase of the charge can be explained by the decreased thickness of the double layer, more charge being necessary to produce the same potential drop over a shorter distance.

In a very accurate investigation of the zeta potential of glass, Rutgers (58) too finds that  $\zeta$  can be very well interpreted as the potential of an ex-

change electrode, the charge density being a variable of only secondary importance, which adapts itself to the potential and thickness of the double layer.

In the case of proteins, interpretation of electrophoresis in terms of charge seems more promising because, in this case, the electrophoretic charge can be compared to the analytical charge as determined by titration.

The electrophoretic data on proteins (and other hydrophilic colloids) fall in two categories: the mobility of the free protein molecules can be determined; on the other hand, the mobility of inert particles covered by adsorption with protein can be measured.

*A priori* one would not expect a simple relation to exist between the mobilities of free and adsorbed protein, because the mobility of the adsorbed protein should depend upon the area covered by one molecule and upon the dissociation properties in the adsorbed form, which might be different from that of the free protein. Even if one assumes that the spreading area is such that—at the same pH—the charge densities (or the zeta potentials) of free and of adsorbed protein are identical, the mobility of the free protein should be considerably lower than that of the adsorbed one, because  $\kappa a$  for the free protein is comparatively small and the Henry correction important.

Nevertheless, in many cases, the two mobilities are nearly identical, a fact that has been pointed out by Abramson (1,2,4) on several occasions. Even if by adsorption a shift of the isoelectric point is found, as is the case for egg albumin, the slope of the  $u$  versus pH curve is the same in both cases. Abramson (2) expressed this curious fact in a very pregnant way by implying that “on adsorption certain proteins take  $\kappa a$  with them.”

A satisfactory explanation of this fact has not been given. A supposition compatible with these experiments is that the form of the free protein molecule is not at all spherical, but more like a flat disk in which the polypeptide chains are parallel to the surface of the disk, the hydrophobic side chains being turned to the interior and the hydrophilic ones to the outside. In adsorption the protein should unfold, so that the hydrophobic chains are attached to the adsorbent, the hydrophilic chains being turned to the water. This supposition would imply that the free protein molecule would have a surface of low curvature and behave more or less like a flat surface with  $\kappa a \rightarrow \infty$ . A test of this supposition would be formed by a comparison of the electrophoretic mobility of the adsorbed and the free form at very low ionic strength, where the double layer around the free protein would be

nearly spherical, thereby depressing the mobility as compared to that of the adsorbed form.

### ***5. Comparison of Electrophoretic Charge with Charge Determined by Other Means***

Apart from the calculation of the charge from electrophoresis, in the case of proteins, at least, two other methods can be used to determine the charge.

The most straightforward method is the determination of the charge from titration data. The titration curve of a protein gives us the number of hydrogen ions taken up or given off by a protein molecule in given circumstances of pH and ionic strength. With each hydrogen ion taken up, the charge increases by  $4.8 \times 10^{-10} \text{e.s.u.}$

Another method has been worked out by Adair and Adair (5). It consists in the calculation of the charge from Donnan equilibria. Although in principle this method looks very attractive because it should include the influence of ions other than  $\text{H}^+$  ions, it should not be forgotten that especially in more concentrated solutions the interpretation of Donnan equilibria entails corrections for activity coefficients, which are difficult to estimate exactly.

Tiselius and Svensson (67) determined the electrophoretic velocity of egg albumin at a constant pH of 7.10 but different values of the ionic strength and calculated the charge by application of Henry's equation combined with our equation (23), assuming  $a = 27.5 \text{ \AA.}$  as the radius of the molecule.

Table VI shows a comparison of the charge thus calculated from electrophoresis and as determined by Adair and Adair from membrane potentials. The agreement is very satisfactory.

A direct comparison of these data with other titration data cannot be given because the titrations, *e.g.*, those of Cannan, Kibrick, and Palmer (16), were made in sodium chloride solutions, whereas the data of Tiselius and Adair are for phosphate buffers. The last column of Table VI gives the charge as determined by titration data. The titration curves have been shifted, so that they pass through the electrophoretic isoelectric point. At low values of the ionic strength, the agreement among the three methods is good, but, at higher values of the ionic strength, the charge as determined by titration is markedly higher than that by the other two methods.

This difference between electrophoresis charge and charge by titration is still more pronounced in an investigation by Longsworth (44). He compared titration data and electrophoresis of egg albumin over a wide range

TABLE VI

Comparison of the Charge of a Molecule of Egg Albumin at pH 7.10 Expressed in the Number of Elementary Charges by Three Different Methods

Ionic strength	$\mu \times 10^4$	$\kappa a$	$Q$ from electrophoresis	$Q$ from membrane potentials	$Q$ from titration curves
0.01	1.16	0.88	12	12	13.8
0.02	(1.00)	1.24	12.4	12.6	14.7
0.05	0.760	1.95	12	13.1	16.0
0.10	0.670	2.75	13.2	13.8	17.0
0.20	0.570	3.9	14.1	15.1	19.1

of pH using only buffers with monovalent ions and, although a beautiful parallelism exists between the two sets of data, the electrophoresis charge is only 60% of the charge by titration (see Fig. 8).

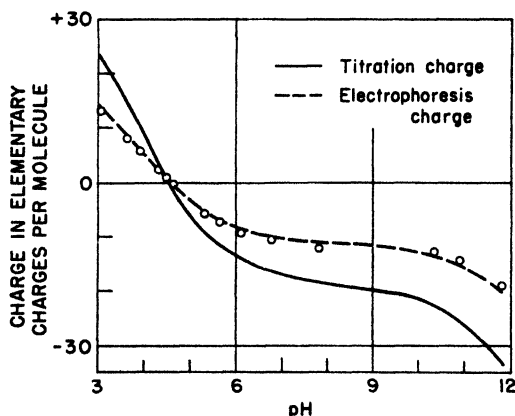


Fig. 8. Charge by titration and electrophoresis charge of egg albumin (44). The broken curve is found from the continuous curve by multiplying the ordinates by 0.60. Ionic strength = 0.1.

In Figure 8 the electrophoresis charge has been calculated using Henry's equation and our equation (23). If the relaxation effect and the correction for large potentials (see Table IV) are taken into account, the electrophoresis charge is increased by less than 5%. Introduction of the Gorin correction for the finite dimension of the ions (Table V) gives a decrease of the charge by some 15%, whereas if the particles are considered to be cylindrical rods instead of spheres the charge is increased by about 20% (4, p. 154). Neither correction is sufficiently large to reconcile the difference between the two sets of data.



The larger difference as compared to the data of Tiselius and Svensson must be ascribed to their use of phosphate buffers, which apparently increase the electrophoretic mobility substantially. This difference cannot be ascribed to the influence of the relaxation effect, which in the circumstances used here is never larger than 1 or 2%. A specific adsorption of phosphate ions seems the more plausible explanation (83).

A similar comparison between the titration curves and the electrophoretic mobility at an ionic strength of 0.02 has been made by Cannan, Palmer, and Kibrick (17). Here again the charge by titration is about 20% higher than the electrophoresis charge and the difference cannot be accounted for by the correction factors of Tables IV and V, nor by the relaxation effect. Gorin and Moyer (28) mention that by their theory they find a quantitative accord between the two sets of data. It is not clear, however, whether they mean the introduction of the assumption that the particle is not spherical but more nearly cylindrical, or their theory that the binding of hydrogen ion is independent of the ionic strength (see below). Both assumptions would be expected to bring the two data nearer to each other.

For serum albumin B the situation is similar to that of egg albumin. Mobility data of Keckwick (37) and Gorin and Moyer (28) can be compared to titration data of Gorin and Moyer (28). For small values of the ionic strength, the agreement between charge by titration and electrophoresis charge is satisfactory. At higher concentrations of electrolyte (ionic strength 0.02 and 0.1), the charge by titration is markedly higher than the electrophoresis charge.

The difference between charge by titration and electrophoresis charge has been interpreted in two different ways. Cannan, Kibrick, and Palmer (16), and Longworth (44) assume that the titration curves give essential information on the hydrogen ion bound to or released by the protein. At higher ionic concentration, however, an important absorption of counterions exists which diminishes the electrophoresis charge. Gorin and Moyer (28), on the contrary, assume that the binding of hydrogen ion is essentially independent of ionic strength, so that at any ionic strength mobility data form a direct measure of hydrogen binding. But the charge by titration is apparently too large, because not only  $H^+$  ions but also undissociated molecules of acid or base are bound to the protein. This assumption seems a bit artificial, especially since the difference in titration curves at different values of the ionic strength can be explained by the electrostatic interaction of the charges on the protein. This interaction is diminished at high ionic strength due to the screening effect of the double layer.

The binding of counterions assumed by Longworth and Cannan need not necessarily be ascribed to specific interaction. It seems possible that

at high ionic strength a part of the counterions is present within the surface of shear (which also contains a certain amount of water of hydration), and by a simple steric effect diminishes the electrophoresis charge.

It cannot, however, be denied that, in the cases mentioned above, which are the only ones forming a real quantitative test of the theory of electrophoresis, the situation is still far from satisfactory. It may be hoped that a better insight in the adsorption of ions other than  $H^+$  and a more accurate knowledge of the form of the proteins will bring about a more complete accord between theory and experiments.

## 6. General Conclusions

Since the influence of the relaxation effect has been included in the theory of electrophoresis, the basis for estimating the zeta potential from electrophoretic mobility seems rather sound.

There are, of course, still additional developments to be desired, essentially:

- (1) An extension of the calculation of the relaxation effect to higher values of  $\zeta$ .
- (2) A theory of electrophoresis for particles of other forms especially for ellipsoidal particles and for randomly kinked long chains.
- (3) A well-founded explanation of the equality of electrophoretic mobility of free and adsorbed proteins.

The relation between the charge and the zeta potential, although in principle much easier to formulate than the relation between  $\mu$  and  $\zeta$ , gives rise to serious difficulties in application, because either the form and dimensions of the particles are not known with sufficient accuracy, or because there really is an essential difference between the electrophoretic and the analytical charge as a consequence of the adsorption of other than hydrogen ions.

The author wants to emphasize a remark made by Booth (11)—that what is most needed in the present state of the theory are better experimental data to compare with the theory. Especially useful information could be derived from:

- (1) Comparisons between electrophoretic and electro-osmotic mobilities of identical surfaces especially at high  $\zeta$  potentials and low values of the ionic strength.
- (2) Comparisons between the electrophoresis of free and adsorbed proteins at low values of ionic strength.
- (3) More data on titration and electrophoresis of the same object, again at low ionic strength.

## References

1. Abramson, H. A., *Electrokinetic Phenomena and Their Application to Biology and Medicine*. Chemical Catalog Co., New York, 1934.
2. Abramson, H. A., *J. Gen. Physiol.*, **15**, 575 (1932); see also ref. 4 below, p. 82.
3. Abramson, H. A., and Mueller, H., *Phys. Rev.*, **41**, 386 (1932); *Cold Spring Harbor Symposia Quant. Biol.*, **1**, (1933).
4. Abramson, H. A., Moyer, L. S., and Gorin, M. H., *Electrophoresis of Proteins*. Reinhold, New York, 1942.
5. Adair, G. S., and Adair, M. E., *Biochem. J.*, **38**, 199, 1230 (1934); *Trans. Faraday Soc.*, **36**, 23 (1940).
6. Bennewitz, K., Wagner, C., and Küchler, K., *Physik. Z.*, **30**, 623 (1929).
7. Bikerman, J. J., *J. Chem. Phys.*, **9**, 880 (1941); *J. Phys. Chem.*, **46**, 724 (1942).
8. Bikerman, J. J., *Z. physik. Chem.*, **A171**, 209 (1934).
9. Bikerman, J. J., *Trans. Faraday Soc.*, **36**, 154 (1940).
10. Bond, W. N., *Phil. Mag.*, **4**, 889 (1927).
11. Booth, F., *Nature*, **161**, 83 (1948) and a series of papers announced there.
- 11a. Booth, F., *Trans. Faraday Soc.*, **44**, 955 (1948).
12. Bull, H. B., and Gortner, R. A., *Physics*, **2**, 21 (1932).
13. Bull, H. B., and Söllner, K., *Kolloid-Z.*, **60**, 263 (1932).
14. Bungenberg De Jong, H. G., in H. R. Kruyt, ed., *Colloid Science*. Vol. II, Elsevier, Amsterdam, 1949.
15. Burton, E. F., *Phil. Mag.*, **11**, 425; **12**, 472 (1906).
16. Cannan, R. K., Kibrick, A., and Palmer, A. H., *Ann. N. Y. Acad. Sci.*, **41**, 243 (1941).
17. Cannan, R. K., Palmer, A. H., and Kibrick, A., *J. Biol. Chem.*, **142**, 803 (1942).
18. Chapman, D. L., *Phil. Mag.*, **25**, 475 (1913).
19. de Bruyn, H., *Rec. trav. chim.*, **61**, 21, 193 (1942).
20. Debye, P., and Hückel, E., *Physik. Z.*, **24**, 185, 305 (1923).
21. Debye, P., and Hückel, E., *ibid.*, **25**, 49 (1924).
22. Fricke, H., and Curtiss, H. J., *J. Phys. Chem.*, **40**, 715 (1936).
23. Frumkin, A., *J. Colloid Sci.*, **1**, 227 (1946).
24. Gorin, M. H., *J. Phys. Chem.*, **45**, 371 (1941).
25. Gorin, M. H., *J. Chem. Phys.*, **7**, 405 (1939).
26. Gorin, M. H., in Abramson, H. A., Gorin, M. H., and Moyer, L. S., *Chem. Revs.*, **24**, 364 (1939).
27. Gorin, M. H., in Abramson, H. A., Moyer, L. S., and Gorin, M. H., *Electrophoresis of Proteins*. Reinhold, New York, 1942, p. 126.
28. Gorin, M. H., and Moyer, L. S., *Electrophoresis of Proteins*, p. 158.
29. Gouy, G., *J. phys. radium*, **9**, 457 (1910); *Ann. phys.*, **7**, 129 (1917).
30. Gronwall, T. H., LaMer, V. K., and Sandved, K., *Physik. Z.*, **29**, 358 (1928).
31. Guggenheim, E. A., *Trans. Faraday Soc.*, **36**, 139 (1940).
32. Hardy, W. D., *Z. physik. Chem.*, **33**, 385 (1900).
33. Helmholtz, H., *Ann. Physik*, **7**, 337 (1879).
34. Henry, D. C., *Proc. Soc. London*, **A133**, 106 (1931).
- 34a. Henry, D. C., *Trans. Faraday Soc.*, **44**, 1021 (1948).
35. Hermans, J. J., *Phil. Mag.*, **26**, 650 (1938).
36. Hückel, E., *Physik. Z.*, **25**, 204 (1924).
37. Keckwick, R. A., *Biochem. J.*, **32**, 552 (1938).

38. Kellermann, A., and Lange, E., *Kolloid-Z.*, **88**, 341 (1939).
39. Komagata, S., *Researches Electrotech. Lab. Tokyo*, No. **387** (1935).
40. Kruyt, H. R., and Klompé, M. A. M., *Kolloid-Beihefte*, **54**, 484 (1943).
41. Lamb, H., *Phil. Mag.*, **25**, 52 (1888).
42. LaMer, V. K., Gronwall, T. H., and Greiff, L. J., *J. Phys. Chem.*, **35**, 2245 (1931).
43. Lange, E., *Handbuch der Experimental Physik*, Vol. XII, Part 2, p. 265, Akadem. Verlagsgesellschaft, Leipzig, 1933. See also Nernst, W., *Z. physik. Chem.*, **9**, 140 (1892); Haber, F., and Beutner, *Ann. Physik*, **26**, 947 (1908).
44. Longworth, L. G., *Ann. N. Y. Acad. Sci.*, **41**, 267 (1941).
45. McBain, J. W., Peaker, C. R., and King, A. M., *J. Am. Chem. Soc.*, **51**, 3294 (1929).
46. McBain, J. W., and Peaker, C. R., *J. Phys. Chem.*, **34**, 1033 (1930).
47. McBain, J. W., and Foster, J. F., *ibid.*, **39**, 331 (1935).
48. Mooney, M., *ibid.*, **35**, 331 (1931).
49. Müller, H., *Kolloid-Beihefte*, **26**, 257 (1928).
50. Onsager, L., *Physik. Z.*, **27**, 388 (1926); **28**, 277 (1928).
51. Overbeek, J. Th. G., *Philips Research Repts.*, **1**, 315 (1946).
52. Overbeek, J. Th. G., *Doctoral Thesis*, Utrecht, 1941.
53. Overbeek, J. Th. G., *Kolloid-Beihefte*, **54**, 287 (1943).
54. Paine, H. H., *Trans. Faraday Soc.*, **24**, 412 (1928); *Proc. Cambridge Phil. Soc.*, **28**, 83 (1931).
55. Powis, F., *Z. physik. Chem.*, **89**, 186 (1915).
56. Quincke, G., *Poggendorf's Ann.*, **113**, 513 (1861).
57. Rutgers, A. J., *Trans. Faraday Soc.*, **36**, 69 (1940).
58. Rutgers, A. J., and De Smet, M., *ibid.*, **41**, 758 (1945).
59. Rutgers, A. J., Verlende, E., and Moorkens, M., *Proc. Acad. Sci. Amsterdam*, **41**, 763 (1938).
60. Rybczyński, W., *Bull. acad. sci. Cracovie, A*, **1911**, 40.
61. Smoluchowski, M., *Graetz Handbuch der Elektrizität und des Magnetismus*, Vol. II, 366, 1914.
62. Smoluchowski, M., *Bull. acad. sci. Cracovie*, **1903**, 182.
63. Steinhardt, J., *Ann. N. Y. Acad. Sci.*, **41**, 287 (1941).
64. Stern, O., *Z. Elektrochem.*, **30**, 508 (1924).
65. Tiselius, A., *Nova Acta Soc. Sci., Upsaliensis, Ser. IV*, **7**, No. 4 (1930).
66. Tiselius, A., *Trans. Faraday Soc.*, **33**, 524 (1937).
67. Tiselius, A., and Svensson, H., *ibid.*, **36**, 16 (1940).
68. Urban, F., Feldman, S., and White, H. L., *J. Phys. Chem.*, **39**, 605 (1935).
69. Verwey, E. J. W., *Doctoral Thesis*, Utrecht, 1934, p. 69.
70. Verwey, E. J. W., *Trans. Faraday Soc.*, **36**, 192 (1940).
71. Verwey, E. J. W., *Philips Research Repts.*, **1**, 33 (1946).
72. Verwey, E. J. W., and Niessen, K. F., *Phil. Mag.*, **28**, 435 (1939).
73. Verwey, E. J. W., and Overbeek, J. Th. G., *Theory of the Stability of Lyophobic Colloids*. Elsevier, Amsterdam, 1948.
74. Verwey, E. J. W., and Overbeek, J. Th. G., *Trans. Faraday Soc.*, **B42**, 117 (1946).
75. White, H. L., Monaghan, B., and Urban, F., *J. Phys. Chem.*, **40**, 207 (1936).
76. White, H. L., Urban, F., and Van Atta, E. A., *ibid.*, **36**, 3152 (1932).
77. Wijga, P. W. O., *Doctoral Thesis*, Utrecht, 1946.



# LYOGELS

E. A. HAUSER

*Massachusetts Institute of Technology and Worcester Polytechnic Institute*

AND

D. S. LE BEAU

*Midwest Rubber Reclaiming Company*

---

I. Introduction.....	137
II. Older Theories of Lyogel Structure.....	139
III. Modern Theories of Lyogel Structure.....	139
IV. Special Types of Lyogels.....	143
1. Thixotropy.....	144
2. Rheopexy.....	145
3. Dilatancy.....	146
V. Elasticity of Lyogels.....	147
1. X-Ray Diffraction.....	148
2. Electron Microscopy.....	150
3. Ultramicroscopy with Incident Light.....	150
VI. Summary.....	158
References.....	159

---

## I. Introduction\*

The term *lyogel*, as it is known today, embodies the development of knowledge over a period of years.

During the seventh meeting of the "Kolloid Gesellschaft," September 20-22, 1928, in Hamburg, Germany, its chairman, Wo. Ostwald, presented a paper entitled, "Survey of the Field of Jellies and Gels" (44). The following sentences have been translated from this publication because they are of historical interest in regard to this contribution.

\* Since this chapter was written, a new book has been published which deserves mention here: *Theory of the Stability of Lyophobic Colloids—The Interaction of Sol Particles Having an Electric Double Layer*, by E. J. W. Verwey and J. T. G. Overbeek (48a). A paper also deserving special attention is "The Influence of Retardation on the London-van der Waals Forces," by H. B. G. Casimir and D. Polder (3a).

The best known and simplest way to obtain a jelly is by cooling a solvated sol, as for example a solution of gelatin. We call the formed matter, which exhibits a series of properties characteristic for solid bodies, jelly or gel, and have for gelatin perhaps the following scheme:



It might be better to speak of a "solvated" gel or *lyogel*.

For lyogels, their liquid content, which can be well over 99%, is characteristic. Coagels, and especially xerogels, are low in liquid, and coagels are by definition of a coarser degree of dispersion than the sols or gels out of which they are formed.

In summing up, Ostwald makes the following statement.

As a general condition for the transformation of a liquid disperse system into a jelly, a uniform subdivision of the system by its structural elements and a corresponding subdivision of the liquid into lyospheres seems essential. Jellies are systems rich in liquid. They can be of varying composition (liquid + liquid, solid + liquid, liquid + solid, etc.), but preferably of colloidal degree of dispersion, the standard elements of which have by mechanical intergrowth or fusion, or by uniform, ordered distribution and sufficiently short distances, subdivided the entire system in such a way that the greater part of the liquid is subdivided into lyospheres.

Lyogels, if dried (*i.e.*, desolvated), have been termed *drygel* by A. Meyer (43) and *xerogel* by Freundlich (9). They are typical examples of reversible colloids. Wagner (49) calls gelatinous systems possessing marked plasticity and elasticity, *plastogels* and *elastogels*, respectively.

If an amorphous or crystalline xerogel imbibes a liquid and swells, the resulting product is termed, according to Ostwald, a *swelling jelly* or *oedogene lyogel* (44).

As can be seen, a great amount of terminology has been established, but it is largely of a descriptive and not definitive nature. To obtain a really satisfactory understanding of the term *lyogel*, a discussion of the theories that have so far been advanced for this state of matter seems the best approach. With this as a basis, their shortcomings, if viewed in the light of the latest discoveries, can be more logically scrutinized.

Before going into further detail, however, we consider it necessary first to make one statement. Colloids, in general, and lyogels, in particular, represent matter in a state in which the ratio of surface to volume is far more responsible for its properties than the chemical composition could account for. Chemistry, in other words, still tries to apply the laws of homogeneous equilibria to colloidal systems, although there is ample proof that they are heterogeneous in composition. It is time that their heterogeneity, in its most modern definition, be recognized and the necessary consequences of such a decision adopted, instead of relying on purely physicochemical considerations, because they have often led astray and will

continue to do so in any attempts to offer an explanation for all properties exhibited by lyogels as long as they are based only on rigid mathematical and thermodynamic concepts (6).

## II. Older Theories of Lyogel Structure

Many mutually incompatible theories for the structure of gels have been proposed. The most important ones can best be grouped under the following headings: (1) the solid solution theory, (2) the liquid-liquid theory, (3) the solid-liquid or micellar theory, and (4) the fibrillar theory.

According to the first hypothesis, the gel is a more or less solid solution of a liquid in the colloid. The same colloidal particles are present in the sol and gel states, which differ only in their respective mechanical properties.

The second hypothesis calls for two liquid phases, where liquid can be synonymous with true solution.

The third hypothesis assumes that gels are composed of molecular complexes, or micelles, with crystalline properties, the dispersion medium being held by molecular attraction forces in the interstices within and between the micelles.

The fourth hypothesis is an alternative to the solid-liquid theory. It differs therefrom only in the assumption that the solid phase is continuous. If it is composed of long-chain molecules or aggregates, the term "fibrillar theory" has been used.

In the light of more recent experimental evidence, which will be discussed next, it is clear that none of the theories (1,2,9,23,24,36,39,42,43,49) offers a truly satisfactory explanation for all typical phenomena and properties exhibited by lyogels.

The two most severe criticisms that can be raised against these theories are their inability to explain gelation of solid-liquid systems at very low concentration of the solid phase, and their complete disregard of the possibility that a system might be composed of only one chemical compound (but one that is present in a wide range of molecular sizes, an arrangement that would correspond to a liquid and solid phase). The latter objection has been met by Ostwald. He termed gels in which "liquid" and "solid" components are of the same chemical constitution *isogels*.

## III. Modern Theories of Lyogel Structure

Hamaker must be credited with having evolved an entirely new point of view for the explanation of various colloidal phenomena by expanding



the van der Waals-London theory. He uses potential curves as a basis. The following are excerpts taken from one of his publications (22).

When forces are acting the energy will vary with the distance between the particles; if we plot energy against distance we get a potential curve and this constitutes the most convenient means to study our present problem.

As long as only repulsive forces are experienced, the energy rises as the distance diminishes and the potential curve will have a shape as curve *R* in Figure 1. Likewise, curve *A* represents a case in which the forces are purely attractive.

As soon as the particles touch the energy rises rapidly owing to strong elastic forces which prevent the particles from penetrating one another; consequently on the left of the line *OY* all potential curves will show a very steep rise.

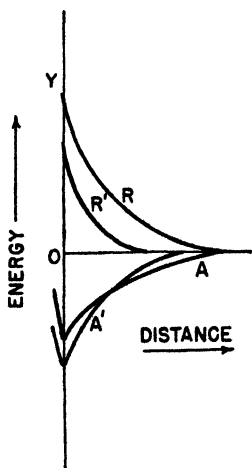


Fig. 1. The general principles of potential curves (22).

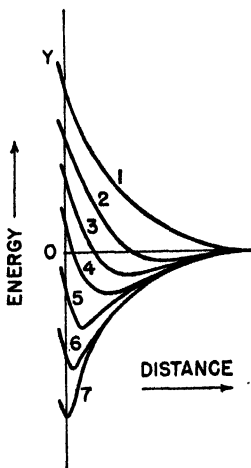


Fig. 2. The transformation of repulsive to attractive force potential curves (22).

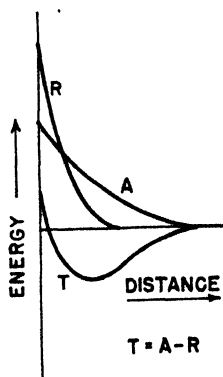


Fig. 3. The construction of intermediate curves by the superposition of attractive and repulsive forces.

A change in the forces, caused by a change in the composition of the sol, will be depicted by a variation in the potential curve. Evidently, however, a transformation of curve *R* to curve *R'* or from *A* to *A'* will not lead to an observable change in the behaviour of the sol, the system being either stable or flocculated all the time. We therefore infer that interesting phenomena will only be encountered during a transformation which gradually carries a curve of type *R* over into a curve of type *A*. A transformation of this kind which readily suggests itself is drawn in Figure 2.

Considering Figure 2 somewhat more closely, it can be said that a force is represented by a slope in the potential curve; for instance on the right side of the minimum in curve 3, where the slope is positive, the force is an attraction and on the left side the force is repulsive, the slope being negative. If such a curve comes into existence by the superposition of a repulsion and an attraction, the latter must be stronger than the former to the right of the minimum but weaker on the left side. And going from com-

plete repulsion (curve 1) to complete attraction (curve 7) the set of curves in Figure 2 originates from the fact that an attractive force begins to preponderate at large distances; the region where the attraction prevails then gradually spreads out to smaller distances, the range where the resultant force is repulsive contracting at the same rate.

Once the different sets of potential curves are studied more closely, it can soon be discovered that Figure 2 provides a surprisingly satisfactory account of many phenomena observed in lyophilic colloids.

Since the particles always strive to take up positions of minimum energy it is easily realized that a transition of curve 7 to curve 3 will be attended by limited swelling; and a transition from curve 7 to 1 will give an unlimited swelling which ends in complete solution.

Transformations in the opposite direction (from curve 1 to 7) will furnish a description of phenomena observed during the setting of a sol to a gel. If the mutual distance between the particles corresponds to the distance of minimum energy, this at once explains the formation of a gel.

Since colloidal particles are mostly of irregular shape, orientations will frequently play a role, especially in the process of gelation. If the interaction is weak it is quite conceivable that orientation is essential for a gel structure, the same system behaving as a fluid when the particles are not oriented.

To simplify this concept the partial energies arising from repulsion and attraction can be added. In Figure 3, curve  $R$  represents again the repulsive energy, and curve  $A$  the attractive one, however, this time with a positive sign. The total energy,  $T$ , can now be obtained by subtracting  $R$  from  $A$ . It can be seen that curve  $T$  corresponds to the shape of the intermediate curves in Figure 2. If we move from the lower numbers of the curves to the higher ones, we can immediately see that the answer is connected with the concentration of the sol.

If the average distance between the particles in the final concentration is not more than their distance at minimum energy, the mass will solidify into a true gel. It must be remarked here that the state of minimum energy is actually reached only when the available fluid is homogeneously distributed throughout the whole mass.

According to the latest theoretical concepts (24,40), which check with the authors' experimental data, it may be assumed that gelation occurs when the kinetic energy,  $kT$ , of neighboring particles is of the same order of magnitude as the electrostatic potential energy of particles at an average distance. If, for example, a particle is negatively charged, it is surrounded by a large number of positive counterions. Their potential energy is large compared to  $kT$ . These ions are bound ions, which reduce the effective charge of the particle. However, those ions of equal sign, which are sufficiently far from the particle so that their energies are not large compared

to  $kT$ , must also be considered. Their distribution is given by the Debye-Hückel theory. The forces of repulsion between the negatively charged particles, if calculated on this assumption, result in distances in accord with the experimental evidence. Whatever the final conclusion might be, it cannot be denied that the introduction of energy *versus* potential curves must be considered a very important step forward in the attempt to offer a comprehensive explanation of the phenomenon of gelation.

If we bear in mind the fact that repulsion not only can be caused by electric double layers formed through the interaction of the disperse phase and the ions present in the dispersion medium but also can be due to electric repulsion caused by the interpenetration of the diffuse ionic atmospheres and to the presence of lyospheres, then this newly advanced concept seems to explain satisfactorily all the data so far obtained experimentally.

These are what one might term the historical facts of the theories promulgated for the formation and structure of lyogels and isogels. It is, however, in our opinion high time to find a more general basis and one that takes the colloidal phenomena exhibited by these systems more into account. First of all, it is necessary to simplify the terminology.

A lyogel is a colloidal semisolid system rich in liquid, its disperse phase characterized by a strong absorptive capacity for the dispersion medium (solvation). The liquid phase, which can be a colloidal sol itself, must solvate but not dissolve the gel-forming colloid. The term lyogel, therefore, embraces any system covered by this definition, independent of the chemical composition of solute and solvent or shape of solute. It also embraces gels caused by the interaction of electric charges located at the surface of the solute and in the diffuse double layer in the dispersion medium surrounding the solute particles, or those resulting from the formation of nonconducting lyospheres by solvation in organic liquids.

As far as the effect of ions is concerned, it must be emphasized that it is not their electric charge or valency that is of primary importance, but their degree of hydration, *i.e.*, their ability to form thick or thin lyospheres. This is best explained by the following experiment.

If a 1% dispersion of montmorillonite having 95 milliequivalents base exchange capacity per 100 grams of clay is prepared in distilled water, a colloidal sol results. If then a few drops of a 3% sodium hydroxide solution are added thereto, the sol immediately sets to a gel, although the concentration of the clay has been somewhat reduced. If an ion of less hydration than sodium, but in equivalent amounts, has been added, either no change in fluidity occurs or the solute is precipitated. The explanation for the formation of this lyogel is the fact that the solute particles in the gel are placed like ions in a crystal but lie at considerable distance from each other (up to 500 millimicrons). Therefore, they appear to be locked into their places by the balance of the

far-reaching attraction and appropriate repulsion forces set up by the interplay of the surface ions and free ions in the dispersion medium (24,29,32). Thus this theory, based on actual observations, was substituted for the so-called mechanical theory, which assumed that the platey clay particles touch each other in random (three-dimensional orientation) (2).

Very similar observations have been made with other inorganic colloids, as, for example, vanadium pentoxide and dialyzed iron oxide.

Another point, which has not been given sufficient consideration and which is of special importance in explaining the structure of some lyogels, is the shape of the particles constituting the disperse phase and their distribution.

As already stated, the structure of lyogels, and particularly those exhibiting elasticity, has been the subject of many publications and controversial opinions (2,3,7,8,15-18,20,28,36,37). Only a very careful scrutiny and logical combination of all recorded findings will give a comprehensive and truly satisfactory explanation. What is meant thereby is most easily demonstrated by again offering some experimental facts.

An unstretched, purified, gelatin gel, if exposed to monochromatic x-rays at low temperatures, or after long storage, will yield a series of admittedly not very sharp Debye-Scherrer rings (38). The same result is obtained with crude natural rubber. If this gelatin gel or the rubber is stretched, the circular diffraction patterns disappear approximately proportionally to the degree of elongation, and interference spots take their place. Their distance from the center corresponds to the respective radii of the diffraction rings. This indicates that in the unstretched samples, regions of matter in oriented condition comparable to the structure of crystals must have been present (18). That they only yield Debye-Scherrer rings, and those only after prolonged storage or cooling, is due to their not being preferentially aligned in respect to the x-ray radiation, as is also the case with crystal powders, and to the fact that the structural elements causing x-ray diffraction are held together only by secondary valence forces. It is well known that the forces acting between the molecules increase with decreasing temperatures, or if the structural elements involved in this reaction have time to orient themselves so that a configuration of least free energy results. The gels, therefore, are composed of structural zones interconnected by molecular fringes (18).

#### IV. Special Types of Lyogels

It is felt that a simplification of the terminology of lyogels would be advantageous because it would help overcome some discrepancies that

still exist in the explanation and definition of some special gelation phenomena like thixotropy, dilatancy, and rheopexy.

It has become customary to term only those gels lyogels that are composed of a solute and solvent of different chemical composition. Gelatin, sodium silicate, and soaps with water as solvent, or rubber in benzene, are specific examples.

However, rubber in itself can be classified as a lyogel, its higher molecular weight fractions representing the solute, and its lower molecular weight fractions representing the solvent.

### 1. Thixotropy

Thixotropy is the isothermal transformation of a gel to a sol by shaking, and its reconversion into a solid state by allowing it to rest. The term is derived from the Greek words *thixis*, meaning the touch, and *trepo*, meaning to change (13,19,24).

Originally it was assumed that this phenomenon is limited to colloidal systems, which have anisometric particles, and that their concentration must be so high that filamentitious aggregates can form (2). This assumption can still be found occasionally in the literature. Besides this, it has been the general opinion that thixotropy is a phenomenon limited to electrocratic systems and that it only occurs in a very narrow range of electrolyte, or to be more specific, counterion concentration. To put this into potential energy terms, it would be represented by a system depending on an energy minimum with only a slight rise with increasing, but a very rapid rise of repulsive energy with decreasing distance between solute particles. These concepts, however, are no longer acceptable. Thixotropic systems are known in which the disperse phase is of such low concentration that the formation of a coherent structure is impossible, even if the particles were pronouncedly anisometric. Thixotropic systems have been prepared, the disperse phase of which is composed of spherical particles, and finally we have thixotropic gels, which are nonaqueous and consequently possess a nonionic liquid continuous phase. Thixotropy is, therefore, not dependent on specific electrocratic properties of the system, but quite generally on the interaction of attractive and repulsive energy between colloidal particles. In the case of typical lyophilic systems, thixotropy depends only on the interaction between the adsorbed lyospheres, which are responsible for repulsion, and the mass attraction forces acting between the disperse particles. This hypothesis, which can easily be proved if the lyosphere is reduced by the addition of an appropriate de-

solvatizing agent, also explains why the minimum concentration of the disperse phase needed for the formation of a thixotropic gel is a function of the anisometry of the dispersed phase.

The change from gel to sol by agitation is primarily due to a shearing off of the lyospheres or at least reduction of their thicknesses.

## 2. Rheopexy

A phenomenon that has so far not received the attention it deserves was first observed by Freundlich and Juliusburger in 1935 (14). They found that an aged, concentrated sol of vanadium pentoxide could be made thixotropic and caused to set to a gel on standing for one hour by adding a

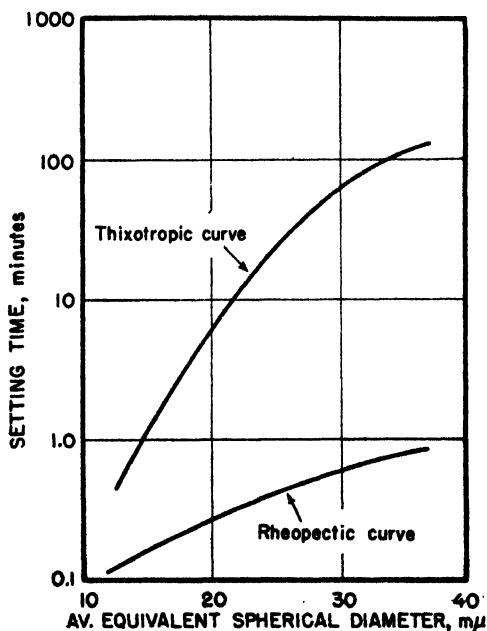


Fig. 4. Setting times of thixotropic and rheopexic systems and influence of particle sizes of the disperse phase.

small amount of sulfuric acid to it. By rolling the container between the palms of the hands, or by gently tapping it on a table top, or simply by swinging it in a circular plane, or moving it like a pendulum at an amplitude of the oscillations of 15–20° from the vertical position, the sol sets to a gel in fifteen seconds. Later the same phenomenon was observed with several other concentrated sols of highly anisometric particles. It was termed

rheopexy, from the Greek words *reo* meaning to flow, and *pectos*, meaning to curdle. Contrary to previous statements, that rheopexy is only possible with highly concentrated sols, Hauser and Reed (26) were not only able to disprove this statement, but they also offered proof that the particle size of the colloidal system is of paramount influence in this gelation phenomenon. The difference in thixotropic and rheoplectic setting time and the influence of particle size is shown in Figure 4 (25,26). Freundlich found that the finest fractions of Solnhofen slate exhibit this phenomenon. This discovery deserves special attention because it offers the most plausible explanation for the formation of the perfect petrifications of jellyfish for which these slates are well known. Similar findings in other parts of the world have always perplexed geologists.

Truly rheoplectic systems seem to be limited to laminar particles and to such systems as are also thixotropic. Ultramicroscopic studies of rheoplectic systems indicate that the rhythmic motion applied to the sols orients and aligns the anisometric particles and thereby accelerates their taking up the equilibrium condition already referred to when discussing the formation of thixotropic gels (25).

### 3. Dilatancy

Attention must also be drawn to a phenomenon often erroneously mentioned as being thixotropy, although it is the direct opposite thereof (24,25). For instance, if starch granules are brought into paste form by adding just enough water to make a barely fluid mixture, the mixture can be stirred as long as it is done slowly. Increasing speed results in increasing resistance until a seemingly dry mass is obtained. This phenomenon seems to be identical with observations first made by Reynolds on moist sand (45). He termed it dilatancy. The best explanation is offered by Freundlich (10) and Verwey (48). According to them, the system at rest must contain particles independent of each other, permitting them to form closely packed sediments with a low sedimentation volume. The external force causes unequal distribution of the particles. They pile up locally, thus forming cavities in other places, which fill up with the liquid. If the external force is removed, the particles will again repel each other and take up their original place. So far, dilatancy has been reported only in systems containing more or less spherical particles. According to the hypothesis just discussed, systems with anisometric particles should also be able to exhibit this phenomenon if the proper conditions are present. The most important of these are: (1) particles must be of sufficient size to permit sedimentation; (2) the particles must be absolutely independent of

each other and free to move; and (3) the correct relation of solid to liquid must be maintained.

Whittaker has actually been able to produce such systems with mono-disperse fractions of kaolin (plates) of  $1\text{--}5\ \mu$  particle diameter (51).

If particle size is not one of the predominant factors controlling thixotropy and dilatancy, then it should be possible to control the characteristics of the disperse part (electrokinetic potential, solvation) in such a way that either one or the other effect appears.

One of the silicone resins known as "bouncing putty" has disproved point one of the enumerated conditions. This high polymer flows if left at rest, leaving a glossy, very sticky surface. However, if rolled between the palms of one's hands, a ball with a dull surface can be obtained, which shows considerable rebound. It is also possible to roll the plastic into a string, which can be extended into very fine threads by slowly pulling. Rapid expansion will, however, cause the string to snap, with the surfaces of the break exhibiting an absolutely dry appearance. After a while flow will again set in and the string flattens on its support. Its surface takes on a glossy appearance. Our knowledge of the structure and molecular weight distribution of these polymers is still too incomplete to be able to offer at present anything more than a hypothesis for this case of dilatancy. If the system is at rest, the particles of the high-molecular fraction are so tangled up that lyosorption is not so pronounced as when the entire surface of the molecule, and thereby all its reactive groups, is exposed and available for lyosorption. It might, however, be stated here that this phenomenon, observed when rapidly expanding the plastic, bears some resemblance to changes other transparent lyogels of high-molecular compounds, like smoked sheet rubber, undergo when subjected to rapid expansion (see Sect. V.1).

## V. Elasticity of Lyogels

It is understandable that of all the colloids, most attention has been focused on natural as well as synthetic rubbers in an effort to explain their outstanding property: elasticity. In spite of the fascinating and frequently ingenious theories postulated, they cannot explain all the phenomena that are of primary interest to the colloid chemist. The main objection to these theories of elasticity (7,8,15-18,30,36,46,47,52), however, is the fact that they are mathematical concepts based primarily on thermodynamic and statistical considerations, necessitating certain assumptions, which cannot always be justified.



Since rubber is the most frequently studied of all known elastic lyogels, it seems appropriate to use it as the basis for the discussion and to ascertain which, if any, of its characteristics is identical with other lyogels exhibiting the property of elasticity.

### 1. X-Ray Diffraction

Natural rubber (*Hevea brasiliensis*, *Cryptostegia grandiflora*, *Guayule madagascariensis*, *Ficus elastica*, etc.) will show a simple amorphous band if exposed to monochromatic x-rays while in unstretched condition at normal

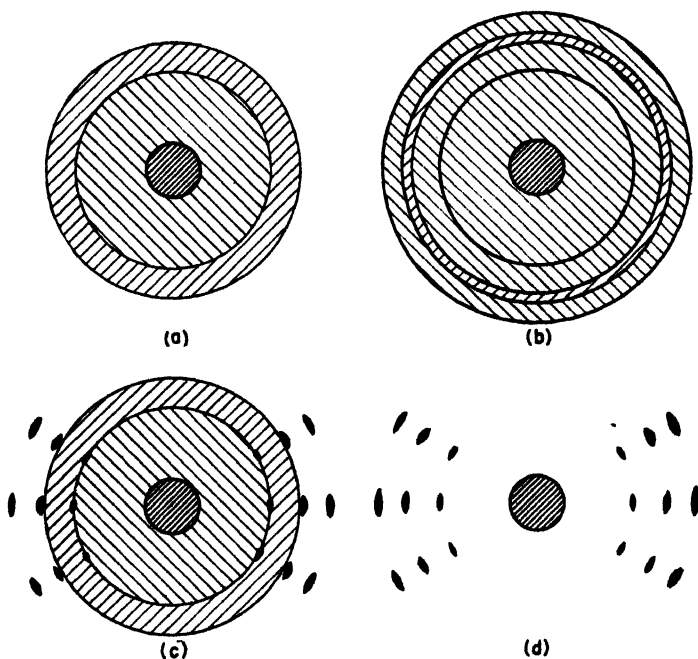


Fig. 5. X-ray diffraction patterns of natural rubber: (a) unstretched; (b) unstretched but frozen; (c) stretched; and (d) racked.

room temperature (Fig. 5a). If the same sample is stored for a prolonged period at low temperatures (below 20° C.), or kept below 0° C. for a few hours before being subjected to x-ray diffraction studies, the amorphous band will be replaced by concentric Debye-Scherrer-Hull rings, characteristic of the pattern obtained with powdered crystals (Fig. 5b). If the rubber is stretched, the amorphous band decreases in intensity and interference spots become evident (Fig. 5c). If frozen rubber is stretched, inter-

ference spots appear superimposed on the Debye-Scherrer-Hull circles. If the sample is racked (adiabatically stretched (4,5)) to an elongation of several thousand per cent, the amorphous band entirely disappears and interference patterns analogous to those obtained with natural fibers take its place (Fig. 5*d*).

From a colloid chemical point of view, the following observations deserve attention. Although standard smoked sheet rubber is transparent, it becomes opaque and hard upon prolonged storage, or if cooled. If racked to the maximum, it also becomes opaque, exhibits practically no elasticity but extraordinarily high tensile strength. Rubber can be separated by dissolution in appropriate solvents into fractions of different molecular weight, thereby proving its inhomogeneous composition. The low-molecular fractions yield upon evaporation of the solvent a very viscous, sticky fluid, the highest molecular fractions a hard, resinous substance exhibiting elasticity only to a very small degree. The former gives no x-ray diffraction pattern except an amorphous band characteristic for liquids, the latter a typical Debye-Scherrer-Hull ring pattern. When mixing the low- and high-molecular fractions and evaporating the solvent, an elastic substance is obtained, which again yields x-ray diffraction patterns typical of the natural product (27).

Similar observations have been made with polyisobutylene. At room temperature, polymers up to 25,000 M.W. are liquids of increasing viscosity, which was to be expected if the increase in length of the molecules is taken into consideration. Polymers with molecular weights of about 400,000 or above are almost solid and exhibit very little elasticity and possess poor rebound. Mixtures of low- and high-molecular fractions, however, are noticeably elastic and possess good rebound. Identical results in regard to elasticity have also been reported for polyvinylidene chloride (Saran) and several acrylic resins.

Hauser and Mark (28) explained the elasticity of rubber on the assumption of a two-phase system composed of a high-molecular fraction swollen in a low-molecular fraction. This concept was later rejected by several investigators, all of whom, however, overlooked the implications of such colloidal phenomena as lyosorption, morphology of molecules in the colloidal range of dimensions, and molecular weight distribution. On the basis of work with other lyogels exhibiting elasticity and the results obtained by applying electron microscopy and, more recently, microscopy with ultraillumination by incident light, elasticity of lyogels can be explained on the assumption of a multiphase system.

Gelatin, for example, can be stretched to 400% if it is first immersed

in a mixture of equal parts of water and glycerin, is allowed to swell therein for several hours, and is then heated to 40° C. It can then be poured into thin films which, after solidification, permit stretching (31). When such a stretched film is heated, it contracts. If the glycerin, however, is removed from the film by extraction with alcohol, it does not retract any more.

Other lyogels exhibiting pronounced elasticity are soaps (12,41), as determined by a rotary type of viscosimeter, or by placing nickel particles into a gel and observing their movement microscopically in an electromagnetic field. The particles return to their original position as soon as the current is cut off. Silica, when freshly formed, yields a jelly possessing elasticity of the same order of magnitude as gelatin jelly (50).

## ***2. Electron Microscopy***

Thin films of high polymers can be prepared by spreading a solution of such a polymer in an organic solvent on water and depositing the film on a very fine wire gauze screen, where it will break into configurations characteristic for the physical structure of the polymer under investigation. If such a preparation is studied under the electron microscope, certain characteristics in the morphology of the preparation can be connected with its molecular sizes and structures. The low-molecular fractions of natural rubber, such as obtained by the fractionation of smoked sheet, exhibit a preponderance of bloblike formations (Fig. 6), whereas the so-called gel fractions (high-molecular fraction) of rubber show thread and network formations (Fig. 7). The total rubber (Fig. 8) combines the characteristics of both.

## ***3. Ultramicroscopy with Incident Light***

However, electron microscopic observations of lyogels can be expected to change the character of their morphology due to the high vacuum and the electron bombardment resulting in a considerable increase in temperature. Indeed, embrittlement of the natural rubber polymer has been definitely observed. The high temperatures also cause secondary effects, which will be discussed later. It was found, however, that good results in observation could be obtained by the use of an ultramicroscope equipped with incident light (31,33-35). Although the magnifications obtained with this instrument in no way compare with those of the electron microscope, the latter's objectionable features, such as embrittlement of the preparation and evolution of heat, do not occur. The use of the ultramicroscope also permits the study of the effect time and temperature have on the mor-

phology of lyogels. The results obtained with this new method give visual proof of the differences in the molecular weight distributions of different natural rubbers of the same chemical compositions (Fig. 9\*), and permit correlating them with their physical properties.

The blobs and strings originally obtained by electron microscopic observation of rubber were found to be secondary morphological formations,



Fig. 6. Electron photomicrograph of the sol fraction of hevea rubber (21).



Fig. 7. Electron photomicrograph of the gel fraction of hevea rubber (21).

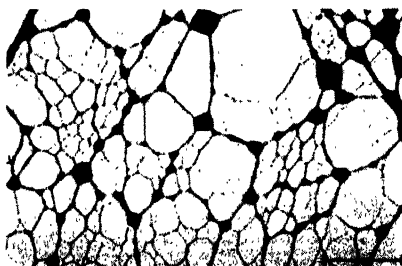


Fig. 8. Electron photomicrograph of hevea rubber (21).

which proved to be a function of time and temperature. A detailed ultramicroscopic study of cryptostegia rubber at room temperature, containing a high percentage of both rather low- and very high-molecular sizes, revealed the changes in the morphological picture of this polymer occurring with time and age of the preparation. Microphotographs of cryptostegia rubber taken immediately after the preparation had been made showed very few blobs and a preponderance of network (Fig. 10a). This was contradictory to the results obtained with the electron microscope, where low-

\* All ultraphotomicrographs reproduced here are reversed prints originally published in *J. Am. Chem. Soc.*, **68**, 153 (1946).

molecular fractions of a polymer were clearly distinguishable by their blob formation, particularly if present in such great quantities as in cryptostegia. However, if this original preparation was left undisturbed over a period of hours and photographed periodically, a radical change in its morphology was noticed (Figs. 10*b*, 10*c*, 10*d*). Blob formation became more and more predominant. At higher temperatures (40°C.), the same phenomenon occurred, but in a much shorter time interval (Figs. 11*a-c*).

If films of sodium oleate are prepared in the same way and observed in the ultramicroscope, preparations containing blobs are at first observed (Fig. 12); later on, however, after storage of the preparation at room temperature, the picture changes and the thornlike formations, identical with those obtained by electron microscopic observations (35), were noticed (Fig. 13).

A rise in temperature ranging considerably above 40°C. is obtained during electron microscopic exposures. Thus it can be expected that the time required for the formation of blobs will be still shorter, so short, in fact, that the original morphology of the lyogel is never observed. Inasmuch as the formation of blobs in polymers has been identified with the presence of low-molecular fractions, the time and temperature needed for their formation can be correlated with the ability of the polymer to flow. It is to be expected that a certain amount of homogeneity exists within a given polymer with regard to the distribution of the various molecular sizes present therein. Molecules of shorter lengths will, upon application of strain, move with greater ease than long-chain molecules. A certain alignment of the molecules in these film preparations can be expected because of the strain present in the threads. This in effect will cause the squeezing out of the low-molecular fraction resulting in the formation of blobs, their shape being controlled by interfacial tension. Actually this phenomenon can be likened to a syneresis effect.

Identical phenomena were obtained from a mixture of carefully prepared and well-defined high- and low-molecular styrene polymers as well as from polyisobutylene (Vistanex) of similar composition (Fig. 14).

Various molecular size fractions of polyisobutylene, ranging from a Staudinger molecular weight of 40,000–300,000 indicated the influence of the length of the polymer chains on the morphology of the polymer. Low-molecular fractions showed indiscriminate flow of such proportions and rate that even blob formation was obscured. As the molecular weight increased, netting with extremely fine blobs became more and more predominant (Fig. 15).

Lack of polymer flow or its hindrance, either due to its structure or



(a)



(b)



(c)

Fig. 9. Ultraphotomicrographs of natural rubbers: (a) *Hevea brasiliensis* (smoked sheet); (b) *Cryptostegia grandiflora*; and (c) *Guayule*.



(a)



(b)

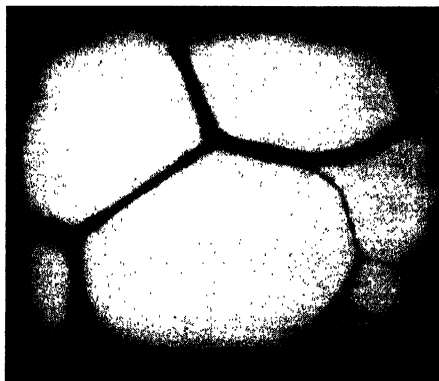


(c)

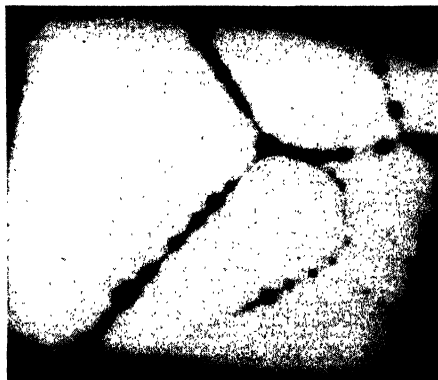
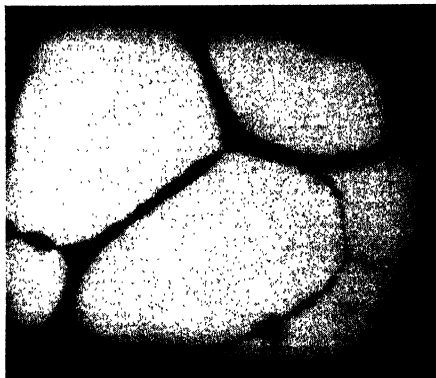


(d)

Fig. 10. Ultraphotomicrographs of cryptostegia rubber at various storage times (35): (a) 0 hour; (b) 7.5 hours; (c) 15 hours; and (d) 30 hours.

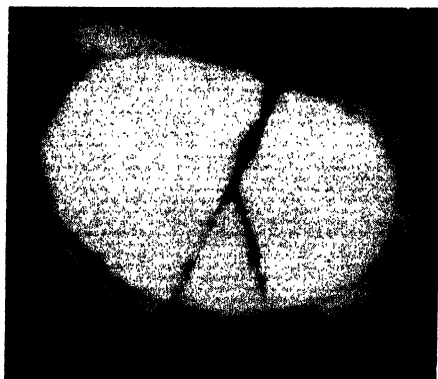


(a)

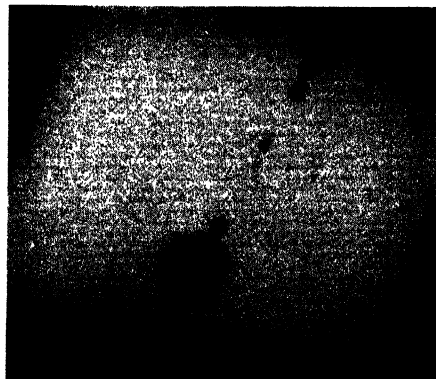


(c)

Fig. 11. Ultraphotomicrographs of cryptostegia rubber at 40°C. at various storage times (35): (a) 0 hour; (b) 1.5 hours; and (c) 3 hours.



(a)



(b)

Fig. 12. Ultraphotomicrograph of sodium oleate (35).





Fig. 13. Electron photomicrograph of sodium oleate (33).

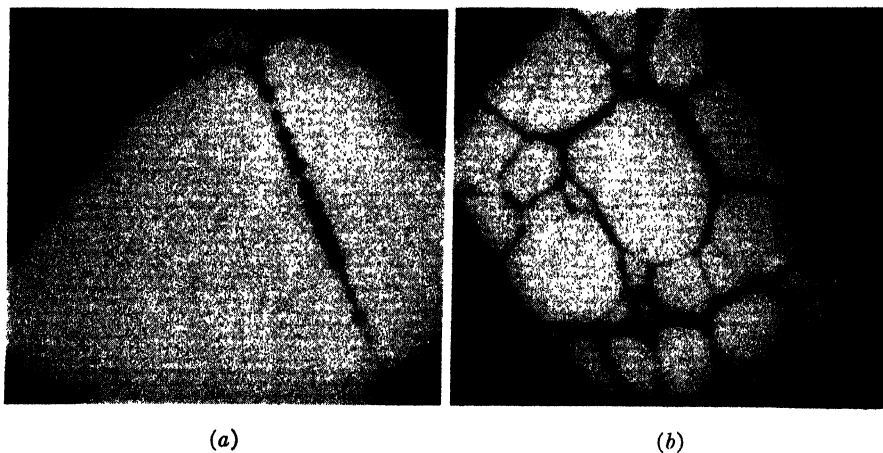


Fig. 14. Ultraphotomicrographs of polyisobutylene: (a) molecular weight 40,000/300,000 in proportion 90/10; and (b) molecular weight 40,000/300,000 in proportion 10/90.



(a)

(b)

Fig. 15. Ultraphotomicrographs of polyisobutylene: (a) molecular weight 40,000; and (b) molecular weight 300,000.



Fig. 16. Ultraphotomicrograph of balata at 25°C.

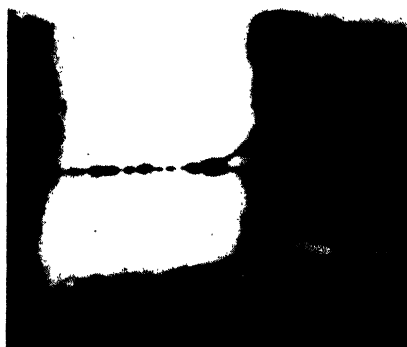


Fig. 17. Ultraphotomicrograph of balata at 65°C.



Fig. 18. Ultraphotomicrograph of balata heated to 65°C. and cooled immediately after break.

molecular size, has been demonstrated by the ultramicroscopic method for certain synthetic rubbers, both in the crude as well as in the milled state.

Changes in the morphological picture of natural rubber occurring during vulcanization were studied under both the electron microscope and the ultramicroscope. Synaeresis of the lower molecular fractions was found to decrease as vulcanization proceeded. At the same time, network formation increased (21,35). All of these results indicate that the explanation of the elasticity of lyogels based on their multiphase structure is in conformity with available evidence.

Gutta-percha or balata, polymers of isoprene, were of particular interest because of their chemical identity with and yet differences in physical properties from natural rubber. These polymers become elastic only above 65°C. Ultramicroscopic studies at room temperature revealed the formation of irregularly breaking, ragged films (Fig. 16). If these films were prepared at elevated temperatures, however, threads could be obtained which, upon heating to 65°C., would form blobs (Fig. 17). Whenever such a thread broke and was cooled to room temperature, it became locked in its position and did not change its morphology (Fig. 18). With natural rubber, however, where even at room temperature flow progresses, though at a slower rate, the whole preparation collapses if a string tears. X-ray diffraction analysis (3) has shown that while rubber crystallizes in the *cis*-configuration, balata and gutta-percha crystallize in the *trans*-configuration. Holding chain bond oscillation responsible for the melting point of the crystallites, it can be deduced that the slightly different position of the methyl group in balata and gutta-percha as compared to natural rubber may exert some influence. The *cis* double bond configuration as encountered in rubber does not offer any obstruction to vibration, such as can be found in gutta-percha. The greater freedom of motion as postulated for the *cis*-configuration of the rubber hydrocarbon polymer should result in flow and synaeresis, as visually observed by use of the ultramicroscope. As the temperature is increased, vibration will be increased until at a given temperature it finally overcomes the obstruction to such an extent that flow can occur even in the *trans*-isoprene polymer.

## VI. Summary

Thus the morphological picture of a lyogel polymer under the ultramicroscope appears largely independent of its chemical composition and has to be considered as a function of its physical structure, chain configuration, and molecular size distribution. The influence of the chemical composition of the lyogel will only be predominant wherever it causes a stif-

fening or steric hindrance in the movability of its parts. However, both steric hindrance and cohesive forces acting between the polymer chains can exert a considerable influence on the behavior of a polymer. Even nonelastic polymers, which in their unadulterated state may be hard and solid, can be rendered elastic to a considerable degree if great amounts of appropriate plasticizers are added. Whether this development of elasticity is of a purely physical nature caused by the weakening of the cohesive forces or whether some interaction between the plasticizer and the polymer takes place has not as yet been determined and will depend on the specific polymer and plasticizer used. Studies to that effect would undoubtedly contribute to the problem of choice and suitability of a given plasticizer for a given polymer on the basis of physicochemical and colloidal considerations of their respective properties. In the final analysis, however, the occurrence of synaeresis will again be noticeable upon electron microscope or ultramicroscopic observation and will be a criterion for the occurrence of elasticity.

### References

1. Bradford, S. C., in J. Alexander, *Colloid Chemistry*. Vol. I, Chemical Catalog Co., New York, 1926, p. 751.
2. Broughton, G., and Squires, L., *J. Phys. Chem.*, **40**, 1041 (1936).
3. Bunn, C. W., in H. Mark and G. S. Whitby, eds., *Advances in Colloid Science*. Vol. II, Interscience, New York, 1946, p. 95.
- 3a. Casimir, H. B. G., and D. Polder, *Phys. Rev.*, **73**, 360 (1948).
4. Feuchter, H., *Kautschuk*, **3**, 149 (1927); **4**, 8 (1928).
5. Feuchter, H., and Hauser, E. A., *ibid.*, **5**, 194, 218, 245, 276 (1929).
6. Fisher, M. H., and Hooker, Marian O., *The Lyophilic Colloids*. C. C. Thomas, Springfield (Ill.), 1933, p. 173.
7. Flory, P. J., and Rehner, J., Jr., *J. Chem. Phys.*, **11**, 512, 521 (1943).
8. Flory, P. J., and Rehner, J., Jr., *ibid.*, **12**, 412 (1944).
9. Freundlich, H., *Kapillarchemie*. Akadem. Verlagsgesellschaft, Leipzig, 1930.
10. Freundlich, H., *Trans. Faraday Soc.*, **34**, 308 (1938).
11. Freundlich, H., *J. Phys. Chem.*, **41**, 901 (1937).
12. Freundlich, H., and Kores, H. J., *Kolloid-Z.*, **36**, 241 (1925).
13. Freundlich, H., *Thixotropy*. Hermann, Paris, 1935.
14. Freundlich, H., and Juliusburger, F., *Trans. Faraday Soc.*, **30**, 333 (1934).
15. Gee, G., in H. Mark and G. S. Whitby, eds., *Advances in Colloid Science*. Vol. II, Interscience, New York, 1946, p. 145.
16. Gee, G., and Orr, W. J. C., *Trans. Faraday Soc.*, **42**, 507 (1946).
17. Gee, G., *ibid.*, **42**, 585 (1946).
18. Gerngross, O., and Hermann, K., *Kautschuk*, **8**, 181 (1932).
19. Green, H., and Weltman, R. N., in J. Alexander, *Colloid Chemistry*. Vol. VI, Reinhold, New York, 1946, p. 328.

20. Guth, E., James, H. M., and Mark, H., in *Advances in Colloid Science*. Vol. II, Interscience, New York, 1946, p. 253.
21. Hall, C. E., Hauser, E. A., le Beau, D. S., Schmitt, F. O., and Talalay, P., *Ind. Eng. Chem.*, **36**, 634 (1944).
22. Hamaker, H. C., *Hydrophobic Colloids*. D. B. Centen, Amsterdam, 1938, p. 16.
23. Hartman, R. J., *Colloid Chemistry*. Houghton Mifflin, Boston, 1938, p. 395.
24. Hauser, E. A., *Colloidal Phenomena*. McGraw-Hill, New York, 1939.
25. Hauser, E. A., *Chem. Revs.*, **37**, 287 (1945).
26. Hauser, E. A., and Reed, C. E., *J. Phys. Chem.*, **40**, 1169 (1936); **41**, 911 (1937); *J. Am. Chem. Soc.*, **58**, 1822 (1936).
27. Hauser, E. A., and Rosbaud, P., *Kautschuk*, **3**, 17 (1927).
28. Hauser, E. A., and Mark, H., *Kolloidchem. Beihefte Ambrohn Festschrift*, 1926, p. 64.
29. Hauser, E. A., and le Beau, D. S., *J. Phys. Chem.*, **42**, 961 (1938); **43**, 1037 (1939).
30. Hauser, E. A., and le Beau, D. S., *India Rubber J.*, **110**, 169 (1946); **111**, 453 (1946).
31. Hauser, E. A., and le Beau, D. S., *Ind. Eng. Chem.*, **37**, 786 (1945).
32. Hauser, E. A., and le Beau, D. S., in H. Mark and G. S. Whitby, eds., *Advances in Colloid Science*. Vol. II, Interscience, New York, 1946, p. 191.
33. Hauser, E. A., and le Beau, D. S., *Ind. Eng. Chem.*, **38**, 335 (1946).
34. Hauser, E. A., and le Beau, D. S., *J. Phys. Chem.*, **50**, 171 (1946).
35. Hauser, E. A., and le Beau, D. S., *J. Phys. & Colloid Chem.*, **51**, 278 (1947); **52**, 27 (1948).
36. Houwink, R., *Elasticity, Plasticity and Structure of Matter*. Cambridge Univ. Press, London, 1937.
37. James, H. M., and Guth, E., *J. Chem. Phys.*, **11**, 455 (1933).
38. Katz, J. R., and Gerngross, O., *Kolloid-Z.*, **39**, 181 (1926).
39. Kuhn, A., *Kolloidchemisches Taschenbuch*. Akadem. Verlagsgesellschaft, Leipzig, 1935.
40. Langmuir, I., *J. Chem. Phys.*, **6**, 873 (1938).
41. Lawrence, A. C. S., *Soap Films*. Bell, London, 1929.
42. Lloyd, Dorothy J., in J. Alexander, *Colloid Chemistry*. Vol. I, Chemical Catalog Co., New York, 1926, p. 767.
43. Meyer, A., *Kolloidchem. Beihefte*, **5**, 1 (1913).
44. Ostwald, Wo., *Kolloid-Z.*, **46**, 248 (1928).
45. Reynolds, O., *Phil. Mag.*, **5**, 469 (1885).
46. Treloar, L. R. G., *Trans. Faraday Soc.*, **36**, 538 (1940).
47. Treloar, L. R. G., *ibid.*, **37**, 84 (1941).
48. Verwey, E. J. W., and J. H. de Boer, *Rec. trav. chim.*, **57**, 383 (1938).
- 48a. Verwey, E. J. W., and J. T. G. Overbeek, *Theory of the Stability of Lyophobic Colloids—The Interaction of Sol Particles Having an Electric Double Layer*. Elsevier, New York-Amsterdam, 1948.
49. Wagner, H., *Kolloid-Z.*, **47**, 19 (1929).
50. Weiser, H. B., *Colloid Chemistry*. Wiley, New York, 1939.
51. Whittaker, H., *Sc.D. Thesis*, Mass. Inst. of Technology, 1937.
52. Wood, L. A., in H. Mark and G. S. Whitby, eds., *Advances in Colloid Science*. Vol. II, Interscience, New York, 1946, p. 57.

# ULTRACENTRIFUGAL SEDIMENTATION OF POLYMOLECULAR SUBSTANCES

PER-OLOF KINELL AND BENGT G. RÄNBY

*Institute of Physical Chemistry, University of Uppsala, Sweden*

---

I. Introduction.....	161
II. Ultracentrifugal Method.....	163
III. Sedimentation Properties of Threadlike Molecules.....	166
1. Threadlike Molecules in Solution.....	166
2. Change of Shape in a Centrifugal Field.....	168
3. Influence of Branching on Sedimentation Velocity.....	170
4. Interaction between Molecules. Solvation.....	172
5. Influence of Shielding Ratio.....	176
6. Sedimentation as a Rate Process.....	177
7. Concentration Dependence.....	177
8. Effects of Polymolecularity.....	181
IV. Information on Polymolecularity from Sedimentation Measure- ments.....	183
1. Average Sedimentation Constants.....	184
2. $dB/dx$ Method According to Gralén.....	185
3. Frequency Functions from Sedimentation Diagrams.....	188
4. Use of Parameter Functions.....	192
V. Polymolecularity Measurements and Fractionation.....	194
1. Cellulose Nitrate.....	198
Selectivity of Fractionation.....	198
Properties of Cellulose Nitrate Molecules.....	202
Frequency Functions.....	204
2. Polymeric Methyl Methacrylate.....	208
3. Polystyrene.....	212
VI. General Conclusions.....	215
References.....	215

---

## I. Introduction

Twenty-five years have elapsed since Svedberg started his work on ultracentrifugation in 1923. Svedberg early realized that the earth's gravitational field was too weak to have any effect on the sedimentation of colloids and high molecular substances. The intensity of the field of force

would have to be increased many thousandfold. This was done by exposing the substance in solution to the influence of a centrifugal field. In collaboration with Nichols (87) he built the first centrifuge by means of which sedimentation could be followed by direct observation and by taking photographs. The first ultracentrifuge, for a speed of 10,000 r.p.m., was built by Svedberg and Rinde (88) in 1924 and proved to be an excellent instrument for the study of different sols and proteins. Since that time the ultracentrifuge has been improved very much and is today a very important scientific tool in the fields of physical chemistry and biochemistry. A comprehensive description of this development and the design of the ultracentrifuge has been given by Svedberg and Pedersen in their monograph (89).

The applications of the ultracentrifugal technique within the field of proteins are numerous. The results gained have been of utmost importance: they have elucidated many questions of fundamental nature in such different fields as chemistry, medicine, zoology, and botany. One of the reasons for the great progress in applying the ultracentrifuge to molecules of the protein type is the fact that these molecules show a rather simple sedimentation behavior. In shape, they are spherical or ellipsoidal, and all molecules belonging to the same species have equal molecular weight (monodispersity) or consist of a few classes of molecular weights (paucidispersity). In some cases the protein has molecules of a filamentous or rod-like shape (virus, muscle proteins).

In the beginning of the 1930's an application of the ultracentrifuge to substances such as cellulose and cellulose derivatives and synthetic high polymers was started. These substances have molecules of another type, namely branched or unbranched threadlike molecules, which do not consist of a single molecular species but show a whole spectrum of molecular weights. The substances are polymolecular.\* Molecules from a certain species, however, show a regularity, because they are built up of the same structural unit. In cellulose, this unit is the glucose molecule; in synthetic and natural high polymers, it consists of different monomers: butadiene, isoprene, styrene, methyl methacrylate, etc. Exceptions from this regularity can occur. In making copolymers, two and even more monomers may be used; they do not need to be arranged in a regular way. This does not, however, influence the general classification of the molecules. In observing the sedimentation behavior of such molecules, one finds marked differences between them and protein molecules. Contrary to the pro-

\* This expression was used by Schulz (69) instead of the earlier "polydisperse."

teins, the sedimentation constant for substances like cellulose shows a very pronounced variation with the concentration of the solute. This is especially true for molecules with high molecular weight at fairly low concentrations. For proteins the spreading of the boundary between solution and solvent is due mainly to diffusion.† For polymolecular substances the spreading of the boundary is almost exclusively dependent upon the differences in molecular weight. The diffusion has in most cases only very little effect, because the diffusion coefficient for threadlike molecules is very small. The study of substances of this type is therefore rather complicated. The experimental difficulties are larger and the interpretation of the data more intricate. Nevertheless the comprehensive work of Gralén (20) on cellulose and cellulose derivatives, Mosimann (59,60), and Julander (30) on cellulose nitrates, and Säverborn (90) on polyuronic acids has contributed very much to our knowledge of these substances. The ultracentrifugal investigations of rubbers and synthetic high polymers are scarcer, but in this field, also, the work is progressing.

The discussions in this article will be concerned mainly with the attempts that have been made to treat the sedimentation properties of threadlike molecules from a theoretical point of view. Furthermore the influence of concentration dependence and polymolecularity on the observed quantities will be discussed. Finally the use of the ultracentrifuge in determining polymolecularity will be treated.

## II. Ultracentrifugal Method

Before we turn to the main subjects, a brief review of the ultracentrifugal method is necessary.

The substance to be investigated is brought into solution and 0.5–1 ml. of this solution is enclosed in a cell of sector-shaped cross section. This cell is placed in a rotor which, by means of two oil turbines (air-driven and electric centrifuges are also used), rotates with a very high speed in an atmosphere of hydrogen at a pressure of 10–15 mm. Hg. In the centrifugal field a force,  $M(1 - V\rho)\omega^2 x$ , is exerted on the particles and, if the forces of inertia are small, this force is balanced by the frictional force,  $f(dx/dt)$ . Hence:

$$M(1 - V\rho)\omega^2 x = f(dx/dt) \quad (1)$$

† This does not seem to be strictly true according to an interpretation given by Bresler (3). He has made an estimation of the statistical spread of molecular weights in the neighborhood of the most probable one and found an average quadratic deviation of 0.8% of the degree of polymerization. This makes a contribution to the spreading of the boundary of about 5%.



where  $M$  is the molecular weight,  $V$  the partial specific volume of the solute,  $\rho$  the density of the solution,  $\omega$  the angular velocity of the rotor,  $x$  the distance from the center of rotation,  $f$  the frictional coefficient per mole, and  $t$  the time. Rewriting this expression we get:

$$\frac{1}{\omega^2 x} \frac{dx}{dt} = \frac{M(1 - V\rho)}{f} \quad (2)$$

For the sedimentation velocity,  $dx/dt$ , reduced to a unit centrifugal field, Svedberg (85) has introduced the notation sedimentation constant,  $s$ . Thus:

$$s = \frac{1}{\omega^2 x} \frac{dx}{dt} \quad (3)$$

This quantity is a characteristic constant for a given molecular species in a given solvent at a given temperature. It is expressed in the unit  $10^{-13}$  c.g.s. called a Svedberg (S).

Integrating equation (3) we get:

$$x = x_0 \exp(\omega^2 s t) \quad (4)$$

which gives the sedimented distance as a function of  $s$ ,  $\omega$ , and  $t$ .  $x_0$  is the position at  $t = 0$  and mostly refers to the meniscus of the solution in the cell.

The frictional coefficient,  $f$ , can be determined from the diffusion constant,  $D$ , that is:

$$f = RT/D \quad (5)$$

where  $R$  is the gas constant and  $T$  the absolute temperature. Equations (2), (3), and (5) give:

$$M = \frac{RTs}{D(1 - V\rho)} \quad (6)$$

which is Svedberg's formula for the determination of molecular weights from sedimentation and diffusion data.

As mentioned above the solution is enclosed in a sector-shaped cell because this is the only way to obtain a convection-free sedimentation. Due to the sector shape and the change of the centrifugal force with the distance from the center of rotation, a uniform decrease of concentration occurs during centrifuging. This effect has been given by Svedberg and Rinde (88) in the equation:

$$c = c_0(x_0/x)^2 = c_0 \exp(-2\omega^2 s t) \quad (7)$$

where  $c_0$  is the original concentration.

All the formulas given are strictly true only if the influence of diffusion is neglected. As a rule, however, there is always some diffusion. Corrections must then be applied but in most cases they are small. For the more detailed theory of sedimentation, where account is also taken of the diffusion, reference is made to the monograph of Svedberg and Pedersen (89). The reader is also referred to this book concerning the influence of electrical charge in the sedimentation of colloidal ions.

The sedimentation constant is always reduced to a standard basis at 20°C. This is made as a reduction of viscosity and density of the solvent and partial specific volume of the solute from the temperature in the run to the standard temperature. The reduced sedimentation constant is designated as  $s_{20}$ . If the compressibility of the solvent is high, an appreciable increase in density and viscosity will occur as a result of the increase in hydrostatic pressure with increasing centrifugal field. A change in the sedimentation constant with the distance from the center of rotation will then occur and a correction for this must then be applied (61,89).

Due to the diffusion, a sedimentation that has been performed for a sufficiently long time will end in an equilibrium, *i.e.*, the quantity of the solute driven by the centrifugal force through a unit surface in the direction of the periphery is equal to that which wanders in the direction of the center of rotation by virtue of diffusion. From this equilibrium distribution of concentration the molecular weight can be calculated:

$$M = \frac{2RT \log (c_2/c_1)}{(1 - V\rho)\omega^2(x_2^2 - x_1^2)} \quad (8)$$

where  $c_1$  and  $c_2$  are the concentrations in the points  $x_1$  and  $x_2$ , respectively (85,86).

To follow the sedimentation three photographic methods have been used, namely, the light-absorption method developed by Svedberg and Rinde (88), the Philpot Schlieren method (65), and the scale method according to Lamm (50-52). As the last method has been used in most of the investigations reported in this review, a brief description of the principles will be given. An equidistant transparent scale is placed on the side of the centrifuge opposite from the camera. The latter is focused on the scale through the cell and exposures are taken at suitable time intervals. As soon as a concentration gradient occurs in the cell, the lines of the scale will be displaced. This line displacement,  $Z$ , is proportional to the magnitude of the concentration gradient in the cell at a place corresponding to the position of that line. Plotting the  $Z$  values against the  $x$  values of the lines, a sedimentation diagram is obtained, *i.e.*, a curve giving the variation of

the concentration gradient throughout the cell. This curve can have one or more maxima depending on the substance under investigation. From the position,  $x_m$ , of these maxima at different times the sedimentation constant,  $s_m$ , is calculated.

### III. Sedimentation Properties of Threadlike Molecules

From equations (2) and (3) in the previous section it follows that the sedimentation constant depends upon the frictional coefficient per mole in the following way:

$$s = M(1 - V\rho)/f \quad (9)$$

Coefficient  $f$  is a function of the shape of the molecules and of their solvation; it may also depend upon the interaction between different molecules. It is evident that the knowledge of  $f$  is of utmost importance in every discussion of the sedimentation properties of different molecules. Already, as in the case of proteins, much work has been done in order to find out how the shape of the molecule influences the frictional resistance. As models for the molecules, spheres, prolate and oblate ellipsoids, cylindrical rods, etc. have been used. The frictional coefficient has been expressed as a function of geometrical quantities of these bodies. Also, in the case of threadlike molecules, it is necessary to have a model for the molecule. Evidently the above-mentioned models can be used only in extreme cases. This section will give a review of the work done on the hitherto most promising model for threadlike molecules, Kuhn's statistical coil, and its use, to describe the sedimentation properties of these molecules. Furthermore the influence of solute concentration, solvation, and polymolecularity will be discussed. Some of the substances having threadlike molecules form heavily charged ions in water solution (polyuronic acids, polyacrylic acids, cellulose xanthates and glycolates, polymetaphosphates, etc.). The influence of the ionic charge on the sedimentation will not be specially discussed, because this influence can be diminished or eliminated by adding strong low-molecular electrolytes to the solutions.\*

#### 1. Threadlike Molecules in Solution

An aliphatic hydrocarbon molecule of low molecular weight can adopt many different configurations, the number depending upon the number of

\* *Note added in proof.* The dimensions of threadlike macroions will change with the amount of low-molecular electrolytes added, as has recently been shown (24a, 49a).

degrees of freedom. The possibility for these different configurations is connected with the existence of a more or less free rotation about C—C bonds. As the number of carbon atoms increases the number of configurations will be larger. If no bending or stretching of valences occurs all these configurational isomers will be equivalent with respect to energy. A threadlike molecule with high molecular weight will constitute a system with so many degrees of freedom that it can be regarded as a system with special statistical properties. This is true even for molecules that do not consist exclusively of C—C chains. The same interpretation can also be applied to molecules having, for instance, a chain built up of glucose residues.

For the statistical treatment the molecular chain is divided into a number,  $N$ , of statistical elements in such a way that the position of the element  $k + 1$  is completely independent of the position of element  $k$ . Generally  $N$  does not coincide with the number,  $Z$ , of monomer units but each element consists of  $j$  such units. The number  $N$  is dependent upon the flexibility of the chain; the more pronounced the steric hindrances, the lower is  $N$ . The shape of the molecule in solution is now given from a statistical point of view by  $N$ . Due to the Brownian movement the shape of the molecule will be continuously changed with time. To each separate molecule, however, we can attribute a configurational probability, which is a function of the distance,  $h$ , between the two end points of the molecule. This function has been given by Kuhn (42,43,45), and Guth and Mark (22). For not too large distances, the probability of the molecule to have an end point separation between  $h$  and  $h + dh$  is given by:

$$W(h) dh = \left( \frac{1}{\sqrt{2/3} NA^2} \right)^3 \frac{4}{\sqrt{\pi}} \exp(-h^2/2/3 NA^2) h^2 dh \quad (10)$$

where  $A$  is the length of the statistical element. The number of chains per unit of volume complying with these requirements is:

$$dG_{h, h + dh} = G W(h) dh \quad (11)$$

where  $G$  is the total number of molecules per unit of volume.  $W(h)$  is normalized to give:

$$\int_0^\infty W(h) dh = 1 \quad (12)$$

Equation (10) is valid for a solution at rest, *i.e.*, free from any sort of internal movement except the Brownian. If the solvent moves relative to the solute as in a centrifugal field, equation (10) does not hold. The effect of this movement will be that the configuration changes. Before we

discuss this influence of the centrifugal field on the shape of the threadlike molecule, some properties of two extreme cases will briefly be discussed.

Kuhn and Kuhn (46) have studied the extreme cases of one threadlike molecule, where the distance between the links of the chain is large enough to permit a free flow of liquid through the molecule—a free-drained coil—and another molecule, where due to the compactness no flow through it is possible—a matted coil. In the latter case, solvent can be immobilized between the links. These two hydrodynamic models are of great importance for the interpretation of experimental data because their sedimentation properties are easily estimated. For the free-drained coil, the frictional coefficient,  $f$ , must be proportional to the molecular weight and, as the centrifugal force also is proportional to the molecular weight, the chain length does not influence the velocity in a centrifugal field. The matted coil, however, has a frictional resistance proportional to the average dimension,  $\bar{h}$ , of the coil. This quantity is proportional to the square root of  $N$  (this is easily seen from equation 10) and hence to the square root of the molecular weight. Thus we have for the two types of molecules:

$$\begin{array}{lll} \text{free-drained coil:} & f \sim M & \text{and} \quad s = \text{const.} \\ \text{matted coil:} & f \sim M^{1/2} & \text{and} \quad s \sim M^{1/2} \end{array}$$

The expressions for the sedimentation constant are obtained from equation (9). To what extent a molecule under investigation will approach one or the other of these extreme cases depends upon the chain length and the internal structure. For lower degrees of polymerization we can expect properties of a free-drained coil. The same is the case even for higher degrees of polymerization if the molecule is rather stiff due to steric hindrances, solvation, etc.

## 2. Change of Shape in a Centrifugal Field

The centrifugal field is proportional to the distance from the center of rotation. Hence a force gradient will occur in the solution contained in the centrifuge cell. This gradient is parallel to the direction of motion of the molecules and causes the force acting on one end of the molecule to differ from that acting on the other end. This difference will be largest for molecules that are moving with their "length" parallel to the centrifugal field. Two consequences of this are obvious: the molecule will be stretched out, and it will show an orientation against the centrifugal field. In order to estimate the magnitude of these effects, the frequency function of the end points of the molecules subjected to the action of the centrifugal force must be calculated. Kuhn and Kuhn (46) have given this function

for threadlike molecules subjected to a shearing stress. Following an analogous treatment, Singer (80) has obtained the expression:

$$w(h, \theta) = \frac{G}{\pi \bar{h}_0^2} \left(1 - \frac{\beta \bar{h}_0^2}{2}\right) \exp \left\{ -\frac{h^2}{\bar{h}_0^2} \left(1 - \frac{\beta \bar{h}_0^2}{2} \cos^2 \theta\right) \right\} \quad (13)$$

where  $\beta = M(1 - V\rho)\omega^2/4RT$  and  $\bar{h}_0^2 = \frac{2}{3}NA^2$ . This function is valid, if the sedimentation velocity is low and if the influence of the internal viscosity introduced by Kuhn and Kuhn (47,48) is neglected. This internal viscosity is concerned with the ability of the molecule to change its configuration while rotating. The lower the internal viscosity, the easier the molecule accommodates itself to forces of deformation exerted from the flowing liquid.

Equation (13) gives the number of molecules,  $dG$ , having an end point separation between  $h$  and  $h + dh$  and for which the angle between the direction of  $h$  and the direction of the centrifugal force has a value between  $\theta$  and  $\theta + d\theta$ , that is:

$$dG = w(h, \theta) h \, dh \, d\theta \quad (14)$$

Integrating this over all value of  $h$  we obtain the total number of molecules which, irrespective of their end point separation, have vectors  $h$  forming an angle between  $\theta$  and  $\theta + d\theta$  with the direction of the centrifugal field. This number is:

$$dG_{\theta, \theta + d\theta} = v(\theta) \, d\theta \quad (15)$$

where:

$$v(\theta) = \frac{G}{2\pi} \left(1 - \frac{\beta \bar{h}_0^2}{2}\right)^{1/2} \frac{1}{1 - (\beta \bar{h}_0^2/2) \cos^2 \theta} \quad (16)$$

It is obvious that the probability of finding molecules fulfilling the requirements of equation (15) has a maximum for a certain angle. For  $\beta \bar{h}_0^2 < 1$  this angle is  $\theta = 0$ , i.e., the molecules have a tendency to orient themselves in the direction of the centrifugal field. This effect, however, is impossible to detect by experimental means because the Brownian motion is too strong compared with the movement of the molecules due to the centrifugal force. This means that the quantity  $\beta \bar{h}_0^2$  is so small (estimated by Singer to be  $10^{-8}$ ) that the change of  $v(\theta)$  with  $\theta$  is quite negligible.

The mean value of  $h^2$  at a constant value of  $\theta$  is given by:

$$\bar{h}_\theta^2 = \frac{\bar{h}_0^2}{1 - (\beta \bar{h}_0^2/2) \cos^2 \theta} \quad (17)$$

which shows, as could be expected, that the molecules will be stretched at all values of  $\theta$ , except  $\theta = \pm 90^\circ$ . The change in  $\overline{h_0^2}$ , however, is small.

In deducing Svedberg's equation (6), the assumption is made that the frictional coefficient,  $f$ , is the same in both diffusion and sedimentation. Especially in a case where a strong centrifugal field distorts and orients the molecule, one could expect that the frictional coefficient in sedimentation,  $f_s$ , should be different from that in diffusion,  $f_D$ . For free-drained coils Singer has calculated the ratio between these two coefficients as a function of the dimension of the molecule and the strength of the centrifugal force. He obtains:

$$f_s/f_D = (1 + 0.420\beta\overline{h_0^2}) (1 - \beta\overline{h_0^2}/2)^{1/2} \quad (18)$$

where  $f_D$  is taken as proportional to  $\overline{h_0^2}$ . For such comparatively high values of  $\beta\overline{h_0^2}$  as 0.05 and 0.001, we find the  $f_s/f_D$  values, 1.0081 and 1.0001, respectively. It is obvious that in ordinary cases the difference between  $f_s$  and  $f_D$  is quite negligible. In order to understand why this is really true we must remember that the orientation of the molecules in the direction of the centrifugal force tends to decrease the frictional resistance, while the stretching of the molecules tends to increase this resistance. Hence we have two effects opposing each other. For molecules with properties of matted coils the difference between  $f_s$  and  $f_D$  is still less, because  $f_D$  is then approximately proportional to  $\sqrt{\overline{h_0^2}}$ .

### 3. Influence of Branching on Sedimentation Velocity

Threadlike molecules are not always of the simple linear structure assumed in the previous paragraphs. They may be more or less branched. Substances such as cellulose and cellulose derivatives have molecules that most likely are unbranched. Other polysaccharides, such as starch, gum arabic, and dextran, have a high degree of branching. Among synthetic high polymers, branching occurs very often especially if the monomer shows multifunctionality.\* In extreme cases branching ends in a complete network structure. Branching can also occur as a result of a chain transfer process. Another possibility for obtaining molecules of this type is by introducing links between linear molecules: vulcanization of rubber. This possibility also exists in the case of cellulose and cellulose derivatives (30g).

\* The formation of three-dimensional molecules and the distribution of molecular weights as well as gel formation have been studied by Flory (14-16) and Stockmayer (82,83).

Regarding two molecules with the same degree of polymerization, one of them unbranched and the other branched, it is evident that the latter will have a more compact structure. It would be expected, therefore, that with increasing degree of branching the molecule would show sedimentation properties, which are growing more and more similar to those of matted coils. No systematic experimental investigations have been done to study the effect of branching on the sedimentation constant. One of the reasons for this is the difficulty to get branched and unbranched molecules with the same molecular weight. From a comparison between polymers of chloroprene obtained in bulk and emulsion polymerization, respectively, Svedberg and Kinell (84) found some evidence that the molecules from bulk polymerization are of the free-drained type, while those from emulsion polymerization show properties of matted coils. Since in emulsion polymerization, as can be judged from the dependence of solubility on degree of conversion, for instance, the polymer formed is of the  $\mu$  type (55), while in bulk polymerization an  $\alpha$ -polymer is obtained, the results of Svedberg and Kinell to some extent show the influence of branching. No comparison can, however, be made from these measurements between the sedimentation constants of branched and unbranched molecules with the same molecular weight.

A theoretical interpretation of this problem has been given by Kuhn and Kuhn (49). These authors consider the statistical volume of a threadlike molecule. This volume can be defined in the following way:

$$V = \frac{4}{3} \pi \bar{R}_e^3 \quad (19)$$

where  $\bar{R}_e$  is the average distance from one end of the chain to that chain element which has the greatest distance from the end point in question. For a branched molecule this volume,  $V'$ , will be less and Kuhn and Kuhn give the following relation:

$$A' = A_m(V'/V) \quad (20)$$

Here  $A'$  and  $A_m$  represent the preference value (*Vorzugswert*) (44) of the length of the statistical element, which has to be used for the branched and unbranched molecules, respectively. As  $V' < V$  then  $A' < A_m$ . Equation (21), relating the sedimentation constant with the degree of polymeriza-

$$s = \frac{M_g}{N_L} \frac{1 - V\rho}{\eta} (k_1 + k_2 \log \frac{A_m}{d_h} + k_3 \sqrt{bZ/A_m}) \quad (21)$$

tion, valid for an unbranched molecule, can then be used even for a branched molecule with the same degree of polymerization, if  $A'$  is substituted for



$A_m$ . In equation (21),  $M_0$  is the molecular weight of the monomer unit,  $N_L$  is Loschmidt's number,  $\eta$  the viscosity of the solvent,  $d_h$ , the hydrodynamic thickness of the monomer units, and  $b$  its hydrodynamic length. ( $k_1$ ,  $k_2$ , and  $k_3$  are numerical constants, to which Kuhn and Kuhn have given the values 0.02,  $0.16 \log_{10} e$ , and 0.1, respectively.) Using equation (21) Kuhn and Kuhn have studied the quotient  $s(\text{branched})/s(\text{unbranched})$  and found that this ratio is  $> 1$  and increases with increasing degree of branching and degree of polymerization.

Equation (21) can be written in the more general form:

$$s = a + b\sqrt{Z} \quad (22)$$

irrespective of the branched or unbranched nature of the molecule. For a branched molecule, however, the intercept,  $a$ , is less and the slope,  $b$ , greater than for the unbranched molecule. This enables us to make comparisons between molecules with different degrees of branching as soon as the relation between sedimentation constant and degree of polymerization is given for molecules that are known to have a linear shape. It is to be noted that equation (22) describes the properties of matted coils if  $a = 0$  and of free-drained coils if  $b = 0$ . A more complete discussion of the extent to which a branched molecule may be regarded as a matted coil cannot be given on the basis of Kuhn and Kuhn's treatment because the nature of the constants  $k$  in equation (21) is not quite clear from their paper. An experimental justification of equation (22) is given by Kuhn and Kuhn (46) using Mosimann's (59) data on cellulose nitrates in acetone, and by Hermans (24) using Gralén's (20e) data on celluloses in cuprammonium (see Sect. 4 below).

#### 4. Interaction between Molecules. Solvation

In the introduction it was briefly mentioned, that the sedimentation constant especially of threadlike molecules, varies very much with concentration. This is due partly to some sort of mechanical interaction (entanglement) between the solute molecules and partly to solvation phenomena. Furthermore, there is a hydrodynamic interaction between the solute molecules.

To get a stringent mathematical treatment of mechanical interaction is certainly difficult. Nevertheless an approximate estimation can be made of the concentration of a solution in which the molecules can move independently of each other. Signer and Gross (74) in some work on polystyrene assumed the volume, which must be occupied by one molecule in order to meet with the above requirements, to be a cube with a side length

equal to the length of the molecule. From this volume they calculated the corresponding concentration,  $c_1$ , and compared this with the lowest concentration,  $c_2$ , which could be used in a sedimentation run. Their result is given in Table I. The ratio  $c_2/c_1$  indicates that a really free sedimentation can only be obtained at extremely low concentrations. This is in agreement with experimental experience.

TABLE I

Concentration for Free Sedimentation ( $c_1$ ) Compared with Lowest Concentration ( $c_2$ ) Used in Sedimentation of Polystyrenes with Various Intrinsic Viscosities in Chloroform (74)

Intrinsic viscosity of polystyrene sample	$c_1$ , base mole	$c_2$ , base mole	$c_2/c_1$
2.7	0.0017	0.05	30:1
5.6	0.00024	0.0017	7:1 <sup>a</sup>
24	0.000023	0.0010	45:1
47	0.000007	0.0010	140:1
110	0.000002	0.0008	400:1

<sup>a</sup> Signer and Gross have given the value 70:1. This is not in agreement with the given values of the concentrations but is obtained if the more reasonable value 0.017 of  $c_2$  is used.

The influence of solvation is twofold: first, the hydrodynamically active volume of a solvated molecule is greater than that calculated from the molecular weight and the partial specific volume; second, due to the solvation mantle a certain amount of solvent moves with the molecules.\* The frictional resistance will not only be dependent upon the shape of the molecule but also upon the degree of solvation. Probably the frictional coefficient will increase because a solvated molecule will be stiffer in proportion to the degree of solvation. The movement of the solvation mantle with the molecule causes a transport of solvent and as the volume of the cell is finite another transport of free solvent in the opposite direction must necessarily occur. Hence the velocity of the solvated molecule relative to the solvent is higher than the velocity relative to the walls of the cell. Enoksson (12) has made an elementary approach to the solution of this problem. He regards the molecule with its solvation mantle as a sedimenting unit with

\* This phenomenon has been used by Sihtola and Svedberg (77) to determine the solvation mantle. The substance is dissolved in a mixture of a solvent and a nonsolvent. These have the same density but different refractive indexes. The amount of nonsolvent will increase above the boundary and the size of the solvation mantle can be calculated from the difference in refractive index between the solutions above and below the sedimenting boundary.

the specific sedimentation volume  $\Phi$ , and obtains the following equation for the sedimentation constant as a function of concentration,  $c$ :

$$s(c) = s'(1 - \Phi c) \quad (23)$$

where  $s'$  is the sedimentation constant relative to the solvent. Generally both  $s'$  and  $\Phi$  have to be regarded as functions of concentration. The complete interpretation of  $s'$  is not yet given. Assuming it is independent of concentration it must necessarily be identical with the sedimentation constant at infinite dilution,  $s_0$ . Then the change of  $s$  with  $c$  is completely determined from the sedimentation volume  $\Phi$ . This quantity is probably not determined by the solvation alone. According to the influence of the sedimenting particles upon the movement of the surrounding medium discussed by Burgers (5), it may be much larger than the solvation mantle. Before knowing something about  $s'$  in the general case, it is not possible to estimate the full applicability of equation (23) to threadlike molecules. A test of the validity of equation (23) has so far only been given for proteins.

The hydrodynamic interaction between solute molecules is due to the above-mentioned influence of a sedimenting particle on the solvent. Another particle will be carried along with a certain velocity,  $u_m$ . The presence of the second particle will, however, experience an induced retardation velocity,  $u_i$ , on the first particle. Both particles will have the same resultant velocity,  $u_{res}$ , which for spherical particles is given by Burgers (5-7):

$$\begin{aligned} u_{res} &= \frac{F}{8\pi\eta} \left( \frac{4}{3a} + u_m + u_i \right) \\ &= \frac{F}{8\pi\eta} \left( \frac{4}{3a} + \frac{1 + \cos^2 \alpha}{r} + \frac{2a^2 (1 - 3 \cos^2 \alpha)}{3r^3} - \frac{5a^3 \cos^2 \alpha}{r^4} \right) \quad (24) \end{aligned}$$

$F$  is the force exerted on the particles,  $\eta$  the viscosity of the medium,  $a$  the radius of the spheres,  $r$  the distance between their centers, and  $\alpha$  the angle between the direction of  $r$  and the direction of motion.

Hermans (23) has made an interesting application of Burgers' theory to threadlike molecules. He regards the molecule in the sense of Kuhn. Under the influence of the force  $F$  each statistical element (length  $A$ ) will get a velocity  $F/3\pi\eta A$  according to Stokes. To this velocity we have to add all the velocities  $u_m$ , which the adjacent statistical elements will exert on the element in question. For this calculation it is necessary to take the mean value over all the statistical elements. Using the expression:

$$f(r) = \exp(-r^2/2\sqrt{3}NA^2) \quad (25)$$

as the density distribution for the middle points of the statistical elements, Hermans gets the following value for the additional velocity:

$$\delta u = \frac{NF}{6\pi\eta} \frac{\int_0^\infty 4\pi r^2 \cdot f/r \cdot dr}{\int_0^\infty 4\pi r^2 f dr} = \frac{F}{3\pi\eta A} \sqrt{\frac{3N}{2\pi}} \quad (26)$$

Only the second and third terms in equation (24) have to be used. The third term has been assumed to be so small that it does not influence this approximate calculation. As the density distribution is highest in the central parts of the molecular coil, Hermans has limited the averaging of equation (24) over  $\alpha$  to central elements and this gives:  $F/6\pi\eta r$ .

Hence the total sedimentation velocity is given by:

$$u \cong \frac{F}{3\pi\eta A} (1 + \sqrt{N}) \quad (27)$$

The contribution from the second term can evidently be quite large since  $N$  is a comparatively large number. Hermans has used equation (27) on Mosimann's (59) data for cellulose nitrate in acetone solution. The result is given in Table II. The constancy of the values in the last column

TABLE II

Relation between Sedimentation Constant and Number of Statistical Elements for Various Cellulose Nitrates in Acetone Solution (23)

$M$	$Z$	$N$	$s_{20}$ , S units	$s/(1 + \sqrt{N})$
613,000	2,320	129	30	2.4
199,000	755	42	18	2.4
80,200	304	17	12.0	2.4
30,000	114	6.3	8.7	2.5
6,200	24	1.3	5.2	2.5

is very striking and in this molecular weight interval the following relation is valid:

$$s = 2.4 \times 10^{-13} (1 + \sqrt{N}) \quad (28)$$

A similar relation also holds for cellulose acetate in the molecular weight interval, 55,000–222,000 (40). The agreement for methyl cellulose and polystyrene is not so good. The reason for this may be experimental difficulties in investigating these substances or insufficiencies in the theory. Finally, Hermans (24) has used some of Gralén's (20e) data for cellulose in cuprammonium solution. As is seen from Figure 1,  $s$  as a function of  $\sqrt{N}$  (i.e.,  $\sqrt{M}$ ) is very near to a linear relationship. It has to be empha-

sized that Gralén's measurements were performed on unfractionated samples.

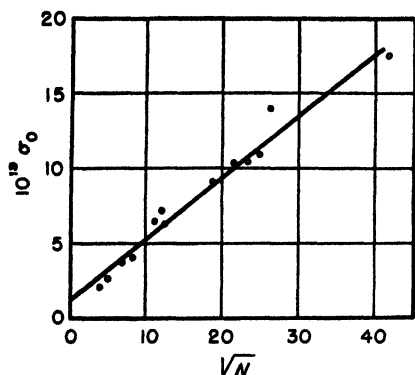


Fig. 1. Sedimentation constant plotted against square root of the number of statistical elements (24). Cellulose in cuprammonium solution.

### 5. Influence of Shielding Ratio

In a theoretical investigation on the intrinsic viscosity of high-polymer solutions, Debye (11,11a) studied how the flow lines are disturbed inside and outside the space covered by a molecule. He has introduced a shielding ratio, defined as the quotient between the size of the occupied space and a shielding length (dependent upon the density of the monomer units in the space). This ratio characterizes the extent to which the bulkiness of the molecules is screening off the space inside the molecule for actions from disturbances in the surrounding medium. Now the frictional coefficient,  $f$ , for threadlike, unbranched molecules can be expressed as a function of this shielding ratio,  $\sigma$ , and the degree of polymerization,  $Z$ , in the following way:

$$f = K \cdot Z^{\epsilon(\sigma)} \quad (29)$$

where  $K$  is a constant and  $\epsilon$  is determined from:

$$\epsilon(\sigma) = \frac{1}{2} + \frac{1}{5} \frac{\sigma}{\psi} \frac{d\psi}{d\sigma} \quad (30)$$

with:

$$\psi(\sigma) = \frac{1 - (1/\sigma) \tanh \sigma}{1 + (3/\sigma^2) (1 - (1/\sigma) \tanh \sigma)} \quad (31)$$

In a case in which the shielding is very weak ( $\sigma = 0$ ),  $f$  will be proportional to  $Z(\epsilon(0) = 1)$  and hence the sedimentation constant independent of

the molecular weight. If the shielding is very strong ( $\sigma = \infty$ ),  $f$  and  $s$  will both be proportional to the square root of  $Z$  and the molecular weight ( $\epsilon(\infty) = 1/2$ ). Thus we find Kuhn's hydrodynamic models as limiting cases in a more general consideration of the behavior of the molecules with respect to their surrounding medium.

### 6. *Sedimentation as a Rate Process*

A molecule in a liquid may be regarded as jumping between equilibrium positions. The motion is quite random but if a force is applied to the molecule it will jump more often in the direction of the force. Between two equilibrium positions the molecule has to pass an energy barrier. It is possible to treat this movement of the molecule from the standpoint of rate processes. Powell and Eyring (66) have performed such a calculation and their final result is:

$$s \cdot \eta = m\lambda_1/h\lambda_2\lambda_3 \quad (32)$$

where  $\eta$  is the viscosity of the solution,  $m$  the mass of the particle,  $\lambda_1$ ,  $\lambda_2$ , and  $\lambda_3$  molecular distances, and  $h$  Planck's constant. Applying this to data of Signer and Gross (74) on polystyrene in chloroform solution, Powell and Eyring have found a rather good constancy of the product  $s \cdot \eta$ . Laufer (54) has found the same result for tobacco mosaic virus. Jullander (30d), however, has shown that for cellulose nitrate in acetone  $s \cdot \eta$  increases with concentration, both for samples with small and large molecular weights.

### 7. *Concentration Dependence*

In all measurements on macromolecules in solution it is quite a common experience that the measured quantities depend upon the concentration of the solute. Thus intrinsic viscosity, diffusion constant, osmotic pressure, sedimentation constant, etc. depend upon the amount of macromolecules dissolved in a given volume of solvent. Earlier in this section we have briefly mentioned the concentration dependence of the sedimentation constant, namely, in connection with molecular entanglement, solvation, hydrodynamic interaction, and rate processes. Nothing, however, has been said about the results from experimental investigations and the relation between quantities characterizing the sedimentation constant as a function of concentration and corresponding quantities for diffusion and osmotic pressure.

From a great number of investigations on substances with threadlike molecules it is known that the sedimentation constant at relatively high

concentrations does not depend very much on concentration. At a certain value, however, the curve shows a rather sharp curvature and then the sedimentation constant increases very much with decreasing concentration. This is especially true for high molecular weights. An example is shown in Figure 2, where the relation between  $s$  and  $c$  has been plotted for four fractions of cellulose nitrate with degrees of polymerization equal to 2400, 1300, 450, and 130, respectively. The solvent is acetone; the measurements have been performed by Rånby (see under Selectivity of Fractionation, Sect. V.1). For  $c > 0.25$  g./100 ml., the sedimentation

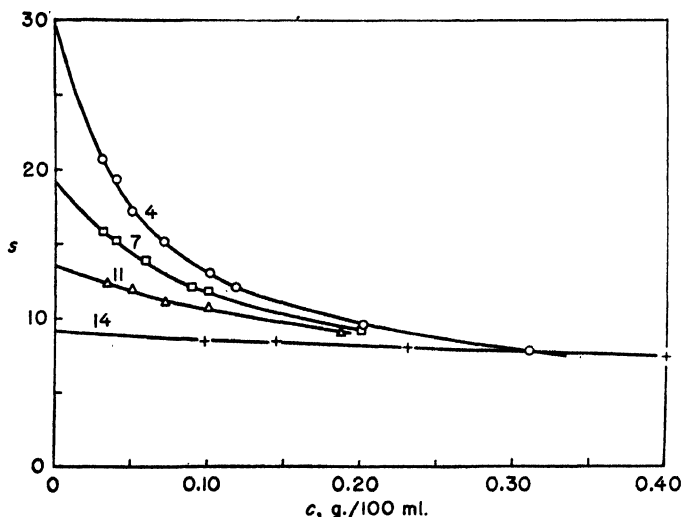


Fig. 2. Sedimentation constant as a function of concentration of solute for cellulose nitrates in acetone solution.

constant has approximately the same value irrespective of the molecular weight (about 8 S). This is probably connected with a very high number of entanglements between the molecules. Each molecule has lost its individual character and there is no free sedimentation. At about  $c = 0.15$  g./100 ml., the molecules seem to begin a more free sedimentation. Below this concentration their velocity increases—the more rapidly, the higher the molecular weight.

Attempts have been made to find a mathematical expression to describe this behavior of the molecules. Signer and Gross (74) found that for polystyrene in chloroform the reciprocal of the sedimentation constant was a linear function of concentration; the same was found by Lauffer (54) on tobacco mosaic virus, and by Gralén (20a) on cellulose in cuprammonium

and on cellulose nitrate in acetone. Gralén, therefore, proposed the following concentration function for the sedimentation constant:

$$s = s_0/(1 + k_s c) \quad (33)$$

$s_0$  is the  $s$  value at infinite dilution and  $k_s$  is a constant characterizing the concentration dependence. This expression is in full agreement with an equation derived by Burgers (7) for spherical particles:

$$s = s_0/(1 + 6.875 Vc) \quad (34)$$

where  $V$  is the partial specific volume of solute. (For most proteins with spherical and ellipsoidal molecules a linear relationship  $s = s_0 (1 - k_s c)$  holds (64).)

Comparing equations (9) and (33) we can write:

$$f_{s,c} = f_{s_0} (1 + k_s c) \quad (35)$$

if the change in density going from solvent to a dilute solution is small in comparison with  $k_s$ . The partial specific volume is independent of concentration in dilute solutions (20,30b). Assuming the driving force of the diffusion process to be the gradient of the free energy of dilution of the system, Singer (81) has expressed the diffusion constant in the following way:

$$D_c = \frac{RT}{f_{D,c}} \left( 1 + \frac{2BM}{RT} c \right) \quad (36)$$

where  $B$  is the constant in the quadratic term of the osmotic pressure relation:  $\pi = (RT/M)c + Bc^2$ . From equations (35) and (36) we obtain:

$$\frac{1 + (2BM/RT)c}{1 + k_s c} = 1 + k_{Dc} + \dots \quad (37)$$

where  $k_{Dc}$  is a constant characterizing the concentration dependence of  $D$  (20d). The value of  $k_{Dc}$  from equation (37) is given by:

$$k_{Dc} = (2BM/RT) - k_s \quad (38)$$

The concentration dependence of the diffusion constant is due to a balancing of two effects: the thermodynamic, tending to increase  $D$ , and the hydrodynamic, tending to decrease  $D$  (compare also Beckmann and Rosenberg) (2). In most cases  $k_{Dc}$  is positive but sometimes it can be slightly negative. Equation (38) has been proved to be valid within experimental errors. For cellulose acetates in acetone Singer has obtained the values of  $2BM/RT$  and  $k_s$  given in Table III. With respect to some of Gralén's (20d) data the two effects do not always seem to balance each other to give



a low  $k_D$  value. Nevertheless, an equation of the type of equation (38) seems to hold even for his substances (79). (Simha has also given an equation similar to equation (38) but including the specific volume of the solute (78).) More data, however, are necessary for the final experimental proof and furthermore, as Singer points out, the specific thermodynamic properties of high-polymer solutions must be taken into account and  $k_s$  and  $k_D$  studied as functions of the entropy and heat of dilution of such solutions.

TABLE III

Comparison between Concentration Dependence in Osmotic Pressure and Sedimentation for Fractions of Cellulose Acetate in Acetone Solution (81)

Fraction	$\frac{\pi}{c}$ , S units	$\frac{D_{90}}{c}$ $\times 10^7$	$M_n$	$M_{s,D}$	$2BM/RT$	$k_s$
15 . . . .	4.07	20.7	11,000	10,350	$14 \pm 2$	$6 \pm 10$
9 . . . .	7.5	7.7	53,000	51,000	$64 \pm 6$	$56 \pm 15$
2 . . . .	10.9	4.0	130,000	143,000	$179 \pm 17$	$143 \pm 20$
2c . . . .	12.5	3.4	—	194,000	$243 \pm 23$	$191 \pm 25$

In the region  $c > 0.25$  g./100 ml. (Fig. 2) the sedimentation constant was practically independent of the concentration and—what is more important—of the molecular weight. Probably the sedimentation in such cases consists of a movement of a gellike structure. Within this the molecular weight of the molecules has no significance with regard to the sedimentation properties. More important are probably the dimension of the monomer units with their solvation mantles and the length of the chain between points of entanglement. From experiments on models and the application of a principle of hydrodynamic similarity,\* Kuhn (41) has arrived at the expression:

$$s = \frac{a(1 - V\rho)}{\eta V(\alpha + \beta\varphi)} \quad (39)$$

where  $a$  is the cross section of the molecular chain,  $\varphi$  the volume fraction of the high polymer, and  $\alpha$  and  $\beta$  constants ( $\alpha = 6.5$  and  $\beta = 515$  in Kuhn's paper). Starting from Mosimann's data (59), Kuhn has used equation (39) to calculate the thickness of the cellulose nitrate molecules in solution. He found the value  $12 \text{ \AA}$ ., which is in rather good agreement with the

\* This principle states that the condition of flow of a liquid in an arbitrary arrangement does not change if this arrangement undergoes a uniform isotropic enlargement or reduction. For the comparison of a model and a gel, Kuhn (44) gives the relation  $\Gamma_{\text{mod}} = \alpha^2 \Gamma_{\text{gel}}$ , where  $\alpha$  is a linear factor of enlargement.

value 8 Å. obtained for nonsolvated molecules by means of x-ray measurements.

In connection with the concentration dependence, another effect must be mentioned. Strictly speaking, equation (7) determines the dilution due to the sector shape of the cell only in a case where the sedimentation velocity does not change with the concentration. If this is the case, the sedimentation velocity will have different values in different parts of the cell and ordinarily increases with the distance from the center of rotation. Furthermore this change in the sedimentation constant must influence the dilution effect. Kinell (32) has given the following relation:

$$\frac{c \cdot s(c)}{c_0 \cdot s(c_0)} = \left(\frac{x_0}{x}\right)^2 \quad (40)$$

valid for a sedimentation dependent on concentration and corresponding to equation (7). Applying this to equation (33) we obtain:

$$s(c) = s_0 - \left(\frac{x_0}{x}\right)^2 (s_0 - s(c_0)) \quad (41a)$$

In this special case  $s(c)$  is a linear function of the inverse square of the distance from the center of rotation. Using equation (7) we get:

$$\frac{1}{s(c)} = \frac{1}{s_0} + \left(\frac{x_0}{x}\right)^2 \left(\frac{1}{s(c_0)} - \frac{1}{s_0}\right) \quad (41b)$$

From the data given by Lauffer (54) on tobacco mosaic virus the regression lines corresponding to equations (41a) and (41b) have been calculated. The coefficients of correlation are 0.81 and 0.75, respectively. The fitting of the line is thus a little better in the case of equation (41a). However, the differences cannot be expected to be large since the concentration dependence of the tobacco mosaic virus is not very pronounced.

### 8. Effects of Polymolecularity

In concluding this section something must be said about the influence of polymolecularity on the sedimentation. The discussion, hitherto, has been concerned exclusively with single molecules or groups of molecules having the same degree of polymerization. In all cases, where the influence of concentration can be neglected each molecule sediments in its own manner and the sedimentation is completely determined from the hydrodynamic properties of the molecules. Theoretically there should be a difference in orientation between short and long molecules but, as has been shown, the orientation is quite negligible even for long molecules. At

higher concentrations, however, certain effects may occur, especially if the molecules have different frictional coefficients. Entangled molecules, for instance, may superpose on each other their specific properties. From an experimental point of view such effects are not too serious because they disappear at a sufficiently low concentration.

Due to the different sedimentation velocities in a polymolecular substance the boundary between solution and solvent will be spread out and this gives rise to a broad concentration gradient curve. As the experimental determination of the sedimentation constant is made from the position of the maximum point of the concentration gradient curve at different times, it can be of interest to study the effect of polymolecularity upon the determined value. Neglecting the influence of concentration dependence, we easily find the following relation between the frequency function,  $dc_0/ds$ , of the sedimentation constants and the concentration gradient curve,  $dc/dx$ :

$$\frac{dc_0}{ds} = \frac{dc}{dx} x_0 \omega^2 t \exp(3\omega^2 st) \quad (42)$$

From this we get a condition for the  $dc/dx$  curve to have a maximum at a definite time  $t$  (32):

$$\frac{d^2c_0}{ds^2} - 3\omega^2 t \frac{dc_0}{ds} = 0 \quad (43)$$

It is immediately seen that the value,  $s_m$ , calculated from the  $x$  coordinate,  $x_m$ , corresponding to the maximum point of the  $dc/dx$  curve does not coincide with the value,  $\bar{s}$ , corresponding to the maximum point of the  $dc_0/ds$  curve. In equation (43),  $3\omega^2 t(dc_0/ds)$  is always positive and hence also  $d^2c_0/ds^2$  must be positive. Consequently:

$$s_m(t) \leq \bar{s} \quad (44)$$

where the equality sign has to be used for  $t = 0$ . From equation (43) we easily find ( $dc_0/ds = \Psi(s_m)$ ):

$$\frac{ds_m(t)}{dt} = \frac{3\omega^2 \Psi(s_m)}{\Psi''(s_m) - (3\omega^2 t)^2 \Psi(s_m)} \quad (45)$$

This displacement effect is primarily determined from the shape of the  $dc_0/ds$  curve in the vicinity of the maximum point. Hence we can get an idea of the influence of the degree of polymolecularity on this displacement by discussing equation (45) at  $t = 0$ . Then we have

$$\left( \frac{ds_m(t)}{dt} \right)_{t=0} = \frac{3\omega^2 \Psi(\bar{s})}{\Psi''(\bar{s})} \quad (46)$$

Consequently the decrease in  $s_m$  is the larger the less the curvature at the maximum point. Thus comparing frequency functions of the same class (only differing in a parameter value) the decrease in  $s_m$  will be the larger the more polymolecular the substance. As an example we solve equation (43) for a logarithmic frequency function (see Sect. IV.4) characterized by a distribution coefficient  $\gamma_s$ . Then we obtain:

$$(\bar{s}/s_m) = (x_m/x_0)^{3\gamma_s/2} \quad (47)$$

For  $\gamma_s < 0.1$  the effect is less than 2 to 3 per thousand,  $\gamma_s = 0.5$  gives  $\bar{s}/s_m = 1.036$  and 1.071 for  $x_m/x_0 = 1.1$  and 1.2, respectively, and  $\gamma_s = 1.0$  gives  $\bar{s}/s_m = 1.154$  and 1.315 for the same  $x_m/x_0$  values. The effect is thus large only for substances with a very high degree of polymolecularity.

#### IV. Information on Polymolecularity from Sedimentation Measurements

We have seen that the shape of the concentration gradient curve will depend upon the nature of the frequency function of the sedimentation constants of the molecules in a polymolecular substance. From the foregoing it is also clear that the sedimentation constant can be regarded as an algebraic function of the molecular weight. Hence the concentration gradient curve will give the general features of the frequency function of the molecular weights. From sedimentation diagrams, therefore, it is possible to deduce the distribution of sizes of particles in a polymolecular substance. Since the development of the ultracentrifugal technique, this method has been widely used, for instance, by Rinde (67) on gold sols and by Nichols *et al.* (89a) on suspensions of ferric oxides and barium sulfates, on emulsions and rubber latex, etc. For substances with a pronounced concentration dependence, the method used by these workers is not directly applicable. The frequency function is very much distorted due to the change in sedimentation velocity with concentration. The skewness of the curve may be altered and, furthermore, for frequency curves with several maxima, the heights of the maxima may change considerably during the sedimentation due to boundary effects. Such effects are most clearly observed if a substance with only two components is sedimenting. The slower moving component will then show an increase in amount if the sedimentation velocity changes when the substance passes the boundary. This effect was first observed by McFarlane (56) and Pedersen (63) in mixtures of proteins. Johnston and Ogston (29) explained it as a boundary effect typical for concentration dependent sedimentation. The influence of this effect on the sedimentation curve of polymolecular substances has

so far not been completely interpreted. Kinell (35), however, in a study of the sedimentation properties of polymeric methyl methacrylates has found that the sedimentation constant determined for the unfractionated material from the maximum of the concentration gradient curve does not coincide with the maximum of the frequency function obtained by adding the functions corresponding to fractions of the original substance. The observed value is 58 S and the value corresponding to the maximum of the frequency function is 70 S. The difference is too large to be explained as only a displacement due to polymolecularity. Notwithstanding the difficulties connected with the interpretation of sedimentation diagrams obtained from polymolecular substances, they have been used rather extensively in the determination of polymolecularity. In this section the methods that have been worked out for this purpose will be discussed.

### 1. Average Sedimentation Constants

From the discussions in Section III.8, it is evident that the sedimentation constant calculated from the movement of the maximum of the concentration gradient curve belongs to only one species in the polymolecular mixture. One of the first questions which arise is then, to what extent it is possible to obtain average values of the sedimentation constants directly from the sedimentation diagram? This is very important in order to get the average sedimentation properties of a system of molecules.

In a case where we can neglect the concentration dependence and the influence of diffusion it is very easy to get any desired average value of the sedimentation constant. This follows from the fact that the relation between the original frequency function,  $dc_0/ds$ , and the concentration gradient curve,  $dc/dx$ , is very simple. From equations (4) and (42) we obtain:

$$\frac{dc_0}{ds} = \frac{dc}{dx} x_0 \omega^2 t \left( \frac{x}{x_0} \right)^3 \quad (48)$$

Thus the  $dc_0/ds$  curve can easily be traced and any desired average values be calculated. When the sedimentation constant varies with the solute concentration this method is not very useful because the relation between the sedimented distance,  $x$ , and the sedimentation constant,  $s(c)$ , for a definite species in the mixture is not known unless the  $k_s$  values have been determined for all species.

A comparatively simple way to calculate the weight average value of  $s$  has been suggested by Kinell (34). By taking the quotient,  $T$ , between the first moment and the area of the concentration gradient curve, that is:

$$T = \frac{\int_{x_1}^{x_2} x (dc/dx) dx}{\int_{x_1}^{x_2} (dc/dx) dx} \quad (49)$$

where  $x_1$  and  $x_2$  are determined from  $(dc/dx)_{x_1} = (dc/dx)_{x_2} = 0$  (this is possible at any time, when all the substance has left the meniscus), it is possible to show that:

$$(s_0)_w = \bar{s}_0 (dT/dx_m)_{t=0} \quad (50)$$

Here suffix 0 indicates that the expression is valid at infinite dilution,  $w$  indicates weight-average value.  $T$  is calculated for sedimentation diagrams obtained at different times from the start of the sedimentation. The derivative taken at  $t = 0$  is then plotted against concentration and extrapolation is made to infinite dilution. In the attempts hitherto made to apply this method to actual cases the results have not been too stimulating. The reason is probably that the sedimentation diagram is not accurate enough to permit the drawing of good base lines. Hence the calculated values of the first moments are not accurate. In case of diffusion diagrams the accuracy is always sufficient to allow a calculation of the weight-average value of the diffusion constant from the second moment and the area.

## 2. $dB/dx$ Method According to Gralén

As a relative measure of the polymolecularity from sedimentation measurements, Gralén (20b) introduced the width,  $B$ , of the sedimentation curve defined as the quotient between the area,  $A$ , and the height,  $H$ , that is:

$$B = A/H \quad (51)$$

According to Gralén the diffusion can be neglected, as, in the case of thread-like molecules, it never involves errors larger than 2 or 3% if the diffusion constant does not exceed  $10 \times 10^{-7}$  c.g.s. Plotting  $B$  against the position of the peak in the cell, Gralén found that in most cases it varied linearly with this distance. It was also evident that the derivative,  $dB/dx$ , varied with the total concentration. By extrapolating to infinite dilution, the value  $(dB/dx)_0$  is obtained. This value is a relative measure of the curve width for free sedimentation. From a simple consideration Gralén stated that the following approximate relation between  $(dB/dx)_0$  and quantities characterizing the frequency function holds:

$$\left(\frac{dB}{dx}\right)_0 = \frac{\int_{s_1}^{s_2} (dc_0/ds_0) ds_0}{(dc_0/ds_0)_{\max} \bar{s}_0} = \frac{\Delta s_0}{\bar{s}_0} \quad (52)$$

where  $\Delta s_0$  is the width which, multiplied by the maximum height, gives the total amount of substance. For the quantity  $(dB/dx)_0$  the name *widening value* of the sedimentation curve has been introduced.

As to the concentration dependence of  $dB/dx$ , Gralén and Lagermalm (21) have shown that in case of symmetrical frequency curves the following approximate relation holds:

$$(dB/dx) = (dB/dx)_0 - K \cdot c \cdot s \quad (53)$$

where  $K$  is a constant. For many substances  $K$  is almost independent of the molecular weight.

An analysis of the factors, which may influence the  $dB/dx$  value, made by Kinell (33) has shown that the width of the sedimentation curve is not only determined from the different sizes of the molecules but also from the increase in the centrifugal field with the distance from the center of rotation. The width of the curve is larger than what would be expected from the polymolecularity. Furthermore the value depends on whether the calculation is carried out in the originally plotted sedimentation diagram or whether it is made in a diagram, where a correction has been made for the dilution due to the sector shape of the centrifuge cell. Finally  $dB/dx$  is affected by the characteristic displacement of the maximum point of the sedimentation curve (see Sect. III.8). The analysis, which has been made for a sedimentation independent of concentration, has given the result, that  $dB/dx$  generally cannot be a linear function of  $x$ . If the calculation is made in the original sedimentation diagram  $dB/dx \geq (dB/dx)_{t=0}$  depending upon the nature of the frequency function. In a corrected diagram  $dB/dx > (dB/dx)_{t=0}$  independent of the frequency function. The deviations are, however, small and no serious errors are introduced, when Gralén's simple procedure is used, assuming that the polymolecularity is not extremely pronounced.

From Kinell's investigation it also follows that the equation (52) is strictly valid only in the case of  $t = 0$ . Defining a width  $\bar{B}$  by the expression:

$$\bar{B} = \frac{c_0}{(\bar{x}/x_0)^2 (dc/dx)_{x=\bar{x}} \log (\bar{x}/x_0)} \quad (54)$$

where  $\bar{x}$  is the  $x$  coordinate corresponding to the maximum height of the frequency function, it is easily shown that:

$$\bar{B} = \frac{\int_{s_1}^{s_2} (dc_0/ds_0) ds_0}{s_0 (dc/ds_0)_{s_0=s_0}} \bar{x} \quad (55)$$

Thus  $\bar{B}$  is a linear function of  $\bar{x}$  and the derivative  $d\bar{B}/d\bar{x}$  is independent of  $\bar{x}$ . The derivative is always related in a simple way to quantities characterizing the frequency function. This method of calculation is even applicable to substances with concentration-dependent sedimentation as shown by Kinell for a sample of polymeric methacrylate in acetone solution. The values of  $d\bar{B}/d\bar{x}$  in Table IV are as constant as can be expected with respect to the experimental accuracy.

TABLE IV

Values of  $d\bar{B}/d\bar{x}$  as a Function of  $\bar{x}$  Calculated at Different Concentrations (Grams per Hundred Milliliters) for Polymeric Methyl Methacrylates in Acetone Solution (33)

$c_0 = 0.396$		$c_0 = 0.298$		$c_0 = 0.198$	
$\bar{x}$	$d\bar{B}/d\bar{x}$	$\bar{x}$	$d\bar{B}/d\bar{x}$	$\bar{x}$	$d\bar{B}/d\bar{x}$
5.991	0.24	5.954	0.40	6.031	0.47
6.045	0.23	6.018	0.34	6.095	0.41
6.101	0.21	6.076	0.28	6.170	0.42
6.213	0.23	6.133	0.32	6.251	0.43
6.333	0.21	6.262	0.32	6.407	0.42
6.462	0.23	6.400	0.32	6.556	0.37
6.595	0.21	6.549	0.31	6.735	0.37
		6.688	0.29	6.881	0.43
$0.22 \pm 0.01$		$0.32 \pm 0.03$		$0.41 \pm 0.02$	
$c_0 = 0.104$		$c_0 = 0.047$		$c_0 = 0$	
$\bar{x}$	$d\bar{B}/d\bar{x}$	$\bar{x}$	$d\bar{B}/d\bar{x}$	$(d\bar{B}/d\bar{x})_0$	
6.109	0.55	6.074	0.49	$0.61$	
6.207	0.48	6.146	0.50		
6.274	0.54	6.228	0.48		
6.404	0.55	6.332	0.61		
6.548	0.50	6.414	0.68		
9.778	0.52				
$0.52 \pm 0.03$		$0.55 \pm 0.07$			

The sedimentation constant depends upon the shape of the molecules. However, it has been shown that the sedimentation constant can be regarded as an algebraic function of the molecular weights. Then it is possible to express  $(d\bar{B}/d\bar{x})_0$  in quantities characterizing the frequency function of molecular weights (real molecular size). Assuming the following relation between  $s$  and  $M$  to be valid:

$$s_0 = \text{const.} \times M^{1-\alpha} \quad (56)$$



we get from equation (52):

$$\left(\frac{dB}{dx}\right)_0 = \frac{\int_{\bar{M}_1}^{M_2} (dc_0/dM) dM}{\bar{M}(dc_0/dM)_{M=\bar{M}}} (1 - a) \quad (57)$$

where  $\bar{M}$  is the molecular weight corresponding to the maximum of the frequency function of the sedimentation constants. The constant  $a$  has the value 1 for free-drained molecules,  $1/2$  for matted coils, and  $1/3$  for spheres. Two  $dB/dx$  values can be compared only if they refer to molecules with similar sedimentation properties.

The simplicity of Gralén's method makes it a very valuable tool to get firsthand information about the distribution of molecular species in a poly-molecular substance. As will be shown in Section V, it can also be used to construct the frequency curve of a substance from the frequency curves of its fractions.

### 3. Frequency Functions from Sedimentation Diagrams

Some of the difficulties encountered in obtaining frequency functions from sedimentation diagrams have been mentioned. In order to avoid all the influences from the concentration dependence, some method of extrapolating the sedimentation diagrams to infinite dilution must be used.

In their work on polystyrene, Signer and Gross (75) have proceeded in the following way. The function  $s = f(M)$  has been determined on fractionated samples by means of sedimentation and equilibrium measurements. (It is also possible to use sedimentation and diffusion.) The sedimentation diagram of the unfractionated sample was then determined and the function  $dc/ds = f(s)$  converted into a function  $dc/dM = f(M)$ . The method is not very accurate since Signer and Gross do not take into consideration the variation of the sedimentation velocity with concentration. Jullander (30e) has improved the method and used it on samples of cellulose nitrate. In order to have the shape of the sedimentation diagram determined accurately, exposures taken at different times from the start of the sedimentation are reduced to a common basis. This is made in a way described by Kraemer (36). The diagram obtained at a time  $t_i$  is reduced to a time  $t_1$  by means of the following equations:

$$x_1 = x_0 \left( \frac{x_i}{x_0} \right)^{(t_i/t_1)} \quad (58)$$

$$h_1 = h_i \left( \frac{x_i}{x_1} \right)^2 \frac{x_i - x_0}{x_1 - x_0} \quad (59)$$

where  $h$  is the height of the curve at a distance  $x$  from the center of rotation and  $x_0$  the position of the meniscus. Figs. 3-5 show the result obtained by

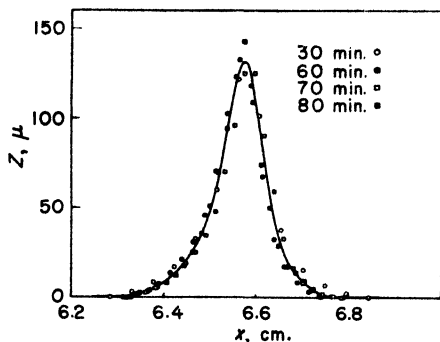


Fig. 3. Comparison between sedimentation diagrams for cellulose nitrate in acetone solution from different exposures (30, 60, 70, 80 min. after full speed of rotor is reached) when reduced to same point of time (30). Original concentration, 0.180 g./100 g.  $Z$  is the scale line displacement in  $\mu$ .

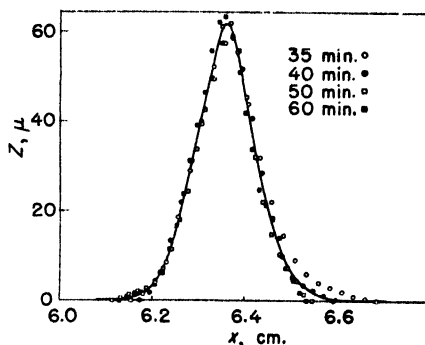


Fig. 4. Comparison between sedimentation diagrams for cellulose nitrate in acetone solution from different exposures (35, 40, 50, 60 min. after full speed of rotor is reached) when reduced to same point of time (30). Original concentration, 0.100 g./100 g.  $Z$  as in Fig. 3.

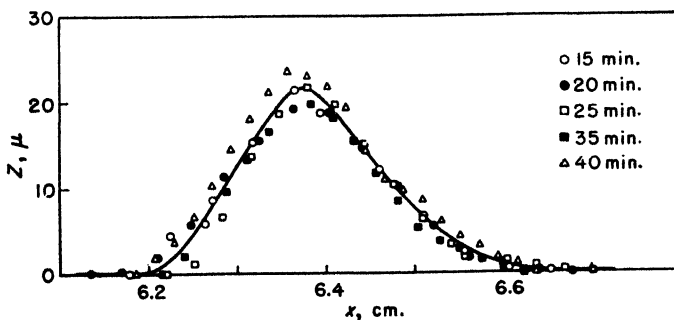


Fig. 5. Comparison between sedimentation diagrams for cellulose nitrate in acetone solution from different exposures (15, 20, 25, 35, 40 min. after full speed of the rotor is reached) when reduced to the same point of time (30). Original concentration, 0.051 g./100 g.  $Z$  is the scale line displacement in  $\mu$ .

Jullander (30c) for a cellulose nitrate with  $M_n = 133,000$  and  $M_v = 151,000$ . No systematic difference appears between the curves derived from exposures at different times. This shows that the diffusion has no influence and

the widening of the curves is due to polymolecularity only. These curves can now be transformed into curves  $dc/ds = f(s)$ . The transformation of the  $x$  axis into an  $s$  axis is easily made from the known value of the sedimentation constant calculated from the maximum or the arithmetic mean

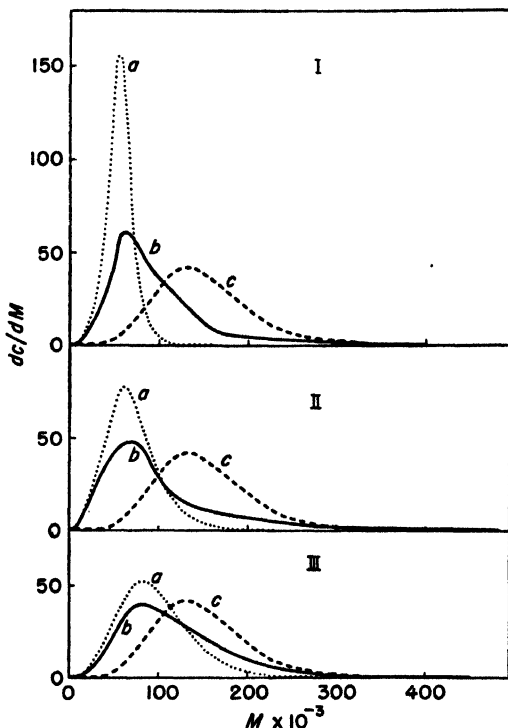


Fig. 6. Frequency functions of cellulose nitrate ( $M_n = 133,000$ ,  $M_w = 151,000$ ) calculated from sedimentation diagrams (Figs. 3-5) (30). Curves *a* calculated according to Signer and Gross; curves *b* corrected for influence of concentration; curves *c* are the corresponding three-parameter function. The areas of the curves are equal. I, II, and III correspond to Figures 3, 4, and 5, respectively.

of the sedimentation curves. The heights need not be changed, because  $dc/dx = dc/ds \cdot ds/dx$ , where  $ds/dx$  is nearly constant. From the data given by Mosimann (59) on fractionated cellulose nitrate, Jullander calculated relations between  $s$  and  $M$  at different concentrations. In order to transform a given  $s_i$  into the equivalent value  $M_i$  the corresponding concentration  $c_i$  is obtained from the integrated  $dc/ds$  curve and from the  $s$ ,

$M$  relation corresponding to this concentration  $M_i$  is read.  $dc/ds$  is then converted into  $dc/dM$  and the curve  $dc/dM = f(M)$  is drawn. A comparison between the original method of Signer and Gross, and Jullander's modified method is given in Figure 6. From curves  $a$  and  $b$  it is obvious that Signer and Gross's method gives too small a polymolecularity. The differences between the curves diminish with decreasing concentration. The curve  $c$  will be discussed later (Sect. 4). In order to make a construction like this it is necessary to know the relation between  $s$  and  $M$  for fractions of the substance. This is not a serious drawback because the same  $s$ ,  $M$  diagram can be used for several substances of the same type.

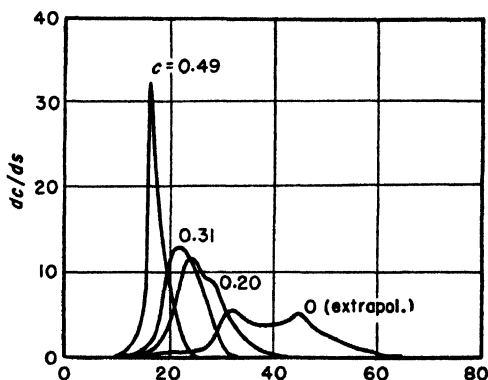


Fig. 7. Frequency functions of polystyrene obtained at different concentrations and extrapolated to infinite dilution (21).

A method to get the  $dc/ds$  curve from the sedimentation diagram has been given by Gralén and Lagermalm (21) in some work on polystyrene. The abscissa,  $x$ , is converted into an abscissa,  $s$ , by means of the expression:

$$s = d \cdot s_m \frac{\log (x/x_0)}{\log (x_m/x_0)} \quad (60)$$

where  $s$  is the sedimentation constant for the point  $x$  and  $d$  is a correction factor for the increase in hydrostatic pressure (61). Equation (60) follows immediately from equation (4), if the correction for hydrostatic pressure is applied.  $dc/ds$  is assumed to be proportional to  $dc/dx$  which, as has been seen, is approximately true. The  $dc/ds$  curves obtained at different concentrations are integrated to give distribution curves. By horizontal equidistant lines the distribution curves are divided into a number of parts (about ten). This means that a theoretical fractionation is performed and the  $s$  value for each "fraction" can be read from the intersections between the horizontal lines and the distribution curves. By means of equation (33) or a similar relation the sedimentation constants of each fraction can,

in the ordinary way, be extrapolated to infinite dilution. This gives the distribution curve for free sedimenting particles. Differentiating this curve gives the corresponding frequency curve for the  $s$  values. The curves obtained at different concentrations are shown in Figure 7. The method is really very simple. It needs, however, very exact measurements and is the more reliable the lower the concentration that can be used. Its importance as a method for obtaining a general estimation of frequency curves is considerable. In this special case it is worth noticing the very good separation of the two maxima that has been reached. The general shape of the curve is in good agreement with results obtained by performing a fractionation (see Sect. V.3).

#### 4. Use of Parameter Functions

In their theoretical treatment of sedimentation equilibrium measurements on polymolecular substances, Lansing and Kraemer (53) introduced a parameter function, which expressed the distribution of molecular weights as a logarithmic relation:

$$dc = K_M \exp(-y^2) dM \quad (61)$$

where:

$$y = (1/\beta) \log(M/M_0) \quad (62)$$

$\beta$  is a parameter defining the spread of the distribution (nonuniformity coefficient),  $M_0$  is the molecular weight corresponding to the maximum of the curve. From sedimentation equilibrium measurements  $M_w$  and  $M_z^*$  can be obtained and  $\beta$  then calculated from:

$$\beta = 2\sqrt{\log M_z/M_w} \quad (63)$$

Gralén (20c) made the assumption that a corresponding distribution could be applied to the sedimentation constants and wrote:

$$dc = K_s \exp(-y^2) ds \quad (64)$$

with:

$$y = (1/\gamma_s) \log(s/s_0) \quad (65)$$

$s_0$  corresponds to the maximum of the curve. The distribution coefficient  $\gamma_s$  can be calculated from  $(dB/dx)_0$  according to equation (52):

$$(dB/dx)_0 = \gamma_s \exp(\gamma_s^2/4) \cdot \sqrt{\pi} \quad (66)$$

\*  $M_z$  is defined by  $\sum_i M_i^2 c_i / \sum_i M_i c_i$ .

The application of this parameter function is, however, limited to cases where the real frequency curve has only one maximum and a positive skewness. When the dispersion has been determined, the shape of the curve is given.

In order to make this method more flexible, Jullander (30a) introduced a function with three parameters,  $K_s$ ,  $\gamma_s$ , and  $k$ :

$$dc = K_s \exp(-y^2) ds \quad (67)$$

with:

$$y = \frac{1}{\gamma_s} \log \frac{1}{k} \left( \frac{s}{s_0} + k - 1 \right) \quad (68)$$

This function is defined for all values of  $s \geq s_0(1 - k)$ . For  $k = 1$  it corresponds to equations (64) and (65). Even this function is limited in its ap-

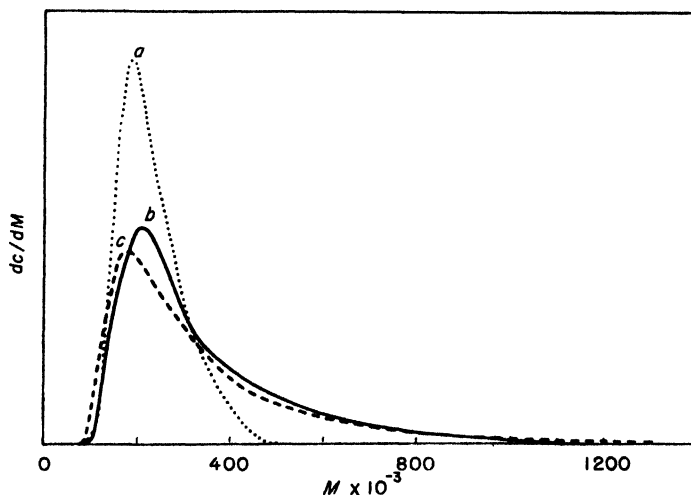


Fig. 8. Frequency functions of cellulose nitrate ( $M_n = 258,000$ ,  $M_w = 386,000$ ) (30).

plication to frequency curves with one maximum but it permits a variation of the skewness from zero to large positive values. For the calculation of the parameters  $\gamma_s$  and  $k$ ,  $(dB/dx)_0$  and the skewness  $\lambda$  of the sedimentation curve defined by:

$$\lambda = \frac{\int_{x_m}^{\infty} (dc/dx) dx}{\int_0^{x_m} (dc/dx) dx} - 1 \quad (69)$$

can be used. The following relations are obtained:

$$(dB/dx)_0 = k\gamma_s \exp(\gamma_s^2/4) \cdot \sqrt{\pi} \quad (70)$$

and:

$$\lambda = \frac{\int_{-\gamma_s/2}^{+\infty} \exp(-x^2) dx}{\int_{-\infty}^{-\gamma_s/2} \exp(-x^2) dx} - 1 \quad (71)$$

Figure 8 illustrates the use of the three-parameter function (curve *c*) given on a molecular weight basis. The substance is a cellulose nitrate investigated by Jullander (30f). Its molecular weight is  $M_n = 258,000$  and  $M_w = 386,000$ . As a comparison are also given the curves *a* and *b* obtained in the way discussed in preceding Section 3. The agreement between *b* and *c* is very good. The curves *c* in Figure 6 are the three-parameter function. The discrepancies here are larger and the reason for this is not clear (30f).

The parameter functions have of course limited applicability. It must, however, be emphasized that, especially for synthetic high polymers where the distribution of molecular weights can be fairly easily calculated from assumed reaction mechanisms, parameters in the obtained expressions may be determined in the way indicated above. So far such an application of the ultracentrifugal technique has not been made.

## V. Polymolecularity Measurements and Fractionation

Hitherto mainly the theoretical problems connected with the sedimentation of threadlike molecules have been treated. Experiments have been described and referred to only as illustrations of the different effects predicted by calculations. Furthermore the information that can be obtained directly from sedimentation diagrams has been discussed. This last section is devoted mainly to experimental investigations, treating some recent work on high polymers. These experiments are of interest especially as a demonstration of the possibilities of the ultracentrifugal method in combination with other methods, mainly fractionation.

In Sections III and IV it is shown that many difficulties are met with in the interpretation of the sedimentation diagrams of threadlike molecules. Many of the effects discussed, for instance, the concentration dependence caused by interaction between the molecular chains and by solvation of the polymer, are functions of the molecular weight and are therefore affected by the polymolecularity of the substance. In fact the difficulties are growing with increasing polymolecularity. As the macromolecular substances with threadlike molecules generally have a very high polymolecular-

ity, it is often necessary to homogenize the substances by fractionation before the measurements are made to study the properties in solution. In this way the measured quantities will be characteristic for definite molecular species, and thus, the properties of the molecules more exactly known.

Using ultracentrifugal sedimentation to characterize high polymeric substances, the measured quantities, as a consequence of the dependence on concentration, must be extrapolated to infinite dilution. Then they obtain a definite physical meaning for the polymer molecules as entities. In sedimentation measurements this procedure must be carried out for the sedimentation constant  $s$  and the widening value  $dB/dx$ . For the extrapolation, measurements at low concentrations are of utmost importance. For a polymolecular substance the concentration gradient in the cell is lower and the maximum less well defined than the gradient for a homogeneous substance. This makes measurements at low concentrations less accurate and at a certain concentration impossible. In many cases the extrapolated  $s_0$  and  $(dB/dx)_0$  values are 30–40% higher than the highest measurable value. Consequently the extrapolation is less reliable. The statistical "standard" errors of the  $s_0$  values caused by the extrapolation alone have been calculated by Bryde and Rånby (4) for unfractionated high-molecular cellulose nitrates in acetone. Errors of  $\pm 10\%$  were obtained.

The polymolecularity causes other effects, too, for which corrections must be introduced. The displacement of the maximum of the sedimentation curves gives too low sedimentation constants. The observed effects are sometimes higher than those expected according to Kinell's treatment (see Sect. III.8). The widening of the sedimentation curves caused by the increase in the centrifugal field makes a correction of the  $dB/dx$  values necessary, when the gradients extend over a large part of the cell. This correction increases approximately as the square of the width of the curve. For unfractionated wood cellulose nitrates with  $dB/dx$  values equal to 1.0, Rånby (68) has found a correction of about 10%.

All the attempts made to calculate the frequency function of a substance with threadlike molecules directly from the sedimentation curves are dependent on the possibility of making accurate experiments at very low concentrations. A rather good separation of molecular species is then obtainable, presupposing, however, that there is a sufficient difference in the molecular weight. This is shown in Figure 9, where the mean molecular weight of the faster peak (cellulose) is about 50 times that of the slower (hemicellulose and low-molecular cellulose).

These facts concerning all the difficulties in measurements on poly-



molecular substances were early realized, and many investigations have been made on substances, the polymolecularities of which were decreased by some fractionation process. The aim of the work was primarily to get information of the properties in solution of the molecules. For instance the work on polystyrene by Signer and Gross (74), on polymeric  $\omega$ -hydroxydecanoic acid and cellulose acetate by Kraemer and Lansing (37,38) was all made on carefully fractionated substances. A complete review up until 1939 is given by Kraemer and Lansing (39).

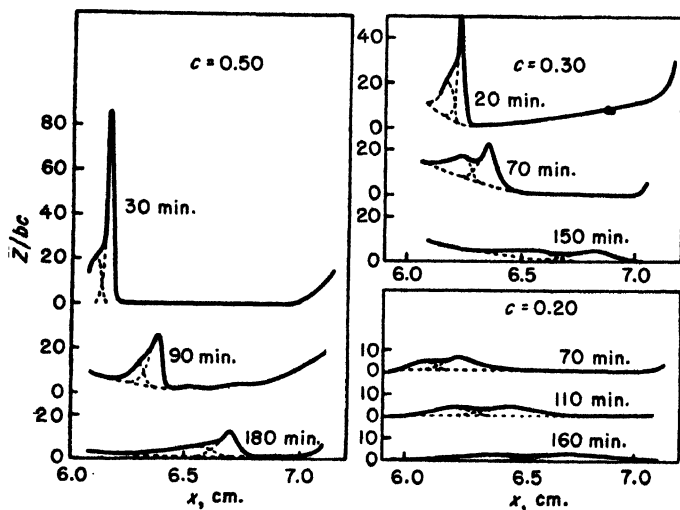


Fig. 9. Sedimentation diagrams for holocellulose from spruce wood in cuprammonium solutions at different concentrations (in g./100 ml.) (20). The peaks correspond to the hemicellulose including some low-molecular cellulose and the cellulose proper, respectively.

Cellulose nitrate has often been studied by ultracentrifugal sedimentation. Mosimann's (59) work dealt with carefully prepared and purified fractions of cellulose nitrates (containing about 12% N) from cotton linters. He made an excellent series of viscosity, sedimentation, diffusion, and double refraction of flow measurements and calculated the shape of the molecules in solution using the theories of Burgers (7). Mosimann's measurements covered a wide range of molecular weights (6,200–613,000 corresponding to degrees of polymerization,  $Z$ , of 25 and 2,300, respectively) and they have been used for further calculations by other authors (see Sect. III.3).

A similar work is published by Campbell and Johnson (8). Their frac-

tions of cellulose nitrates covered a smaller range of molecular weights ( $Z$  values 100 to 600–700, calculated from the viscosity data) and their measurements were not quite as comprehensive as those of Mosimann (59). The relation obtained between the intrinsic viscosity  $[\eta]^*$ , and sedimentation constant does not agree with measurements of Rånby (68); the  $[\eta]$  values are too low compared with the  $s_0$  values. This is perhaps an effect of depolymerization during the work. The authors used technical cellulose nitrates, which were not quite stable during the measurements (28). The stability of these cellulose nitrates in solution has been further studied by Campbell and Johnson (8a).

The work of Mosimann (59) and Campbell and Johnson (8) has given experimental evidence that the cellulose nitrate molecules in acetone solution are long, rather stiff chains, whose thickness is considerably increased by solvation. At low molecular weights ( $Z < 300$ ) the chain seemed to be almost completely stretched. No attempts were made in these investigations to estimate the polymolecularity of the fractions.

During World War II, the polymolecularity measurements on high polymers mainly followed two different lines. Gralén (20) and Jullander (30) used the ultracentrifuge directly on unfractionated samples and analyzed the sedimentation diagrams. Many other authors used fractionation, especially fractional precipitation, for polymolecularity studies (this work is reviewed by Cragg and Hammerschlag (9)). With none of these methods alone could complete and reliable distribution functions of the molecular weights be obtained. Therefore, during the last five years a combination of fractionation and sedimentation measurements has been used. In this way the advantages of both methods can be utilized. Three different substances have hitherto been studied: nitrates from wood and cotton cellulose (68,76), polymeric methyl methacrylate (35), and polystyrene (21). This more intensive work has been directed mainly to three important problems:

(1) To obtain information on the polymolecularity of the fractions and find the best working conditions for a selective fractionation.

(2) To obtain frequency curves of the molecular weight by summation of the fractions.

(3) To use fractions of highest possible purity and homogeneity for accurate determination of the properties in solution of the polymer molecules.

The first of these problems was studied only for fractions of cellulose nitrate. To date only a part of these investigations has been published in

\* The intrinsic viscosity is given by  $[\eta] = \lim_{c \rightarrow 0} (\eta_{sp}/c)$ ;  $c$  in g./100 ml.

commonly available journals. As the results obtained are interesting and some important conclusions may already be drawn from them, it is worth while giving an account of the measurements here.

### *1. Cellulose Nitrate*

From the work of Mosimann (61), Gralén (20), and Jullander (30,31), it was quite evident that much information on the molecular properties of cellulose and cellulose derivatives in solution could be obtained by ultracentrifugal sedimentation. Nitration with nitric acid-phosphoric acid mixtures at a low temperature (0°C.) seems to be the best way to get a well-defined and easily soluble cellulose derivative possible to prepare without any considerable depolymerization. As Gralén (20) has shown, the nitration causes only about one broken bond per 3000 glucose units. Hence the chain-length distribution of such a cellulose nitrate may be assumed to correspond to that of the original cellulose sample. The cellulose nitrate is an important model substance for physicochemical measurements on rather stiff chain molecules. That is the reason why the work on this substance has been given the largest space in this section. The work reported has mainly been done by Rånby (68) on wood and cotton cellulose. As to the nitration of the original cellulose samples (13.8% N), it can be mentioned that Davidson's (10) method was used. The nitrates were stabilized by boiling with distilled water. Nitrates from wood cellulose containing lignin were extracted by cold methanol instead of boiling (4) to remove the nitrolignin formed. The cellulose nitrates prepared in this way were stable for some months, if not exposed to daylight.

### *Selectivity of Fractionation*

Fractional precipitation of high polymers has been extensively used during the last three decades. For references see a paper by Cragg and Hammerschlag (9). One of the most important problems is to get a solvent-nonsolvent system, which gives the best selectivity. By selectivity is then meant the possibility of getting fractions of low polymolecularity, which here is measured as  $dB/dx$  values. Theoretical work, mostly by statistical thermodynamics (17-19,25,26,72,73), has shown that the selectivity is a function of the precipitation conditions. Low initial concentration of the polymer and big volume ratio supernatant to precipitated phase should favor good separation. Very few experimental investigations, however, have been made to test the validity of these theo-

ries. A few authors have given some experimental verification of these predictions (9), but in recent articles, Morey and Tamblyn (57,58), after a comprehensive study, were of the opinion that the selectivity is hardly affected by the original polymer concentration. They did not measure the polymolecularity of the fractions directly but draw their conclusions from the distribution curves obtained from the fractionation. Sedimentation measurements in the ultracentrifuge seem to be one of the best methods now available for testing the selectivity. Using Gralén's  $dB/dx$  method (see Sect. IV.2) to measure the width of the fraction from the sedimentation diagrams, a good basis for comparisons is obtained.

The fractional precipitation was made by Rånby (68) in the following way. A precipitating agent was slowly added to acetone solutions of cellulose nitrates. When the solution became turbid at the critical concentration, the temperature was raised to 35–40°C. until the solution became clear. The temperature of the bath was then lowered to 20° for about 10 hours and held constant within 0.05°. After about two days the finely divided precipitation had settled as a gelatinous layer and could easily be separated by pouring off the supernatant liquid. Precipitations were made by two agents, distilled water and petroleum ether (a petroleum fraction, b.p. 60–75°C.), at different initial polymer concentrations. Twelve to sixteen fractions of about equal size were obtained (in one case only six). Viscosity and sedimentation measurements were made on the fractions dissolved in acetone. Generally the fractions precipitated out with decreasing  $[\eta]$  values.

The sedimentation curves of the fractions all had a well-defined maximum (Fig. 10). Accurate measurements could be made in concentrations as low as 0.02 g./100 ml. and sometimes still lower, and consequently the extrapolation of the sedimentation constant,  $s_0$ , and the widening value  $(dB/dx)_0$ , to infinite dilution was much more reliable than for unfractionated substances (Fig. 11). For these fractions having a rather low polymolecularity no corrections were necessary as regards the broadening of the sedimentation curves due to the increase in the centrifugal field and the displacement of the peaks due to polymolecularity according to Kinell (see Sections III.8, and IV.2). The total corrections of this kind were estimated to be only a few per cent of the  $(dB/dx)_0$  values.

To study the selectivity of the fractionation, the  $(dB/dx)_0$  values are plotted as a function of the  $[\eta]$  values for different series of fractionation in Figure 12. The  $(dB/dx)_0$  values seem to have a minimum for  $[\eta] = 10$  to 20. The polymolecularity of the fractions depends on the nonsolvent used. With petroleum ether the polymolecularity is lower than with water. Also

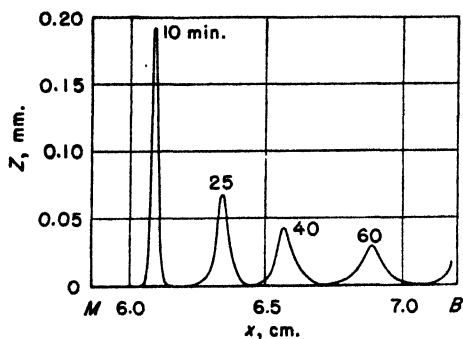


Fig. 10. Sedimentation diagrams for a fraction of nitrated wood cellulose ( $c = 0.040 \text{ g./100 ml.}$ ) at different time intervals. Velocity, 50,000 r.p.m., giving a centrifugal field of 180,000 g. at the distance 6.5 cm. from the axis.  $M$  = meniscus.  $B$  = bottom of cell.

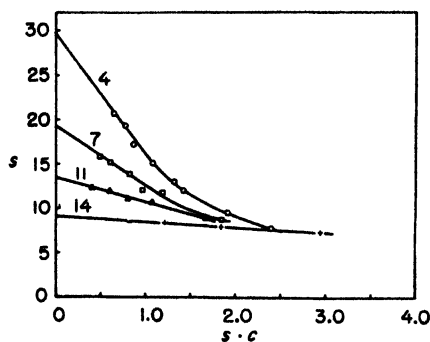


Fig. 11. Sedimentation constants  $s$  vs.  $s \cdot c$  for the same fractions as in Figure 2.

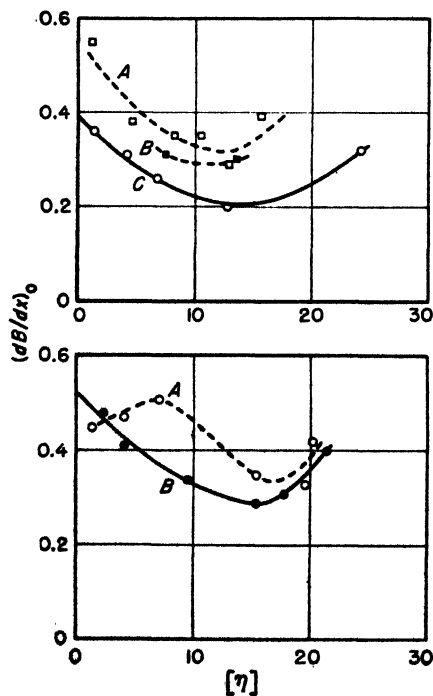


Fig. 12.  $(dB/dx)_0$  values of fractions of cellulose nitrates as a function of the intrinsic viscosity  $[\eta]$ . Upper, precipitation by petroleum ether: curve A ( $c = 1.2 \text{ g./100 ml.}$ ), curve C ( $c = 0.33 \text{ g./100 ml.}$ ), and curve B ( $c = 0.20 \text{ g./100 ml.}$ ) (only 6 fractions), respectively. Lower, precipitation by water: curve A ( $c = 0.67 \text{ g./100 ml.}$ ) and curve B ( $c = 0.10 \text{ g./100 ml.}$ ).

lower polymer concentration gives better selectivity, in the case of both water and petroleum ether. This is in agreement with the theory. The difference between the effects of water and petroleum ether is a question of great interest, because these two precipitating agents act in not quite analogous ways. With water the precipitation occurs at a solvent-non-solvent ratio of 10:1 to 10:2; with petroleum ether the ratio is 10:10 to 10:15. The dissolution of water in acetone to these proportions is an exothermic process and that of petroleum ether in acetone an endothermic. The dissolution gives a decrease and an increase, respectively, in the final volumes (68a).

Conclusions as to the selectivity of the fractionation in different molecular weight intervals might not be drawn directly from the  $(dB/dx)_0$  values, because the solution properties depend on the molecular weight (see below). The first and the last fractions in a series always have higher polymolecularity than the others. This is easy to understand. In the first fractions, easily precipitated impurities, gel particles, etc. may be found; the last fraction, obtained by evaporation of the final solvent-nonsolvent mixture, contains many easily soluble impurities.

An important question that can be elucidated by means of ultracentrifugal sedimentation is the limit of selectivity obtainable by fractional precipitation. An experiment with a sample, which had an original  $(dB/dx)_0$  value of 1.1, gave the following result. By only one precipitation, made under conditions shown to have given the highest selectivity ( $c = 0.33$  g./100 ml., precipitation by petroleum ether), a  $(dB/dx)_0$  minimum value of 0.20 was obtained (see Fig. 12). Naturally the fractions must be rather small ( $\sim 0.5$  g.), making refractionation of the fractions impossible. Another fractionation was made with higher initial concentration (1.2 g./100 ml.) giving 12 fractions with a  $(dB/dx)_0 \text{ min} = 0.31$ . The third of these fractions, I:3, 15.9% of the original substance, was refractionated at a lower concentration (0.4 g./100 ml.) to 4 fractions. A value for  $(dB/dx)_0 \text{ min}$  of 0.24 was obtained for the second fraction (II:2) containing 46.2% of the fraction I:3. Still another refractionation was made. Fraction II:2 was separated into 3 fractions; for the second (III:2, 60% of II:2) the  $(dB/dx)_0$  value of 0.21 was obtained. No further refractionation was carried out. From these experiments it can be concluded, that the possibility to homogenize the fractions by refractionation seems to be limited. This also shows the importance of finding the "optimum" conditions of fractionation for any given substance. In such a way a satisfactory result can be obtained without all the work connected with repeated refractionations.  $(dB/dx)_0$  values of 0.20 seem to be the experimental limit obtained

for this solvent nonsolvent system. The question as to whether or not this is the theoretical limit may still be open.

### *Properties of Cellulose Nitrate Molecules*

From the data obtained by viscosity and sedimentation measurements on the cellulose nitrate fractions, it is possible to study the properties of the molecules. The relation between  $[\eta]$  and  $s_0$  for fractionated and unfractionated cellulose nitrates is given in Figure 13. The curve is drawn

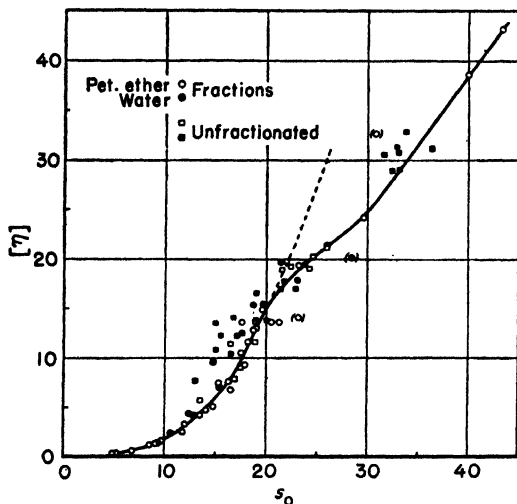


Fig. 13. Intrinsic viscosity  $[\eta]$  vs. sedimentation constant  $s_0$  for cellulose nitrate dissolved in acetone. The broken curve represents equation (72).

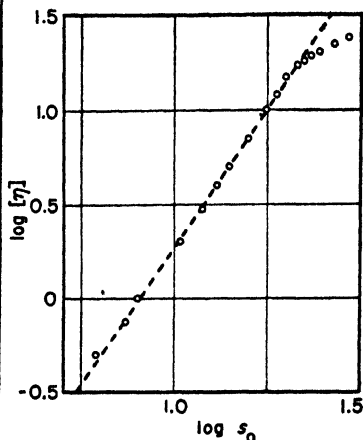


Fig. 14.  $\log_{10} [\eta]$  vs.  $\log_{10} s_0$ . Points graphically determined from curve of Figure 13.

through points representing the fractions. This curve can be regarded as composed of two parts meeting at  $s_0 = 18$  to  $20$  S. The unfractionated samples have sedimentation constants generally 10–15% lower than fractions with the same  $[\eta]$  values. Part of this discrepancy may be due to effects of polymolecularity (see Sect. III.8). If  $\log_{10} [\eta]$  is plotted as a function of  $\log_{10} s_0$  (Fig. 14) the relation obtained is approximately a straight line within the interval  $s_0 = 5$  to  $21$  S, corresponding to the  $[\eta]$  interval of  $0.4$  to  $17$ .

According to measurements of Mosimann (59) and Jullander (30) the simple Staudinger law is approximately valid for cellulose nitrates to  $Z$  values of about 2000. The  $K_m$  constant varies with the nitrogen content.

For a nitrate with 13.8% N, Jullander has given the value  $10.5 \times 10^{-3}$  ( $c$  in g./100 ml.). The linear relationship in Figure 14 means that:

$$s_0 = k_1[\eta]^{k_2} \quad (72)$$

From the intercept and the slope of the line in Figure 14, we get  $k_1 = 8.1$  and  $k_2 = 0.34$ . In this range, however, the Staudinger relation also holds:

$$[\eta] = K_m Z \quad (73)$$

Combining equations (72) and (73) and introducing  $M = mZ$ , where  $m$  is the molecular weight of the monomer unit, we obtain:

$$s_0 = k_1 \left( \frac{K_m}{m} \right)^{k_2} M^{k_2} \quad (74)$$

For cellulose nitrate (13.8% N,  $m = 291$ ) in acetone solution we then have:

$$s_0 = 0.24 M^{0.34} \quad (75)$$

Equation (75) is identical in form with equation (56). The constant  $a$  in this case is 0.66, showing that the molecules in solution have sedimentation properties between those of matted and free-drained coils or in the Debye terminology (11), a shielding ratio of about 3. At still higher molecular weights ( $Z > 2000$ ), the constant  $a$  shows a tendency to decrease indicating a denser coiling of the chains. Accurate measurements of  $a$  values in this interval have so far not been possible, because of the difficulty of getting absolute values of the molecular weights.

Another indication of a change of the solution properties at high molecular weights is obtained from the viscosity measurements. According to Huggins (27) concentration dependence of the viscosity of high polymers in solution generally follows the equation:

$$\eta_{sp}/c = [\eta] (1 + k'[\eta]c) \quad (76)$$

where  $k'$  is a constant characterizing a given high-polymer-solvent system and experimentally shown to be independent of the molecular weight (1). The value  $k' = 0.38$  has been obtained for many different unbranched high polymers in good solvents (13). In a poor solvent  $[\eta]$  generally has a lower and  $k'$  a higher value. For the cellulose nitrate fractions of very high molecular weights ( $[\eta] > 30$ ), the relation  $(\eta_{sp}/c, c)$  is not always a straight line and the  $k'$  values must be calculated from the measurements at very low concentrations. To avoid mistakes from the curvature, extrapolations were also made from logarithmic diagrams ( $\log \eta_{sp}/c, c$ ) according to the equation:



$$\eta_{sp}/c = [\eta] \times 10^{k''[\eta]c} \quad (77)$$

giving fairly good straight lines. Equation (76) is identical with (77) at the first approximation with  $k' = 2.303 k''$ .

From the diagrams containing  $k'$  and  $k''$  as a function of the  $[\eta]$  values (Fig. 15), it is evident that the value of both  $k'$  and  $k''$  increases at higher

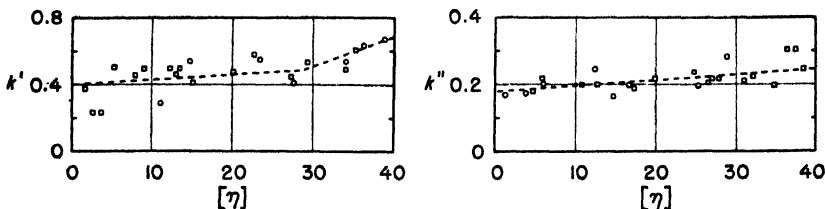


Fig. 15. Viscometric constants  $k'$  and  $k''$  vs. intrinsic viscosity  $[\eta]$  for fractions of cellulose nitrates dissolved in acetone.

$[\eta]$  values, indicating a change of the solution properties. Acetone is a good solvent for cellulose nitrate at low  $Z$  values but gradually becomes not so good at very high  $Z$  values ( $Z > 2000$ ). This is in agreement with the conclusions from the  $([\eta], s_0)$  diagrams (Figs. 13 and 14).

The cellulose nitrate molecules seem to be unbranched chains at low molecular weights ( $Z < 2000$ ). The change in properties at higher  $Z$  values is most probably an effect of a denser coiling of the chains. The possibility of branching is not quite excluded, however, and Pascu (62) has in recent papers made the assumption that cross linking by acetal and hemiacetal groups is frequently occurring in the cellulose. Pascu's conclusions are based on data especially from degradation reactions.

### Frequency Functions

Summation of the fractions to get frequency curves of the original substances is usually made by taking the derivative of the "smoothed" step diagrams (a distribution curve) with the intrinsic viscosity  $[\eta]_n$  of the  $n$ th fraction as a function of the quantity:

$$\sum_{1}^{n-1} p_m + \frac{1}{2} p_n$$

where  $p_m$  denotes the amount in per cent of the  $m$ th fraction according to Schulz (70). This method is not quite satisfactory as the fractions are not summed with their polymolecularity taken into account. The three

curves *A*, *B*, and *C* in Figure 16 correspond to three different fractionations of the same cellulose nitrate. The selectivity increases from *A* to *C*. The frequency functions obtained by derivation of the three curves do not coincide very well. This demonstrates the uncertainty of the method. It gives, however, a rough estimation of the distribution of the molecular species.

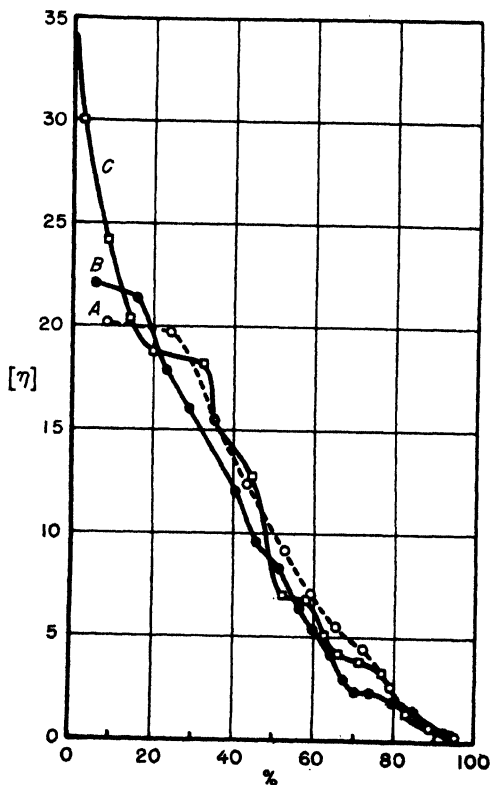


Fig. 16. Intrinsic viscosity  $[\eta]$  vs. amount of substance for three series of fractionation of a wood cellulose nitrate with increasing selectivity in order *A*, *B*, and *C*.

In principle it is better to assume a frequency function for fractions, which approximately gives their shape and which is easy to treat mathematically. Rånby (68) has introduced triangular frequency functions. The area of each triangle is proportional to the percentage amount of each fraction, the mode is the measured  $s_0$  value and the base is  $2 \times s_0 \times (dB/dx)_0$ . As a first approximation symmetrical triangles have been used. If the sedimentation curves are skew the skewness can be measured (30h) and corresponding nonsymmetrical triangles constructed. The use of

symmetrical triangles introduces, however, only a small error. The skewness of the sedimentation curves of the fractions is generally very small as in

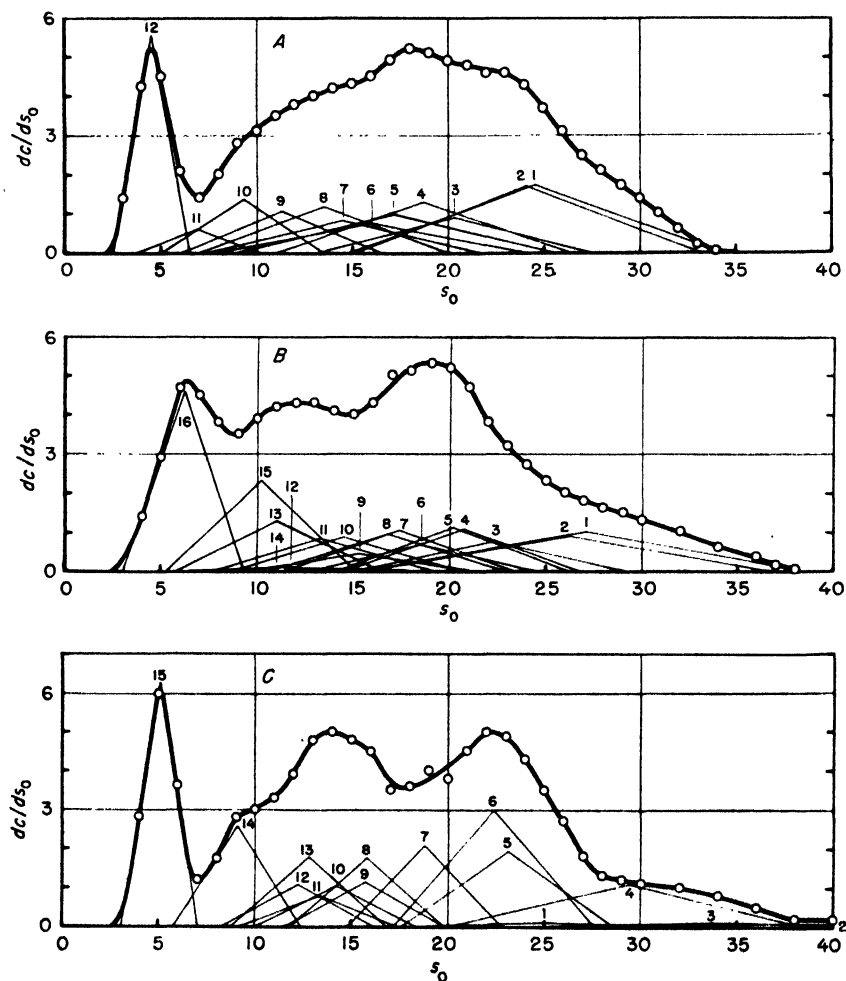


Fig. 17. Construction of frequency curves by summation of fractions as symmetrical triangles. Fractionation of wood cellulose nitrate by water (*A* and *B*) and by petroleum ether (*C*).

Figure 10. Summation of triangular frequency functions has been applied to the same experiments as in Figure 16. It is evident from Figure 17

that the frequency curves of the original substances are richer in details, the higher the selectivity of the fractional precipitation. Only in the last case

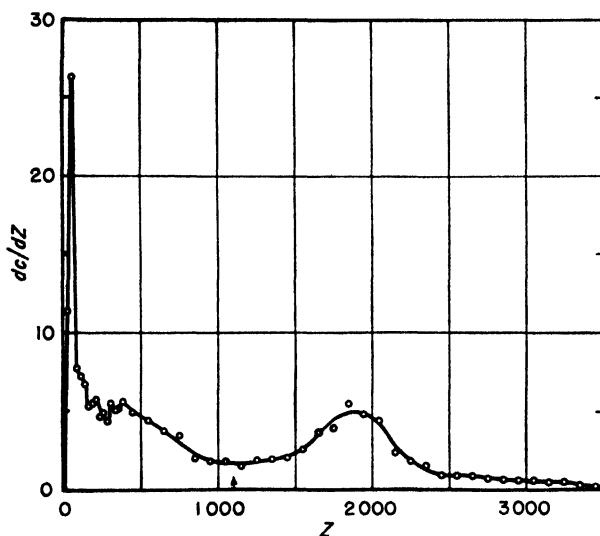


Fig. 18. Frequency curve ( $dc/dZ$ ,  $Z$ ) recalculated from curve  $C$  of Figure 17.

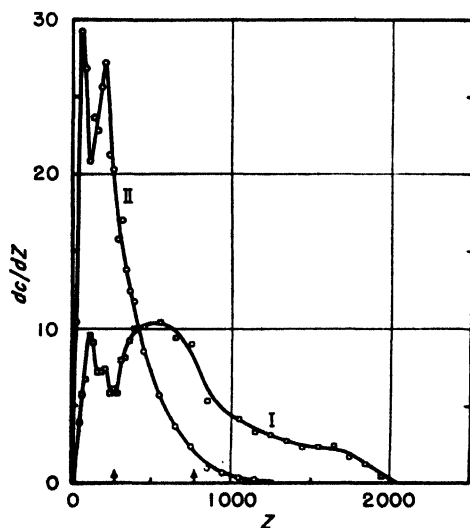


Fig. 19. Frequency curves for two cotton cellulose nitrates, depolymerized by boiling in pure water in an autoclave (76).

is the polymolecularity of the fractions smaller than that of the separate maxima of the resulting frequency function. Thus, it is very important to get the highest possible selectivity in the fractional precipitation.

Construction of frequency functions in  $Z$  values can be made from the  $s_0$  curves when the relation between  $s_0$  and  $Z$  is known. This is done graphically for curve  $C$  of Figure 17 using the  $s_0, [\eta]$  relation of Fig. 13 and Eq. 73 proved to hold for  $Z$  values up to about 2000; the transformation of the  $(dc/ds_0, s_0)$  curve to a  $(dc/dZ, Z)$  curve is made section by section. From the diagram of Figure 18 it is evident that the frequency function has the principal maxima at  $Z$  values of 70 and 1800 and smaller ones at about 100, 200, 300, and 400. The first one ( $Z = 70$ ) contains mainly hemicelluloses. The last four seem to be multiples of a unit of about 100 glucose residues. The weight average value of  $Z$  of the original substance calculated from the curve and checked by viscosity measurements is 1100, thus lying between the two principal maxima. Evidently a value of this kind determined on the original sample is of little real importance without knowledge of the frequency curve. Frequency curves of two depolymerized cotton cellulose nitrates (Fig. 19), obtained in the same way as that of Figure 18, also show maxima for  $Z$  values of 100 and 200. Also here an indication of the existence of multiple degradation products is obtained. Most probably this is an effect of the crystallinity of the native cellulose.\*

## 2. Polymeric Methyl Methacrylate

A similar study on two commercial polymeric methyl methacrylates has been made by Kinell (35). The samples (B and E) dissolved in acetone were characterized by sedimentation and diffusion measurements (Table V). The  $(dB/dx)_0$  values indicate a very high polymolecularity.

A fractional precipitation was made by adding cyclohexane to benzene solutions (71) in about the same way as described for cellulose nitrate (see (Sect. V.1)). The polymer concentration of the original solutions was as high as about 2% and has probably decreased the selectivity of the fractionation. The polymolecularity of the fractions measured as  $(dB/dx)_0$  values is therefore rather high (Table VI).

The relation between sedimentation constant,  $s_0$ , and intrinsic viscosity,  $[\eta]$ , shown in Figure 20, indicates a rather complicated behavior of the

\* *Note added in proof.* This assumption has been verified by later experiments (cf. 86a). Cellulose crystallites, micelles, with a length of 500 Å. (corresponding to 100 glucose units) have been obtained in aqueous colloidal solution (68b). They have been isolated and studied morphologically and structurally (68c). The micelles were earlier postulated from x-ray diffraction patterns of cellulose fibers.

TABLE V

Sedimentation and Diffusion Measurements on Unfractionated Samples of Polymeric Methyl Methacrylates (35)

Sample	$s_0$	$(dB/dx)_0$	$D_0$	$M^a$
B.....	37.2	1.80	4.31	570,000
E.....	58.2	1.23	3.31	1,170,000

<sup>a</sup> Molecular weight  $M$  is calculated by equation (6).

TABLE VI

Sedimentation and Viscosity Measurements on a Series of Fractions of Polymeric Methyl Methacrylates (35)

Fraction	$s_0$	$(dB/dx)_0$	$[\eta]$
E (2) I.....	94	0.58	2.82
II.....	97	0.56	2.40
III.....	80	0.60	1.91
IV.....	70	0.53	1.75
V.....	60	0.43	1.36
VI.....	53	0.42	1.20
VII.....	39	0.44	1.05
VIII.....	34	0.51	0.74
IX.....	26	0.40	0.58

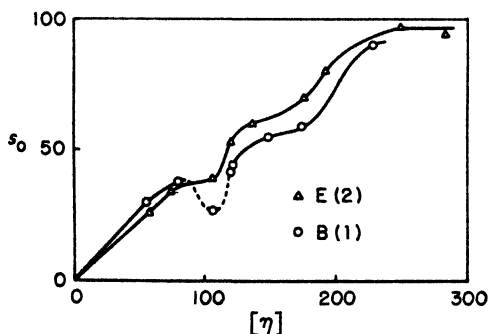


Fig. 20. Relation between sedimentation constant  $s_0$  and intrinsic viscosity  $[\eta]$  for fractions of two samples of polymeric methyl methacrylate ( $c$  in g./ml.) (35).

molecules in solution. Whether this is an effect of branching, cross linking or folding cannot be decided. The  $k'$  values according to equation (76) indicate differences in structure. These questions are discussed in Section 3 below.

The two samples investigated showed frequency curves with more than one maximum, probably three for each sample. Distribution and frequency curves from viscosity data (Fig. 21) generally agree with the curves

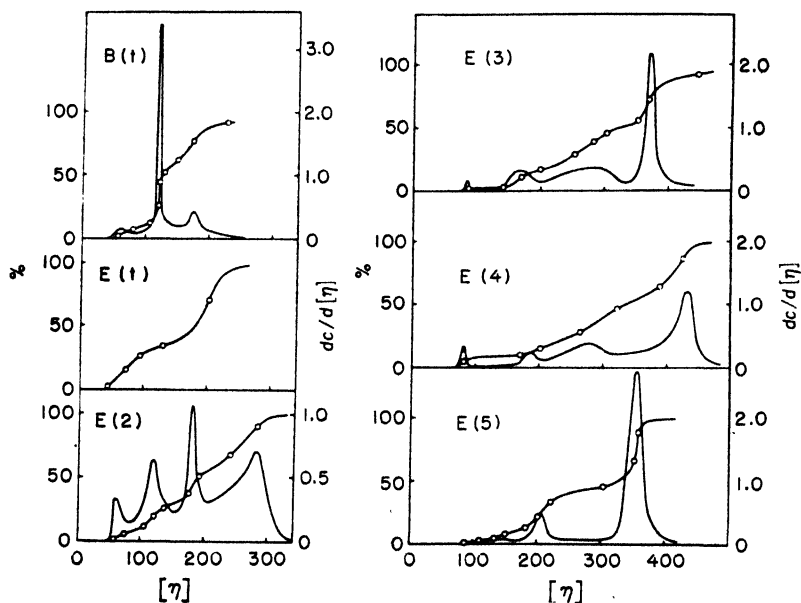


Fig. 21. Distribution and frequency curves for polymeric methyl methacrylate from viscosity data (35).

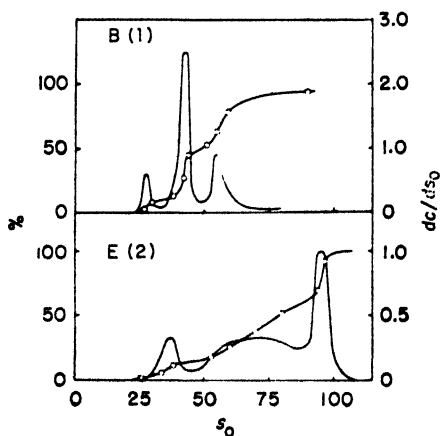


Fig. 22. Distribution and frequency curves for polymeric methyl methacrylate from sedimentation data (35).

from sedimentation measurements (Fig. 22). The sedimentation diagrams of the unfractionated substances (Fig. 23) also indicate the existence of three maxima. Summation of the fractions, assumed to have triangular

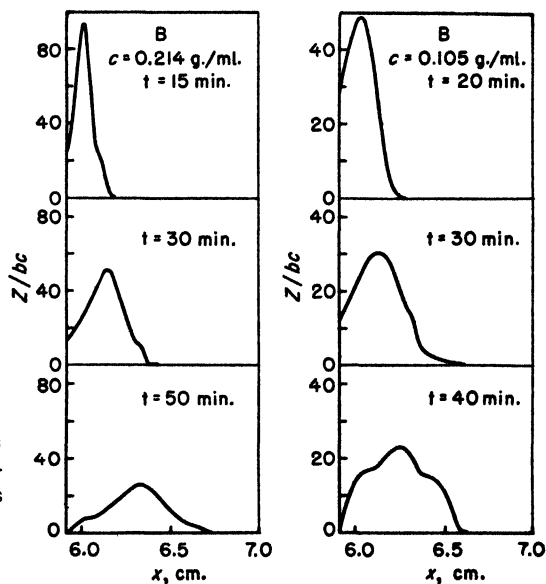


Fig. 23. Sedimentation diagrams of polymeric methyl methacrylate at different concentrations and different times (35).

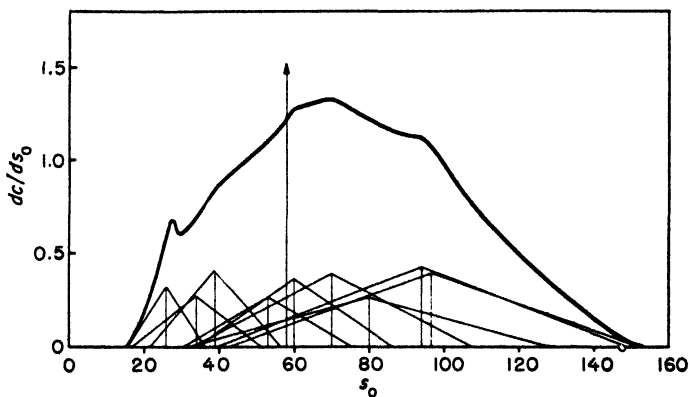


Fig. 24. Frequency curve of polymeric methyl methacrylate obtained by summation of fractions as triangular functions (35).



frequency curves based on the sedimentation constants, did not give a curve with separate maxima (Fig. 24) but an indication of at least three. This bad separation is certainly an effect of the low selectivity of the fractionation giving fractions with high polymolecularity. In examining Figure 24, we find that the determined  $s_0$  value of 58 S for the unfractionated sample does not correspond to the highest maximum. This is partly an effect of the concentration dependence of the sedimentation of a polymolecular substance (see Sect. IV). So far it cannot be completely interpreted quantitatively for this substance with threadlike molecules and many maxima in the frequency function.

A synthetic high polymer giving a frequency function of the shape shown in Figures 21, 22, and 24 must have been formed by a rather complicated mechanism of reaction. Both of the samples were probably formed by a homogeneous polymerization.

### 3. Polystyrene

Gralén and Lagermalm (21) quite recently published some work on the polymolecularity of polystyrene. They used a sample polymerized at

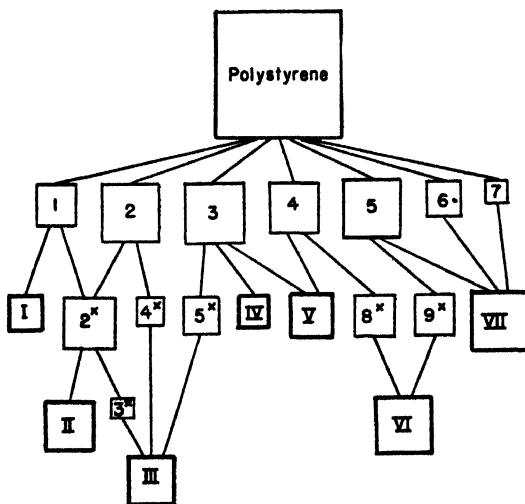


Fig. 25. Fractionation scheme of polystyrene (21). The area of the squares is proportional to the size of the fractions.

60°C. in a nitrogen atmosphere from a purified monomer without any catalyst. The fractional precipitation was made by *n*-butanol from 0.4% solutions in methyl ethyl ketone. The alcohol was first added to a con-

centration slightly below the critical precipitation and its concentration was increased by successive evaporation of the solvent-nonsolvent mixture at a low pressure (10 mm. Hg). At the fractionation temperature (40°C.) the ketone is much more volatile than the alcohol and the evaporation gives an increase in the relative amount of butanol. The fractions were precipitated during intense stirring. The precipitate settled and

Fig. 26. Frequency curve of the sedimentation constants obtained by summation of fractions (21).

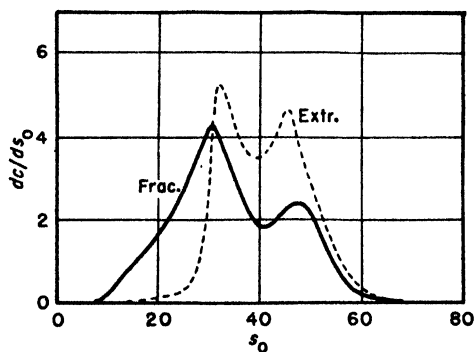
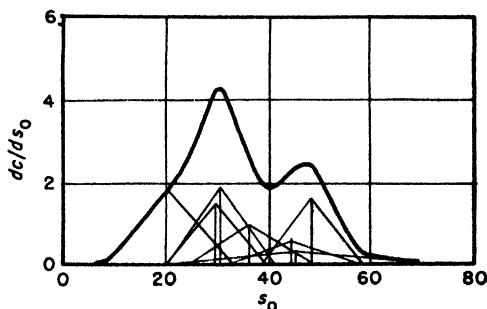


Fig. 27. Frequency curves of polystyrene obtained by extrapolation and summation of fractions (21).

formed a liquid gel, which could be easily pipetted off. The fractions were regrouped and refractionated according to the scheme of Figure 25, finally forming 7 fractions for measurements. The original samples and the fractions were characterized by viscosity and sedimentation measurements in methyl ethyl ketone (Table VII). The selectivity of the fractionation was higher than in the case of polymeric methyl methacrylate (preceding Sect. 2) and the same minimum value of  $(dB/dx)_0 = 0.20$  was reached as with cellulose nitrate when precipitating with petroleum ether.

The frequency function in  $s_0$  values of the original substance was constructed by summation of the fractions as symmetrical triangles (Fig. 26) in the way described under Frequency Functions, Section V,1. A fre-

quency curve was also obtained by graphical extrapolation of the sedimentation diagrams to infinite dilution. The method is treated in Section IV,3 and the result given in Figure 7. Figure 27 gives a comparison between the results from the fractionation and the extrapolation. In consideration of the graphical methods involved the agreement is rather good, especially the coincidence of the two maxima.

As regards the sedimentation properties of polystyrene molecules, it is seen from Table VII that the  $s_0$  values first increase with  $[\eta]$ . At  $[\eta]$  equal to 1.2 and 1.4 we have about the same  $s_0$  value of 30 S. Then  $s_0$  increases again to 45 and 48 S for  $[\eta]$  equal to 2.3 and 2.1. Hence this relationship is of the same general character as in the case of polymeric methyl methacrylate (Fig. 20). It is, however, not so pronounced. A striking fact is that in both cases the  $s_0$  ranges, where the variation of  $s_0$  with  $[\eta]$  is relatively small, coincide fairly well with the position of the maxima of the corresponding frequency functions. This should mean that the molecules represented in the maxima should be of a free-drained type. They cannot, however, be of the same linear structure in all the maxima. The increase in

TABLE VII  
Sedimentation and Viscosity Measurements on Polystyrene (21)

Sample	Per cent	$s_0$	$(dB/dx)_0$	$[\eta]$
Original.....	100	35	1.04	1.6
Fraction I.....	8	45	0.55	2.3
II.....	15	48	0.20	2.1
III.....	14	30	0.32	1.4
IV.....	7	45	0.27	2.1
V.....	11	37	0.33	1.6
VI.....	19	31	0.34	1.2
VII.....	21	21	0.58	0.8

$s_0$  values between the ranges discussed corresponds to a decrease in the frictional resistance. During the polymerization the structure of the molecules most probably is changed and it seems likely that an originally linear molecule through a branching or cross-linking process may get a structure, which again gives it properties of free-drained coils. The frictional resistance depends on the molecular weight and on other quantities, for instance, shape factors and solvation. The final decision of the properties of the molecules cannot be made before both  $[\eta]$  and  $s_0$  have been related to absolute values of the molecular weight. So far it might be emphasized, that the maxima in the  $(dc/ds_0, s_0)$  frequency curves do not

necessarily mean corresponding maxima in  $(dc/dM, M)$  curves. In every range, where the molecules turn over to a free-drained type, we can expect to find a maximum in the frequency curves based on  $s_0$  values.

## VI. General Conclusions

In this chapter the use of the ultracentrifuge to study high polymers in solution has been described. The sedimentation properties of threadlike molecules have been discussed and a review of the theoretical work so far published is given. Attention has been drawn to the concentration dependence of the sedimentation velocity and the effects of polymolecularity. The possibilities of getting information about polymolecularity from sedimentation measurements have been extensively treated, especially in combination with fractionation.

Many of the properties of high-polymer molecules in solution have not yet been interpreted from a theoretical point of view. The attempts hitherto made seem to be very promising and further work will undoubtedly throw light upon unexplained experimental facts. The formal theory of the influence of concentration is not yet complete. Only tentative attempts have so far been made on this problem. The effects of polymolecularity are also difficult to interpret quantitatively. In spite of that, the ultracentrifuge has proved to be a versatile tool, and a good illustration of this is the useful results obtained in applying the ultracentrifuge to fractional-precipitation experiments.

During the last few years, two new instruments applicable to the study of high-polymer molecules have appeared: the osmotic balance and the apparatus for light-scattering measurements. Without a doubt the combination of the ultracentrifuge, these new instruments, and all the other well-known methods (viscosity, diffusion, stream double refraction, etc.) forms the means for fruitful investigations of the high-polymer molecules, giving quite as successful results as those obtained earlier on globular proteins.

## References

1. Alfrey, T., Bartovics, A., and Mark, H., *J. Am. Chem. Soc.*, **64**, 1557 (1942).
2. Beckmann, C. O., and Rosenberg, J. L., *Ann. N. Y. Acad. Sci.*, **46**(5), 329 (1945).
3. Bresler, S., *Compt. rend. Acad. Sci. U. R. S. S.*, **43**, 310 (1944).
4. Bryde, Ø., and Rånby, B., *Svensk Papperstidn.*, **50**, No. 11B (1947).
5. Burgers, J. M., in *Second Report on Viscosity and Plasticity*. Royal Netherlands Academy of Sciences, Noord-Hollandsche, Amsterdam; Interscience, New York, 1938, p. 128.
6. Burgers, J. M., *Proc. Acad. Sci. Amsterdam*, **44**,<sup>\*</sup> 1045, 1177 (1941).
7. Burgers, J. M., *ibid.*, **45**, 9, 126 (1942).

8. Campbell, H., and Johnson, P., *Trans. Faraday Soc.*, **40**, 221 (1944).
- 8a. Campbell, H., and Johnson, P., *J. Polymer Sci.*, **3**, 735 (1948).
9. Cragg, L. H., and Hammerschlag, H., *Chem. Revs.*, **39**, 79 (1946).
10. Davidson, G. F., *J. Textile Inst.*, **29**, 195T (1938).
11. Debye, P., paper read before the XIth International Congress of Pure and Applied Chemistry, London, July 17-25, 1947.
- 11a. Debye, P., and Bueche, A. M., *J. Chem. Phys.*, **16**, 573 (1948).
12. Enoksson, B., *Nature*, **161**, 934 (1948).
13. Ewart, R. H., in H. Mark and G. S. Whitby, eds., *Advances in Colloid Science*. Vol. II, Interscience, New York, 1946, p. 210.
14. Flory, P. J., *J. Am. Chem. Soc.*, **63**, 3083, 3091, 3096 (1941).
15. Flory, P. J., *ibid.*, **69**, 30 (1947).
16. Flory, P. J., *J. Phys. Chem.*, **46**, 132 (1942).
17. Flory, P. J., *J. Chem. Phys.*, **10**, 51 (1942).
18. Flory, P. J., *ibid.*, **12**, 425 (1944).
19. Gee, G., *Ann. Repts. on Progress Chem. London*, **39**, 7 (1942); and in H. Mark and G. S. Whitby, eds., *Advances in Colloid Science*, Vol. II, Interscience, New York 1946, p. 145.
20. Gralén, N., *Sedimentation and Diffusion Measurements on Cellulose and Cellulose Derivatives*, Almqvist & Wiksells, Uppsala, 1944. (a) *Ibid.*, p. 12. (b) *Ibid.*, p. 18. (c) *Ibid.*, p. 19. (d) *Ibid.*, p. 62. (e) *Ibid.*, p. 89.
21. Gralén, N., and Lagermalm, G., in *Festskrift tillägnad J. Arvid Hedvall*. Elmders Boktryckeri, Göteborg, 1948, p. 215.
22. Guth, E., and Mark, H., *Monatsh.*, **65**, 93 (1935).
23. Hermans, J. J., *Rec. trav. chim.*, **63**, 219 (1944).
24. Hermans, J. J., *J. Polymer Sci.*, **1**, 233 (1946).
- 24a. Hermans, J. J., and Overbeek, J. Th. G., *Bull. soc. chim. Belg.*, **57**, 154 (1948).
25. Huggins, M. L., *Ann. N. Y. Acad. Sci.*, **43**, 1 (1942).
26. Huggins, M. L., *ibid.*, **44**, 431 (1943).
27. Huggins, M. L., *J. Am. Chem. Soc.*, **64**, 1712 (1942).
28. Johnson, P., *private communication*.
29. Johnston, J. P., and Ogston, A. G., *Trans. Faraday Soc.*, **42**, 789 (1946).
30. Jullander, I., *Arkiv Kemi Mineral. Geol.*, **A21**, No. 8 (1945). (a) *Ibid.*, p. 18. (b) *Ibid.*, p. 42. (c) *Ibid.*, p. 76. (d) *Ibid.*, p. 55. (e) *Ibid.*, p. 73. (f) *Ibid.*, p. 80. (g) *Ibid.*, p. 109. (h) p. 68 *et seq.*
31. Jullander, I., *J. Polymer Sci.*, **2**, 329 (1947).
32. Kinell, P.-O., *J. chim. phys.*, **44**, 53 (1947).
33. Kinell, P.-O., *Acta Chem. Scand.*, **1**, 335 (1947).
34. Kinell, P.-O., paper read before the Symposium on Coal, Petroleum, and Their Newer Derivatives, University of St. Andrews, Scotland, July 7-12, 1947; *Svensk Kem. Tidskrift*, **61**, 19 (1949).
35. Kinell, P.-O., *Acta Chem. Scand.*, **1**, 832 (1947).
36. Kraemer, E. O., in T. Svedberg and K. O. Pedersen, *The Ultracentrifuge*. Clarendon Press, Oxford, 1940, p. 327.
37. Kraemer, E. O., and Lansing, W. D., *J. Am. Chem. Soc.*, **55**, 4319 (1933).
38. Kraemer, E. O., and Lansing, W. D., *J. Phys. Chem.*, **39**, 153 (1935).
39. Kraemer, E. O., and Lansing, W. D., in T. Svedberg and K. O. Pedersen, *The Ultracentrifuge*, Clarendon Press, Oxford, 1940, p. 416.

40. Kraemer, E. O., and Nichols, J. B., in *The Ultracentrifuge*, p. 430.
41. Kuhn, H., *Experientia*, **2**, 64 (1946).
42. Kuhn, W., *Kolloid-Z.*, **68**, 2 (1934).
43. Kuhn, W., *Experientia*, **1**, 6 (1945).
44. Kuhn, W., *ibid.*, **1**, 9 (1945).
45. Kuhn, W., and Grün, F., *J. Polymer Sci.*, **1**, 183 (1946).
46. Kuhn, W., and Kuhn, H., *Helv. Chim. Acta*, **26**, 1394 (1943).
47. Kuhn, W., and Kuhn, H., *ibid.*, **28**, 1533 (1945).
48. Kuhn, W., and Kuhn, H., *ibid.*, **29**, 71 (1946).
49. Kuhn, W., and Kuhn, H., *ibid.*, **30**, 1233 (1947).
- 49a. Kuhn, W., Künzle, O., and Katchalsky, A., *Bull. soc. chim. Belg.*, **57**, 421 (1948); *Helv. Chim. Acta*, **31**, 1994 (1948).
50. Lamm, O., *Z. physik. Chem.*, **A138**, 313 (1928).
51. Lamm, O., *ibid.*, **A143**, 177 (1929).
52. Lamm, O., *Nova Acta Regiae Soc. Sci. Upsaliensis, Ser. IV*, **10**, No. 6 (1937).
53. Lansing, W. D., and Kraemer, E. O., *J. Am. Chem. Soc.*, **57**, 1369 (1935).
54. Lauffer, M. A., *J. Am. Chem. Soc.*, **66**, 1195 (1944).
55. Mark, H., and Whitby, G. S., eds., *Collected Papers of W. H. Carothers on High Polymeric Substances* (High Polymers, Vol. I). Interscience, New York, 1940, p. 274.
56. McFarlane, A. S., *Biochem. J.*, **29**, 407, 660 (1935).
57. Morey, D. R., and Tumblyn, J. W., *J. Phys. Colloid Chem.*, **50**, 12 (1946).
58. Morey, D. R., and Tumblyn, J. W., *ibid.*, **51**, 721 (1947).
59. Mosimann, H., *Helv. Chim. Acta*, **26**, 61 (1943).
60. Mosimann, H., *ibid.*, **26**, 369 (1943).
61. Mosimann, H., and Signer, R., *Helv. Chim. Acta*, **27**, 1123 (1944).
62. Pascu, E., *J. Polymer Sci.*, **2**, 565 (1947).
63. Pederson, K. O., *Compt. rend. trav. lab. Carlsberg, Sér. chim.*, **22**, 427 (1938).
64. Pedersen, K. O., *Ultracentrifugal Studies on Serum and Serum Fractions*. Almqvist & Wiksells, Uppsala, 1945, p. 148.
65. Philpot, J. St. L., *Nature*, **141**, 283 (1938).
66. Powell, R. E., and Eyring, H., in Kraemer, ed., *Advances in Colloid Science*. Vol. I, Interscience, New York, 1942, p. 210.
67. Rinde, H., *The Distribution of Sizes of Particles in Gold Sols*. Almqvist & Wiksells, Uppsala, 1928.
68. Rånby, B. G., *unpublished work*.
- 68a. Rånby, B. G., papers read before the XIth International Congress of Pure and Applied Chemistry, London, July 17–25, 1947, and Sjötte Nordiska Kemistmötet, Lund, Sweden, August 25–29, 1947.
- 68b. Rånby, B. G., *Acta Chem. Scand.*, **3**, 649 (1949).
- 68c. Rånby, B. G., and E. Ribi, *Experientia*, **6**, 12 (1950).
69. Schulz, G. V., *Z. Elektrochem.*, **44**, 102 (1938).
70. Schulz, G. V., *Z. physik. Chem.*, **B47**, 155 (1940).
71. Schulz, G. V., and Dinglinger, A., *J. prakt. Chem.*, **158**, 136 (1941).
72. Scott, R. L., *J. Chem. Phys.*, **13**, 178 (1945).
73. Scott, R. L., and Magat, M., *J. Chem. Phys.*, **13**, 172 (1945).
74. Signer, R., and Gross, H., *Helv. Chim. Acta*, **17**, 59 (1934).
75. Signer, R., and Gross, H., *ibid.*, **17**, 726 (1934).
76. Sihtola, H., *unpublished work*, and Rånby, B. G., and Sihtola, H., *to be published*.

77. Sihtola, H., and Svedberg, T., *Acta Chem. Scand.*, **2**, 474 (1948).
78. Simha, R., *J. Applied Phys.*, **17**, 406 (1946).
79. Simha, R., *private communication*.
80. Singer, S., *J. Polymer Sci.*, **2**, 290 (1947).
81. Singer, S., *J. Chem. Phys.*, **15**, 341 (1947).
82. Stockmayer, W. H., *J. Chem. Phys.*, **11**, 45 (1943).
83. Stockmayer, W. H., *ibid.*, **12**, 125 (1944).
84. Svedberg, I., and Kinell, P.-O., in *Harald Nordenson 60 år*. Esselte, Stockholm, 1946, p. 321.
85. Svedberg, T., *Kolloid-Z.*, Supplement to **36**, 53 (1925).
86. Svedberg, T., *Z. physik. Chem.*, **121**, 65 (1926).
- 86a. Svedberg, T., *Svensk Papperstidn.*, **52**, 157 (1949).
87. Svedberg, T., and Nichols, J. B., *J. Am. Chem. Soc.*, **45**, 2910 (1923).
88. Svedberg, T., and Rinde, H., *J. Am. Chem. Soc.*, **46**, 2677 (1924).
89. Svedberg, T., and Pedersen, K. O., *The Ultracentrifuge*, Clarendon Press, Oxford, 1940. (a) *Ibid.*, p. 331.
90. Säverborn, S., *A Contribution to the Knowledge of the Acid Polyuronides*. Almqvist & Wiksells, Uppsala, 1945.

# FATIGUE PHENOMENA IN HIGH POLYMERS

J. H. DILLON

*The Textile Foundation and Textile Research Institute, Princeton, New Jersey*

---

I. Definitions of Fatigue.....	220
II. Classification of High Polymers.....	221
III. Basic Phenomena Occurring with Fatigue.....	222
1. Molecular Flow and Secondary Bond Slippage.....	222
2. Physical Rupture of Molecular Chains.....	223
3. Orientation.....	223
4. Crystallization.....	225
5. Second-Order Transition.....	226
6. Chemical Scission and Cross Linking.....	226
IV. Generalized Fatigue Tests.....	227
1. Class A Fatigue.....	229
2. Class B Fatigue.....	229
3. Class C Fatigue.....	229
4. Class D Fatigue.....	229
5. Class E Fatigue.....	232
6. Class F Fatigue.....	232
V. Fatigue of Rubbers.....	233
1. General Characteristics.....	233
2. Fatigue Tests with Hysteretic Temperature Rise.....	233
3. Hysteresis.....	237
4. Stress-Strain Characteristics.....	243
5. Dynamic Fatigue Experiments.....	246
6. Qualitative Theory of the Effect of Strain Magnitudes and Limits upon Dynamic Fatigue Life.....	254
7. Fatigue of Rubbers as Related to Weathering.....	263
8. Fatigue Effects as Influenced by Oxidation.....	265
9. Static Fatigue at Intermediate and Low Temperatures.....	270
VI. Fatigue of Fibers.....	272
1. General Characteristics.....	272
2. Resilience.....	273
3. Stress-Strain and Primary Creep Characteristics.....	275
4. Static Fatigue-Rupture, Long-Term Creep, and Relaxation....	282
5. Dynamic Fatigue.....	286
VII. Fatigue of Plastics.....	306
1. General Characteristics.....	306
2. Stress-Strain, Creep, and Hysteresis.....	307
3. Static and Dynamic Fatigue to Rupture.....	309
VIII. Summary.....	315
References.....	316

---



## I. Definitions of Fatigue

The term "fatigue," in the broadest sense, denotes change in a property of a material or structure taking place in a finite interval of time under a given set of conditions. The property that undergoes change might be chemical or physical in nature, but, since the majority of so-called physical properties of high polymers may be related to the ultimate chemical structure of the material, this distinction is usually unnecessary. In certain cases, of course, the rate of fatigue depends primarily upon the growth of surface flaws where the stress is concentrated and there is some difficulty in attributing failure to chemical changes. Yet the interatomic binding stresses that must be exceeded for a flaw to develop or grow larger may be classed as chemical in nature. Only to the extent that the stress distribution in the vicinity of a growing flaw changes, then, can the fatigue be termed physical. Another form of fatigue that possesses purely physical features is the permanent change of shape, which occurs in plastic deformations. But here also molecular rearrangements usually take place, which result in such physical effects as strain hardening and embrittlement. Thus, only when dimensional changes are the sole observable effect of the deformation can the fatigue be classed as entirely physical.

The idea of elapsed time is fundamental in the use of the word fatigue to describe a process. In the strict sense, however, even impact rupture might be called a fatigue effect since the time of stress application, although very short, is still finite and measurable. The conventional engineering concept of fatigue usually infers failure or decay of properties after a series of repeated stress applications, but, to discuss the true chemical and physical nature of fatigue, it would be unfortunate to neglect the important limiting case where the frequency of stressing is zero.

The conditions of fatigue may be generally described in terms of the parameters: applied stress or strain, frequency and wave form of stress or strain, temperature, moisture content, the chemical environment, and the intensity and frequency of radiation impinging upon the sample. Unfortunately, many fatigue tests have been designed in a manner that prohibits clear-cut specification of one or more of these parameters. Often, for example, only the over-all maximum load on the sample is known while the true natures and magnitudes of the stresses are indeterminate. The prevalence of tests of this type makes difficult the quantitative comparison of data for various materials provided by the different fatigue testers.

It is apparent from these very general considerations that many phenomena might be classed as fatigue effects. A partial list would include:

(1) dynamic cycling tests, (2) static aging tests, (3) creep and relaxation phenomena, (4) swelling and solubility measurements, (5) impact and single-cycle rupture tests, and (6) complex phenomena involving abrasion, tearing, cutting, etc. In order to narrow this discussion to a reasonable scope, the following qualifications have been arbitrarily imposed upon the definition of fatigue:

(a) An external stress greater than zero must be imposed upon the material, either dynamically or statically in the course of the experiment.

(b) Time must be an explicit variable, expressed either in absolute units or indirectly as the number of cycles at a specified frequency.

(c) When actual rupture is not achieved, the property chosen for study must change irreversibly.

(d) Tests in which the stress-strain-time relationships cannot be defined such as those involving complicated indexes as in abrasion loss or depth of cut will be excluded from the discussion.

(e) Tests designed to evaluate engineering structures composed of several different materials will not be discussed.

These qualifications immediately eliminate all save the phenomena (1), (2), and (3) listed above. In a positive sense, fatigue will be considered as *that phenomenon wherein a material ruptures or changes one or more of its properties permanently, after a measured "fatigue time" during which a system of finite stresses has been imposed.* Even with this limited definition of fatigue, there exists a very great amount of published material, which comes within its scope. For example, creep and relaxation data have been presented in great volume. It is obvious then that no attempt at bibliographic completeness can be made in this brief survey. Rather, this discussion will be aimed at a better understanding of the chemical and physical processes occurring in fatigue experiments; references to the literature will be made only where essential to the explanation of these basic phenomena. Special attention will be given experiments involving dynamic fatigue to rupture because of its great practical importance.

## II. Classification of High Polymers

In this discussion of fatigue phenomena, high polymers are classified in the usual way as rubbers, fibers, and solid plastics. It must be recognized, of course, that a given polymer may exist in each of the following states: hard crystalline, hard amorphous, rubbery, and liquid, depending on its temperature-time history. This matter has been amply discussed by Mark (1). Furthermore, it is possible for a polymer to exist simultaneously in two or more states at a given temperature. For example, natural rubber may be stretched to a moderate elongation at which only a por-

tion of its structure will be sufficiently ordered to form crystallites. If held at that elongation, it is true that relaxation will take place with a corresponding change in the ratio of amorphous to crystalline polymer; thus, the state may be considered metastable. In a native cellulose fiber where the interchain binding forces are higher, however, crystalline and amorphous regions exist simultaneously with no external stress required to maintain that condition. Returning to natural rubber, this material in unvulcanized form may be extended to a high elongation and then vulcanized at room temperature in sulfur chloride vapor. The result is a material with the high tensile strength and low extensibility characteristic of a highly oriented crystalline fiber.

In the light of these facts, it is clear that the classification of a polymer as a rubber, fiber, or plastic and the state in which it exists are functions of its history, as defined by the parameters temperature, strain, and chemical environment. Fatigue phenomena are essentially time phenomena and, in the case of dynamic fatigue, heat is developed by the hysteresis mechanism, which raises the temperature above the surroundings. Furthermore, seldom is a fatigue test conducted in the absence of reactive agents such as oxygen. Hence, careful classification and definition of state are particularly necessary in discussing fatigue phenomena of high polymers.

### III. Basic Phenomena Occurring with Fatigue

Before entering into a study of the literature on fatigue, it is desirable to consider briefly the various physicochemical phenomena that can occur during a controlled fatigue operation, *i.e.*, in a high polymer sample held for a period of time under stress in air at known but possibly varying temperature. The major effects may be listed as: (a) molecular flow and secondary bond slippage resulting only in a change of shape; (b) physical rupture of chains by stress concentration in a localized region; (c) orientation of chains with or without crystallization; (d) crystallization by cooling or orientation; (e) second-order transition; and (f) chemical scission of chains and cross linking.

#### 1. *Molecular Flow and Secondary Bond Slippage*

The first-listed phenomenon, molecular flow and secondary bond slippage, is very common for amorphous high polymers when held for long periods under a static stress. It is variously referred to as set, flow, plastic deformation, etc. Often secondary bond slippage is not truly irreversible since the original dimensions may sometimes be regained or approached by

increasing the temperature or the moisture content. The type of flow treated by Eyring and co-workers (2-4) is mainly of this quasi-permanent type and thus does not fall strictly within our definition of fatigue. Nevertheless, quasi-permanent flow is often an important factor in true fatigue tests since the resulting dimensional changes increase the applied stress concentrations and thus hasten the process of dynamic or static rupture.

## *2. Physical Rupture of Molecular Chains*

The second phenomenon, physical rupture of molecular chains, occurs principally in the region of high localized stresses or where the whole sample is subjected to a stress near the static rupture value. It is quite often difficult to separate this effect from others such as secondary bond slippage, chemical scission, and cross linking. The rupture of primary valence bonds by mechanical stresses is at present receiving considerable attention. An expression for the critical shear stress necessary to rupture a macromolecule of given length has been discussed in connection with the shear breakdown of concentrated high polymer solutions (5).

## *3. Orientation*

Orientation of the long molecular chains in the direction of the principal stress is a property common to all high polymers possessing molecular asymmetry. Orientation may be of three major types: (*A*) alignment of the chain molecules of the noncrystallizing regions of a polymer parallel to the stretch axis to produce order in the plane normal to the axis, (*B*) ordering of crystallites initially present with long axes along the stretch axis, and (*C*) ordering of the molecules into a three-dimensional crystalline phase.

The first type of orientation (*A*) yields the lowest degree of order and is difficult to measure. It occurs in copolymers, which are not sufficiently regular in molecular constitution to permit the higher degrees of order (*B*) and (*C*). In general, type *A* orientation produces no change in the amorphous x-ray pattern but it has been reported (6) that the "noncrystallizing copolymer" of butadiene and acrylonitrile, Buna N, does show at high elongations a splitting of the amorphous halo into two arcs symmetric about the axis of stretch. More recently, Hanson and Halverson (7) have observed similar patterns for raw polymers stretched and then frozen. These polymers, which by ordinary techniques appear to be "noncrystallizing," included emulsion polymers of butadiene, isoprene, and dimethylbutadiene and mass-polymerized (sodium catalyst) polybutadiene and polyisoprene. This effect can be attributed to an ordering in the plane normal

to the axis of stretch. For crystallizing rubbers such as Hevea, type *A* orientation should be considered as a necessary condition for the formation of crystallites when the temperature is above the crystallization range for zero strain. Type *A* orientation can be "frozen in" by reducing the temperature quickly below the second-order transition point. For fibers such as regenerated cellulose, type *A* orientation certainly exists in the amorphous regions after stretching and plays a salient role in orienting the crystallites initially present.

Type *B* orientation is characteristic of many fibers such as regenerated cellulose where a large amount of crystallization exists in the unoriented unstrained state. Here orientation can be measured simply by observing the alignment of the initial crystallites by changes in the x-ray diffraction patterns (8). The cellulose crystallites do not grow in size or number with increased orientation and hence serve as convenient "markers" to trace the course of over-all molecular alignment. Orientation can be "set" or made permanent by drying the wet-stretched fiber under tension.

Type *C* orientation occurs with many rubbers and some fibers (9). Upon stretching, certain regions of the polymer develop three-dimensional order, which gives sharp diffraction patterns. In general, the crystallites so formed increase in number but not in size with increasing strain. The amorphous regions of the polymer must be oriented according to type *A* but this is masked by the crystallizing effect. This important phenomenon is often referred to as "crystallization" and will be discussed in some detail under that heading.

Orientation of type *A* or *B* always results in increased stiffness, breaking strength, and decreased extensibility in the direction of the principal stress. Here it will be noted that the term stiffness (sometimes referred to as secant modulus) is employed to represent the ratio of stress to strain rather than modulus, which must be defined more explicitly. The changes in properties in the plane normal to the principal stress are not as easily specified but, for the special case of axial tension, both the axial and radial stiffnesses of the material increase with orientation (10). The question of radial strength is somewhat obscure since it is difficult to evaluate experimentally. A reasonably clear picture of the variation of radial strength can be derived, however, by adopting a naive viewpoint wherein the oriented polymer is considered as a bundle of elongated coil springs for rubbers, or rigid rods for a cellulosic fiber—held parallel by an external force or by weak radial forces introduced by cooling or deswelling from a wet condition. Here, it might be expected that the radial breaking stress would be low in tension. This conclusion is borne out by observations on ramie

fibers, which are very strong axially but brittle in the transverse direction. In compression, however, the value of the radial breaking stress would depend on the rigidity of the oriented molecules and its approximate value would be difficult to predict.

#### *4. Crystallization*

Crystallization of high polymers is another very important factor in their fatigue behavior. As pointed out by Alfrey and Mark in a comprehensive review of phase transitions in rubber (11), crystallization phenomena in rubbers are much more complex than for low-molecular compounds in that crystallization takes place over a range of temperatures as a function of time. For example, in unstrained natural rubber, Wood and Bekkedahl (12) have shown this range to extend from  $-50^{\circ}$  to  $+15^{\circ}\text{C}$ . with the maximum rate of crystallization taking place at  $-25^{\circ}\text{C}$ . There is an appreciable decrease of volume, 2.0 to 2.7%. They further showed that the melting point of rubber depends upon the temperature at which the rubber was crystallized, the melting point being  $4-7^{\circ}\text{C}$ . above the crystallization temperature for natural rubber. This unsharpness of crystallization and melting is explained qualitatively (11) on the basis of the current ideas of high polymer crystallites, which appear to be distributed among the molecular chains in such a manner that several chains may pass through a given crystalline region while some of these chains may enter other neighboring crystallites. When a rubber polymer is strained, crystallization can take place at temperatures considerably above the upper limit of the range observed for the case of zero strain. For example, Field (13) has shown with vulcanized gum rubber stocks that observable crystallization sets in at about 200% extension and increases with increasing extension until, at 700%, approximately 80% of the polymer is crystallized, as judged by the ratio of intensities of the diffraction spots and the amorphous halo. Wildschut (14), employing extrapolations of stress-temperature curves, calculated the crystallinity at 600% elongation as only 30-32%. Thus the determination of the absolute amount of crystallinity is still a subject for continuing research.

In general, it may be said that low temperature and high extension favor crystallinity in those rubbers that are sufficiently regular in molecular chain constitution to permit true three-dimensional order. Stretching at a given temperature greatly increases the rate of crystallization, more rapid rates of stretching giving a higher degree of crystallinity (15). Heating stretched rubber reduces the crystallinity; conversely, chilling crude natural rubber ( $-5^{\circ}\text{C}$ . for 18 hours), which is held at as low an elongation as

30%, brings out clearly the diffraction pattern of the crystalline phase. This result obtained by Gehman and Field (16) was interpreted by them to mean that localized ordered regions caused by stretching act like nuclei for crystallization when freezing occurs. Field (13) gives other valuable data on the variation of crystallinity with extension, temperature, and state of cure. In particular, he shows that extended creep (a true fatigue effect) results in increased crystallinity in natural rubber.

On the basis of this very brief discussion, then, it seems safe to conclude that crystallization has the following effects pertinent to the study of fatigue phenomena in high polymers: (1) increased strength and stiffness in the axis of crystallite orientation, (2) increased brittleness (for fibers, not necessarily for rubbers), and (3) a volume decrease.

### ***5. Second-Order Transition***

The so-called second-order transition takes place at a temperature or within a range of temperatures that marks the boundary between the rubbery and the hard brittle state, which defines many noncrystallizing plastics. The transition is characterized by changes in the first derivatives of the principal thermodynamic variables (coefficient of expansion, specific heat, etc.). The effect can be explained by assuming that the chain segments are restrained from rotation below the second-order transition temperature. All rubbers experience a second-order transition at some temperature,  $-70^{\circ}\text{C.}$  for Hevea rubber,  $+70^{\circ}\text{C.}$  for polymethyl methacrylate. The effect appears quite independent of crystallization and results in increased stiffness and brittleness below the transition temperature. Crystallization of rubbers does not, in general, result in brittleness. There is no evidence that the second-order transition is influenced by an applied stress although this would seem possible. The effect is not as slow as crystallization under no stress but its sharpness is influenced by the speed of mechanical testing (17).

Fatigue tests are seldom made in the region of the second-order transition for obvious reasons. However, when rubber products are required to operate at low temperatures, the phenomenon must be taken into account as well as crystallization. Such fatigue phenomena generally consist in rupture within the first few cycles or rapid hysteretic heating, which brings the product safely through the transition into a satisfactory rubbery state.

### ***6. Chemical Scission and Cross Linking***

It has been demonstrated by Tobolsky and co-workers (18) that two different types of oxidation occur in many rubbers when held at a fixed

strain in air at temperatures above 70°C. The long-term, stress-relaxation experiments employed may be considered as static fatigue studies. In brief it was found that, after the relatively rapid secondary bond relaxation is complete, another process of relaxation takes place, which is caused by oxidative scission of the extended molecular chains. The rate of relaxation was found to obey simple laws of chemical reactions and was independent of the elongation employed in a range of 50–200%. Now since these experiments were made with the elongation fixed, the effects of any possible crosslinking were largely excluded and the scission reaction was effectively isolated in a convenient manner. This was not true, however, when they employed another technique termed “intermittent relaxation” wherein the rubber samples were maintained at zero elongation except for short intervals in which they were stretched to a fixed elongation and the stress measured. In this latter experiment, the stress change would be the resultant of those due to scission of chains (a stress decrease) and to cross linking (a stress increase). In all cases, of course, “continuous relaxation” gave a decreasing stress but some rubbers, GR-S, for example, showed an increasing stress in the “intermittent” test, indicating that the cross-linking reaction predominated. In other cases, natural rubber, butyl, etc., the scission reaction was greater but, by combining the results of both types of tests, it was evident that, in general, both cross linking and scission take place concurrently. Since most fatigue tests are conducted in air, often at elevated temperature, the importance of these findings is obvious. Oxidative scission results in reduced stiffness and lower breaking strength; cross linking produces increased stiffness and brittleness.

#### IV. Generalized Fatigue Tests

Thus far in this chapter, fatigue has been defined and the various basic physicochemical phenomena, which may occur in the course of a fatigue experiment, have been listed and briefly discussed. The next step in our considerations is the analysis of the mechanical conditions employed in fatigue testing. This is accomplished by selecting several distinct types of fatigue experiments and discussing the special cases for each and their relation to actual test conditions. There are numerous possible systems of classification of fatigue experiments but the following system seems to combine the objectives of reasonable generality and clarity. This system consists of four general classes of alternating fatigue defined according to four quantities: dynamic strain amplitude  $Y$ , dynamic stress amplitude  $X$ , average static strain  $y_a$ , and average static stress  $x_a$ . In addition, two other classes of fatigue are considered to embrace repeated stress-strain



cycling at constant rate of strain and constant rate of loading, respectively. In each class of alternating fatigue, two of these quantities are specified as constant while the other two vary as functions of time. The total number of possible combinations, of course, would be six. However, two of these are physically impossible, *i.e.*, both static stress and static strain constant and both dynamic stress and dynamic strain constant. Hence, we have the four main classes of alternating fatigue A, B, C, and D illustrated in Figures 1 to 4.

Now before discussing these classes of fatigue, it is well to recognize the limitations of this system. First of all, the matter of wave form is treated very lightly, approximately sinusoidal strain and stress being assumed. However, since most dynamic fatigue machines impose sinusoidal or connecting rod motion with a reasonably large ratio of connecting rod length to amplitude, very little generality is sacrificed by this assumption. Nevertheless, it must be remembered that some products undergo quite complicated stress cycles. For example, a given region of a tire tread is subjected to very rapid rates of stressing as it strikes the pavement and as it leaves it, but is under a condition of steady stress during most of the period of rotation of the wheel. Thus, it has been estimated (19) that the effective frequency of stressing in a truck tire tread is of the order of 100 cycles/second, with rest periods intervening between stressings and destressings. It will be noted in the illustrations of Figures 1 to 4 that stress and strain appear to be in phase. In reality, of course, the strain may lag behind the stress because of hysteresis. However, except at resonance, which is generally avoided in a fatigue test, the phase angle is usually only a few degrees and, for simplicity of drafting, no phase angle is shown. It should be noted that the important case of shear fatigue is omitted from consideration in Figures 1 to 4. Since shear strains and stresses can be resolved into tension and compression components, classes A to D can be considered to include the shear cases also. Temperature and moisture content are other variables not included specifically in these classifications but it is clear that their values must be considered in each individual experiment because of their profound effect upon the fatigue results. Ordinarily, the temperature of a dynamically fatiguing sample soon reaches an equilibrium value where the rate of hysteretic heat generation is just balanced by the losses to the surroundings. In a few instances, however, temperature is deliberately varied periodically and valuable data on cellulosic fibers, perhaps not truly fatigue data since the load was zero during heating, have been obtained (20). It should be noted that the strains  $y_a$ ,  $y_m$ , and  $y$  given in the diagrams are total strains, *i.e.*, they correspond to settings of a ma-

chine that cannot distinguish between elastic and plastic strains. Acknowledging, then, the limitations of this system of classification, it is necessary to give some consideration to each of the six principal classes of fatigue.

### ***1. Class A Fatigue***

This type of fatigue experiment is most common in work with rubbers. It is not always realized that even though a test is set up with a constant strain amplitude well within the tension region initially (see strain-time plot of Fig. 1), the dynamic stress may eventually enter the compression region because of stress relaxation (see stress-time plot of Fig. 1). However, the average static stress  $\bar{\sigma}_a$  can never change from tension to compression in this type of experiment. Class A fatigue also embraces stress-relaxation experiments when the dynamic strain amplitude vanishes (see subclasses 5, 6, and 7); thus, it is important for tests on fibers and plastics as well as rubbers.

### ***2. Class B Fatigue***

The class B type of experiment includes many of the fatigue studies on yarns and cords where it is experimentally convenient to apply a steady load but subject the sample to a constant alternating strain. Creep tests of various types are also included under the classification, simply by equating the dynamic strain to zero (see subclasses 5, 6, and 7).

### ***3. Class C Fatigue***

This type of fatigue is formally almost equivalent to class A, if stress and strain are interchanged as variables. However, dynamic and static strain increase with time whereas, in class A, dynamic and static stress decrease with time. When the stress amplitude  $X$  is equated to zero, this class overlaps class B (subclasses 5, 6, and 7). Subclasses 1, 2, and 3 are seldom employed, which is rather surprising since there is little experimental difficulty in maintaining both static strain and dynamic stress constant (neglecting changes in cross section resulting from creep).

### ***4. Class D Fatigue***

Subclasses 1, 2, 3, and 4 of this type of fatigue (see Fig. 4) have never been employed with high polymers as far as the available literature indicates. Class D overlaps class A in subclasses 5, 6, and 7.

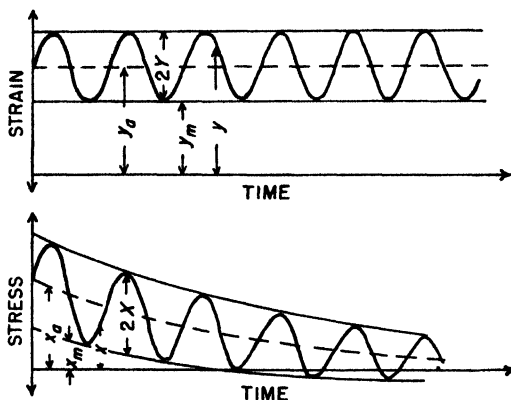


Fig. 1. Class A fatigue. Alternating dynamic stress and strain; dynamic strain amplitude  $Y$  constant; average static strain  $y_a$  constant. Subclasses are:

1. Dynamic tension fatigue:  $Y > 0$ ;  $y_m \geq 0$ .
2. Dynamic compression fatigue:  $Y > 0$ ;  $y_m \leq -2Y$ .
3. Asymmetric fatigue:  $Y > 0$ ;  $|y_a| < Y$ .
4. Symmetric fatigue:  $Y > 0$ ;  $y_a = 0$ .
5. Static tension relaxation:  $Y = 0$ ;  $y_a > 0$ .
6. Static compression relaxation:  $Y = 0$ ;  $y_a < 0$ .
7. Intermittent relaxation:  $Y = 0$ ;  $y_a = 0$ .

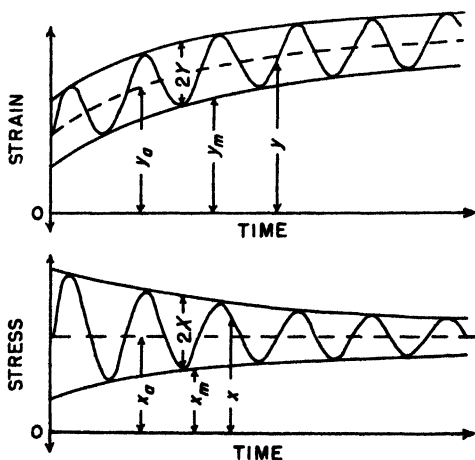


Fig. 2. Class B fatigue. Alternating dynamic stress and strain; dynamic strain amplitude  $Y$  constant; average static stress  $x_a$  constant. Subclasses are:

1. Dynamic tension fatigue:  $Y > 0$ ;  $x_m \geq 0$ .
2. Dynamic compression fatigue:  $Y > 0$ ;  $x_m \leq -2X$ .
3. Asymmetric fatigue:  $Y > 0$ ;  $|x_a| < X$ .
4. Symmetric fatigue:  $Y > 0$ ;  $x_a = 0$ .
5. Static tension creep:  $Y = 0$ ;  $x_a > 0$ .
6. Static compression creep:  $Y = 0$ ;  $x_a < 0$ .
7. Intermittent creep:  $Y = 0$ ;  $x_a = 0$ .

Fig. 3. Class C fatigue. Alternating dynamic stress and strain; dynamic stress amplitude constant; average static stress constant. Subclasses are:

- |                                 |                            |
|---------------------------------|----------------------------|
| 1. Dynamic tension fatigue:     | $X > 0$ ; $x_m \geq 0$ .   |
| 2. Dynamic compression fatigue: | $X > 0$ ; $x_m \leq -2X$ . |
| 3. Asymmetric fatigue:          | $X > 0$ ; $ x_a  < X$ .    |
| 4. Symmetric fatigue:           | $X > 0$ ; $x_a = 0$ .      |
| 5. Static tension creep:        | $X = 0$ ; $x_a > 0$ .      |
| 6. Static compression creep:    | $X = 0$ ; $x_a < 0$ .      |
| 7. Intermittent creep:          | $X = 0$ ; $x_a = 0$ .      |

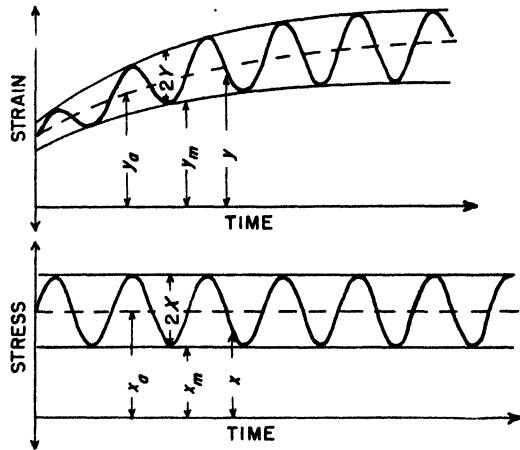
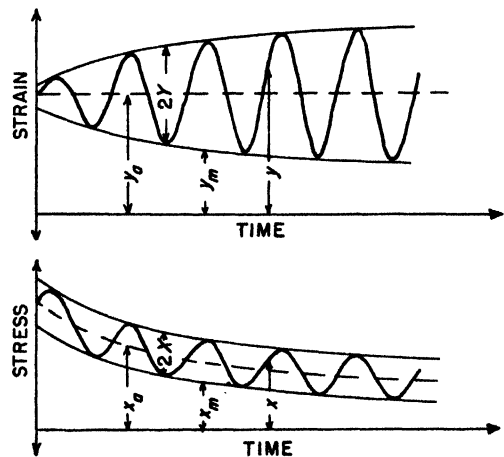


Fig. 4. Class D fatigue. Alternating dynamic stress and strain; dynamic stress amplitude constant; average static strain constant. Subclasses are:

- |                                   |                            |
|-----------------------------------|----------------------------|
| 1. Dynamic tension fatigue:       | $X > 0$ ; $y_m \geq 0$ .   |
| 2. Dynamic compression fatigue:   | $X > 0$ ; $y_m \leq -2Y$ . |
| 3. Asymmetric fatigue:            | $X > 0$ ; $ y_a  < Y$ .    |
| 4. Symmetric fatigue:             | $X > 0$ ; $y_a = 0$ .      |
| 5. Static tension relaxation:     | $X = 0$ ; $y_a > 0$ .      |
| 6. Static compression relaxation: | $X = 0$ ; $y_a < 0$ .      |
| 7. Intermittent relaxation:       | $X = 0$ ; $y_a = 0$ .      |



### 5. *Class E Fatigue*

Experiments involving repeated stress-strain cycles with constant rate of increasing and decreasing strain have been performed in great number on all varieties of high polymers. Unfortunately few of these studies have been made with the controlled strain cycle illustrated in Figure 5 and hence the results are difficult to interpret from the viewpoint of fatigue. Nevertheless, this type of experiment with rather low rates of strain appears to offer great possibilities for elucidating the molecular changes that take

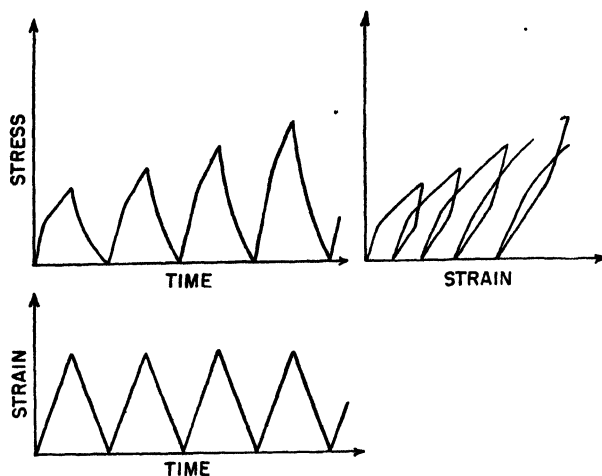


Fig. 5. Class E fatigue. Constant rate of strain; constant maximum strain.

place, and will probably find increased favor. It is obvious, of course, that the shape of each stress-time curve depends on the particular material under test and the choice of strain cycle. With wool and rubbers, for examples, the extension curve generally shows an upward inflection at the higher stresses, the retraction curves (on a stress-strain diagram) nearly coincide and there is a much greater tendency for elastic reversibility than is shown in Figure 5. Because of the almost limitless variations possible in this type of experiment, it would be unwise to attempt to develop subclasses.

### 6. *Class F Fatigue*

Constant rate of loading stress-strain tests are common, particularly in textile yarn research. The data are somewhat more difficult to analyze

than those obtained at constant rate of strain. Otherwise, all the statements made for class E tests apply.

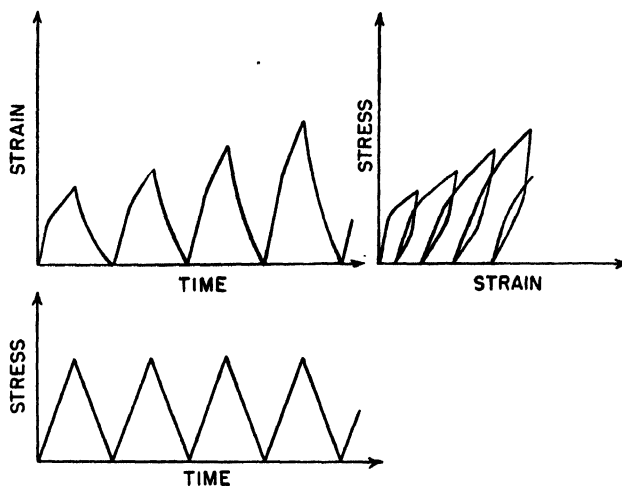


Fig. 6. Class F fatigue. Constant rate of loading; constant maximum load.

## V. Fatigue of Rubbers

### 1. General Characteristics

Rubbers, when vulcanized sufficiently to reduce creep effects, are ideally suited for many applications where dynamic fatigue is a problem because of their high reversible extensibility. All rubbers are limited in this respect by their hysteretic properties and by the fact that most of them tend to develop surface cracks as a result of their susceptibility to the action of oxygen and ozone. Consequently, rubber products are usually designed to operate at a maximum dynamic strain, which is much below the breaking strain. Nevertheless, high strains do occur in regions of incipient failure, at the base of a cut or crack, for example. Hence, the fatigue failure of a rubber product is often dependent both upon the tendency for tiny cracks to develop and for them to grow in depth and length.

### 2. Fatigue Tests with Hysteretic Temperature Rise

Hysteretic heat generation is a very important factor in the fatigue of rubbers since, in a dynamically strained sample, there is always a rise of

temperature in the initial period of cycling. Neglecting changes in the temperature of the environment, an equilibrium state is generally reached where the rates of loss by conduction, convection, and radiation are equal to the rate of heat generation. As the sample fatigues and its mechanical properties change permanently, the equilibrium may be disturbed and another temperature rise occurs. Often this final rise of temperature leads to thermal failure or "blowout" of the sample. A number of fatigue tests for rubber stocks have employed this principle (21-24). They have proved very useful in the development of rubber stocks for tires and other products. However, the machines employed in these tests are designed to operate under known dynamic and static loads and deflections rather than known stresses and strains. Hence, the published data are somewhat difficult to interpret in terms of the basic properties of fatiguing polymers. Nevertheless, the work of Havenhill (23) with the St. Joe flexometer is of interest because of the variety of properties that he studied as functions of fatigue time. With this machine, it is possible to vibrate rubber samples in shear under conditions of constant shear force (horizontal load) or constant shear strain (horizontal deflection). The sample may be held either at constant compressive (vertical) load or compressive deflection (vertical compression), normal to the shearing force. Some of the data obtained are given in Figures 7 to 11. By varying the direction of the grain of the sample with respect to the plane of shear, it was possible to study the anisotropic effect of pigment orientation as well as that of the rubber molecules. Havenhill concluded that it is possible for rubber compounds "to exhibit simultaneously a plastic flow in one direction and a marked stiffening in another direction resulting from the elimination of plastic flow by flexing." Lessig (22) employed a somewhat simpler fatigue machine, the Goodrich Flexometer, which operates with a constant compressive static load and a constant compressional amplitude. This test was thus essentially of class B-2 although the constant compressional amplitude was not a true strain amplitude because of the fact that the end areas of the sample were constant, resulting in a lateral bulging. It should be noted that constant amplitude flexing tends to penalize a stiff stock as shown in Figures 12 and 13. Lessig also studied the anisotropic effects of pigments, obtaining results shown in Figure 14. Gough and Parkinson (24) have obtained rather interesting results with the Dunlop Fatigue Tester, which is a device providing compressional fatigue of rubber blocks, class A or class B, or with constant power input. It was found that all properties that progressively changed during a run varied linearly with the logarithm of the life  $L$  (expressed in minutes). Several rather interesting empirical relationships were de-

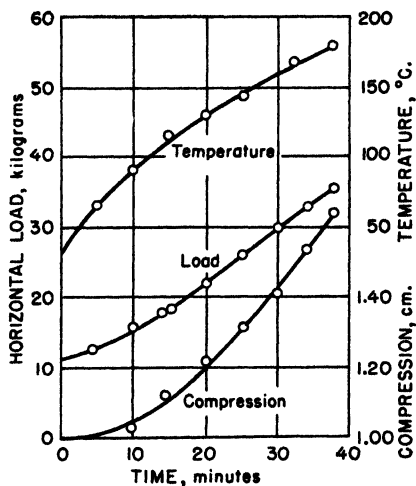


Fig. 7. Constant horizontal deflection test (vertical load, 250 kg.; horizontal deflection, 0.673 cm.) (23).

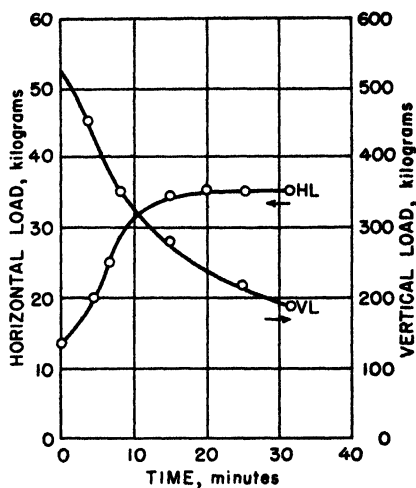


Fig. 8. Constant vertical compression test (vertical compression, 1.61 cm.; horizontal deflection, 0.714 cm.) (23).

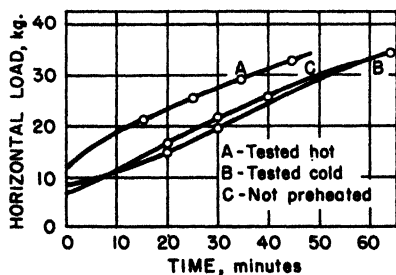


Fig. 9. Constant horizontal deflection tests on preheated specimens (vertical load, 250 kg.; horizontal deflection, 0.610 cm.) (23).

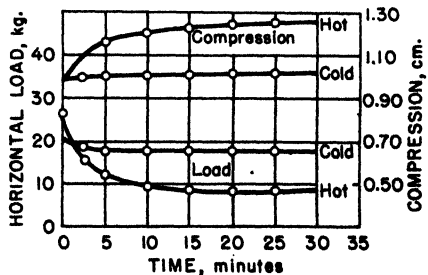


Fig. 10. Static compression test on hot and cold plugs (vertical load, 250 kg.; horizontal deflection, 0.714 cm.) (23).



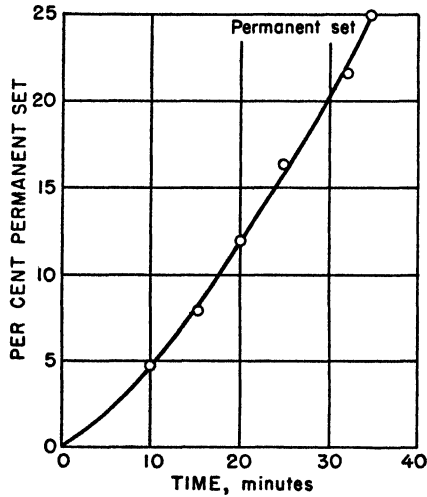


Fig. 11. Permanent set acquired during flexometer test (vertical load, 250 kg.; horizontal deflection, 0.673 cm.) (23).

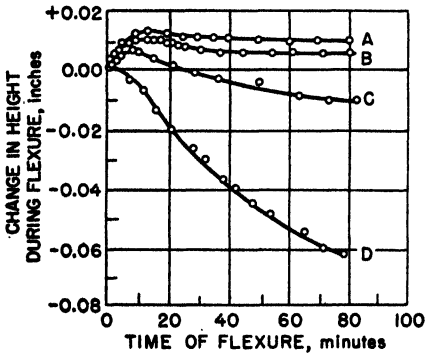


Fig. 12. Changes in height during flexure using various percentages of carbon black (22). Volume loading: A, 0%; B, 10%; C, 20%; D, 30%.

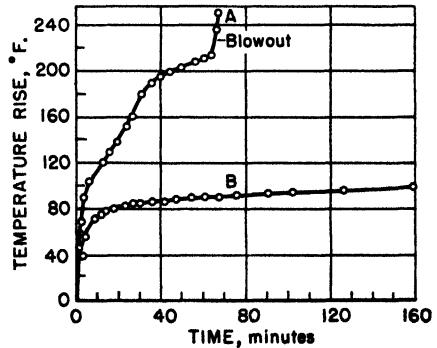


Fig. 13. Fatigue test (22). A, loaded with 25 parts channel black and 132 parts zinc oxide; B, loaded with 51 parts soft black and 10 parts zinc oxide. Applied load, 180 p.s.i.; compression stroke, 0.25 in.

rived from this work. Fatigue resistance  $R$  was defined as  $\log L$  and it was found that:

$$R = \log L = A - BT \quad (1)$$

where  $T$  is the mean running temperature, and  $A$  and  $B$  are constants. Another empirical relation found was:

$$R = \log L_{100} + \log n + (100 - T)/D \quad (2)$$

where  $R$  is the fatigue resistance at a mean running temperature  $T$ ,  $L_{100}$  is the life at  $100^\circ\text{C}.$ ,  $n$  is the frequency, and  $D$  is a constant for a given rubber stock.

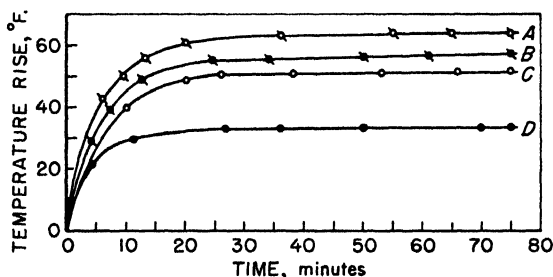


Fig. 14. Anisotropy (22). *A*, suprex-clay filler, flexure parallel to plate surface of pigment; *B*, suprex-clay filler, flexure normal to plate surface of pigment; *C*, asbestine filler, flexure parallel to long axis of pigment; *D*, asbestine filler, flexure normal to long axis of pigment. Applied load, 143 p.s.i.; compression stroke, 0.25 in.; filler, 25.6 volumes.

### 3. Hysteresis

The hysteresis of rubbers has been studied by many workers using various different techniques. The work done in this field has been summarized quite completely by Dillon and Gehman (25) who give a comprehensive bibliography. They point out that the methods employed fall into five principal classes: (1) low-speed stress-strain loop, (2) impact resilience, (3) free vibration, (4) forced vibration at resonance, and (5) forced vibration at nonresonance. These methods are analyzed mathematically and the devices used by the various investigators are broken down into simple models for comparison. Measuring the area of the stress-strain loop obtained with an ordinary testing machine is a simple means of measuring hysteresis but the results often do not correlate with

those obtained by the dynamic methods (2) to (4). The results thus are not always significant in relation to dynamic fatigue tests. Method (5) generally involves the direct measurement of operating temperature and thus is very simple and effective for predicting the temperature of a fatiguing sample, providing the stress-strain-time conditions are properly chosen. It has been shown (26-28), however, that the rate of heat generation depends greatly upon the choice of the vibration conditions; for examples, at a given frequency, it is proportional to the internal friction  $\eta$  for constant strain amplitude vibrations, but to  $\eta/E^2$  (where  $E$  is the dynamic modulus) for constant stress amplitude vibrations. Hence, great care must be exercised in interpreting hysteresis data. For convenience of reference,  $\eta$  and  $E$  are defined by the differential equations for longitudinal vibrations:

$$\frac{h}{A} M \frac{d^2 y}{dt^2} + \eta \frac{dy}{dt} + Ey = X \cos \omega t \quad (3)$$

and

$$\frac{h}{A} M \frac{d^2 y}{dt^2} + \eta \frac{dy}{dt} + Ey = 0 \quad (4)$$

where  $y$  is the strain,  $t$  is the time,  $M$  is the vibrating mass,  $A$  is the cross-sectional area,  $h$  is the length of the sample in the  $y$ -direction,  $\omega$  is the radian frequency, and  $X$  is the stress amplitude. Obviously, equations (3) and (4) apply equally well to shear vibrations when  $y$  is the shear strain,  $X$  is the shear-stress amplitude,  $E$  is the shear modulus, and  $h$  is the distance between shear planes of area  $A$ . The internal friction  $\eta$  then has dimensions of viscosity. Equation (3) applies to forced vibrations and the special case (4) applies either to free vibrations or to impact-resilience experiments. Solving (3) and applying the approximate condition for resonance:

$$E = \frac{h}{A} M \omega_0^2 \quad (5)$$

it is found that:

$$\eta = \frac{X}{\omega_0 y_0} \quad (6)$$

where the subscript zero refers to the resonance condition. Likewise, for the case of free vibrations, there is obtained from (4) the relation:

$$R = \left( \frac{y_{n+1}}{y_n} \right)^2 = \exp (-2\pi\omega_0\eta/E) \quad (7)$$

where  $y_{n+1}$  and  $y_n$  are successive strain amplitudes separated by a time interval of  $2\pi/\omega_0$ . The quantity  $R$  is commonly called the "dynamic resilience" and obviously can be calculated either from free- or forced-vibration data. With appropriate geometrical assumptions,  $R$  can be calculated also from impact-resilience tests (28). Similarly, the quantities  $\eta$  and  $E$  can be obtained from forced-vibration tests by equations (5) and (6) and from free-vibration tests by (5) and (7). Now equations (3) and (4) are based upon the assumption of Hookean elasticity and viscous damping. Thus, for the small vibrations, both  $E$  and  $\eta$  should be independent of both amplitude and frequency. For pure-gum stocks of natural rubber and GR-S in simple shear vibration it has been shown (28) that both  $E$  and  $\eta$  are independent of strain amplitude up to about 10% strain. The dynamic modulus  $E$  is independent of frequency in the range of 20–200 cycles/second but is slightly greater than the static modulus;  $\eta$  decreases with increasing frequency in such a manner that  $\omega\eta$  is nearly independent of frequency. The relationships are almost as simple for tread stocks except that  $E$  decreases with increasing strain amplitude.

Both  $\eta$  and  $E$  decrease markedly with increasing temperature for all rubber polymers investigated (28). It appears safe to state, furthermore, that all synthetic rubbers thus far developed have a greater internal friction (hysteresis defect) than does natural rubber at temperatures of 20°C. and above. However, it has been shown (28) that butadiene-styrene copolymers high in butadiene (in a gum formula) have a lower temperature coefficient of  $\eta$  than does natural rubber; thus, at a temperature of 0°C., polybutadiene is better than natural rubber from the hysteresis standpoint. This is not true for corresponding tread compounds, however.

The marked frequency dependence of  $\eta$  indicates that the assumptions upon which equations (3) and (4) are based are incorrect; yet, for a given frequency they apply fairly well. Obviously, to compare different polymers, measurements should be made at the same frequency. This is simple to accomplish with forced vibrations, very difficult with free vibrations; hence, the former method seems better adapted to studying the hysteretic aspects of fatigue. It must be remembered, however, that, while the over-all strain amplitude of a fatigue experiment may be small and thus within the range of forced-vibration hysteresis tests, the localized strains in the region of incipient failure of the fatiguing test piece may be very high. Wiegand and Braendle (29,30) have called attention to this matter. They performed stress-strain cycling tests (class E fatigue, rate of strain, 18 inches/minute) at a series of maximum elongations (see Fig. 15) and demonstrated that the relative hysteresis of GR-S and natural rubber (in

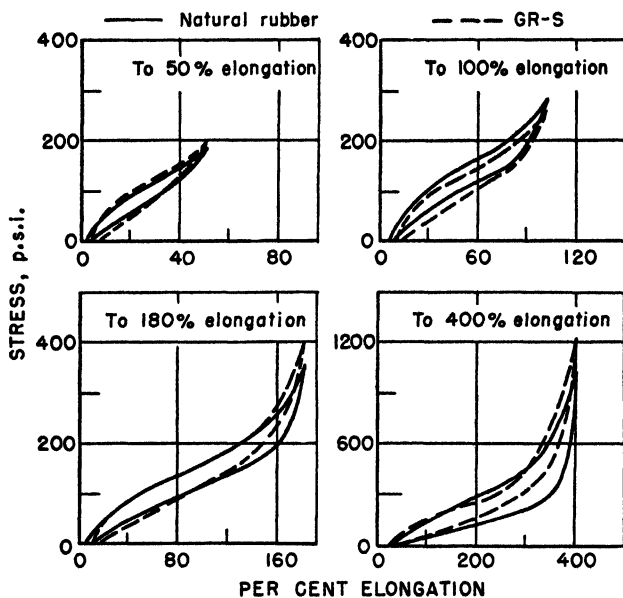


Fig. 15. Hysteresis loops, natural rubber and GR-S treads (10th loop) (29).

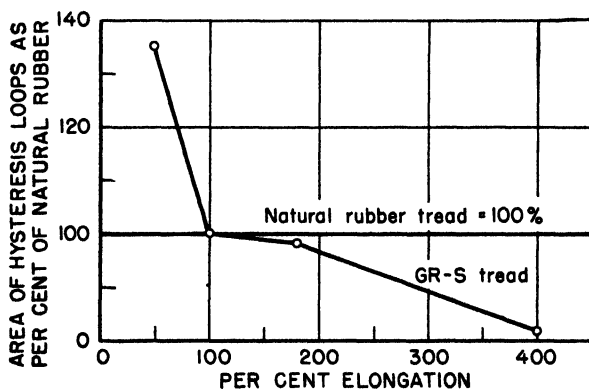


Fig. 16. Effect of elongation on hysteresis of GR-S and natural rubber (29).

tread formulations) decreased with increasing maximum elongation (see Fig. 16) so that for loops carried above 200% elongation, GR-S actually was lower in hysteresis than natural rubber. They also showed by flexing the GR-S and natural rubber to 400% elongation ten times and taking stress-strain loops on flexed and unflexed samples that, at elongations

above 500%, the natural rubber became much softer while, in that region of elongation, the before and after curves for GR-S coincided (see Fig. 17).

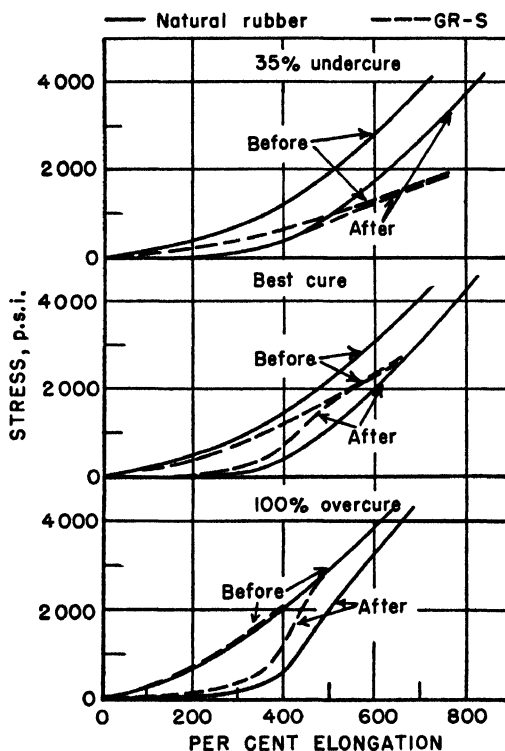


Fig. 17. Effect of 10 flexings to 400% elongation on GR-S and natural rubber treads at comparable cures (29).

Their interpretation of this phenomenon was as follows:

“Because of the lower hysteresis of GR-S at the higher elongations, it relaxes less than natural rubber. On both the extension and retraction cycles the developed stresses are greater. When these occur at a flex cut, they increase greatly the total force on the element of rubber at the apex of the cut. This relaxation-failure effect of GR-S acts as a lever to multiply the force at the apex of the cut. At ordinary or room temperatures, GR-S treads have a tensile strength about 60% of similarly reinforced natural rubber treads but a flex life rating of only about 10%. The relaxation-failure effect is thus the equivalent of a 6 to 1 leverage. These factors coupled with the higher heat build-up of GR-S under flexures of small amplitude and its high negative temperature coefficient of tensile strength, all contribute to the acceleration of cut growth.”

The work of Braendle and Wiegand is rather significant in developing a qualitative theory of hysteresis in rubber polymers since it indicates that,

within the crystallization region of natural rubber, it becomes more hysteretic than noncrystallizing GR-S. Naturally, the results of Braendle and Wiegand would have been more conclusive had they been obtained under dynamic conditions. However, in the light of the difficulties of performing hysteresis tests at high frequencies and high strains, we must accept their conclusions for the moment. In any event, their results suggest that the crystallization of natural rubber is not necessarily a reason for its low hysteresis at low strains, as compared to GR-S. In fact, Gee and Treloar (31) conclude that crystallization can be considered as a sort of cross linking and that it is largely responsible for hysteresis in natural rubber. That there is hysteresis in crystallization itself has been shown by Clark and co-workers (32). This does not mean, however, that the "regularity" of the natural rubber molecule, which makes crystallization possible—CH<sub>3</sub> side groups occurring at regular intervals along the almost completely linear chain—is not a factor in its low hysteresis.

The theory of hysteresis of rubberlike polymers is still in a somewhat chaotic state but, in the light of its importance to fatigue phenomena, it seems pertinent to consider it at this point. First of all, it seems quite clear that large pendular groups such as the benzene ring of the styrene molecule must increase the hysteresis of a network. But it must be remembered that the linearity of GR-S is increased by the presence of the benzene side group. Taking into account the increase in  $\eta$  with increasing proportions of styrene in GR-S type polymers (28), it seems that this pendular group does more hysteretic damage than it achieves in linearity benefits. The affect of branching is not as easily appraised for it could conceivably increase or decrease the hysteresis defect. It is almost certain, however, that a certain amount of branching could reduce hysteresis just as it might increase rate of crack growth; certainly, tightness of cure, a similar phenomenon, operates in this manner. The presence of heavy polar side groups as in neoprene should theoretically increase hysteresis and, as far as the data extend, this appears to be confirmed. Increasing the molecular weight, providing this is done in a manner that balances properly the linearity and branching, should reduce hysteresis. In the main, however, we can only conclude that developing a rubber polymer must depend upon empiricism based upon the particular chemical system employed rather than soundly established general principles. Certainly, in view of the importance of hysteresis to the usefulness of rubber polymers, more carefully planned work in this field should be carried out with the object of elucidating the effects of the various molecular structure parameters upon the internal friction. An encouraging beginning has been

made in this undertaking by Nolle (33). Using the concept of a complex modulus, which includes the elastic and viscous components as real and imaginary components, he employed some six different methods of measurement to study the variation of the elastic modulus and loss factor of several rubbers over a wide range of frequencies ( $10^{-1}$  to  $1.5 \times 10^7$  cycles/second) and a range of temperatures ( $-55^\circ$  to  $100^\circ\text{C}.$ ). He found that the behavior of the complex compliance or reciprocal modulus in the temperature-frequency plane is qualitatively similar to that which has been found for the dielectric constant of substances that have a wide frequency range of dispersion. He interpreted the results in terms of the kinetic theory of elasticity and the Frenkel and Eyring activation energy concepts of relaxation. The large values found for some of the activation energies suggested to Nolle that some of the relaxation effects may be due to hindrances, which oppose the motion of molecular segments composed of several monomer units. This mode of attack appears to have very great possibilities for revealing the nature of hysteresis in high polymers and the work should be continued and expanded with this objective.

#### 4. Stress-Strain Characteristics

The fact that the area and location of the stress-strain hysteresis loop change with progressive cycling of rubber has received considerable attention. Some of the most significant data of this type on natural rubber were

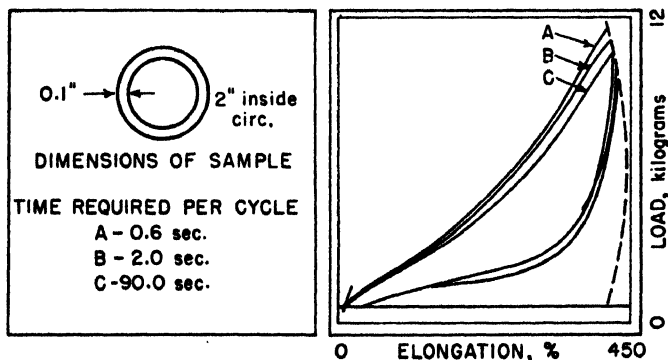


Fig. 18. Effect of speed of stretch on stress-strain properties, showing curves for duplicate samples recorded at three different speeds (34).

obtained by Holt (34) who maintained the maximum elongation and rate of elongation constant (class E fatigue). He also made observations at varying rates of strain with sinusoidally varying load with apparatus specially devised for this purpose, which was capable of giving 100 stress-strain cycles



per minute. The effect of varying the testing speed is shown in Figure 18. While no great differences in the stress-strain loops at different rates are observed for vulcanized specimens, the use of high speeds (30 cycles/minute) did make possible the testing of crude rubbers. Repeated cycles at this rate are shown in Figure 19. It is of great interest to note that the re-

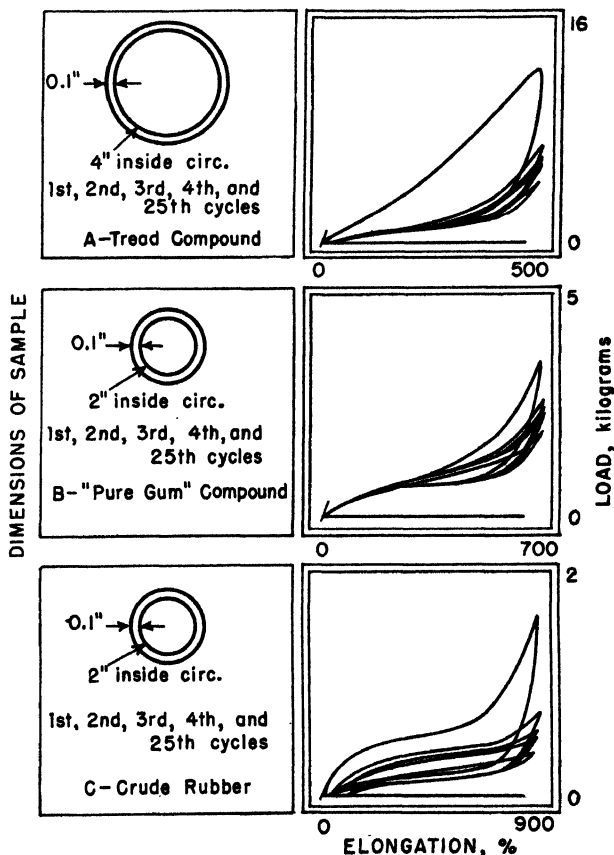


Fig. 19. Charts from stress-strain apparatus, showing successive cycles as recorded for three types of rubber (34).

traction curves for the vulcanized gum compound coincide and that, after resting at zero strain, a considerable recovery takes place (see Figs. 20 and 21). This behavior is very similar to that of wet wool fibers and will be discussed later in that connection. While some progress has been made in developing an understanding of stress-strain phenomena in rubbers (35-47), an accurate explanation of thixotropic breakdown, *i.e.*, dropping of the

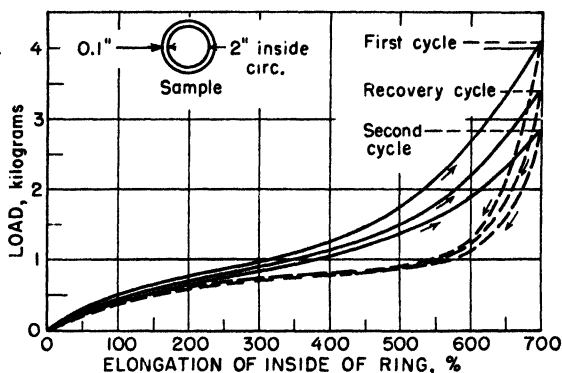


Fig. 20. Recovery of ring sample of pure gum rubber after strain (34).  
Recovery curve shows effect of 24 hours at room temperature.

extension curve with repeated cycling, has never been given. On the basis of the kinetic theory of elasticity, the general thermodynamic relationship can be written:

$$f = \left( \frac{\partial E}{\partial l} \right)_T - T \left( \frac{\partial S}{\partial l} \right)_T \quad (8)$$

relating the restoring stress  $f$  exerted by a strained molecular network to the length derivatives of the internal energy  $E$  and entropy  $S$  at constant absolute temperature  $T$ . For strains of 10% and higher, if the rubber is allowed to relax to an equilibrium state at some temperature  $T_1$  (343°K. or lower to minimize oxidation effects) and then the temperature is reduced, it is found that the stress is proportional to the absolute temperature  $T$  (48). Since the entropy is purely a configurational quantity, it is concluded that the stress must be entirely due to the entropy term of (8), *i.e.*,  $(\partial E / \partial l)_T$  is zero. By writing the usual entropy-probability relationship:

$$S = k \ln P \quad (9)$$

and working out the probability of configuration, on the basis of a Gaussian distribution function, there results the well-known stress-strain relation for tension:

$$f_\alpha = NkT \left( \alpha - \frac{1}{\alpha^2} \right) \quad (10)$$

where  $\alpha$  is the ratio of stretched to unstretched length,  $k$  is Boltzmann's constant, and  $N$  is the number of "molecules" per unit volume, a "mole-

cule" being the length of chain between junction points of the network. For the case of simple shear, the relation is simpler:

$$f_s = NkT\sigma \quad (11)$$

where  $f_s$  is the shear stress and  $\sigma$  the shear strain.

Equations (10) and (11) have been found to agree with the extension curves of rubbers at low and intermediate strains. Employing the Flory

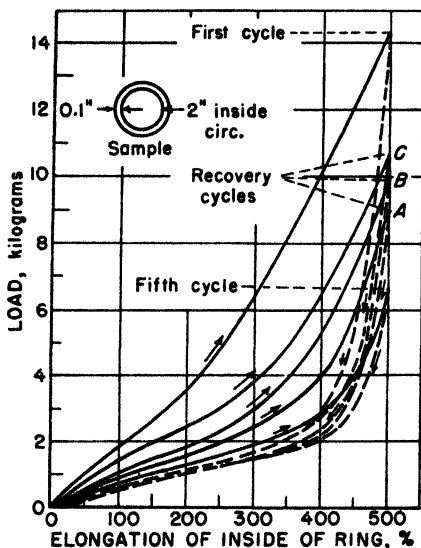


Fig. 21. Recovery of ring sample of tread compound after strain (34). *A*, effect of 2 hours' rest at room temperature; *B*, effect of 10 minutes at 100°C.; *C*, effect of 45 minutes at 100°C. and 40 hours at room temperature.

and Rehner (46) theory of non-Gaussian probability distributions of molecular length, Treloar (49) calculated more accurately the stress-strain relationships for simple tension and two-dimensional tension (compression) and found excellent agreement between theory and experiment up to the breaking point for polyisoprene rubbers of various molecular weights. But, important as this achievement is, it must be remembered that it amounts only to explanation of a single extension curve and does not explain the phenomena observed with repeated cycling.

### 5. Dynamic Fatigue Experiments

Roelig (50) has performed some interesting experiments with a forced vibrator, which can be cataloged under class C-2 fatigue. With this apparatus, the actual dynamic hysteresis loop was recorded and thus rather complete data obtained. He did not employ large enough stress amplitudes

to produce actual fatigue failure but changes with time of cycling of other properties were obtained as illustrated in Figure 22.

Many of the dynamic fatigue tests on rubbers have been devised to evaluate the cracking resistance under conditions simulating the service of rubber products, especially tires. As such, they have served a practical useful purpose but have yielded little basic scientific information. An example of work of this type is that of Torrance and Peterson (51). The apparatus used was a wheel with slots radiating toward the axis from the circumference. Rubber samples molded with grooves were inserted in the

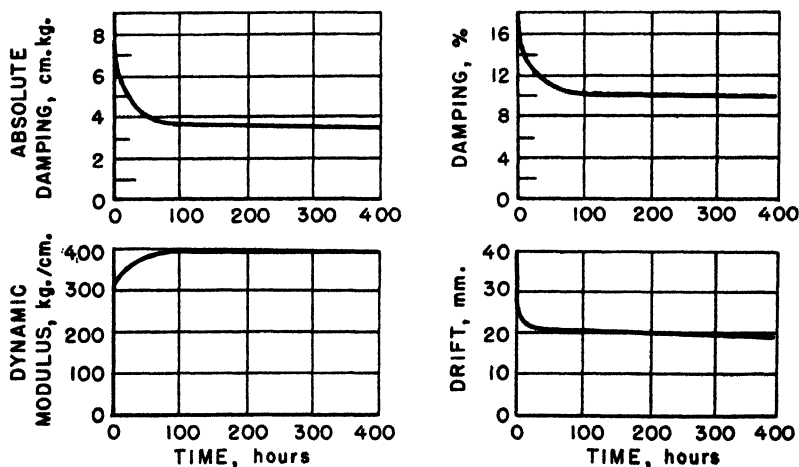


Fig. 22. Dynamic modulus, drift, and damping over a 400-hour period (50).

slots in such a manner that they were bent through  $90^\circ$  on each revolution by striking a stationary pin so that the grooves opened and closed. The test thus was essentially of class A-3 with  $y_a = 0$ , if the strains in the rubber in the base of the groove only are considered. Unfortunately, no data were given but the statement was made that the results correlated with tire service in showing antioxidants beneficial in reducing cracking of tread stocks. Cooper (52), however, in developing a practical tire sidewall flexing test noticed that black-loaded rubber samples must be returned to zero elongation in each cycle in order to make them fail in a reasonably short time. The importance of this observation will be discussed later. Another practical test of class A-4 was that described by Neal and Northam (53) who employed a molded grooved rubber belt running over pulleys in such a manner that the rubber at the base of the groove was subjected both to tension and compression. They concluded that failure on flexing was due

to oxidation rather than mechanical fatigue, or the action of ozone, which might be generated during flexing by triboelectric effects. They also concluded that antioxidants of the secondary aromatic amine type improved flexing in the presence of oxygen but had no influence on the action of ozone. It should be noted that, like Torrance and Peterson (51), they did not employ initial cuts at the bases of the grooves but they did measure both the time required for cracks to appear and the subsequent time to failure. Rainer and Gerke (54), however, stated that a fatigue test should: (1) measure crack growth, (2) operate within constant strain limits, and (3) employ strains comparable to those in tires. Their test, designed on these principles, was essentially of class A since it employed grooved samples and

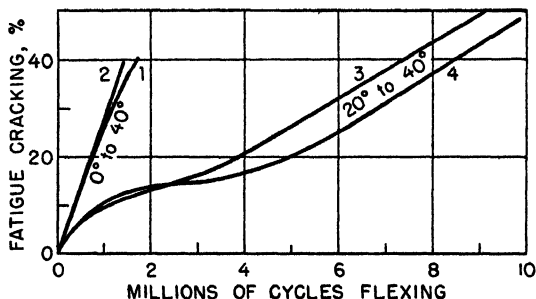


Fig. 23. Effect of minimum strain (54).

it was possible to strain dynamically the rubber in the base of the groove over a range—30% compression to 100% tension. These strains were produced by bending the samples between various angular settings ranging from  $-20^{\circ}$  to  $+85^{\circ}$ . Initial cracks were produced by an ozone treatment and the amount of crack growth measured quantitatively by the change in bending moment of the samples, which was shown to be roughly proportional to the depth of the flex cracks. The effect of varying the maximum strain was studied and an empirical relationship:

$$R = k/S^n \quad (12)$$

was found to hold in which  $R$  was the number of kilocycles required to give 1% reduction in bending moment,  $S$  was the maximum surface strain, and  $k$  and  $n$  were constants for any stock and cure. The effect of varying the minimum strain for a given strain amplitude was also studied and it was found that, in agreement with Cooper (52), a minimum fatigue life was obtained for zero minimum strain (see Fig. 23). It was also found that the rate of cracking was independent of the frequency of flexing if the fatigue

time was measured in cycles. The rate of cracking increased as the temperature was raised. No "endurance limit" was found, *i.e.*, even for very small strain amplitudes, some cracking was observed. Antioxidants were found to increase the fatigue life and overcure decreased it.

Cassie *et al.* (55) also reached the conclusion that the minimum fatigue life for a given strain amplitude occurs with zero minimum strain. Their fatigue tester was a constant stroke rocker machine that maintained the average stress constant and thus provided class B-1 fatigue conditions. They attributed the rapid fatigue at zero minimum strain to the maximum in the frictional losses (hysteresis) in the vicinity of zero strain, which they observed with a torsional free-vibration test. This rather interesting speculation involves the rather doubtful assumption that irreversible elastic effects and fatigue rupture effects derive from the same molecular structure characteristics. They also derived an empirical equation relating the fatigue life  $L$  to the observed drop in tensile strength ( $T_0 - T$ ) and the frictional loss  $f$  (hysteresis):

$$L = \frac{K}{T_0 - T} - \alpha f \quad (13)$$

where  $\alpha$  and  $K$  are constants. This equation can hardly be widely obeyed and probably has no basic scientific significance.

Springer (56), presumably using apparatus similar to that of Roelig (50) (class C-2 fatigue), emphasized the role of chemical reactions in fatigue. While he considered that the reactions are too complicated to be analyzed separately, he proposed that the fatigue life under dynamic conditions should be inversely proportional to the net rate of the reactions. Thus, the life  $L$  and the absolute temperature should be related by the Arrhenius law:

$$L = Ce^{E/RT} \quad (14)$$

where  $E$  is the energy of activation,  $R$  the gas constant, and  $C$  a constant. Thus, an equation of the type:

$$\ln L = A + B/T \quad (15)$$

should hold. This reasonable equation is not in accord with that proposed by Gough and Parkinson (24) (Eq. 1). Springer found rather convincing agreement between equation (15) and experiment, using the data of Roberts (57), as shown in Figure 24.

Quite a number of fatigue experiments have been made with no effort at theoretical interpretation, for example, those of Carlton and Reinbold (58)

and Breckley (59), and it is therefore unnecessary to discuss the results, important as they may have been from an engineering development standpoint. The work of Prettyman (60), however, while designed to evaluate groove cracking in tire treads, yielded a number of interesting experimental relationships and deserves comment. He employed a fatigue machine that forced grooved samples (either molded or cut from tire treads) through a cycle of combined bending, tension, and compression at 1140 cycles/minute (class A test). The tension-compression cycle, calculated for the rubber in the base of the groove, could be varied over wide limits but, in most cases, he employed a cycle of 43% compression to a suitable tension to give a reasonable fatigue life. The maximum tensile strains ranged from 21.5 to 93.0%. With a prototype machine, he also varied the compression and found evidence of a minimum fatigue life when the minimum strain

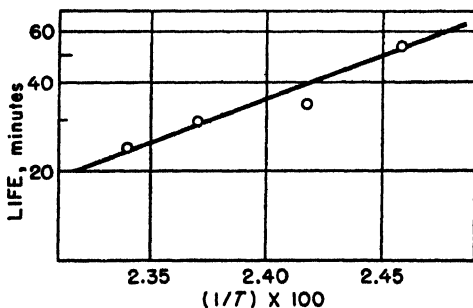


Fig. 24. Relation between length of life and temperature developed (56).

was near zero. Both crack incipience (time to form cracks) and crack growth (time for a precut to grow to a length of 0.3 in.) were measured. In agreement with other workers (54) he found that maximum fatigue life (crack growth) occurred at a low state of cure (see Fig. 25). Very interesting results were obtained with various tread stocks based upon blends of Hevea with GR-S, Hevea with reclaim, guayule with GR-S, and reclaim with GR-S. The results are given in Figure 26 where it is seen that tensile strength can hardly be used as a criterion of resistance to crack growth or incipience. It is interesting to note that, while Hevea shows about 280 to 1 superiority over GR-S in crack growth, it is actually inferior by a factor 4 to 1 in respect to crack incipience. Prettyman suggested that this superiority for Hevea in crack growth may be closely allied to the orientation or crystallization effect, which produces "knotty tear" in Hevea stocks loaded with gas black, as discussed by Busse (61). On this basis, it is necessary to consider the GR-S polymer superior to Hevea in fatigue resistance except where a flaw is present, which permits crack growth to take

place unhindered by the crystallization effect present in Hevea. He also pointed out that the GR-S stocks acquired a higher running temperature, which also probably explained part of the inferiority of GR-S in crack growth. That temperature was a major factor in this test is doubtful since

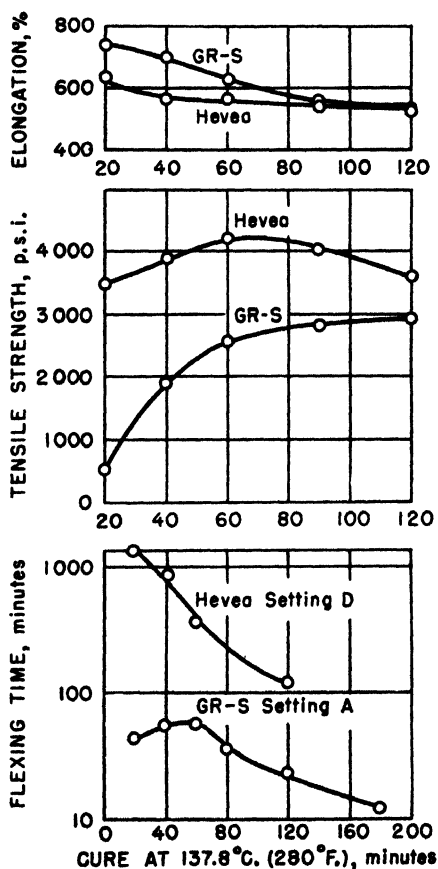


Fig. 25. Effect of cure of Hevea and GR-S stocks on elongation at break, tensile strength, and crack growth (60). (Time to grow 0.3 in.; precut samples.)

GR-S was actually superior to Hevea in crack incipience. This difference in the relative crack growth characteristics of Hevea and GR-S was noted also by Parkinson and Bloxham (62) but they concluded that the differences in running temperatures of GR-S and Hevea stocks explained the phenomenon entirely. White *et al.* (63) interpreted the inferiority of GR-S



in crack-growth resistance as resulting from the presence of a branched gel structure, which might act like a reinforcing pigment in the more linear regions of the molecular matrix, thus stiffening the stock to a degree that increased the localized stresses appreciably. This conclusion may be correct, of course, but it appears to be based upon an oversimplified picture.

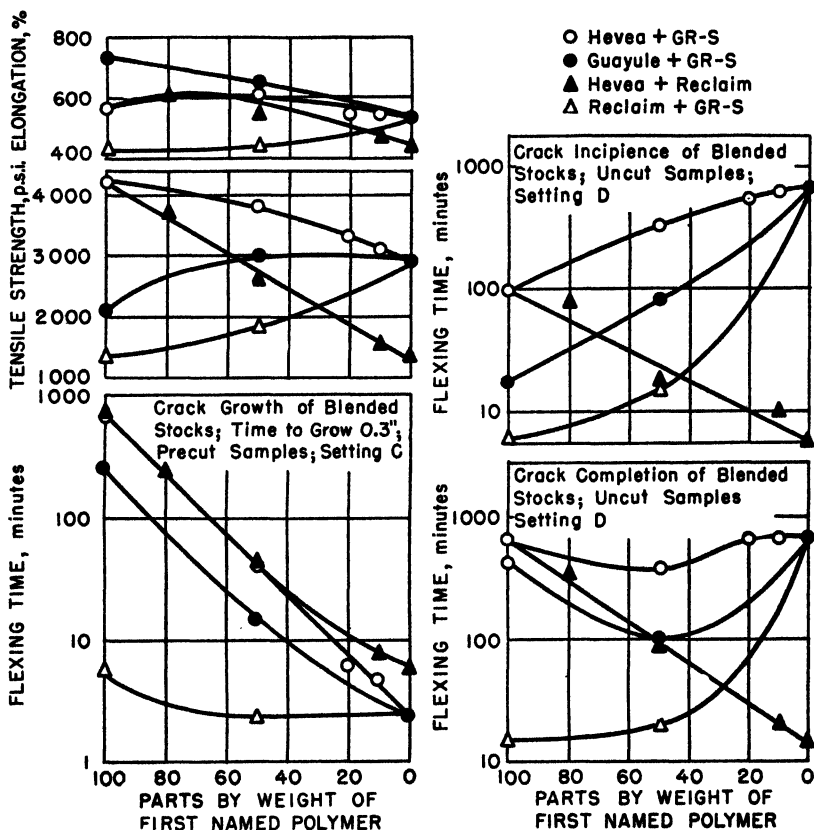


Fig. 26. Physical properties of blended stocks (60).

What were probably the most carefully controlled experiments on the effects on dynamic fatigue of varying the limits and amplitudes of strain are those of Cadwell *et al.* (63a, 64) and Yost (65). These workers made very comprehensive studies employing rubber samples bonded to metal end plates so that the strain cycle could include varying amounts of tension and compression. They also made tests with balanced shear samples

(sandwiches). Several different machines were used giving fatigue of class A and class B at various frequencies (180–3600 cycles/minute). For their class A tests, the several types of conditions used are shown in Figure 27. Their class A dynamic fatigue data on a natural rubber stock are plotted as the logarithm of the fatigue life *versus* the minimum strain for several values of the strain amplitude in Figure 28. The existence of a minimum fatigue life when the minimum dynamic strain is zero, for each of the several constant strain amplitudes, is clearly shown. A maximum life occurs in the region where the minimum strain  $y_m$  is positive, *i.e.*, tension, for all amplitudes. Where  $2Y$  is 50% or less, another maximum occurs in the compression region. Cadwell *et al.* state that similar sets of curves were

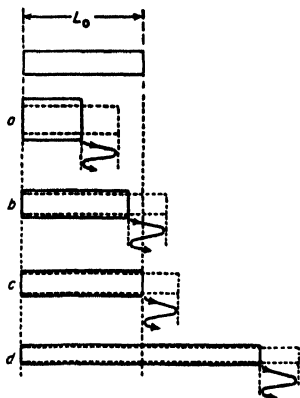


Fig. 27. Types of oscillation conditions for constant oscillation stroke  $\Delta L$  (63a).

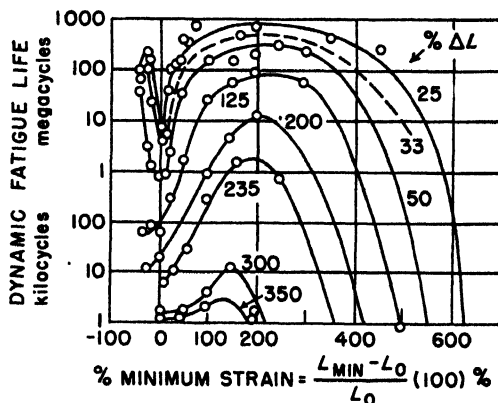


Fig. 28. Experimental data on 50 durometer stock (63a).

obtained for all stocks tested and these ranged in hardness from 30 to 80 on the Shore Durometer scale, depending on the loading of channel black. They also stated that similar curves were obtained at all frequencies (180–3600 cycles/minute) for crack growth as well as crack initiation, and even for class B tests where the samples were subjected to a constant static load with a constant dynamic strain amplitude. In the latter case, the peaks were somewhat narrower. The curves of Figure 28 were not corrected for differences in running temperature resulting from higher amplitudes but it is stated that, when the curves were thus corrected to 100°F., no essential difference in their general nature was found. When shear sandwiches were tested, equivalent results were obtained if the obvious consideration of the effect of lateral strains upon the minimum shear strain in the sand-

wiches was given (see Fig. 29). Static fatigue studies of classes A-5 and B-5 were carried out for long enough times for the occurrence of rupture. A static fatigue curve of class A-5 (for a series of constant strains, *i.e.*, relaxation to rupture) is plotted together with dynamic class A curves for three different frequencies in Figure 30. As might be expected, the static fatigue curve is the limiting envelope of the dynamic fatigue curves.

The importance of the results of Cadwell *et al.* (64,65) can hardly be overestimated both from a practical and a fundamental point of view. Unfortunately, they made no attempt to explain these phenomena on the basis of molecular structure except to state: "We believe it (static fatigue) is due










SHEAR CYCLE	LATERAL STRAIN		
	None	12½% Compression	25% Extension
-25% to +25%	A  7 Million	D  20 Million	G  12 Million
0% to 50%	B  1 Million	E  2 Million	H  2 Million
75% to 125%	C  15 Million	F  2 Million	I  40 Million

Fig. 29. Dynamic fatigue results on shear samples of 50 durometer stock (63a).

to the existence within the body of the material of randomly oriented regions of weakness, to stress concentrations, or to variations in elastic or plastic properties."

## 6. Qualitative Theory of the Effect of Strain Magnitudes and Limits upon Dynamic Fatigue Life

There is no difficulty in explaining the observed decrease of dynamic fatigue life with increasing strain amplitude for a given minimum strain (see Fig. 28) on a molecular basis. Since a rubber is characterized by its "entropy conscience," *i.e.*, its tendency to return to the most probable state of zero strain, when it is strained through increasing amplitudes, the chance of occurrence of abnormally high local molecular strains that could

cause local failures increases. This reasoning applies equally well at ordinary and elevated temperatures where oxidation in air is appreciable. Now oxidation involves concomitant scission and cross-linking reactions (18). Scission of the molecular chains induces a softening but also a weakening of the rubber and is not a function of elongation in the range of 0-200%; hence, it would be difficult to predict exactly what effect it would have on the fatigue *versus* amplitude relationship except for strains above 300% elongation where the reaction is known to increase with increasing strain (18). Oxidative cross linking, however, should be a factor since it

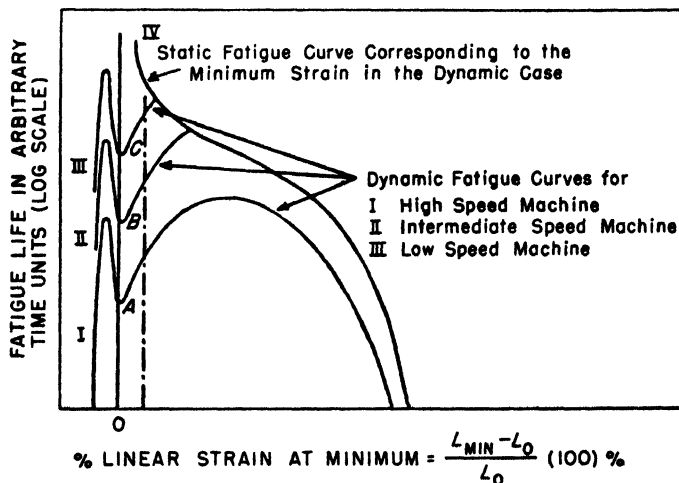


Fig. 30. Static and dynamic fatigue of rubber stocks (64).

results in an embrittlement as well as a weakening of the rubber. Here embrittlement is considered to be synonymous with reduction of extensibility of individual oxidatively cross-linked regions of the polymer, which must fracture more frequently than other regions as the amplitude is increased. It is also obvious that the fatigue life should fall to zero at some high value of  $y_m$ , which approaches the static strain at which failure occurs (see Fig. 30).

The matter of the decrease of dynamic fatigue life as the minimum strain approaches zero is not as easily understood. Busse (61) has given a quite reasonable interpretation of this phenomenon in terms of anisotropy effects, which he terms "semiracking" in gum stocks and "a mechanically fibrous structure" for gas-black stocks. Fielding (66) has followed up the suggestions of Busse and has particularized them to mean that crystalliza-

tion upon stretching is the dominant factor. Neither of these investigators, however, has attempted to explain in detail how orientation or, more specifically, crystallization effects can cause all of the observed fatigue-strain phenomena. The following is an attempt, admittedly speculative, in this direction.

Let us break down the fatigue life *versus* minimum strain phenomenon into two special cases (see Figs. 31*a* and *b*). For simplicity, sinusoidal vibrations of a given frequency are assumed in both cases. Where the minimum strain is zero (Fig. 31*a*), it is apparent immediately that the rubber

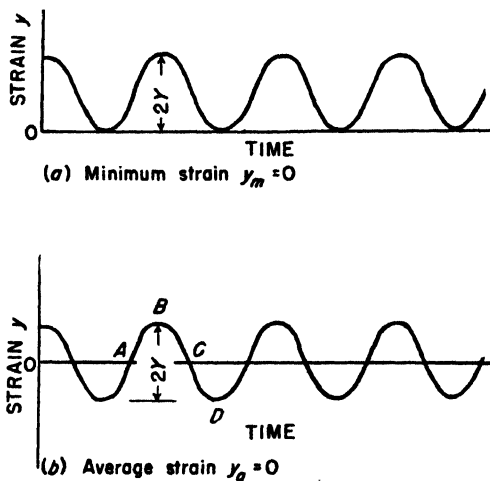


Fig. 31. Fatigue *vs.* strain conditions.

sample spends a much larger portion of its time at the extremes of vibration ( $y = 0$  and  $y = 2Y$ ) than at the intermediate strains ( $0 < y < 2Y$ ). This situation is even more pronounced for connecting rod motion; hence, the assumption of simple harmonic motion does not limit this argument. In the region of minimum static strain, therefore, any orientation and/or crystallization effects have a rather good opportunity to vanish because of the relatively long time interval provided by the periodic nature of the vibration. It has been shown by Aken, Singer, and Davey (67) that there is a definite (but not accurately determined) time lag of fibering in natural rubber, as observed by x-ray diffraction techniques. Hence, it seems reasonable that any orientation effects, which are generally associated with increase of strength in the direction of stretch, are most easily dissipated when the minimum dynamic strain coincides with zero static strain. Thus,

on the average, the desirable state of orientation and/or crystallization should be a minimum when  $y_m = 0$ , as observed.

The above explanation is essentially that given by Busse in connection with his very informative work on tear resistance and dynamic fatigue (61). However, he feels that the phenomena occurring in gum stocks

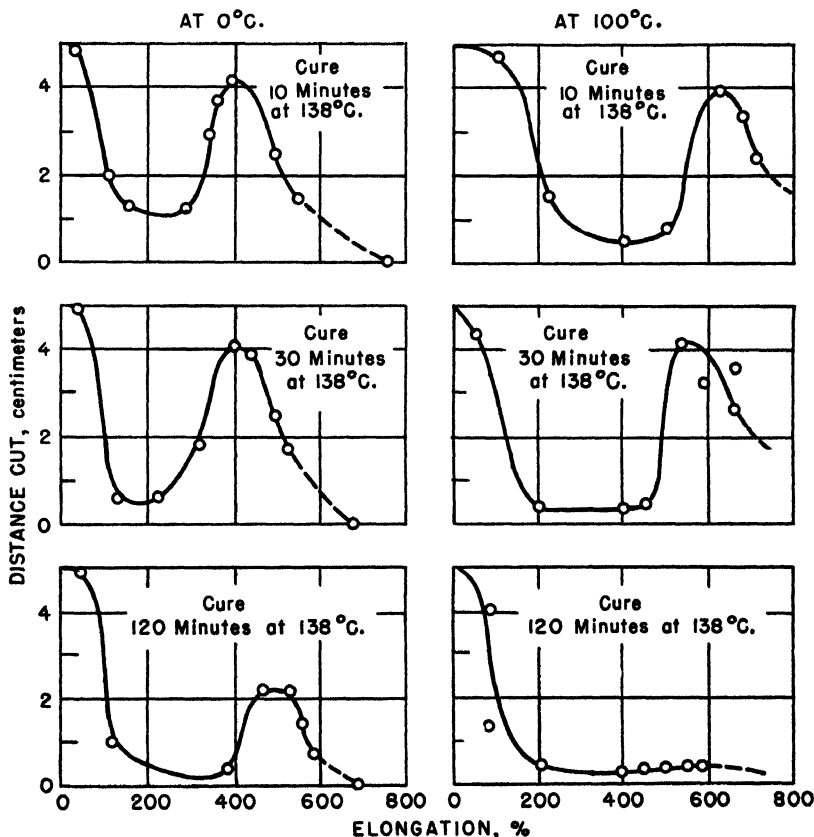


Fig. 32. Distance cut to cause failure *vs.* elongation; Captax high-gum stock (61).

("semiracking") and black-loaded stocks ("mechanically fibrous structure") may not result from the same molecular configurational situation. He has good reason for this reservation in the light of the "knotty tear" found frequently in gas-black stocks but seldom in gum stocks, and on the basis of his studies of the length of transverse cut necessary to cause samples to tear completely across *vs.* the initial elongation. These latter results,

given in Figures 32 and 33, show a complete absence of the second maximum for gas-black stocks which, in gum stocks, he reasonably attributes to crystallization upon stretching. In view of more recent work (68), however, it is known that the presence of gas black simply reduces the minimum elongation at which the diffraction pattern appears. Thus, it seems reasonable to assume that gas black has the effect of causing high local strains among the rubber molecules within the black-rubber matrix. On the basis of this argument, the absence of the second maximum (see Fig. 33)

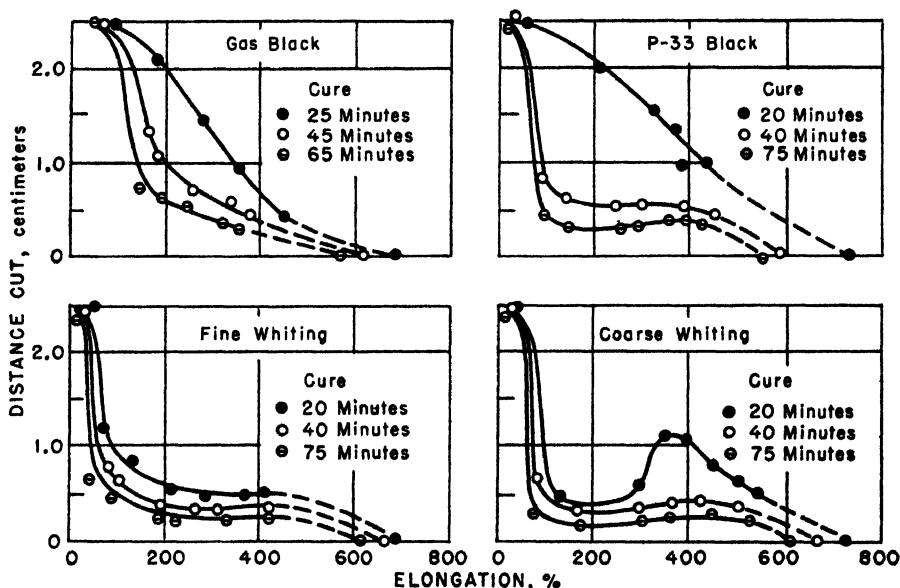


Fig. 33. Distance cut to cause failure *vs.* elongation; pigmented stocks (cured at 146°C.) (61).

could be anticipated. The phenomenon of "knotty tear," which is so characteristic of gas-black stocks (see Fig. 34 and Table I), is shown clearly in strips tested by Busse under dynamic conditions (200 cycles/minute). "Knotty tear" appears to be an excellent pictorial proof of the existence of the orientation and probably crystallization of the rubber molecules in the black-rubber matrix. In fact, it is difficult, on the basis of our concept of orientation, to understand why "knotty tear" does not occur more frequently with gum stocks at higher elongations. Certainly, there must be the same tendency for weakness to develop normal to the direction of stretch for any sort of one-dimensional orientation. Possibly the absence of "knotty tear" in gum stocks is only a matter of lower rigidity of the

matrix, as compared with that of a gas-black stock, or perhaps the distribution of stress within the gas-black stock is sufficiently irregular to initiate splitting between oriented "fibers." In any event, in the light of more recent experimental results and theoretical interpretations, Busse's conclusions cannot be criticized except that they are perhaps a little conservative.

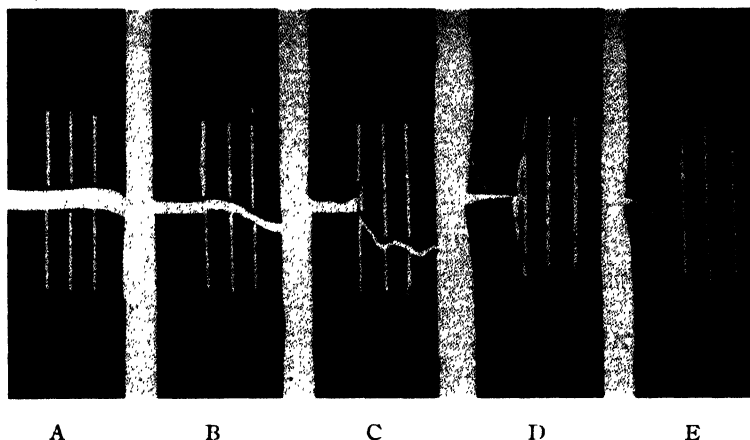


Fig. 34. Characteristic tears formed in tread stocks flexed through cycles having different minimum elongations (61).

TABLE I

Effect of Minimum Elongation of Stretching Cycle on Flexing Life of a Tread Compound (61)

Sample	Stretching cycle, %	Life, minutes
A.....	5-60.....	10
B.....	10-60.....	25
C.....	15-60.....	90
D.....	17-60.....	150+
E.....	20-60.....	Infinite

Thus far, the explanation is quite straightforward for it is easy to assume that the average orientation, whether or not crystallization is involved, can influence the dynamic fatigue life just as it appears to control the static stiffness and strength. But when the rubber sample passes through zero static strain in the fatigue cycle, it is not quite as clear why the fatigue life achieves another maximum in the region of compression.



To elucidate this result, it is convenient to refer to the special case of symmetric (class A-4) fatigue, illustrated in Figure 31*b*. Recognizing the importance of time in orientation and/or crystallization effects, let us write the time derivative of the simple harmonic relation:

$$y = Y \sin \omega t \quad (16)$$

which is, of course:

$$\frac{dy}{dt} = \omega Y \cos \omega t = \omega Y [1 - (y/Y)^2]^{1/2} \quad (17)$$

At the extremes of vibration,  $y = Y$  and  $dy/dt = 0$ ; at  $y = 0$ ,  $dy/dt = \omega Y$ . This last boundary condition is of great importance for it signifies the relatively rapid passage of the sample through the condition of zero static strain where, if it were allowed to remain for a reasonable period of time, relaxation of the desirable orientation might take place. But, on the basis of the results of Aken, Singer, and Davey (67), it is possible that the rate of "deorientation" and/or "decrystallization" could be exceeded by the rate of strain in the vicinity of  $y_m = 0$  where  $dy/dt \cong \omega Y$ . In that event, the strain could pass from the condition of maximum dynamic tension  $B$  to maximum compression  $D$  without "tensional" deorientation occurring to an appreciable extent. At this point, we must be careful to specify the direction of orientation since orientation is positively associated with tension and, upon going into compression (as referred to the direction of the applied stress), the rubber passes into a state of two-dimensional tension normal to the applied stress. If, for simplicity, we consider a cylindrical sample with the applied stress axial, the radial tension strain is one-half the axial compressional strain. Hence, assuming, as seems permissible for reasonably small strains, an approximate proportionality between stress and strain, the radial stresses tending to separate the tension-oriented molecules radially asunder must always be somewhat less than the compressional stress. This compressional stress may be considered as a "column stress" which, because the end areas of the sample are fixed, produces a radial "bulging" of the sample. This bulging effect is important since it indicates that the surface of the sample, which is more subject to fatigue failure than the interior (because of availability to oxygen and effects of surface flaws as stress centers), tends to maintain a state of tension although the sample, as a whole, is subjected to compression. To summarize these arguments, then, it is conceivable that the orientation produced in the tensional part of the vibration  $AB$  might persist in the half-cycle  $BD$  to an appreciable extent. Furthermore, some of the molecules

lying in the plane normal to the applied stress and therefore not oriented in the tension cycle would be oriented by the radial tension due to the applied compressive stress. They would thus oppose radial fracture to some extent. Thus, the fatigue life for the condition  $y_a = 0$  (Fig. 31b) could be greater than that for  $y_m = 0$  (Fig. 31a), as observed for natural rubber stocks. It is obvious, of course, that, when the strain cycle lies entirely within the region of compression, radial orientation would be the dominant type. Just how radial orientation would affect fatigue life is not as clear.

Now, it must be emphasized that the dynamic fatigue *versus* strain data discussed up to this point have been obtained on gas-black stocks of natural

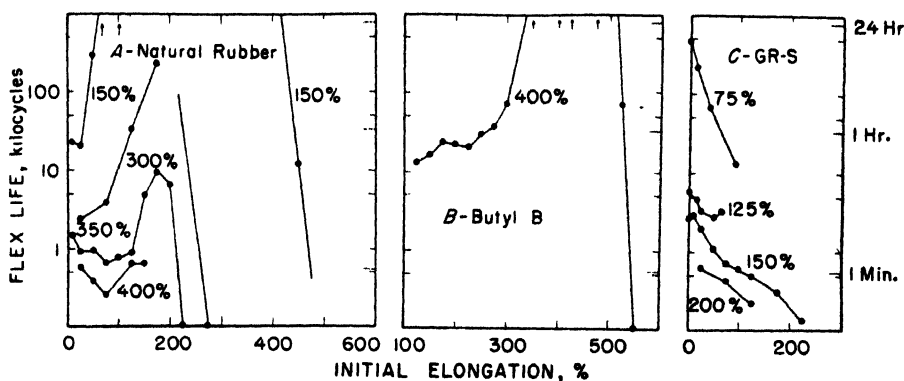


Fig. 35. Fatigue data of Fielding (66).

rubber. It is not entirely certain that identical results would be obtained on gum stocks. Since our arguments have largely been based on the established time dependence of crystallization phenomena, we might expect, as pointed out by Aleksandrov and Lazurkin (69), that the frequency of a fatigue test might have a profound effect upon the fatigue *versus* strain relationship. Apparently testing frequencies have not been varied over wide enough ranges to permit observations of this kind. This is unfortunate since important additional knowledge of the nature of dynamic fatigue might thus be obtained. It would also be of interest to examine samples of rubber that have been subjected to class A-4 fatigue for the presence of internal longitudinal cracks but no work of this type has been reported either.

Considerable information on the nature of dynamic fatigue has been obtained by studying synthetic rubbers that do not crystallize on stretching. Fielding (66) has employed the cycle of Figure 1 with natural, butyl,

and GR-S tread stocks. He found a minimum fatigue life with the minimum dynamic strain in the low strain region for natural rubber and butyl stocks but the life *versus* minimum strain curves for GR-S, a noncrystallizing polymer, showed no definite minima (see Fig. 35). Presumably Fielding did not employ an initial cut in his ring samples. His test was a class A with a frequency of 550 cycles/minute. Taken by themselves, Fielding's results bear out quite well his conclusion that the existence of a minimum dynamic fatigue life in the vicinity of zero strain for a given strain amplitude is entirely caused by the crystallizing tendency of a rubber. However, a single fatigue life *versus* minimum strain curve for a GR-S stock (see Fig. 36) given by Dillon (70), in the discussion of a paper by Yost (65), appears to contradict Fielding's data. A closer examination of Fielding's

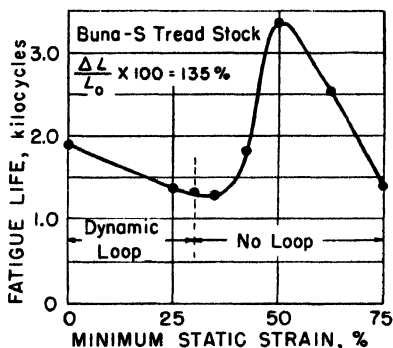


Fig. 36. Fatigue data on GR-S (70).

curve for an amplitude of 125% in GR-S suggests the remote possibility that he may have failed to observe the peak by not carrying his data to higher values of  $y_m$  (Dillon's amplitude was 135% and the frequency of 400 cycles/minute was close to Fielding's). If Dillon's admittedly meager data are accepted as significant, it appears that some sort of orientation effect, which does not involve actual crystallization but which requires a finite time to relax, may also contribute to the fatigue life–minimum strain relationship. It is interesting to note that the fatigue minimum fell at about 30% minimum static strain rather than zero. Yost (65) also mentions observing such an effect with "synthetics" of a type not specified. Dillon attributes his result to the fact that the cross section of his sample was so small as compared to its length that bending or "looping" took place when the sample was in the decreasing strain portion of the cycle. Because of the high hysteresis of the GR-S stock it was unable to return to

zero minimum strain when the machine was set for this condition; thus a loop formed in the sample. The minimum fatigue life appeared to occur at the minimum dynamic elongation where the loop just disappeared. Obviously more extensive data of this type should be obtained before further attempts at interpretation are made.

To sum up our discussion of the dynamic fatigue life-strain relationship, it appears that it can be explained qualitatively by assuming finite times for the oriented structure produced by tension to disappear during the short interval when the minimum dynamic strain is near zero. The maximum fatigue life found within the compression region is more difficult to understand than the tension fatigue maximum. By assuming, however, a columnar structure of oriented chains with reasonable interchain binding forces persisting as the sample goes rapidly from tension to compression, the compression fatigue maximum can also be explained. In the light of results obtained on crystallizing and noncrystallizing polymers, it appears that the dynamic fatigue life-strain behavior of natural rubber is largely governed by crystallization-time phenomena in a rather straightforward manner. There are still far too few data available on dynamic fatigue life as a function of strain amplitude, minimum strain, frequency, and temperature to permit more than a qualitative theoretical discussion at this time.

### ***7. Fatigue of Rubbers as Related to Weathering***

The "weathering" of rubbers is an exceedingly complicated subject which has received much attention in the literature. The principal observed effects of weathering are "cracking," which takes place at right angles to the direction of the applied stress, which must be finite for the effect to occur, and "crazing" of the surface, which is nondirectional and can occur with an unstrained sample. The subject of weathering is so broad and complicated that a detailed discussion of it is not within the scope of this chapter. Nevertheless, because of its importance in causing fatigue, a few of the salient features of weathering must be discussed in relation to dynamic and static fatigue. For detailed discussions of weathering, the reader is referred to the excellent papers by Newton (71) and by Crabtree and Kemp (72).

It is now known that weather cracking is entirely due to the action of ozone, which diffuses down to the earth's surface from the stratosphere where it is formed by the action of ultraviolet radiation upon oxygen. Ozone is unstable and decomposes under the action of sunlight and is absorbed in various ways, particularly by organic materials. According to

Crabtree and Kemp (72), the ozone concentration at Murray Hill, New Jersey, varied from 0.2 to 6 parts per 100 million over a period of a year. Even these small concentrations of ozone can cause observable cracking in strained rubber samples within a few hours. However, the rubber must be strained for cracking to occur but the necessary threshold strain is so small that its value has never definitely been established. Ozone cracking takes place in the dark just as rapidly as in the light and thus is not catalyzed by irradiation. The other weathering phenomenon, "crazing" of the surface, on the other hand, takes place in rubber at zero strain in the presence of oxygen and is accelerated by irradiation. Crazing appears to be the result of the formation of an oxidized surface layer which, under some circumstances, influences the type of ozone cracking observed by providing a discontinuous protective film on the stretched sample.

Newton (71) measures ozone cracking both by its effect on tensile strength, which he terms "degree of cracking," and by microscopic observations of the number and size of the cracks. He concludes that the rate of *formation* of cracks increases with increase of strain until a maximum is reached at about 75% elongation, but that the mean rate of *growth* of cracks is most rapid at 20% elongation. This situation holds only at room temperatures for, as shown by Crabtree and Kemp (72), increasing the temperature increases the number and decreases the size of ozone cracks at a given elongation. Cracks occur at temperatures as low as  $-40^{\circ}\text{C}$ . Ozone cracking occurs in many rubbers, Hevea, GR-S, Perbunan, etc., but has not been reported in butyl rubber and in only a few highly loaded neoprene-GN compounds. In general, at room temperatures, only a few large cracks appear at the lower elongations but their number increases and size decreases with increasing strain until, at 100% elongation, several hundred tiny cracks per square millimeter of surface appear. Antioxidants have no effect upon ozone cracking but retard the light-catalyzed oxidation resulting in crazing.

Crabtree and Kemp (72) discuss very thoroughly the effects upon ozone cracking of elongation, concentration of ozone, time of exposure, temperature, humidity, wind velocity, cure, grain, time between stretching and exposure, light irradiation, and compounding ingredients. Suffice it to say that no completely satisfactory way of protecting rubber against ozone has been developed and it must always be considered as a contributing effect to fatigue, both as regards crack initiation and growth. Crazing also affects fatigue life but probably mainly through its influence upon the type of ozone cracks formed.

### 8. Fatigue Effects as Influenced by Oxidation

Several investigators (51,53,54) have noted the beneficial effects of antioxidants upon the fatigue life of rubber stocks and thus recognized that oxidation is important in fatigue phenomena. It remained for Tobolsky and co-workers (18) to point out, however, that two distinctly different oxidation processes, scission and cross linking, take place concurrently in rubbers. A brief discussion of this paper has already been given in the section "Chemical Scission and Cross Linking," but further consideration will be given to this work because of its importance in regard to both static and dynamic fatigue.

In the early work of Tobolsky *et al.* (18), simple stress-relaxation apparatus was employed by which both continuous relaxation (elongation held constant and stress measured at various times) and intermittent relaxation (elongation zero and stress measured at 50% elongation periodically) could be studied. Some 30 different rubber polymers were thus evaluated at various temperatures in both gum- and tread-stock formulas. Continuous relaxation for natural rubber (Hevea) gum and tread stocks at 3 temperatures is shown in Figure 37 with time plotted logarithmically for convenience. Similar curves were obtained for all other polymers tested. It is seen that, at 100°C., the relaxation is nearly complete at 100 hours and the over-all rates of relaxation of the gum and tread stocks are about equal. In Figure 38 the fraction of the 0.01 hour stress remaining is plotted against logarithmic time at 100°C. for various elongations. The rate is seen to be independent of elongation up to 100% and probably higher. A comparison of Hevea and GR-S, gum and tread stocks, is given in Figure 39 where it is seen that the continuous relaxation of GR-S is slower than that of Hevea. Examination of the form of the curve for Hevea rubber revealed it was that predicted by a simple unimolecular chemical reaction:

$$x = x_0 e^{-Kt} \quad (18)$$

where:

$$K = (kT/h) e^{-\Delta F^\ddagger/RT} \quad (19)$$

and  $x$  is the stress at time  $t$ ,  $x_0$  the initial stress,  $K$  a rate constant,  $k$  Boltzmann's constant,  $h$  Planck's constant,  $\Delta F^\ddagger$  the free energy of activation,  $R$  the gas constant, and  $T$  the absolute temperature. On the basis of this law, it was found possible to predict data accurately at various temperatures from the value of  $K$  determined at a single temperature (see curves of Fig. 40). The energy of activation for all polymers studied was within

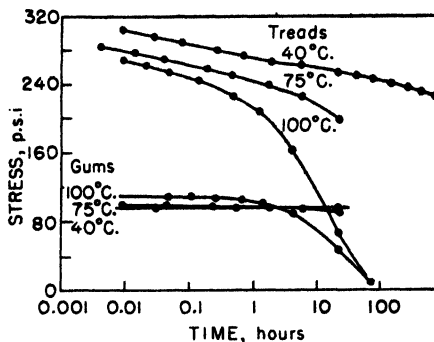


Fig. 37. Hevea stocks, 50% elongation (18).

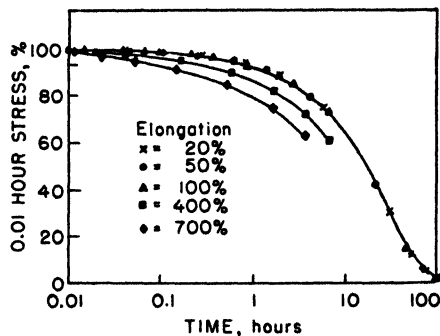


Fig. 38. Hevea gum, effect of elongation on relaxation rate, 100°C. (18).

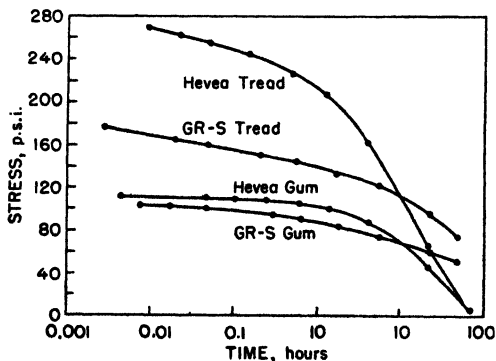


Fig. 39. Hevea and GR-S stocks, 100°C., 50% elongation (18).

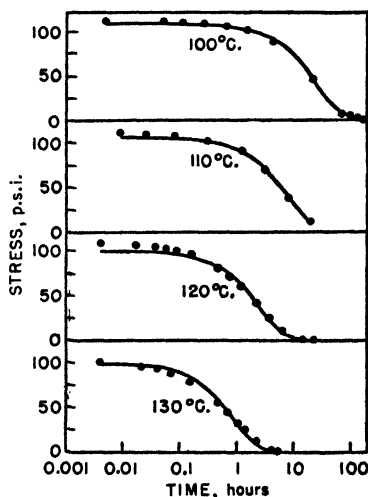


Fig. 40. Hevea gum stock, 50% elongation (experimental points, theoretical curves) (18).

the range  $30 \pm 2$  kcal./mole. Now it was natural to assume that this reaction was one of oxidative scission on the molecular chains and, in fact, this was verified by later experiments (73) where the relaxation was carried out in highly purified nitrogen and the rate was reduced by a factor 1000. Similarly, creep experiments at 110°C. in vacuum at a pressure of

$10^{-5}$  mm. mercury showed a 1000-fold reduction of rate over that in air at atmospheric pressure.

The continuous relaxation process should be due almost entirely to chain scission since any oxygen cross links formed should have only a small effect on the stress. With intermittent relaxation, however, each time the rubber is extended to measure the stress the cross links formed in the previous interval should resist the stress in such a manner as to counteract to some extent the reduction of stress resulting from chain scission. This effect was observed, as seen in Figures 41 and 42. In fact, for GR-S, the

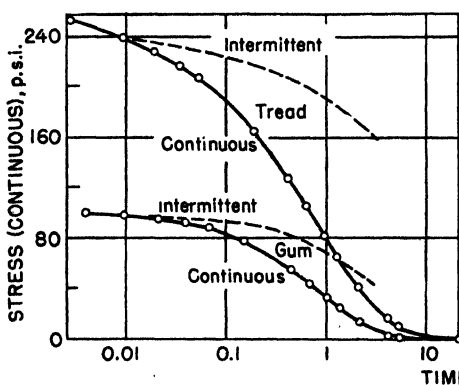


Fig. 41. Hevea stocks, continuous and intermittent stress relaxation,  $130^{\circ}\text{C}$ ., 50% elongation (73). (Intermittent stress set equal to continuous at 0.01 hour.)

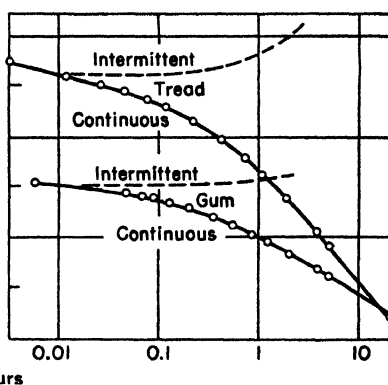


Fig. 42. GR-S stocks, continuous and intermittent stress relaxation,  $130^{\circ}\text{C}$ ., 50% elongation (73). (Intermittent stress set equal to continuous at 0.01 hour.)

stress actually increased when measured by the intermittent method, indicating that oxidative cross linking predominated. For Hevea, although the cross-linking reaction was present, the scission reaction exceeded it in rate. Similar experiments were carried out with creep and analogous results obtained. Only one type of rubber, the polysulfide polymers, appears to relax not by oxidation but by some other reaction (74).

It should be noted at this point that these primary bond relaxation phenomena were observed at temperatures of  $100^{\circ}\text{C}$ . and above where secondary bond relaxation would be so rapid as to be unobserved by the experimental techniques used. Secondary bond relaxation, which is partially reversible and therefore not strictly a fatigue effect, has been studied by Roth and Wood (75) and by Mooney, Wolstenholme, and Vil-



lars (76). It has also been discussed at length in relation to primary bond relaxation (oxidative) by Tobolsky and Andrews (73).

The primary bond relaxation and creep studies of Tobolsky *et al.* are important from the fatigue viewpoint since they give a rather complete molecular explanation of static fatigue phenomena of classes A-5, A-7, B-5, and B-7, provided the rubber samples are thin so that the diffusion rate of oxygen is unimportant. Even for thicker samples they give useful qualitative information since fatigue failures usually start from surface defects. Furthermore, it has been demonstrated that true permanent set can be calculated from relaxation data by Andrews, Tobolsky, and Hanson

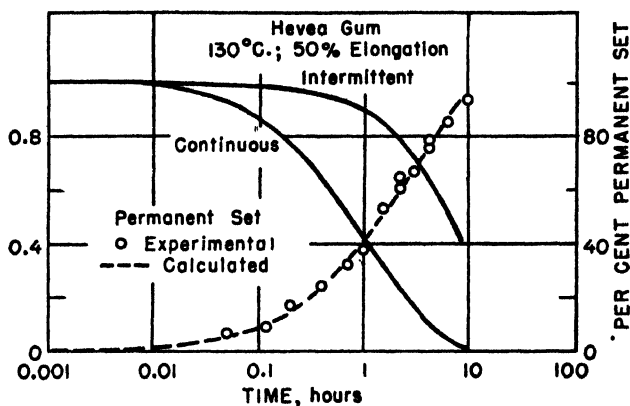


Fig. 43. Permanent set ( $f/f_0$ ) as a function of time for Hevea gum stock, 130°C., 50% elongation (77).

(77). A sample of their data, showing the agreement of theory and experiment, is given in Figure 43. They also show that, if continuous relaxation is carried to extreme times, the stress for some polymers begins to increase and rises to high values, indicating that cross linking can sometimes be observed by continuous relaxation techniques (see Fig. 44).

The role of oxygen on the dynamic fatigue of a GR-S tread stock has been studied by Winn and Shelton (78), using grooved specimens in a de Mattia-type flexing machine (class A fatigue), enclosed in a constant-temperature case to permit tests in air and nitrogen atmospheres. Reproducible initial "nicks" were made in the rubber at the base of the groove by means of an automatic lance. Both nicked and unnicked samples were tested. The oxygen content of the nitrogen passed through the testing chamber was measured for each test. In agreement with previous work

on natural rubber (54,60), it was found that undercures were superior in fatigue life (see Fig. 45). The log life *versus* temperature curves obtained (see Fig. 46) indicated a temperature coefficient of  $1.3/10^{\circ}\text{C}.$ , which is rather low for an ordinary chemical reaction. In contrast to work on

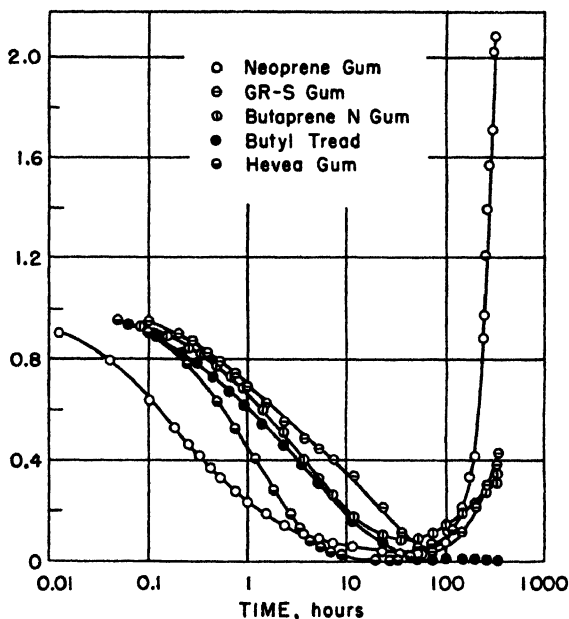


Fig. 44. Continuous relaxation curves for extended periods for various rubber types,  $130^{\circ}\text{C}.$ , 50% elongation (77). Ordinate is stress.

natural rubber (51,53,54), an antioxidant, phenyl- $\beta$ -naphthalamine, had no effect on the fatigue life. Nevertheless, reducing the oxygen content of the nitrogen atmosphere below 0.37% by volume did produce a considerable improvement in fatigue life (see Table II).

TABLE II  
Improvement in Life in Low-Oxygen Atmosphere (78)

O <sub>2</sub> content, by volume per cent	Percentage improvement in:			
	Initial cut to failure	Appearance of first cut	First crack to failure	Total to failure
0.37	0	0	0	0
0.27	30	39	48	45
0.05	27	70	57	60

The work of Winn and Shelton clearly establishes that oxygen is an important factor in dynamic fatigue. They pointed out that because the testing period employed was rather short, their results probably minimized the effect of oxygen, which might be a greater factor in the long period cracking of a tire tread in service. Their results do not indicate whether oxidative cross linking or chain scission is more important although it is probably the former, in the light of its known embrittling action and the fact that softer stocks usually have longer lives in class A fatigue. It would

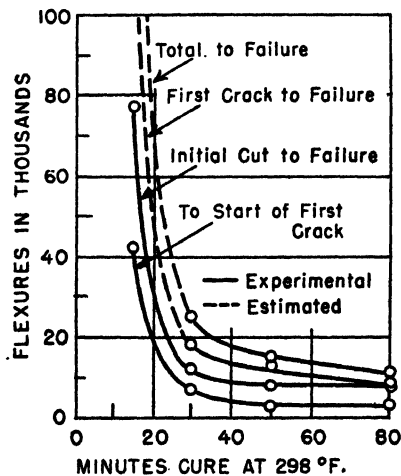


Fig. 45. Effect of cure (78).

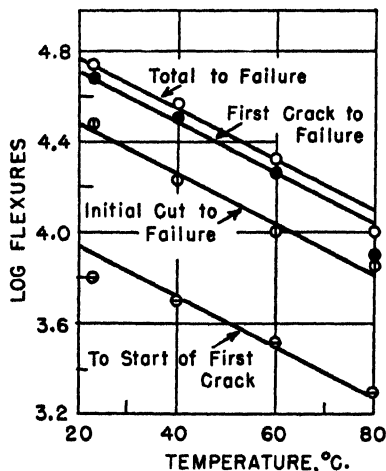


Fig. 46. Effect of testing temperature (78).

be of great interest to perform similar experiments with several different polymers, employing thin samples at various amplitudes so as to make possible direct comparison of the results with other fatigue phenomena such as relaxation.

### 9. Static Fatigue at Intermediate and Low Temperatures

We have already speculated at some length concerning the effects of orientation and crystallization upon dynamic fatigue. It is also of interest to learn what effects crystallization has on long period creep phenomena, as studied by Field (13). He employed a gum and a tread stock of natural rubber at 35°C. and performed a series of creep experiments with each stock, using different loads to give various initial elongations. He plotted as "per cent creep" the ratio of the increase in elongation to the initial

elongation. The creep curves obtained are shown in Figures 47 and 48. At the end of the 3.5 month creep period, the samples were clamped to aluminum strips while still under stress and x-ray diffraction patterns were recorded. The crystallinity as a function of the final elongation is plotted

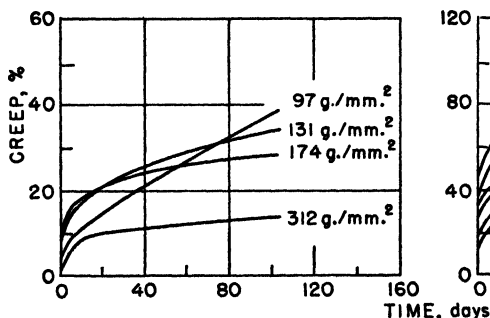


Fig. 47. Creep curves for vulcanized gum stock (13).

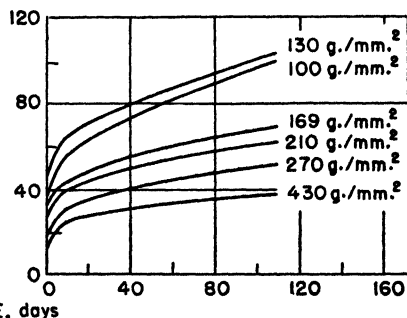


Fig. 48. Creep curves for vulcanized carbon black stock (13).

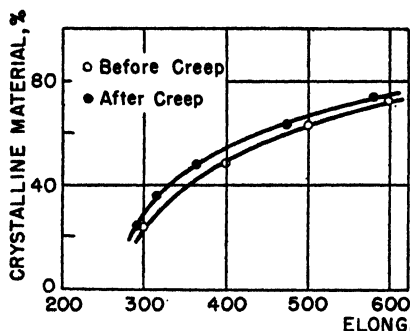


Fig. 49. Crystallization in gum stock before and after creep (13).

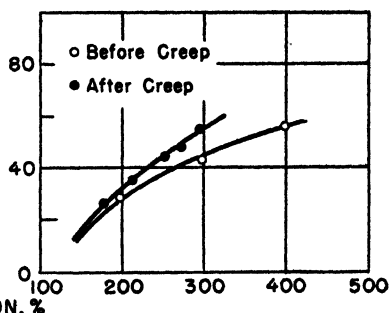


Fig. 50. Crystallization in carbon black stock before and after creep (13).

in Figures 49 and 50. The control curve in each case was obtained from diffraction data obtained immediately after stretching. For both the gum and the tread stock the crystallinity is seen to have been increased by creep. This result is not unexpected since it would seem probable that additional crystallites might form as the molecular flow and secondary bond slippage associated with creep should make higher forms of order more probable. From a practical fatigue standpoint, these results indicate that rubber becomes stiffer by crystallization during low-temperature creep while, at

high temperatures, it becomes softer because of the excess of oxidative scission over cross linking. It would be of interest to superimpose a small dynamic strain amplitude upon the long period creep at high and low temperatures to ascertain what effects, if any, a dynamic strain has upon crystallization and the oxidative phenomena.

## VI. Fatigue of Fibers

### 1. *General Characteristics*

It has already been indicated that fibers are a class of high polymers in which longitudinal strength and low extensibility are induced by molecular orientation, crystallization, and high intermolecular bonding forces. These properties along the axis of a fiber are basic, of course, but equally important is the fact that fibers are of small diameter and thus may be bent through large angles without the development of internal shearing stresses of sufficient magnitudes to cause rupture. The uses of fibers vary between the extremes of decorative fabrics where no appreciable stress exists and tire cords that must withstand superposed high static and dynamic stresses at elevated temperatures. Yet fiber fatigue is important even in the decorative fabrics for the various textile processes by which they are produced such as spinning and weaving impose both static and dynamic stresses of considerable magnitudes. It may be said, then, that fiber fatigue is of vital importance whenever a yarn is spun, or a fabric is woven or knitted. In the light of this fact, it is truly amazing that so little attention has been given to fatigue phenomena in fibers, yarns, and fabrics. Possibly the paucity of fatigue data on fibers is explained by the difficulties inherent in all single-fiber tests and by the discouraging variability of properties among fibers and along a given fiber. In any event, this discussion of the fatigue of fibers appears to resolve itself essentially into perhaps too extended a consideration of the few available data; yet it may serve to indicate what should be done in this field. The fatigue of yarns and fabrics has received increasing attention, justifiably from a practical viewpoint, because the constituent fibers are subjected to the types of strains incurred in processing and service (bending and torsion as well as tension). Unfortunately, this procedure leaves us in a state of quantitative ignorance of the fatigue characteristics of the fibers themselves. Thus, it is difficult to design a new fiber or modify an old one intelligently in the direction of increased fatigue resistance.

## 2. Resilience

The often misused term "resilience" is employed here advisedly, since in the majority of fiber applications (clothing textiles) interest is centered on the ability of a fiber to recover from a deformation rather than upon the inverse phenomenon—the ability to develop heat in repeated cycling, *i.e.*, hysteresis. But, whatever term is employed, the hysteretic imperfection in the elasticity is always important in fatigue phenomena. Mark (79) has discussed the meaning of the resilience of fibers in relation to desirable properties of clothing fabrics on the basis of current concepts of fiber structure. Dillon (80) has surveyed the literature on resilience of textiles with the object of clarifying its definition which, in the majority of cases, is the ratio of the energy of retraction to the energy of deformation. He considers separately the resilience of single fibers and yarns, bulk fibers, and fabrics, and points out that a fiber that may be considered as an outstanding example of resilience for clothing applications, wool for example, may be hopelessly unresilient (hysteretic) when used for tire cord. It is thus emphasized that resilience depends on the factors: temperature, moisture content, rate of strain, rate of retraction, strain history, rest period between cycles, nature of cycle, etc. Hence, "resilience" must be considered an arbitrary quantity that is defined only in form, and which must be measured under the particular conditions of service (or processing) of the product under consideration. Hoffman (81) has given a very illuminating but still qualitative discussion of resilience of fibers wherein a three-dimensional plot of the parameters, stiffness, elastic recovery, and the time effect, is given to represent a broad concept of resilience. Comparison of the different types of resilience of the various fibers on this basis appears to offer possibilities in directing research in the development of new fibers.

The resilience of textiles has been the subject of study from the practical angle (82–90) for some time but most of the work published does not apply directly to the understanding of fatigue phenomena. The classic work of Smith (82) is an exception in that he developed expressions for the resilience, toughness, etc., which are pertinent both to static and dynamic fatigue. The earliest dynamic measurements on fibers were made at acoustic frequencies by Meyer and Lotmar (91). They determined only the moduli at these high frequencies. Similarly, Ballou and Silverman (92) obtained dynamic moduli of rayon and nylon filaments by a greatly refined acoustic method and later Ballou and Smith (93), using the theory de-

veloped by Nolle (94), studied the attenuation and thus the dissipative properties of fibers at high frequencies. By using several methods of measurement, they were able to measure the modulus and internal friction over a range of frequencies 3–30,000 c.p.s. For a polyethylene terephthalate yarn, they found the modulus practically constant over a frequency range 8–34,000 c.p.s., but the internal friction decreased markedly with frequency. However, the product of internal friction and frequency was not constant over the whole range.

Recently, other measurements at sonic frequencies have been made on various cords and yarns by Lyons and Prettyman (19,95), using an electrically driven tension forced vibrator operative in the frequency range of 60–320 cycles/second. They tuned the system to resonance by varying the vibrating mass or the length of the cord and yarn samples and calculated the dynamic modulus and "internal friction," assuming the usual relationships based on "viscous damping." In agreement with previous analogous work on rubbers (27,28), the dynamic modulus  $E$  was found to be independent of frequency whereas the internal friction  $\mu$  was inversely proportional to frequency. They also calculated the absolute damping energy/cycle  $R$  from the product of the driving force  $F$  and the resonance amplitude  $S_m$  ( $R = \pi FS_m$ ) and found  $R$  to be independent of frequency. Values for 10 different samples measured at 180 cycles/second are given in Table III. In spite of the fact that several of the samples were measured at higher humidities (64–69%), all these were of materials possessing very small moisture absorptions except the ramie cord. Thus, with the exception of ramie, all the samples can be compared against the cotton, viscose rayon, and nylon cords, which were studied at 51–52% relative humidity. The data were all obtained with the same static tension of 2 kg. and ostensibly the same dynamic force  $F$ . In view of this choice of conditions and the known dependence of  $\mu$ ,  $E$ , and  $R$  upon static tension and strain amplitude, the authors recognized that care must be exercised in interpreting the data of Table III. Thus, it is not surprising that they obtained a value of  $H_e$ , the damping energy/gram cycle of  $2.6 \times 10^4$  ergs/gram cycle for cotton whereas Wakeham and Honold (97), using a frequency of 1 cycle/second and higher strain amplitudes found a value  $2.12 \times 10^5$ . The agreement was somewhat better for values of the dynamic modulus  $E$  of cotton cords— $7 \times 10^{10}$  dynes/cm.<sup>2</sup> vs. 2.5 to  $5.0 \times 10^{10}$  found by Wakeham and Honold. It should be noted that the values of internal friction  $\mu$  must depend somewhat on the cord or yarn construction; in fact, comparison of values of  $\mu$  determined on single fibers and yarns, respectively, might be used to estimate the frictional effects between fibers in the yarns. In any

event, it is hoped that similar data will be obtained on single fibers and filaments as well as yarns and cords. The results of Wakeham and co-workers (96-98) are also very interesting from the hysteresis viewpoint but, since their data apply directly to dynamic fatigue, their work will be discussed under that heading.

TABLE III  
Dynamic Properties of Various Cords, Yarns, and Filaments (19,95)

Sample		Dynamic measurements			
		Dynamic modulus, $E$ , $10^{10}$ dynes/cm. <sup>2</sup>	Internal friction, $\mu$ at 180 cycles/sec., $10^6$ poises	Temperature, ° C.	Relative humidity, %
Fiber	Construction				
Cotton.....	11/4/2	10.2	5.2	25	51
Viscose rayon.....	1100/2	15.2	4.0	21	52
Nylon.....	210/3/3	8.7	2.3	23	51
Du Pont					
fiber V.....	75/16/2	10.9	3.1	21	69
fiber A.....	300-den. yarn	16.4	8.9	21	68
Vinyon N.....	300-den. yarn	10.6	4.0	22	64
Velon.....	0.012-in. monofil	6.4	10.0	21	64
Ramie.....	3-ply cord	31.9	7.5	21	64
Fiberglas.....	7-ply cord	53.9	11.3	21	65
Steel cord.....	6 × 3 × 0.0058 in.	106.2	—	21	50

### 3. Stress-Strain and Primary Creep Characteristics

The general nature of repeated stress-strain curves obtained on fibers and yarns has been studied by many workers (85,99-104) but only in a few cases, for example, Shorter (103), did the earlier workers attempt explanations of stress-strain phenomena in terms of a molecular model. The importance of creep phenomena was not clearly understood until Peirce (105) made studies of torsional creep on raw and mercerized cotton, viscose rayon, acetate rayon, silk and wool yarns, and tin wires. He arrived at some useful empirical laws of creep but, in general, did not interpret his results beyond that point. Smith (106) and Smith and Eisenschitz (107) performed probably the first creep and relaxation experiments on single filaments of silk, viscose rayon, and acetate rayon using a modified Polanyi tester (106). They made observations over a wide range of temperatures and moisture contents and employed the Maxwell-Boltzmann theory of relaxation with some success. Steinberger (108,109) made careful studies both of stress-strain curves and primary creep data on single fibers and made some progress in interpretation by the use of the Maxwell-Boltzmann theory. Later, Leaderman (110) made comprehensive studies of creep phenomena in fibers of various types and employed the Boltzmann super-



position principle quite effectively to explain his data quantitatively. He distinguished between primary creep, which may be termed recoverable delayed elasticity, and secondary creep, which is the truly permanent part of a deformation. While he did obtain some quite encouraging agreement between theory and experiment, he recognized that the linear model inferred by the Boltzmann theory has definite limitations, even when generalized by assuming a distribution of relaxation times such as that of Wiechert. For example, the linear model provides proportionality between rate of creep and load, which is contrary to experiment.

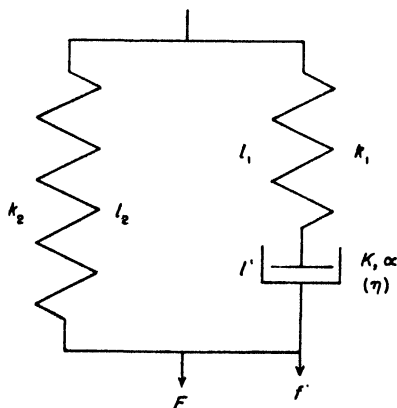


Fig. 51. Three-element model.

The next phase of research on stress-strain and primary creep phenomena in fibers saw the introduction of the Eyring non-Newtonian dashpot into a three-element model (3) to represent the structure and mechanical behavior of a fiber. Without going into the Eyring theory of flow (111) we shall simply write down its results. Suppose we represent a fiber by the three-element model shown in Figure 51 composed of an open Hookean spring with spring constant  $k_2$ , a closed Hookean spring with spring constant  $k_1$  and a non-Newtonian dashpot characterized by two constants  $K$  and  $\alpha$ . Let the total force on the model be  $F$  and the force on the Maxwell element  $f$ . If the total strain on the model is  $l$  and the strains  $l_1$  and  $l'$  apply to the closed spring and dashpot, respectively, then:

$$F - f = k_2 l \quad (20)$$

and the force on the dashpot is:

$$f = (1/\alpha) \sinh^{-1} (\dot{l}'/K) \quad (21)$$

Equation (21) is an expression of the Eyring flow law for the case of a symmetric energy barrier. The more general expression may be written:

$$\dot{l}' = K e^{(2\mu - 1)\alpha f} \sinh \alpha f \quad (22)$$

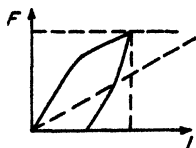
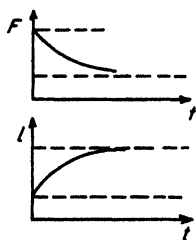
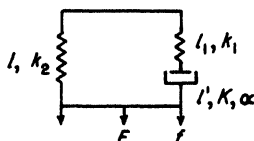
where  $\mu$  is the symmetry constant. For  $\mu = 1/2$ , (22) is equivalent to (21).

For the simple symmetrical case, then, the total force on the model is:

$$F = k_2 l + (1/\alpha) \sinh^{-1} (\dot{l}' / K) \quad (23)$$

and the rate of strain is:

$$\dot{l} = (1/k_1) \dot{l}' + K \sinh \alpha f \quad (24)$$



General relations:

$$F = k_2 l + \frac{1}{\alpha} \sinh^{-1} \left( \frac{\dot{l}'}{K} \right) = k_2 l + k_1 l_1$$

$$\dot{l} = \frac{1}{k_1} \dot{l}' + K \sinh \alpha f$$

Relaxation ( $l = \text{const.}$ ):

$$F = l \left\{ k_2 + \frac{2}{\alpha l} \tanh^{-1} \left[ \tanh \left( \frac{\alpha k_1 l}{2} \right) e^{-\alpha K k_1 t} \right] \right\}$$

Creep ( $F = \text{const.}$ ):

$$l = \frac{F}{k_2} \left\{ 1 - \frac{2}{\alpha F} \tanh^{-1} \left[ \tanh \left( \frac{\alpha k_1 F}{2(k_1 + k_2)} \right) \times e^{-[(\alpha K k_1 k_2)/(k_1 + k_2)] t} \right] \right\}$$

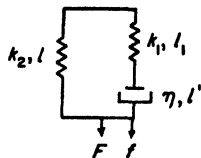
Constant rate of strain ( $\beta = \rho/K = \text{const.}$ ):

$$F = k_2 l + \frac{1}{\alpha} \ln \left\{ \beta + \sqrt{1 + \beta^2} \tanh \left[ \frac{\sqrt{1 + \beta^2}}{2\beta} \alpha k_1 l \right] + \tanh^{-1} \frac{1 - \beta}{\sqrt{1 + \beta^2}} \right\} \quad \text{Extension}$$

$$F = k_2 l + \frac{1}{\alpha} \ln \left\{ -\beta + \sqrt{1 + \beta^2} \tanh \left[ \frac{\sqrt{1 + \beta^2}}{2\beta} \alpha k_1 (l_m - l) \right] + \tanh^{-1} \left( \frac{e^{\alpha(F_m - k_1 l_m) + \beta}}{\sqrt{1 + \beta^2}} \right) \right\} \quad \text{Retraction}$$

Fig. 52. Eyring three-element model.

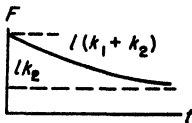
From the general equations (23) and (24), special equations can be derived to represent relaxation ( $l = \text{constant}$ ), creep ( $F = \text{constant}$ ), and constant rate of strain ( $\rho = \dot{l} = \text{constant}$ ) experiments. These are given



General equation:

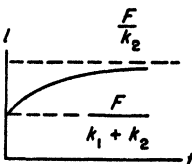
$$F = k_2 l + \eta \dot{l}' = k_2 l + k_1 l_1$$

$$\dot{l} = \frac{1}{k_1} \dot{f} + \frac{1}{\eta} f$$



Relaxation ( $\dot{l} = \text{const.}$ ):

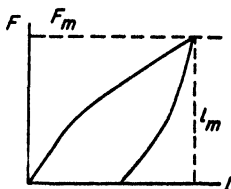
$$F = l(k_2 + k_1 e^{-t/\tau_1}); \quad \tau_1 = \frac{\eta}{k_1}$$



Creep ( $F = \text{const.}$ ):

$$l = \frac{F}{k_2} \left( 1 - \frac{k_1}{k_1 + k_2} e^{-t/\tau_c} \right);$$

$$\tau_c = \frac{(k_1 + k_2)\eta}{k_1 k_2}$$



Constant rate of strain ( $\dot{l} = \rho = \text{const.}$ ):

$$F = \rho \eta (1 - e^{-k_1 l / \eta \rho} + \frac{k_2}{\rho} l)$$

Extension

$$F = F_m e^{-k_2 (l_m - l) / \eta \rho}$$

$$- \rho \eta (1 - e^{-k_1 (l_m - l) / \eta \rho} + \frac{k_2}{\rho} (l_m - l))$$

Retraction

Fig. 53. Linear three-element model.

in Figure 52, which may be compared with the simpler relationships found for the linear three-element model given in Figure 53. For the linear model, of course, the dashpot is assumed to have a constant viscosity  $\eta$  so that it flows according to the law:

$$f = \eta \dot{l}' \quad (25)$$

and:

$$F = k_2 l + \eta \dot{l}' \quad (26)$$

$$\dot{l} = \frac{1}{k_1} \dot{f} + \frac{1}{\eta} f \quad (27)$$

Now the advantages of the Eyring model over the linear model are not at once apparent from Figures 52 and 53. A careful examination of the relationships will show, however, that the Eyring equations accomplish the following objectives toward better agreement with experiment: (a) creep is not proportional to the load, (b) relaxation is not proportional to the strain, (c) stress-strain properties are more realistically related to the rate of strain, and (d) creep and relaxation are extended over a reasonable

region of log time (the same aim was accomplished by distributions of relaxation times for the linear model).

There have appeared some ten papers (3,112-120) employing this concept, which have been adequately summarized and correlated by Halsey (121). Since this work deals only with primary creep and stress-strain

Fig. 54. Experimental and theoretical creep curves (3). The experimental points are taken from Leaderman (110). The solid curve was obtained from theory using Hooke's law and a hyperbolic sine law for viscous flow. If a single linear viscous element were used, the curves could at best be fitted over one-third the time range.

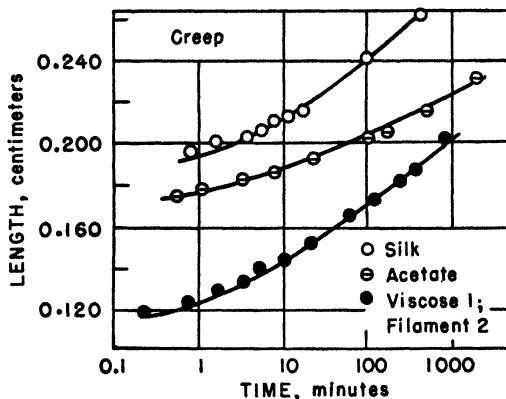
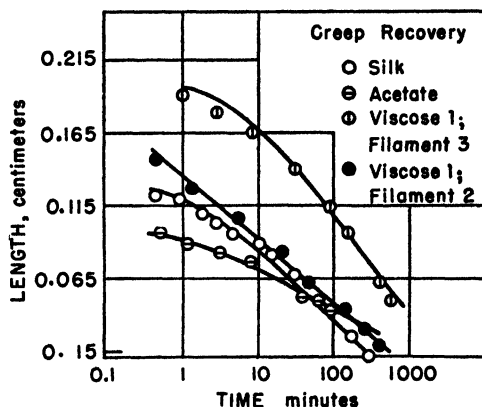


Fig. 55. Experimental and theoretical creep recovery curves (as in Fig. 54) (3). The points are from Leaderman (110); the solid curves are theoretical.



phenomena and is therefore only indirectly related to true fatigue effects, a further detailed discussion is not justified here. Suffice it to say that the application of the Eyring concept of flow to textile fibers has had considerable success with some fibers such as acetate rayon and somewhat less with others, for example, wool. A few of the cases where the simple Eyring three-element model theory gave good agreement with experiment are illustrated in Figures 54, 55, and 56. An historical treatment of the

development of theories of fiber behavior has been given in Part I of a paper by Burte, Halsey, and Dillon (4). The reader is referred to this paper for an over-all picture of the results obtained with both linear and nonlinear (Eyring) models.

As pointed out by Burte *et al.* (4), the simple Eyring three-element model described in Figure 54 was completely effective in explaining the stress-strain-time phenomena for only a limited number of fibers. Its use was extended to other more complicated fibers by several generalizing

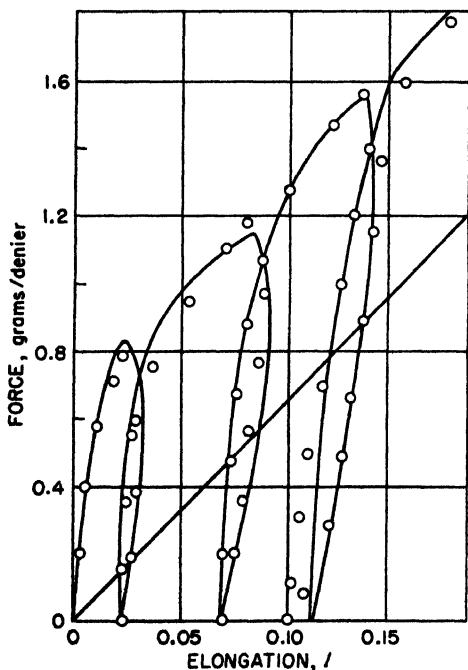


Fig. 56. Loasby's curve for viscose at a constant rate of loading of 4 grams per denier per minute,  $\beta = 30$  (112). The circles are calculated on the basis of the three-element model.

steps (4), such as the use of asymmetric energy barriers, non-Hookean springs, and increases in the number of elements in the model. For some fibers such as nylon and wool, however, a more drastic procedure was necessary. Burte and Halsey (122) and Burte, Halsey, and Dillon (4) have developed a new theory, which appears to have possibilities for explaining the thixotropic behavior of wool in repeated stress-strain experiments. This theory involves a concept of energy states with populations changing as the fiber is extended. The reaction-rate techniques of Eyring are used to develop the mathematical formulas for relaxation, creep, and stress-strain behavior. The theory appears to explain qualitatively the phenomena of

thixotropy and the final upward inflection of stress-strain curves for wool, nylon, and rubber. There are also preliminary indications that the theory has some quantitative significance in regard to wet wool. Incidentally, the similarity of the curves for a wet wool fiber, given in Figure 57, to those for rubber (see Fig. 19) is striking. This similarity is still more surprising when it is remembered that the elastic behavior of rubber is generally considered to be an entropy phenomenon whereas that for wool is supposed to involve principally changes in internal energy.

Now it must be remembered that all the linear and nonlinear models and probably also the newer Burte-Halsey concepts are not intended as de-

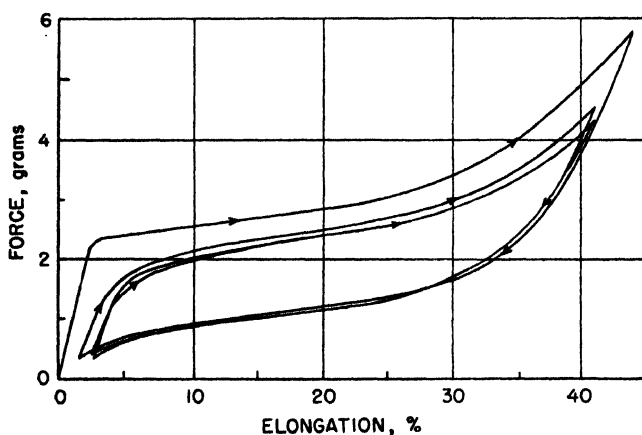


Fig. 57. Repeated stress-strain curves for a wet wool fiber.

tailed representations of the internal structures of fibers. However, when a model is successful, *i.e.*, the behavior calculated from it agrees with experiment, considerable benefit accrues since certain "constants" of the model can be evaluated and compared for different fibers. Thus the models offer a convenient means of cataloging the behavior of fibers in terms of measurable quantities. The ultimate objective, of course, would be to associate the elements of a model with chemical elements of structure of the fiber; this aim is far from accomplishment at the present time. While the fiber theories of Eyring and co-workers (112-122) have not found wide use up to the present time, they do offer the possibility of calculating the size of the flowing units. Burleigh and Wakeham (123) have applied these principles to the study of the relaxation of cotton and rayon cords and, assuming the strength of a fiber to be the force necessary to cause all cellulose chains to move as individual flow units, have

calculated the strengths of rayon and cotton to be  $6.1 \times 10^9$  and  $7.9 \times 10^9$  dynes/cm.<sup>2</sup>, respectively. These values are rather close to those observed ( $4.5 \times 10^9$  and  $3.5 \times 10^9$  dynes/cm.<sup>2</sup>, respectively). O'Shaughnessy (124) has given a pertinent discussion of the Eyring concept of fiber behavior in connection with comprehensive studies of the creep of viscose rayon yarns.

#### 4. Static Fatigue-Rupture, Long-Term Creep, and Relaxation

Static fatigue to rupture for singles yarns of cellulosic fibers has received some early attention (126-128). A rather definite linearity between breaking load and log time was found in most cases, for example, see Figures 58 and 59 representing data of Peirce (128). Karrer, Grant,

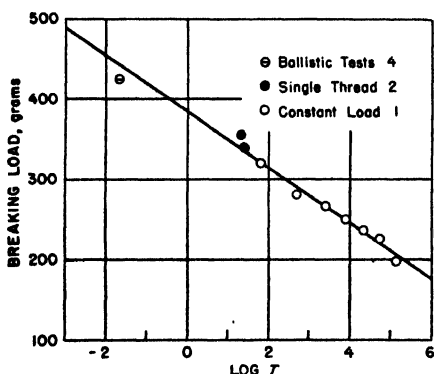


Fig. 58. Time effect on apparent strength of 36's Sakel yarn (128). ( $T$  = time in seconds.)

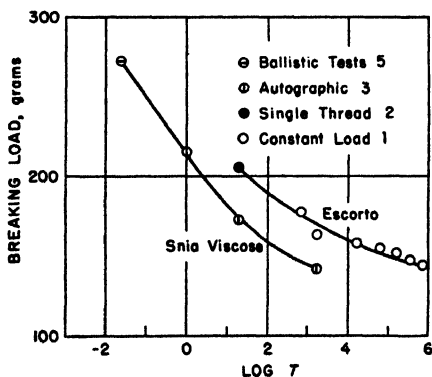


Fig. 59. Time effect on apparent strength of rayon yarns (128).

and Orr (129) performed static fatigue experiments with cotton and rayon tire cords as well as with the individual fibers constituting them. For cotton cords, the linear relationship between the load and the logarithm of the time to rupture was observed. This was not true for the viscose rayon cords. The relationships for the various single fibers were found to be very nearly the same as those of the cords fabricated from them. Thus, rupture in the cords appeared to be the terminal condition of flow of microelements of the fibers themselves rather than a phenomenon of fiber slippage. The load *versus* log time relationship will be discussed later under the heading, "Dynamic Fatigue." Hind and Speakman (130) have studied "true permanent set" of animal fibers resulting from treatments in high-temperature steam, steam at atmospheric pressure, and boiling water, under load. Speakman (131,132) has studied relaxation of wool under

similar conditions and interprets permanent effects as the results of breakage of the cystine bond, promoting dissipation of the stress, and subsequent cross-linkage formation, fixing the relaxed structure in its deformed state.

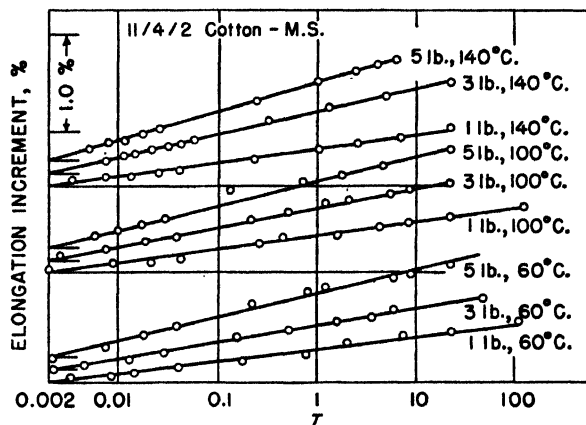


Fig. 60. Cotton *MS* (medium stretch) — elongation increment *vs.* logarithmic time (in hours) (133).

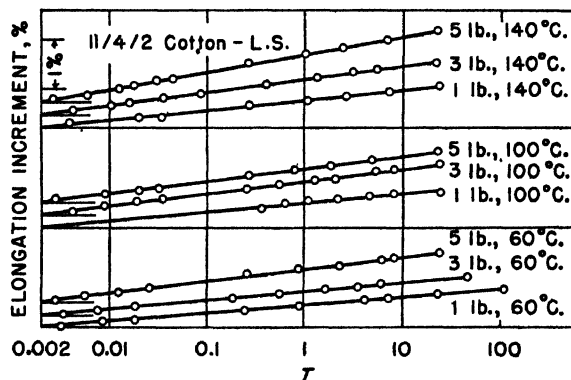


Fig. 61. Cotton *LS* (low stretch) — elongation increment *vs.* logarithmic time (in hours) (133).

The importance of creep in tire cords has stimulated such studies as those of Dillon and Prettyman (133) and Lyons (134). Creep curves at various temperatures and loads obtained by the former authors (133) on cords of low- and medium-stretch cotton, viscose rayon, Fortisan (saponified acetate), and nylon are given in Figures 60–64. The approximate



linearity of the curves at the lower loads is of interest and the departure from linearity for nylon at the higher temperature has been explained plausibly by Lyons (134). Now these measurements are technically not within the defined scope of this chapter, since they were made with cord

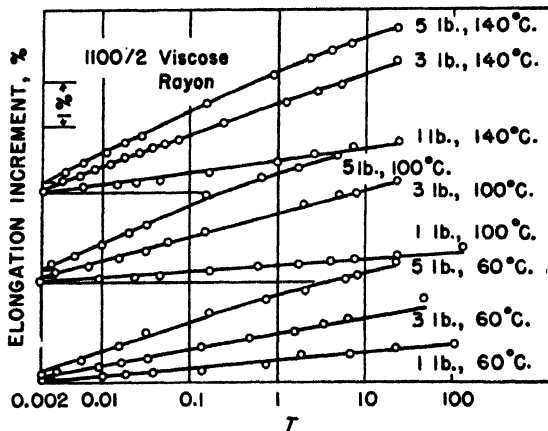


Fig. 62. Rayon — elongation increment vs. logarithmic time (in hours) (133).

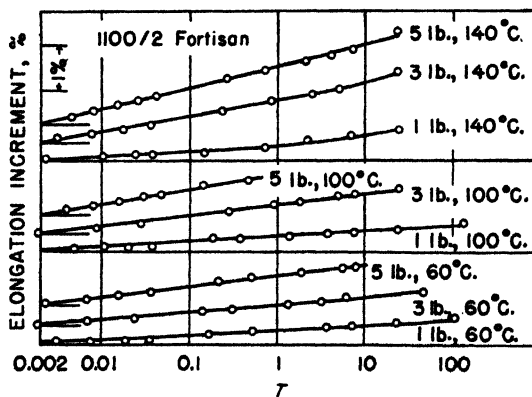


Fig. 63. Fortisan — elongation increment vs. logarithmic time (in hours) (133).

“structures”; nevertheless, the temperature dependence of creep establishes that “tire growth” is largely a matter of the flow of the individual fibers or filaments of the cords. Dillon and Prettyman distinguish between the rapid initial elongation and the slope of the long period creep

curves, defining two corresponding arbitrary indexes, "initial compliance" (= elongation at 0.002 hour divided by the unit load in grams/grex\*), and "weighted creep" (= slope of logarithmic creep curve divided by the unit load in grams/grex). A rather interesting comparison on the basis of these indexes of the five types of cord studied is given in Table IV.

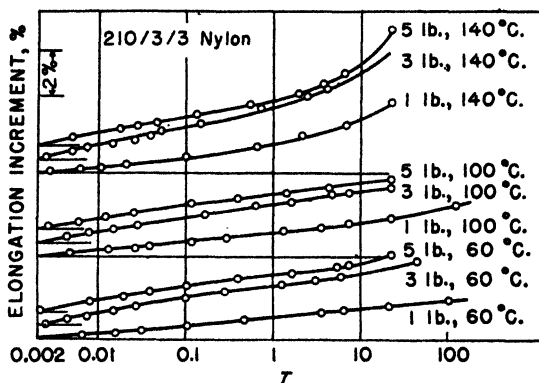


Fig. 64. Nylon — elongation increment vs. logarithmic time (in hours) (133).

TABLE IV  
Weighted Creep ( $S/P$ ) and Initial Compliance ( $e_0/P$ )

Temp., °C.	Index	Medium-stretch cotton	Low-stretch cotton	Viscose rayon	Fortisan	Nylon
100	$e_0/P$	20.8	14.1	2.9	5.1	10.4
	$S/P$	1.3	0.52	1.0	0.48	1.0
140	$e_0/P$	24.6	14.3	5.0	5.6	14.0
	$S/P$	1.5	0.74	1.3	0.71	1.5

Lyons (134) discusses the validity of various equations for creep and concludes that an expression of the form:

$$\epsilon = \epsilon_1 + at + b \log t \quad (28)$$

represents the variation of the strain  $\epsilon$  with time  $t$ , where  $\epsilon_1$  is the initial strain and  $a$   $b$  are constants, quite well for cotton and rayon cords at various loads at room temperature. He discusses this equation in its relationship to the Eyring theory of flow. The corresponding equation for relaxation at constant strain:

$$\sigma = \sigma_1 - \beta \log t \quad (29)$$

\* A grex unit is the weight in grams of 10,000 meters of filament or yarn.

where  $\sigma$  is the stress at time  $t$ ,  $\sigma_1$  is the initial stress, and  $\beta$  a constant, is also treated but no relaxation data are presented. The experimental creep curves for cotton and viscose rayon cords were extended to times greater than  $10^4$  minutes whereas those of Dillon and Prettyman were of somewhat shorter duration. Hence, the absence of the final upward inflection from most of their curves is not inconsistent with Lyons' results, which are given in Figures 65, 66, and 67.

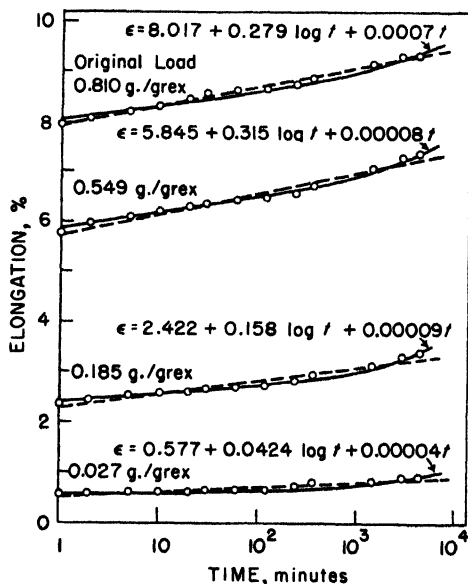


Fig. 65. Creep in a regular, wet-twisted 29/5/3 cotton cord (134).

Numerous other relaxation and creep experiments on fibers and yarns have been made in tension (124) or torsion (135); however, in many cases, the experiments have not been carried out for sufficiently long times to permit accurate interpretation. Often, no attempt whatever at interpretation has been made.

### 5. Dynamic Fatigue

Very few dynamic fatigue results have been reported on individual fibers, as far as the available literature reveals. A description of a fiber fatigue tester, which operates by rotating a fiber between chucks with axes at various angles, has been given (125), but no data obtained with it are

presented. Apparatus that imposes repeated bending stresses on single fibers has been described by Franz and Henning (136). Hermans (137) employed this device to study the effect of varying the orientation of viscose rayon filaments upon the "bending endurance." The viscose fila-

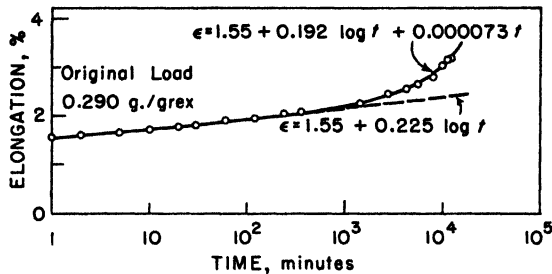


Fig. 66. Creep in a continuous filament, 1100/2 viscose rayon cord (134).

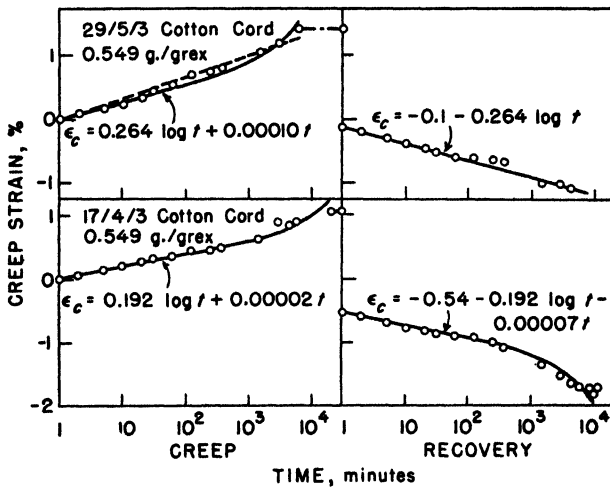


Fig. 67. Creep and recovery in a regular 29/5/3 and a dual stretched 17/4/3 cotton cord (134). Creep in both cords took place under an original load of 0.549 gram/grex.

ments employed were specially prepared with negligible initial orientation and various degrees of orientation were then produced by stretching to different elongations. He found an optimum bending endurance (number of cycles to rupture) with an orientation corresponding to 40% prior elongation. Above this value the bending endurance decreased rapidly with

increasing orientation. Observations were also made with cotton fibers, which showed very high bending endurance, which Hermans ascribed to their spiral structure rather than their high orientation. Consistent with this conclusion was the lower bending endurance of highly oriented ramie in which the spiral structure is absent. Thomson and Traill (138) have employed a modified version of the Franz and Henning apparatus to study the bending endurance of various fibers: wool, nylon, cotton, silk, viscose rayon, soya bean, cellulose acetate, casein, saponified cellulose acetate, and glass. Their results given in Table V are not strictly comparable since they were all obtained at the same static tension and angle of bend (1 g. and  $180^\circ$ , respectively), while the fiber diameters necessarily varied. Nevertheless, the superiority of wool and nylon over other fibers of corresponding diameters is evident, in fact very striking. Thomson and Traill also studied the effects of varying the static tension and angle of bend and they show photomicrographs of partially fractured fibers. Fibrillation appeared at the point of bending in wool fibers but not in cotton.

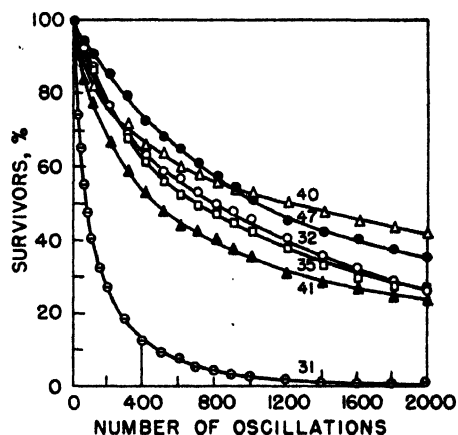
TABLE V  
Single Filaments Bent to Fracture Through  $180^\circ$  under 1 Gram Tension (138)

Fiber	Breaking load, grams	Diameter, $\mu$	Average number of bends
Wool.....	4	24	Some unbroken at 20,000
Nylon.....	6	14	Some unbroken at 20,000
Sea Island cotton.....	4.5	17	3,200
Natural silk.....	6	15	1,800
"Tenasco".....	6	16	950
"Delustra".....	4	21	660
Boiled off silk.....	4	11	370
Soya bean fiber.....	3	21	150
Cellulose acetate.....	4	19	100
Viscose.....	4	13	75
Casein fiber.....	3	25	23
Deacetylated cellulose acetate.....	3	7	1
Glass.....	—	8	1

The effects of varying the rate of loading on yarns has been investigated (126–128) and, in general, it has been found that the breaking strength increases with increasing rate—for the ranges of rates employed. The dynamic fatigue of cotton singles yarns has been studied at rather low frequencies, about 100 cycles/minute, by Oxley (139) and by Owen and Oxley (140). The test employed was of class B-1. The tension was about 40% of the static breaking load. An effective technique used was to record the number of cycles for each yarn as it broke and plot the number of sur-

viving yarns *versus* this number of oscillations. Owen (141) used this method in studying the effect of starch sizes on the fatigue lives of cotton yarns (see Fig. 68). The extension at break of the yarns as a function of number of cycles was also plotted and distinct differences in the curves for sized and unsized yarns were found (see Figs. 69 and 70). New and Gregson (142) have described the behavior of flax yarns under repeated impacts. Their method was to apply an impact force to a yarn by means of a falling weight the height of which was continuously adjusted to follow the extension of the yarns and produce a constant energy of impact. Aside from these simple but very useful experiments, the dynamic fatigue of

Fig. 68. Effect of starch sizes on the fatigue lives of cotton yarns (141). Sample 31: 36's unsized. Sample 32: 36's grey, sized farina and tallow. Sample 35: 36's grey, sized wheat flour and tallow. Sample 40: 36's bleached, sized farina and tallow. Sample 41: 36's bleached, sized wheat flour and tallow. Sample 47: 36's grey, sized sago flour and tallow. Load: 111.4 grams. Speed: 120 r.p.m.



clothing textile yarns has not been studied except for abrasion tests on yarns and fabrics which, by definition, do not fall within the scope of this discussion.

The dynamic fatigue of tire cords, because of its obvious importance in tire life has received more attention (143-159). Among the earlier investigators, Staveland and Shepard (144) flexed cords threaded over a system of pulleys under constant load. While they had some success in predicting cord performance in tires, their tester, essentially of class B-1, operated at a low frequency at room temperature, and fatigue failure resulted partly from abrasion produced by the pulleys. They recognized the importance of hysteresis in tire cords but measured only that calculated from stress-strain cycles performed at low rates of strain. More recently, several cord fatigue testers based on quite different principles have been developed (146-149). The Goodyear machine (148) probably approaches more closely the conditions of tire service than any of the others. In it, a

cord is cured along the surface of a rubber-fabric cylinder, which is rotated between chucks, the axes of which are not parallel. Thus, the cord goes through cycles of tension and compression (probably a class A-4 test) much as it would in a tire. The method also offers the possibility of evaluating cord to rubber adhesion. This machine has been reported to be very successful but no detailed data obtained with it have been published except those of Venable (150), which will be mentioned presently. The Firestone Snap-Cycle Machine (147) is interesting in that it operates with a cam

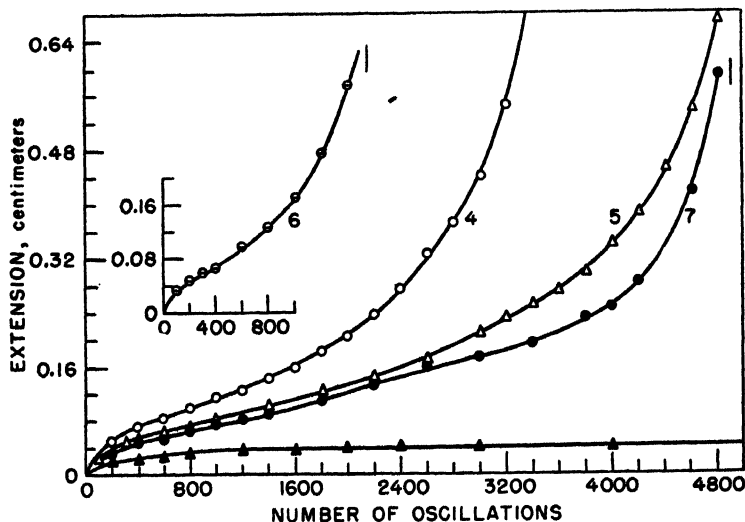


Fig. 69. Extension of the yarns at break as a function of number of cycles (141). Sample: Cop 49, 32's mule yarn, unsized. Load on specimens: 45 grams. Speed: Nos. 4, 5, and 6, 122 r.p.m.; Nos. 7 and 8, 120 r.p.m. Length of specimens: 6 cm. except No. 5 where length is 12 cm. but ordinates are halved.

that produces a gradually increasing periodic load with a rapid and complete release of tension in each cycle, simulating the dynamic cord conditions in a tire. An automatic device takes up the slack produced by creep of each cord during the test and maintains the maximum dynamic and the average static tensions approximately constant. It thus fits class C-1 approximately but the asymmetric strain cycle makes it unique. Valuable results have been obtained with this machine also but detailed data have not been published. The author's own experience with this machine indicates that it has some advantages for predicting cord fatigue in tire sidewalls but that the action is so severe that results are sometimes mis-

leading and the machine is subject to periodic breakdowns. The U. S. Rubber Company Cord Fatigue Tester (146,152) and the Goodrich Cord Vibrator (149) are essentially class B-1 tests but are quite different in other respects. Results obtained with them will be discussed later.

Comparative data on the above four fatigue testers as well as several others have been obtained on a series of specially selected viscose rayon cords by Venable (150). The fatigue ratings of the machines were evaluated in terms of supposedly known tire service characteristics of the various types of rayon cords. While it would be difficult to criticize this procedure

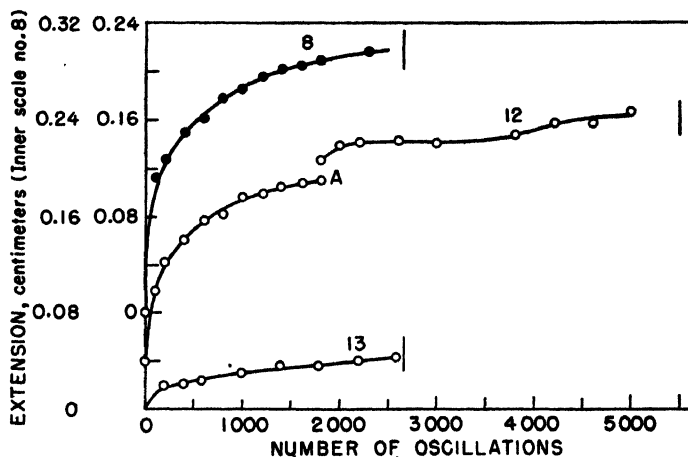


Fig. 70. Extension of the yarns at break as a function of number of cycles (141). Sample: 28's, sized 9.35% farina. Length of specimen: 21 cm. Speed: 120 r.p.m. Load: No. 8, 157.6 grams: Nos. 12 and 13, 185.9 grams.

in detail, still there was a possibility that it was not entirely based on objective concepts. Venable's conclusion that all of the machines were useful and could differentiate "good from bad" but that none of them was sufficiently reliable to be adopted as an A.S.T.M. standard appears quite justified in view of the data obtained. Budd and Larrick (151) have made a statistical study of the data of Venable and conclude that the Goodrich tester correlates best with the other machines. The four machines (146-149) have been discussed by Bradshaw (152). He also made the recommendation that none of the machines be adopted by the A.S.T.M. as a standard test. Bradshaw gave a very good discussion of the natures of the stresses and strains in cords within an operating tire. Some of his statements, particularly those on the unimportance of the rate of stressing,



are difficult to understand in the light of conflicting data in the literature. In general, however, his conclusions concerning the various testers were sound. He gives quite a detailed description of the U. S. Rubber Company Fatigue Tester and the procedure employed with it. It has been pointed out (153) that all the various cord fatigue testers have been useful but, since the stress-strain-time conditions for cords in various regions of a tire vary significantly, it would require great optimism to expect any one machine to predict over-all cord fatigue in a completely reliable manner.

The first extensive studies of tire-cord fatigue, which gave careful consideration of the physical and chemical principles involved, were made by Busse, Lessig, Loughborough, and Larrick (154). They employed the Goodrich Cord Vibrator (149), as did Scholes (155) and Larrick (156).

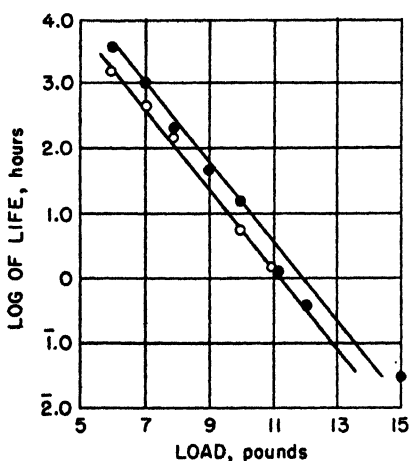


Fig. 71. Effect of dead load on the life of two cotton cords (154).

This machine operates with cords suspended by dead weights vibrated with rather small dynamic strains of 0.4 to 0.8%. The cords pass through a constant-temperature oven. Busse *et al.* (154) studied cord creep and static fatigue to rupture as well as dynamic fatigue with cotton, staple viscose rayon, continuous filament viscose rayon, and nylon cords. By varying the length of cotton cords between grips, they showed that static fatigue failure does not result from fiber slippage but probably from creep effects within the individual fibers. A linear relation between the logarithm of the static fatigue life and the load was found with cotton cord, as shown in Figure 71. Thus, the equation governing the life ( $L$ )-load ( $W$ ) relationship was:

$$W = A \log L + B \quad (30)$$

In the dynamic studies, the frequency was varied over a range of 0-3700 cycles/minute but, because of resonance effects in the machine, results were significant only in the range of 2000-3700 cycles/minute where no variation in the fatigue life (in hours) of a rayon cord was found. With temperature and amplitude constant, the logarithm of the dynamic life

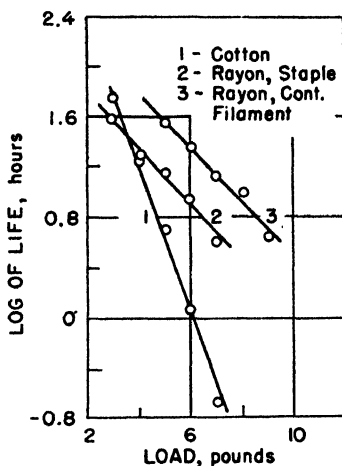


Fig. 72. Effect of load on vibration life (154).

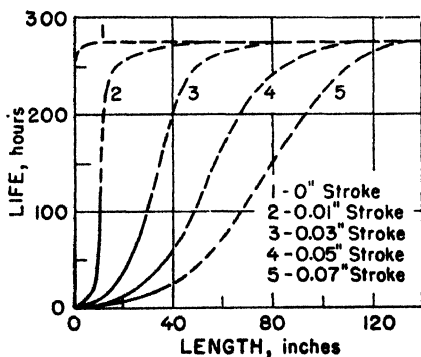


Fig. 73. Effect of stroke and length on life (154).

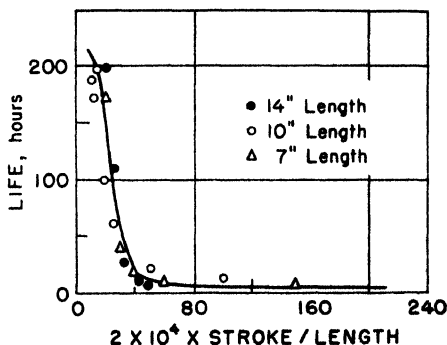


Fig. 74. Vibration life as a function of reduced stroke (stroke/length) (154).

was found to vary linearly with the load, as in the case of the static test. Curves for cords of cotton, continuous filament high-tenacity viscose rayon, and staple viscose rayon are given in Figure 72. A "probable" relation between life, amplitude (stroke), and cord length was proposed as shown in Figure 73. The observed effect of varying the strain amplitude

is given in Figure 74. It was shown rather convincingly that the dynamic fatigue effects were irreversible, long aging periods, wetting with water, etc. failing to cause even partial recovery of initial properties. That the dynamic fatigue phenomenon was not entirely a heat-aging effect was demonstrated by comparing the tensile strength of cords fatigued dynamically with that of cords held at the same temperature (280°F.) under the same static load for various times. The dynamic fatigue was much more rapid than the static. Having shown that fiber slippage was not involved in fatigue, Busse *et al.* attempted to explain the phenomenon in terms of the Eyring theory of flow (111) of the constituent fibers. This would require the life-temperature relationship to be:

$$\ln L = (E/RT) + B \quad (31)$$

where  $E$  is the activation energy for flow and  $R$  is the gas constant. Indeed the data bore out this assumption (see Figs. 75 and 76). Values for the activation energy calculated are given in Table VI. Busse *et al.* did

TABLE VI  
Activation Energies (154)

Cord	Activation energy, kcal./mole
Nylon.....	45.7
Cotton.....	28.8
Rayon.....	19.0

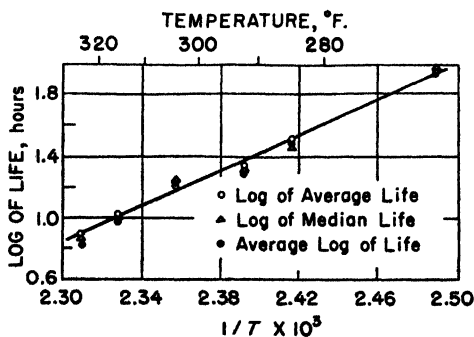


Fig. 75. Effect of temperature on the life of a cotton cord (154).

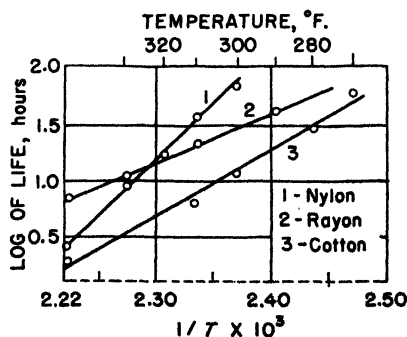


Fig. 76. Change of vibration life with temperature (154).

not maintain that flow of the fibers is the only cause of fatigue failure since cord construction, twist, etc. are known to affect the results. However, they did establish quite conclusively that fiber flow is one important factor and demonstrated that scientific reasoning can be extremely valuable in clarifying even such a complex phenomenon as cord fatigue. Scholes (155) gave further data obtained with the Goodrich Cord Vibrator (149) on various rayon and cotton cords. He demonstrated the known superiority of high-tenacity viscose rayon in dynamic fatigue but also gave data on the greater creep of the rayon cords. He compared fatigue life with tensile strength and showed that the two indexes do not always correlate. Larrick (156) gave further results on the same device and presented curves showing the changes in fatigue life produced by the conditions of tire-cord service.

Waller and Roseveare (157) have made a thorough study of viscose rayon cord and yarn fatigue, using both the Goodrich vibrator (149) and the U. S. Rubber Company tester (146,152). The basic test conditions A, B, and C employed are given in Table VII. While the Goodrich tester

TABLE VII  
Fatigue Test Conditions (157)

Test	Tester	Class	Load, gram/denier	Temp., °C.	Moisture regain, %	Frequency, cycles/min.
A	U. S. Rubber	III	0.14 (min.)	49	3.7	360
B	Goodrich	IV	1.0 (av.)	100	2.0	3000
C	Goodrich	IV	0.65 (av.)	170	"Dry"	3600

is essentially of our class B-1, Waller and Roseveare pointed out a distinction between their classifications III and IV. In the U. S. Rubber tester, termed class III, the slack in the cords under a constant minimum static load  $x_m$  is taken up by a ratchet mechanism operating at the point of minimum strain  $y_m$  in the cycle. Thus the strain amplitude remains constant and the minimum static strain  $y_m$  increases. This is the only significant type of fatigue reported in the literature that does not fall within our classifications of Figures 1-6. The Goodrich tester, termed class IV, falls within our class B-1 where the strain amplitude  $Y$  and the average static stress  $x_a$  are constant. To facilitate reference to Waller and Roseveare's work, their classifications III and IV and test designations A, B, and C (see Table VII) will be used here. It should be noted that test C conditions (low stroke, high temperature, high frequency) were those employed by Busse *et al.* (154). The basic conditions of Table VII were varied in some cases by Waller and Roseveare. For example, the fre-

quency was varied in the type B test and a linear decrease of fatigue life was observed (see Fig. 77), contrary to the results of Busse *et al.* (154) using test C. Waller and Roseveare suggested that this discrepancy probably resulted partly from the heat aging involved in test C. In agreement with

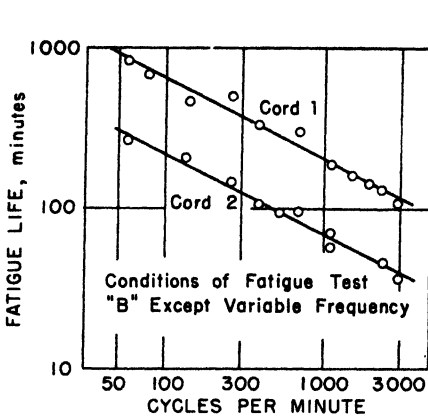


Fig. 77. Effect of frequency of stresses on fatigue life (157).

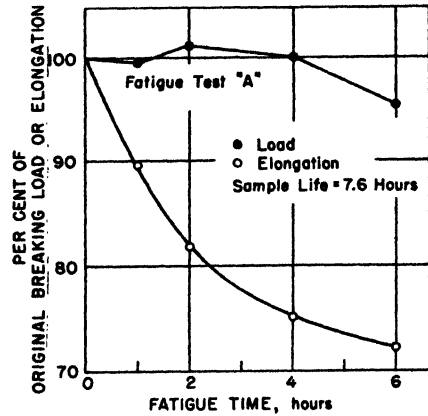


Fig. 78. Effect of fatiguing on breaking load and elongation of a tire cord (157).

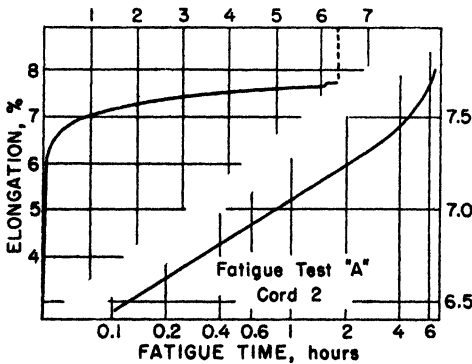


Fig. 79. Growth behavior during fatiguing (157).

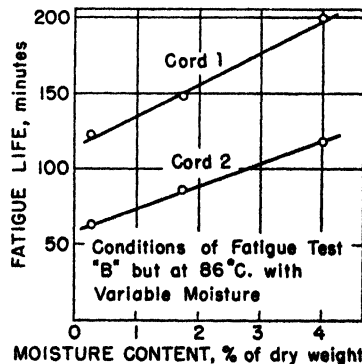


Fig. 80. Effect of moisture on fatigue life (157).

Busse *et al.* (154), it was found that the fatigue phenomena were irreversible for conditions A. The effects of fatiguing, for various times short of failure, upon the breaking load and elongation are shown in Figure 78. The creep or growth behavior of the cords (conditions A) during fatiguing is illustrated in Figure 79 and the effect upon fatigue life of increasing moisture content (conditions B) in Figure 80. The observed increase of dy-

dynamic life with increasing moisture (conditions B) is the opposite of the effect found in the case of static fatigue and probably results from the lower cyclic stresses present in moist cord. The effect would not be expected at higher temperatures where the combination of moisture and high temperature is very effective in reducing fatigue life. This matter is treated in detail by Waller, Bass, and Roseveare (158).

The effects of temperature on fatigue were studied for conditions B and C and for creep failure (static fatigue) under two static loads. In agreement with Busse *et al.* (154), the Arrhenius equation (31) was found to hold

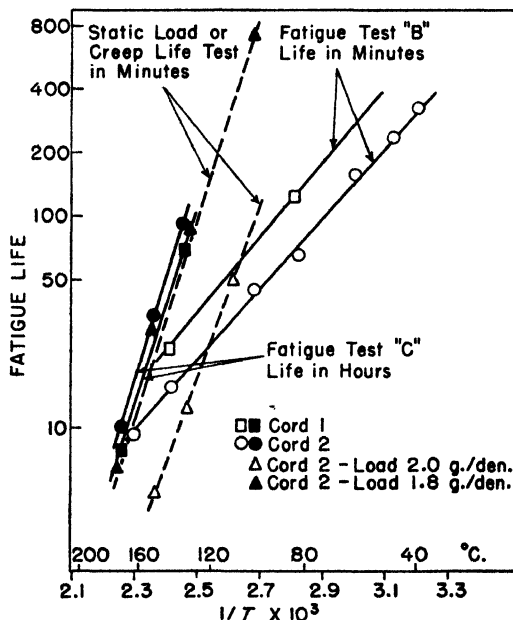


Fig. 81. Effect of temperature on fatigue life (157).

(see Fig. 81). However, the calculated activation energy for dynamic fatigue with the high temperature-low amplitude conditions C, used by Busse *et al.*, was about equal to that for static fatigue but much higher than that for the lower temperature-higher amplitude conditions B. Hence, the conclusions of Busse *et al.* that their fatigue effects were largely results of flow within individual fibers are borne out but it appears that "heat aging" may be a larger factor than they supposed. A tabulation of the calculated activation energies is given in Table VIII. It appears that the process governing fatigue with conditions B is not the same as that involved either in heat aging or creep under static load.

TABLE VIII  
Activation Energies

Cord test	Activation energy, kcal./mole
Fatigue test B.....	7.8
Fatigue test C.....	23.0
Fatigue test of Busse <i>et al.</i> .....	19.0
Creep (1.8 g./denier).....	22.0
Creep (2.0 g./denier).....	19.0
Thermal degradation of cord.....	25.0

Waller and Roseveare also studied the effects upon fatigue of varying the static load and stroke and compared data on yarns and cords. They observed surface fibrillation of filaments in fatigued cords, an effect not found in cords broken in the usual tensile test. They failed also to find this effect in fatigue-ruptured cords taken from tires but fibrillation would be hard to observe because of the presence of the adhesive. Thus, they suggest that the fatigue of tire cord may be associated with an internal rupturing of the filaments and that surface fibrillation is important only in cords not coated with an adhesive. They also consider the work on fatigue of rubber by Cadwell *et al.* (64) and Fielding (66) and accept the interpretation of the latter that the existence of a fatigue life minimum at zero minimum static strain is associated with crystallization on stretching. Thus, they conclude that this effect is not to be expected with rayon tire cords where the filaments are already highly crystallized and oriented. While this conclusion is probably justified, it would still seem of interest to investigate the fatigue life *versus* strain and amplitude relationships of single filament or low-twist yarns.

Wakeham and co-workers (96-98) have attacked the problem of tire cord fatigue from an entirely different viewpoint. Instead of measuring cycles or time to rupture, they have developed apparatus that allows observation of changes in absolute hysteresis, elongation, and modulus with increasing times of cycling at a frequency of 1 cycle/second. This apparatus, essentially a fatigue tester of class B-1, is simply a nonresonance vibrator with provision for measuring stress and strain at various times during each cycle so that hysteresis loops can be plotted as the cycling progresses. Likewise the strain and elastic modulus can be followed during the fatigue process. Provision for varying the temperature and moisture content of the cords is also provided. Typical changes observed in the hysteresis loop with progressive cycling are shown in Figure 82 for a nylon cord. Un-

doubtedly, the early portion of the decrease in hysteresis resulted from geometrical "compacting" of the cord but the later changes must have been due principally to changes of the elastic properties of the individual fibers. The general trend, for a cotton cord, of hysteresis, modulus, and elonga-

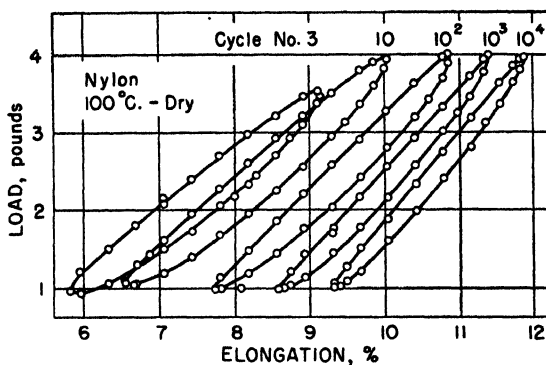


Fig. 82. Typical mechanical hysteresis loops at various cycle numbers for dry nylon at 100°C. (97).

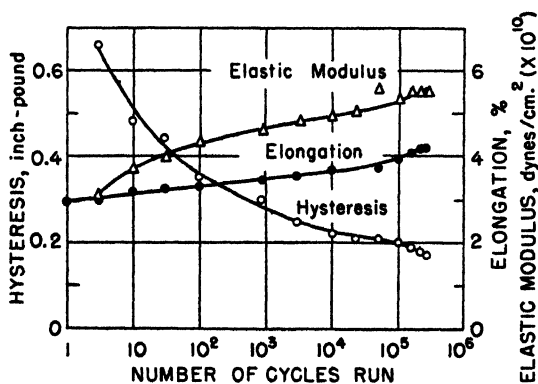


Fig. 83. Hysteresis, elastic modulus, and elongation vs. cycle number to point of rupture for dry experimental cotton cord-2 at 145°C. (97).

tion as fatigue effects is shown in Figure 83. The appreciable effects of moisture upon the hysteresis changes are given in Figures 84 and 85, the variation of modulus with cycling in Figure 86. It is interesting to note the large moisture effect in the case of nylon (Fig. 85). The relation between elongation and number of cycles for dry cords at 25°C. is given in Figure 87 and the rate of growth (creep) *versus* moisture content in Figure 88. The



effect upon the hysteresis of varying the temperature is shown in Figures 89 and 90. Nylon shows the largest temperature effect, cotton the smallest, as might be expected. The rate of growth *versus* temperature rela-

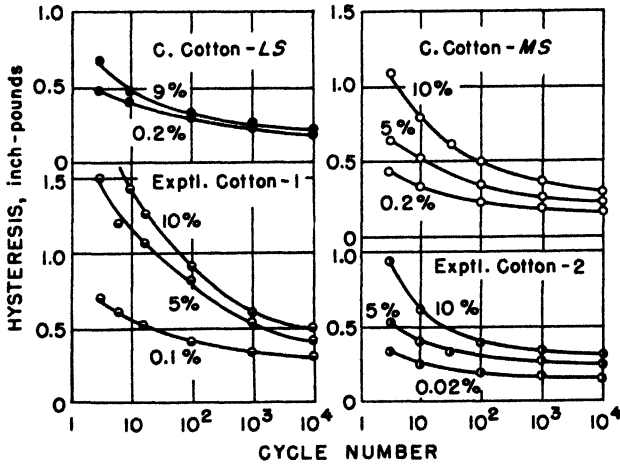


Fig. 84. Hysteresis *vs.* cycle number for cotton cords at constant moisture and 25°C. (97).

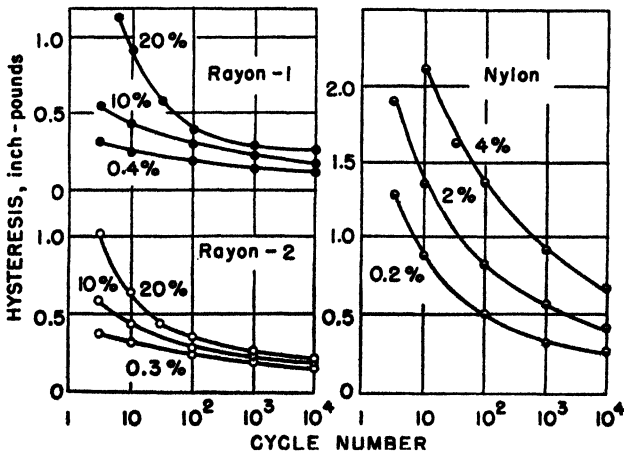


Fig. 85. Hysteresis *vs.* cycle number for rayon and nylon cords at constant moisture and 25°C. (97).

tionship is given in Figure 91. Values of the various indexes for the different cords after 1000 cycles are compared in Table IX. It would be dangerous to draw conclusions concerning the properties of the individual

fibers from this table since cord construction is obviously an important factor. However, the data should be extremely useful in predicting performance of the various cords in tires, particularly in regard to the portion of the hysteretic heating contributed by the cords as compared to that of the

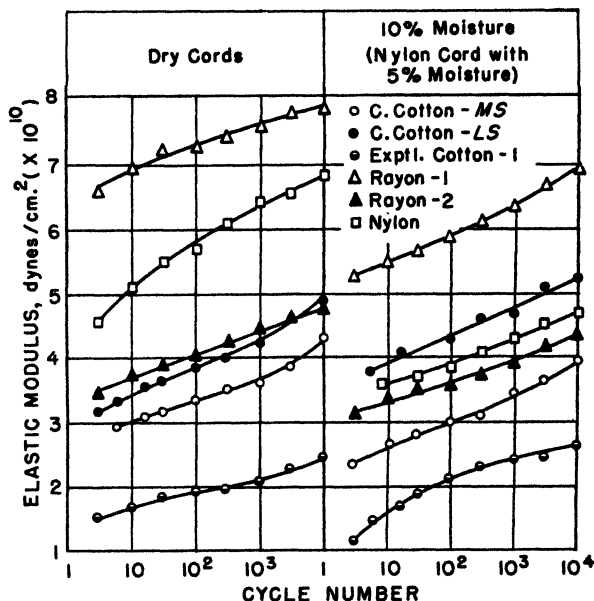


Fig. 86. Elastic modulus vs. cycle number at constant moisture and 25°C. (97).

rubber. Again it would appear highly desirable to perform similar experiments with single fibers and thus deduce the actual performances of the individual materials.

TABLE IX

Comparison of Properties of Tire Cords (Dry) after 1000 Cycles at 25°C. (Load 0.1 to 0.4 Gram/Grex)<sup>a</sup>

Cord <sup>a</sup>	Construction	Grex	Modulus, dynes/cm. <sup>2</sup>	Growth rate at 0.2 g./grex, %	Hysteresis	
					Inch-lb. per 100 in.	Cal. per g.
Nylon.....	210/4/2	1986	$6.00 \times 10^{10}$	0.247	0.098	$5.26 \times 10^{-3}$
Viscose r.....	1100/2	2444	7.66	0.105	0.072	3.10
Viscose r.....	2200/3	5366	4.60	0.215	0.258	5.10
Med.-stretch c.....	18/4/3	4342	3.56	0.073	0.207	5.07
Low-stretch c.....	16/4/3	5064	5.16	0.130	0.278	5.83
Exptl. low-stretch c..	17/4/3	4446	4.37	0.086	0.169	4.05

<sup>a</sup> r. = rayon; med. = medium; c. = cotton.

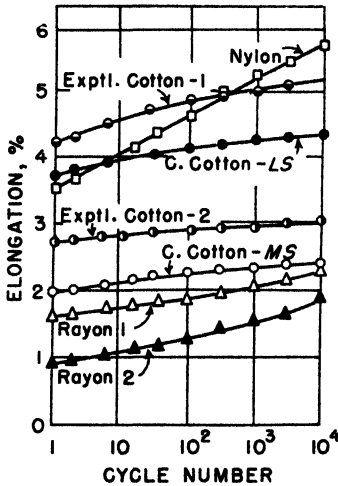


Fig. 87. Elongation vs. cycle number for dry cords at 25°C. (97).

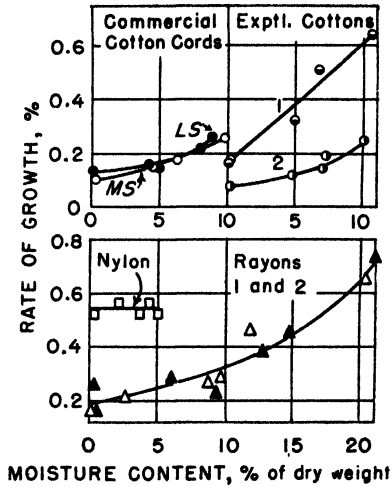


Fig. 88. Rate of growth vs. moisture for cords at 25°C. (97).

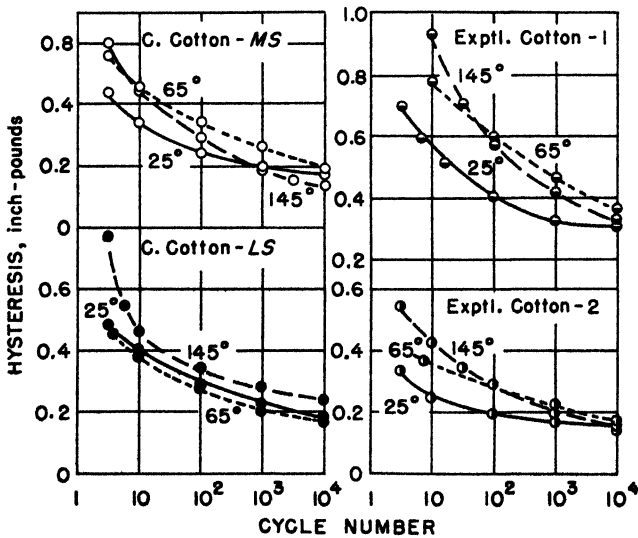


Fig. 89. Hysteresis vs. cycle number at constant temperature for dry cotton cords (97).

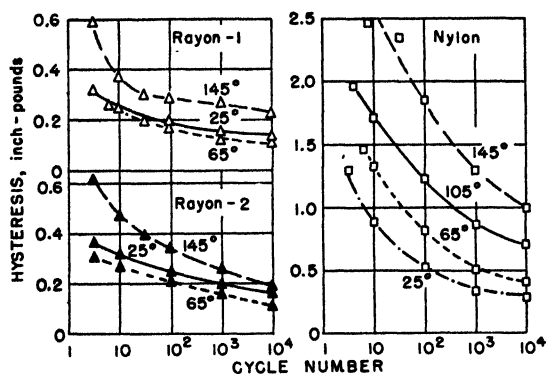


Fig. 90. Hysteresis *vs.* cycle number at constant temperature for dry rayon and nylon cords (97).

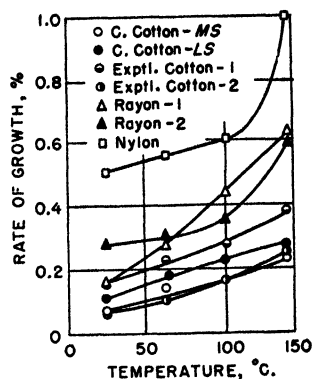


Fig. 91. Rate of growth *vs.* temperature for dry cords (97).

Recently, Meredith and Peirce (159) have described experiments on the "cumulative extension" of yarns and cords. The apparatus used was a class B-1 fatigue tester, which provides a continuous record of the extension of a sample as it is flexed with a fixed amplitude at a rather low frequency (normally 60 cycles/minute), under a fixed static load. Means are also provided for measuring the maximum tension in the sample at intervals during the test. The wave form of the imposed strain is essentially sinusoidal with negative half-waves omitted, *i.e.*, each full cycle consists of a single sinusoidal peak followed by a rest period of equal duration. In some but not all cases, samples were run to rupture. All measurements were made at 65% relative humidity and 21.1°C. The extensions were expressed in the logarithmic manner of Hencky, *i.e.*, extension:

$$E_n = \ln (l_n/l_0)$$

where  $l_n$  is the length after  $n$  cycles and  $l_0$  the initial length of the specimen. The value of the constant static load selected was termed the "residual tension." It was expressed as a fraction of the weight of one kilometer length of each specimen. Thus, different cords tested at a given value of the residual tension were compared on essentially an "equal count" basis.

A large number of materials was employed in these experiments: cottons, viscose rayons, acetate rayons, nylon, silk, wool, casein, camel hair, etc. Particularly interesting data are given in Tables X and XI comparing cotton and viscose rayon cords with varying load (residual tension) and frequency, respectively. The strain amplitude used was 3%. The greater dynamic fatigue life of viscose rayon, as compared to cotton, is quite clearly

TABLE X  
Effect of Residual Tension on Cumulative Extension

Sample and conditions	Residual tension, km. wt.	Cumulative extension, % $\frac{\bar{E}_1}{E_1} - \frac{E_{10} - E_1}{E_1}$	Extension to reach length at 1 km. tension, %	Cumulative extension to break + imposed extension, %	Extension at break from length at 1 km. tension, %	Cycles to break, <i>N</i>	Maximum tension in 10th cycle, km. wt.
Cotton cord C, at 3%, 60 c.p.m.	0.19	0.25	1.2	—	—	—	2.1
	0.38	0.36	2.1	14.9	12.6	1245	3.6
	0.77	0.78	4.2	13.5	12.8	189	7.6
	1.54	1.47	5.4	12.1	13.3	35	14.1
	3.08	1.85	5.8	10.9	14.2	13	22.9
Viscose rayon cord H, at 3%, 60 c.p.m.	0.19	0.29	1.2	—	—	—	4.8
	0.38	0.40	2.0	15.9	15.5	2325	6.4
	0.77	0.53	2.7	16.6	16.5	1357	7.1
	1.54	0.82	4.2	16.9	17.3	403	8.2
	3.08	1.61	7.4	17.9	19.3	49	12.8

TABLE XI  
Effect of Frequency of Extension on Cumulative Extension

Sample and conditions	Frequency, cycles/min.	Cumulative extension, %		Cumulative extension at break + imposed extension, %	Maximum tension in 10th cycle, km. wt.	Maximum tension at 10% extension, km. wt.	Cycles to break, <i>N</i>	Life, minutes
		$\bar{E}_1$	$E_{10}$					
Cotton cord C, at 3% and 1 km. wt.	6	1.8	6.6	—	13.1	11.7	52	7.7
	20	1.3	5.7	11.4 <sup>a</sup>	14.0	12.0	74	4.7
	60	1.0	4.7	10.7	13.7	12.5	118	2.0
Viscose rayon cord H, at 3% and 1 km. wt.	120	1.3	4.4	10.4	13.9	12.7	140	1.1
	6	1.6	4.8	11.1	16.0	9.7	308	51.4
	20	1.7	4.0	10.3	16.3	9.9	456	22.9
	60	1.1	3.0	9.3	16.2	10.1	560	9.3
	120	1.3	3.1	8.6	16.0	10.7	635	5.3

<sup>a</sup> Extrapolated.

shown. However, the expected greater creep, "cumulative extension," of rayon is not found for all test conditions. This situation probably resulted from the selection of the "residual tension" on the basis of total count (fraction of one kilometer weight of specimen). This really amounts to assuming that rate of creep is proportional to load which, of course, is not true. In fact, the data of Table X show that it is not true. Hence, the comparative results of this test, like all fatigue tests, mean very little unless the

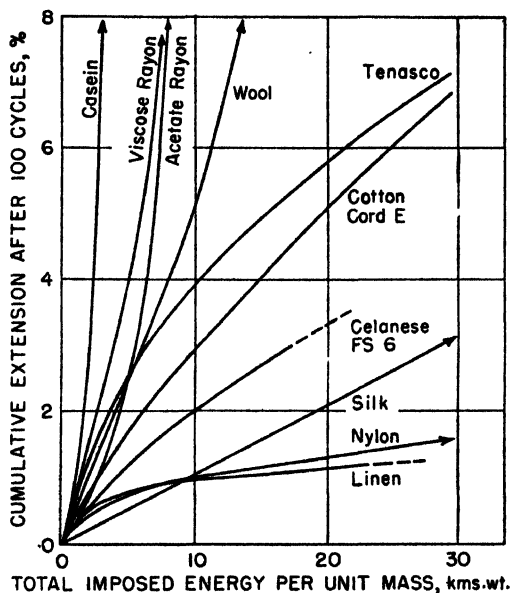


Fig. 92. Cumulative extension vs. imposed energy (159).

counts of the different cords compared are nearly the same. For this reason relative values of cumulative extension and fatigue life given by Meredith and Peirce for the different cords must not be taken too seriously, even when plotted against the imposed energy per unit mass, as in Figure 92. The shape of the curves was significant, however, and was discussed effectively in the paper. For example, the following conclusion is possibly correct since it is qualitative. "On the above basis (equal imposed energy/unit mass), the cords showing the least plasticity, *i.e.*, low cumulative extension, are linen, nylon, and silk, and these are followed in order by Durafil, stretched cotton cord, and Fortisan. Hair, wool, Tenasco, and unstretched cotton cord form the next group with intermediate plasticity, whilst ordinary viscose rayon, acetate rayon, and casein fiber show considerable

plasticity." It must be remembered, however, that these measurements were made at room temperature and at 65% relative humidity, that the static loads were quite large, and that the frequency was low. Thus, the results have little meaning in relation to tire cord fatigue.

## VII. Fatigue of Plastics

### 1. General Characteristics

The term plastics has come to include almost anything nonmetallic that is not in the vapor or gas phase. Even a simple inorganic compound such as silver chloride may, under certain circumstances, be classed as plastic. Indeed glasses may quite properly be termed plastics and, in fact, inorganic high polymers. The term plastics is unfortunate since, in the usual physical sense, any solid or liquid material possesses plasticity, *i.e.*, the ability to deform under stress in an incompletely reversible manner. The terms "rubber" and "fiber" are relatively quite definite since they denote special characteristics, long-range elasticity and extremely anisotropic elasticity, respectively. But all rubbers become plastics, in the stricter sense, as they are cooled below the "second-order transition." Polymethyl methacrylate is rubbery above 70°C.; natural rubber is a hard amorphous "plastic" when cooled quickly below -70°C. Nylon makes an excellent fiber when extruded and oriented; yet it may be molded by conventional methods to form a "plastic." Often "plastics" are thus christened even before they are deposited as coatings or cements from a solution or dispersion. It is obviously important, then, that we carefully limit our discussion in this brief chapter.

We have already given some thought to those important plastics—rubbers and fibers; hence, they may be excluded henceforth. Only minor apologies are required for the elimination of inorganic "plastics" and solutions or dispersions, which cannot fatigue as such since they are incapable of supporting stress for reasonable periods of time. There then remain two general classes of *hard organic plastics*: (1) thermosetting resins and (2) thermoplastic resins. But in their consideration it must always be remembered that most plastics become rubbers when the temperature is raised above the second-order transition providing the temperature of decomposition is sufficiently high. A further complication in this definition is the fact that otherwise hard plastics may be "plasticized" to form flexible materials which, in some cases, behave suspiciously like rubbers although with considerably retarded elasticity. But, in the light of the requirements of logic and brevity, plasticized polymers may be discussed only as

special cases of the basic materials. Furthermore, in view of our "Definitions of Fatigue," the numerous experiments on laminates should not be treated; yet some data on them must be included where results on the molded polymers themselves are lacking.

The solid plastics, both thermoplastic and thermosetting, for obvious reasons have been susceptible to study by practical engineering techniques to a much greater degree than rubbers and fibers. Their relatively small deformations under ordinary loadings suggest that they may behave in much the same manner as metals, providing the temperature range is properly selected. Thus creep, static fatigue, and dynamic fatigue studies have been made on plastics with the object of evaluating them as components of a structure, which is specified to deform a certain amount, last a certain time at a given stress, or withstand a predetermined number of cyclic loadings before rupture. In one sense, this situation has been fortunate since it has made possible rapid advances in the applications of plastics. On the other hand, the result has been a tendency to neglect the basic physical properties and thus create an enormous fund of engineering data unsuitable for interpretation in terms of the chemical structures of the base materials.

## ***2. Stress-Strain, Creep, and Hysteresis***

The significance of the different types of stress-strain curves obtained with various plastics has been discussed effectively by Carswell and Nason (160) in terms of engineering concepts such as softness, hardness, toughness, and strength. They also present data upon the effects of temperature, moisture, rate of strain, and exposure to various chemicals on the tensile and impact properties. Couzens and Wearmouth (161) investigated the effect of increasing the rate of strain with cellulose nitrate and several vinyl polymers and found that the yield stress increased with increasing rate. They also concluded that there is a critical stress below which creep does not take place. Morey (162) discussed impact strength in relation to the structure and constitution of plastics, essentially upon the basis of linear models, and arrived at an expression for the total deflection, which appeared to represent his data with fair accuracy. Turner and Thomason (163) have made extensive studies in the attempt to correlate various mechanical properties of plastics. In fact, the literature is replete with stress-strain and impact data on plastics. However, because of the large amount of flow that usually occurs after the yield point has been reached, it is seldom practicable to perform more than a single cycle of extension. The results thus cannot be considered as directly related to fatigue.



Long-period creep and static-rupture studies of hard plastics are numerous but, in many cases, the work has been largely concerned with the establishment of an empirical law (164-171). Haward (164), for example, found linear relationships between the rate of strain and the time to rupture and the rupture stress when plotted on log-log charts. Findley and co-workers (165-168) have made extensive studies of creep and have shown that the data on long-term creep can usually be expressed as power functions in the time. They also present data establishing the existence of a "critical creep stress" (165) in agreement with other workers (161). Unfortunately, such power functions are difficult to interpret in terms of current theories of flow. Telfair, Carswell, and Nason, however, obtain the more interpretable creep equation discussed by Lyons (134) (see Eq. 28) indicating that phenolic plastics and tire cord obey similar laws of flow. Some work has been done in the direction of theoretical interpretation of the mechanical properties of plastics. Leaderman (172), for example, applied the Boltzmann superposition principle to the creep and creep recovery of Bakelite under torsion. He found some plastic flow (secondary creep) occurring in the first cycle of creep and recovery. On subsequent cycles, however, primary creep appeared to be the controlling factor and the Boltzmann law was obeyed. He also developed relationships based on the Boltzmann law, which allowed calculation of specific damping capacity from static step-by-step cyclic loading tests and from free-vibration measurements. Fair agreement was found between the values calculated from the two types of experiments. Leaderman also had some success in explaining the creep and creep recovery of plasticized polyvinyl chloride by means of the Boltzmann principle (173). He found that, after "mechanical preconditioning," the flow was recoverable (primary creep); thus, he concluded that points of entanglement must exist between the chains in the plasticized polyvinyl chloride, which are strong enough to prevent slippage under the conditions of test. Other significant work of this nature aimed at explaining the action of plasticizers in various vinyl polymers has been done by Aiken *et al.* (174). The field has been reviewed by Alfrey (175) although perhaps not as completely as might be desired. Robinson *et al.* (176) have given very interesting results on the creep of polymethyl methacrylate, supplementing the creep data with optical birefringence measurements. They arrived at a law of creep,

$$y = y_0 + \sum_i b_i [1 - \exp(-Q_i t)] + Kt, \quad (32)$$

where  $y_0$  is the instantaneous elongation,  $b_i$ ,  $Q_i$ , and  $K$  are constants. The

number of rate constants  $1/Q_i$  necessary to describe creep decreased as the temperature increased. Plotting " $1/Q_i$ " against reciprocal absolute temperature, they calculated activation energies for flow of the order of 30 kcal./mole.

Alfrey (175) has made some progress in explaining theoretically the static rupture of plastics under prolonged loading but it is apparent that insufficient experimental data exist to permit a test of the theory. His treatment of ultimate strength of high polymers in general, as related to molecular weight distribution, crystallization, and orientation, is particularly valuable. It is of interest to note that his conclusion that orientation rather than crystallization is the dominant factor in rupture strength is quite in accord with the theoretical arguments given in the early part of this chapter.

Hysteresis effects in solid plastics have been given deserved attention, particularly in respect to their interrelationship with dynamic fatigue phenomena (165,172,177,178). There is one important distinction between the internal friction of solid thermoplastics as compared to that of rubbers. For thermoplastics the internal friction increases with increasing temperature (178), while that of rubbers decreases.

### ***3. Static and Dynamic Fatigue to Rupture***

Numerous papers have appeared in recent years describing dynamic fatigue experiments on hard plastics. The apparatus employed has been, in the main, of three types:

(1) Rotating beam type in which a sample of circular cross section is rotated between chucks with a static load applied in such a manner as to give a constant bending moment with the speed of rotation zero. When the sample rotates, a given region passes through cycles of alternating longitudinal tension and compression. This type is, therefore, of class A-3.

(2) Constant strain amplitude type with the sample subjected to repeated bending, torsion, tension, or compression deflections, which are usually symmetric about the condition of zero strain. Sometimes a dynamometer arrangement is provided to measure the maximum alternating stress. This test may be of class A-3 or A-4.

(3) Constant stress amplitude type with the sample subjected to repeated bending, torsion, tension, or compression stresses, which are usually produced by the centrifugal force of a rotating mass. Tests of this type fall within classes C and D.

Methods of representation of fatigue data on plastics are often quite different from those employed with rubbers and fibers. Frequently the maximum dynamic stress ("fatigue stress") is plotted against the number of cycles to failure. As the "fatigue stress" is decreased, the number of cycles to failure, "fatigue life," increases until finally a region is reached

where further reductions in "fatigue stress" give no further increases in the life, *i.e.*, the fatigue life becomes infinite at a certain value of the fatigue stress, which is often referred to as the "endurance limit." Typical fatigue stress *versus* cycles to failure curves have been presented by Lazan and Yorgiadis (179) (see Fig. 93) who give an excellent review of fatigue phenomena in plastics from an engineering viewpoint. These curves, plotted with logarithmic abscissas, appear linear. However, because of the wide statistical variations of dynamic fatigue data, it does not seem entirely certain that the curves are linear or that a definite "endurance limit" exists except within the limits of error of present fatigue testing techniques. For examples, the curves of Findley (168) for different mean static

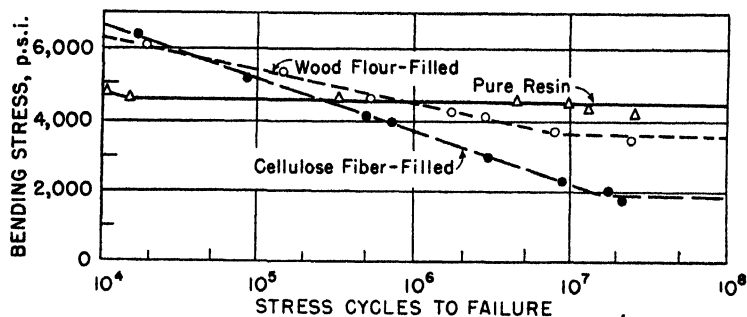


Fig. 93. Fatigue bending stress *vs.* cycles to failure for three phenolic plastics (179).

stresses, obtained with phenolic molding materials, are given in Figure 94. Fatigue stress *versus* mean static stress is plotted in Figure 95. Findley also presents interesting data on the variation of mean static stress with time for various stress amplitudes (Fig. 96) and the fatigue stress-frequency relationship (Fig. 97).

Returning to the summary of Lazan and Yorgiadis (179), another effective but unusual method of presenting fatigue data is given in the stress range diagram of Figure 98. This type of plot is useful since it shows the manner in which the permissible stress amplitude decreases as the superposed static load increases. Lazan and Yorgiadis also give a comprehensive discussion of the various types of fatigue testers now in use and point out that either crack initiation or growth can be considered as evidence of fatigue failure. They emphasize the greater reliability of constant-stress amplitude tests (class C or D) as compared to constant-strain amplitude tests (class A or B) since the former provide a more definite time of failure; "when fracture starts, the effective specimen area de-

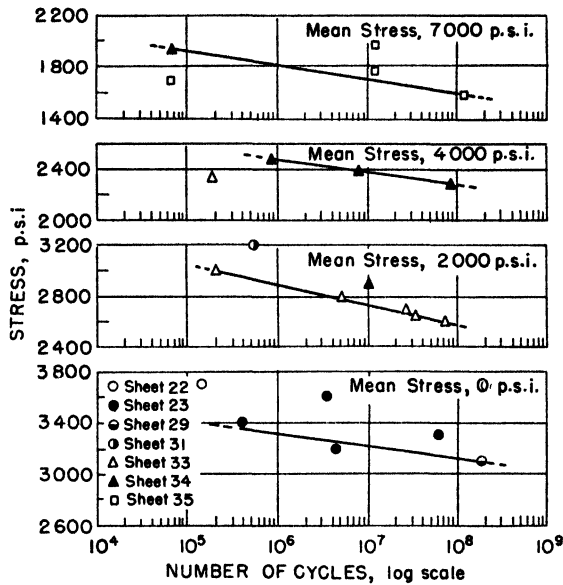


Fig. 94. Fatigue stress *vs.* cycles to failure for several mean static stresses (168).

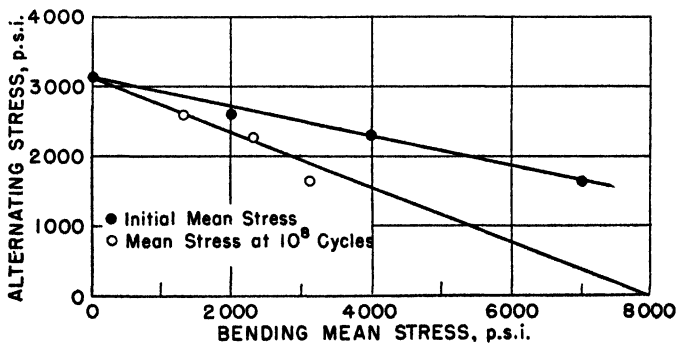


Fig. 95. Fatigue stress at  $10^8$  cycles *vs.* mean stress (168).

creases, causing an increase in unit stress which accelerates the progress of the fracture." Another important feature of the article of Lazan and Yorgiadis (179) is the presentation in tabular form of fatigue results on several important plastics obtained by various investigators. They further give a comprehensive bibliography on the fatigue of plastics. The existence of this bibliography obviates the necessity of listing here all the

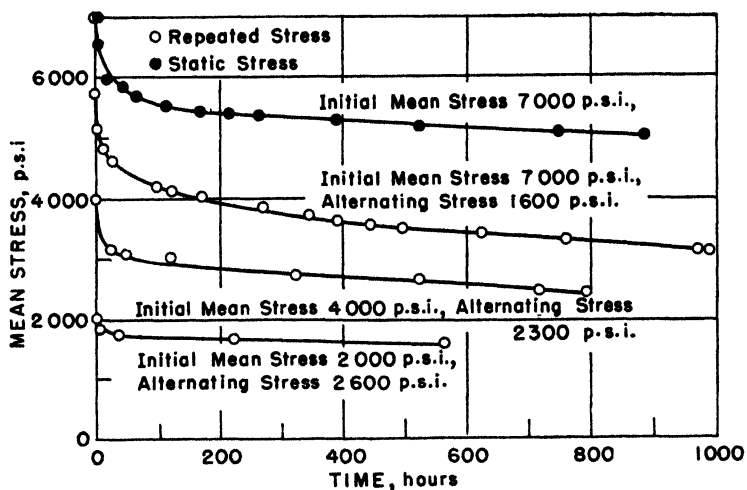


Fig. 96. Mean static stress vs. time for various stress amplitudes (168).

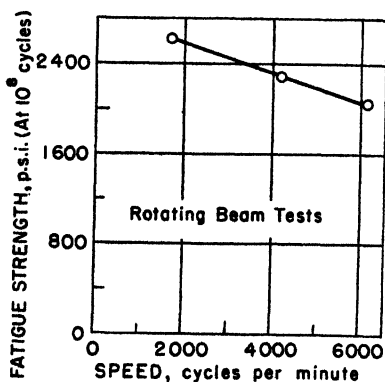


Fig. 97. Fatigue stress vs. frequency (168).

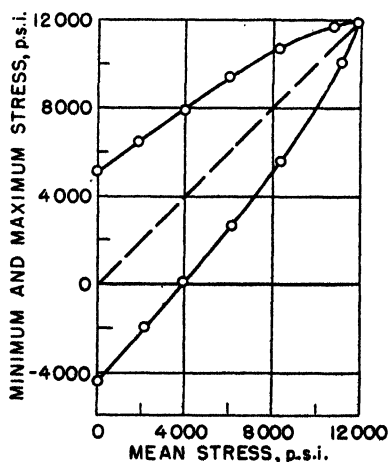


Fig. 98. Stress range diagram for a phenolic resin with cellulose fiber filler (179).

many papers on fatigue of plastics except where results of fundamental scientific interest have been obtained. A very interesting paper is that of Findley and Hintz (180) who compared the results of repeated impact tests with those of constant strain amplitude fatigue. An ingenious impact device that dropped steel balls on the test piece at a fixed rate and retrieved them as they bounced was employed. The maximum stress was

calculated for each of the two types of test and both values plotted, with a scale adjustment, against cycles to failure. A surprisingly good correlation between constant force impact and constant strain amplitude alternating fatigue results was obtained. Furthermore, failures in both tests appeared to result from the same sort of progressive fracture. It is of interest to note that the energy per impact blow corresponding to the endurance limit was less than 1% of the energy required to fracture the specimen in a single blow. The nature of fatigue fracture, static or dynamic, in hard plastics appears to be a combination of chemical and purely physical effects. Haward (164) found that if a sample of cellulose acetate under static stress was released before rupture, allowed to recover at 65°C., and then again subjected to load, it was more easily extended and broke after a short time. Thus, the initial period of static fatigue had produced a truly irreversible change without any visible cracks. Whether or not cracks would have been detected by microscopic examination is a matter of conjecture. Tobolsky (181) observed complete relaxation of stress in a sample of polystyrene held at constant compression strain (1%) but, upon examination by microscope found that the complete relaxation was caused by the formation of many tiny internal fractures. This effect did not disappear at higher temperatures. Chasman (170) reported that surface crazing appeared on specimens of methyl methacrylate and cellulose acetate almost from the beginning of a static fatigue test. It thus seems apparent that any attempts to explain creep phenomena in hard plastics must recognize the possibility that the phenomenon is partly one of progressive fracture. When creep tests on phenolic compounds were carried out by Gailus and Telfair (171) at 192°F., it was noted that shrinkage took place during the creep tests, as observed on dummy samples under zero load, presumably because the condensation reaction continued at this temperature. Hence, it may be necessary to consider competing chemical reactions in creep tests at higher temperatures. Static and dynamic fatigue tests do not always correlate, as pointed out by Telfair, Adams, and Mohrman (182), in connection with their studies of phenolic and melamine plastics. As expected, the more highly cross-linked melamine resins showed better static fatigue characteristics, yet the phenolic compounds were superior in dynamic fatigue stress. The total creep of the two types of resins was about equal. The effect of wide variation of specimen temperature upon the fatigue properties has been studied by Oberg *et al.* (183) with several plastics such as methyl methacrylate and phenolic resins. They concluded that fatigue characteristics are not adversely affected by low temperatures. Likewise Findley (184) showed for paper laminates

that the dynamic fatigue stress decreases continuously with increasing temperature in the range of  $-75^{\circ}$  to  $+425^{\circ}\text{F}$ . He also found a decrease in dynamic fatigue stress as the testing frequency was increased from 500 to 14,000 cycles/minute. However, the frequency effect was greatly reduced when the effect of operating temperature was taken into account. The effects of several other parameters were also studied by Findley (184) but, because he employed laminates, it is difficult to interpret the results in terms of the base phenolic resin employed.

The dynamic fatigue of flexible vinyl sheetings has been investigated by Duggan and Fligor (185) by means of a de Mattia machine (class A test). As was to be expected, increasing the bending or tension strain amplitude decreased the fatigue life. However, in contrast to results on solid plastics

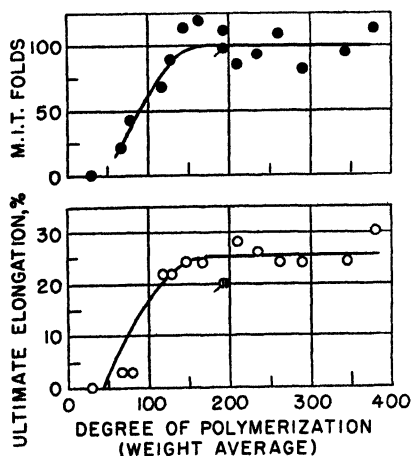


Fig. 99. Ultimate elongations and folding endurance of cellulose acetate fractions as a function of the viscometrically estimated DP. The starting material is designated by tagged circles (186).

(183,184), decreasing the temperature from  $25^{\circ}$  to  $0^{\circ}\text{C}$ . gave a large reduction in fatigue life. It is thus apparent that plasticized resins have fatigue properties intermediate between those of the base resins and true rubbers. Sookne and Harris (186,187) have given valuable results on the mechanical properties of films prepared from a series of fractions of cellulose acetate. Fractions of DP (degree of polymerization) higher than 30 showed a rapid improvement in ultimate elongation, strength, and fatigue life, as judged by results of the M.I.T. fold tester with a fixed static tension (class B-1 test). The fatigue life correlated very well with ultimate elongation. Above a DP of 150 only slight improvements in the properties occurred (see Fig. 99). The effects of variation of both the weight-average and number-average DP were studied and it was found that, at any

weight-average DP, the fractions were superior to the blends and, furthermore, those blends containing fractions of low DP were inferior to those which did not. However, for any given number-average DP, the properties of the fractions and all of the blends were approximately equal. Similar work of Spurlin (188) on nitrocellulose fractions gave results consistent with those of Sookne and Harris. More data of this type on various polymers are badly needed to obtain a better understanding of the meaning of fatigue life in terms of basic molecular properties. At the same time, the various physical parameters of fatigue should be more carefully studied for each fraction or blend of fractions, for examples, static strain, dynamic strain, limits of strain, frequency, temperature, etc.

### VIII. Summary

In conclusion, it is clear that a vast fund of data on the fatigue of high polymers already exists but that only a few of the experimental conditions chosen have been capable of producing relationships between the various parameters that are necessary for a clear understanding of the phenomena. It seems that a broad concept of fatigue and recognition of the six, or possibly more, basic phenomena occurring in a fatigue test may be helpful in interpreting future experiments. It further seems desirable to classify the fatigue tests in some manner similar to that which we have suggested in order that future experiments may be set up to yield the optimum in scientific as well as directly applicable engineering information.

Only one law of fatigue, the fatigue life-temperature relationship of equation (15), appears possible, at present, for general application to rubbers and fibers, possibly plastics also. Use of this law to calculate activation energies for the fatigue process has already aided greatly in clarifying the nature of fatigue failure in fibers constituting tire cords. High-temperature relaxation phenomena in thin rubber specimens have been explained quite conclusively on the basis of oxidative scission and cross linking but these concepts have not yet been extended to dynamic fatigue phenomena. The study of all types of fatigue by the use of existing theories such as those of Leaderman and Eyring has been confined mainly to a few fibers and plastics. Further tests of these theories with the object of generalizing them to cover a wider range of high polymers should add much to our knowledge of the mechanism of deformation and rupture as well as the structures of the materials. A rather general law of fatigue for rubbers has been developed in respect to the dependence of fatigue life upon the minimum dynamic strain. Yet the data at hand are insufficient to permit more than the very qualitative explanation on the basis of time effects in



orientation offered in this chapter. Obviously, wide variations in frequency and temperature of fatigue as well as examination of nonrubber polymers would go far in elucidating the important fatigue-strain relationship. The concepts of endurance limit and critical creep stress have been very useful, indeed, in the engineering of plastics, yet it may be necessary to set these practical indexes aside, at least temporarily, in order to pry deeper into the true nature of fatigue in high polymers.

### References

1. Mark, H., *Ind. Eng. Chem.*, **34**, 1343 (1942).
2. Tobolsky, A. V., and Eyring, H., *J. Chem. Phys.*, **11**, 125 (1943).
3. Halsey, G., White, H. J., Jr., and Eyring, H., *Textile Research J.*, **15**, 295 (1945).
4. Burte, H., Halsey, G., and Dillon, J. H., *ibid.*, **18**, 449 (1948).
5. Morris, W. J., and Schnurman, R., *Nature*, **160**, 674 (1947).
6. Sebrell, L. B., and Dinsmore, R. P., *Rubber Chem. and Technol.*, **16**, 857 (1943).
7. Hanson, E. E., and Halverson, G., *J. Am. Chem. Soc.*, **70**, 779 (1948).
8. Sisson, W. A., in Ott, E., ed., *Cellulose and Cellulose Derivatives*. Interscience, New York, 1943, Chapter III-A.
9. Baker, W. O., and Fuller, C. S., *Ann. N. Y. Acad. Sci.*, **44** (Art. 4), 329 (1943).  
See also Baker, W. O., in Twiss, S., ed., *High Polymers* (Advancing Fronts in Chemistry, Vol. I), Reinhold, New York, 1945, Chapter 8.
10. Ariano, R., *Gomma*, **3**, 31 (1939); *Rubber Chem. and Technol.*, **13**, 92 (1940).
11. Alfrey, T., and Mark, H., *Rubber Chem. and Technol.*, **14**, 525 (1941).
12. Wood, L. A., and Bekkedahl, N., *J. Applied Phys.*, **17**, 362 (1946).
13. Field, J. E., *ibid.*, **12**, 23 (1941).
14. Wildschut, A. J., *ibid.*, **17**, 51 (1946).
15. Hünemörder, H., and Rosbaud, P., *Kautschuk*, **3**, 228 (1927).
16. Gehman, S. D., and Field, J. E., *J. Applied Phys.*, **10**, 564 (1939).
17. Spencer, R. S., and Boyer, R. F., *ibid.*, **17**, 398 (1946).
18. Tobolsky, A. V., Prettyman, I. B., and Dillon, J. H., *ibid.*, **15**, 380 (1944).
19. Lyons, W. J., and Prettyman, I. B., *ibid.*, **19**, 473 (1948).
20. Lewis, W. S., *Textile Research J.*, **17**, 431 (1947).
21. Cooper, L. V., *Ind. Eng. Chem., Anal. Ed.*, **5**, 350 (1933).
22. Lessig, E. T., *ibid.*, **9**, 582 (1937).
23. Havenhill, R. S., *Physics*, **7**, 179 (1936).
24. Gough, V. E., and Parkinson, D., *Trans. Inst. Rubber Ind.*, **17**, 168 (1941).
25. Dillon, J. H., and Gehman, S. D., *India Rubber World*, **115**, No. 1, 61 (1946); No. 2, 217 (1946); *Rubber Chem. and Technol.*, **20**, 827 (1947).
26. Naunton, W. J. S., and Waring, J. R., *Proceedings of the Rubber Technology Conference*, Heffer, Cambridge, 1938, p. 805; *Rubber Chem. and Technol.*, **12**, 332 (1939).
27. Gehman, S. D., Woodford, D. E., and Stambaugh, R. B., *Ind. Eng. Chem.*, **33**, 1032 (1941).
28. Dillon, J. H., Prettyman, I. B., and Hall, G. L., *J. Applied Phys.*, **15**, 309 (1944).
29. Braendle, H. A., and Wiegand, W. B., *ibid.*, **15**, 304 (1944).
30. Wiegand, W. B., and Braendle, H. A., *Ind. Eng. Chem.*, **36**, 699 (1944).
31. Gee, G., and Treloar, L. R. G., *Rubber Chem. and Technol.*, **18**, 707 (1945).

32. Clark, G. L., Kabler, M., Blaker, E., and Ball, J. M., *Ind. Eng. Chem.*, **32**, 1474 (1940). Clark, G. L., Letourneau, R. L., and Ball, J. M., *Rubber Chem. and Technol.*, **14**, 546 (1941).
33. Nolle, A. W., *Doctoral Thesis*, Massachusetts Institute of Technology, 1947.
34. Holt, W. L., *Ind. Eng. Chem.*, **23**, 1471 (1931).
35. Meyer, K. H., von Susich, G., and Valkó, E., *Kolloid-Z.*, **59**, 208 (1932).
36. Busse, W. F., *J. Phys. Chem.*, **36**, 2862 (1932).
37. Kuhn, W., *Kolloid-Z.*, **68**, 2 (1934); **76**, 258 (1936); **87**, 3 (1939).
38. Guth, E., and Mark, H., *Monatsh.*, **65**, 93 (1934).
39. Meyer, K. H., and Ferri, C., *Helv. Chim. Acta*, **18**, 570 (1935).
40. Guth, E., *Kautschuk*, **13**, 201 (1937).
41. Pelzer, H., *Monatsh.*, **71**, 444 (1938).
42. Mooney, M., *J. Applied Phys.*, **11**, 582 (1940).
43. James, H. M., and Guth, E., *Phys. Rev.*, **59**, 111 (1941); *J. Chem. Phys.*, **11**, 455 (1943).
44. Wall, F. T., *J. Phys. Chem.*, **10**, 132, 485 (1942); **11**, 527 (1943).
45. Treloar, L. R. G., *Trans. Faraday Soc.*, **39**, 36, 241 (1943); **40**, 59, 109 (1944); **42**, 83 (1946).
46. Flory, P. J., and Rehner, J., *J. Chem. Phys.*, **11**, 512 (1943).
47. Huggins, M. L., *J. Polymer Research*, **1**, 1 (1946).
48. Anthony, R. L., Caston, R. H., and Guth, E., *J. Phys. Chem.*, **46**, 826 (1942).
49. Treloar, L. R. G., *Trans. Faraday Soc.*, **42**, 83 (1946).
50. Roelig, H., *Rubber Chem. and Technol.*, **12**, 394 (1939).
51. Torrance, P. M., and Peterson, L. C., *India Rubber World*, **80**, 62 (1929).
52. Cooper, L. V., *Ind. Eng. Chem., Anal. Ed.*, **2**, 391 (1930).
53. Neal, A. M., and Northam, A. J., *Ind. Eng. Chem.*, **23**, 1449 (1931).
54. Rainer, E. T., and Gerke, R. H., *Ind. Eng. Chem., Anal. Ed.*, **7**, 368 (1935).
55. Cassie, A. B. D., Jones, M., and Naunton, W. J. S., *Trans. Inst. Rubber Ind.*, **12**, 49 (1936).
56. Springer, A., *Kautschuk*, **19**, 55 (1943); *Rubber Chem. and Technol.*, **18**, 71 (1945).
57. Roberts, G. L., *India Rubber World*, **100**, 31 (1939).
58. Carlton, C. A., and Reinbold, E. B., *ibid.*, **108**, 141 (1943).
59. Breckley, J., *Rubber Age N. Y.*, **53**, 331 (1943).
60. Prettyman, I. B., *Ind. Eng. Chem.*, **36**, 29 (1944).
61. Busse, W. F., *ibid.*, **26**, 1194 (1934).
62. Parkinson, D., and Bloxham, J. L., *Trans. Inst. Rubber Ind.*, **21**, 67 (1945).
63. White, L. M., Ebers, E. S., Schriver, G. E., and Breck, S., *Ind. Eng. Chem.*, **37**, 770 (1945).
- 63a. Cadwell, S. M., Merrill, R. A., Sloman, C. M., and Yost, F. L., *Ind. Eng. Chem., Anal. Ed.*, **12**, 19 (1940).
64. Cadwell, S. M., Merrill, R. A., Sloman, C. M., and Yost, F. L., *Ind. Eng. Chem.*, **33**, 370 (1941).
65. Yost, F. L., *Trans. Am. Soc. Mech. Engrs.*, **65**, 881 (1943).
66. Fielding, J. H., *Ind. Eng. Chem.*, **35**, 1259 (1943).
67. Aken, M. E., Singer, W. E., and Davey, W. P., *ibid.*, **24**, 54 (1932).
68. Gehman, S. D., and Field, J. E., *ibid.*, **32**, 1401 (1940).
69. Aleksandrov, A. P., and Lazurkin, J. S., *Compt. rend. acad. sci. U. R. S. S.*, **45**, 291 (1944); *Rubber Chem. and Technol.*, **19**, 42 (1946).
70. Dillon, J. H., *Trans. Am. Soc. Mech. Engrs.*, **65**, 888 (1943).

71. Newton, R. G., *J. Rubber Research*, **14**, 27, 41 (1945); *Rubber Chem. and Technol.*, **18**, 504 (1945).
72. Crabtree, J., and Kemp, A. R., *Ind. Eng. Chem.*, **38**, 278 (1946).
73. Tobolsky, A. V., and Andrews, R. D., *J. Chem. Phys.*, **13**, 3 (1945).
74. Stern, M. D., and Tobolsky, A. V., *ibid.*, **14**, 93 (1946).
75. Roth, F. L., and Wood, I. A., *J. Applied Phys.*, **15**, 749 (1944).
76. Mooney, M., Wolstenholme, W. E., and Villars, D. S., *ibid.*, **15**, 324 (1944).
77. Andrews, R. D., Tobolsky, A. V., and Hanson, E. E., *ibid.*, **17**, 352 (1946).
78. Winn, H., and Shelton, J. R., *Ind. Eng. Chem.*, **37**, 67 (1945).
79. Mark, H., *Textile Research J.*, **16**, 361 (1946).
80. Dillon, J. H., *ibid.*, **17**, 207 (1947).
81. Hoffman, R. M., *ibid.*, **18**, 141 (1948).
82. Smith, H. DeWitt, *Am. Soc. Testing Materials, Proc.*, **44**, 543 (1944).
83. Fox, K. R., and Schwarz, E. R., *Textile Research*, **11**, 227 (1941).
84. Hamburger, W. J., *Am. Dyestuff Repr.*, **34**, 146P (1945).
85. Meredith, R., *J. Textile Inst.*, **36**, 147T (1945).
86. Harris, M., Mizell, L. R., and Fourn, L., *J. Research Natl. Bur. Standards*, **29**, 73 (1942).
87. Winson, C. G., *J. Textile Inst.*, **23**, 386T (1932).
88. Schiefer, H. F., *Textile Research*, **3**, 505 (1933).
89. Schiefer, H. F., *ibid.*, **3**, 388 (1933).
90. Hansen, A. M., and Fletcher, H. M., *Textile Research J.*, **16**, 571 (1946).
91. Meyer, K. H., and Lotmar, W., *Helv. Chim. Acta*, **19**, 68 (1936).
92. Ballou, J. W., and Silverman, S., *Textile Research*, **14**, 282 (1944); *J. Acoust. Soc. Am.*, **16**, 113 (1944).
93. Ballou, J. W., and Smith, J. C., *J. Applied Phys.*, **20**, 493 (1949).
94. Nolle, A. W., *J. Acoust. Soc. Am.*, **19**, 194 (1947).
95. Lyons, W. J., and Prettyman, I. B., *J. Applied Phys.*, **18**, 586 (1947).
96. Wakeham, H. R. R., Honold, E., and Skau, E. L., *ibid.*, **16**, 388 (1945).
97. Wakeham, H. R. R., and Honold, E., *ibid.*, **17**, 698 (1946).
98. Honold, E., and Wakeham, H. R. R., *Ind. Eng. Chem.*, **40**, 131 (1948).
99. Barratt, T., *J. Textile Inst.*, **13**, 17T (1922).
100. New, G. F., *ibid.*, **13**, 25T (1922).
101. Matthew, J. A., *ibid.*, **13**, 45T (1922).
102. Shorter, S. A., and Hall, W. J., *ibid.*, **14**, 493T (1923).
103. Shorter, S. A., *ibid.*, **15**, 207T (1924).
104. Loasby, G., *ibid.*, **34**, 45P (1943).
105. Peirce, F. T., *ibid.*, **14**, 390T (1923).
106. Smith, H. DeWitt, *ibid.*, **22**, 158T (1931).
107. Smith, H. DeWitt, and Eisenschitz, R., *ibid.*, **22**, 170T (1931).
108. Steinberger, R. L., *Physics*, **5**, 53 (1934); *Textile Research*, **4**, 207, 271 (1934).
109. Steinberger, R. L., *Textile Research*, **6**, 191, 267, 325 (1936); **7**, 83 (1936).
110. Leaderman, H., *Elastic and Creep Properties of Filamentous Materials and Other High Polymers*, Textile Foundation, Washington, D. C., 1943.
111. Glasstone, S., Laidler, K. J., and Eyring, H., *The Theory of Rate Processes*. McGraw-Hill, New York, 1941.
112. Eyring, H., and Halsey, G., *Textile Research J.*, **16**, 13 (1946).
113. Stein, R., Halsey, G., and Eyring, H., *ibid.*, **16**, 53 (1946).

114. Eyring, H., and Halsey, G., *ibid.*, **16**, 124 (1946).
115. Holland, H. D., Halsey, G., and Eyring, H., *ibid.*, **16**, 201 (1946).
116. Halsey, G., and Eyring, H., *ibid.*, **16**, 329 (1946).
117. Eyring, H., and Halsey, G., *ibid.*, **16**, 335 (1946).
118. Katz, S., Halsey, G., and Eyring, H., *ibid.*, **16**, 378 (1946).
119. Reichardt, C. H., Halsey, G., and Eyring, H., *ibid.*, **16**, 382 (1946).
120. Reichardt, C. H., and Eyring, H., *ibid.*, **16**, 635 (1946).
121. Halsey, G., *J. Applied Phys.*, **18**, 1072 (1947).
122. Burte, H., and Halsey, G., *Textile Research J.*, **17**, 465 (1947).
123. Burleigh, E. G., and Wakeham, H. R. R., *ibid.*, **17**, 245 (1947).
124. O'Shaughnessy, M. T., *ibid.*, **18**, 263-286 (1948).
125. Schiefer, H. F., Fourt, L., and Kropf, R. T., *ibid.*, **18**, 89 (1948).
126. Mann, J. C., and Peirce, F. T., *Shirley Institute Memoirs*, **5**, 7 (1926).
127. Midgley, E., and Peirce, F. T., *ibid.*, **5**, 102, 255 (1926).
128. Peirce, F. T., *J. Textile Inst.*, **15**, 207T (1924); **18**, 475T (1927).
129. Karrer, E., Grant, J. N., and Orr, R. S., *Textile Research J.*, **17**, 314 (1947).
130. Hind, J. R., and Speakman, J. B., *J. Textile Inst.*, **36**, 19T (1945).
131. Speakman, J. B., *ibid.*, **17**, 472T (1926).
132. Speakman, J. B., *ibid.*, **38**, 102T (1947).
133. Dillon, J. H., and Prettyman, I. B., *J. Applied Phys.*, **16**, 159 (1945).
134. Lyons, W. J., *ibid.*, **17**, 472 (1946).
135. Morton, W. E., and Permanyer, F., *J. Textile Inst.*, **38**, 54T (1947).
136. Franz, E., and Henning, H. J., *Melliand Textilber.*, **17**, 121 (1936).
137. Hermans, P. H., *Kolloid-Z.*, **108**, 180 (1944).
138. Thomson, R. H. K., and Traill, D., *J. Textile Inst.*, **38**, 43T (1947).
139. Oxley, A. E., *ibid.*, **13**, 54T (1922).
140. Owen A. E., and Oxley, A. E., *ibid.*, **14**, 18T (1923).
141. Owen, A. E., *ibid.*, **14**, 375T (1923).
142. New, G. F., and Gregson, A. L., *ibid.*, **17**, 437T (1926).
143. King, F. W. C., and Truesdale, R., *Textile Recorder*, **40**, No. 481, 88; **41**, No. 482, 86; **41**, No. 483, 99; **41**, No. 484, 105 (1923).
144. Stavely, F. W., and Shepard, N. A., *Ind. Eng. Chem.*, **19**, 296 (1927).
145. Gurney, H. P., and Davis, E. H., *J. Textile Inst.*, **21**, 463T (1930).
146. Castricum, M., U. S. Pat. 1,923,296 (1933).
147. Allen, R. W., and TeGrotenhuis, T. A., U. S. Pat. 2,157,092 (1936).
148. Ray, F., U. S. Pat. 2,235,622 (1941) Mallory, G. D., U. S. Pat. 2,412,524.
149. Lessig, E. T., U. S. Pat. 2,240,505 (1941).
150. Venable, C. S., *ASTM Bull.*, No. 136, 17 (1945).
151. Budd, C. B., and Larrick, L., *ibid.*, No. 136, 19 (1945).
152. Bradshaw, W. H., *ibid.*, No. 136, 13 (1945).
153. Dillon, J. H., *Am. Dyestuff Repr.*, **36**, No. 14, 385P (1947).
154. Busse, W. F., Lessig, E. T., Loughborough, D. L., and Larrick, L., *J. Applied Phys.*, **13**, 715 (1942); **16**, 120 (1945).
155. Scholes, A., *J. Textile Inst.*, **35**, 99P (1944).
156. Larrick, L., *Textile World*, **95**, 107 (1945).
157. Waller, R. C., and Roseveare, W. E., *J. Applied Phys.*, **17**, 482 (1946).
158. Waller, R. C., Bass, K. C., and Roseveare, W. E., *Ind. Eng. Chem.*, **40**, 138 (1948).
159. Meredith, R., and Peirce, F. T., *Shirley Institute Memoirs*, **21**, 115 (1947).

160. Carswell, T. S., and Nason, H. K., *Symposium on Plastics* (Philadelphia District Meeting, Feb. 22-23, 1944), A.S.T.M., Philadelphia, 1944, pp. 22-45.
161. Couzens, E. G., and Wearmouth, W. G., *J. Soc. Chem. Ind. London*, **61**, 69 (May, 1942).
162. Morey, D. R., *Ind. Eng. Chem.*, **37**, 255 (1945).
163. Turner, P. S., and Thomason, R. H., *Modern Plastics*, **23**, 146 (May, 1946); **23**, 155 (July, 1946).
164. Haward, R. N., *Trans. Faraday Soc.*, **38**, 394 (1942); **39**, 267 (1943).
165. Findley, W. N., *Modern Plastics*, **19**, 71 (Aug., 1942); **20**, 99 (March, 1943).
166. Findley, W. N., and Worley, W. T., *ibid.*, **22**, 143 (June, 1945).
167. Findley, W. N., *Symposium on Plastics*. (Philadelphia District Meeting, Feb. 22-23, 1944), A.S.T.M., Philadelphia, 1944, pp. 118-134.
168. Findley, W. N., *Modern Plastics*, **25**, 145 (Dec., 1947).
169. Telfair, D., Carswell, T. S., and Nason, H. K., *ibid.*, **21**, 137 (Feb., 1944).
170. Chasman, B., *ibid.*, **21**, 145 (Feb., 1944).
171. Gailus, W. J., and Telfair, D., *ibid.*, **22**, 149 (May, 1945).
172. Leaderman, H., *J. Applied Mechanics*, **6**, 79A (1939).
173. Leaderman, H., *Ind. Eng. Chem.*, **35**, 374 (1943).
174. Aiken, W., Alfrey, T., Jaussen, A., and Mark, H., *J. Polymer Sci.*, **2**, 178 (1948).
175. Alfrey, T., *The Mechanical Behavior of High Polymers*. Interscience, New York, 1948.
176. Robinson, H. A., Ruggy, R., and Slantz, E., *J. Applied Phys.*, **15**, 343 (1944).
177. Lazan, B. J., *Modern Plastics*, **20**, 83 (Nov., 1942).
178. Rinehart, J. S., *J. Applied Phys.*, **12**, 811 (1941).
179. Lazan, B. J., and Yorgiadis, A., *Symposium on Plastics*. (Philadelphia District Meeting, Feb. 22-23, 1944), A.S.T.M., Philadelphia, 1944, pp. 66-90.
180. Findley, W. N., and Hintz, O. E., Jr., *Modern Plastics*, **21**, 119 (Dec., 1943).
181. Tobolsky, A. V., *private communication*.
182. Telfair, D., Adams, C. H., and Mohrman, H. W., *Modern Plastics*, **24**, 151 (May, 1947).
183. Oberg, T. P., Schwartz, R. T., and Shinn, D. A., *ibid.*, **20**, 87 (April, 1943).
184. Findley, W. T., *Am. Soc. Testing Materials, Proc.*, **45**, 878 (1945).
185. Duggan, F. W., and Fligor, K. K., *Ind. Eng. Chem.*, **35**, 172 (1943).
186. Sookne, A. M., and Harris, M., *Textile Research*, **13**, 17 (1943).
187. Sookne, A. M., and Harris, M., *Ind. Eng. Chem.*, **37**, 478 (1945).
188. Spurlin, H. M., *ibid.*, **30**, 538 (1938).

# FLOTATION

STRATHMORE R. B. COOKE

*University of Minnesota School of Mines and Metallurgy*

---

I. Introduction.....	321
II. Colloid Production in Grinding.....	323
III. Flotation Reagents.....	324
1. Frothers.....	325
Two-Phase Systems.....	325
Structure of Frothers.....	328
Three-Phase Systems.....	330
Aeration.....	331
Frothers in Practice.....	334
2. Collectors.....	336
Mechanism of Collection.....	338
Orientation of the Collector Coating on the Mineral.....	346
Effect of Slimes on Collection.....	347
Flocculation and Collection.....	353
Classification of Flotation Collectors.....	354
3. Activators.....	357
4. Depressants.....	368
References.....	372

---

## I. Introduction

Flotation is one of the most recently devised methods for the concentration of minerals, but it leads all other concentrating processes in tonnage of material treated. Because of the early development of flotation under the strains of industrial needs and empirical experimentation, flotation theory has lagged behind technological application, and even today, pragmatically speaking, flotation is more of an art than a science. In recent years, however, a number of noteworthy attempts have been made in an endeavor to discover the fundamental principles underlying the process, and this chapter is a résumé of the more recent important contributions to our understanding of the field.

Flotation is a specialized method of gravity concentration, whereby certain minerals are rendered of lower specific gravity than water by modifi-

cation of their surfaces by chemical processes, and by the subsequent attachment of air bubbles. The air bubbles so lighten the mineral particles that they are "rafted" to the surface of the fluid and are removed as a concentrate. Associated and undesirable minerals, either by correct choice of reagent or by addition of specific reagent, remain hydrophile and are removed with the body of the fluid as a tailing product.

Necessarily ores are reduced to some size approximating the "size of liberation" before concentration. This is that size at which the valuable mineral is mechanically freed from the worthless constituents (gangue). Achievement of the precise size of liberation is rarely necessary for successful concentration by flotation, for under the proper conditions an exposed mineral particle physically locked with gangue is capable of attaching itself to an air bubble, and will normally appear in the concentrate as a "middling" grain. The greater the amount of middling in the concentrate, the lower the grade of that product so that the fineness to which the ore should be ground becomes a matter of economics.

The mineral dressing engineer could very well dispense with colloidal particles produced from the ore, and as will be described later, the usual size range through which froth flotation is successful is from about 400 to about 1 micron. If we accept the upper limit of particle size of a colloidal dispersion as 0.5 micron, it can be seen that flotation utilizes material just without the colloidal range as conventionally defined. Nevertheless, because there is no natural line of demarcation between the range of coarse dispersions and that of colloidal dispersions, the two merging insensibly into each other, in flotation there are systems analogous to sols (solid-in-liquid), emulsions (liquid-in-liquid), and froths or foams (gas-in-liquid). Further, ore grinds correspond to hydrosol systems; and the flocculated system is the analog of the colloidal hydrogel. Surface energy and surface properties play an important part, for the surface per cubic centimeter of mineral ranges from 150 to 60,000 square centimeters or more. The situation is complicated by admixture of true colloids contributed by the ore and by the engineer in controlling the mineral separation.

As froth flotation can be employed only in sizes finer than 300 or 400 microns (about 35 or 48 mesh), and as overgrinding of soft minerals is undesirable, stage comminution is employed, involving coarse crushing, fine crushing, and grinding, the last step being performed in revolving cylinder mills operating in closed circuit with sizing devices such as classifiers. In the final stage of size reduction, reagents are frequently added to the ore pulp for control of the chemical conditions, and it is here that colloid phenomena become important. Subsequent treatment involves fur-

ther chemical conditioning of the pulp before it is admitted to the flotation cells for separation and removal of concentrate and tailing.

## II. Colloid Production in Grinding

As the presence of colloidal and of very fine particles may materially affect flotation performance, some consideration should be given to the ability of a cylinder mill to produce such material. Weinig (76) is of the opinion that the lower limit of an ore grind is about one micron, and he designates material finer than this as colloidal material, *i.e.*, material which does not settle out after a sedimentation balance has reached substantially constant weight. Any material finer than one micron which occurs in the ground pulp is ascribed to the physical liberation of naturally occurring colloids within the ore itself, known as primary slimes. Bond and Maxson (9), on the basis of an extensive investigation of the grinding of ores, come to substantially the same conclusion and place the limit of the ore grind at approximately 0.8 micron, stating that "determinations show that most of the clayey material in an ore is released by crushing to about minus 10 mesh, and further grinding, even all through 200 mesh, results in the production of little or no additional colloidal material."

On the other hand, Gaudin (33) is of the opinion that the finest particles resulting from comminution are of the order of 0.001 micron, that is, of the order of size of the unit crystal, and the application of Gaudin's equation would certainly indicate extension of an ore grind to very fine sizes. However, the relative quantity of such fine material (secondary slimes) must be very small, and it is safe to assert that the ordinary ore grind, involving the comminution through 100 or 200 mesh (149 and 74 microns, respectively), produces negligible quantities of colloidal material other than freeing that which is inherent to the ore. The importance of the amount of primary slimes in an ore is demonstrated by an example from a recent paper by Gaudin and Preller (37). These investigators determined the specific surfaces of Morenci tailing, feed, and concentrate to be, respectively, 4.047, 4.069, and 0.976 square meters per grams, *i.e.*, the specific surface of the concentrate is approximately only one-quarter of that of the tailing. A screen analysis of the concentrate and tailing gave the following results:

Mesh	Tailing	Concentrate
Minus 100, per cent. ....	77.5. ....	95
Minus 200, per cent. ....	59.0. ....	69

As the tailing has more coarse material than the concentrate, the greater specific surface of the former must be due to the presence of very consider-



able quantities of primary slimes, liberated in grinding and largely rejected by the concentrate during the roughing and cleaning stages of flotation. Products from other ores exhibit the same phenomenon.

This primary slime can be, in many cases, highly detrimental to flotation, and occasionally it is necessary to remove it by desliming prior to flotation, even though such a procedure involves considerable economic loss. Such colloidal material shows a high  $\text{Al}_2\text{O}_3$  to  $\text{SiO}_2$  ratio, indicating the presence of minerals such as kaolin, talc, sericite, and aluminum hydroxide, and frequently high iron, indicative of ferric hydroxide. Substances of this nature, possessing large surface area, may cause high reagent consumption by adsorption or chemical reaction, depression of minerals by closure of surface, or they may adversely affect frothing. Difficulties of this kind frequently accompany the flotation of ores derived from near-surface ore deposits, and from the oxidized and enriched zones of an ore body, for it is in these places that minerals possessing colloidal properties are formed in abundance.

A secondary, but no less important effect resulting from the treatment of oxidized ores is the liberation of heavy-metal ions and of anions during grinding. Cations may cause undesirable activation of some minerals; their reaction with anions may cause precipitation of colloidal hydroxides; they will precipitate collector ions and prevent their proper function; and anions will undesirably activate gangue minerals. For these reasons, and others, flotation is today performed almost universally in circuits made alkaline with lime or sodium carbonate. Additions of these reagents frequently are made to the ore fed to the cylinder mill so that precipitation of the offending ions is effected at the earliest possible moment. Another reason for the early addition of alkali is its protective effect on cyanide ion, often used in preferential flotation. Cyanide ion is destroyed by heavy-metal cations and by acids resulting from the oxidation of sulfide minerals.

Another unfortunate effect of grinding, practically unavoidable under present conditions, is the overgrinding of the relatively softer sulfide minerals. As will be pointed out later, extremely fine sulfide particles do not respond readily to flotation.

### III. Flotation Reagents

Reagents are those substances added to the pulp to modify or control the chemical conditions and so enhance the selectivity of the process. Many substances so added serve dual purposes, but the simplest classification is as follows: *frothers*, *collectors*, *activators*, and *depressants*.

In froth flotation it is essential to create a large air-water interfacial area, and frothing agents are used for this purpose. They are not employed in agglomerate tabling, however, for in this case the natural air-water surface is large enough to permit efficient separation of aerophilic from hydrophilic minerals.

Collecting agents are used to create the aerophilic surface on minerals, this serving as a bond between the mineral proper and the air bubble. Modern flotation practice is almost entirely dependent on the use of the so-called "chemical collectors," as contrasted with the earlier use of "oily" collectors.

Some minerals do not respond to collection unless their surfaces are first modified by resurfacing or in some other manner. Reagents that form a bond between the mineral surface and the collector ions are known as activators. In a sense, depressants function in the converse manner; that is, they so modify the chemical atmosphere of the ore pulp that collector ions either cannot attach themselves to specified mineral surfaces, or, should they become attached, they cannot function as collectors.

### ***1. Frothers***

#### *Two-Phase Systems*

If a container half full of a pure liquid is vigorously shaken, it will be noticed that the entrapped air rises as bubbles, which on reaching the surface of the liquid collapse almost instantaneously. If a small quantity of frother is added to the liquid and shaken, a change is immediately manifested; first, the life period of the bubbles at the surface is greatly increased, so that an appreciable depth of froth is formed; second, the dispersion or state of subdivision of the individual bubbles is greatly increased, attributable to the lowered surface tension. Further additions of frother continue to increase the froth depth and to decrease the size of the most stable bubbles, but it will be noted that at the air-froth interface the bubbles collapse and coalesce. At a certain concentration of frother the froth depth will reach a maximum, and froth coalescence will be at a minimum. Addition of frother beyond this point causes a lowering of froth depth, and vigorous bubble collapse, accompanied by "showering" or the formation of a fine spray over the froth surface. The relationship between frother concentration and resulting froth stability is shown qualitatively in Figure 1.

It should be noted that froth production is accompanied by a large increase in surface area, which, allowing for the decrease in surface tension,

necessarily implies an increase in total surface-free energy. Froth systems are therefore inherently unstable.

Explanation of the phenomena described above is based in part upon the concentration of the frother at the air-water interface. The adsorption is expressed, at equilibrium, by the Gibbs equation:

$$a = -(c/RT)(dt/dc)$$

in which  $a$  is the amount of solute adsorbed or concentrated per square centimeter of surface,  $c$  is the concentration of solute in moles per liter,  $R$

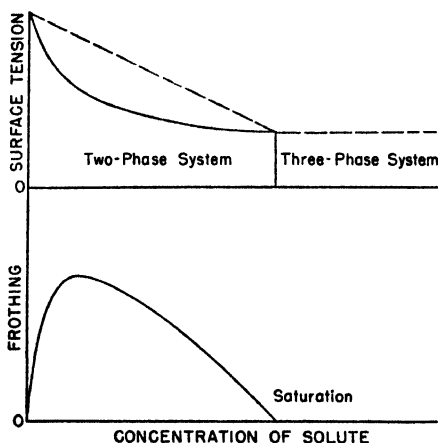


Fig. 1. Surface tension and frothing of aqueous solutions (33).

is the gas constant, and  $T$  is the temperature in degrees Kelvin. For ionized solutes, the dissociation constant  $i$  appears in the equation.

For positively adsorbed solutes such as those used as frothers in flotation,  $dt/dc$  is negative, as may be seen from Figure 2, in which the surface tension-concentration curve for butyric acid is given.

The surface tensions of most salt solutions are greater than the surface tension of pure water, and inspection of the Gibbs equation shows that the salt ions must be negatively adsorbed. Stating this another way, the water is positively adsorbed at the surfaces of such solutions;  $dt/dc$  is negative, as is shown by the surface tension-concentration curve for calcium chloride.

Taggart and Gaudin (60) have shown that maximum frothing occurs at approximately that concentration of the solute at which  $dt/dc$  is changing most rapidly, and Figure 1 illustrates this.

The most rational explanation of the stability of froths involves both surface tension (or surface free energy) changes, and adsorption of the solute. As has been mentioned, in the case of organic solutes a marked lowering of surface tension occurs with increase in bulk concentration. When an air bubble is formed in an aqueous solution of such a substance, new surface is created. By diffusion the solute molecules will distribute themselves in this surface, and the bubble will attain equilibrium. If the equilibrium is now disturbed by a force tending to increase the total surface of the bubble, there will be dilution of the solute in the interface by water molecules, and the surface tension will rise. This increase in surface

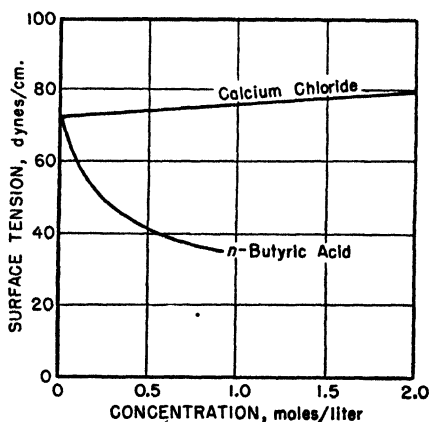


Fig. 2. Relation between surface tension and solute concentration.

tension acts as a restoring force, which resists that force increasing the bubble surface, and the result is that the bubble adjusts itself to the new conditions. Too rapid application of the externally applied force, however, will result in rupture, for diffusion in the liquid state is rather slow. Conversely, any force tending to reduce surface area favors stability, for then solute molecules diffuse from the bulk of the solution to the interface and the surface free energy is thereby diminished. High solute vapor pressure will lower froth stability, but the effect is negligible in flotation. High viscosity favors froth stability, but the small amount of frother used in practice has no noticeable effect on film viscosity. However, the effect of increase in viscosity can be employed in a very practical way. When a froth column in a flotation cell tends to instability by showering and dropping its mineral load, a froth stiffener is added, usually in the form of a creosote oil. Presumably such substances are forced into the

surface film by mutual solubility with the frother molecules. The froth stiffening ability of collector-coated mineral particles will be discussed later under "Three-Phase Systems."

### *Structure of Frothers*

Pure saturated hydrocarbon oils do not spread at the surface of water. Oils that possess an active group in the molecule will spread to form layers one molecule thick. This spreading of polar nonpolar substances was shown by Langmuir (44) to be due to orientation of the solute molecules in the air-water interface, with the hydrophilic group in the molecule immersed in the water phase, and the hydrophobic carbon chain directed to the gas phase.

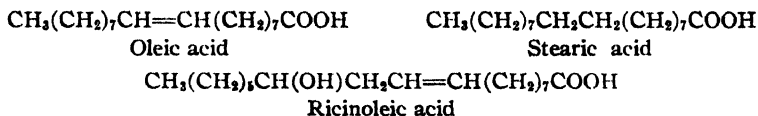
Taggart (63) has made a remarkably complete investigation of the relationship between chemical constitution and frothing ability in respect to a large number of organic compounds. For substances to possess frothing ability in the absence of collecting property, Taggart says (63):

... a reagent should contain an oxygen-bearing water-avid group. Preferably OH, COOH, CO, or COO(COOR) and preferably, also, one such group only. The amide (CONH<sub>2</sub>) group will serve as the water-avid group, but appears in many substances to have a harmful effect on collecting and should, therefore, be avoided. Attached to the oxygen-bearing group there should be a structure composed of carbon and hydrogen atoms, containing preferably at least six carbon atoms that are not directly attached to the oxygen-bearing group. There must be appreciable solubility but the solubility rating should preferably be "slight"; *i.e.*, around 1000 mg. per liter, although many more soluble substances are satisfactory frothers.

Elsewhere (66) Taggart states that in alkyl compounds the solubilizing effect of the water-avid groups is COOH > NH<sub>2</sub> > OH > CO; in aryl compounds the order is OH > NH<sub>2</sub> > CO > COOH. In any homologous series the length of the chain has a marked effect on the frothing ability. The short-chain members are highly soluble and are poor frothers. With increase in chain length, frothing reaches a maximum, then declines, for with long chains and with the polar groups listed above, the secondary valence characteristics are so masked that the compounds become practically water-insoluble, and adsorption is minimized. Two or more water-avid groups decrease or entirely prevent frothing ability, the effect depending to some extent on the position and relative polarities of the competing groups. Glycerol is a poor frother, and all three hydroxyl groups probably lie in the aqueous phase for those molecules that are adsorbed, with the chain lying parallel to the surface. The four oxygen-bearing groups of pentaerythritol tetrapalmitate lie in the water phase on being

adsorbed, and it is evident that, in spite of the blocking effect of the palmitate chains, the cohesional forces must be large enough to materially distort the structure of the solute.

An unsaturated bond increases water avidity. Oleic acid is strongly adsorbed at a water surface, and Devaux (21) has shown that molecules of this substance are attached to the aqueous phase by both the carboxyl group and by the double bond. In this case the presence of two polar groups in the molecule markedly favors the frothing ability of the substance, which is widely used in nonsulfide flotation, because stearic acid, the saturated analog of oleic acid, is a poor frother and is but slightly soluble in water. Introduction of a third polar bond into the oleic acid structure, as in ricinoleic acid, causes the molecule to lie almost flat on the surface of the water, and frothing ability is very poor. On the other hand,



the alkali metal salts of most of the normal alkyl carboxylic acids are powerful frothers and collectors due to their ready ionization in water and the liberation of anions, which adsorb at the water-air interface and at the mineral-water interface. Harris (19), by utilizing hydrophilic groups having much greater water avidity than those mentioned above, has successfully balanced very long hydrophobic groups, and has made a number of compounds, which possess many desirable properties, particularly that of functioning as frothers without accompanying collection of the mineral. As an example, cetyl alcohol,  $\text{CH}_3(\text{CH}_2)_{14}\text{OH}$ , is too insoluble to be a frother. By replacing the hydroxyl group by more strongly polar groups, compounds are obtained that are highly surface active, and which, from work by Dean (20) and his colleagues, appear to have useful applications in flotation. Thus cetyl hydrogen sulfate and cetyl sulfonic acid are unaffected by the presence of alkaline earth metal salts in solution, and function well as frothers in either acid or alkaline pulps. Their frothing characteristics may be modified by oils such as kerosene. Some of these compounds are interesting in that they possess complex polar groupings, such as phosphate, sulfoacetate, and glycolate.

Certain mixtures of frothing agents behave as if the substances were mutually antagonistic. Thus sodium oleate or stearate in the presence of a small amount of the commercial detergent Dreft (the sodium salt of a long-chain alkyl sulfate,  $\text{RCH}_2\text{OSO}_3\text{Na}$ ) produce their characteristic froths. Likewise, the presence of a small quantity of oleate or stearate does not

hinder the production of froth when the organic sulfate is in excess. With intermediate quantities of both substances in solution, no froth is produced. Coghill and Clemmer (15) remarked on the same phenomenon when certain mixtures of pine oil and soap were used in nonsulfide mineral flotation, saying: "If colloid chemists have tested the frothing properties of mixtures of pine oil and soap, they must have reported that in certain ratios these reagents are incompatible. When a dilute soap solution is shaken in a test tube in the presence of an increasing amount of pine oil, its sudsing proclivities gradually disappear until no froth can be formed by shaking. With an excess of pine oil a froth again appears." Wark (72) and Bartsch (6) have both commented on this effect, which Bartsch ascribes to mutual lowering of solubility. An investigation by the writer indicates that, in the case of the incompatibility of pine oil and sodium oleate, it is due to emulsification of the pine oil by oleate ions. If pine oil is added to an agitated and frothing solution of sodium oleate, the froth diminishes because oleate ion is being abstracted to stabilize the freshly forming pine oil emulsion. At certain relative concentrations of pine oil and oleate ion, no free oleate is available to form a frothing system, and the froth collapses. Further addition of pine oil now results in the formation of the normal pine oil froth. Such an explanation does not seem applicable to the incompatibility of sodium oleate and Dreft. The subject has some importance because mixture of frothers are sometimes used, particularly in the flotation of nonsulfide minerals.

### *Three-Phase Systems*

Three-phase frothing systems may consist of two mutually immiscible liquids and a gas phase (Fig. 1) or of solid, liquid, and gas. The first type is of little importance in flotation, for frothers are rarely added in such quantity, except accidentally, that their solubility in water is exceeded. Sometimes two liquid phases are formed when an insoluble oil is added, but nothing is known about the characteristics of such a system.

The second type represents normal operating practice, and the presence of quantities of water-repellent collector-coated mineral particles profoundly modifies froth stability. This may be demonstrated readily by shaking fine particles of galena in a test tube with a dilute solution of potassium ethyl xanthate. It is found that a very stable froth is formed, consisting of air bubbles heavily armored with the galena. Now short-chain xanthates have practically no effect on the surface tension of water, particularly in the small concentrations used in flotation, and as it may be readily shown that a dilute solution of such a compound is incapable of pro-

ducing a froth, the stable froth produced in the presence of galena is obviously not due to adsorption of xanthate at the water surface. On the other hand, *clean*, that is, unoiled or uncoated galena particles in pure water are incapable of producing a froth. The explanation is that the galena is rendered aerophilic by the xanthate and upon being shaken adheres tenaciously to the air-water interface. Because of the resistance to movement effected by the keying action of the galena particles, a phenomenon akin to viscosity, the bubbles resist externally imposed strains and the froth is stabilized. In fact, as the solid particles lack diffusivity and cannot evaporate, such froths are inherently much more stable than those produced with soluble frothing agents. The presence of freely floating mineral particles, then, stabilizes froths and as would be expected reduces the quantity of organic frother required in the circuit.

In the case of a normally operating flotation cell, the intercellular liquid of the froth also contains hydrophilic gangue particles, which resist flow and thereby increase froth stability. Obviously, if the froth is too rigid, these gangue particles cannot drain into the machine and the concentrates will be contaminated and of low grade. Under these conditions froth modification or change of frother is necessary. The reverse phenomenon, that of a brittle, poorly mineralized froth, is due either to insufficient stiffness in the froth, corrected, as already mentioned, by addition of a froth stiffener, or to inadequate collection. Either way, remedial steps must be taken, because a weak froth will yield a concentrate high in grade but representing a poor recovery.

Fine material, especially naturally occurring colloidal material from an ore, adversely affects frothing by causing overfrothing, a condition characterized by the production of copious quantities of large bubbles carrying little of the mineral which it is desired to float. This effect is due to colloids of high surface activity closing the air-water interface to occupancy by the mineral. Addition of too much soap or alkali in soap flotation will similarly cause surface closure by solid or micellar soap. Gelatin and saponin apparently cause the same effect, although it is questionable whether the depression of collected sulfides by gelatin is due to this or to the reciprocal effect of mineral surface closure by a film of hydrophilic colloid.

### *Aeration*

Flotation in modern cells requires delivery of large quantities of air to the pulp, upward of 1000 cu. ft. per cubic foot of solids floated. This delivery is performed in two types of machine: (a) pneumatic machines, in which air bubbles are formed by blowing air through the pores of a sep-



tum or by dispersion in the pulp by an air lift, and (b) subaeration machines in which dispersion of air bubbles in the pulp is effected by mechanically beating a stream of air with an impeller. For an enlightening discussion of the role played by aeration in flotation the reader is referred to papers by Rose (55) and Fahrenwald (24).

The effect of composition of the gas phase on affecting contact with the collector-coated mineral has been investigated by Wark and Cox (69), who found that air, oxygen, hydrogen, nitrogen, and carbon dioxide all gave the same angle of contact with xanthate-coated mineral surfaces.

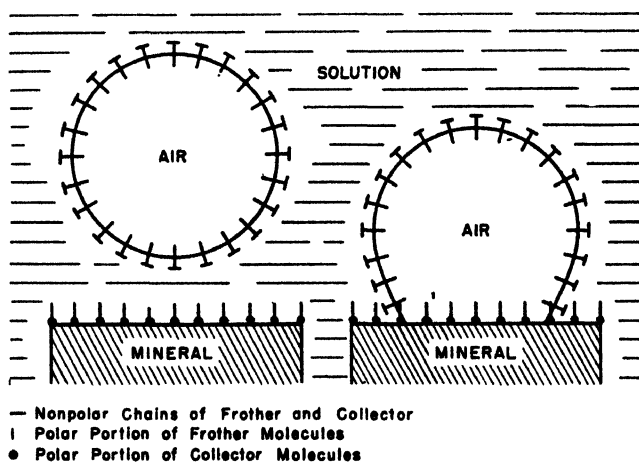


Fig. 3. Distribution of frother and collector ions.

Sulfur dioxide gave a markedly lower angle of contact than the other gases mentioned, but it seems probable that this was due to decomposition of the xanthate by the highly acid solution. This independence of contact angle with gas composition is surprising in view of Adams' (1) work, which showed that the floatability of a mineral depended on the nature of the gas, and in the light of adsorption experiments with platinum and charcoal, which show that the amount of adsorption depends greatly on this variable. In fact Dean (17) developed a theory of flotation based on differential gas adsorption. While the subject has little more than academic interest in view of the universal use of air in practice, it requires further investigation.

The influence of the adsorbed solutes at the gas-water interface on contact of the gas phase with the mineral surface is not well understood. Hysteresis, in establishing contact in the presence of a collector only, is at-

tributed by Wark (72) to the necessity of squeezing adsorbed collector ions away from the contacting air-water surface, and he remarks that if a frother is present too, the ease of making contact will be still further decreased, as shown in Figure 3.

However, in a recent paper Taggart (67) has pointed out that an air bubble failed to make contact with a sphalerite surface immersed in a potassium ethyl xanthate solution even after 60 minutes of exposure to the bubble, but that addition of cresol caused contact to be immediately established. This is a decrease in induction period of at least 3600 to 1, and in his words:

The undissolved cresol in this case was the key to the difference in induction times. It coated the test bubble with a film of oily liquid. The contact to be established was then between this and the xanthated particle. It has been observed many times that the wetting of a xanthated particle with a droplet of oil is much more rapid than with a bubble of air. In the absence of undissolved oil, the effect of the frother, while still noticeable, is nowhere near so great.

Taggart goes on to point out that the oil used in underground mining alone will range from 0.04 to 0.06 lb. per ton of ore, and that:

This oil, in the presence of a frother agent spreads over the bubbles in the bubble column and is the effective phase to which bubble attachment is made.

It seems difficult to picture the mechanism whereby this contact of air and collector-coated mineral is accelerated. If there is a Gibbs adsorption film on the bubble, surface contact should be hindered until by diffusion or squeezing the solute molecules are removed from the contacting surfaces. Possibly it is due to emulsified droplets of oil smearing the collector-coated mineral, but in the presence of a heteropolar substance, such as cresol, the droplets should be armored with water-avid hydroxyl groups. It is interesting to note that Barsky and Falconer (4), using an independent method for determining displacement pressure of one liquid over another, came to the conclusion that collecting agents favor wetting of the collector-coated mineral surface by pine oil, with the inference that wetting by this substance is a *sine qua non* for floatability. Likewise Christmann (10) postulates mutual dependence of collector and frother in effecting flotation. Wark (72) specifically denies this function of a frother, pointing out that all his contact angle measurements were made in the absence of frothing agents. However, he notes that in supersaturated solutions of air in water, air will be precipitated on xanthate-coated galena when it is not precipitated on clean galena. As extraordinary precautions must be taken in contact angle work to prevent contamination of specimens

by oily or greasy particles suspended in air, the lack of such contamination in air, which is blown into a captive bubble, must be questioned. If Taggart's interpretation of his experimental work is correct, a trace of oil in the air bubble would cause immediate contact.

Elsewhere (66) Taggart in discussing the use of neutral oils as collectors with soaps says:

Quantity of oil must be kept down to such an amount that the film is less than about 4 molecules in thickness; below this thickness the layer, on a solid surface, has the characteristics of a solid, above it the characteristics are those of a liquid, and gas bubbles will neither precipitate at nor adhere to a liquid oil-water interface.

The physical principles governing bubble attachment to aerophilic surfaces and the wetting of hydrophilic surfaces are well understood and the reader is referred to Taggart (66), Gaudin (33), Wark (72), and Coghill and Anderson (14).

In a special flotation process known as agglomerate tabling or table flotation, frothing agents are not used. Only certain deslimed mineral associations can be concentrated by this method, which consists of mixing a collector and nonpolar oil into a thick pulp of the sandy material. The mineral that is to be floated becomes coated with the collector ion and this surface is in turn smeared with a highly water-repellent coating of the oil. The associated gangue mineral remains water avid. The pulp is fed to a shaking table or to a conveyor belt, this mechanical act entrapping air bubbles, which become heavily armored with the oiled mineral particles. The entrapped air lowers the specific gravity of the agglomerated and oiled particles so that they float on the surface of the water and pass as a concentrate over the side of the shaking table or over the edge of the conveyor. The unoled and unagglomerated minerals remain submerged in the water and are discharged as a tailing.

### *Frothers in Practice*

For practical purposes, authorities are agreed on the following desirable properties for a frother: (1) They should lack collecting properties. (2) Their range of water solubility should be limited, Gaudin giving the limits of from 0.2 to 5 mg. per liter. (3) Their cost must be reasonably low.

The most commonly used frothers are pine oil, cresylic acid, the soaps, and synthetic alcohols.

Pine oil is a complex mixture of the following approximate composition (8):

Tertiary alcohols (chiefly terpineol).....	55-65%
Secondary alcohols (borneol and fenchyl alcohols).....	10-20%
Hydrocarbons (monocyclic terpenes such as dipentene, etc.)...	10-20%
Ethers (anethole and estragole).....	5-10%
Ketones (camphor).....	5-10%

Bishop points out that the double bond in terpineol plays an important role in the frothing ability of the compound and that the saturated equivalent of terpineol, dihydroterpineol, is a poorer frother. The ether and keto groupings in the other compounds confer frothability, but the weakly water-avid double bonds in the unsaturated hydrocarbons do not make these very active frothers.

Pine oil is probably the most widely used frother in practice, possessing practically no collecting power for most sulfide and nonsulfide minerals. Eucalyptus oil is used as a substitute for pine oil when economic considerations so dictate. During the war synthetic pine oil was used extensively in place of the extracted oil.

Cresylic acid consists of a mixture of three isomeric cresols, the six xylenols, and of higher homologs, but contains no phenol. Coal tar cresylic acid contains only small quantities of neutral oils and sulfur compounds, but petroleum cresylic acid contains more sulfur in the form of thiophenol and thiocresols (7). Such compounds, carrying an active thio alcohol grouping, confer on the frother the undesirable function of being a weak sulfide-mineral collector. Cresylic acid gives a more brittle froth than pine oil, although the froth will carry more gangue, and it is widely used in the flotation of galena and of the copper sulfides and the copper-iron sulfide minerals.

Soaps are extensively employed in nonsulfide mineral flotation, primarily as collectors, secondarily as frothers, although this dual function is undesirable. Soap froths are temperamental and are usually modified by the simultaneous addition of frothers such as pine oil or the synthetic alcohols. Commonly used soaps are the alkali metal salts (usually sodium) of oleic, palmitic, and fish oil carboxylic acids. At Anaconda rhodochrosite is floated with a mixture of the sodium salts of linoleic, oleic, and palmitic acids prepared from cottonseed oil foots. Mixtures of fatty and resin acid soaps derived from sulfate paper mill liquors are attractive from the point of low cost. They contain abietic acid and its derivatives.

The synthetic aliphatic alcohols are coming into wide practical use because of their closely controlled composition and reproducible frothing characteristics. Average molecular weights of these frothers, which contain not only primary and secondary alcohols, but also ketones and esters,

range from 100–150. An interesting suggested application is the use of esters as frothers, for by slow hydrolysis, frothing can be maintained in a series of flotation cells without exhaustion of frother.

The amount of frother used in practice depends on local conditions, but normally lies somewhere in the range of 0.01 to 0.25 lb. per ton of ore. Rose (54) points out that in one plant at least frother concentration may be extremely critical and that:

In some parts of the circuit at least a change of as little as one one-thousandth of a pound of frother per ton of ore, in either direction, will give a measurable difference in assay. This is perhaps true in many plants.

## 2. Collectors

Froth flotation of mineral particles is dependent upon their attachment to air bubbles, the net buoyancy resulting in their being rafted to the surface of the fluid pulp. Reagents, added to the pulp for the purpose of creating surface conditions on the particles such that they become attachable to air bubbles, are called collecting agents or collectors.

Much of the recent theory of collection is based upon experimental work employing the "captive bubble" method (63,69). In this procedure a clean mineral surface is immersed in an aqueous solution of the reagent to be tested, and an air bubble is presented to the mineral. In the absence of contact between air and mineral, the angle of contact is zero (Fig. 4), and the work done by the system ( $W$ ) is zero, according to the equation:

$$W = Twa(1 - \cos \theta)$$

In this equation, as Wark (72) has shown, the work done is a measure of tenacity of adhesion, or in other words it is a criterion of the floatability of the mineral.  $Twa$  is the surface free energy of an air–water interface and  $\theta$  is the angle of contact between the mineral surface and the air bubble measured through the water phase. Obviously, with  $\theta = 0^\circ$ ,  $W$  is zero, and under these conditions the mineral is not floatable. For a finite value of  $\theta$ , work is done by the system, and the mineral is floatable. Figure 5 shows contact between an air bubble and a polished surface of galena in a solution of potassium ethyl xanthate.

By observation of the contact between air bubbles and mineral surfaces under a wide variety of solution conditions, Wark and his co-workers have made significant contributions to the knowledge of many phases of flotation theory.

For small values of  $\theta$  (less than approximately  $10^\circ$ ) the method is insensitive, primarily because of the difficulty of measuring such small angles

under the prevailing conditions. Reference to this method and to results obtained by its employment will be made in the succeeding pages.

It is claimed that certain minerals possess an inherent floatability (28, 33) and this statement is certainly true with respect to naturally occurring hydrocarbons (which, being composed of nonpolar hydrocarbons would naturally be water-repellent) and perhaps to soft coals. The easy floatability of naturally occurring sulfur and graphite poses another problem, for whereas Taggart and his associates (65) found that progressive purification of both these substances leads to decreasing floatability, attributing this phenomenon to oily contamination, Wark and his co-workers (71,72)

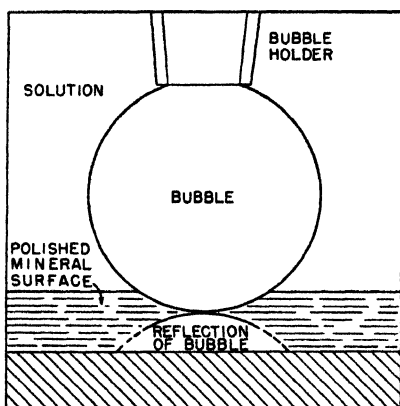


Fig. 4. Lack of contact of air bubble at a sphalerite surface in a dilute potassium ethyl xanthate solution.

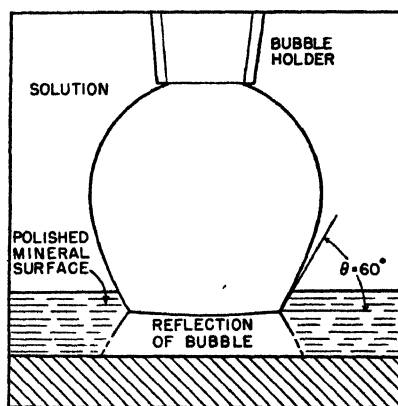


Fig. 5. Contact of air bubble on polished galena surface in a dilute potassium ethyl xanthate solution.

disagree with both their theory and their experimental results. Molybdenite, graphite, and cinnabar are often quoted as minerals that possess inherent floatability. This property may be due to their unusual lattice structures permitting adsorption of nonpolar impurities. However, all investigators agree that under adequately controlled conditions, hydrophilic surfaces of sulfide minerals can be prepared. Unfortunately it is difficult to prevent such surfaces from being almost immediately contaminated by impurities. Even a brief exposure of a freshly prepared hydrophilic sulfide mineral surface to air leads to a measurable contact angle when the specimen is immersed in water and a bubble is presented. Further, any contamination in the water interface may be dragged in with the specimen and may vitiate the results. As this is the case, it is obvious

that mineral particles may readily be soiled by the grease or oil-bearing atmosphere of a mine or a mill.

The chemical atmosphere of an ore pulp is an important variable, one which has led to difficulty in extrapolation from laboratory experiments to plant-scale practice. In the laboratory, contact angle experiments are conducted under carefully controlled conditions in which distilled water and reagents of the highest purity are employed. In practice, flotation pulps carry not only cations (such as  $H^+$ ,  $Na^+$ ,  $K^+$ ,  $Ca^{++}$ ,  $Mg^{++}$ ,  $Al^{+++}$ ,  $Fe^{++}$ ,  $Fe^{+++}$ , and almost invariably in the case of sulfide mineral flotation,  $Cu^{++}$ ,  $Pb^{++}$ , and  $Zn^{++}$ ), anions (such as silicates, carbonate, sulfide, sulfoxy, and complex ions), and the particular organic anions or cations used as collectors, but also colloidal substances such as the iron and aluminum hydroxides, kaolin, and colloids specifically added for control purposes.

### *Mechanism of Collection*

Collecting agents in froth flotation are polar nonpolar substances and they function by creating a nonpolar surface on the mineral to be floated. To this point most authorities are in agreement, but beyond it there is considerable controversy due in many cases to disagreement in the interpretation of terminology and in the exact mechanism of the process. The two prevailing theories are the "chemical theory" and the "adsorption theory." Taggart (64), the foremost proponent of the chemical theory, has summarized his stand in the following words:

All dissolved reagents which, in flotation pulps, either by action on the to-be-floated or on the not-to-be-floated particles affect their floatability, function by reason of chemical reactions of well-recognized types between the reagent and the particle affected.

The best available summation of the adsorption theory, adopted by Wark (74) and others, and favored by Gaudin, is given by Gaudin (33):

All ions dissolved in a flotation pulp adsorbed at mineral surfaces. At each mineral surface, the adsorption of each dissolved ion is specific, *i.e.*, it depends on the dissolved ion and on the mineral; this specific ion adsorption is also a function of the concentration of the dissolved ion under consideration and that of other dissolved ions. If and when a sufficient proportion of the mineral surface is covered by the collector ions, the particle becomes floatable.

A third theory, which may be called the detergent theory, has been advanced by Dean (18,20) and co-workers, and as it possesses some interesting features, may be summed up as follows:

Flotation of a mineral depends upon maintenance of an aerophilic coating on its surface during the operation, and depression depends on removal of this coating or superimposition of a hydrophilic coating. Any flotation mixture, exclusive of solid and gas,

consists of a two-phase system in which a lipophile phase is distributed through the water phase that contains a dispersion or emulsifying agent. When a mineral particle is introduced, the dispersed lipophile phase tends to collect at the mineral-water interface, and this collection is resisted by the dispersing agent. Accordingly, flotation is determined by a balance of these conditions.

Most of the work that is held to substantiate the chemical theory has been done on galena, although the behavior of a fair number of other minerals has been investigated. Xanthates have been generally used as collectors and are particularly useful in this type of work because of their ease of preparation and the high purity in which they may be obtained. Xanthates, introduced in 1923 as collectors for sulfide minerals, are alkali metal salts of the monoalkyl dithiocarbonates, and are prepared by reacting together stoichiometric quantities of alkali hydroxide, primary or secondary monohydric alcohols, and carbon disulfide. The xanthates are polar nonpolar substances, as is shown by the constitution of potassium ethyl xanthate,  $C_2H_5OSSK$ .

The salient points regarding collection of galena with xanthate may be summarized, following Gaudin's lead (33), in the following manner.

(1) Finely ground galena abstracts xanthate ion from aqueous solution, but the concentration of alkali metal ion is unchanged (68).

(2) Sulfate, carbonate, hydroxyl, and ions of the type  $(S_mO_n)^{--}$ , where  $m/n < 4$ , are exchanged by a galena surface for the abstracted xanthate ion (30,63,68).

(3) Within the limits of detectability (72) no sulfide ion is exchanged for xanthate ion (63,68).

(4) Lead xanthate can be leached by suitable solvents from a galena surface that has been treated by xanthate solution. By increasing the time of treatment the amount of recoverable xanthate decreases, being replaced by sulfur and oily decomposition products (29,30). At no time is the recoverable lead xanthate stoichiometrically equivalent to the xanthate ion abstracted (30).

(5) Unoxidized galena possesses inherent floatability and can be floated with xanthate in the absence of oxygen. Oxidizing agents suppress subsequent flotation of unoxidized galena with xanthate (51,53).

(6) Galena, resurfaced with sulfide ion, is not aerophilic, but immediately floats on addition of a collector (72).

(7) Xanthate coating of galena occurs when the solubility product of lead ethyl xanthate is exceeded, not otherwise (67).

(8) The angle of contact, air-galena, is not independent of the concentration of xanthate ion in solution (34).



Taggart's theory, specifically applied to the collection of galena with xanthates, is as follows.

(a) Under normal conditions, galena ground in water in the presence of air (oxygen) is coated with a film of oxidation products, such as lead sulfate, carbonate, hydroxide (or basic lead carbonate), and lead sulfoxides.

(b) Addition of an alkali metal xanthate to the pulp of galena in water leads to metathetical chemical reaction whereby the solubility product of lead xanthate is exceeded and an oriented molecular film of that substance coats the galena particles, the surface-released anions passing into solution.

(c) The oriented film of lead xanthate presents an aerophilic surface directed into the water phase, and such a surface is readily attachable to an air bubble and will float.

Points 1, 2, 3, 4, and 7 are in accord with this theory. On the other hand, points 1, 3, 4, 5, 6, and 8 are in accord with the adsorption theory as previously outlined. It should be noted that points 5 and 6 are mutually exclusive and that more experimental work is needed to determine the validity of one or the other.

The solubility of lead sulfide is given as  $4.4 \times 10^{-12}$  g. per liter (40). Assuming the galena to be the only source of lead ions by the mineral surface, then using Taggart's value (67) for the solubility product of lead ethyl xanthate ( $6.7 \times 10^{-16}$ ), the concentration of ethyl xanthate ion required to exceed the solubility product and obtain precipitation on the galena surface is  $1.9 \times 10^{-1}$  mole per liter, or 30 g. per liter of water. Actually, the amount of ethyl xanthate required for flotation may be less than 0.02 lb. per ton of ore, or (assuming 25% solids in the pulp) less than 0.0029 g. ethyl xanthate ion per liter, and some of this is consumed by heavy-metal ions in solution, other than lead. In other words, flotation by direct metathesis with the galena surface does not seem feasible. On the other hand, the solubility of lead sulfate is given as  $1.4 \times 10^{-4}$  mole per liter (40). Assuming this to be the reactive surface of galena, and assuming the solubility of this lead sulfate to have the same solubility as massive anglesite (see below), then the concentration of ethyl xanthate ion required to exceed the solubility product of lead ethyl xanthate is 0.00035 g. per liter, which, remembering that xanthate is consumed by reactions other than collection, is much more in accord with practice.

A difficulty arises when discussing solubilities. If air-ground galena is shaken with water, both lead and sulfate ions pass into solution. Addition of alkali metal xanthate liberates a great deal more sulfate ion. As

the initial liberation of sulfate ion does not equal that which would be furnished by a monomolecular layer of lead sulfate, and is in any event less than that which would be equivalent to a saturated lead sulfate solution, it is difficult to avoid the conclusion that the sulfate is retained on the galena by other than chemical forces. In other words, the solubility of the lead sulfate coating is less than the solubility of lead sulfate in bulk. This is admitted and is ascribed (68) to orientation of the initially formed lead sulfate film with the galena structure, this sulfate being isomorphous with galena and having a solubility less than that of ordinary lead sulfate. This is manifestly adsorption.

Taggart has extended his theory to cover the flotation of all minerals. Thus in the collection of other sulfides by xanthates, surface oxidation is also required to furnish sufficient cation concentration to precipitate the metal xanthate on the surface of the mineral. It encounters a number of difficulties, exemplified by the flotation of pyrite. Ferrous xanthates are very soluble in water and on the basis of the chemical theory cannot be held responsible for the collection of pyrite. Ferric xanthate is insoluble in water, and pyrite is assumed to be filmed by this compound. For this to happen, it is necessary to predicate that ferrous ions are oxidized to ferric ions at the surface of pyrite, and that these ions, presumably as ferric sulfate, are there retained by van der Waals' forces or by unsaturated surface forces. As ferric oxide (hematite) and ferric hydroxide (limonite) are not collected by xanthate, it does not seem feasible to invoke compounds of this type in any reaction with the collector. If the reaction really is between xanthate ion and ferric sulfate, then, as Gaudin (33) has pointed out, this indicates an extraordinarily selective retention of sulfate ion rather than hydroxide ion at the pyrite surface, for pyrite can be floated with xanthate to a pH of 10.5, *i.e.*, at a ferric ion concentration of only  $10^{-25}$ . Gaudin found that only a small recovery of ferric xanthate is obtained if xanthate-collected pyrite is leached with organic solvents, and then only if the pyrite has been collected in the absence of oxygen conditions. Similarly, his results of investigations (30,32) on the collection of chalcocite with amyl xanthate do not tally with the chemical theory.

The most specific description of the mechanism of collection is given by Gaudin (33):

- (1) Prior to addition of the collector, all water-wet minerals are the seat of adsorption of ions from solution, a phenomenon that is selective as to the ions involved.
- (2) Addition of collectors results in adsorption of the effective collector ion as a replacement for some of the ions already there. This substitutional adsorption, or exchange adsorption, is selective also. Its extent is controlled by the concentration of the

effective collector ion, the concentration of the displaced ion, the solubility product for each ion pair, and the relationship between adsorbed-ion density at the mineral surface with subsaturation concentration. (If in this statement the existence of a relationship between adsorbed-ion density and concentration is denied, the present hypothesis becomes the chemical-reaction hypothesis.)

(3) The adsorbed-ion density *versus* concentration relationship is specific to the adsorbent and adsorbate.

Wark (72,74), in an extended discussion, states his belief that collection proceeds through adsorption of the collector ion and that "adsorption of xanthate by a given mineral is related to but is not determined exclusively by solubility of the salt formed by the xanthate with the metal of the mineral," and this has led to his adoption of the term "adsorption solubility product" having a smaller value than the normal solubility product. According to this concept, adsorption will occur if the metal and xanthate ionic concentration product exceeds this constant, and not otherwise. For a criticism of this concept, the reader is referred to Taggart (67), whose work, in the case of galena and xanthate, does not confirm Wark's conclusions.

Interesting pioneer work has been carried out not by Gaudin and his associates at the Richards Mineral Dressing Laboratories on the mechanism of collection (35,36,37,38). From the structure of organic compounds, Gaudin calculated the covering areas of certain collector ions, assuming them to be oriented on the mineral surfaces so that the polar ends are directed to the mineral, and the nonpolar ends are directed into the water phase. The covering area is taken to be the same as the maximum cross-sectional area of the ions projected on a plane normal to their lengths. For the oleate ion the specific covering area was determined to be 20.5 square angstroms. For a normal xanthate the value is 29 square angstroms, and for the dicresyl dithiophosphate ion, 53 square angstroms. For the sulphydric collectors given, the computed values are based on assumed but reasonable structures.

By measurement of specific surface areas of mill products by the B.E.T. method (23a), and knowing the ratio of concentration, the quantity of reagent used per ton of ore, the reagent purity, and the molecular weight of the reagent, Gaudin calculated the area of mineral covered per ion of collector. His results are given in Table I.

By comparison of columns 4 and 5, these data show that in no case is a monoionic coating formed on the mineral floated and that such a coating is not necessarily a requirement for flotation, a situation that has been recognized for a number of years. On the other hand, the area covered may

TABLE I  
Correlation between Covering Area of Collecting Ions and Area Covered (37)

Sample	Specific surface, m. <sup>2</sup> /g.	Collector	Area available per ion, sq. Å.	Area coverable by collecting ions on close-packed basis, sq. Å.
Morenci copper cons.....	0.98	Na dipropyl dithio-phosphate	96.4	45
Manganese oxide cons.....	6.88	Oleic acid	82	20.5
Western pyrite cons.....	1.87	K ethyl xanthate	64.2	29
Western galena cons.....	0.43	" " "	64.2	29
Western sphalerite cons.....	0.6	" " "	64.2	29
Anaconda copper cons.....	1.5	Na ethyl xanthate	237.6	29
Utah copper cons.....	1.4	Na dicresyl dithio-phosphate	182	53
Sullivan galena cons.....	0.64	K isopropyl xanthate	32.5	29
Sullivan marmatite cons.....	0.65	K isopropyl xanthate	71	29
Laboratory galena cons.....	0.41	K ethyl xanthate	32.8 <sup>a</sup>	29

<sup>a</sup> This was obtained by taking all the galena surface, *i.e.*, not only the floated material.

approach that which is theoretically coverable. Gaudin points out that the values given in column 4 depend on the validity of the following assumptions:

(1) All the collecting agent is utilized, *i.e.*, the residual collector concentration in the liquor is negligible.

(2) No collector is wasted, that is, there is no loss of collector by evaporation or by the formation of insoluble precipitates.

(3) The otherwise collectable mineral actually not collected has not consumed any collector.

(4) The concentrate surface as measured is entirely due to the collected minerals, and not to diluents of small weight but large surface area, such as clay minerals.

(5) The surface accessible to nitrogen in the gas-adsorption method is the same as the surface accessible to the collector ion.

In his analysis, Gaudin believes that assumptions 1, 2, and 5 are justifiable, but that the validity of 3 and 4 is more debatable. On the basis of carefully controlled laboratory flotation experiments on galena of known specific surface, Gaudin concludes that "when the recovery is substantially complete, the xanthate requirement is near enough to form a complete monolayer."

Figure 6, from Gaudin and Preller, shows both the close-packed arrangement of xanthate ions requiring an area of 29 square angstroms per

ion, and the more probable arrangement calling for 35.4 square angstroms per ion. The last-mentioned array involves twofold coordination, *i.e.*, two lead ions per ion of xanthate. For geometric reasons the stoichiometric ratio of two xanthate ions per lead ion required for lead xanthate seems impossible on the galena cube face, yet contact angle work proves that such a surface becomes xanthate-coated. The more probable arrangement places the sulfur atoms of the xanthate ion almost directly above the lead ions

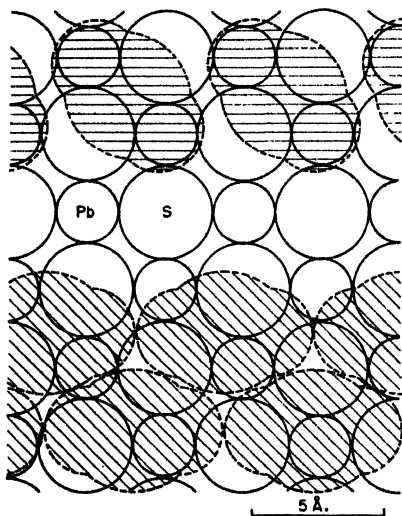


Fig. 6. Close register of xanthate ions (top) and closest packing arrangement (bottom) on a galena surface (after Gaudin and Preller, 37).

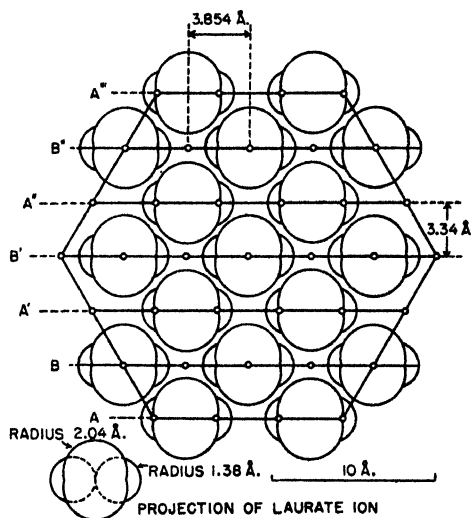


Fig. 7. Arrangement of laurate ions on octahedral face of fluorite (according to Gaudin) on assumption that cleavage has given a face occupied by Ca ions alone. This configuration gives electrostatic neutrality (36).

of the galena lattice, and this excellent "fit" may explain the ready collection of galena by xanthate. Other lead minerals do not respond so easily to collection by this substance. Gaudin points out in this paper that if the adsorbed ions can dispose themselves in register with the mineral lattice, a complete monomolecular collector coating is merely a matter of supplying sufficient collector. By plausible argument he shows (37) that fatty acid (laurate) ions can be fitted to the calcium ions on a cleaved octahedral surface of fluorite, even though there will be considerable asymmetry in the bonding of the collector ion to the calcium, considerable unevenness in spacing the adsorbed ions, or a different bonding between alternate rows.

The arrangement shown in Figure 7, possessing equalization of charges, seems the more probable.

A further example is given by Gaudin. With a mixture of fluorite and quartz in water, calcium ions can be adsorbed by the quartz, and in the presence of a collector the calcium ions on both minerals will compete for collector ions. That the fluorite surface is selectively coated by the collector under these conditions is ascribable to the orderly arrangement of calcium ions on the fluorite lattice and hence to the better "fit" of the absorbate.

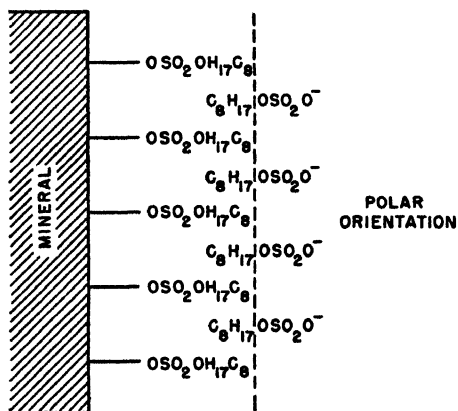


Fig. 8. Formation of a hydrophilic coating by double coating.

This picture of the mechanism of collection is by far the most attractive that has been hitherto offered and seemingly fits the observed facts better than any other that has been advanced.

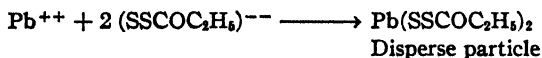
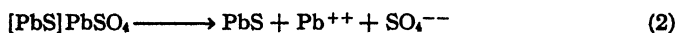
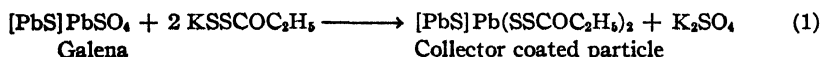
Dean's theory of collection involves elements of adsorption and the chemical theory can be shown to be a special case of the detergent theory. Thus, in a solution saturated with sodium and potassium chloride, solid particles of sylvite (KCl) can be selectively and almost completely floated from solid particles of halite (NaCl) with relatively small additions of sodium normal octyl sulfate. The astonishing fact is that by washing the sylvite concentrate with fresh brine the reagent can be collected and used over again (16). By recycling brine in this manner, reagent consumption can be reduced to a very small quantity. Obviously, most of the reagent is adsorbed from the brine by the sylvite, and it is apparent that the reagent is very loosely bonded with the mineral. Excess of collector depresses the sylvite, a fact attributed by Dean to detergency of the

collector coating, but just as readily ascribed, in the lack of experimental evidence to the contrary, to deposition of a hydrophilic coating by double layer formation, as shown in Figure 8.

The almost complete removal of the octyl sulfate from solution by the sylvite, and its subsequent removal from the sylvite by brine free of collector, in spite of the excess potassium ion in solution, indicates that a surface adsorption rather than a metathetical chemical reaction is occurring, for the relative solubilities of the potassium and sodium octyl sulfates differ but little. The washed sylvite is almost completely depressed, and requires recoating to be floated.

As Dean, Clemmer, and Cooke (18) point out, the flotation of galena with xanthate and pine oil can be explained by the detergent theory:

The dispersed lipophile phase is formed *in situ*, and since the frother used, such as pine oil or cresylic acid, is a very mild detergent, the lipophile coating persists. Formation of the lipophile phase *in situ* evidently is not necessary. On a thermodynamic basis the conditions that bring about its formation and retention are the same as those that would insure its aggregation at the surface if formed in the solution. That is, an equivalent change in free energy takes place in floating galena with xanthate, whether it is regarded as taking place according to the first or second of the following processes:



Dietrich (20) has shown that emulsions of lead ethyl xanthate in cresylic acid and pine oil give recoveries of galena comparable with that effected by normal flotation with potassium ethyl xanthate and cresylic acid, and that similar emulsions of lead xanthate in saponin, sodium oleate, and other emulsifying reagents can give successful flotation of the same mineral.

### *Orientation of the Collector Coating on the Mineral*

Irrespective of the theories that have been advanced regarding the interaction between mineral and collector, it is generally accepted that the polar portion of the collector ion is directed toward the mineral surface. Remembering that collectors are polar nonpolar substances, this necessarily implies that the nonpolar portion is directed away from the mineral surface toward the surrounding liquid phase. In all cases this aerophilic portion is either an alkyl or an aryl grouping. In the case of the

commercially used xanthates the chain ranges in length from  $C_2$  to  $C_6$ . In some cases the chain may be branched, as with isopropyl xanthate. With the aerofloats the aerophilic loading is either an alkyl or an aryl group. The constitution of the alkylamines and soaps used in nonsulfide flotation is apparent.

The most convincing indirect proof of orientation was first furnished by Wark and Cox (69) who showed that the equilibrium contact angle obtained on collector-coated minerals was independent of the nature of the mineral and was a function of the number of carbon atoms in the chain of the normal alkyl xanthates. Figure 9, taken from their paper, shows this relationship. It should be noted that the angle of contact of air against a

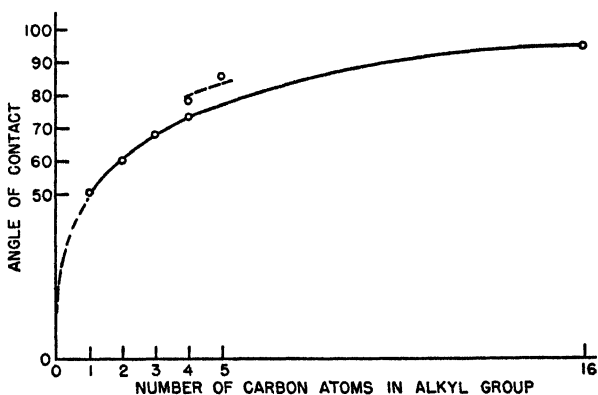


Fig. 9. Dependence of contact angle on alkyl group (69).

long-chain solid paraffin is  $105^\circ$ , the value which the curve approaches asymptotically. The curve for the more condensed iso compounds lies above that for the normal compounds. The constancy of the angle for any given alkyl or aryl group, irrespective of the nature of the polar group, is shown in Table II.

Independence of angle of contact with the mineral is shown by Table III. It is apparent that as chain length is increased, the polar portion of the collector ion or of the mineral is more completely masked by the aerophilic collector chain, with an approximation to the behavior of solid paraffin in the long-chain members. Consonant with their structure, the iso compounds give more covering than the normal compounds.

#### *Effect of Slimes on Collection*

It has long been known that colloids or particles of near-colloid size have a profound effect on flotation. The influence of fine particles on froth-



TABLE II  
Contact Angles (in Degrees) for Various Minerals and Xanthates<sup>a</sup> (69)

Minerals	Xanthate									
	Methyl	Ethyl	n-Propyl	n-Butyl	Isobutyl	Isoamyl	Cetyl	Benzyl	Phenyl ethyl	Cyclohexanol
Galena.....	50X	59	68	74	77	88	100	71	70	73
Sphalerite.....	51X	61X	69X	74X	79X	84X	97	71X	71X	75X
Pyrrhotite.....	—	59X	—	—	—	86X	95	72X	—	—
Pyrite.....	49X	60	67	74	78	82	95	71	70	75
Bornite.....	51	60	68	73	78	86	95	70	71	75
Chalcocopyrite.....	52X	60	69	76	78	90	94	75	72	74
Chalcocite.....	—	60	—	—	—	—	—	—	—	—
Anglesite.....	—	58	—	—	—	—	—	—	—	—
Cerussite.....	—	57	—	—	—	—	—	—	—	—
Cleophane.....	50X	61	—	—	—	—	—	—	—	—
Crocoite.....	—	63	—	—	—	—	—	—	—	—
Tetrahedrite.....	—	60	—	—	—	—	—	—	—	—
Mean value.....	50	60	68	74	78	86	96	72	71	75
										73

<sup>a</sup> With the copper minerals the figures given represent the contact angle obtained before dioxanthogen begins to form. This generally implies that the measurements be made before 2 hours' contact between mineral and solution, but this time is variable. X indicates that activation was necessary.

TABLE III

Contact Angles in a Solution (25 Milligrams per Liter) of Potassium Propyl Xanthate

Mineral	Activator	Angle of contact, degrees	Time of reading
Galena.....	None	64	10 min.
	"	67	45 min.
	"	68	100 min.
	"	70	1 day
Sphalerite.....	10 mg. per liter CuSO <sub>4</sub> .5H <sub>2</sub> O	66	5 min.
	"	69	35 min.
	"	(86)	1 day <sup>a</sup>
Pyrite.....	None	67	25 min. <sup>b</sup>
	"	67	60 min.
Bornite.....	None	65	10 min.
	"	68	50 min.
Chalcopyrite.....	None	69	15 min. <sup>c</sup>
	"	(78)	40 min.

<sup>a</sup> Dixanthogen effect (note presence of copper as activator).<sup>b</sup> Full angle developed within 1 minute.<sup>c</sup> Dixanthogen effect noticed very early.

ing has already been mentioned. Hydrophilic colloids such as glue, starch, tannin, or saponin, in sufficient quantity, will completely depress collector-coated minerals. Starch can be used to selectively depress molybdenite occurring in a xanthate-collected bulk concentrate of that mineral and copper sulfides, and a number of patents cover the use of starch and of modified starch products in the anionic flotation of silica from iron ores. Tannic acid is used to depress calcite and dolomite in the soap flotation of fluorite.

Protective colloids added to a pulp prior to collector addition apparently prevent interaction between collector ion and mineral surface. Added subsequently to collectors they apparently prevent collection by superimposition of a hydrophilic coating on the collector film. Most of these substances form micellar suspensions in water and are well loaded with hydrophilic groups. Reagents of this type are added to the flotation pulp for certain desired effects, and of course their action is controlled by the quantity or type added. Sodium silicate, in sparing quantities, is frequently used in cleaner circuits to produce high-grade concentrates. It may function in two ways: (a) by increasing silicate ion concentration and thus increasing specific adsorption by gangue minerals such as quartz and car-

bonates; the coating of hydrophilic ions prevents flotation; and (b) by causing increased dispersion or deflocculation of fine gangue minerals and so preventing them from entering the froth. Excess of sodium silicate depresses collector-coated minerals.

Since colloids are sensitive to changes in hydrogen ion concentration, the pH of the pulp will in many cases determine the efficacy of the colloid.

Fine mineral particles are difficult to float, and in sulfide flotation at least, a respectable proportion of mineral lost in the tailing occurs in the fine sizes. Table IV shows the assay per cent of zinc in a series of sized products prepared from the feed to, and the tailing from, a flotation circuit, together with recovery of zinc from each size (12). The decrease in recovery in the material finer than 5 microns is marked.

TABLE IV  
Assays of Sized Products from Flotation Feed and Tailing (12)

Size	Weight, feed	Per cent tailing	Assay, feed	Per cent Zn tailing	Extraction, per cent
+48 mesh.....	1.2	1.5	1.58	0.53	66
-48 +65 .....	6.6	10.3	1.41	0.39	72
-65 + 100.....	19.1	22.5	2.01	0.39	81
-100 +150.....	14.0	11.6	2.57	0.52	80
-150 +200.....	8.4	8.1	7.00	0.63	91
-200 +270.....	10.2	8.9	10.34	0.54	95
-270 +400 (38 $\mu$ )....	9.3	7.4	11.24	0.49	96
-38 +25 .....	2.0	9.2	16.08	0.75	95
-25 +15 .....	9.5	3.6	9.60	0.71	93
-15 +10 .....	10.0	7.5	6.68	0.96	86
-10 +5 .....	3.6	—	6.92	—	—
-5 .....	6.1	9.4	6.36	2.43	62
Total.....	100.0	100.0	6.14	0.75	88

On the basis of certain simplifying assumptions, Gaudin has shown (28) that if particle size is small compared with bubble size, the probability of collision between bubble and the "sphere of rotation" of the particle varies directly with the size of particle, *i.e.*, the probability of collision diminishes with decreasing size of particle. Elsewhere (27), Gaudin, Groh, and Henderson, working with results obtained in the laboratory and in practice, showed that there is a size range through which maximum recovery is obtained, but that at both coarser and finer sizes, recovery is decreased. The size range of optimum recovery lies between 52 and 25 microns (compare Table IV).

Explanation of the lack of floatability of the finest sizes is shown by

Gaudin and Malozemoff (31) to be due to two factors. The first is the low probability of collision between a gas bubble and a fine particle, already mentioned. The second is due to the aging of the surfaces of fine particles in the chemical atmosphere of the ore pulp. Necessarily, fine particles have statistically older surfaces than coarse particles, if only because in the act of grinding the coarse particles continue to be broken while the finer particles, having greater mobility, escape the grinding media. Under these conditions the finer and older particles may have their surfaces profoundly altered, the sulfides adsorbing anions released by the gangue minerals, and the gangue minerals adsorbing cations released by the sulfides. Thus the fine particles tend to reach a level whereby, upon addition of collector, the sulfides will not be collector-coated, and the gangue minerals will. Data presented by Gaudin and Malozemoff confirm these conclusions. A further point is that increase of surface area produced by fine grinding would necessitate expenditure of more collector per unit weight of mineral to be floated, for under constant reagent addition, the older and less reactive fine particles would be starved for reagent and would fail to float. To these considerations, Wark (72) adds three more: a greatly increased air-water interfacial area would be required to float a large quantity of fine mineral, fine bubbles on the surfaces of the fine particles would tend to pass into solution, and adsorption of ions by the fine particles would give each particle a high charge and tend to repel collector ions. A partial remedy for the effect of fine grinding and one used in practice, is to add collector to the grinding circuit.

Tailing losses due to nonflotation of coarse particles may be due to two causes. These are: (a) The particles are too large or too massive for levitation. Under normal conditions the maximum floatable size is governed by well-understood factors, such as the specific gravities of mineral particles and of pulp, the surface tension of the fluid, the completeness of the collector coating on the mineral, and the angle of contact between air and mineral surface. Thus gold particles, of high specific gravity, cannot be floated at the same coarse size at which calcite can be floated (45). (b) Tailing losses are high in flotation circuits where very fine grinding is required to liberate valuable mineral from gangue, and these losses are not all attributable to poor flotation of fine sizes, *i.e.*, coarse particles refuse to float as they should. Taggart (61) explain this on the basis of "slime-coating," that is, precipitation of slime particles on the mineral surface with physical interference of contact between air bubble and mineral.

The subject of slime-coating has since received a great deal of attention. Ince (42) explained it as being caused by differential electrical

charge between the surface of the mineral and the slime particles. He pointed out that dispersion agents could be used to control the magnitude and sign of the charges and therefore to control the amount of slime-coating. Later, del Giudice (39), expressing dissatisfaction with the electrical charge theory, advanced a chemical explanation. In the specific example discussed by him, a clean galena surface immersed in a pulp of fine calcite particles rapidly acquired a surface coating of these particles. He explained this as being due to chemical reaction between the lead sulfate coating on the galena and carbonate ion in solution to give the less soluble lead carbonate, which acted as a bond between galena and the particles. Fluorite particles did not coat galena, explained by him on the basis that lead fluorite and calcium sulfate are more soluble than calcium fluoride and no bonding substance could be formed. Unfortunately, calcite slimes coat calcite, galena slimes coat galena, and any slimes near the isoelectric point will coat any nonreactive surfaces.

Bankoff (3) also observed heavy slime coatings under conditions precluding formation of a cementing compound by metathesis, and concluded that the most satisfactory explanation was that it was caused by the same conditions that control flocculation of mineral particles in water. Correlating this with Taggart's theory of Brownian movement as a result of surface ionization (62), Bankoff concluded that reagents that favor Brownian movement by increasing surface ionization will inhibit slime-coating, and, conversely, those that stop Brownian movement will facilitate slime-coating. Sun (57), in an excellent paper, points out that Brownian movement is an incomplete guide to the mechanism of slime-coating, for according to Bankoff's theory, quartz slime should not coat calcite, yet both exhibit active Brownian movement in water. Using a slit ultramicroscope and Mattson's cataphoretic cell (47), Sun measured the sign and magnitude of the charge on fine particles of a number of minerals under controlled solution conditions, and concluded that slime-coating is governed by the sign and magnitude of the ionic charge of both particle and slime.

Sun says (57):

Mutual attraction induces slime-coating and repulsion prevents slime-coating. Ionic charges of mineral surfaces, as represented by the zeta potential, is determined by the domination of anions or cations and can be regulated by chemical reagents. The relationship between slime-coating and zeta potential is established by the experimental data of the cataphoretic cell and of slime coatings. The results of experiments can be summarized as follows.

(1) Slime-coating is heavy when zeta potentials of particle and slime are both high but opposite in sign.

- (2) Slime-coating is light when the zeta potential of slime is high and that of the particle is low.
- (3) Slime-coating is heavy when the zeta potential of slime is low.
- (4) Slime-coating is prevented when the zeta potentials of slime and the particle are both high and alike in sign.
- (5) Slime-coating is facilitated by the decrease of slime particle size when the other factors are kept constant.
- (6) Slime-coating is increased by the increase of the agitation process.
- (7) The least but still effective amount of inhibiting reagents for the prevention of slime-coating is shown on the turning points of the cataphoretic curves.
- (8) A high zeta potential is accompanied by Brownian movement and dispersion. A low zeta potential is associated with flocculation and shows no Brownian movement.

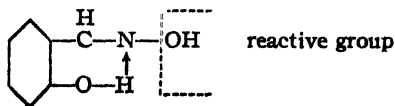
Slime-coating is thus shown to be a special case of the mutual coagulation (flocculation) of two sols of opposite charge, and there is general agreement with the Schulze-Hardy rule. Following this interpretation slime-coating should show some dependence upon temperature changes in the system.

The validity of Sun's second statement under (8) above is questionable. The writer has found that Brownian movement occurs in any flocculated system, the amount of movement depending upon the floc size. In heavily coagulated quartz, calcite, and hematite systems, occasional single particles occur, and these, when small, show as active motion as similarly sized particles in a disperse system. Floccules of two or more particles also show motion, but it becomes imperceptible when the total floc mass is roughly equal to that of a single particle which is motionless in a disperse system. Conversely, in a coagulated system, flocs may be disintegrated into individual particles or aggregates of a few particles, which resume motion. Thus Taggart's theory of Brownian movement by ionization does not seem valid. Kellogg (43), after a comprehensive investigation, comes to the same conclusions.

### *Flocculation and Collection*

For many years a correlation has been claimed between the state of flocculation or dispersion of the mineral pulp and the efficacy of flotation. Many writers report that the mineral to be floated should be in a state of flocculation, and that which should not float should be dispersed. Coghill and Clemmer (15) claim that overflocculation (flocculation of both gangue and economic mineral) leads to contamination of the froth by the gangue and Ralston and Barker (50) correlate flocculation with flotation of pyritic copper ore.

Gaudin and Malozemoff (31) point out that flocculation of the mineral



**Dithiocarbonates.** Xanthates,  $\text{ROCSSH}$ , in which R is an alkyl group, or an aryl group linked through an alkyl group. These compounds, used as the alkali metal salts, are, with the dithiophosphates, the most commonly used sulfide collectors. The most commonly used xanthates are the ethyl, isopropyl, secondary butyl, and amyl xanthates (77).

**Dithiophosphates.** Aerofloats,  $(\text{RO})_2\text{PSSH}$ , in which R is alkyl or aryl, are used either as the acids or as the alkali metal salts. The aerofloats seem to be more complex in composition than the simple formula given would indicate (58).

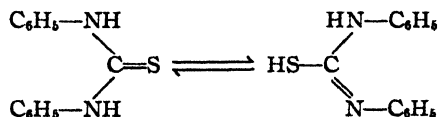
**Dithiocarbamates.**  $\text{R}_2\text{NCSSM}$ , in which R is alkyl or aryl, and M is an alkali metal. Dithiocarbamic acid is unstable, so these compounds do not function in acid circuit. The dithiocarbamates are reported to be more powerful collectors for the sulfides than the xanthates, but being more expensive are not used outside of the laboratory.

**Thio Alcohols.**  $\text{RSH}$ , in which R is alkyl or aryl. The mercaptans are good collectors for sulfide minerals, but their expenses and odor prevent their use. They are only very slightly soluble in water, but the mercaptides, formed in alkaline pulps, ionize to furnish reactive groups.

**Alkyl Sulfates.**  $\text{ROSO}_2\text{OM}$ , in which R is a normal alkyl grouping or a chain containing other than hydrocarbon groups, and M is an alkali metal. Short-chain sulfates are not effective as collectors.

**Alkyl Sulfonates.**  $\text{RSO}_2\text{OM}$  are obtained in impure form as a by-product from petroleum refining. R is a long alkyl chain. Dean and Ambrose (20) discuss applications of the alkyl sulfates and sulfonates in flotation.

Other compounds of interest are diphenylthiourea and mercaptobenzothiazole. The first mentioned (thiocarbanilide) is an excellent collector for galena, but is highly insoluble in water. Collection is effected through the acid tautomer:



Mercaptobenzothiazole and its sodium salt have been used in the flotation of cerussite (75).

Both these compounds contain the active trivalent nitrogen and bivalent sulfur atoms, but their collecting action is probably mainly through the sulfurs.

**Cationic Collectors.** Cationic collectors carry the aerophilic hydrocarbon and the reactive polar group in the cation. The functions and



applications of these collectors are not too well known for they are of only fairly recent introduction and are difficult to obtain in high purity.

*Amines.*  $\text{RNH}_2$ ,  $\text{R}_2\text{NH}$ ,  $\text{R}_3\text{N}$ , and  $\text{R}_4\text{NX}$ , where R is an alkyl group and X is a halide. Primary, secondary, and tertiary amines and the quaternary ammonium salts have been used in the flotation of the non-metalliferous minerals. When amines function as cationic collectors, Taggart (2,66) postulates a reaction between the amine hydroxide and an anionic film at the surface of the mineral. When they function as anionic collectors he states (66) that:

Collecting reaction of amines with heavy metal sulfides apparently results in the formation of a metal-amine compound in which the metal and amine constitute an amine-metal complex ion similar to the metal-ammonium ions. Laurylamine is a collector for all of the metallic minerals tested which form water-stable coordination complexes with ammonia (Cu, Pt, Ag, Zn, Ni, Cd,  $\text{Fe}^{++}$ , Sn) and is not a collector for those tested which do not form such water-stable ammonia complexes (Mg, Al, Pb).

The use of quaternary ammonium salts is reported by Wark (72) and by Dean and Ambrose (20). Pyridinium salts, obtained by addition of alkyl halide to pyridine, have been used in the flotation of quartz from magnetite (18).

*Sulfonium* ( $\text{R}_3\text{SX}$ ) and *phosphonium* ( $\text{R}_4\text{PX}$ ) salts are reported to be cationic collectors.

**Oil Collectors.** A small group of compounds functions by the solubility of its constituents in the nonpolar portion of an established collector film. Hydrocarbon oils are used to implement the flotation of soap-coated minerals, as in table flotation (23). The oil smears itself over the coated mineral, mechanically reinforcing the hydrophobic coating, and thereby permits establishment of a larger angle of contact and increase in tenacity of adhesion.

Organic sulfides of the monoxanthogen and dixanthogen types seem to function as oily collectors. In the flotation of copper sulfide ores, cupric ion in solution oxidizes xanthates to dixanthogen, and this will tend to form a second coat on the xanthated mineral surface. According to Wark (72) the angle of contact with an ethyl xanthate film is  $60^\circ$ , and with a second film of dixanthogen it is  $80^\circ$ . It is probable that the reported excellent collection of some copper minerals is due to this mechanism. Hassialis (41) has shown that the collection of sulfide copper minerals by diphenyl sulfide is due not to the organic compound itself, but to an impurity, possibly thiophenol, and he postulates that the diphenyl sulfide oil smears the thiophenol coated mineral.

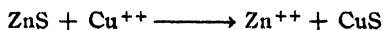
### 3. Activators

The classic example of activation is the resurfacing of sphalerite with copper ion to permit collection with sulfhydryc collectors. A clean sphalerite surface is not coated by xanthates having alkyl groups of less than 6 or 8 carbon atoms. Introduction of a small quantity of copper ion under either acid or alkaline conditions rapidly modifies the surface so that it will accept a short-chain xanthate. The mechanism of the process has been much discussed, and the prevailing theory is that a monomolecular layer of copper sulfide is formed on the sphalerite surface. Some workers claim that a visible surface coating is formed (25), but this cannot be confirmed by others.

The Schürman (56) series is an arrangement of the sulfides of the metals in increasing order of solubility. An abbreviated list, with the corresponding solubility products (40), is given below:

HgS.....	$4 \times 10^{-53}$ to $2 \times 10^{-49}$
Ag <sub>2</sub> S.....	$1.6 \times 10^{-49}$
CuS.....	$8.5 \times 10^{-45}$
PbS.....	$3.4 \times 10^{-28}$
ZnS.....	$1.2 \times 10^{-23}$

According to this series, any cation lying above a given sulfide should be capable of replacing the cation of that sulfide. Thus:



As the sulfides of mercury, silver, copper, and lead can be collected by ethyl xanthate ion, and the sulfide of zinc cannot be so collected, it follows that resurfacing of the zinc sulfide by any of the first-mentioned cations should permit collection. This is realized in practice.

The writer recently investigated the nature of the coatings formed on sphalerite by exposure to fairly concentrated (0.1 molal) solutions of the nitrates of silver and lead, and the chlorides of copper and mercury, at a temperature of about 100° C. After 50 days of exposure it was found that sphalerite in the lead and mercuric solutions showed very little surface alteration. Occasional areas of the sphalerite treated with lead showed replacement with what was apparently lead sulfide, but the thickness of the material was too small for removal and identification. Sphalerite treated with mercuric chloride has a roughened surface coating in places, but no replacement to depth, and the coating could not be removed for identification. Cupric ion gave a rather thick coating of a deep blue color over the entire sphalerite surface. This was identified by x-ray

analysis as covellite ( $\text{CuS}$ ). Chemical analysis showed that the copper removed from solution was stoichiometrically equivalent to the zinc passing into solution, so the equation given above expresses the reaction for the conditions prevailing.

Under the same conditions, the silver nitrate completely disintegrated the sphalerite, leaving a black powder, which x-ray analysis identified as argentite ( $\text{Ag}_2\text{S}$ ).

Just why silver and copper can replace zinc in the sphalerite lattice, under the conditions given, and lead and mercury do so with difficulty, is not known. The galena and cinnabar lattices are simple compared with those of covellite and argentite, and the mercuric ion has a radius nearly identical with that of silver. Extrapolation from massive reaction of this type, at elevated temperature, to resurfacing under flotation conditions is hazardous and probably impossible.

Ravitz and Wall (52) have shown from flotation tests that maximum recovery of sphalerite particles ranging in size from 295 to 147 microns (48 to 100 mesh) corresponds to formation of a monolayer of cupric ion. At finer sizes substantially less copper ion than is required for a monoionic film suffices to give optimum recovery, confirming other investigations, which indicate that a complete monolayer of activator or collector is unnecessary for flotation of fine sizes. In some abstraction tests Ravitz and Wall used copper ion concentrations in excess of those used in flotation practice, and found that the adsorbed or chemically formed layer was either many atoms thick or that the mosaic structure of sphalerite was responsible for the enhancement of deposition in the coarser sizes. The apparent thickness of the deposited film decreased in the finer sizes, and extrapolation of their results gave a monolayer of cupric ion at 0.37 micron—presumably the size of the mosaic structure.

Wentworth (78) points out that sphalerite treated with dilute copper sulfate solution becomes a good electrical conductor. As sphalerite has low electrical conductivity and covellite is a good conductor, this supports the theory that a covellite film is formed in activation.

In an interesting paper (49), Ralston and Hunter describe activation and flotation of marmatite ( $(\text{Zn},\text{Fe})\text{S}$  containing up to 20% iron) using a variety of activating cations. They found that cuprous ion functioned much the same as cupric ion, both in grade of concentrate produced and in equivalence of copper required to give a desired result. It is obvious that the large amount of oxygen in a flotation cell would be almost certain to oxidize the copper to the cupric condition, and that cupric ions were probably those responsible for activation. Cuprous amyl xanthate, a sub-

stance of very low solubility, gave practically no recovery of marmatite when used as a combined activator and collector, and from this it appears that activation must precede collection, a conclusion in accord with the theory that the activator prepares the mineral surface for adsorption of, or reaction with, the collector ions. Ralston and Hunter found that mercuric and mercurous ions both activated marmatite and in general gave recoveries, presumably with xanthate as collector, comparable with those furnished by cupric and cuprous ions. Activation may have been effected by the mercuric ion alone, for mercurous ion would readily oxidize in a flotation cell. Table V, taken from their paper, shows the activating effect of these and of other ions.

TABLE V  
Effects of Metallic Salts of Which Cations Should Be Discharged by Zinc (49)

Cations used	Activation in		Remarks
	Grade	Extraction	
Ag <sup>+</sup> .....	Slight	Fair	Excess caused depression
Hg <sup>+</sup> .....	Fair	Good	Probably oxidized to Hg <sup>++</sup>
Hg <sup>++</sup> .....	Fair	Good	
Cu <sup>+</sup> .....	Good	Very good	Probably oxidized to Cu <sup>++</sup>
Cu <sup>++</sup> .....	Best	Best	Slightly better than Cu <sup>+</sup>
Pb <sup>++</sup> .....	None <sup>a</sup>	None <sup>a</sup>	Practically inert
Cd <sup>++</sup> .....	Depressed	Depressed	
Zn <sup>++</sup> .....	Depressed	Depressed	

<sup>a</sup> The alkaline pulp would give a very low lead ion concentration.

In practice, activation of sphalerite with silver ion does not occur because of the scarcity of that ion. Activation with lead ion may occur in the grinding circuit when the pulp is acid, but undesirable activation (sphalerite is floated *after* galena) is prevented by grinding in the presence of lime or soda ash. Undesirable activation of sphalerite with copper ions from the ore is prevented by addition of cyanide in alkaline circuit. Intentional activation is effected by the use of copper sulfate, the cheapest source of copper ions. Wark and Cox (70) have shown that iron-free zinc blende and marmatite containing up to 13% iron show no essential difference in behavior to collection. Mortenson (48), however, reports that the time required to activate blende with copper ion increases with the iron content of the lattice, and also with rise in temperature and increase in hydrogen ion concentration.

Wark and Cox (70), by contact angle experiments, have shown that copper-activated sphalerite surfaces, in the presence of potassium ethyl

xanthate, do not respond to prevention of contact by cyanide ion as does massive covellite. Figure 10 illustrates this dissimilarity in the behavior and simultaneously shows that a copper-activated sphalerite surface responds to depression by cyanide ion in a manner markedly similar to chalcopyrite. This last-mentioned similarity is further emphasized by results given in a later paper by Sutherland (59). However, exact correspondence in behavior between a monolayer of cupric ion and of a surface of massive

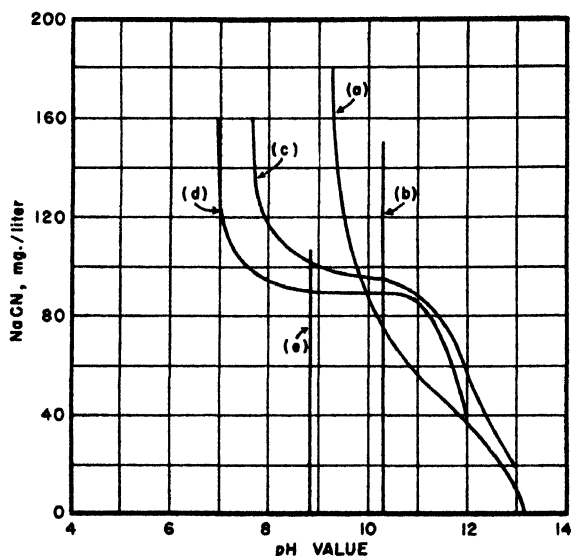
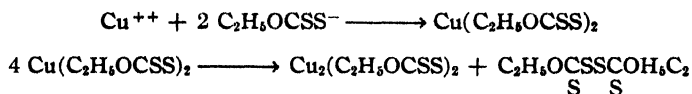


Fig. 10. Contact curves for covellite (a), galena (b), chalcopyrite (c), sphalerite pre-activated with  $\text{Cu}^{++}$  (d), and sphalerite pre-activated with  $\text{Pb}^{++}$  (e). Potassium ethyl xanthate, 25 mg./liter, except for curve (e) (5 mg./liter). Contact possible only to left of curves. After Sutherland (59), and Wark and Cox (70).

covellite should not be expected, if only because of the lattice strain involved when zinc atoms are replaced by copper atoms of different radius and activity. It would be interesting to ascertain the behavior of wurtzite (the hexagonal form of zinc sulfide) to cupric ion as an activator and to normal collectors with and without activation.

Excess of activating ion usually prevents subsequent flotation with a collector. This is attributed to precipitation of the collector by the excess cation. Thus cupric ion reacts with xanthate ion to form cupric xanthate, which immediately decomposes to form cuprous xanthate and dioxanthogen:



With excess cupric ion, ionization of the cuprous xanthate is so suppressed that insufficient xanthate ion is available for collection.

A summation of published opinion leads to the following conclusions regarding the activation of sphalerite with heavy-metal cations.

(1) Cupric ion replaces zinc atoms at the surface of the zinc blende lattice.

(2) Under the low  $\text{Cu}^{++}$  concentrations prevailing in flotation, an incomplete monolayer is formed on the zinc blende. A complete monolayer is unnecessary for successful collection and flotation.

(3) The deposited copper forms a bond between the substratum of zinc blende and the superstrate of collector ions. Collection is presumably governed by the same factors that control collection of minerals, which do not require activation.

(4) Zinc blende resurface with copper at concentrations and under conditions equivalent to those employed in practice does not respond to imposed conditions precisely as if it were filmed with covellite. This is attributed to the known differences in behavior between two-dimensional and three-dimensional lattices.

(5) Silver, mercury, and lead ions will activate zinc blende under the proper conditions, and of these lead is the only ion that may accidentally activate zinc blende.

Both pyrite and arsenopyrite seem to be activated by copper ion, but the mechanism in these examples is obscure.

Natural processes will oxidize galena *in situ* to anglesite ( $\text{PbSO}_4$ ) and cerussite ( $\text{PbCO}_3$ ) and in the presence of certain cations, other oxidized lead minerals, some quite complex, may be formed. On the basis of the adsorption theory of collection as it now stands it is impossible to predict how anglesite and cerussite will respond to sulfhydryc collectors. As lead xanthate has a lower solubility than lead sulfate or carbonate, the chemical theory predicts that collection is possible. Unfortunately, another factor, the relatively high solubility of the sulfate, and to a less extent that of the carbonate, modifies the situation. Xanthates will collect these two minerals but only when large and uneconomic quantities are used, *i.e.*, the lead ion in solution must first be precipitated by xanthate prior to collection. This is particularly true of anglesite. For this reason anionic collection of the oxidized lead minerals, in the absence of an activator, is costly and

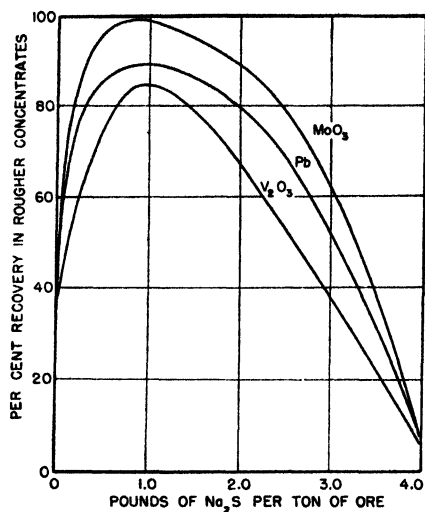


Fig. 11. Effect of sodium sulfide on recovery of oxidized lead minerals (13).

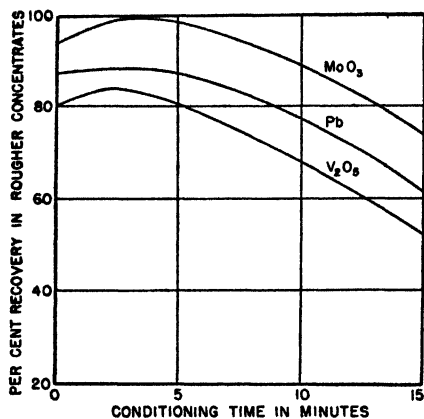


Fig. 12. Effect of conditioning time on recovery of oxidized lead minerals (13).

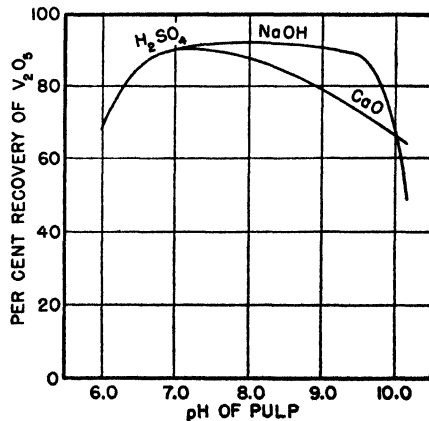


Fig. 13. Influence of pH on recovery of V<sub>2</sub>O<sub>5</sub> as vanadinite and descloizite (13).

usually impractical. A partial remedy consists in resurfacing the minerals with sulfide ion, supplied by sodium sulfide. With cerussite the reaction is:



The resurfaced mineral functions somewhat as galena and is amenable to collection by normal sulfide-mineral collectors, although less efficiently than galena.

Clemmer and Cooke (13) report that wulfenite ( $\text{PbMoO}_4$ ), vanadinite ( $\text{PbCl}_2 \cdot 3\text{Pb}_3\text{V}_2\text{O}_8$ ), descloizite ( $(\text{Pb,Zn})_2\text{V}_2\text{O}_8 \cdot (\text{Pb,Zn})(\text{OH})_2$ ), and cerussite may be floated with relatively large quantities of a mixture of ethyl or amyl xanthate and aerofloat. Sulfidization with sodium sulfide markedly reduced the amount of collector required, and permitted more rapid flotation of the minerals. It was noted that treatment of the minerals listed with a dilute solution of sodium sulfide gave immediately visible surface coatings of lead sulfide in the case of cerussite and wulfenite, that vanadinite coated at a much slower rate, and that no visible coating formed on the descloizite. For effective flotation of these minerals it was found that both the amount of alkali sulfide added and the time of conditioning were critical. Figures 11 and 12 show the effects of quantity of sulfide added and of conditioning time, respectively, using moderate quantities of amyl xanthate and aerofloat as collectors.

A high pH is detrimental to flotation of sulfidized minerals. This is shown in Figure 13. A secondary effect caused by the cation of the compound furnishing hydroxyl ion is apparent.

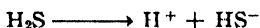
Anglesite is not readily sulfidized and recovery is poor when an oxidized lead ore containing this mineral is activated with sulfide ion and floated with sulphydric collectors. This may be due to two causes. (a) The solubility of lead sulfate is  $1.4 \times 10^{-4}$  mole per liter, that of lead carbonate  $4.13 \times 10^{-6}$  mole per liter. The greater solubility of the sulfate necessarily implies the use of larger quantities of sulfide, and as will be explained later, high sulfide addition depresses lead sulfide. (b) The "fit" of the sulfide on the anglesite lattice is poor, or it may easily be removed by the scouring action of the flotation pulp.

Wark (72) has shown that depression at high sulfide concentration is due to two effects, the depressing effect of hydrosulfide ion and the depressing effect of high hydroxyl ion concentration. Wark and Cox (73), using contact measurements, show that in the presence of 25 mg. per liter potassium ethyl xanthate, small quantities of sodium sulfide act as a depressant for galena through a pH range of 6 to 10.4, the higher value being the critical pH for that mineral, *i.e.*, the pH above which the mineral will not float. This is shown in Figure 14. Figure 16 shows the influence of pH and concentration of sodium sulfide on contact at an anglesite surface, and Figure 15 the influence of the same variables on contact with cerussite.

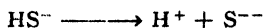
The similarity of the left-hand portions of the curves in Figures 14 and 16 implies that there is essentially a galena or galenalike surface on sulfide-activated cerussite and anglesite. In the case of lead-activated sphalerite, the cessation of contact at a pH of more than 10.4 carries the same implica-



tion. In the case of the sulfide-activated lead minerals, however, there is another factor. A dibasic acid such as  $\text{H}_2\text{S}$  ionizes in two stages:



and



From the ionization constants for the respective stages, it is possible to calculate the concentrations of  $\text{H}_2\text{S}$ ,  $\text{HS}^-$ , and  $\text{S}^{--}$  per mg. or  $\text{Na}_2\text{S} \cdot 9\text{H}_2\text{O}$

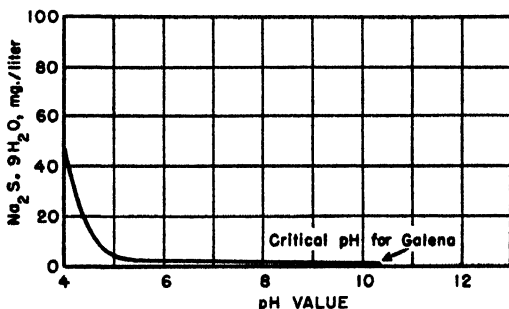


Fig. 14. Relationship between pH value and concentration of sodium sulfide to prevent contact at surface of galena (potassium ethyl xanthate, 25 mg./liter) (after Wark and Cox).

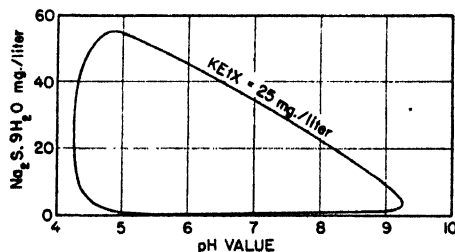


Fig. 15. Influence of pH value and concentration of sodium sulfide on contact at a surface of cerussite (contact possible inside curve) (73).

added per liter. From these data it may be shown that through a pH range of 4.0 to 10.0 and along the curve of Figure 14, the  $\text{H}_2\text{S}$  concentration varies by a factor of  $2.4 \times 10^4$ , the  $\text{HS}^-$  by a factor of 40, and the  $\text{S}^{--}$  by a factor of  $2 \times 10^8$ . It would therefore seem that the hydrosulfide ion concentration is the only reasonably constant figure, and, therefore, that this ion is responsible for the depression. The actual mechanism seems to be that of competition between the hydrosulfide ion and collector ion at the activated mineral surface.

Taggart (66) attributes depression in the presence of excess sulfide ion to two effects: (a) the formation of sulfide surfaces, on the oxidized minerals, of lower solubility than the corresponding metal-collector salt, *e.g.*, lead sulfide is less soluble than lead xanthate, and (b) the maintenance of reducing conditions by the sulfide ion, rather than oxidizing conditions. It will be remembered that Taggart postulates oxidation of sulfide surfaces before collection with sulfhydryl collectors becomes permissible.

In practice, hydrogen sulfide, the alkali metal, and ammonium sulfides, and calcium and barium polysulfides have been used for sulfidization, al-

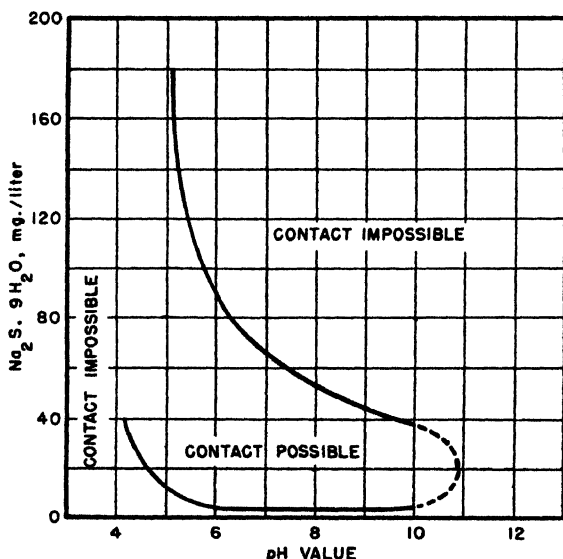


Fig. 16. Influence of pH value and concentration of sodium sulfide on contact at a surface of anglesite (potassium ethyl xanthate, 25 mg./liter) (after Wark and Cox).

though sodium sulfide is the most commonly used activator. To avoid high alkalinity and high hydrosulfide ion concentration, the sulfidizer is usually added in stage addition, alternating with collector addition.

Gaudin and Rizo-Patrón (35) have investigated the mechanism of the activation of quartz with barium ion, using oleate ion as collector. They found that barium abstraction is a function of pH, being nil in acid solution, small at or near neutrality, and substantial in alkaline solution. Because acid or alkali added to aqueous suspensions of quartz does not lower or raise, respectively, the pH by the calculated amount, they conclude that the quartz surfaces are covered with both hydrogen and hydroxyl ions. Addi-

tion of alkali, such as sodium hydroxide, to a suspension of quartz in water, presumably either liberates hydrogen ion and causes simultaneous adsorption of hydroxyl ion, or else hydroxyl ion alone is removed from the solution. Either mechanism will explain the observed facts. A further conclusion is that sodium ions will exchange with hydrogen ions on the surface of the quartz. When barium ions are added to the suspension they are adsorbed by exchange with the sodium. The quartz, activated in this manner can be floated by addition of oleate ion and an oily collector. However, Gaudin and Rizo-Patrón found that maximum recovery of quartz was obtained when the molecular ratio of oleate to barium was 1:1, and that almost complete depression of the quartz resulted when the ratio of collector to activator was 2:1. Elaborating on these results with some ingenious reasoning, these writers demonstrate that the loci of ruptured bonds on quartz occur with an average frequency of two loci (one with anionic preference, one with cationic preference) per 23.4 square angstroms of surface. In water,  $4.27 \times 10^{14}$  hydrogen ions and the same number of hydroxyl ions may be accommodated, then, per square centimeter of surface. By predicating "adsorption of one barium ion at every locus of ruptured bond on the quartz surface" they compute the maximum adsorbability of barium ion to be  $1.7 \times 10^{-6}$  mole per gram of the quartz used, which had a calculated specific surface of 1240 sq. cm. per gram. Their determined value, for conditions not necessarily representing maximum adsorbability, was  $1.27 \times 10^{-6}$  mole per gram, a result in good agreement with the theoretical.

These investigators conclude that with an oleate-barium ratio of unity, one valency of the barium ion is directed toward the quartz, leaving the other valence bond directed to the oleate ion. Lack of flotation at a ratio of 2 is ascribed to adsorption of a second layer of oleate ion with the polar bonds directed into the water phase. Interestingly enough, this means that the ion  $(\text{BaOl})^+$  functions as a cationic collector, although oleate ion is considered as an anionic collector. Similarly flotation of calcite, fluorite, and silica using calcium ion as activator would be cationic rather than anionic.

By extension of this reasoning, these authors advance the thought-provoking suggestion that, should activation by the mechanism described prove of general application, the nonactivated minerals, galena, pyrite, and the copper sulfides are actually floated, not by the collector ion, but by a cation formed from the monovalent anion of the collector and the bivalent cation of the mineral. Galena, then, would be floated by the cation  $\text{Pb}(\text{SSCOC}_2\text{H}_5)^+$  and not by the anion  $(\text{SSCOC}_2\text{H}_5)^-$ . The converse reasoning is applicable to the function of the so-called cationic collectors.

If, as is frequently asserted, quartz in water has silicate ions available at its surface, then flotation with lauryl pyridinium iodide may be attributable to the bonding of these ions, the anion  $(C_8H_5N.C_{16}H_{33}.SiO_3)^-$  acting as an *anionic* collector.

Clemmer (11) has been unable to confirm Gaudin and Rizo-Patrón's work regarding the pertinent influence of collector-activator ratio when floating silica from iron oxide minerals; and he states that: "an excess of activator is more deleterious than an excess of collector." With respect to the activation of quartz with cations, Clemmer has found that the relatively insoluble compounds formed between anionic collectors (such as soaps, and alkyl sulfates and sulfonates) and metals (such as calcium, magnesium, barium, strontium, and lead) are efficient activators, provided that the proper quantity is used at an optimum pH. He also notes that copper, aluminum, iron, and zinc salts have been used for the same purpose. Table VI is taken from Clemmer's paper and shows the permissible pH range and optimum pH at which the listed cations function as quartz activators.

TABLE VI  
Permissible and Optimum pH for Metal-Salt Activation of Quartz (11)

Cation	Permissible pH range	Optimum pH
Cu.....	5.0- 9.0.....	6.0
Mg.....	7.5-12.0.....	10.4
Ca.....	9.5-12.5.....	11.0
Ba.....	5.5-14.0.....	10.0
Zn.....	5.5-11.0.....	9.5
Pb.....	4.5-14.0.....	11.0
Fe(III).....	3.0- 8.0.....	5.0

Another type of activation is referred to by Taggart (66) as "common-ion activation." Remembering that the chemical theory of collection postulates a film of metal salt, on the sulfide mineral surface, of lower solubility than the equivalent salt in bulk, then by the law of mass-action addition of a metal ion common to this metal of the salt will load the surface with metal ion, and this in turn should require less activator. Thus Wark and Cox found that zinc would activate sphalerite, which was uncollectable with ethyl xanthate, and that copper ion activates chalcopyrite, which is otherwise not collected with methyl xanthate. However, an alternative explanation for these examples is that addition of the common ion so lowers the solubility of the metal xanthate in water that it is precipitated on the

mineral surfaces. Wark and Cox (69) found this explanation valid for the collection of sphalerite in the presence of amyl xanthate and zinc ion, *i.e.*, bubble attachment was impossible until precipitation of zinc amyl xanthate occurred in solution. In the case of sphalerite and ethyl xanthate no collection occurred even when the solubility product of zinc ethyl xanthate was exceeded by adding zinc ion. Likewise, the writer has found that contact between air and galena is immediate in a saturated solution of lead ethyl xanthate but that addition of lead ion inhibits contact.

Some minerals can be apparently "activated" by the small quantities of grease or oil used in mining operations. On occasion the writer has found that this activating film is very tenacious, and that up to 20 lb. cyanide per ton of ore has not sufficed to depress marmatite. Cleaning of the mineral surfaces with small quantities of emulsifying agents, together with cyanide, has effected complete depression.

#### **4. Depressants**

The reader will understand by now that depression is the converse of activation, usually involving the addition of reagents to the pulp to prevent certain minerals from floating. Separation of galena, sphalerite, and pyrite from one another is accomplished by judicious use of activators and depressants. Calcium hydroxide and cyanide added to the ball mill during grinding inhibit flotation of sphalerite and pyrite when a sulfhydrylic collector is later added to float the galena. High hydroxyl ion concentration and cyanide ion both depress the pyrite, and cyanide ion depresses the sphalerite. The next step consists of addition of copper ion, which destroys the cyanide ion and activates the sphalerite so that it may be floated with the customary reagents. The pyrite, now depressed by the hydroxyl ion alone, is subsequently floated by acidifying the circuit.

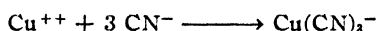
Depression of the types mentioned above are fairly well understood, but there are a number of other ways of accomplishing the same end, and in general the mechanism of depression is a poorly investigated field. Depression is effected in one or more of the following ways.

- (1) Removal of an activating superstrate by a solubilizing agent.
- (2) Formation of a hydrophilic coating on the mineral by adsorption of a colloidal depressant or of a hydrophilic ion.
- (3) Resurfacing of the mineral by a coating that is more readily adsorbed by the mineral than is the collector, or is more insoluble than the compound formed between collector and mineral.
- (4) Removal of adsorbed or chemically formed collector coating by emulsification (detergency) or by chemical reaction.

- (5) Depression by slime-coating.
- (6) Dispersion.
- (7) Selective depression of mineral by starvation feeding of collector.

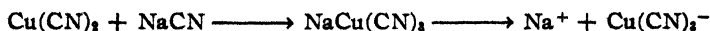
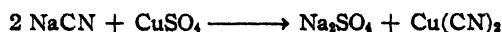
This classification is incomplete, for other mechanisms are available for effecting depression.

The classic example of (1) is the deactivation or depression of copper-coated sphalerite in the preferential flotation of sulfide lead-zinc ores. The mechanism of this reaction has been discussed at great length in the technical literature (70). Christmann (10) offers a mechanism for the observation that cyanide ion is abstracted by sphalerite (42). On the other hand, Gaudin (26) and his co-workers do not believe that cyanide ion is abstracted, and Gaudin (33) is explicit in attributing deactivation to removal of the copper ion as a cupric cyanide, which is unable to furnish sufficient copper ions to maintain activation:



Taggart (66) is also of this opinion. Dean (20) believes that the cyanide functions by preventing the formation of, or by removing, a collector superstrate by detergency. Other theories have been advanced involving preferential coating by slime.

Wark (72) and his colleagues have made a very thorough investigation of the deactivation of sphalerite, employing the contact angle method and varying such factors as pH, cyanide concentration, type of collector, temperature, and cation concentration. They found a relationship between the cyanide and alkali concentration necessary to prevent precipitation of cuprous xanthate at constant copper sulfate and xanthate concentrations, which was paralleled over a given pH range by the contact curve for pre-activated sphalerite. Hydrocyanic acid is a weak acid and as Barsky (5) pointed out, the cyanide ion concentration will be greatly influenced by the alkali concentration. It is significant that over the aforementioned range the ratio of NaCN to  $\text{CuSO}_4$  is slightly greater than 3:1, *i.e.*, there is approximate correspondence to the following reaction:



By the extension of their experimental work to other minerals, Wark and Cox have shown that for most minerals there is a critical cyanide ion concentration, below which contact is possible and above which contact is impossible. Except for the copper minerals, it does not seem possible to predicate a reaction of the type given above, although it may be significant

that the metal ion of those minerals that are depressed can form complex compounds with cyanide. As Wark points out, the significance of their results is not always clear, and it is possible that cyanide ion, when present in sufficient quantity, competes with collector ion for the mineral surface. In such cases the mechanism would correspond to (2) above.

Wark has also shown that there is a critical hydroxyl ion concentration above which contact is impossible, and in the soap flotation of iron ores, Clemmer (11) attributes depression of the iron oxide minerals to high hydroxyl ion concentration. Figure 17 shows the relation between the

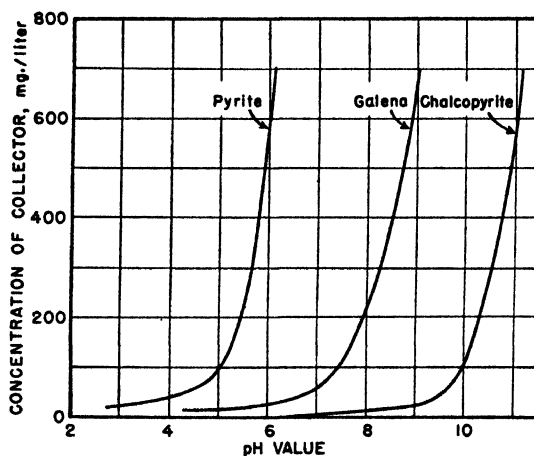


Fig. 17. Relation between concentration of sodium diethyl dithiophosphate and critical pH value for pyrite, galena, and chalcopyrite (70).

concentration of sodium diethyl dithiophosphate and critical pH value for three minerals. Contact is possible only to the left of each curve. In Wark's words (72):

Barsky drew attention to the fact that the corresponding curve for galena and ethyl xanthate conforms to the relationship:

$$[X^-] \times [H^+] = \text{constant} \quad (1)$$

in which  $[X^-]$  and  $[H^+]$  represent the concentrations of the xanthate and hydrogen ions, respectively. Similar equations hold for the other curves. Now since in any system containing water:

$$[H^+] \times [OH^-] = \text{constant} = 10^{-14} \quad (2)$$

it follows from (1) and (2) that, along any of these curves:

$$[X^-]/[OH^-] = K \text{ (a constant)} \quad (3)$$

From this, if a mineral is placed in a solution and the value of  $[X^-]/[OH^+]$  is greater than  $K$ , collector ion will be adsorbed by the mineral surface, and contact will be possible. If less than  $K$ , hydroxyl ion will be adsorbed and contact becomes impossible.

There seems to be competition between collector ions and hydroxyl ions at the mineral surface, and as hydroxyl ions are hydrophilic, depression results when these are in possession of the mineral surface, as in (2).

It must be admitted, in the lack of more experimental evidence, that much of this is speculation, and that other theories are capable of explaining the depression caused by cyanide and hydroxyl ions. It is common experience in practice to find that additions of zinc ion markedly improve the deactivation of sphalerite by cyanide ion, yet no reasonable theory has been advanced to explain this effect. Cyanide is a most effective depressant for pyrite, and since pyrite is collectable without activation, it is not a deactivator in the same sense that it is for sphalerite. Taggart (66) explains depression in this case as the result of closure of the pyrite surface to oxidation (oxidation being a requirement for collection according to his theory) by surface-precipitated ferrous or ferric ferrocyanides. Similarly he attributes depression of the copper-ion minerals (chalcopyrite, bornite) to closure of surface by copper ferrocyanide.

Galena is not depressed by cyanide ion in the presence of sulfhydrylic collectors. Yet Dean, Clemmer, and Cooke (18) have shown that when lauryl pyridinium iodide is used as a collector, cyanide is a marked depressant for the same mineral, which Dean (20) attributes to an increase in detergency by the cyanide.

An instance of (3) is possibly afforded by the depression of galena by potassium chromate and dichromate, or by chromic acid. A bulk concentrate of galena and chalcopyrite can be floated from sphalerite by using normal collectors, cyanide, and high lime. Separation of the two minerals in the bulk concentrate may then be effected by addition of chromate or dichromate ion, the galena being depressed after adequate conditioning time, the chalcopyrite readily floating. The galena can be reactivated with reducing reagents such as ferrous ion or sulfur dioxide. As lead chromate is less soluble than lead xanthate, Taggart (66) attributes depression of the galena to formation of a multicoating of lead chromate. Wark (72), however, points out that lead chromate (in the form of the mineral crocoite) is floatable by ethyl xanthate.

Depression of pyrite with chromate, dichromate, and permanganate ion has been attributed not to formation of an insoluble coating (the iron chromates are soluble) but to oxidation of the collector. This explanation



is unsatisfactory, for collector-coated chalcopyrite will float at high chromate and dichromate ion concentrations.

Depression caused by overdetergency (4) has already been discussed under "Collection." Such a phenomenon may be due to other causes such as formation of a second layer of surface-active compound on the collector-coated mineral (page 345) or to solidification of the compound at the bubble surface. Wark discusses at some length the mechanism of the last-mentioned process (72). Taggart (66) states: "Acid and alkali in soap flotation form acid and basic soaps at coated particle surfaces; these ionize and thus decrease the tendency to levitation."

Depression by slime-coating (5) is usually accidental, and as far as the writer knows is not intentionally employed as a method of depression. Slime-coating prevents flotation by interference with the attachment of air bubble to the mineral surface.

An example of (6) is the use of protective colloids to selectively coat with a water-avid film that mineral that is to be depressed. Silicate minerals are depressed in sulfide flotation by surfacing the mineral particles with the hydrophilic silicate ion. The use of glue and related colloidal substances for this purpose has already been mentioned.

Mechanism (7) is rarely employed, and then only as a last resort. Of two minerals that can adsorb or react with a collector ion, that mineral with the greater adsorbability will float preferentially when the collector ion concentration is kept low.

## References

1. Adams, A. S., "Flotation Practice," *A.I.M.E.*, 1928, p. 216. Papers and discussions presented at meetings held at Salt Lake City (August, 1927) and New York (February, 1928).
2. Arbiter, N., Kellogg, H. H., and Taggart, A. F., *A.I.M.E.*, **Trans.** 153, 517 (1943).
3. Bankoff, S. G., *A.I.M.E.*, **T.P.** 1391 (1941).
4. Barsky, G., and Falconer, S. A., *Trans. Electrochem. Soc.*, **60**, 343 (1931).
5. Barsky, G., *A.I.M.E.*, **Trans.** 112, 236 (1934).
6. Bartsch, O., *Kolloidchem. Beihefte*, **20**, 1 (1924).
7. Bates, W. A., and Miller, R. J., *A.I.M.E.*, **T.P.** 2015 (1946).
8. Bishop, W. T., *A.I.M.E.*, **T.P.** 2011 (1946).
9. Bond, F. C., and Maxson, W. L., *A.I.M.E.*, **T.P.** 888 (1938).
10. Christmann, L. J., *American Cyanamid Company*, **T.P.** 17 (1930).
11. Clemmer, J. B., *Flotation of Iron Ores*. Center for Continuation Study, Univ. Minnesota, Minneapolis, 1947.
12. Clemmer, J. B., and Coghill, W. H., *Eng. Mining J.*, **129**, 551 (1930).
13. Clemmer, J. B., and Cooke, S. R. B., *U. S. Bur. Mines, Rept. Invest.* 3333 (1937).
14. Coghill, W. H., and Anderson, C. O., *U. S. Bur. Mines*, **T.P.** 262 (1923).
15. Coghill, W. H., and Clemmer, J. B., *A.I.M.E.*, **Trans.** 112, 449 (1934).

16. Coghill, W. H., DeVaney, F. D., Clemmer, J. B., and Cooke, S. R. B., *U. S. Bur. Mines, Rept. Invest.* **3271** (1935).
17. Dean, R. S., *Mining Sci. Press*, **122**, 291 (1921).
18. Dean, R. S., Clemmer, J. B., and Cooke, S. R. B., *U. S. Bur. Mines. Rept. Invest.* **3333** (1937).
19. Dean, R. S., and Hersberger, A. B., *A.I.M.E., Trans.* **134**, 81 (1939).
20. Dean, R. S., and Ambrose, P. M., *U. S. Bur. Mines, Bull.* **449** (1944).
21. Devaux, H., *J. phys. radium* **2**, 237 (1931).
22. De Witt, C. C., and von Batchelder, F., *J. Am. Chem. Soc.*, **61**, 1247 (1939).
23. Diener, F. P., Clemmer, J. B., and Cooke, S. R. B., *U. S. Bur. Mines, Rept. Invest.* **3247** (1935).
- 23a. Emmett, P. H., S. Brunauer, and E. Teller, *J. Am. Chem. Soc.*, **59**, 2682 (1937).
24. Fahrenwald, A. W., *Idaho Bur. Mines Geol., Pamphlet* **64** (1943).
25. Gates, J. F., and Jacobsen, L. K., *Univ. Utah Research Invest., Bull.* **16** (Vol. 16, No. 4) (1925).
26. Gaudin, A. M., Haynes, C. B., and Haas, E. C., *Univ. Utah and U. S. Bur. Mines, T.P.* **7** (1930).
27. Gaudin, A. M., Groh, J. O., and Henderson, H. B., *A.I.M.E., T.P.* **414** (1931).
28. Gaudin, A. M., *Flotation*. 1st ed., McGraw-Hill, New York, 1932.
29. Gaudin, A. M., and Wilkinson, W. D., *J. Phys. Chem.*, **37**, 833 (1933).
30. Gaudin, A. M., *et al.*, *A.I.M.E., Trans.* **112**, 319 (1934).
31. Gaudin, A. M., and Malozemoff, P., *A.I.M.E., Trans.* **112**, 303 (1934).
32. Gaudin, A. M., and Schuhmann, R., *J. Phys. Chem.*, **40**, 257 (1936).
33. Gaudin, A. M., *Principles of Mineral Dressing*. 1st ed., McGraw-Hill, New York, 1939.
34. Gaudin, A. M., *A.I.M.E., T.P.* **1242** (1940).
35. Gaudin, A. M., and Rizo-Patrón, A., *A.I.M.E., Trans.* **153**, 462 (1943).
36. Gaudin, A. M., *Eng. Mining J.*, **146**, 91 (1945).
37. Gaudin, A. M., and Preller, G. S., *A.I.M.E., T.P.* **2002** (1946).
38. Gaudin, A. M., and Sun, S. C., *A.I.M.E., T.P.* **2005** (1946).
39. del Giudice, G. R. M., *A.I.M.E., Trans.* **112**, 398 (1934).
40. *Handbook of Chemistry and Physics*. 26th ed., Chemical Rubber Pub. Co., Cleveland, 1942.
41. Hassialis, M. D., *A.I.M.E., T.P.* **1583** (1943).
42. Ince, C. R., *A.I.M.E., Trans.* **87**, 261 (1930).
43. Kellogg, H. H., *A.I.M.E., T.P.*, **1841** (1945).
44. Langmuir, I., *J. Am. Chem. Soc.*, **39**, 1848 (1917).
45. Leaver, E. S., Woolf, J. A., and Head, R. E., *U. S. Bur. Mines, Rept. Invest.* **3226** (1934).
46. Malozemoff, P., and Wilkinson, W. D., *A.I.M.E., Trans.* **112**, 465 (1934).
47. Mattson, S., *J. Phys. Chem.*, **32**, 1531 (1928).
48. Mortenson, M., *Tids. Kjem. Bergvesen*, **10**, 118 (1930).
49. Ralston, O. C., and Hunter, W. C., *A.I.M.E., Trans.* **87**, 401 (1930).
50. Ralston, O. C., and Barker, L. M., *Trans. Electrochem. Soc.*, **60**, 319 (1931).
51. Ravitz, S. F., and Porter, R. R., *A.I.M.E., T.P.* **513** (1934).
52. Ravitz, S. F., and Wall, W. A., *J. Phys. Chem.*, **38**, 13 (1934).
53. Ravitz, S. F., *A.I.M.E., Trans.* **153**, 528 (1943).
54. Rose, E. H., *A.I.M.E., T.P.* **1679** (1944).

55. Rose, E. H., *A.I.M.E.*, T.P. 1702 (1944).
56. Schürman, *Ann.*, 249, 326 (1888).
57. Sun, S. C., *A.I.M.E.*, Trans. 153, 479 (1943).
58. Sutherland, K. L., *A.I.M.E.*, T.P. 1098 (1939).
59. Sutherland, K. L., *A.I.M.E.*, Trans. 153, 453 (1943).
60. Taggart, A. F., and Gaudin, A. M., *A.I.M.E.*, Trans. 68, 479 (1923).
61. Taggart, A. F., *Handbook of Ore Dressing*. Wiley, New York, 1927.
62. Taggart, A. F., Taylor, T. C., and Knoll, A. F., *A.I.M.E.*, Trans. 87, 217 (1930).
63. Taggart, A. F., Taylor, T. C., and Ince, C. R., *A.I.M.E.*, Trans. 87, 285 (1930).
64. Taggart, A. F., del Giudice, G. R. M., and Ziehl, O. A., *A.I.M.E.*, Trans. 112, 348 (1934).
65. Taggart, A. F., del Giudice, G. R. M., Sadler, A. M., and Hassialis, M. D., *A.I.M.E.*, T.P. 838 (1937).
66. Taggart, A. F., *Handbook of Mineral Dressing*. 2nd ed., Wiley, New York (1945).
67. Taggart, A. F., and Hassialis, M. D., *A.I.M.E.*, T.P. 2078 (1946).
68. Taylor, T. C., and Knoll, A. F., *A.I.M.E.*, Trans. 112, 382 (1934).
69. Wark, I. W., and Cox, A. B., *A.I.M.E.*, Trans. 112, 189 (1934).
70. Wark, I. W., and Cox, A. B., *A.I.M.E.*, Trans. 112, 245 (1934).
71. Wark, I. W., and Cox, A. B., *J. Phys. Chem.*, 39, 551 (1935).
72. Wark, I. W., *Principles of Flotation*. Australasian Inst. Mining & Met., Melbourne, 1938.
73. Wark, I. W., and Cox, A. B., *A.I.M.E.*, Trans. 134, 7 (1939).
74. Wark, I. W., and Cox, A. B., *A.I.M.E.*, Trans. 134, 26 (1939).
75. Wark, I. W., and Sutherland, K. L., *A.I.M.E.*, Trans. 134, 53 (1939).
76. Weinig, A. J., *Quarterly Colorado School Mines*, 28, No. 3 (1933).
77. Weiss, N., *A.I.M.E.*, T.P. 2213 (1947).
78. Wentworth, H. A., *Eng. Mining J.*, 90, 15 (1910).

## SUBJECT INDEX

### A

Absorption, and adsorption, 60  
 Acetamide monolayers, configurations, 77  
 Acrylates, 80  
 Activated adsorption, 60-63  
   and chemisorption, 60  
 Activation, classic example, 357  
   common-ion, 367  
 Activation energy, for dynamic fatigue, 297  
   of various cord tests, 298  
 Activators as flotation reagents, 324, 357-368  
 Active spots, of crystals, 11, 16  
   and healing of crystals, 11  
   and recrystallization, 11  
   and sintering, 11  
 Adsorbed films, 70  
   of proteins, 75  
 Adsorbed ions, interaction with surface, 8-20  
   polarization of dielectric surface, 13  
 Adsorbed molecule(s), changes in, 60-63  
   electrostatic polarization, 36-38  
   mutual van der Waals' forces, 49-52  
 Adsorbing surface, changes in, 58-60  
 Adsorption, and absorption, 60  
   activated, 60-63  
   and atomic forces, 1-66  
   of atoms, by nonpolar van der Waals' forces, 24-27  
   collaboration between various forces, 38-58  
   and covalent bond formation, 20  
   on metal surfaces by van der Waals' forces, 29-32  
   physical, 20-21  
   of single atom or molecule, various forces collaborating in, 38-46  
   van der Waals', 20  
 Adsorption energy, 6, 9  
   of cesium ion, 52  
   at crystal corners, 10  
   at crystal edges, 10  
   of dipole molecule on metallic surface, 41  
   due to electrostatic induction of a dielectric, 14  
   of a growing crystal, 11  
   of ion on an ionic surface, 42  
   on metal surface, 12, 44  
   of molecule with nonperipheral dipole on ionic surface, 40

Adsorption energy (*continued*):  
   with peripheral dipole on ionic surface, 41  
   and repulsion forces, 7  
 Adsorption force, 2  
 Adsorption kinetics, at air-water interfaces, 80-82  
   at oil-water interfaces, 80-82  
 Adsorption rate, at air-water interfaces, 80  
 Adsorption solubility product, 342  
 Adsorption theory, of collection of minerals, 338  
 Aeration, in flotation, 331-334  
 Agglomerate tabling, 334  
 Air-water interfaces, kinetics of adsorption, 80-82  
 Alkyl sulfates as flotation collectors, 355  
 Alkyl sulfonates as flotation collectors, 355  
 Amines as flotation collectors, 356  
 Amorphous polymers, 80  
 Anionic flotation collectors, 354-355, 367  
 Anthelmintic activity, of hexylresorcinol in presence of soaps, 92-94  
 Antibody-antigen monolayers, 74  
 Antigen-antibody monolayers, 74  
 Atom adsorption by nonpolar van der Waals' forces, 24-27  
 Atom size and nonpolar van der Waals' forces, 25  
 Atomic diamagnetic susceptibility, 23  
 Atomic forces, and adsorption, 1-66  
 Atoms, on surfaces, 17-20  
 Attraction forces, collaborating in adsorption of single atom or molecule, 38-46  
   and repulsion, 2-8

### B

Bending endurance of fibers, 287  
 Biological activity, of homologous series, 91  
 Biological problems, and surface phenomena, 91-95  
 Blended stocks of rubber, physical properties, 252  
 Birefringence, 28  
 Boltzmann superposition principle, 308  
 Boltzmann's constant, 100  
 Boltzmann's theorem, 100  
 Bouncing putty, and gelation, 147  
 Brownian movement, as factor in electrophoretic theories, 113  
 Brunauer's concept of physical adsorption, 21

Burger's theory, for threadlike molecules, 174

## C

Capillary rise method, for surface studies, 70  
 Captive bubble method, of collection of minerals, 336  
 Carboxylic flotation collectors, 354  
 Catalase monolayers, 74  
 Cataphoresis, 97. See also *Electrophoresis*.  
 Cationic flotation collectors, 355-356  
 Cellulose and ultracentrifuge, 162  
 Cellulose nitrate, frequency functions, 204-208  
   molecules, properties of, 202-204  
   stable preparations for sedimentation studies, 198  
   ultracentrifugal sedimentation studies, 198-208  
   validity of Staudinger law, 202  
 Centrifugal field, change of molecular shape in, 168-170  
 Chains, molecular, physical rupture in fatigue, 223  
 Charge, electrophoretic, compared to Donnan equilibrium data, 130  
   compared to membrane potential data, 130, 131  
   compared to titration data, 130, 131  
   and potential, 120-122, 133  
   and zeta potential, applications, 128-130  
 Charge density, in double layer, 101  
   relation to potential, 114  
   on surface, 103  
 Chemical collectors in flotation, 325  
 Chemical scission and fatigue, 226-227  
 Chemical theory, of collection of minerals, 338  
 Chemisorbed molecules, additional forces emanating from, 52-54  
 Chemisorption, 17, 19, 20  
   and activated adsorption, 60  
   and Fischer-Tropsch synthesis, 19  
   and temperature, 60  
 Class A fatigue, 229, 230  
 Class B fatigue, 229, 230  
 Class C fatigue, 229, 231  
 Class D fatigue, 229, 231  
 Class E fatigue, 232  
 Class F fatigue, 232-233  
 Coacervation, 98  
 Coagels, liquid content, 138  
 Collection, effect of slimes, 347-353  
   and flocculation, 353-354  
   mechanism, 338-346  
 Collectors, flotation, 324, 336-356  
   flotation, alkyl sulfates, 355  
   alkyl sulfonates, 355

Collectors (*continued*):

- amines, 356
- anionic, 354-355
- carboxylic, 354
- cationic, 355-356
- classification, 354-356
- dithiocarbamates, 355
- dithiocarbonates, 355
- dithiophosphates, 355
- oil, 356
- phosphonium, 356
- sulfonium, 356
- thio alcohols, 355

Collector coating, orientation on the mineral, 346-347

Colloid(s), electrophoretic velocity, quantitative interpretation, 97-135  
   hydrophilic, and electrophoresis, 98  
   hydrophobic, and electrophoresis, 98  
   and surface chemistry, 67-96

Colloidal systems, applications of surface chemistry to, 70-95

Colloid production in grinding, 323-324

Common ion activation, 367

Compensation charge of suspended particle, 99

Concentration dependence, comparison between osmotic pressure and sedimentation, 180  
   and sedimentation, 177-181  
   of viscosity of high polymers, 203

Concentration gradient curve, 182, 183, 184

Condensed monolayers, 88

Conductance, surface, influence, 117-118

Conduction electron, 18

Conductivity of particle and electrophoresis, 107-108

Configurational probability, of molecules, 167

Cords, cumulative extension, 303

Cord tests, activation energies, 298

Cotton, hysteresis, 299

Cotton cords compared to viscose rayon cords, 303, 304

Coulomb forces, 3

Coulomb interaction, between surface and adsorbed ion, 8-11

Covalent bonds, and exchange forces, 3  
   and nonpolar van der Waals' forces, 45-46

Covalent bond formation and adsorption, 20

Crack growth of rubber, 250

Crack incipience of rubber, 250

Creep, of fibers, long-term, 282-286  
   law, 308

of plastics, 307-309

and relaxation phenomena, and fatigue, 221

Creep failure, effects of temperature on fatigue, 297  
 Critical creep stress, 308  
 Critical potential, 98  
 Cross linking, and fatigue, 226-227  
 Crystallization of high polymers and fatigue, 225-226  
 Cumulative extension, effect of frequency, 304  
     effect of residual tension, 304  
     *vs.* imposed energy, 305  
     of yarns and cords, 303  
 Cyanide ion, use in preferential flotation, 324

D

$dB/dx$  method of Gralén, 185-188  
 Debye-Hückel ionic atmosphere, 100  
 Debye induction effect, 21  
 Degrees of freedom and molecular configuration, 166-167  
 De Mattia machine for testing dynamic fatigue, 314  
 Depressants as flotation reagents, 324, 368-372  
 Depression, methods of achieving, 368  
 Desorption from interfaces, 82-83  
 Detergent theory of collection of minerals, 338  
 Dichroism, 28  
 Dielectric constant, 14, 100  
     of liquid, in Smoluchowski derivation, 101  
 Dielectric surface, polarization by adsorbed ion, 13-16  
 Diffusion constant and concentration, 177  
 Dilatancy, 146-147  
 Dipole molecule on metallic surface, adsorption energy, 41  
 Dipole moment, 14  
 Dispersion forces, 3, 21, 24  
 Displacement effect in sedimentation studies, 182  
 Dithiocarbamates as flotation collectors, 355  
 Dithiocarbonates as flotation collectors, 355  
 Dithiophosphates as flotation collectors, 355  
 Double layer, electric moment, 103  
 Double layer charge, and specific surface conductivity, 117  
 Double layer deformation, influence on electrophoresis, 109-120  
 Dreft, chemical composition, 329  
 Drygel, 138  
 Dunlop fatigue tester, 234  
 Dynamic cycling tests and fatigue, 221  
 Dynamic fatigue, of fibers, 286-306

Dynamic fatigue (*continued*):  
     to rupture, 309-315  
     of viscose rayon, compared to cotton, 303, 304  
 Dynamic fatigue experiments, 246-254  
 Dynamic fatigue life, qualitative theory of effect of strain magnitudes and limits on, 254-263  
 Dynamic resilience, 239

E

Elastogels, 138  
 Electric conductance of liquid in Smoluchowski's derivation, 101  
 Electric dipole, 52  
 Electric field and electrophoresis, 101  
 Electric image, 11  
 Electron microscopy and lyogel elasticity, 150  
 Electro-osmosis and electrophoresis, 99  
     comparison, 119  
 Electro-osmotic mobility and electrophoretic mobility, 112  
 Electrophoresis, definition, 97  
     and electro-osmosis, 99  
     comparison, 119  
     and hydrophilic colloids, 98  
     and hydrophobic colloids, 98  
     influence of double layer deformation, 109-120  
     and isoelectric point determinations, 98  
     of liquid droplets, 108-109  
     of mercury drops, 107, 108  
     of oil drops, 119  
     and particle conductivity, 107-108  
     and zeta potential, 118-119  
 Electrophoretic charge, comparison with charge determined otherwise, 130-133  
 Electrophoretic data on proteins, 129  
 Electrophoretic equation, for symmetrical electrolytes, 114  
     for unsymmetrical electrolytes, 114  
 Electrophoretic mobility 98  
     and electro-osmotic mobility, 112  
     Henry's equation for calculation, 105  
     of infinitely long cylindrical particles, 107  
     of microscopic particles, 111  
     in symmetrical electrolytes, 116  
     in unsymmetrical electrolytes, 116  
 Electrophoretic retardation, 103, 109  
 Electrophoretic theories, and Brownian movement, 113  
     experimental tests, 119-120  
 Electrophoretic velocity, and charge of particles, 120-133  
     classical concepts, 99-109  
     of colloids, quantitative interpretation, 97-135

Electrophoretic velocity (*continued*):  
  of particle, calculation, 102  
  total influence of Henry's correction on, 115, 116  
Electrostatic polarization, of an adsorbed molecule, 36-38  
  of atoms, 3  
  and nonpolar van der Waals' forces, 39-40  
Emulsions, 80-89  
  structure of stabilizing film, 83-89  
Emulsion systems, reactions, 89  
End positions, of crystals, significance, 11, 16  
Endurance limit, in fatigue, 310  
Energy versus potential curves, and theories of gelation, 141  
Entropy changes, significance, 56-58  
Enzymes as monolayers, 74  
Epsilon potential, 100  
  and zeta potential, difference, 100  
Equilibrium distance, 6  
Exchange forces, 3  
Eyring non-Newtonian dashpot, 276  
Eyring theory of flow, 276, 285, 294

## F

Fat absorption, mechanism, 91-92  
Fatigue, basic phenomena occurring with, 222-227  
  chemical and physical, 220  
  and chemical scission, 226-227  
  class A, 229, 230  
  class B, 229, 230  
  class C, 229, 231  
  class D, 229, 231  
  class E, 232  
  class F, 232-233  
  and cross linking, 226-227  
  and crystallization, 225-226  
  definitions, 220-221  
  dynamic, to rupture, 309-315  
    of viscose rayon, compared to cotton, 303, 304  
  effect of temperature, 297  
  endurance limit, 309  
  of fibers, 272-306  
  as influenced by oxidation, 265-270  
  and molecular flow, 222-223  
  and molecular orientation, 223-225  
  parameters, 220  
  and physical rupture of molecular chains, 223  
  of plastics, 306-315  
  and quasi-permanent flow, 223  
  of rubbers, 233-272  
    general characteristics, 233  
    as related to weathering, 263-264  
  and secondary bond slippage, 222-223

Fatigue (*continued*):  
  and second-order transition, 226  
  static, effects of temperature, 297  
    at intermediate and low temperatures, 270-272  
    to rupture, 309-315  
Fatigue life, 309  
Fatigue life-temperature relationship, 315  
Fatigue phenomena, of high polymers, 219-320  
Fatigue resistance, 237  
Fatigue stress, 309  
Fatigue tests, generalized, 227-233  
  with hysteretic temperature rise, 233-237  
Fibers, bending endurance, 287  
  fatigue, 272-306  
    dynamic, 286-306  
    initial compliance, 285  
    long-term creep, 282-286  
    primary creep characteristics, 275-282  
    relaxation, 282-286  
    resilience, 273-275  
    static fatigue-rupture, 282-286  
    stress-strain, 275-282  
    weighted creep, 285  
Fibrillar theory of lyogel structure, 139  
Field strength, calculation, 101  
Film(s), adsorbed, 70  
  stabilizing, structure in emulsions, 83-89  
  structure in foams, 83-89  
Firestone Snap-Cycle machine, 290  
Fischer-Tropsch synthesis and chemisorption, 19  
Fixed liquid layer on particle surface, 100  
Flexometer, St. Joe, 234  
Floatability, inherent, 337  
Flocculation, and collection, 353-354  
  pseudo, 354  
  true, 354  
Flotation, 321-374  
  aeration in, 331-334  
  collectors, classification, 354-356  
  froth, 322  
  preferential, use of cyanide ion, 324  
  reagents, 324-372  
    definition, 324  
    frothers, 325-336  
  size range where recovery is maximum, 350  
  successful size range, 322  
  theory, based on differential gas adsorption, 332  
Foams, 80-89  
  structure of stabilizing film, 83-89  
Foam stability, Hardy's technique, 89  
Forces, types, 3  
Fractional precipitation, limit of selectivity and ultracentrifugal sedimentation, 201

Fractionation, and polymolecularity measurements, 194-215  
 selectivity, 198-202  
 Free radicals on surfaces, 17-20  
 Free valency electron, 17, 18  
 Frequency functions, of cellulose nitrate sedimentation studies, 204-208  
 from sedimentation diagrams, 188-192  
 triangular, 205  
 Frictional coefficient, in diffusion and sedimentation, 170  
 and molecular characteristics, 166  
 and sedimentation constant, 166  
 and shielding ratio, 176  
 Frictional resistance, and molecular shape, 166  
 Frother(s), desirable properties, 334  
 as flotation reagents, 324, 325-336  
 in practice, 334-336  
 structure, 328-330  
 two-phase systems, 325-328  
 Frother ions, distribution, 332  
 Froth flotation, 322  
 size range, 322  
 Frothing, and surface tension, 326  
 three-phase systems, 330-331  
 Froths, stability, explanations, 327  
 Froth stiffener, 327

## G

Gangue, 322  
 Gelation, and energy versus potential curves, 141  
 and ions, 142  
 and kinetic energy of neighboring particles, 141  
 Gibbs equation and frothers, 326  
 Goodrich Cord Vibrator, 291, 292, 295  
 Goodrich flexometer, 234  
 Gorin correction to electrophoresis theory, 125, 126, 131  
 Gouy-Chapman type double layer, 113  
 Gralén  $dB/dx$  method, 185-188  
 Gravity concentration. See *Flotation*.

## H

Hamaker's theory of lyogel structure, 139-140  
 Hanging plate method for surface studies, 70  
 Hardy technique for studying foam stability, 89  
 Heat aging of fibers, 297  
 Helmholtz unit, 103  
 Helmholtz-Smoluchowski equation, 99-103  
 Helmholtz theory of electrokinetic phenomena, 99

Henry equation, application to proteins, justification, 117  
 for calculating electrophoretic mobility, 105  
 Henry solution, of Smoluchowski and Hückel contradiction, 104-107  
 Henry's correction, total influence on electrophoretic velocity, 115, 116  
 Hexylresorcinol, anthelmintic activity, in presence of soaps, 92-94  
 High polymers. See also *Plastics*.  
 classification, 221-222  
 fatigue phenomena, 219-320  
 Hookean elasticity, 239  
 Horse-serum globulin, monolayer, 74  
 Hückel equation, 103-104  
 for coulomb forces, 9  
 Hückel-Smoluchowski theories, contradiction, 104-107  
 Hydrodynamic similarity principle, 180  
 Hydrogen bonding, 33  
 in protein and protein monolayers, 76-78  
 Hydrophilic colloids and electrophoresis, 98. See also *Water-avid groups*.  
 Hydrophobic colloids and zeta potential, 98  
 Hysteresis, of cotton, 299  
 of nylon, 299  
 of plastics, 307-309  
 of rayon, 300  
 of rubbers, 237-243  
 Hysteresis defect, 239  
 Hysteretic heat generation, 233

## I

Impact and single-cycle rupture tests, and fatigue, 221  
 Influence effect, 37  
 Initial compliance, of fibers, 285  
 Interfacial complexes, 85  
 Interfacial phenomena and surface chemistry, 67  
 Intermittent relaxation and fatigue, 227  
 Internal plasticization, 79  
 Intestinal emulsifying systems, 92  
 Intrinsic viscosity and concentration, 177  
 and sedimentation constant, 197, 209  
 Ion(s), adsorbed, and surface, interaction, 8-20  
 at fixed distance, energy contribution by various forces, 16  
 and gelation, 142  
 on ionic surface, adsorption energy of, 42  
 on metallic surface, adsorption energy, 44  
 Ion distances on crystal surfaces, 4  
 relation to second layer, 5  
 Ion interaction with a metal surface, 11-13



Ionic atmosphere of Debye-Hückel, 100  
 Isoelectric point, determination by electrophoresis, 98  
 Isogels, 139  
 Isopropyl alcohol, as spreading medium for protein monolayers, 71

## K

Keesom's alignment effect, 21  
 Knotty tear phenomenon, 257, 258  
 Kuhn's statistical coil, and sedimentation properties of molecules, 166

## L

Lamm scale method, for following sedimentation, 165  
 principles, 165  
 Laplace operator, 100  
 Light absorption method, for following sedimentation, 165  
 Lipide-protein films, 75  
 Liquid droplets, electrophoresis, 108-109  
 Liquid-liquid theory of lyogel structure, 139  
 London equation for mutual energy of interaction of a pair of atoms, 22  
 Loschmidt's number, 172  
 Lyogel(s), 137-160  
   desolvated, 138  
   elastic, x-ray diffraction, 148-150  
   elasticity, 147-158  
     and electron microscopy, 150  
     and ultramicroscopy with incident light, 150-158  
   special types, 143-147  
   structure, theories, 139-143  
   shape of particles, 143  
   water content, 138  
 Lyospheres around ions, 142

## M

Mechanical preconditioning, 308  
 Mercury drops, electrophoresis, 107, 108  
 Metastable state of high polymers, 222  
 Micellar theory of lyogel structure, 139  
 Microscopic particles, electrophoretic mobility, 111  
 Molecular branching, influence on sedimentation velocity, 170-172  
 Molecular chains, physical rupture in fatigue, 223  
 Molecular configuration and degrees of freedom, 166-167  
 Molecular entanglement, 172, 178  
 Molecular flow and fatigue, 222-223  
 Molecular shape, changes in centrifugal field, 168-170  
   and frictional resistance, 166

Molecular weights from monolayer measurements, 71-72  
 Molecule(s), adsorbed, changes in, 60-63  
   interaction between, 172-176  
   threadlike, sedimentation properties, 166-183  
 Monodispersity, 162  
 Monolayer(s), acetamide, configurations of, 77  
   antibodies, 74  
   condensed, 88  
   elasticity, 88  
   enzymes, 74  
   of long-chain amides, 74  
   polymers, 78-80  
   of ureas, 74

## N

Navier and Stokes equations, 104  
 Nernst equation, 100  
 Noncrystallizing copolymer, 223  
 Nonperipheral dipole on ionic surface, adsorption energy of molecule with, 40  
 Nonpolar van der Waals' forces, 21  
   additive character, results, 27-29  
   adsorption of atoms, 24-27  
   and atom size, 25  
   and covalent bonds, 45-46  
   and electrostatic polarization, 39-40  
   nature, 21-24  
 Nonspherical particles, 127-128  
 Nylon, hysteresis loops, 299

## O

Oedogene lyogel, 138  
 Oil absorption of pastes, 89  
 Oil collectors in flotation, 356  
 Oil-water interfaces, kinetics of adsorption, 80-82  
 Oily collectors in flotation, 325  
 Onsager correction of Debye-Hückel theory, 113  
 Ore grind, size limit, 323  
 Orientation of molecule and fatigue, 223-225  
 Oscillating jet technique for surface studies, 70  
 Osmotic pressure, and concentration, 177  
   and sedimentation, comparison of concentration dependence, 180  
 Overdetergency, 372  
 Overfilm, 79  
 Overfloculation, 353  
 Oxidation, effect on fatigue, 265-270

## P

Parameter functions, use in sedimentation studies, 192-194

- Particles, microscopic, electrophoretic mobility, 111  
nonspherical, 127-128  
spherical, 122-127
- Particle charge and electrophoretic velocity, 120-133
- Particle conduction in Smoluchowski derivation, 101
- Particle conductivity and electrophoresis, 107-108
- Particle dimensions, in Smoluchowski derivation, 100
- Particle form in Smoluchowski derivation, 100
- Pastes, 89-90  
flow behavior, 89  
sedimentation volume, 89
- Paucidispersity, 162
- Pauli principle, 3
- Pendant drop method for surface studies, 70
- Peripheral dipole on ionic surface, adsorption energy of molecule with, 41
- Phosphonium, as flotation collector, 356
- Philpot Schlieren method for following sedimentation, 165
- Pine oil as frother, 335
- Plasticity, definition, 306
- Plastics. See also *Polymers*.  
creep, 307-309  
definition, 306  
fatigue, 306-315  
hard organic, 306  
hysteresis, 307-309  
stress-strain, 307-309
- Plastogels, 138
- Pneumococcus antibody as monolayer, 74
- Poiseuille equation, 69
- Poisson equation, 100
- Polanyi tester, 275
- Polar van der Waals' forces, 32-36
- Polarization, of dielectric surface by adsorbed ion, 13-16  
electrostatic, of an adsorbed molecule, 36-38  
and nonpolar van der Waals' forces, 39-40
- Polymeric methyl methacrylate, sedimentation studies on, 208-212
- Polymerization, bulk, 171  
emulsion, 171
- Polymers. See also *Plastics*.  
amorphous, 80  
fatigue phenomena, 219-320  
monolayer studies, 78-80  
synthetic linear, 74
- Polymolecular substances, 162  
ultracentrifugal sedimentation, 161-218
- Polymolecularity, corrections, 195  
effects on sedimentation, 181-183
- Polymolecularity (*continued*):  
information from sedimentation measurements, 183-194  
measurements, and fractionation, 194-215
- Polystyrene, fractionation scheme, 212  
polymolecularity, 212  
sedimentation studies, 212-215  
viscosity measurements, 214
- Potential, and charge, 120-122  
relation to charge density, 114  
total, in double layer, 100
- Potential energy and repulsion forces, 6
- Potentiometry for determination of zeta potential, 119
- Preconditioning, mechanical, 308
- Preference value of length of statistical element, 171
- Preferential flotation, use of cyanide ion, 324
- Primary creep, 308  
of fibers, 275-282
- Propyl alcohol as spreading medium for protein monolayers, 71
- Proteins, adsorbed films, 75-76  
application of Henry's equation, 117  
electrophoretic data, 129  
as foam and emulsion stabilizers, 87-88  
hydrogen bonding, 76-78  
layers, hydrogen bonding, 76-78  
molecular weight in monolayers, 72  
monolayers, 71  
at air-water and oil-water interfaces, 73-75  
and interface behavior, 88  
and molecular weight determination, 71  
use of isopropyl alcohol, 71  
of propyl alcohol, 71  
purity, determination by Tiselius method, 98  
strength of salt linkages, 78  
and surface chemistry, 71-78  
surface denaturation, 74
- Protein-lipide films, artificial, 75
- Pseudoflocculation, and true flocculation, 354

## Q

Quasi-permanent flow and fatigue, 223

## R

Radial strength of molecule, 224

Radicals, adsorbed, and surface, interaction, 8-20

Rayon cords, viscose, compared to cotton cords, 303, 304

- Relaxation, of colloids, 112  
   in electrophoresis, 109-117  
   of fibers, 282-286  
   relation to size of zeta potential, 117
- Repulsion forces, 6-7  
   and adsorption energy, 7  
   and attraction, 2-8  
   and potential energy, 6
- Residual tension, 303, 305
- Resilience of fibers, 273-275
- Resins, thermoplastic, 306  
   thermosetting, 306
- Rheopexy, 145-146
- Rideal-Walker tests, 94
- Ring method for surface studies, 70
- Rubber, blended stocks, physical properties, 252  
   fatigue, 233-272  
     as related to weathering, 263-264  
   hysteresis, 237-243  
   stress-strain characteristics, 243-246
- S**
- Saccharase monolayers, 74
- Salt linkages in proteins, 78
- Schulze-Hardy rule, 353
- Schürman series of metals, 357
- Scission, chemical, and fatigue, 226-227
- Secant modulus, 224
- Secondary bond slippage and fatigue, 222-223
- Second-order transition and fatigue, 226
- Sedimentation, and concentration dependence, 177-181  
   curve, widening value, 186  
   in determination of limit of selectivity of fractional precipitation, 201  
   diagrams, frequency functions from, 188-192  
   effects of polymolecularity, 181-183  
   measurements, information on polymolecularity, 183-194  
   and osmotic pressure, comparison of concentration dependence, 180  
   properties, of threadlike molecules, 166-183  
     of molecules, and Kuhn's statistical coil, 166  
   as a rate process, 177  
   studies on cellulose nitrate, 198-208  
     on polymeric methyl methacrylate, 208-212  
     on polystyrene, 212-215  
   use of parameter functions, 192-194  
   velocity, 175  
     influence of molecular branching, 170-172
- Sedimentation constant, 164  
   average, 184-185
- Sedimentation constant (*continued*):  
   and frictional coefficient, 166  
   at infinite dilution, 174  
   and intrinsic viscosity, 197, 209  
   and molecular concentration, 172  
   and molecular weight, 183  
   and number of statistical elements, 175, 176
- Selective hydrogenation and specific adsorption, 61
- Selectivity of fractionation of high polymers, 198-202
- Semiconductors and covalent bond formation at surfaces, 20
- Semiracking, 255, 257
- Shielding ratio, and frictional coefficient, 176  
   influence on sedimentation, 176-177
- Slater-Kirkwood equation for van der Waals' interaction energy, 22
- Slimes, effect on collection, 347-353
- Slime coating, 351  
   relation to zeta potential, 352-353
- Slip boundary phenomenon, 100
- Smoluchowski derivation, assumptions, 100
- Smoluchowski-Helmholtz equation, 99-103
- Smoluchowski and Hückel theories, contradiction, 104-107
- Sodium chloride, distance of ions on crystal surface, 4
- Solid-liquid theory of lyogel structure, 139
- Solid solution theory of lyogel structure, 139
- Solvation, 142, 172-176  
   Solvatized gel, 138. See also *Lyogel*.
- Specific sedimentation volume, 174
- Specific surface conductivity, and double layer charge, 117
- Spherical particles, 122-127
- Stabilizing film, thickness, 83
- Static aging tests and fatigue, 221
- Static fatigue, effects of temperature, 297  
   at intermediate and low temperatures, 270-272  
   to rupture, 309-315
- Static fatigue-rupture, of fibers, 282-286
- Static polarizability of a metal, 30, 31
- Static rupture value, 223
- Staudinger law, validity for cellulose nitrates, 202
- Stokes-Navier equations, 104
- Stiffness and molecular orientation, 224
- St. Joe flexometer, 234
- Strain magnitudes, qualitative theory of effect on dynamic fatigue life, 254-263
- Stress-strain, of fibers, 275-282  
   of plastics, 307-309

**Stress-strain (*continued*):**

- relationship, for tension, 245
- of rubber, 243-246
- Sucrase (saccharase) monolayers, 74
- Sulfonium as flotation collector, 356
- Surface, and adsorbed ions, interaction, 8-20
  - adsorbing, changes in, 58-60
  - atoms on, 17-20
  - forms of van der Waals' interaction, 46-49
  - free radicals, on, 17-21
  - ionic, 54-55
  - metal, adsorption by van der Waals' forces, 29-32
  - reactions, 58-63
  - structure, 4-6
  - and visiting molecule, van der Waals' forces between, 20-38
- Surface aging phenomenon, 80
- Surface charge density, 103
- Surface chemistry, applications to problems in colloidal systems, 70-95
  - and colloids, 67-96
  - experimental techniques, 68-70
- Surface complex formation, 84
- Surface conductance, influence, 117-118
- Surface denaturation of proteins, 74, 88
- Surface phenomena and biological problems, 91-95
- Surface physical chemistry. *See Surface chemistry.*
- Surface potential, 69
- Surface pressure, 68
- Surface tension, relation to solute concentrations, 326, 327
- Surface viscosity, 69
- Surplus electron, 8
- Svedberg's formula, for determination of molecular weights, 164
- Svedberg-Rinde method, for following sedimentation, 165
- Svedberg unit, 164
- Swelling, due to adsorbing, 58-60
  - and solubility measurements, and fatigue, 221
- Swelling jelly, 138
- Synthetic linear polymers, 74

**T**

- Tension, residual, 303, 305
- Thermoplastic resins, 306
- Thermosetting resins, 306
- Thio alcohols, as flotation collectors, 355
- Thixotropic behavior of wool, explanation, 280
- Thixotropic breakdown, 244
- Thixotropy, 144-145
- Threadlike molecule(s), statistical volume, 171

**Threadlike molecule(s) (*continued*):**

- sedimentation properties, 166-183
  - in solution, 166-168
- Tire cords, comparison of properties, 301
- Tiselius method, for determination of purity of proteins, 98
  - of electrophoretic mobility, 98
- Total potential in double layer, 100
- Triangular frequency functions, 205

**U**

- Ultracentrifugal sedimentation of poly-molecular substances, 161-218
- Ultracentrifuge, application to cellulose, 162
  - of Svedberg and Rinde, 162
  - technique, theory, 163-166
- Ultramicroscopy with incident light, and lyogel elasticity, 150-158
- Urease monolayers, 74
- U. S. Rubber Company Cord Fatigue Tester, 291, 292, 295

**V**

- Valency electron, 8
- Van der Waals' adsorption, 20
- Van der Waals' forces, 3, 6, 7
  - adsorption on metal surfaces, 29-32
  - mutual, between adsorbed molecules, 49-52
  - nonpolar, 21
    - nature, 21-24
  - polar, 32-36
    - between surface and visiting molecule, 20-38
- Van der Waals' interaction at different spots of surface, 46-49
- Van der Waals' interaction energy, equations, 22
- Van der Waals'-London theory of lyogel structure, after Hamaker, 140
- Viscose rayon cords compared to cotton, 303, 304
- Viscosity, of high polymers, concentration dependence, 203
  - of liquid, in Smoluchowski derivation, 101
- Viscous damping, 274
- Viscous friction, 103
- Visiting molecule, and surface, van der Waals' forces, 20-38
- Vorzugswert*, 171

**W**

- Water-avid groups, 328. *See also Hydrophilic colloids.*
- Water avidity and unsaturated bonds, 329

Wave equation and behavior of atoms, 3  
Weathering of rubbers, 263-264  
Weighted creep of fibers, 285  
Wilhelmy plate method in surface chemistry, 71  
Work function of metal, 52

### X

Xerogel(s), 138  
  liquid content, 138  
X-ray diffraction of elastic lyogels, 148-150

### Y

Yarns, cumulative extension, 303

### Z

Zeta potential, 98  
  calculations from electrophoretic mobility, 98  
  and charge, applications, 128-130  
  conditions for evaluation from electrophoresis, 118  
  determination by electroosmosis, 119  
    by potentiometry, 119  
    by streaming potential, 119  
  and electrophoresis, 118-119  
  and epsilon potential, difference, 100  
  minimal, 98  
  of particle surface, 100  
  relation to slime coating, 352-353  
  size and relation to relaxation effect, 117





